JOURNAL OF THE

Electrochemical Society

l. 114, No. 3

March 1967

Dallas Meeting Program Issue

No more eyeballing.

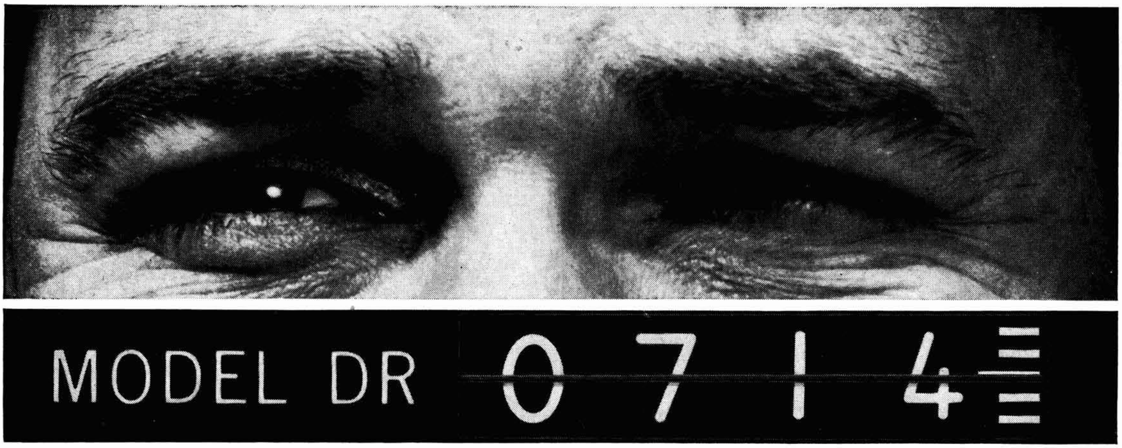

You can read Sargent's DR pH Meter to 0.001 pH at a glance.

You'd need a pH scale 35 feet in length to get readability equivalent to that of our DR pH Meter. There's no switching or recalibration required to get a reading to 0.001 pH. The DR reads directly, in digits, to the second decimal; a graduated scale shows the third decimal.

The DR's relative accuracy is ± 0.002 pH (within 4 pH of buffer set point). This accuracy is unchanged by any mechanical or electrical wear in its automatic, self-balancing, measuring system. There's no drift, either. Restandardization is dictated only by the type of electrode used. Three controls are all it takes to realize the DR's full capability: one each for standardization, operating mode, and temperature compensation.

The DR's high input impedance lets you work with any commonly used electrode. And the automatic isopotential setting adapts to electrodes of any isopotential from 0 to 14 pH —without adjustment.

The Model DR pH Meter is designed and manufactured by E. H. Sargent & Co. So you know that it's made for dependable, trouble-free service. And that it's been carefully assembled and thoroughly tested.

This unique combination of readability, accuracy, and reliability is priced at $630.00 (with electrodes and solutions). If you'd like a demonstration of the Model DR pH Meter, just call your Sargent man or write directly to us.

7-212

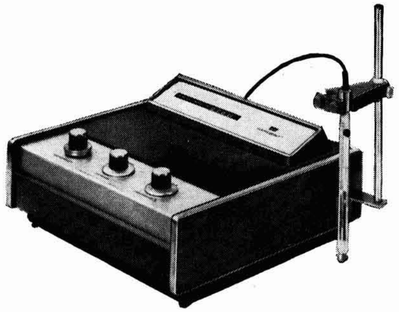

Sargent Model DR
Direct-Reading
pH Meter

SARGENT® SCIENTIFIC LABORATORY INSTRUMENTS • APPARATUS • CHEMICALS

E. H. SARGENT & CO.
4647 West Foster Avenue
Chicago, Illinois 60630

Chicago • Anaheim, Calif. • Birmingham • Cincinnati • Cleveland
Dallas • Denver • Detroit • Springfield, N.J. • Toronto, Canada

JOURNAL OF THE

C. L. Faust, Chairman, Publication Committee
Charles B. Moore, Director of Publications

EDITORIAL STAFF

Cecil V. King, Editor
Norman Hackerman, Technical Editor
Ruth G. Sterns, Managing Editor
Julius Klerer, Book Review Editor
Daniel J. Immediato, Assistant Editor

DIVISIONAL EDITORS

W. C. Vosburgh, Battery
Paul C. Milner, Battery
Z. A. Foroulis, Corrosion
A. C. Makrides, Corrosion
Morris Cohen, Corrosion
Jerome Kruger, Corrosion
J. Paul Pemsler, Corrosion
Harry C. Gatos, Corrosion—Semiconductors
Newton Schwartz, Dielectrics and Insulation
Seymour Senderoff, Electrodeposition
Ephraim Banks, Electronics
Simon Larach, Electronics
F. A. Trumbore, Electronics—Semiconductors
P. Wang, Electronics—Semiconductors
George R. Cronin, Electronics—Semiconductors
H. Clay Gorton, Electronics—Semiconductors
Sherlock Swann, Jr., Electro-Organic
Stanley Wawzonek, Electro-Organic
John M. Blocher, Jr., Electrothermics & Metallurgy
J. H. Westbrook, Electrothermics & Metallurgy
Scott Lynn, Industrial Electrolytic
C. W. Tobias, Theoretical Electrochemistry
A. J. deBethune, Theoretical Electrochemistry
R. M. Hurd, Theoretical Electrochemistry
M. W. Breiter, Theoretical Electrochemistry

ADVERTISING OFFICE
ECS

Daniel J. Immediato, Assistant Editor
Journal of The Electrochemical Society
30 East 42 St., New York, N. Y., 10017

ECS OFFICERS

H. J. Read, President
Dept. of Metallurgy
Pennsylvania State University
University Park, Pa.

H. C. Gatos, Vice-President
Depts. of Met. & Electrical Eng.
Massachusetts Institute of Technology
Cambridge, Mass. 02139

Ivor E. Campbell, Vice-President
220 Gentry Rd.
Coraopolis, Pa.

N. C. Cahoon, Vice-President
Union Carbide Corp.
Consumer Products Division, Cleveland, Ohio

Ralph A. Schaefer, Treasurer
The Electric Storage Battery Co.
Yardley, Pa.

R. F. Bechtold, Secretary
Dow Chemical International A.G.,
Alfred Escher Strasse 39,
Zurich, Switzerland

Ernest G. Enck, Executive Secretary
National Headquarters, The ECS,
30 East 42 St., New York, N. Y., 10017

MARCH 1967

EDITORIAL

ELECTROCHEMICAL SCIENCE

TECHNICAL PAPERS

TECHNICAL NOTES

BRIEF COMMUNICATIONS

ELECTROCHEMICAL SOCIETY

VOL. 114 • NO. 3

SOLID STATE SCIENCE

TECHNICAL PAPERS

TECHNICAL NOTE

BRIEF COMMUNICATION

ELECTROCHEMICAL SOCIETY NEWS

DALLAS MEETING PROGRAM

Manuscripts submitted to the Journal should be sent, in triplicate, to the Editorial Office at 30 East 42 St., New York, N. Y., 10017. They should conform to the revised Instructions to Authors published on pp. 299C-300C of the Nov. 1966 issue. Manuscripts so submitted become the property of The Electrochemical Society and may not be published elsewhere, in whole or in part, unless permission is requested of and granted by the Editor.

The Electrochemical Society does not maintain a supply of reprints of papers appearing in its Journal. A photoprint copy of any particular paper, however, may be obtained by corresponding direct with the Engineering Societies Library, 345 E. 47 St., New York, N. Y., 10017.

Inquiries re positive microfilm copies of volumes should be addressed to University Microfilms, Inc., 313 N. First St., Ann Arbor, Mich.

Walter J. Johnson, Inc., 111 Fifth Ave., New York, N. Y., 10003, have reprint rights to out-of-print volumes of the Journal, and also have available for sale back volumes and single issues, with the exception of the current calendar year. Anyone interested in securing back copies should correspond direct with them.

Published monthly by The Electrochemical Society, Inc., at 215 Canal St., Manchester, N. H.; **Executive Offices, Editorial Office and Circulation Dept.,** and **Advertising Office** at 30 East 42 St., New York, N. Y., 10017, combining the JOURNAL and TRANSACTIONS OF THE ELECTROCHEMICAL SOCIETY. Statements and opinions given in articles and papers in the JOURNAL OF THE ELECTROCHEMICAL SOCIETY are those of the contributors, and The Electrochemical Society assumes no responsibility for them.

Claims for missing numbers will not be allowed if received more than 60 days from date of mailing plus time normally required for postal delivery of JOURNAL and claim. No claims allowed because of failure to notify the Circulation Dept., The Electrochemical Society, 30 East 42 St., New York, N. Y., 10017, of a change of address, or because copy is "missing from files." Subscription to members as part of membership service; subscription to nonmembers $24.00 plus $1.50 for postage outside U.S. and Canada. Single copies $1.70 to members, $2.25 to nonmembers. Entered as second-class matter at the Post Office at Manchester N. H., under the act of August 24, 1912. Postage paid at Manchester, N. H.

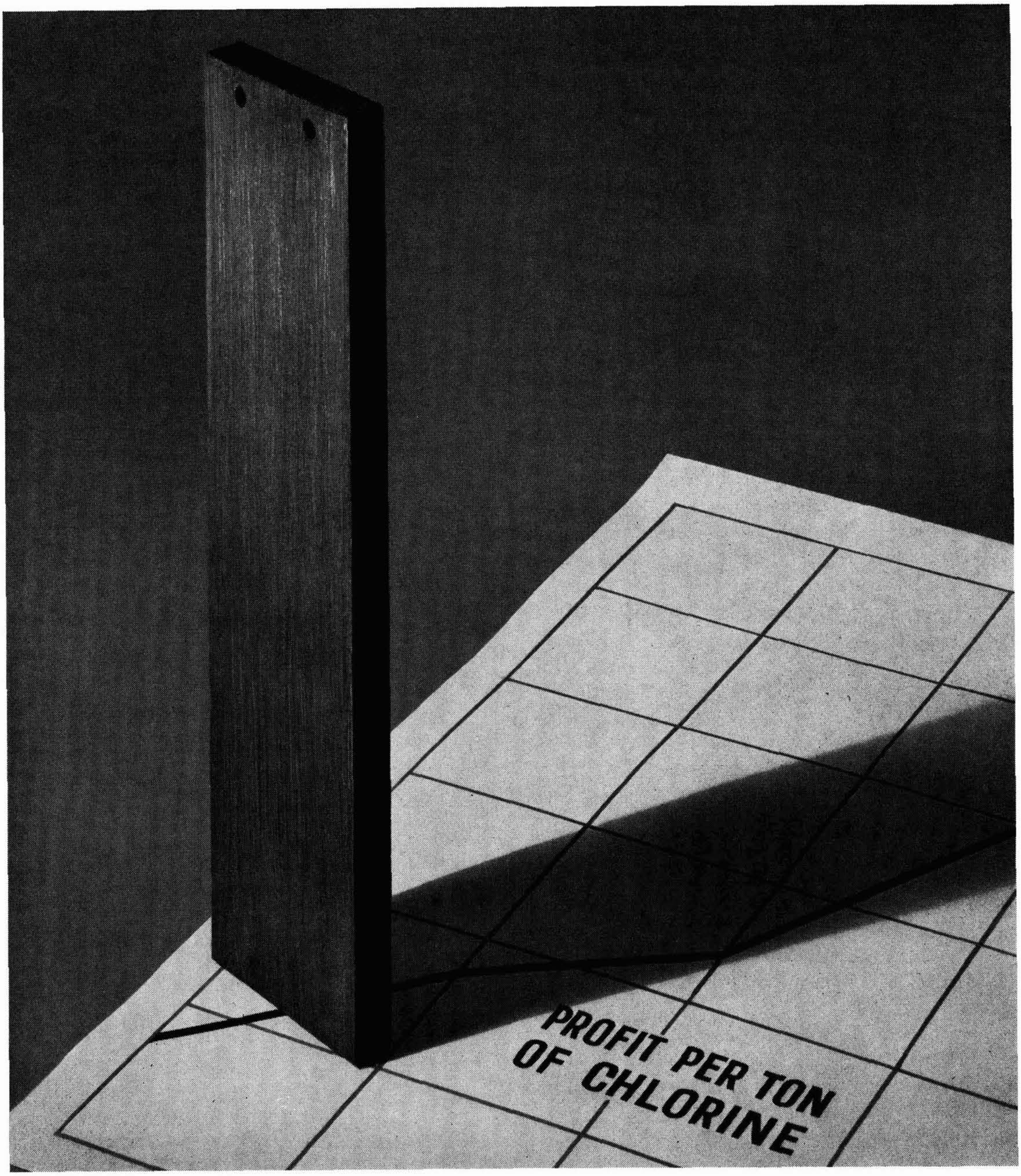
PROFIT PER TON
OF CHLORINE

Information Required

We are working hard toward an expanded publications program, such that Society members and *Journal* readers will:

First, consider Society journals the primary and favored target for their professional output, and,

Second, agree that Society journals fully serve their professional needs.

My editorial in December reported the Publication Committee's recommendations of a three-way split in existing journals. Progress has been made since, and January's meeting of the Board of Directors might even be termed exciting in the vistas evoked and questions provoked.

We have not yet decided on a course of action, and feel that you will approve our careful approach. One more investigation, and a decision can be achieved.

Early in March, we will investigate *you,* all those receiving the *Journal,* through a short and painless questionnaire. An ad hoc committee, consisting of Publication Committee Chairman, C. L. Faust, Treasurer, R. A. Schaefer, and myself, has been empowered by the Board of Directors to conduct the survey, evaluate returns along with other facts, and recommend action to the Board.

At meetings, by telephone and letter, many have suggested ways toward an expanded publications program. But these may not be the Society, nor even a sizable percentage of *Journal* readers. *We urge that you, all of you, fill out and return the questionnaire promptly.* Tell us whether our present publication program serves *your* needs, or if not, why not. The questionnaire will enable you to express your reader preference. We give away no prizes. But we do dangle prospects of publication tailored to your publishing and reader interests.

—Harold J. Read, President
The Electrochemical Society

Is the discrete semiconductor business here to stay?

It depends upon your point of view — your attitude — your method of attack. Some of us have found ways to maximize our position in this industry through unique product innovation, strategic planning and market specialization; others in the industry have plodded along, pushing out the same old product with the same old technology — and have, as a result, fallen behind. Still others have pursued short-term strategies which maximize today's profitability but suggest extremely vulnerable positions under changed market conditions.

Question: Will hybrid micro circuits or monolithic integrateds severely deteriorate the market for small signal transistors?

Answer: We think so — probably within the next year or two.

Question: Will I.C. technology severely deteriorate the market for a sophisticated family of medium power SCR's?

Answer: Absolutely — but probably not for another decade.

Question: Where will we be in 5 years? — or 10?

Answer: We'll be building a new future — and probably at 4 or 5 times our present size.

Question: How have we done so far?

Answer: Very well, thank you. And we can show you a business performance to prove it. SSPI has enjoyed a solid position in the industry for each one of its 8 years. We were "in the black" when the industry was failing in 1961 and 1962.

Question: Who will obsolete SSPI's products?

Answer: SSPI will.

If you're uncertain about where your company will be in this industry when today's boom is passed, you should talk to SSPI.

Call or come in and let us tell you about where we have been and where we're going. We have new openings for good people in every area of semiconductor product and process technology as well as related areas of sales, application and equipment development.

We're excited about our company and the future we're planning for it in this industry. We think you'll be excited about it, too! Your inquiry by phone or mail to Mr. Richard J. Bronstein is invited.

SOLID STATE Products, Inc.

An Equal Opportunity Employer.

ONE PINGREE STREET, SALEM, MASS.
617 - 745-2900

ELECTROCHEMICAL SCIENCE

Fused-Organic Electrolytes for Thermal Cells

Richard A. Wallace[1] **and Paul F. Bruins**

Department of Chemical Engineering, Polytechnic Institute of Brooklyn, Brooklyn, New York

ABSTRACT

The low-melting ($<200°C$) fused electrolytes tested were salts of organic acids, substituted pyridinium halides, and acetamide salt solutions. Methylpyridinium bromide and several alkali acetates were found to be thermally stable and good conductors, but they entered into spontaneous reactions with cathodic oxidants. Salts in molten acetamide, however, made suitable low-melting electrolytes for organic thermal cells. Potentials of some fused-acetamide cells were measured as a function of temperature, and the behavior on discharge was observed.

An organic fused-salt cell is a reserve-type thermal cell which produces electrical energy of long duration on application of a requisite amount of heat. The organic electrolyte of this cell is solid and nonconducting at ordinary temperatures, but, on activation, the heat rapidly applied to the cell causes the electrolyte to melt and become conducting.

Organic thermal cells have not been studied thoroughly in the past, chiefly because of a lack of reliable data of the physical and electrochemical behavior of suitable low melting salts. The literature on fused-salt thermal cells relates chiefly to inorganic ones of the type reported by Hamer and Schrodt (1) and Goodrich and Evans (2). Special inorganic types have been treated by Rubin and Malmberg (3), McKee (4), Doan (5), Selis (6), and Jennings (7). Panzer (8) carried out exploratory test surveys on a wide variety of organic and inorganic salts for possible application as suitable electrolytes in fused-salt thermal cells. Unfortunately, most fused-salt cell studies are largely qualitative in nature.

The three most important disadvantages of current inorganic thermal cells are (*a*) high operating temperatures (400°-600°C), (*b*) cell life limited to 5-10 min, and (*c*) marked cathodic polarization.

Organic electrolytes can be divided into two classes. The first is organic salts that conduct electrolytically in the molten state, *e.g.*, the sulfonates, formates, acetates, and substituted pyridinium salts. The second class includes solutions of salts in organic solvents, *e.g.*, molten acetamide salt solutions (9).

Experimental

Reagents.—Methylpyridinium chloride was prepared by the method of Rozhdestvenskii (10). The hygroscopic crystalline solid melted at 138°C, in agreement with that reported in the literature. On melting, the salt forms a clear, water-white melt that did not decompose up to 200°C for 2 hr. This chloride salt was extremely hygroscopic and difficult to obtain in high yields. On the other hand, the corresponding bromide pyridinium salt was appreciably less hygroscopic and was obtainable in yields greater than 80%.

Methylpyridinium bromide was prepared by passing excess methyl bromide into a mixture of equal volumes of pyridine and benzene at room temperature. After about 4 min, the exothermic addition reaction between pyridine and methyl bromide occurred. At this time the addition reaction was stopped, and the resulting white slurry removed and washed with large volumes of benzene to ensure removal of trace amounts of pyridine adsorbed on the salt. The salt was purified further by crystallization from anhydrous ethyl alcohol at —40°C. This purification procedure was repeated three times. The salt was vacuum-dried for two days; its melting point is 150°-151°C. The bromide salt forms a clear, water-white melt that did not char or otherwise decompose up to 200°C for several hours.

Acetamide crystals (Mallinckrodt analytical reagent) were further purified by recrystallization from pure benzene and then vacuum-dried for two days. The salts $MgCl_2$, $AlCl_3$, $ZnCl_2$, and $CdCl_2$ (Baker and Adamson reagents) were used without further purification; they were dried at about 200°C and kept in a desiccator.

Metal rod electrodes (Fisher Scientific) were at least 99.5% pure. Silver-silver chloride electrode was prepared electrolytically. Cathodic oxidants such as $CaCrO_4$ and K_2CrO_4 were supplied by Eagle-Picher. All electrode materials were washed with acetone and dried at 120°C prior to use in cells.

Electrolytic cell.—Figure 1 depicts the electrolytic cell used to measure the potentials of organic fused-salt cells as a function of temperature. The cells were constructed of Pyrex glass unless noted otherwise. All

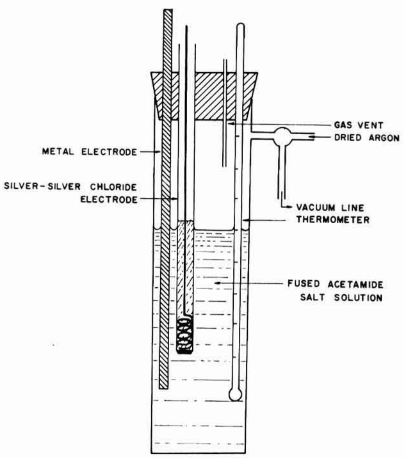

Fig. 1. Fused-acetamide salt cell

---

[1] Present address: Department of Chemical Engineering, University of California, Berkeley, California.

negative electrodes were 1/8-in. commercially pure metal rods. The positive electrode was nickel mesh with $CaCrO_4$ or K_2CrO_4 oxidants for fused acetate and pyridinium cells. For fused acetamide salt cells, a 1/16-in. Ag/AgCl rod immersed in 0.10M KCl-Acetamide and contained in a fritted glass tube, shown in Fig. 1. A positive liquid head was maintained in the tube compartment of this Ag/AgCl electrode to prevent contamination of the acetamide salt solution. Interelectrode distance was about 1.0 cm. Approximately 100g of a tenth molal metal chloride solution was placed in the cell, immersed in a thermonitor-controlled oil bath by Sargent.

Upon fusion of the organic salt mixture, the cell was vacuum-pumped for 2 hr through the side arm to remove water vapor from the electrolyte. Then dry argon gas was allowed to enter, bringing the system to atmospheric pressure. Argon was continuously maintained above the organic melt and allowed to escape via a small exit tube in the stopper. Once constant temperature was attained, the emf of the system was measured with an L&N K-3 potentiometer.

Results and Discussion

Potassium methylsulfonate and the sodium salts of benzene and p-toluene sulfonic acids all failed to melt. Molten sodium formate did not decompose for several hours at 270°C, but readily reduced AgCl, $CaCrO_4$, and K_2CrO_4 cathodic reactants.

A eutectic mixture (11) of sodium, potassium, and lithium acetates (37.5/11.9/50.6 w/o) melted at 157°C and remained thermally stable and conductive at 200°C for 5 hr. The fused acetate eutectic also reacted spontaneously with $CaCrO_4$ and K_2CrO_4. The cell Mg/alkali acetate eutectic/$CaCrO_4$,Ni failed to deliver useful amounts of current at 250°C.

Substituted pyridinium halides have better thermal and conductive properties than unsubstituted pyridinium halides (12). Methylpyridinium chloride and bromide were thus synthesized and evaluated as molten electrolytes for organic thermal cells. Figure 2 presents the electrical conductivity of molten methylpyridinium bromide. Clearly, this salt conducts very well in the molten state.

The organic salt cell, Mg/methylpyridinium bromide/$CaCrO_4$,Ni gave an open-circuit potential of 1.15v at 200°C. Appreciable currents, however, were not obtained when this cell was under load. At the magnesium electrode, two reactions took place during discharge: the electrochemical cell reaction and the redox reaction between magnesium and methylpyridinium bromide.

Potential-temperature data of several fused acetamide salt systems were measured in our experimental cell. Calcium is not included here because of its vigorous reaction with fused acetamide to generate hydrogen. Conductance data for several alkali and alkaline earth chlorides in molten acetamide are given by Wallace (9) and Winkler (13).

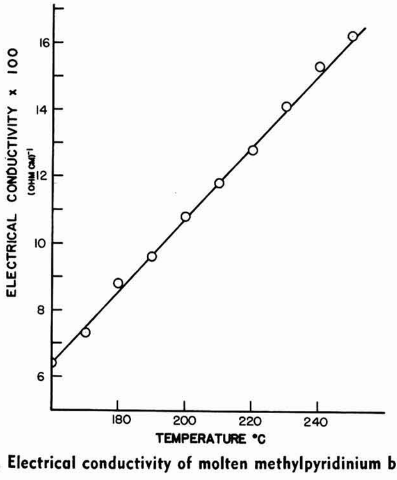

Fig. 2. Electrical conductivity of molten methylpyridinium bromide

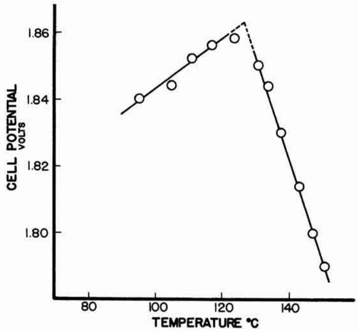

Fig. 3. Cell potential of Mg/0.10M $MgCl_2$-acetamide/AgCl,Ag. Hydrogen was evolved above 125°C.

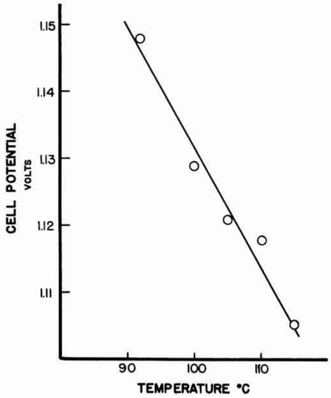

Fig. 4. Cell potential of Al/0.10M $AlCl_3$-acetamide/AgCl,Ag. Hydrogen was evolved both on open circuit and discharge.

Magnesium.—The open-circuit potential of Mg/0.10*M* $MgCl_2$-acetamide/AgCl,Ag cell is shown in Fig. 3 as a function of temperature. The potential (1.835v at 90°C) increased with temperature up to about 125°C (1.860v) where hydrogen evolution began. Above 125°C the cell potential rapidly decreased. The extent of magnesium corrosion with molten acetamide increased slowly up to 125°C and then accelerated in an exponential-like manner with rising temperature.

Much hydrogen gassing occurred in these cells when placed on discharge. On replacing chloride solutions with bromide salt solutions in magnesium-acetamide thermal cells, however, hydrogen evolution was reduced markedly.

Aluminum.—The open-circuit potential of Al/0.10*M* $AlCl_3$-acetamide/AgCl,Ag cell was measured as a function of temperature. Figure 4 shows the cell potentially (1.150v at 90°C) falling sharply with increasing temperature. Hydrogen evolution occurred rapidly with aluminum due chiefly to the high acidity of molten $AlCl_3$-acetamide. When aluminum-acetamide cells were placed on discharge, very vigorous hydrogen evolution was noted.

Zinc.—The equilibrium voltage of Zn/0.10*M* $ZnCl_2$-acetamide/AgCl,Ag decreases linearly with increasing temperature, as shown in Fig. 5. The potential of the cell reaction: $Zn + 2AgCl = ZnCl_2\ (0.10M) + 2Ag$ with a zinc chloride concentration of 0.10*M* in molten

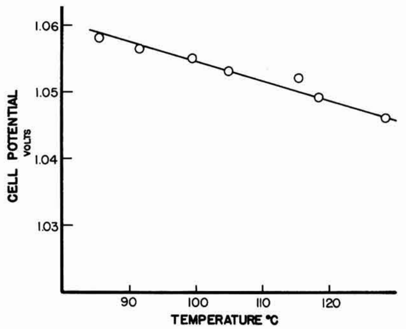

Fig. 5. Cell potential of Zn/0.10*M* $ZnCl_2$-acetamide/AgCl,Ag

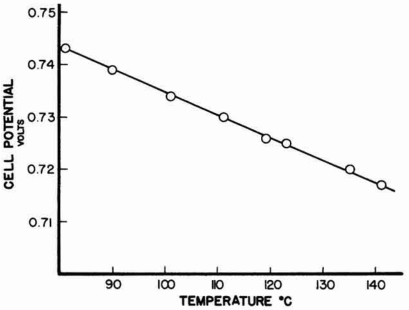

Fig. 6. Cell potential of Cd/0.10*M* $CdCl_2$-acetamide/AgCl,Ag

acetamide is 1.058v at 90°C. By use of the Gibbs-Helmholtz relation, the heat of reaction is calculated to be —56.3 kcal/mole and entropy change, —25.3 e.u. For comparison, ΔH of —55.6 kcal/mole and ΔS of —34.5 e.u. are recorded at 25°C for the aqueous cell reaction: $Zn + 2AgCl = ZnCl_2$ ($a = 1$) $+ 2Ag$ with unit zinc chloride activity in water (14).

The discharge behavior of this galvanic cell system was determined at 90° and 130°C. Several silver chloride-zinc cells were held at these temperatures for 8 hr before discharging. No harmful effects or cell deterioration was observed. Even under maximum current drains, the zinc electrode did not gas. The initial maximum current output from these cells were largely limited by the resistance offered by the molten electrolyte. Values for the conductivity of molten 0.10*M* $ZnCl_2$-acetamide were 0.5 x 10^{-3} ohms-cm^{-1} at 90°C and 0.9 x 10^{-3} ohms-cm^{-1} at 130°C. Discharge cell performance and limitations for silver chloride-zinc cells are presented in another paper (15).

Cadmium.—In Fig. 6 is given the equilibrium cell potential of Cd/0.10*M* $CdCl_2$-acetamide/AgCl,Ag cell as a function of temperature. The potential of the cell reaction: $Cd + 2AgCl = CdCl_2$ (0.10*M*) $+ 2Ag$ with a cadmium chloride concentration of 0.10*M* in molten acetamide is 0.739v at 90°C. The heat of reaction is calculated to be —42.3 kcal/mole and entropy change, —23.0 e.u. For comparison, ΔH of —36.5 kcal/mole and ΔS of —26.1 e.u. are recorded at 25°C for the aqueous cell reaction: $Cd + 2AgCl = CdCl_2$ ($a = 1$) $+ 2Ag$ with unit cadmium chloride activity in water (14).

The discharge behavior of this galvanic cell system was also determined at 90° and 130°C. No cell deterioration or gassing was noted on discharge. Likewise, maximum current output from these silver chloride-cadmium thermal cells were initially limited by the conductivity of 0.10*M* $CdCl_2$-acetamide melt, 0.3 x 10^{-3} ohms-cm^{-1} at 90°C, and 0.7 x 10^{-3} ohms-cm^{-1} at 130°C. Discharge behavior of these cells was similar to silver chloride-zinc thermal cells.

Acknowledgments

The authors wish to thank the Sandia Power Sources Laboratory in Albuquerque, New Mexico, for their sponsorship. Thanks are due to Dr. Charles Jennings and Dr. Frank Hudson for stimulating discussions.

Manuscript received Aug. 12, 1966; revised manuscript received Oct. 12, 1966. This paper was delivered before the New York Meeting Oct. 1-3, 1963. This work was done in partial fulfillment of the requirements for the Ph.D. degree at Polytechnic Institute of Brooklyn by R. A. Wallace.

Any discussion of this paper will appear in a Discussion Section to be published in the December 1967 JOURNAL.

REFERENCES

1. W. J. Hamer and J. P. Schrodt, *J. Am. Chem. Soc.*, **71**, 2347 (1949).
2. R. B. Goodrich and R. C. Evans, *This Journal*, **99**, 207 (1952).
3. B. Rubin and M. S. Malmberg, National Bureau Standards Report 3081, Washington, D. C. (1954).
4. E. S. McKee, Proc. Tenth Annual Battery Conference, Power Sources Div., Signal Corps Engineering Lab., Fort Monmouth, N. J. (1956).
5. D. J. Doan, Proc. Eleventh Annual Battery Conference, Power Sources Div., Signal Corps Engineering Lab., Fort Monmouth, N. J. (1957).
6. S. M. Selis, Proc. Twelfth Annual Battery Conference, Power Sources Div., Signal Corps Engineering Lab., Fort Monmouth, N. J. (1958).
7. C. W. Jennings, *This Journal*, **103**, 531 (1956).
8. R. E. Panzer, Technical Memorandum 44-7, U. S. Naval Ordnance Laboratory, Corona, Calif. (1960).
9. R. A. Wallace, Dissertation, Investigation of Organic Fused-Salt Cells, Polytechnic Institute of Brooklyn, New York (1963).
10. M. S. Rozhdestvenskii and L. M. Broude, *J. Appl. Chem. (USSR)*, **10**, 722 (1937).
11. N. M. Sokolov, *J. Russian General Chem.*, **24**, 1145 (1954).
12. R. C. Elderfield, "Heterocyclic Compounds," Vol. 1, p. 414, John Wiley & Sons, Inc., New York (1950).
13. G. Winkler in "Chemistry in Nonaqueous Ionizing Solvents," G. Jander, H. Spandau, and C. Addison, Editors, Vol. IV, Part 3, Vieweg and Sohn, Braunschweig, Germany (1963).
14. W. M. Latimer, "Oxidation Potentials," Prentice-Hall, New York (1953).
15. R. A. Wallace and P. F. Bruins, *This Journal*, **114**, 212 (1967).

Fused-Acetamide Thermal Cells

Richard A. Wallace[1] **and Paul F. Bruins**

Department of Chemical Engineering, Polytechnic Institute of Brooklyn, Brooklyn, New York

ABSTRACT

Low-temperature ($<200°C$) fused-acetamide thermal cells, using highly porous cathodes, furnish appreciable electrical energy on discharge. The cell, Zn/2.5% KCl-acetamide/AgCl,Ag had an average discharge voltage of 0.970v (at 2.0 ma/cm^2 and 100°C) for 360 min. Cathodic polarization was principally responsible for termination. Voltage regulation and uniform discharge depended to a very large degree on silver chloride electrode. Effects of charge rate and addition of small amounts of water on cell discharge were also measured.

In the previous paper (1) we reported that low-temperature ($<200°C$) organic thermal cells generated appreciable electrical energy on discharge and molten acetamide salt solutions made good cell electrolytes. In this paper, the fused acetamide cell, Zn/2.5% KCl-acetamide/AgCl,Ag has been studied.

Existing information on the physical and chemical properties of solid and molten acetamide has been reviewed by Winkler (2) and Wallace (3). In 1957 Jander and Winkler (4) made careful potentiometric and conductometric titrations of a relatively large number of acid-base neutralization reactions in molten acetamide. Early in 1960, Wallace (3) measured several physical and electrochemical properties of molten KCl-acetamide and KBr-acetamide systems over their full solubility and temperature ranges and reported their use as low-temperature thermal cell electrolytes. We found that molten saturated KCl-acetamide meets most of the basic criteria set down for a suitable electrolyte for organic fused-salt cell usage (1). Its effective liquid range, and hence the temperature range of the cells, lies between 77°C (melting point) and 180°C (200 mm Hg vapor pressure).

Acidic (H_2SO_4) and basic (KOH) solutes are not suitable for cell usage because they decompose acetamide. A nonhygroscopic, neutral salt having good solubility and conductance in molten acetamide is needed and KCl was found suitable. The molten acetamide salt solution (see Fig. 1) should be nearly saturated (2.5g KCl/100g acetamide or 0.33*M*). Such a KCl-acetamide solution is preferred because it provides maximum conductance while still assuring complete solution of KCl at any temperature.

Silver chloride was selected as the cathodic reactant. Preliminary experiments showed that it provides excellent voltage stability and an unusually flat discharge curve in working acetamide cells. Also, it is slightly soluble in saturated KCl-acetamide solutions.

Zinc was the most convenient working anode for a study of fused-acetamide salt cells under discharge for long periods (hours) at moderately high current drains. Zinc did not gas in the organic thermal cell, Zn/KCl-acetamide/AgCl,Ag on dicsharge. It has a high electrochemical capacity (49.2 amp-min/g), and $ZnCl_2$ is highly soluble in molten acetamide.

Experimental

Reagents.—Acetamide crystals (Mallinckrodt analytical reagent grade) were further purified by recrystallization from pure benzene. Recrystallized acetamide was vacuum-dried for two days and then kept in a desiccator. The salts KCl and $ZnCl_2$ (Baker and Adamson reagents) were used without further purification; the salts were dried at about 150°C and the dried salts kept in a desiccator. Dry argon gas was used to minimize dissolved oxygen in fused acetamide. Zinc sheet (N. J. Zinc) was 99.95% containing less than 0.005% Cu, 0.005% Fe, 0.005% Cd, the major impurity being Pb. Rectangular sheets of high-purity, fused AgCl electrodes with a surface skin of Ag to make electronic contact were supplied by Eagle-Picher. Our analysis showed these electrodes contained 99.5% AgCl and 0.5% Ag.

Reference electrode.—The $Ag/AgCl/Cl^-$ reference electrode has been used successfully in both aqueous and molten salt electrochemistry and found by Wallace (3) to be a stable and reproducible reference electrode in molten acetamide systems. The $Ag/AgCl/Cl^-$ reference electrode is described in Fig. 2. The glass container for this reference electrode (Fig. 2) was a small glass tube of about ½-in. diameter with a fritted glass bottom (medium porosity) that acted as a salt bridge between the reference electrode and test cell electrodes. The electrode proper was prepared by chloridizing a 1.6 mm silver wire in 1*N* HCl at 25°C for 2 hr at 10 ma/cm^2 current density. The lower portion of the electrode was wound spirally to provide not only greater electrolytic contact area, but also a snug fit with the inside of the tube, thereby fixing the position of the electrode. Excess solid KCl was added to the tube compartment in order to keep the chloride activity constant.

Conductometric measurements.—Conductances of molten electrolytes were measured with an industrial instrument (model RC-16B2) conductivity bridge using a dip-type cell with a 0.630 cell constant. The measurements were made at a frequency of 1000 Hz; preliminary runs showed that electrolyte resistances were independent of frequency.

Temperatures of molten acetamide solutions were controlled to 0.3°C by a forced-draft electric furnace. A period of 20 min was allowed after each salt addition before a resistance reading was taken. During this period the melt was shaken to ensure complete solution of the added salt and to hasten equilibrium.

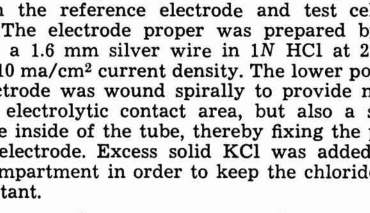

Fig. 1. Solubility of KCl in molten acetamide

---

[1] Present address: Department of Chemical Engineering, University of California, Berkeley, California.

Cell design and testing.—Experimental acetamide cells consisted of a Ag-AgCl rectangular cathode (3.3 x 3.3 x 0.091 cm) sandwiched between two parallel zinc anodes (3.3 x 3.3 x 0.059 cm). Electrode separation was effected by four tiny glass strips (0.80 cm long and 0.40 cm wide) cemented to the top and bottom edges of each electrode with a high-temperature epoxy adhesive. The parallel-electrode arrangement (Fig. 2) was used because it was simple in geometrical design, provided as nearly uniform current density as possible over the surfaces of the plane electrodes, and allowed the acetamide melt to circulate freely between working electrodes. Electrical contact was made by soldering a thin Zn tab to the two outside Zn sheets and by silver-soldering a thin Ag wire to the silver-coated AgCl electrode, or in the case of electroformed Ag-AgCl, to the Ag mesh screen itself. This sandwich cell was sturdy and did not buckle under thermal stresses produced during testing.

More porous Ag-AgCl cathodes were also prepared by chloridizing spongy silver sheets, incorporated on silver grids of about 50 by 50 mesh supplied by Eagle-Picher. Silver was electrolytically converted into active AgCl by chloridizing in a 1*N* HCl at 25°C and a current density of 10 ma/cm². Formation was continued until the remaining silver was reduced to about one-half its original thickness.

All cells were immersed in a 400 ml Pyrex beaker containing 2.5% KCl-acetamide solution maintained at a constant temperature in an electric oven. Cell voltages were measured with a Sargent (Model MR) multirange potentiometric recorder, calibrated periodically against a Weston standard cell whose emf was 1.0193v. These cells were discharged at a constant current by manually adjusting the load. Charging of the cells was done either on an automatic constant current charger supplied by Ray-O-Vac, Division of Electric Storage Battery Company, or manually.

Electrode polarization.—Polarization potential of the working electrodes were measured at 100°C by means of the reference electrode in the same acetamide electrolyte. Included in these polarization potentials was the ohmic drop in the electrolyte between the reference electrode and the surface of the working electrode. To minimize this voltage drop, the reference electrode was placed in close proximity to the outer edge of both working electrodes, a region where the current flux is minimal.

Results and Discussion

A systematic conductometric analysis of the role and influence of $ZnCl_2$ in molten $KCl_{(sat.)}$-acetamide was made by Wallace (3). In Fig. 3 is presented the specific electrical conductance of $ZnCl_2$-$KCl_{(sat.)}$-acetamide solutions, as a function of zinc salt concentration and temperature. When added in small amounts, $ZnCl_2$ markedly diminished the conductivity of the molten KCl-acetamide electrolyte. On further additions, the conductivity reached a minimum and then increased fairly rapidly thereafter until it attained a maximum value occurring in the 1-3*M* zinc salt region.

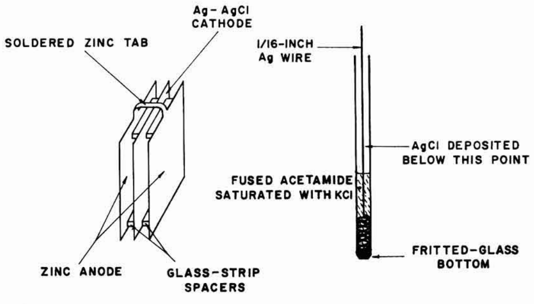

Fig. 2. Diagrams of experimental cell (left) and silver-silver chloride reference electrode (right).

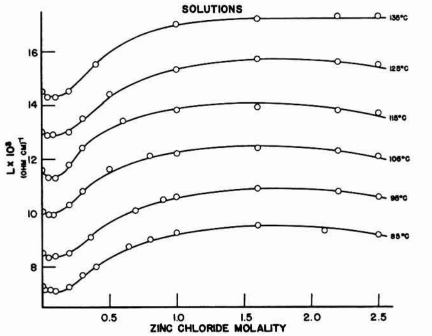

Fig. 3. Specific conductance of molten $ZnCl_2$-$KCl_{(sat.)}$-acetamide solutions.

These conductance deviations were attributed to the formation of chlorozinc complex and coordination molecules in the saturated KCl-acetamide melt; these effects resulted in minimum-maximum curves. The precise location of the minima and maxima points depend upon the temperature and amount of KCl in acetamide. In Fig. 3 it is of interest to point out that the large temperature coefficient of conductance may be due to two factors: (*i*) less stability of chlorozinc complexes with increasing temperature, putting more chloride ions in solution, and (*ii*) increased KCl solubility with temperature, putting more potassium and chloride ions in solution.

Cell performance.—The performance characteristics of experimental Zn/2.5% KCl-acetamide/AgCl,Ag cells were measured with temperature, electrode spacing, and discharge current density as parameters. Typical performance curves for cells using fused Ag/AgCl cathodes are shown in Fig. 4. On applying a load, the cell voltage falls almost instantaneously to a steady value and remains fairly constant throughout discharge.

The magnitude of the maximum current drains increased with an increase in operating temperature and, to a lesser extent, with a decrease in electrode spacing. Discharge current densities exceeding 30 ma/cm² could not be obtained from these experimental cells, although it is likely that higher current densities could be attained in cells using more porous cathodes, operating at higher temperatures with closer electrode spacings.

Temperature effect.—In all experimental cells, the cell voltage and maximum current output increased

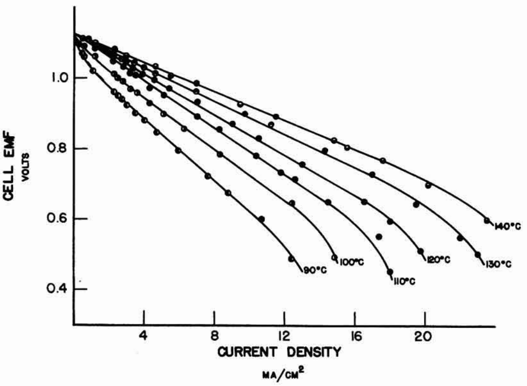

Fig. 4. Performance of Zn/KCl-acetamide/AgCl,Ag cells (0.312 cm electrode spacing) at various temperatures.

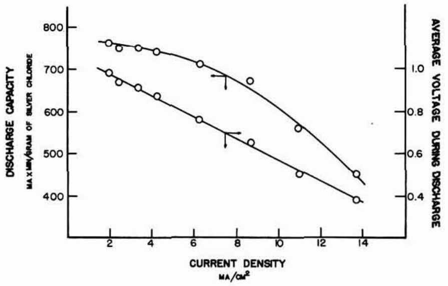

Fig. 5. Discharge capacity and average voltage of acetamide cells on discharge at 100°C.

materially with temperature. Figure 4 illustrates the large temperature effect on cell output.

Discharge capacity.—The discharge capacity, in milliamps-minutes per gram of fused AgCl, was calculated from cell performance curves and given in Fig. 5 as a function of current density. Also included in Fig. 5 is the variation of the average cell voltage with current density. Figure 5 points out that Zn/2.5% KCl-acetamide/AgCl,Ag cells do not furnish as great a capacity when discharging at high current densities as when discharging at low densities.

A more porous, electroformed silver chloride cathode was fabricated and tested. Approximately 1.40g of AgCl was electrolytically formed on the silver mesh grid (22 cm² exposed geometric surface area). Several Zn/2.5% KCl-acetamide/AgCl,Ag cells, with this electroformed AgCl were discharged at 100°C at a current density of 2 ma/cm². These cells had a 0.970 average discharge voltage and a 360-min cell life, which is equivalent to 1.3g of converted AgCl. In comparing cells using fused AgCl electrodes with an average cell capacity of only 0.762 amp-min/g AgCl with electroformed AgCl electrodes with a cell capacity 11.1 amp-min/g AgCl, a striking increase in cell capacity is revealed. It should be pointed out that this higher cell capacity is close to the theoretical capacity of 11.2 amp-min/g. AgCl. Longer discharge times were also obtained by electroforming even greater amounts of AgCl on silver grids.

Individual electrode behavior.—For the purpose of pinpointing the cause of cell termination and improving performance, individual electrode polarizations were measured at 100°C at a variety of discharge rates. Generally, the current drain had much more effect on cathodic than on anodic polarization. Cathodic polarization increased with time much more rapidly under high current drains and was principally responsible for discharge termination.

Anodic polarization, on the other hand, was comparatively small and did not significantly alter cell performance. The magnitude of anodic polarization was in the 5-15 mv range and increased with an increase in current drain, and only slightly with length of discharge. This was attributed entirely to concentration polarization effects.

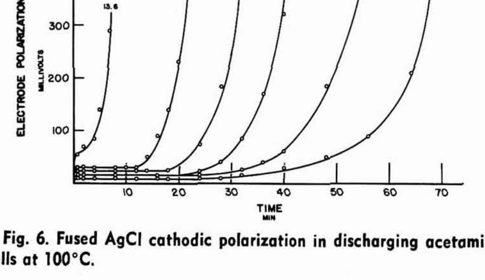

Fig. 6. Fused AgCl cathodic polarization in discharging acetamide cells at 100°C.

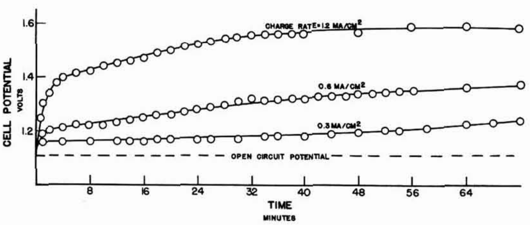

Fig. 7. Performance of Zn/KCl-acetamide/AgCl,Ag cells (0.12 cm electrode spacing) on charging at 100°C.

Cathodic polarization results in Fig. 6, clearly point out that the silver chloride cathode contributes most to cell termination. The polarizations remain fairly constant over much of the discharge until, at the inverted knee of the curve, there is a sudden large increase.

At the end of cell discharge, the AgCl on the cathode surface was observed to be reduced to spongy silver. Chloride ions must diffuse from within this dense, fused AgCl electrode. As a result, severe polarization took place. At current drains greater than 15 ma/cm², cell output was virtually dependent on the amount of KCl in immediate contact with active layers of AgCl. These polarization results accentuate the need to use a cathode of high porosity for usage in fused-acetamide thermal cells.

Charge rate.—Figure 7 shows the effect of charge rate on cell performance at low current densities at 100°C. These cells consisted of a zinc sheet (17.0 cm² exposed surface area) and a silver grid of the same area. On charge, their terminal cell voltage increased sharply. This abrupt rise in charge voltage was caused by the sudden drop in KCl concentration at the silver electrode and by hydrogen evolution coming from the zinc electrode. All cells were arbitrarily charged for 72 min and then discharged at 4.0 ma/cm² current density; on the average, about 60-70% charge was recovered. These experiments demonstrate that Zn/KCl-acetamide/AgCl,Ag molten acetamide cells are capable of being recharged.

Water addition.—Water is completely miscible with molten acetamide and allows the slightly aqueous acetamide to dissolve greater amounts of salt. The effect of water on melting point of solid 2.5% KCl-acetamide solution is recorded in Fig. 8.

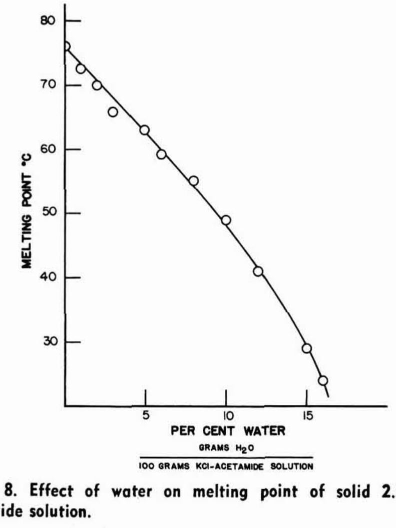

Fig. 8. Effect of water on melting point of solid 2.5% KCl-acetamide solution.

Addition of small amounts of water permitted the operating temperatures of acetamide thermal cells to be extended downwards. For example, three acetamide cells were discharged at 80°C in saturated KCl-2% H_2O-acetamide, melting point 70°C. The discharge performance of these cells at 80°C were similar to anhydrous cells at 100°C.

Acknowledgments

The authors wish to express their thanks to the Sandia Power Sources Laboratory in Albuquerque, New Mexico for their sponsorship, and to Dr. Charles Jennings and Dr. Frank Hudson for stimulating discussions.

Manuscript received Aug. 12, 1966; revised manuscript received Oct. 12, 1966. This paper was delivered before the New York Meeting, Oct. 1-3, 1963. This work was done in partial fulfillment of the requirements for the Ph.D. degree at Polytechnic Institute of Brooklyn by R. A. Wallace.

Any discussion of this paper will appear in a Discussion Section to be published in the December 1967 JOURNAL.

REFERENCES

1. R. A. Wallace and P. F. Bruins, *This Journal*, **114**, 209 (1967).
2. G. Winkler in "Chemistry in Nonaqueous Ionizing Solvents," G. Jander, H. Spandau, and C. Addison, Editors, Vol. IV, Part 3, Vieweg and Sohn, Braunschieveig, Germany (1963).
3. R. A. Wallace, Dissertation, Investigation of Fused-Organic Salt Cells, Polytechnic Institute of Brooklyn, New York (1963).
4. G. Jander and G. Winkler, *J. Inorg. Nuclear Chem.*, 2, 24 (1959).

Infrared Spectroscopic Investigation of Charged Nickel Hydroxide Electrodes

Frederick P. Kober

General Telephone & Electronics Laboratories Incorporated, Bayside, New York

ABSTRACT

Through the use of deuterated samples of Ni(OH)$_2$ electrodes at various stages of charge, it has been possible to make definitive band assignments for the structures of the active material. The relative intensity of the band due to hydrogen bonding in the charged state is shown to be a measure of the electrochemical capacity of the system. The charging reaction gives rise to the formation of active oxygen sites (as defined by Aia) through a site alteration mechanism in addition to the formation of hydrogen bonded sites within the charged phase. The mechanistic and structural implications of these spectral data are discussed in detail.

In a previous publication (1), the characteristic structural changes which occur in the hydrated nickel-oxide electrode during charge-discharge were examined. It was shown that the discharged state is characterized by nonhydrogen bonded hydroxyl groups whereas the charged state is a hydrogen bonded structure. In addition, Labat (2) and more recently Aia (3) have demonstrated the role of active oxygen[1] in the electrochemical capacity of the charged state. In fact, there is quantitative agreement between the equivalents of active oxygen "stored" in the higher oxide structure and the observed electrochemical capacity (3).

The nickel hydroxide electrode reaction, particularly the charged state, has been re-examined using high resolution infrared spectroscopy. By means of deuterium substitution, more definitive band assignments are made for the structure of the active materials. The formation of active oxygen which accompanies the charging reaction is shown to be closely associated with the formation of hydrogen bonding within the solid phase. The relative intensity of the absorption band due to hydrogen bonded groups is found to be proportional to the electrochemical activity of the higher oxide and, hence, its active oxygen content.

Experimental Procedure

Preparation of sintered electrode samples for infrared analysis is given in detail elsewhere (1). For this particular study, Nujol mulls were employed throughout. In the region from 4000 to 2500 cm^{-1} both CaF$_2$ and Irtran II windows were used, whereas polyethylene windows were used for the far infrared measurements (600-280 cm^{-1}). All measurements were made using a Beckman IR-7 double-beam instrument equipped with CsBr optics.

Deuteration of the discharged electrode material was accomplished by washing ground samples several times with D$_2$O (99.99%) using the method of Cabannes-Ott (4). This method takes advantage of the rapid exchange of hydrogen with deuterium in the Ni(OH)$_2$ system (5). When applied to the charged electrode material, this method of deuteration proved unsuccessful. Deuteration was achieved by immersing the discharged electrode in 31% KOD (D$_2$O), cycling several times, and subsequently washing the charged electrode in D$_2$O. This result indicates that protons are considerably more tightly bound in the higher oxide thus limiting exchange with D$_2$O.

The spectra of deuterium-free samples were measured against pure Nujol placed in the reference beam. In order to clearly discern spectral shifts due to deuteration, it was necessary to place undeuterated samples in the reference beam. The necessity of this differential technique was a consequence of the fact that the deuteration procedures employed yielded only partial exchange with hydrogen.

Results and Discussion

4000-2500 cm^{-1} Region.—Deuteration of the discharged electrode caused the sharp intense band observed at 3650 cm^{-1} to shift to 2705 cm^{-1}. This result is in agreement with that of Cabannes-Ott (4) and is illustrated in Fig. 1. These frequencies are in the ratio 1.35 substantiating the assumption that this absorption is the stretching fundamental of the nonhydrogen bonded hydroxyl groups.[2] During charging, the stretching fundamental is replaced by a broad diffuse absorption having a center at approximately 3450 cm^{-1} and attributed to hydrogen bond forma-

---

[1] The concept of active oxygen formation resulting from the anodic polarization of Ni(OH)$_2$ is discussed by Labat (2) and by Aia (3).

[2] To a first approximation, the frequency in wave numbers of a classical harmonic oscillator is given by γ (cm^{-1}) = $(1/2\pi C)$ $(k/\mu)^{1/2}$ where k is the Hook's law force constant and μ is the reduced mass. Consequently, the ratio of frequencies will be inversely proportional to the square-root of the ratios of reduced masses. The theoretical ratio $(\mu_{OD}/\mu_{OH})^{1/2}$ is found to be 1.36.

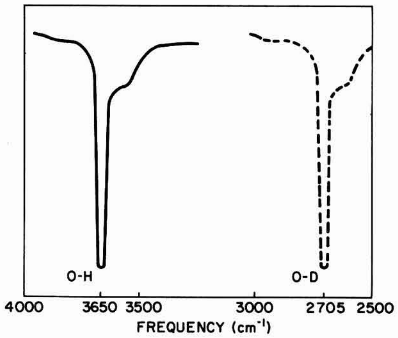

Fig. 1. Shift in OH stretching fundamental due to deuterium substitution.

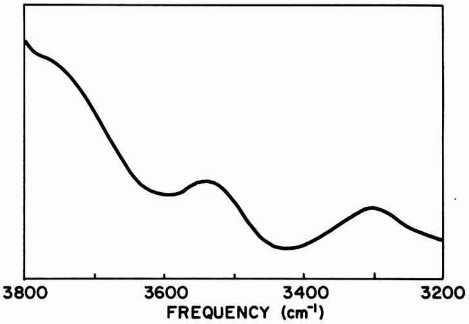

Fig. 2. Spectrum of charged Ni-O electrode in 3μ region

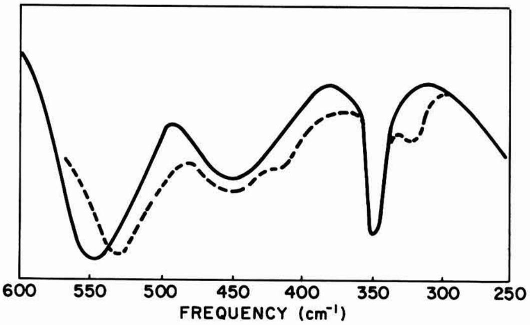

Fig. 3. Spectra of discharged Ni-O electrodes in the region 600 to 250 cm^{-1}; —Ni(OH)$_2$, - - - - Ni(OD)$_2$.

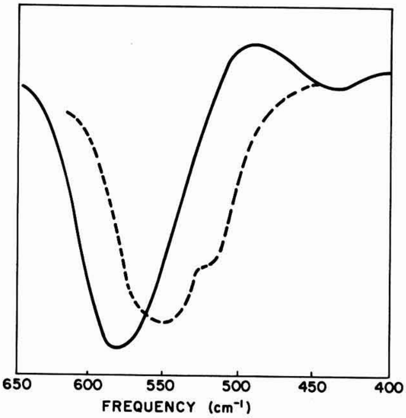

Fig. 4. Spectra of charged Ni-O electrodes in the region 650-400 cm^{-1}; —Ni-O(H); - - - Ni-O(D).

tion (1). Examination of this band under high resolution (greater than 1 cm^{-1}) reveals that, in fact, two or perhaps three bands are superimposed. These bands are shown in Fig. 2. Due to the nature of the samples, it was not possible to achieve better resolution of these absorptions even with deuterium substitution.

The broad diffuse nature of these bands suggests that they arise from lattice modes of the hydrogen bonded hydroxyl layers. Similar spectral features in the three micron region are observed for the minerals boehmite (γ-AlOOH) (6) and lepidocrocite (γ-FeOOH). These minerals are hydrogen bonded layer structures in which the central cations are surrounded by distorted octahedra of oxygens, the over-all symmetry being orthorhombic. Although the spectrum of the charged nickel-oxide electrode is not truly definitive with regard to structure, there is indication that similarities exist between the structure of the higher nickel oxides and that of boehmite (or lepedocrocite).

650-250 cm^{-1} Region.—The spectra, in this region, of both discharged and charged electrodes have been reported previously (1). Upon deuterium substitution, several frequency shifts are observed. These shifts are illustrated in Fig. 3. The band at 325 cm^{-1} in the deuterated sample is associated with the librational mode at 350 cm^{-1}.[3] In addition to the absorption at 325 cm^{-1}, there are bands observed at 415 and 525 cm^{-1}. Since the absorption at 450 cm^{-1} in the undeuterated sample is due to the nickel-oxygen lattice mode and does not involve proton vibration (1), the two vibrations observed for deuterated electrodes must be associated with shifts in the band having a center at 540 cm^{-1}. Consequently, this absorption is actually the superposition of two vibrations. From group theoretical considerations (7), the band at 540 cm^{-1} appears to arise from the singly degenerate lattice vibration associated with the motion of hydroxyl groups along the 001 direction relative to the nickel ion sites. The shift from 550-540 to 525 cm^{-1} is a manifestation of this assignment. Superimposed on this lattice mode is the torsional mode of the weakly bound lattice water also having a band center at 550-540 cm^{-1} (1). Upon deuteration, a shift to 415 cm^{-1} is observed.

The spectral changes which result from charging of the electrode have also been discussed in ref. (1). The broad but intense band having a center at 575-580 cm^{-1} was shown to arise from hydrogen bonding of the hydroxyl groups. For deuterated samples, this band shifts to 540-550 cm^{-1} with the appearance of a shoulder at approximately 520 cm^{-1}. These shifts are illustrated in Fig. 4. The ratios of these frequencies indicate that the 580 cm^{-1} absorption is a lattice mode(s) caused by the motion of hydrogen bonded linkages, *i.e.*, ---H–O–H--, relative to the nickel sites. This band is discussed in greater detail below. All frequencies together with possible assignments are listed in Table I.

580 cm^{-1} Band.—This band, which arises from the motion of hydrogen bonded linkages, appears to be characteristic of the charged state. As was shown by Aia (3), the charging reaction is accompanied by the continuous formation of active oxygen, the equivalents being in quantitative agreement with the electrochemical capacity. Thus, it is not unlikely that hydrogen bond formation is a consequence of structural changes brought about by the formation of active oxygen sites during the charging reaction. This suppo-

---

[3] The assignment in ref. (1) for the band at 350 cm^{-1} as a combination band arising from an interaction of the nickel-oxygen lattice mode with a low frequency librational mode (<100 cm^{-1}) now appears to be incorrect. Reconsideration of the data leads to the conclusion that the band at 350 cm^{-1} is, in fact, the true librational mode of the free OH groups. For a theoretical discussion of the OH librational mode in nonhydrogen bonded hydroxides see: C. K. Coogan, *J. Chem. Phys.*, 43, 823 (1965).

Table I. Infrared active vibrations (cm^{-1}) of nickel-oxide electrodes

Discharged electrode, $Ni(OH)_2$	$Ni(OD)_2$	Charged electrode	Deuterated charged electrode	Frequency assignments (8)
3650, sh	2705, sh			OH stretching fundamental
		3580, br 3450, str, br	— —	Lattice modes of H-bonded hydroxyl layers
540-550, int.	415, w			Lattice water libration
	525, br, int.			Hydroxyl group lattice mode
		580, br, int.	545 (525)	Lattice mode(s) of H-bonded linkages
450, br	450	450, v. dif.	450, v. dif.	Ni-O lattice mode
350, sh, int.	325			Free hydroxyl libration

sh—sharp, Int.—intense, br—broad, w—weak, v. dif.—very diffuse.

sition is supported by the fact that the formation of hydrogen bonding is also found to be a continuous function of charge (1). Consequently, any change in active oxygen content should manifest itself as a change in intensity of the band at 580 cm^{-1}.

Thermal decomposition of charged electrodes at various temperatures is accompanied by a loss of active oxygen, leading to a loss in electrochemical capacity (3). This loss of active oxygen does indeed result in a decrease in relative intensity of the absorption due to hydrogen bonded linkages at 580 cm^{-1} (Fig. 5). In fact, this decrease in relative intensity is a direct measure of the remaining electrochemical activity of the electrode.

If we assume that the intensity of the 580 cm^{-1} band for an electrode dried at 25°C represents 100% capacity, the relative intensity of this band as a function of drying temperature is then a measure of the remaining capacity (active oxygen content) after thermal treatment. These data are plotted in Fig. 6 together with actual capacity measurements of charged electrodes thermally treated at various temperatures. The excellent agreement between the capacity values predicted from infrared data with those measured experimentally strongly indicates that the formation of active oxygen is associated with the formation of hydrogen bonding. This conclusion is further supported by the thermal and stoichiometric results of Aia (3).

Mechanistic Implications

It has been demonstrated that the local site of electrochemical activity in the $Ni(OH)_2$ structure is at adjacent nonhydrogen bonded hydroxyl groups (8). Also, from the above results we see that the formation of active oxygen sites (electrochemical capacity) during charging of the electrode causes hydrogen bonding to occur within the solid phase. These data imply the following mechanistic steps.

The charging reaction involves the interaction of a "free" hydroxyl group with the electrolyte, resulting in an alteration of the electron density (electronic structure) at that given hydroxyl site. Since the reaction is initiated at the hydroxyl sites any change in the electronic structure of the nickel ion sites must be the result of electron transfer across the nickel-to-oxygen bonds. The change in the d^8 electronic configuration of the nickel sites brought about in this manner results in the formation of a hydrogen bonded structure possessing an over-all symmetry lower than D_{3d}. Thus, the appearance of active oxygen is a manifestation of a change in electronic structure at a hydroxyl site. A theoretical treatment of the changes in electronic structure which occur at the hydroxyl and nickel ion sites as a result of the interaction of a free hydroxyl site with the electrolyte will be presented in a subsequent paper.

The magnetic susceptibility data of Labat (2) clearly demonstrates that the charging reaction causes a decrease in electron-spin density about the nickel ion sites, thus effecting a change in electronic structure. Since the charging reaction alters the electronic structure of both the hydroxyl and nickel ion sites, a resulting change in crystal structure is anticipated. This over-all change in symmetry of the OH groups about the nickel ion sites has been discussed by Aia (3). Infrared data observed for the charged state in the 3μ region suggests that similarities exist between the structure of the higher oxide and that of boehmite (or lepidocrocite). This possibility is indeed compatible with the mechanistic implications discussed above. The beohmite structure is a hydrogen bonded layer lattice comprising brucite-type subunits linked through the sharing of oxygen atoms at the corners

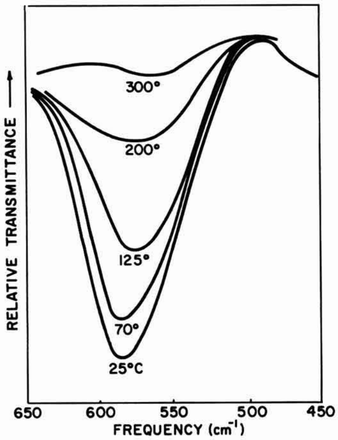

Fig. 5. Relative intensity of lattice mode due to hydrogen bonded linkages as a function of drying temperature.

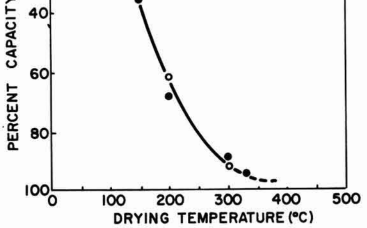

Fig. 6. Predicted and experimental electrochemical capacity remaining after thermal treatment at various temperatures.

of MO_6 octahedra (9). The fact that the nickel-to-oxygen coordination remains essentially octahedral upon charging has been previously shown (1, 8). It is not difficult to envision the conversion of the $Ni(OH)_2$ brucite-type structure into the orthorhombic boehmite-type structure via a change in symmetry at the hydroxyl sites.

Acknowledgment

The author wishes to thank M. Fucci for his aid with the experimental work and M. A. Aia for stimulating discussions concerning this work.

Manuscript received Sept. 14, 1966; revised manuscript received Nov. 21, 1966.

Any discussion of this paper will appear in a Discussion Section to be published in the December 1967 JOURNAL.

REFERENCES

1. F. P. Kober, *This Journal*, **112**, 1064 (1965).
2. J. Labat, Thesis, Univ. Bordaux, *Ann. Chim.* (*Paris*) **9**, 399 (1964); A. Pacault and J. Labat, *Compt. rend.*, **258**, 541 (1964).
3. M. A. Aia, Ext. Abstracts, Battery Div., Philadelphia Meeting of the Society (1966).
4. *Mme.* C. Cabannes-Ott, *Ann. Chim.* (*Paris*), **5**, 905 (1960).
5. For an analysis of the exchange kinetics of H with tritium in $Ni(OH)_2$ see W. Feitknecht, A. Wyttenback, and W. Buser, Proc. 4th Inter. Symp. Reactivity of Solids, Amsterdam (1960), pp. 234-239.
6. L. D. Fredrickson, Jr., *Anal. Chem*, **26**, 1883 (1964); K. A. Wickersheim and G. K. Korpi, *J. Chem. Phys.*, **42**, 579 (1962); E. Schwatzmann, *J. Anorgan. Chem.*, **317**, 176 (1962).
7. For a complete group theoretical analysis of the brucite-type structure see S. S. Mitra, *Solid State Phys.*, **13**, 1 (1962).
8. F. P. Kober, Proc. 5th Internat. Battery Symp., Brighton, September (1966).
9. A. F. Wells, "Structural Inorganic Chemistry," pp. 556-560, Oxford University Press, London (1962).

Kinetics of the Fluorination of Iron

Patricia M. O'Donnell

Lewis Research Center, National Aeronautics and Space Administration, Cleveland, Ohio

ABSTRACT

The effect of temperature and pressure on the reaction of fluorine gas on solid iron samples was studied at various pressures up to 200 Torr over the temperature range of 225° to 525°C. The reaction was found to follow the logarithmic rate law, and logarithmic rate constants are reported. The probable mechanism of film growth is movement of fluorine through defects in the fluoride film to the iron surface.

The purposes of this report are (*i*) to present the results of a kinetic study of the fluorination of iron in the temperature range of 225°-525°C and (*ii*) to propose a mechanism for this reaction. The kinetics of this reaction are interesting since the only data available in the literature are the corrosion type where the reaction of fluorine on iron has been observed by taking a few measurements at long incremental time periods and linearly extrapolating them to give results reported as inches of penetration per month or per year at varying temperatures (1). A linear extrapolation of this type does not give a detailed picture of the reaction but merely defines maximum gross effects. This kinetic study was, therefore, undertaken in order to observe the details of the reaction of fluorine on iron. A few detailed studies of the reaction of fluorine gas with other metals have been reported. By studying the reaction between copper powder and fluorine gas from room temperature up to 250°C and at pressures up to 60 Torr, Brown, Crabtree, and Duncan (2) found that the reaction obeys a logarithmic rate law and is not pressure dependent. This law is widely applicable to corrosion kinetics (3) and relates the amount of reaction y with time t by

$$y = K \log (at + 1) \qquad [1]$$

and where K and a are constants for a given system and temperature. In a study of the reaction of fluorine on plate copper (4, 5), it was found that the reaction followed a logarithmic law above 538°C, but that below that temperature a simple power law was applicable. The reaction was observed to be pressure dependent. Other studies have been made of the reaction kinetics of fluorine with copper (6), nickel (7), and zirconium compounds (8) under various conditions. Although there have been extensive kinetic studies of the rates of oxidation of iron, there are no similar studies on the rates of the fluorination of iron.

Experimental

The vacuum apparatus used to measure the rate of fluorination of iron has been described previously (5).

The general experimental method used to determine the rate of fluorine consumption by iron was to measure the pressure decrease in a vessel of known volume containing the iron sample. In order to maintain approximately constant fluorine pressure, the pressure was allowed to drop only about 2 Torr, whereupon additional fluorine was admitted to return the pressure to its initial value. The perfect gas law was used to calculate the amount of fluorine consumed after each of these steps, from the incremental pressure drop, the vessel volume, and the temperature. Fluorine consumed was expressed in milliliters at standard temperature and pressure. Standard volumetric procedures were used to calibrate the volume of the furnace, storage vessel, and connecting lines. The glass system was passivated by introducing fluorine at increasing pressures and temperatures until further reaction of fluorine with the system was insignificant. The blank after passivation represented a correction of less than 1%.

To determine the temperature gradient along the iron strip, a special strip was made with eight Chromel-Alumel thermocouples attached along it. The leads came through a special end plug to a recording system. The temperature profile along the strip varied ±0.5°C at the low temperatures and ±3° for the 525°C temperature in a nitrogen atmosphere.

The iron samples were machined from spectrographically pure iron having the following impurities in parts per million: manganese, 2; silicon, 2; magnesium, 1; nickel, 1; silver, 1; and copper, 1. The samples were 1.27 x 15.24 x 0.012 cm with a 0.5-cm hole drilled in one end to facilitate handling. All samples were degreased in trichloroethylene, cleaned in 20% hydrochloric acid for 3 min, and washed in distilled water, acetone, and alcohol. Samples were immediately inserted into the furnace under flowing argon and were positioned the same for each run. The system was sealed and pumped down to about 0.1μ pressure. All samples were preheated 0.5 hr at 525°C under vacuum before running. After the pretreatment, the temperature was adjusted to the operating temperature, and fluorine was introduced to the desired pressure. The recorder plotted the amount of fluorine consumed on a continuous time trace. Some experimental points from the traces are shown on Fig. 1 and 2. When the consumption of fluorine had decreased to a negligible value, the heaters were turned off, the system was allowed to cool to 25°C, and the fluorine was pumped out of the system through the soda lime traps. The test sample was removed to a glass tube holder, which was attached to the end of the reaction section, and was sealed under flowing argon for later visual and instrumental analysis. Some of the films scraped from the strips were analyzed by x-ray diffraction.

For cross-sectional analysis, samples were embedded in plastic, cut, and polished. They were then examined on a metallograph and photographed. The cross section was etched and dyed in order to determine if there was any grain boundary attack. Microscopic analysis was performed to reveal the topology of the samples.

Results and Discussion

The fluorine consumption by the iron samples was measured at several temperatures and pressures (Table I). Figures 1 and 2 illustrate the results; the milliliters of fluorine consumed per square centimeter of iron surface are plotted against the time in minutes. Some duplicate runs (solid symbols) have been plotted in order to show the reproducibility of the data. The effect of temperature on the reaction is shown in Fig. 1 where the data are plotted at temperatures from 225° to 525°C at a constant pressure of 60 Torr. Figures 2(a) and (b) show the effect of pressure on the reaction. In Fig. 2(a) the pressure effect is plotted at a constant temperature of 225°C and in Fig. 2(b) at a constant temperature of 525°C. In Fig. 1 the runs at 375° and 425°C cross at $t = 90$ min. Similar behavior is noted in Fig. 2 where the runs at 60 and 100 Torr at 525°C cross at $t = 70$ min. This type of crossover phenomena has also been observed in the oxidation of iron (9). In the 525°C 15-Torr run [Fig. 2(b)], the fluorine was pumped out after 125 min while the sample was kept at 525°C in order to determine the effect of heat and vacuum on the reaction. New fluorine was introduced to 15 Torr (point B), and the reaction appeared to start again. Copper plate and fluorine showed similar behavior (5); however, the reaction between copper powder and fluorine did not start again under similar conditions (2).

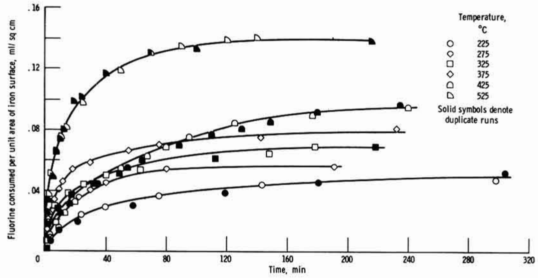

Fig. 1. Effect of temperature on the fluorination of iron at 60 Torr.

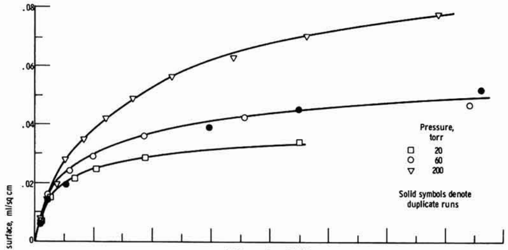

(a) Temperature, 225° C.

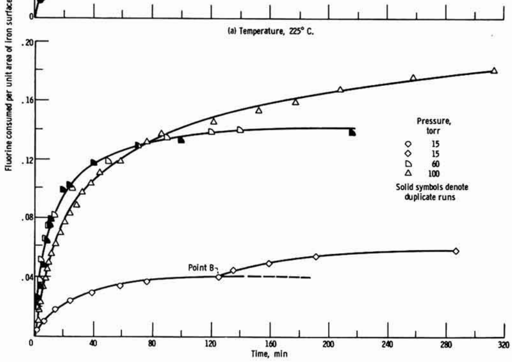

(b) Temperature, 525° C.

Fig. 2. Effect of pressure on fluorination of iron

Table I. Summary of temperature and pressure conditions and calculated logarithmic rate constants

Temperature, °C	Pressure, Torr	Logarithmic rate constant, ml/cm^2
225	60	0.024
275	↓	0.026
325		0.029
375		0.031
425		0.057
525		0.064
225	20	0.016
225	60	0.024
225	200	0.046
525	15	0.022, 0.013
525	60	0.064
525	100	0.089

Product identification and volume ratio.—X-ray diffraction patterns were run on both the low and high temperature films and the product was identified as ferric fluoride (FeF_3); no ferrous fluoride (FeF_2) was detected. The over-all reaction may be described by

$$2Fe + 3F_2 \rightarrow 2FeF_3 \qquad [2]$$

In this reaction, the fluoride occupies a larger volume than the metal destroyed. The volume ratio (10) is defined as $\Phi = Wd/wD$ where W is the molecular weight of the film formed, w the formula weight of the metal, D the density of the film formed, and d the density of the metal. The volume ratio Φ for this reaction has a value of 4.9 at 25°C.

Logarithmic equation.—The data from Fig. 1 and 2 are replotted in Fig. 3 and 4 on a log time as a function of fluorine consumed basis. The straight lines shown on Fig. 3 and 4 fit a logarithmic equation that is similar to Eq. [1]. This equation is

$$y = K(\log at) + c \qquad [3]$$

where y is the fluorine consumed (at STP), ml/cm^2; t time, min; K the logarithmic rate constant; a the constant with dimensions of reciprocal min; and c the intercept. The constant a is unity for the lines drawn on Fig. 3 and 4. Figure 3 shows the data at constant pressure of 60 Torr for various temperatures. In Fig. 4(a) the 225°C data are plotted at 20, 60, and 200 Torr, and in Fig. 4(b) the 525°C data are plotted at 15, 60, and 100 Torr showing the effect of pressure at constant temperature. It can be seen that the logarithmic equation fits all the data within the experimental error except at short times. Figure 2 indicates that heat and vacuum have an effect on the passivity of the metal strip. At point B the metal strip had reached a point

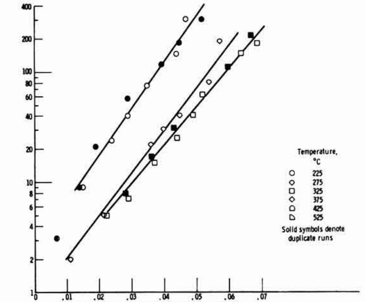

(a) Temperatures, 225°, 275°, and 325° C.

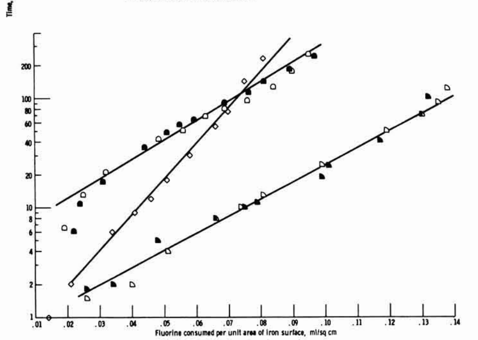

(b) Temperatures, 375°, 425°, and 525° C.

Fig. 3. Temperature effect at 60 Torr

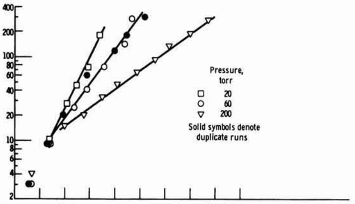

(a) Pressures of 20, 60, and 200 torr at 225° C.

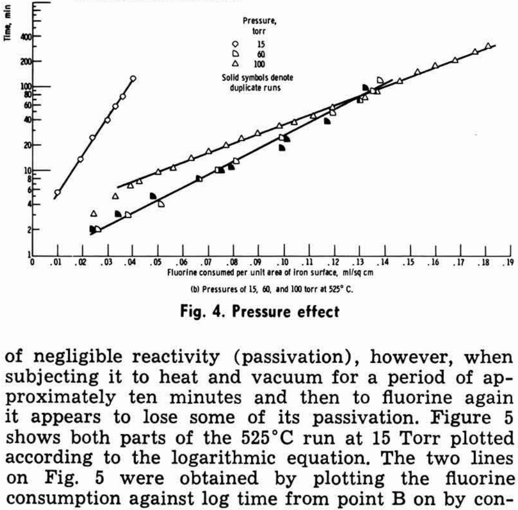

(b) Pressures of 15, 60, and 100 torr at 525° C.

Fig. 4. Pressure effect

of negligible reactivity (passivation), however, when subjecting it to heat and vacuum for a period of approximately ten minutes and then to fluorine again it appears to lose some of its passivation. Figure 5 shows both parts of the 525°C run at 15 Torr plotted according to the logarithmic equation. The two lines on Fig. 5 were obtained by plotting the fluorine consumption against log time from point B on by considering the fluorine consumption for this second part of the reaction as the difference between reaction 1 (dashed line) and reaction [2] and B as the zero time point for reaction [2]. The rate for this second reaction is, however, lower than the original rate. The values of K for these reactions are 0.022 and 0.013 ml/cm^2, respectively, and are listed in Table I along with the values of the other rate constants.

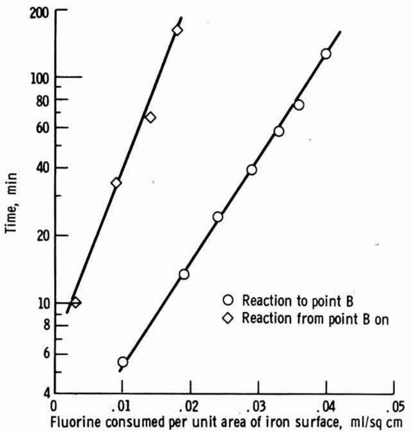

Fig 5. Interrupted fluorination of iron at 525°C and 15 Torr

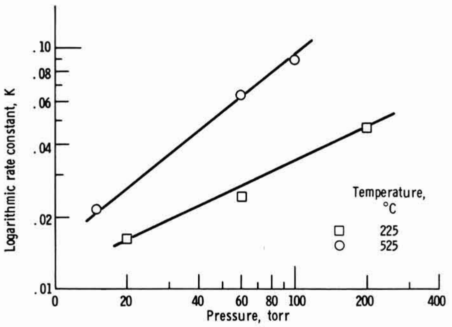

Fig. 6. Effect of pressure on rate constant

From the data of Fig. 1 and 2, the reaction between iron and fluorine is seen to be both temperature and pressure dependent. The effect of pressure on the logarithmic rate constant is shown in Fig. 6 where the log of this constant is plotted as a function of pressure at constant temperature according to the equation $\log K = m \log P + B$. The slope m is the order of the reaction with respect to the fluorine pressure. At 225°C, m has a value of 0.87, and at 525°C m is 0.48.

Metallographic studies.—Cross sections of the fluorine-corroded iron strips were prepared by standard metallographic techniques. Photomicrographs of typical cross sections are shown in Fig. 7. These photographs show that the boundary between the fluoride and the iron is very sharply defined. The fluoride film does not grow preferentially along grain boundaries in the iron. This was confirmed by etching and staining of polished cross sections. Near the iron-fluoride interface, the fluoride appears to be uniformly dense. Near the surface of the fluoride film, the fluoride appears somewhat broken and imperfect. This is to be expected, since the fluoride film occupies a volume 4.9 times larger than the iron from which it is formed, and this volume expansion must result in stresses which can fracture the film when it is thick enough.

Mechanism of fluorine attack.—The rate-determining process in growth of corrosion films on metals can be deduced by consideration of the growth law of the film. For example, if the film grows by diffusion of lattice vacancies through the film, the film thickness will increase with the square root of time. In the experiments reported here, the fluorine uptake, and hence the film thickness, varied directly with the logarithm of time except at short times, where the

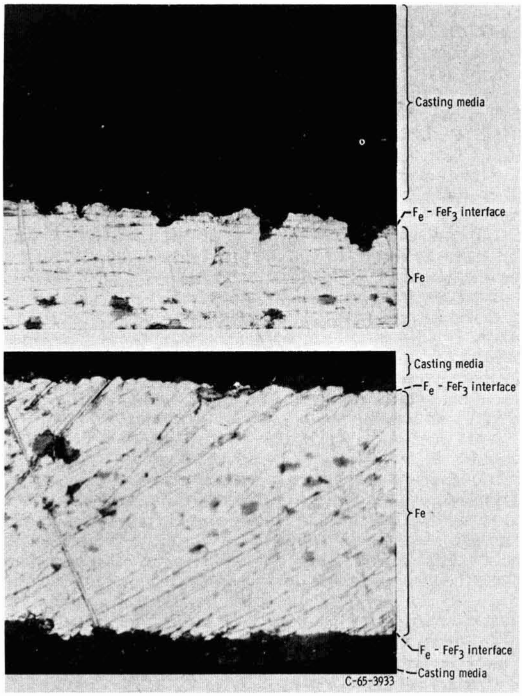

Fig. 7. Cross-section views (Fe + F_2 at 500°C). X500

film thickness is less than about 350Å. Theoretical analyses (3) have shown that such a direct logarithmic dependence can arise from either of two mechanisms: (*i*) when the growth rate is controlled by tunneling of electrons through the film, or (*ii*) when the growth rate is controlled by passage of gas through pores or other defects in the film to the metal surface. Tunneling is important only for films thinner than a few hundred angstroms. The film thicknesses in this research were much larger, so that this mechanism can be discarded. The second mechanism, that of passage of gas through pores in the film, is the most likely process. The pores through which the gas moves may be the intersection of three grains, the intersection of two slip-planes, screw, and edge dislocations, or simply fractures in the film. When the compressional stress in one pore exerts a pressure on neighboring pores, some of these will be blocked as the film grows. This is the case of mutually blocking pores and leads to the direct logarithmic growth law as found in this research. At low temperatures, the logarithmic law is found to be obeyed for the oxidation of iron and copper, where the expansion which occurs when metal is transformed to oxide tends to close up neighboring pores. In this research, the fluoride occupies a volume 4.9 times that of the metal from which it is formed, so that mutual blockage by compression can be expected. It is concluded that above a film thickness of about 350Å the fluoride film on the iron grows by passage of fluorine through pores in the film, and that these pores tend to block one another as the film thickness increases.

Manuscript received June 20, 1966; revised manuscript received Nov. 22, 1966.

Any discussion of this paper will appear in a Discussion Section to be published in the December 1967 JOURNAL.

REFERENCES

1. E. Skinner, *Chem. Eng.*, **65**, 137 (1958).
2. P. E. Brown, J. M. Crabtree, and J. F. Duncan, *J. Inorg. Nuclear Chem.*, **1**, 202 (1955).
3. U. R. Evans, "The Corrosion and Oxidation of Metals: Scientific Principles and Practical Applications," St. Martin's Press, Inc. (1960).
4. P. M. O'Donnell and A. E. Spakowski, Reaction of Copper and Fluorine from 800° to 1200°F, NASA TN D-768, 1961.
5. P. M. O'Donnell and A. E. Spakowski, *This Journal*, **111**, 633 (1964).
6. Yu. A. Luk'yanychev, N. S. Nikolaev, I. I. Astakhov, and V. I. Luk'yanycheva, *Dokl. Akad. Nauk. SSSR*, **147**, 1130 (1962).
7. R. L. Jarry, J. Fischer, and W. H. Gunther, *This Journal*, **110**, 346 (1963).
8. A. K. Kuriakose and J. L. Margrave, *J. Phys. Chem.*, **68**, 290 (1964).
9. E. A. Gulbransen, *Trans. Electrochem. Soc.*, **81**, 327 (1942).
10. N. B. Pilling and R. E. Bedworth, *J. Inst. Metals*, **29**, 529 (1923).

Electrochemical Aspects of the Interaction Between Materials and Blood

Dennis B. Matthews and Avery Catlin

Department of Materials Science, School of Engineering and Applied Science,
University of Virginia, Charlottesville, Virginia

ABSTRACT

Electrolysis of human plasma, collected under various conditions, and of bovine fibrinogen (a protein normally present in blood) was carried out in order to verify conclusions made by earlier investigators. Electrolysis of recalcified plasma, ACD-plasma (plasma to which an acid solution of dextrose and sodium citrate has been added), citrated-plasma (plasma to which sodium citrate has been added), and heparinized plasma (plasma containing heparin anticoagulant) in glass, plastic, and silvered tubes did not support the conclusion that electrolysis produced inhibitors of, or catalysts for, the enzymatic blood coagulation reaction. The results were interpreted in terms of the effect of *p*H on the rate of coagulation.

Blood, withdrawn from a human and placed in contact with various materials, clots at a rate dependent on the material with which it is in contact. The rate of clotting is a maximum for such materials as glass, kaolin, celite (diatomaceous silica), and barium carbonate; it is a minimum for such materials as the normal vascular endothelium (the inside lining of blood vessels), paraffin, plastics including cellophane, and siliconized glass. For use as vascular prostheses such as artificial arteries, heart valves, and hearts, a material must, besides other requirements, not initiate blood coagulation.

The intrinsic enzyme mechanism of blood coagulation, initiated by contact with a foreign surface, is fairly well documented, and the mechanism currently accepted by a large number of the workers in this area is shown below.

Surface contact
↓
XII → XIIa
↓
XI → XIa
↓
IX → IXa
↓
VIII → VIIIa
↓
X → Xa
↓
V → Va
↓
II → IIa (Thrombin)
↓
I (Fibrinogen → Ia (Fibrin)

This enzyme cascade (1, 2) sequence or bioamplifier (3, 4) system is believed to be initiated by adsorption of factor XII (Hageman factor). The adsorbed factor XII is in an active state, designated as XIIa and capable of activating factor XI to give XIa which in turn activates factor IX, and so on, until the enzyme IIa (thrombin) attacks factor I (fibrinogen), converting it to fibrin which polymerizes, both end-to-end polymerization and crosslinking occurring, forming a net which enmeshes blood cells and serum.

There exists at present in the literature sufficient evidence to be able to conclude that electrical and possibly electrochemical factors play a role in the interaction between materials and blood, both *"in vitro"* and *"in vivo"* (21, 25).

This paper is concerned with the analysis of existing data in the light of some new results reported herein.

Despite the fact that the dependence of blood coagulation on electrolysis was observed as early as 1824, the first significant and systematic work on this subject was not carried out until 1953. In 1953, Sawyer, Pate, and Weldon (5, 7) observed that the potential difference across the canine artery wall changed sign upon injury being —3 to —15 mv (inside negative with respect to the outside) before injury and +1 to +10 mv after injury. The current flowing across the artery wall was also observed to change its sign and magnitude upon injury. The reversal of sign of the potential difference and the appearance of an "injury current" was accompanied by the formation of a thrombus, or blood clot, within the injured artery. A similar result was reported by Sawyer and Pate (6, 7) for the canine aorta.

Electrolysis of heparinized or citrated canine blood between platinum electrodes in a glass tube at 0.2-10 ma for 30 min resulted in the formation of a precipitate at the anode (8). The precipitate contained platelets, red blood cells (erythrocytes), and white blood cells (leukocytes). In the case of heparinized blood, fibrin strands were also reported to be part of the precipitate. No precipitate was formed at the cathode. It was demonstrated by Sawyer and Pate (8) that this precipitate was not caused by gross changes in *p*H. As the anode and cathode were situated in the same vessel separated only by 1 cm of solution it is not surprising that no gross changes of *p*H were observed.

The results of Sawyer and Pate (8) have been repeated by Lamb *et al.* (14) who used platinum wires 5 mm apart in the electrolysis of heparinized whole blood and plasma. The nature and amount of deposit formed on the anode was noted for various potentials between the anode and cathode and for various quantities of charge passed.

Passage of current across a blood vessel wall or across the blood vessel *in vivo* was also found to produce a deposit, or thrombus, on the vessel wall nearest the anode. On the basis of these experiments it was postulated by Sawyer, Deutch, and Pate (9) in 1955 that reversal of the normal potential difference across the canine blood vessel wall results in an electrophoretic migration of platelets, other cellular elements, and negatively charged proteins to the injured vascular wall thus precipitating a thrombus (blood clot). In later years, however, Sawyer (15) has concluded that electrolysis interferes with the intrinsic enzyme mechanism of blood coagulation.

In 1956 the investigations proceeded one step further when it was found by Sawyer and Deutch (10) that thrombosis (blood clot formation) was delayed at the cathode during electrolysis. Currents greater than 30 μa, when passed between a platinum cathode, placed around crushed canine arteries and veins, and an anode located at a distant position in the dog, were able to delay thrombosis compared to a control experiment where no current was passed.

These results were confirmed in 1959 by Schwartz (11) who observed *in vivo* thrombosis at the anode during electrolysis and who found that cathodic polarization was able to delay thrombin-induced thrombosis. Several other workers (12, 13, 16, 17) have since been able to produce *in vivo* thrombi by anodic polarization.

The experiments of Sawyer and Pate (8) were repeated by Sawyer, Dennis, and Wesolowski (15) with platinum electrodes in separate glass tubes connected by a salt bridge. Currents of 0.1-1.0 μa were found to produce a deposit on the anode in heparinized or citrated blood. A solution of fibrinogen in sodium chloride was also electrolyzed, and a deposit was observed at the anode. This deposit was thought to be fibrin produced from fibrinogen by electrolysis. It was conjectured that electrolysis can cause blood coagulation by bypassing all but the final steps in the intrinsic enzyme clotting mechanism.

In all the above *in vitro* experiments the blood was heparinized or citrated. The intrinsic blood coagulation mechanism was thus checked; in particular, the activation of factor IX is inhibited under these conditions.

In 1964 Naumovski and Dejanov (21) reported some results on the effect of electrolysis on *in vitro* clotting. Currents of 1.6 ma were passed through citrated plasma for 1 hr. At the cathode the plasma was found to have a markedly prolonged recalcification time, more than 80 times the average spread. The plasma *p*H was 9.6-9.8. Diluting the cathode plasma by imadazole buffer (*p*H 7.4) did not change the anticoagulant effect. Plasma at the anode changed negligibly, and the *p*H was 6.6-6.8.

On the other hand, Lavelle (21) concluded that direct electric current does not appear to initiate, or accelerate, the enzymatic coagulation system in circulating native blood. Lavelle's work, however, suffered from the disadvantage that the anode and cathode were not in separate chambers. Any material oxidized at the anode may well have been reduced at the cathode. In 1964 Sawyer, Brattain, and Boddy (18) observed that erythrocytes and leukocytes in Krebs solution (an electrolyte of ionic composition similar to that of blood) at *p*H 7.4 migrate and adhere to a platinum electrode at potentials greater than or equal to +0.33v (against NHE). Decrease of this potential led to desorption of the blood cells.

A similar behavior was observed with platelet suspensions (19) except that the adsorption of platelets was irreversible, the platelets visibly disintegrating at the electrode. Fibrinogen in buffer solution, however, was not found to deposit under these conditions (20).

The above results obtained by Sawyer and his coworkers and by others have led Sawyer to believe (21) that electrolysis is capable of interfering with the intrinsic enzyme mechanism of blood coagulation, the rate of blood coagulation being catalyzed at an anode and an inhibitor being produced at the cathode.

It was the aim of the present work to substantiate if possible the above viewpoint by repeating the *in vitro* experiments of Sawyer and co-workers under conditions where the intrinsic enzyme mechanism of coagulation is operative.

Experimental

Blood was collected in 450 ml quantities from healthy male donors. The blood was withdrawn under vacuum into a double plastic pack containing acid citrate-dextrose (ACD) anticoagulant. In some experiments sodium citrate or heparin anticoagulant was used in the place of ACD. The blood was centrifuged at either 1000g (platelet poor plasma, p.p.p.) or 300g (platelet rich plasma, p.r.p.) for 30 min to remove red cells and white cells. The plasma was squeezed off from the packed cells into the second plastic pack. Aliquots of about 4 ml were gravity fed from the pack into siliconized glass or polystyrene tubes, sealed and stored at either 4° or —20°C. Immediately prior to an experiment a plasma aliquot was thermostatted in a water bath at 37°C. In the case of plasma stored at —20°C, this procedure disrupts the platelets, producing lysed plasma.

To initiate clotting, 0.20 ml of 0.25M $CaCl_2$ was added to 2 ml of plasma. The rate of coagulation was followed with a photometric system (23). Light from a voltage regulated 0.25 amp 6-volt lamp was passed through the sample, contained in a block of aluminum thermostated at 37° ± 0.5°C, and the transmitted light was monitored with a CdS photocell. The resistance of the photocell was measured with a Wheatstone bridge, and the change of resistance with time was continuously recorded with a potentiometric recorder. The measuring system is shown in Fig. 1. The type of recording obtained is idealized in Fig. 2. The times t_0 and t_1 mark the onset and completion of fibrin polymerization, respectively. The shape of the curve obtained depended on the experimental conditions. In the case of a simple sigmoidal curve the time $t_{1/2}$ was used as a measure of the rate of coagulation. For more complex curves. *e.g.*, double sigmoidal, linear + sigmoidal, the times t_0 and t_1 were tabulated.

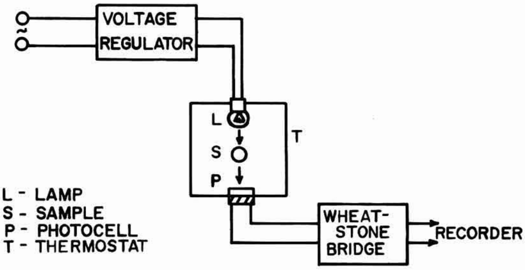

Fig. 1. Apparatus for photometric determination of the rate of blood coagulation.

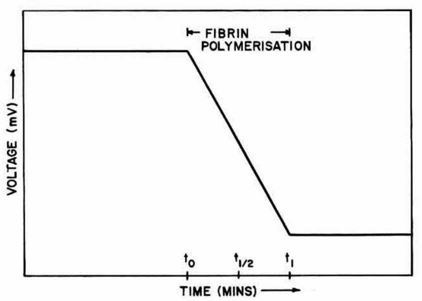

Fig. 2. Idealized representation of the photometric clotting curve.

Table I. Effect of electrolysis on the rate of coagulation of human plasma at 37°C

Polarity	Current, ma	Platelet content	Anti-coagulant	Storage temperature, °C	t_0, min
Control	0	Poor	Na citrate	−20	3.2 ± 0.2
Cathode	0.5	Poor	Na citrate	−20	3.5 ± 0.3
Anode	0.5	Poor	Na citrate	−20	3.1 ± 0.2
Control	0	Poor	ACD	−20	2.2 ± 0.1
Cathode	2.0	Poor	ACD	−20	2.7 ± 0.1
Anode	2.0	Poor	ACD	−20	2.4 ± 0.1
Control	0	Poor	ACD	4	6.9 ± 0.7
Cathode	2.0	Poor	ACD	4	6.4 ± 0.1
Anode	2.0	Poor	ACD	4	6.5
Control	0	Rich	ACD	4	3.9 ± 0.4
Cathode	2.0	Rich	ACD	4	3.4 ± 0.4
Anode	2.0	Rich	ACD	4	4.2 ± 0.2
Control	0	Rich	ACD	4	5.6 ± 0.3
Cathode	1.0	Rich	ACD	4	4.8 ± 0.1
Anode	1.0	Rich	ACD	4	6.3 ± 0.3
Control	0	Poor	Na citrate	4	4.9 ± 0.3
Cathode	1.0	Poor	Na citrate	4	4.2 ± 0.7
Anode	1.0	Poor	Na citrate	4	5.1 ± 0.2

Electrodes used were, except where otherwise indicated, platinum wire spirals approximately 1 cm^2 in area. The cathode and anode were placed in separate tubes connected by a saturated KCl-gelatin salt bridge. The salt bridge was constructed either of siliconized glass tubing or of polyethylene tubing. The platinum electrodes were cleaned in 1:1 mixture of concentrated HCl-concentrated H_2SO_4, rinsed with distilled water, and heated to red heat in a flame.

Bovine fibrinogen obtained from Warner-Chilcott was dissolved by standing at 37°C with distilled water.

All pipettes and other glassware used in handling plasma were siliconized with Clay-Adams Siliclad. Test tubes were discarded after use, fresh tubes being used in each test.

Polystyrene tubes were silver coated according to a well-known procedure (22) and dried at 60°C for 5 hr or more.

Results

The effect of electrolysis, after recalcification, of various types of plasma, collected and stored under various conditions, is summarized in Table I and Fig. 3. The tests were carried out in glass tubes at 37°C. In these experiments the plasma was in contact with both glass and an electrode.

In order to eliminate uncertainties brought about by contact with glass, a polystyrene tube coated internally with electrically conducting silver was used both as container and cathode. The effect of cathodic electrolysis was tested in these tubes by electrolyzing citrated plasma for a given time, t_a, and then transferring the plasma to a polystyrene tube containing $CaCl_2$. The experiments were carried out at 37°C with

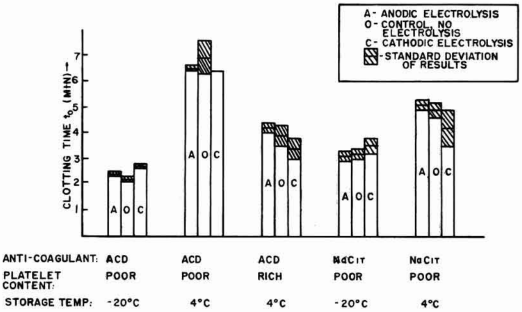

Fig. 3. Effect of electrolysis on the rate of coagulation of human plasma in glass at 37°C.

Table II. Effect of electrolysis at a silver cathode on the rate of coagulation of platelet poor lysed plasma at 37°C

t_a, min	Current, ma	$t_{1/2}$, min
5	0	8.1 ± 0.1
5	2	6.8 ± 0.1
5	0	7.8 ± 0.7*
5	2	6.6 ± 0.4*
12	0	7.6 ± 0.9
12	2	5.6 ± 0.9

* Plasma was deaerated with nitrogen.

platelet poor plasma (lysed) collected in ACD. Results are given in Table II.

The experiment of Sawyer, Dennis, and Wesolowski (15) on the electrolysis of fibrinogen was repeated. Purified bovine fibrinogen (2.0 ml) was electrolyzed with platinum electrodes in separate glass tubes connected by a salt bridge. At 1 ma a deposit formed on the anode within 25 sec. The deposit consisted of a white precipitate mixed with bubbles of O_2 causing the precipitate to adhere to the anode. No reason was seen for believing the deposit to be fibrin rather than fibrinogen. Addition of sodium citrate to fibrinogen was found to inhibit the formation of a deposit. Only after 15 min of electrolysis at 1 ma did a very fine precipitate form, and this tended to remain in suspension. Electrolysis of citrated plasma itself, which contained the same concentration of fibrinogen as in the above experiments, resulted in the formation of a very fine precipitate only after 15 min of electrolysis at 1 ma. The possibility of fibrinogen being precipitated by a decrease in *p*H of the solution in the anode compartment was checked both by calculation and actual measurement of the *p*H change. In the absence of buffer the *p*H changed from 6.00 to 3.61 after 1 min of electrolysis at 1 ma, while in the presence of sodium citrate the *p*H change was from 8.16 to 7.58.

The experiments of Naumovski and Dejanov on the electrolysis of citrated plasma were repeated using platelet poor plasma. Electrolysis was carried out at 1.6 ma with 10 ml of plasma in polystyrene tubes using Pt electrodes. After 60 min electrolysis the plasma was thermostatted at 37°C and 2 ml recalcified in glass tubes at 37°C. Results obtained are shown in Table III. Both cooled and lysed plasma were tested.

The above experiments were repeated with heparinized platelet poor plasma. Electrolysis was conducted in polystyrene tubes at 3.2 ma for 30 min using 10 ml of fresh plasma. After electrolysis 2 ml of the sample was contacted for 10 min in glass tubes at 37°C, 0.20 ml of protamine sulfate was then added to neutralize the heparin. This experiment was repeated with a 1:1 sample of fresh plasma and veronal buffer ($pH = 7.5$), in order to inhibit the *p*H changes brought about by electrolysis. The results of the experiments with heparinized plasma are given in Table IV.

Table III. Effect of prolonged electrolysis on the rate of clotting of citrated platelet-poor plasma at 37°C

Electrolysis carried out for 60 min at 1.6 ma in polystyrene tubes with Pt electrodes. Vol. of plasma = 10 cc. Plasma recalcified in glass tubes.

A. Fresh plasma

Electrode	*p*H	t_o, min
Anode	6.59	16.7 ± 2.3
Cathode	7.29	7.7 ± 0.2

B. Lysed plasma

Electrode	*p*H	t_o, min
Anode	6.47	9.0 ± 0.5
Cathode	7.35	3.7 ± 0.5
No current	7.01	4.7 ± 0.2

Table IV. Effect of prolonged electrolysis on the rate of clotting of heparinized platelet-poor fresh plasma at 37°C

Electrolysis carried out for 30 min at 3.2 ma in polystyrene tubes with Pt electrodes. Volume of plasma = 10 cc. Plasma contacted with glass for 10 min. Heparin neutralized with protamine sulfate.

	Polarity	*p*H	$t_{1/2}$, min
A.	Unbuffered		
	Control, no current	7.66	5.5 ± 0.4
	Cathode	8.20	8.9 ± 0.2
	Anode	7.25	6.2 ± 0.1
B.	Buffered		
	Control, no current	7.52	6.3 ± 0.4
	Cathode	7.90	5.6 ± 0.3
	Anode	7.18	6.7

Discussion

Table I shows that for plasma collected in either ACD or sodium citrate there is little effect of electrolysis either on t_o or t_1. This result is independent of whether the plasma was platelet rich or platelet poor and whether or not the platelets were lysed by freezing and thawing. The variations in clotting time as a function of platelet concentration and platelet condition are not meaningful since each set of results refers to a different batch of plasma. Variations in plasma obtained from different donors or from the same donor on different days are such as to allow comparison only between results obtained within a given batch of plasma. Such experiments yield the result that the clotting time t_o is less for platelet rich than for platelet poor plasma. With platelet rich plasma clot retraction was very pronounced and prevented determination of t_1. Platelet lysis led to a decrease in clotting times t_o and t_1, but the decrease in t_o was almost independent of the original platelet concentration indicating the release of an enzyme from the platelets. The decrease in t_1 was dependent on the original platelet concentration, but when the platelet fragments were removed by centrifugation at 2500g then lysis caused no change in $t_1 - t_o$.

A small increase in the rate of clotting was produced by cathodic electrolysis, but this effect is much smaller and of opposite sign to that previously reported for plasma and whole blood containing anticoagulant. Moreover, in the presence of anticoagulant (ACD), Table II shows that electrolysis in silvered tubes did not inhibit the formation of contact factor (factor XIa) nor did it produce an inhibitor to clotting, rather, a small increase in coagulatibility was observed.

Electrolysis of fibrinogen in unbuffered solutions was shown to produce a rapid and large decrease of *p*H in the anode compartment with the resultant precipitation of fibrinogen.

Prolonged electrolysis of plasma in polystyrene tubes with Pt electrodes did not produce an inhibitor in the plasma. The recalcification time was not greatly increased by cathodic electrolysis contrary to the observation of Naumovski and Dejanov, rather, the clotting time for ACD-plasma was slightly decreased by cathodic electrolysis. Anodic electrolysis caused an increase in clotting time compared to unelectrolyzed ACD-plasma. These results may be attributed to the *p*H changes produced in the plasma by electrolysis. It is well known (24) that the clotting time for blood is a minimum at $pH = 7.5$ and increases rapidly with either increase or decrease of *p*H. Inspection of Table III for lysed plasma shows that cathode plasma with *p*H 7.35 has the smallest clotting time. Unelectrolyzed plasma of *p*H 7.01 (due to presence of ACD) has a slightly larger clotting time and anode plasma with *p*H 6.47 has a much larger clotting time. Similar effects were noted on electrolysis of heparinized plasma.

The present results on the electrolysis of human plasma and bovine fibrinogen indicate no interference with the intrinsic enzyme mechanism of blood coagulation, and it is concluded that the results of Sawyer and others on the electrolysis of blood were caused by an electrophoresis mechanism, negatively charged erythrocytes, leukocytes and platelets migrating in the field between the anode and the cathode.

The results do not exclude the possibility of electrochemically influencing the intrinsic enzyme mechanism of blood coagulation. One might reasonably hope to influence the adsorption of Hageman factor (factor XII) on a given material by altering the charge on the material. However, the conditions under which specific proteins are adsorbed and desorbed are by no means obvious and information is required on factors which influence protein adsorption at the solid-liquid interface. Such information would be of great value not only to the study of blood-materials interaction but to the general area of compatability of prosthetic materials and the human body.

Acknowledgments

This work was supported by the National Institute of Dental Research, Grant DE-2111-02. The authors acknowledge the cooperation of the University of Virginia Medical Center and, in particular, the continued interest and assistance of Doctors Oscar A. Thorup, Jr., Phillip M. Allen, and Mary Lou Abram.

Manuscript received Aug. 16, 1966.

Any discussion of this paper will appear in a Discussion Section to be published in the December 1967 JOURNAL.

REFERENCES

1. R. G. Macfarlane, *Nature,* **202**, 498 (1964).
2. E. W. Davie and O. D. Ratnoff, *Science,* **145**, 1310 (1962).
3. G. Wald, *ibid.,* **150**, 1028 (1965).
4. S. N. Levine, *ibid.,* **152**, 651 (1966).
5. P. N. Sawyer, J. W. Pate, and C. S. Weldon, *Am. J. Physiol.,* **175**, 108 (1953).
6. P. N. Sawyer and J. W. Pate, *ibid.,* **175**, 113 (1953).
7. P. N. Sawyer and J. W. Pate, *Surgery,* **34**, 491 (1953).
8. P. N. Sawyer and J. W. Pate, *Am. J. Physiol.,* **175**, 103 (1953).
9. P. N. Sawyer, B. Deutch, and J. W. Pate, Thrombosis and Embolism, Proceedings of the first *International Conference,* 1954, Basil, Switzerland, Schwabe (1955).
10. P. N. Sawyer and B. Deutch, *Am. J. Physiol.,* **187**, 473 (1956).
11. S. I. Schwartz, *Surg. Gyn. Obst.,* **113**, 324 (1961).
12. R. D. Williams and L. C. Carey, *Annals Surgery,* **149**, 381 (1959).
13. R. R. Bradham, *Surg. Gyn. Obst.,* **113**, 324 (1961).
14. J. C. Lamb, J. P. Isaacs, W. L. Bloom, and D. S. Harmer, *Am. J. Physiol.,* **208**, 1006 (1965).
15. P. N. Sawyer, C. Dennis, and S. A. Wesolowski, *Ann. Surg.,* **154**, 556 (1961).
16. J. W. Richardson and S. I. Schwartz, *Surgery,* **52**, 636 (1962).
17. S. I. Schwartz, *Surg. Forum, Am. Coll. Surgeons,* **12**, 46 (1961).
18. P. N. Sawyer, W. H. Brattain, and P. J. Boddy, *J. Proc. Nat. Acad. Sci.,* **51**, 428 (1964).
19. P. N. Sawyer, J. H. Reardon, and I. C. Oganiak, *ibid.,* **53**, 200 (1965).
20. J. C. Oganiak and P. N. Sawyer, *ibid.,* **53**, 572 (1965).
21. "Biophysical Mechanisms in Vascular Hemostasis and Intravascular Thrombosis," P. N. Sawyer, Editor, Appleton-Century-Crofts, New York (1965).
22. "Handbook of Chemistry and Physics," 39th ed., p. 3051, Chemical Rubber Publishing Co. (1957-58).
23. H. W. Hanover and D. L. Brook, *Ann. Surgery,* **160**, 870 (1964).
24. "Blood Coagulation, Hemorrhage and Thrombosis," L. M. Tocantins and L. A. Kazal, Editors, Grune and Stratton, New York (1964).
25. S. I. Schwartz, *Monographs of the Surgical Sciences,* **2**, 159 (1965).

Surface Tensions of Co-Ce and Pu-Co-Ce Alloys as Determined from Frozen Menisci

John C. Biery

University of California, Los Alamos Scientific Laboratory, Los Alamos, New Mexico

ABSTRACT

The surface tensions of three Pu-Co-Ce and three Co-Ce alloys at their freezing point were determined from their frozen menisci. A new calculational procedure was used in which calculated menisci were compared with the experimental menisci. The meniscus shapes were calculated by numerically integrating the Laplace-Young equation. The best surface tension for a given meniscus was found by comparing the computed and experimental menisci at 25 points across the meniscus and by varying the surface tension and contact angle at the outside of the meniscus section until various restraints were satisfied. The meniscus comparing techniques satisfactorily detected and discarded distorted menisci. Of the 28 menisci studied, 15 were found to be acceptable.

Molten plutonium alloys with cobalt and cerium were tested as possible fast nuclear reactor fuels. These studies indicated that unusual phenomena occur at and above the liquid/gas interface of the molten fuel when it is contained in tantalum capsules. Since some of these phenomena may be associated with the energy in the interface, the surface tensions of these alloys should be known to understand the systems better. The usual methods of determining surface tension such as capillary rise, pendant drop, sessile drop, and bubble pressure require expensive and time-consuming experiments when plutonium is involved. Therefore, a technique was developed to generate surface tensions from photographs of menisci since in many cases well-formed menisci are observed in sectioned capsules containing the Pu-Co-Ce alloys. The initial mathematical and numerical techniques for making these determinations from menisci and the test of the method with mercury and water are reported elsewhere (1). Here, the results from analyzing frozen menisci of Co-Ce, Pu-Co-Ce, and Ni-Ce/NaK are presented.

The previously published geometrical and computational methods (1) were tested experimentally with liquid menisci. An important objective of this paper is to test the applicability of the methods as applied to frozen menisci. The tests of the methods were made by (*i*) processing many capsules and comparing the acceptable results from capsules with similar radii, (*ii*) comparing results from menisci formed in capsules with significantly different radii, and (*iii*) comparing results for Pu-Co-Ce with one value obtained from a capillary rise experiment.

Experimental and Calculational Procedure

The frozen menisci were analyzed by an experimental and calculational procedure that has been previously described in detail (1). Below are summarized the important features of the analysis.

Experimental procedure.—The capsule containing the frozen alloy is sectioned longitudinally and is then polished to the centerline position.[1] For best results the void space above the alloy should be filled with epoxy resin. The meniscus is then photographed, and the photograph is enlarged to 25 cm across the diameter of the tube. Meniscus heights at 25[2] positions across the radius are read from a graph onto which the meniscus curve had been traced. These heights are replotted on a graph of expanded scale, and a smooth curve is drawn through the points. Values from this curve are read into the computer for comparison with the computed curves.

Also, from the experimental heights, the sine of the tangent angle at the outside of each radial increment is calculated. A smooth curve is drawn through these points. This "adjusted" sine curve is positioned after calculations have been made to produce a constant surface tension when these sines are used as boundary conditions in the calculations.

Calculational procedure.—The analysis as developed includes a mathematical procedure for calculating the meniscus curve and a method for comparing the computed and experimental curves. The comparison is made in such a manner as to produce the best surface tension value and to throw out the distorted menisci. The meniscus curve is generated by numerically solving a modified form of the Laplace-Young equation shown below.[3]

$$z = \frac{\gamma}{rg(\rho_1 - \rho_2)} \frac{\partial}{\partial r} (r \sin \theta) \qquad [1]$$

The determination of the surface tension and the testing of the distortion of the meniscus involves the selection of γ and ϕ to produce a best fit between the computed and experimental meniscus curves. The procedure involves the following steps:

1. A γ_{optimum} *vs.* $\sin\phi$ curve is calculated for portions of the meniscus out to radial increments 21 through 25.[4] The range of $\sin\phi$ for each sized meniscus is determined by a ± 0.015 range about the smoothed experimental $\sin\theta$ curve. For each $\sin\phi$, γ_{optimum} is found by satisfying the "sum of mass restraint." A series of menisci are calculated with various surface tension values, γ_{as}, for each $\sin\phi$. The capillary rise, z_0, calculated at the center of the capsule for each γ_{as}, when combined with the experimental meniscus curve, allows a γ_{cal} to be calculated by equating the net weight of fluid between the meniscus and the datum plane to the peripheral surface tension force. When the γ_{as} and γ_{cal} agree, this common value is the desired surface tension which satisfies the "sum of mass restraint" for the chosen $\sin\phi$.

2. An "adjusted" experimental $\sin\theta$ curve is drawn to fit the experimental $\sin\theta$ points best and to give the same value of surface tension for the calculations at increments 21 through 25. The γ_{optimum} *vs.* $\sin\phi$ curves calculated in 1 above are used to determine the surface tension at each radial position.

3. For each calculation, standard deviations, s and s_7, between the calculated and experimental meniscus heights are calculated. For an undistorted meniscus at the correct values of γ and ϕ, these standard deviations should be a minimum and should have a value less than 0.0015 cm. If such a minimum occurs with $\sin\phi$ within a ± 0.015 range of the "adjusted" experimental sine curve, then this surface tension is allowed as an acceptable value.

Thus, the primary test as to whether or not a meniscus is undistorted and the surface tension value is acceptable is that the s and s_7 standard deviation values calculated at the conditions where the "sum of mass restraint" is satisfied have minima which are less than some arbitrarily chosen value. Also, the $\sin\phi$ values at these minima in s and s_7 must be within ± 0.015 range of the "adjusted" experimental sine curve. Averaging methods 1, 2, 3 as listed below are versions of this set of requirements with increasing limits on the maximum allowable values of s and s_7 at the minima. In the original formulation of the averaging methods, additional less stringent requirements were proposed as methods 4 through 9. These methods were tested in the present study but are not listed below. Their requirements can be formed elsewhere (1).

Method 1.[5] Average of all surface tension values as determined by the "sum of mass restraint" and a minimum in s or s_7 where $|(\sin\phi_{\min} - \sin\phi_{\text{adj}})| < 0.015$ and s and $s_7 < 15 \times 10^{-4}$ cm.

Method 2.[5] Same as method 1 except s and $s_7 < 25 \times 10^{-4}$ cm.

Method 3. Same as method 1 except s and $s_7 < 35 \times 10^{-4}$ cm.

The above restricting procedures were designed to separate the undistorted from the distorted menisci. The possible sources of distortion in both liquid and frozen menisci that require detection are as follows: (*a*) optical distortion when meniscus is viewed through a cylindrical surface; (*b*) distortion produced by local wetting such that the meniscus is not a surface of revolution; (*c*) variation of the surface with time where wetting conditions or temperature conditions are not stabilized to produce an equilibrium meniscus; and (*d*) errors introduced by sectioning of a frozen meniscus where the cut may be off center or not parallel to the axis of the cylinder.

Specific tests in the initial paper (1) or in this paper have not been performed to determine specifically the limits of distortion which the various restricting techniques detect. In both cases the applicability of the methods is inferred by the comparison of numerical results from a number of menisci and the comparison of surface tensions with known values as determined by other methods.

---

[1] Most of the capsules utilized in this study were not carefully polished to the centerline position since the sectioning was done for metallographic purposes in conjunction with another project.

[2] The value of N, the number of increments across the radius of the tube, is arbitrary and should be chosen small enough to limit computation time but large enough to allow accurate reproduction of the highly curved section of the meniscus near the wall. For the present system with surface tensions in the 600 to 1000 d/cm range, densities near 10 g/cc, and tube radii between 0.45 and 1.2 cm, the choice of N equal to 25 was found to give good results. However, with larger capsules N should be increased to insure that the highly curved section near the wall is divided into at least 5 and preferably 10 increments. Also, with a smaller ratio of $\gamma/(\rho_1 - \rho_2)$ and a resulting flatter meniscus, more increments may have to be used.

[3] See Nomenclature at end of paper.

[4] In all of the calculations and comparisons, the section of the meniscus used was that portion from the centerline out to some arbitrary radial position less than or equal to the radius of the tube. The effect of utilizing successively smaller portions of the meniscus was studied by discarding increments of the meniscus at the outside perimeter. As each increment was discarded and the comparison between computed and experimental data was made, a better or worse value of surface tension was obtained. The change depended on whether or not the discarded increment was more or less distorted than the remaining inside portion of the meniscus. Many calculations were run with 21, 22, 23, 24, and 25 increments retained when the radius was divided into 25 increments. The results indicated that the 25th increment, which was next to the tube wall, was many times distorted and that the most consistent data were obtained when the calculations were made for 24/25 or 23/25 of the total meniscus. Because of the increased curvature near the wall, the most readily detectable surface tension data were contained in the outside 10/25th of the meniscus. Therefore, the quality of the surface tension results deteriorated when as many as 4 increments were discarded.

[5] The limits on methods 1 and 2 were revised somewhat as compared to those used in the Hg, water calculations (1). The changes were made to make methods 1, 2, and 3 consistent. In these three methods the limit on the sines is held constant while the restraint on s and s_7 is progressively relaxed.

Surface Tensions of Co-Ce Alloys from Frozen Menisci

The surface tensions of 6, 12, and 18 w/o Co in Co-Ce alloys were determined from their frozen menisci. A total of 12 menisci were analyzed, and of this number 7 produced minima in the s and s_7 curves that met the demands of methods 1, 2, or 3. The best data came from the 12 w/o Co-Ce melts. For this composition, 6 samples were run, and four of them gave acceptable s and s_7 minima.

In Tables VII and VIII in the Appendix,[6] are compiled the physical properties and chemical analyses of the alloys, characteristics of the menisci, and the computation data for the three alloys. The densities at melting of the alloys were obtained from a paper by Perkins *et al.* (2). These density studies show the 12 and 18 w/o Co-Ce alloys to be near eutectics and to melt at nearly constant temperatures of 425° and 440°C. The 6 w/o alloy is not a eutectic and melts over a range from 420° to 625°C. Therefore, the surface tension for the 6 w/o material does not accurately represent the surface tension of the alloy, but probably shows the properties of a melt near 12 w/o Co which is the last material to solidify at 420°C.

All of these alloys expand on freezing. Thus, the shape of the meniscus is quite well preserved since a crust tends to form first over the meniscus and excess liquid is squeezed upward by the freezing action and usually escapes up on the meniscus crust through cracks. The upward pressure of the unsolidified melt does not seem to distort the meniscus unduly. The characteristics of each alloy and its surface tension determination are discussed below.

6 w/o Co-Ce *alloy.*—The surface tensions for the 6 w/o alloy are shown in Table I. Because of a large s value greater than 0.0025, only those methods that did not include or relaxed the s and s_7 size restrictions gave any useful results. Acceptable minima in s were obtained when s was allowed to be as large as 0.0035 cm in method 3, and the average surface tension, 685 ± 38.2 dynes/cm, obtained with these restrictions had the smallest 95% confidence intervals. Methods 8 and 9 gave comparable results, 677 dynes/cm, but with a larger confidence interval of ±96.8 dynes/cm.

In these determinations the radius of the capsule ranged from 0.47 to 0.57 cm. The meniscus in this sized capsule had maximum heights above the meniscus bottom of 0.32 cm, and the calculated capillary depression varied between 0.23 and 0.29 cm for the two acceptable menisci. In Table X in the Appendix, is tabulated a summary of the computation results for the three menisci.

Table I. Summary of surface tension data

Type of av	No. of menisci in av	No. of surface tension determinations in av	Range of surface tensions in av, dynes/cm	95% Confidence interval for av value of surface tension, dynes/cm	Av value of surface tension, dynes/cm
			6 w/o Co-94 w/o Ce		
1	None	—	—	—	—
2	None	—	—	—	—
3	2	2	628-688	±38.2	685.0
4	None	—	—	—	—
5	1	1	699	—	699
6	1	1	632	—	632
7	None	—	—	—	—
8	2	3	632-700	±96.8	677.0
9	2	3	632-700	±96.8	677.0
			12 w/o Co-88 w/o Ce		
1	4	10	628-660	±7.7	644.5
2	Ditto				
3	Ditto				
4	3	3	617-668	±65.9	646.7
5	5	5	617-1029	±219.0	719.2
6	6	6	617-1029	±175.8	744.0
7	4	9	617-669	±16.5	647.7
8	5	12	617-880	±56.3	682.6
9	4	9	617-669	±16.5	647.7
			18 w/o Co-82 w/o Ce		
1	1	2	897-943	±293	920.0
2	Ditto				
3	Ditto				
4	None	—	—	—	—
5	1	1	872	—	872
6	2	2	872-880	±51.0	876
7	None	—	—	—	—
8	None	—	—	—	—
9	None	—	—	—	—

12 w/o Co-Ce *alloy.*—The analyses of the 12 w/o Co-Ce menisci gave the best and most consistent results. Six menisci were studied, and these were formed in three different size tubes of 0.46, 0.57, and 1.2 cm radii. Acceptable minima in the s and s_7 curves were obtained from all three sizes of menisci. These menisci produced surface tensions with an average value of 644.5 dynes/cm with a 95% confidence interval of ±7.7 dynes/cm. The menisci with the largest radius were most easily analyzed. The minima in s and s_7 were much sharper, and the surface tension was much more insensitive to changes in $\sin\phi$. Also, in the larger radius capsules the value of z_0 was smaller, and its influence on the total calculation was less.

The results from the 12 w/o Co-Ce menisci gave the best indication that distortion was not significant when the criteria of method 1 were satisfied. Menisci from three different radii tubes were analyzed, and the results from all three agreed very satisfactorily. Since the cooling histories of the melts in the capsules were considerably different, the probability of all menisci distorting in such a manner to meet the demands of method 1 and still give the same value of surface tension is quite small. In Fig. 1 and 2 are shown the menisci for capsule 3 (1.21 cm radius) and capsule 277 (0.459 cm radius), both of which produced surface tensions which met the requirements of method 1. The large diameter capsule exhibited distortion in the center. However, the outside portions of the meniscus were undistorted and produced acceptable values of surface tension. Capsule 277 meniscus appears visually to be undistorted, and the computations supported

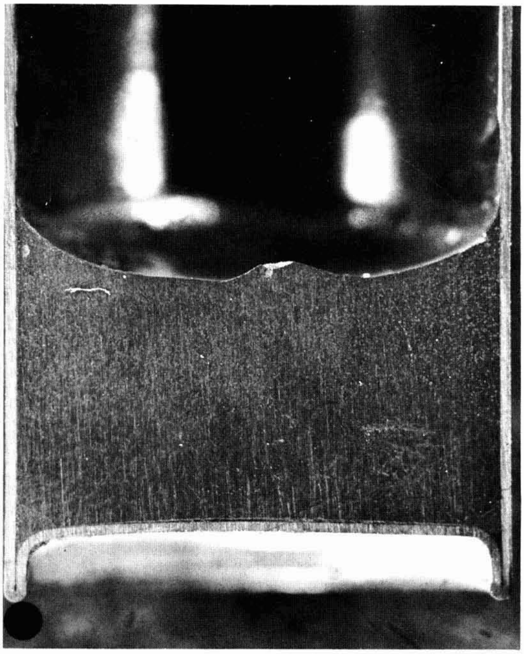

Fig. 1. Meniscus in capsule 3 with 1.21 cm radius; 12 w/o Co-88 w/o Ce.

---

[6] The Appendix has been deposited as Document No. 9231 with the American Documentation Institute Photoduplication Service, Library of Congress, Washington 25, D. C., and may be obtained for $3.75 for photoprints or $2.00 for 35 mm microfilm.

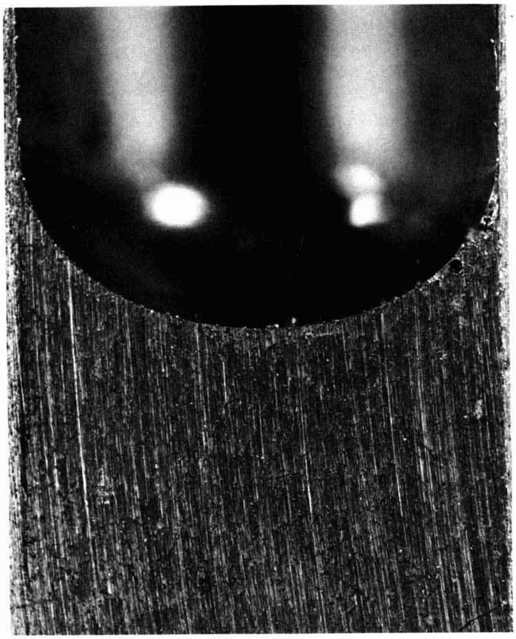

Fig. 2. Meniscus in capsule 277 with 0.459 cm radius; 12 w/o Co-88 w/o Ce.

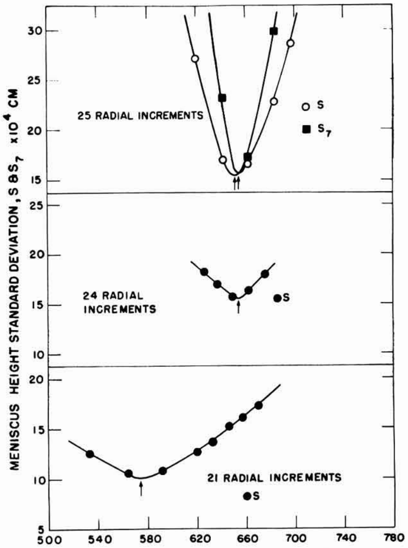

Fig. 3. Meniscus height standard deviations, s and s_7 vs. "optimum" surface tension for capsule 3; radius = 1.21 cm, 12 w/o Co-Ce.

this contention. In Fig. 3 and 4 are shown the s and s_7 curves for these two capsules.[7] The "adjusted" and experimental sine curves for these two capsules are shown in Fig. 5 and 6. Visual comparison of Fig. 3 *vs.* 4 and of Fig. 5 *vs.* 6 indicates that the methods used to treat the data permit satisfactory results to be obtained from both symmetric and distorted menisci provided only that the region of obvious distortion is not in the curved section near the outside perimeter of the meniscus.

In Table X in the Appendix are summarized the computational results for the 12 w/o Co-Ce alloys.

18 w/o Co-Ce *alloy.*—The surface tension results for the 18 w/o Co-Ce melts are summarized in Table I. Only one of the three menisci gave acceptable minima in the s and s_7 curves. However, the limitation of method 6 allowed two results from two capsules to be averaged and gave a result of 876 ± 51 dynes/cm. The two acceptable menisci for method 6 had significantly different radii of 0.57 and 1.21 cm. The computational

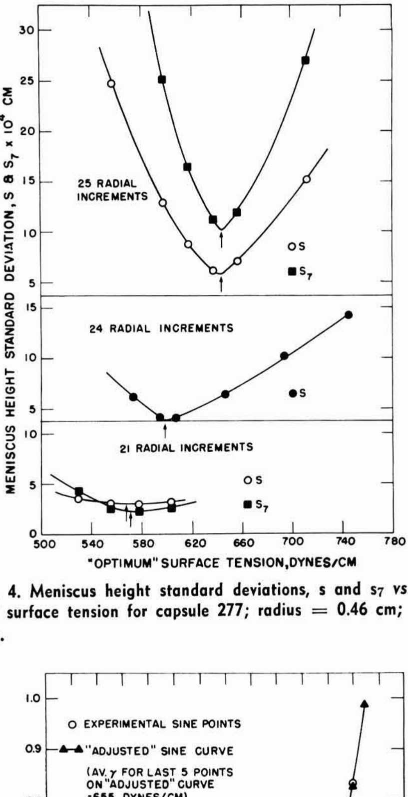

Fig. 4. Meniscus height standard deviations, s and s_7 vs. "optimum" surface tension for capsule 277; radius = 0.46 cm; 12 w/o Co-Ce.

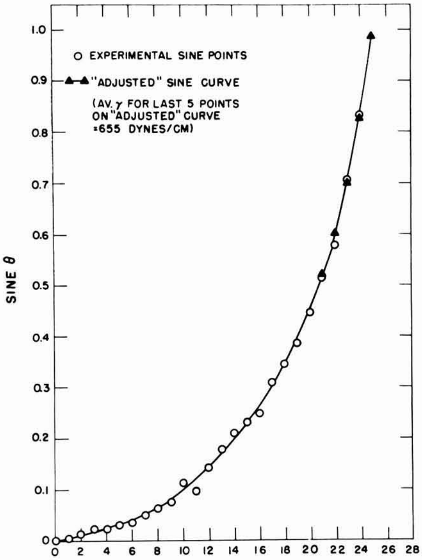

Fig. 5. Experimental and "adjusted" sine curve for capsule 3; radius = 1.21 cm, 12 w/o Co-Ce.

---

[7] In each case the radius was divided into 25 increments. Three calculations are shown for the cases where the inside 21, 24, and 25 increments are retained in the comparison.

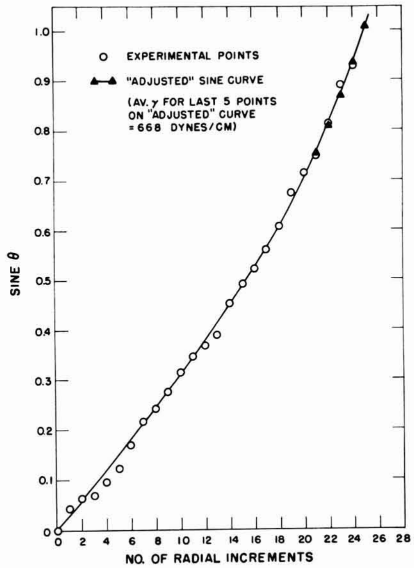

Fig. 6. Experimental and "adjusted" sine curve for capsule 277; radius = 0.46 cm; 12 w/o Co-Ce.

Table III. Summary of surface tension data

Type of av	No. of menisci in av	No. of surface tension determinations in av	Range of surface tensions in av, dynes/cm	95% Confidence interval for av value of surface tension, dynes/cm	Av value of surface tension, dynes/cm
			3 g/cc Pu-Co-Ce		
1	2	10	628-687	±14.9	653.6
2	Ditto				
3	Ditto				
4	2	2	616-648	±415	648.5
5	3	3	616-1124	±663	807.0
6	3	3	616-1124	±663	807.0
7	3	8	615-1124	±144	704.0
8	5	13	397-1124	±143	728.8
9	5	10	397-1124	±130	662.6
			5 g/cc Pu-Co-Ce		
1	None				
2	2	8	927-1340	±151	1125.3
3	Ditto				
4	1	1	1148.0		1148.0
5	2	2	979-1148	±1074	1063.5
6	3	3	629-1148	±633	918.7
7	2	5	977-1148	±115.6	1079.8
8	4	8	629-1279	±164.8	1035.8
9	3	7	629-1148	±171.4	1001.0
			8 g/cc Pu-Co-Ce		
1	None				
2	None				
3	3	5	935-1135	±117.5	1019.0
4	None				
5	1	1	918.0		918.0
6	3	3	918-1184	±334.0	1041.0
7	None				
8	3	5	918-1187	±163.6	1044.0
9	3	4	918-1187	±205.5	1076.3

and comparison results for the 18 w/o Co-Ce alloys are presented in Table XI in the Appendix.

Surface Tensions of Pu-Co-Ce Alloys

The Pu-Co-Ce system forms a series of low melting alloys in which the plutonium concentration can be varied over a wide range of concentrations without significantly changing the melting temperature. These alloys are of interest in a liquid metal nuclear reactor because of the possibility of changing the plutonium concentration and the power density without changing the temperature requirements of the coolant system. Alloys from this system have been extensively tested as to their corrosion characteristics in tantalum containers, and some usable menisci were observed when photomicrographs were made from the sectioned capsules. The three alloys of interest are the 3, 5, and 8g Pu/cc concentrations. The nominal weight per cent compositions for the three alloys are listed in Table II. Also, listed are the melting ranges of these materials. These alloys are not true ternary eutectics, but their compositions do reside near the bottom of a temperature trough running through the ternary diagram. Therefore, the 3 and 5g Pu/cc materials do melt over a very narrow range of 10°C while the 8 g/cc melts over a 25°C range.

The data reported here were obtained from various capsules that were run for other purposes. As a result, many menisci were asymmetrical and distorted from not being in an exact vertical position on freezing. Also, no great care was taken to section the capsule exactly in the center. However, the number of undistorted menisci was sufficiently large to give reasonable estimates of the surface tension of the melts on freezing. In Tables XII and XIII, in the Appendix, are listed the chemical analyses for many of the melts tested. Also, the physical properties of the menisci and the computation requirements for the three alloys are tabulated in Table XIV of the Appendix.

Table II. Nominal compositions and melting ranges for Pu-Co-Ce alloys

Alloys Pu conc., g/cc	Nominal composition, w/o			Melting range, °C
	Pu	Co	Ce	
3	33.5	10.2	56.3	436 ± 5
5	49.3	9.9	40.8	440 ± 5
8	68.1	8.3	23.6	420-445

3 g/cc Pu-Co-Ce *alloy.*—Five menisci were analyzed for the 3 g/cc alloy; the results are shown in Table III. Two of the menisci produced acceptable minima in the s and s_7 curves as required by method 1, with a resulting average surface tension of 653.6 ± 14.9 dynes/cm. For this alloy only methods 1, 2, and 3 produced averages with small enough confidence intervals to be meaningful.

One of the 5 menisci was obtained by radiographing a sealed capsule in which the meniscus was frozen. Added uncertainty was produced by the fuzzy nature of the radiograph, and the resulting s and s_7 values were excessively large. However, the average γ from the "adjusted" sine curve was 598 dynes/cm which compares surprisingly well with the 654 dynes/cm value from the two acceptable mensici. A summary of the computational and comparison results for the 3 g/cc alloy is presented in Table XV of the Appendix.

5 g/cc Pu-Co-Ce *alloy.*—Five menisci from the 5 g/cc alloy were studied, and two of the menisci produced minima acceptable by method 2. However, in this case the range of the surface tensions from these minima was very large, 927 to 1340 dynes/cm. The average surface tension from method 2 was 1125 ± 151 dynes/cm. Method 7 actually produced an average with a smaller confidence interval, 1079.8 ± 116 dynes/cm. This wide confidence interval indicates that some distortion was being allowed in method 2 and that more menisci should be studied as they become available. The tabulation of comparison results is given in Table XVI in the Appendix.

The radiographed meniscus again had very large s values. The average value from the adjusted sine curve was 629 dynes/cm which does not compare favorably with the above averages.

8 g/cc Pu-Co-Ce *alloy.*—The average surface tensions found for the 8 g/cc alloy are presented in Table III. Of the 5 menisci tested none met the requirements of methods 1 and 2. However, the minima in s and s_7 were acceptable from three of the menisci when the size restriction of s and s_7 was relaxed to

35×10^{-4} cm in method 3. This result of 1019 ± 118 dynes/cm had the smallest 95% confidence interval for all of the 9 averaging methods. All other restricting methods had confidence limits of ±164 dynes/cm or greater. Table XVII in the Appendix contains the computational and comparison results for the various menisci.

The radiographed capsule had very large s and s_7 values and gave an average surface tension of 740 dynes/cm. The fuzziness of the radiograph produced some of the distortion indicated by the size of the s and s_7.

Capillary rise surface tension determination.—The surface tensions of these alloys have not been determined by other methods in experiments designed for such determinations. However, one independent calculation of the surface tension of 6.2g Pu/cc Pu-Co-Ce (57.7 w/o Pu-9.4 w/o Co-32.8 w/o Ce) was made possible from a radiograph of the fluid contained in an electromagnetic pump experimental apparatus (3). The reservoir and manometer legs provided a system in which capillary rise in the legs could be measured. At 530°C the rise in the manometer tube along with the assumption of 0° contact angle gave a surface tension of 1050 dynes/cm. This value compares very favorably with the values of 1125 ± 151 and 1019 ± 118 dynes/cm for the 5 and 8g Pu/cc Pu-Co-Ce alloys.

Interfacial Tension of a Co-Ni Alloy Covered with NaK

In density studies made with a NaK volumeter (2) the density specimen is held in direct contact with the indicating NaK fluid. Many of the specimens formed well-shaped concave menisci between the alloy and the NaK. At this time one of these menisci from an 18 w/o Ni-Ce alloy has been analyzed. The results presented in Table IV indicate that the meniscus was relatively undistorted since acceptable minima in s and s_7 at three of the four radial increments tested were obtained. The best result came from method 3 where a tension of 421.3 ± 16.1 dynes/cm was produced. Since only one sample was run, most of the analyzing methods could not give a 95% confidence interval. The physical data for the mensicus and the computation times are given in Table XIX in the Appendix. The computation results for each radial increment are included as Table XX in the Appendix. As indicated in Table XVIII the Ni-Ce alloy melted over a temperature range of 450°-490°C and is not a true eutectic. A complete tabulation of the experimental meniscus heights for all of the menisci studied are presented in Table XX in the Appendix.

Results and Conclusions

Surface tensions of 6, 12, and 18 w/o Co-Ce, 3, 5, and 8g Pu/cc Pu-Co-Ce alloys, and the interfacial tension of 18 w/o Ni-Ce/NaK were determined from frozen menisci of the alloys. A total of 28 menisci were analyzed and, of this number, 15 produced minima in the standard deviations, s and s_7, that met the limitation of size of s and s_7 and of deviation in $\sin\phi$, as required by averaging methods 1, 2, and 3. Nine methods of testing the surface tension data for distortion were tested on the menisci, and methods 1, 2, and 3 which require acceptable minima in s and s_7 were consistently the best. Of the more liberal restricting techniques, methods 7, 8, and 9 most consistently produced results that agreed with methods 1, 2, and 3. These last restrictive methods invariably had 95% confidence intervals that were from 1½ to 10 times as large as those from methods 1, 2, and 3. In one case, for 18 w/o Co-Ce, method 6 which only requires that experimental and adjusted sine curves be nearly parallel gave the most acceptable results with the smallest 95% confidence interval. The surface tensions obtained from the analyses are summarized in Table V.

Table IV. Summary of interfacial tension data
18 w/o Ni—81 w/o Ce/78 w/o NaK

Type of av	No. of menisci in av	No. of surface tension determination in av	Range of surface tensions in av, dynes/cm	95% Confidence interval for av value of surface tension, dynes/cm	Av value of surface tension, dynes/cm
1	1	4	408.0-440.0	±22.8	423.0
2	Ditto				
3	1	5	408.0-444.0	±16.1	421.4
4	None				
5	1	1	423.1		423.1
6	1	1	423.1		423.1
7	1	1	423.0		423.0
8	1	1	423.0		423.0
9	1	1	423.0		423.0

The surface tension calculation and restriction procedure was designed such that if averaging method 1 was satisfied the meniscus could be assumed to have no significant distortion from freezing. Averaging methods 2 and 3 also should minimize the possibility of distortion, but because of the larger allowable standard deviation in meniscus differential heights, more distortion is permitted. The analysis of the 28 menisci in this study indicate that the restrictions of method 1 are sufficient to eliminate distorted menisci. Methods 2 and 3 with their relaxation on the size of the standard deviation also give good results in general. Three tests of the restricting procedures were possible from the computations. Comparisons of surface tensions from capsules of similar size could be made. Also, surface tension comparisons from capsules with significantly different radii were possible. And finally, one independent surface tension determination was available for comparison.

In the first test, the surface tension of a given alloy was determined from a number of capsules of approximately the same diameter, and these values were compared. Since the cooling histories of the capsules were probably dissimilar, the surface tension values from the capsules could be significantly different if distortion were allowed to influence the results. Also, the values from the various capsules could vary from asymmetries resulting from nonvertical freezing and noncenterline cutting. The minima methods were designed to detect and discard nonmeniscus type of shapes. Thus, if the methods are operating satisfactorily, the remaining acceptable menisci should produce comparable values of surface tension. In Table VI are summarized the data obtained from capsules of comparable size for the alloys tested. The surface tensions of the capsules accepted and from those rejected are noted. Also, the type of minima method used is listed. Three sets of capsule pairs from two alloys met the requirements of method 1. The range of the dual values was for each set within ±1.8, ± 1.2, and ± 0.23% of the average for the two capsules. As the magnitude of the standard deviations, s and s_7, was relaxed in methods 2 and 3, the spread in surface tensions became greater. For the 5g Pu/cc Pu-Co-Ce with method 2, the range was ± 13.4%. Method 3 gave very good results for 6 w/o Co-Ce with a range of ± 0.43%. However, the range with method 3 for 8g Pu/cc Pu-Co-Ce was ± 10.5%. These results tend to indicate that method 1 is sufficiently stringent to insure that the shape being studied was formed by surface tension forces. However, some dis-

Table V. Summary of surface tensions obtained from frozen menisci

Material	Method No.	Surface tension, dynes/cm	95% Confidence interval
6 w/o Co-94 w/o Ce	3	685.0	±38.2
12 w/o Co-88 w/o Ce	1	644.5	±7.7
18 w/o Co-82 w/o Ce	6	876	±51
3 g/cc Pu-Co-Ce	1	653.6	±14.9
5 g/cc Pu-Co-Ce	2	1125	±151
8 g/cc Pu-Co-Ce	3	1019	±118
18 w/o Ni-82 w/o Ce/NaK	1	423.0	±22.8

Table VI. Comparison of surface tension values from capsules of comparable size which satisfy averaging methods 1, 2, and 3

Material	No. of menisci tested with similar radii	Radius range, cm	No. of menisci acceptable	Averaging method used	Average values of surface tension for each capsule accepted	Average values of surface tension for each capsule not accepted
6 w/o Co-94 w/o Ce	3	0.47-0.57	2	3	682, 688	405
12 w/o Co-88 w/o Ce	4	0.46-0.57	2	1	645, 642	853, 1073
	2	1.21	2	1	654, 637	
18 w/o Co-82 w/o Ce	1	0.57	1	1	920	
	2	1.21	0	—	—	808, 541
3 g Pu/cc-Pu-Co-Ce	5	0.46-0.48	2	1	668, 644	303, 1360, 412
5 g Pu/cc-Pu-Co-Ce	5	0.46-0.48	2	2	1260, 962	1279. 629, 1137
8 g Pu/cc-Pu-Co-Ce	5	0.47-0.48	3	3	1121, 985, 937	510, 735

tortion in the meniscus can be expected if methods 2 or 3 are used.

A second test of averaging method 1 was made available by the data from the 12 w/o Co-Ce menisci. Here two sets of capsules with significantly different radii met the requirements of method 1. The shapes of these menisci were quite different as indicated in Fig. 1 and 2, and their thermal cooling histories had to be very different because of the different radii. As shown in Table VI, the average values for these two sets of capsules were 643 and 645 dynes/cm.

Finally, a surface tension value was obtained by a capillary rise experiment for the 6.2g Pu/cc Pu-Co-Ce fuel. This value was 1050 dynes/cm which falls right between the values obtained for the 5 and 8g Pu/cc fuels as determined by methods 2 and 3.

These calculational and experimental results show that good surface tension values can be obtained from frozen menisci with the comparison and restricting procedures utilized. However, the less stringent averaging procedures, methods 4 through 9, should be used with care and should be utilized only to indicate the general range of the surface tension for a given liquid metal.

Acknowledgment

The author wishes to thank Carl R. Cushing and John M. Oblak for their help in obtaining and preparing the experimental data. Also, the efforts of Marguerite Coleman and Doreen Bourne in preparing the manuscript are greatly appreciated.

This work was performed under the auspices of the United States Atomic Energy Commission.

Manuscript received March 7, 1966; revised manuscript received Oct. 31, 1966. This paper was presented at the Washington Meeting, Oct. 11-15, 1964.

Any discussion of this paper will appear in a Discussion Section to be published in the December 1967 JOURNAL.

REFERENCES

1. J. C. Biery and J. N. Oblak, *Ind. & Eng. Chem. Fundamentals*, **5**, 121 (1966).
2. R. H. Perkins, L. A. Geoffrion, and J. C. Biery, *Trans. Met. Soc. AIME*, **233**, 1703 (1965).
3. G. L. Caldwell, "An Experimental dc Electromagnetic Pump for a Molten Plutonium Alloy," Los Alamos Scientific Lab. LA-3240, Dec. 9, 1965.

NOMENCLATURE

g	acceleration due to gravity, cm/sec^2
s	sample standard deviation between calculated and experimental heights at all N radial positions, cm
s_7	sample standard deviation between calculated and experimental meniscus heights at outside seven radial positions, cm
z	height of meniscus above datum plane at radial position r, cm
z_o	height of meniscus above datum plane at $r = 0$, cm
$z'_{m-1/2(\mathrm{exp})}$	experimental meniscus height above horizontal tangent plane, cm
$z'_{m-1/2(\mathrm{num})}$	numerically calculated meniscus height above horizontal tangent plane, cm
ρ_1	density of fluid, below meniscus, g/cc
ρ_2	density of fluid, above meniscus, g/cc
θ	angle between tangent to surface tension curve and horizontal line at radial position r, radians
θ_{exp}	experimental angles calculated from $z'_{m-1/2(\mathrm{exp})}$, radians
θ_{adj}	values of θ on a smoothed curve through $\sin\theta_{\mathrm{exp}}$ points. Values from this curve when used for boundary condition of $\sin\phi$ give approximately a constant value of γ at all radial positions tested
ϕ	angle of tangent to meniscus curve at outside of meniscus. This is the boundary condition required in the numerical computation, radians
ϕ_{min}	value of ϕ at minimum in s or s_7, radians
ϕ_{as}	external tangent angle assumed for a computation, radians
γ	surface tension, dynes/cm
γ_{as}	surface tension assumed for a computation, dynes/cm
γ_{cal}	surface tension calculated with sum of mass restraint dynes/cm
$\gamma_{\mathrm{optimum}}$	surface tension calculated with sum of mass restraint where $\gamma_{\mathrm{as}} = \gamma_{\mathrm{cal}}$, dynes/cm

Technical Notes

The Application of Ultraviolet Analytical Techniques to Lead Acid Systems

Thomas F. Sharpe

Research Laboratories, General Motors Corporation, Warren, Michigan

The use of ultraviolet (uv) spectrophotometric techniques to clarify the role of organic additives in electrolytic systems has been restricted to some extent because portions of the spectra of the organic materials have been obscured. In studies of adsorption at copper, nickel, and silver electrodes, Barradas and Conway reported (1) that traces of metal ions and/or complexes formed between the metal ion and the organic compounds tended to distort the uv absorption bands of the organic adsorbate. To minimize these effects, the study was confined to alkaline and weakly acidic solutions at electrode potentials near the reversible hydrogen potential for the given solution.

Similarly, the application of uv methods for studying the reactions of conjugated organic compounds in experimental lead-acid battery systems is limited because of inorganic uv-absorbing materials in the electrolyte.

This paper reports on attempts to characterize the various inorganic uv-absorbing constituents in lead-acid cells to find ways to minimize their interference with the evaluation of concentration and structural changes of the organic materials. The experimental approach was to measure the uv absorbance of sulfuric acid solutions exposed to lead surfaces on open circuit and during polarization, and then to compare these results with the absorbance exhibited by lead and lead-antimony corrosion products added to the acid as the reagent grade chemicals. Absorbance measurements were made with a dual beam spectrophotometer[1] using distilled water as a reference. The sulfuric acid solutions were prepared by diluting the reagent grade acid to the desired specific gravity with distilled water. The absorbance exhibited by these solutions was negligible throughout the range 350-210 mμ.

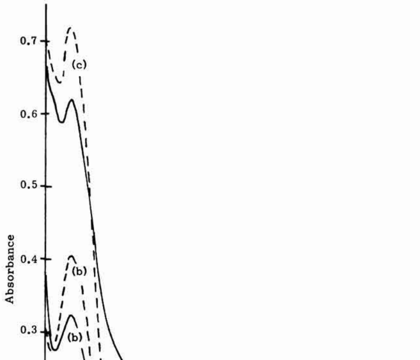

Fig. 1. The ultraviolet absorbance exhibited by 1.21 sp gr H_2SO_4 solutions containing: ——— lead power, (a) 10 g/liter, (b) 100 g/liter, and (c) 500 g/liter; — — — PbO_2, (a) 1 g/liter, (b) 10 g/liter, and (c) 100 g/liter; and . . . . $PbSO_4$ (saturated).

The absorption spectra presented in Fig. 1 were obtained following the additions of pure lead powder, lead sulfate ($PbSO_4$), or lead dioxide (PbO_2) to 1.21 sp gr H_2SO_4. To insure equilibrium, the solutions were stirred thoroughly for several hours; then the excess solid material was allowed to settle before making the absorbance measurements.

The magnitude of absorbance exhibited by the $PbSO_4$ is attributed to the sparingly soluble Pb^{2+} ion, since quantities of $PbSO_4$ greater than those required for saturation did not affect the absorbance. Increasing the amount of excess PbO_2, however, caused an increase in absorbance. Since PbO_2 can oxidize the water in the solution, the absorbance may be caused by Pb^{2+} ion present in greater quantity than normal saturation, or by the formation of an oxygen-containing complex, such as $PbO \cdot PbSO_4$. The absorbance of the acid exposed to the pure lead powder reached its maximum in 18 hr and is similar to that resulting from additions of PbO_2.

Since the increase in absorbance of H_2SO_4 solutions exposed to the lead may be caused by the reaction of lead with oxygen, some experiments were conducted in nitrogen stirred solutions to determine whether the absorbance was minimized. Electrodes (3.0 x 4.0-cm portions of a lead-3% antimony gauze) were polarized in an H-type cell whose two electrode compartments were separated by a glass frit. Figure 2 shows the effect of both anodic and cathodic polarization on absorbance of the acid determined by sampling the appropriate compartment of the H-cell for spectrophotometric analysis.

No increase in absorbance was found after an 18-hr open-circuit exposure of the electrodes in nitrogen stirred solution. However, anodic polarization in nitrogen stirred solution, even at very low current densities, gave measurable increases in absorbance.

Prolonged cathodic polarization in nitrogen stirred solution at low current density gave no increase in absorbance. However, when nitrogen stirring was replaced by air stirring (without interrupting the current), the absorbance increased in a manner similar to that found in the solution from the anode compartment. In the presence of air, the absorption con-

---

[1] Cary Model 15, Applied Physics Corporation, Monrovia, California.

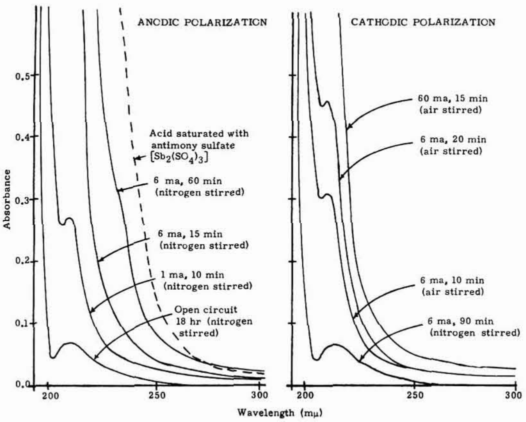

Fig. 2. Effect of anodic and cathodic polarizations of lead-3% antimony electrodes on the absorbance of 1.30 sp gr H_2SO_4. (Acid saturated with $PbSO_4$ before test.)

tinued to increase even at much higher cathodic current densities.

The spectrum (broken line in Fig. 2) resulting from the addition of antimony sulfate [$Sb_2(SO_4)_3$] to the acid suggests that a substantial portion of the absorbance shown in Fig. 2 was because of dissolution of the antimony. It appears that in nitrogen stirred solutions the electrode potential is sufficiently noble so that there is no metal dissolution. However, in the presence of oxygen (air), even when applying a low cathodic current, the potential is sufficiently active to allow metal dissolution to take place.

It has been suggested that an additional cause for absorption is the possible formation of hydrogen peroxide (H_2O_2) by reduction of oxygen (2) at the cathode. Small quantities of H_2O_2 in H_2SO_4 give uv absorbance patterns similar to those shown by the acid exposed to the lead surfaces. The minimum quantity of H_2O_2 detectable by the uv method is 0.001%, which was established by measuring the absorbance of H_2SO_4 solutions containing known quantities of H_2O_2. During the experiment represented in Fig. 2, quantities of solution in the cathode compartment were checked periodically for H_2O_2. Using the standard peroxytitanic acid test (3), the presence of H_2O_2 was not indicated. Since this test is sensitive to $< 0.001\%$ H_2O_2, it appears that H_2O_2 is not a contributor to absorption in these experiments. The absence of H_2O_2 in lead-acid systems is not surprising, however, since lead surfaces are reported (4) to be excellent peroxide decomposers.

To summarize, these experiments indicate that when ultraviolet techniques are applied to lead-acid systems, conditions should be maintained to minimize buildup of corrosion products of lead and lead-antimony alloys. Therefore, the reactions of conjugated organic compounds at lead surfaces should be studied in nitrogen stirred solutions at potentials more cathodic than the corrosion potential of the lead surface.

Manuscript received Nov. 1, 1966; revised manuscript received Dec. 7, 1966.

Any discussion of this paper will appear in a Discussion Section to be published in the December 1967 JOURNAL.

REFERENCES

1. R. G. Barradas and B. E. Conway, *J. Electroanal. Chem.*, **6**, 314 (1963).
2. M. Taube, *Ber. Chem. Deutsch. Ges.*, **15**, 2434 (1882).
3. G. M. Eisenberg, *Ind. Eng. Chem.*, **15**, 327 (1943).
4. W. C. Schumb, C. N. Satterfield, and R. W. Wentworth, "Hydrogen Peroxide," pp. 168, 402, Reinhold Publishing Corp., New York (1955).

Studies of Hydrocarbon Fuel Cell Anodes by the Multipulse Potentiodynamic Method

IV. Effect of Various Electrolytes on the Behavior of Hydrocarbons on Conducting Porous Teflon Electrodes

L. W. Niedrach and M. Tochner[1]

General Electric Research & Development Center, Schenectady, New York

Important variables in fuel cell studies are the electrocatalyst, electrode structure, electrolyte, and fuel structure. A systematic study of these variables using the multipulse potentiodynamic (MPP) method has been under way in this Laboratory (1-5). Previous papers in the present series have dealt with the behavior of methane, ethane, and propane on Teflon bonded platinum black electrodes with a perchloric acid electrolyte (3, 4) and with methane through butane with a phosphoric acid electrolyte (5).

Recent observations in fuel cell studies that higher current densities can be sustained by hydrocarbons with a hydrofluoric acid azeotrope electrolyte than a concentrated phosphoric acid electrolyte (6) initiated the present examination of the effects of various electrolytes. Of particular interest was any difference in behavior that could account for the higher, steady-state current densities that can be supported in hydrofluoric acid cells without the appearance of voltage decay and oscillations. The electrolytes that were compared in this study were H_3PO_4, $HClO_4$, and HF at 60°C. Ethane served as the model hydrocarbon for the comparison.

Experimental

A three-compartment Teflon cell described elsewhere (3) was used in these experiments. A miniature version (0.2 cm diameter) of a previously described (7) conducting-porous "Teflon" fuel cell electrode containing platinum black as the catalyst was employed. That used in this work was designated as ME-16.

Both the hydrogen reference and counter electrodes were platinized platinum flags. The hydrogen reference communicated with the working electrode by a Luggin capillary. All potentials are referred to this electrode. The cell was operated in an air thermostat enabling control of the temperature to within 0.1°C.

The acids employed in the study were 4.3*N* perchloric acid, 5*N* phosphoric acid, 36*N* (75%) phosphoric acid, and 22*N* (azeotrope) hydrofluoric acid. All were prepared by diluting reagent grade acids with quartz distilled water. Electrolytic grade hydrogen was used in the reference electrode chamber, and

---

[1] Present address: Silicone Products Department, General Electric Company, Waterford, New York.

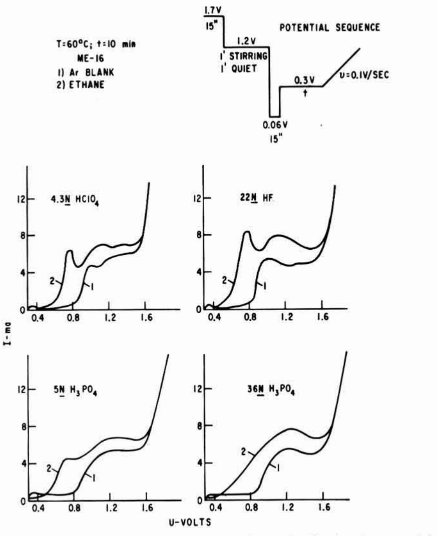

Fig. 1. Current-potential (time) traces for adsorbed ethane with various electrolytes.

Phillips research grade ethane was used as the fuel. Tank argon deoxygenated by passage over heated copper turnings was substituted for the fuel for obtaining solvent blanks. Tank argon was also used for degassing the electrolyte.

As in the earlier work linear anodic sweeps were applied to the electrode to determine the behavior of the ad-layer as well as the amount of fuel adsorbed after equilibrations at various potentials for varying times. Prior to each equilibration the electrode was pretreated with a series of potential steps which have previously been found to result in reproducible conditions. The sequence of steps is shown in Fig. 1 and the details are discussed elsewhere (3).

Briefly, oxidizable impurities are removed from the electrode during the period at 1.7v. During the step at 1.2v, oxygen evolution ceases, and free oxygen is removed from the vicinity of the electrode. Adsorption of fuel is blocked at this time by "adsorbed oxygen" on the electrode. The brief excursion to 0.06v results in reduction of the "adsorbed oxygen" layer at a potential at which hydrocarbons are themselves not adsorbed. The potential is then stepped to that at which adsorption and performance data are required. After the desired equilibration time a linear anodic sweep is applied in order to determine the number of coulombs associated with oxidation of the carbonaceous ad-layer. This information is obtained by integrating the area between the trace for the equilibrated electrode and that obtained when argon is substituted for the fuel. In the latter case the wave starting at about 0.8v corresponds to the formation of the adsorbed oxygen layer. When fuel is present on the electrode some ad-species may be oxidized prior to the formation of the oxygen ad-layer while others may be oxidized concurrently over the same potential range. In the latter case, the wave obtained over the potential range 0.8-1.6v is enhanced over that obtained during an argon blank. The final sharp rise in all of the traces marks the onset of oxygen evolution.

Polarization curves were obtained by measuring the currents during the longer equilibrations just prior to application of the linear anodic sweeps. These curves, of course, differ in form from the current-voltage traces obtained during linear anodic sweeps. The former reflect quasi steady-state performance while the latter are associated with complete oxidation of all of the ad-species on the surface. It is to be noted that the steady-state currents are much smaller than those flowing during the linear anodic sweeps. They therefore introduce a negligible error in the determination of the charge associated with oxidation of the ad-layer.

Results and Discussion

The general form of the current-voltage traces obtained with linear anodic sweeps for adsorbed ethane in the presence of the four electrolytes is shown in Fig. 1 after 10-min equilibrations at 0.3v. Traces obtained after shorter and longer equilibrations were of the same form. In all cases the ad-layer is oxidized over a range of potentials. With the perchloric and hydrofluoric acid electrolytes two distinct waves can be detected. The first occurs at potentials below those (approximately 0.8v) at which the surface itself is normally oxidized. The second wave exhibits a flat maximum which extends from 0.8v to oxygen evolution potentials. In the case of the perchloric acid electrolyte the first wave has been attributed to the oxidation of C_1 species and the second to C_2 species (1-4).

With the phosphoric acid electrolytes oxidation of the ad-layer is again initiated at potentials below those required for platinum surface oxidation, but the resolution of two discrete waves is less pronounced than with the other electrolytes. It has been noted, however, that at higher temperatures resolution of the two waves occurs (5).

As the equilibration potential is increased from about 0.2v the magnitudes of both waves decline, indicating that the surface coverage with the assorted species decreases (3, 5). This occurs in order that the rate of adsorption may keep pace with the increasing steady-state currents being drawn from the electrode as the potential increases (1-5). The change in coverages with equilibration potential, as reflected by changes in Q_{E1} and $Q_{E\text{tot}}$, the charges required for oxidation of the species of wave 1 and the entire ad-layer, respectively, are illustrated in Fig. 2 through 5. Because of the incomplete identification of the precise oxidation states of the species involved, it is not possible to relate these data to the actual number of surface sites obscured. The values of $Q_{E\text{tot}}$ were obtained from linear anodic sweeps by integrating the area between the ethane trace and that of the argon blank as described above. Q_{E1} was obtained by a similar integration to the left of a perpendicular at about 0.85v. In the cases of the perchloric and hydrofluoric acid electrolytes this potential corresponded to the minimum on the fuel oxidation trace.

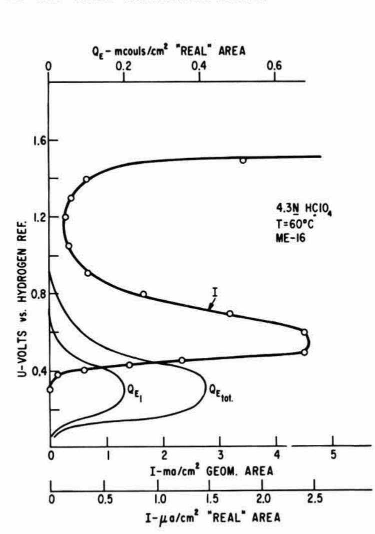

Fig. 2. Polarization and surface charge curves for ethane with a perchloric acid electrolyte.

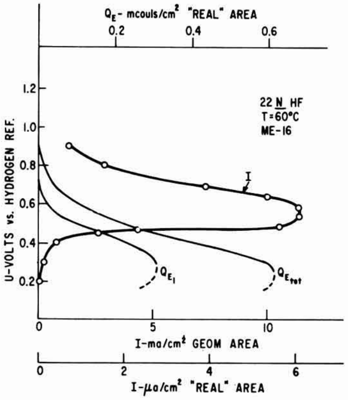

Fig. 3. Polarization and surface charge curves for ethane with a hydrofluoric acid electrolyte.

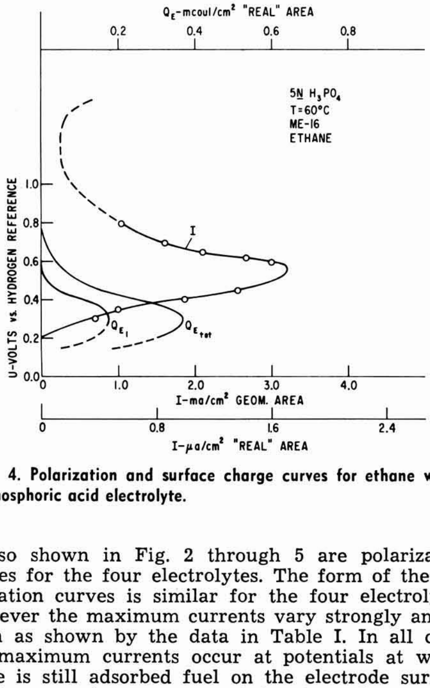

Fig. 4. Polarization and surface charge curves for ethane with a 5N phosphoric acid electrolyte.

Also shown in Fig. 2 through 5 are polarization curves for the four electrolytes. The form of the polarization curves is similar for the four electrolytes. However the maximum currents vary strongly among them as shown by the data in Table I. In all cases the maximum currents occur at potentials at which there is still adsorbed fuel on the electrode surface. Maximum surface coverage of the electrode occurs at 0.2-0.3v in all cases.

Table I. Effect of electrolyte on maximum current

Electrolyte	Maximum current density ma/cm² (geom.)	Relative
4*N* $HClO_4$	4.6	1.0
22*N* HF	11.4	2.5
5*N* H_3PO_4	3.2	0.7
36*N* H_3PO_4	1.5	0.3

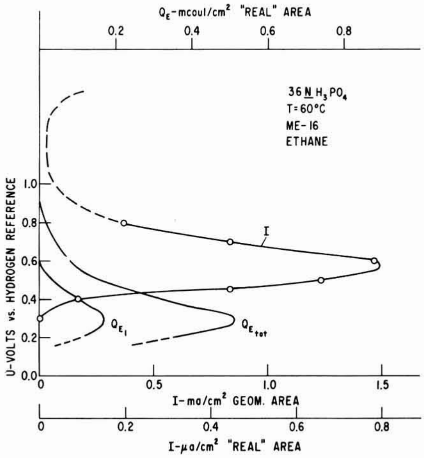

Fig. 5. Polarization and surface charge curves for ethane with a 36*N* phosphoric acid electrolyte.

Summary and Conclusions

Linear anodic sweep data obtained with ethane as a model hydrocarbon with perchloric acid, hydrofluoric acid, and phosphoric acid electrolytes indicate that in a qualitative sense the behavior is similar with all of the electrolytes. In view of the similarities of the behaviors of ethane, propane, and butane in previous studies (3,5) it is anticipated that the present observations with ethane will extend to higher hydrocarbons as well. Quantitative effects therefore appear to account for the differences in performance of hydrocarbons in fuel cells employing different acidic electrolytes. These are probably associated with changes in the double layer structure and may also reflect differences in the solubility of the hydrocarbons in the various electrolytes.

Acknowledgment

This work is a part of the program under contracts DA-44-009-AMC-479(T) and DA-44-009-ENG-4909, ARPA Order No. 247 with the U.S. Army Engineer Research and Development Laboratories, Fort Belvoir, Virginia, to develop a technology which will facilitate the design and fabrication of practical military fuel cell power plants for operation on ambient air and hydrocarbon fuels.

Manuscript received March 15, 1966; revised manuscript received Dec. 1, 1966.

Any discussion of this paper will appear in a Discussion Section to be published in the December 1967 JOURNAL.

REFERENCES

1. S. Gilman, *Trans. Faraday Soc.*, **61**, 2546, 2561 (1965).
2. S. Gilman in "Hydrocarbon Fuel Cell Technology," B. S. Baker, Editor, p. 349, Academic Press, New York (1965).
3. L. W. Niedrach, S. Gilman, and I. Weinstock, *This Journal*, **112**, 1161 (1965).
4. L. W. Niedrach, *ibid.*, **113**, 645 (1966).
5. L. W. Niedrach and M. Tochner, *ibid.*, **114**, 17 (1967).
6. E. J. Cairns in "Hydrocarbon Fuel Cell Technology," B. S. Baker, Editor, p. 465, Academic Press, New York (1965).
7. L. W. Niedrach and H. R. Alford, *This Journal*, **112**, 117 (1965).

A New Air Electrode for Fuel Cells

Harold I. Zeliger[1]

General Electric Research & Development Center, Schenectady, New York

It is believed that a porous structure will allow better mass transport of reactant gases to the active sites of fuel cell electrodes and thereby give higher performances. With the thought that the incorporation of high surface area inert material would yield a highly porous structure, electrodes containing silica were prepared and evaluated in fuel cells.

Standard Teflon bonded electrodes (1) (pressed at 350°C) were prepared incorporating silica. These electrodes were extremely hydrophobic, showed no porosity when placed in fuel cells, and would not perform on hydrogen. They apparently were impervious to hydrogen. Leaching them with sodium hydroxide or hydrofluoric acid for periods of up to 3 days improved their fuel cell performances only slightly. (Apparently the Teflon protected the silica from the leaching media.)

If, however, the electrodes were pressed cold (room temperature) the resulting structures were highly porous and readily wetable, and the electrodes showed moderate fuel cell performance. Further experimentation led to an electrode fabrication procedure which gave very high performance electrodes. It is as follows:

A mix was prepared consisting of 0.15g John Cabot Cab-O-Sil silica (surface area: 175-200 m^2/g), 0.15g graphite,[2] 0.12cc Dupont T-30 Teflon suspension (0.108g Teflon), 5 drops Rohm and Haas Triton X-100 wetting agent, the appropriate quantity of chloroplatinic acid (from Engelhardt Industries, 40% platinum), and sufficient water to give a free flowing slurry. The slurry was applied on alternate sides of a 17.7 cm^2 (1⅞ in. diameter) 45 mesh platinum screen (woven from 8 mil wire) with a single quill camel's hair brush or medicine dropper and dried above a 350°C hot plate after each application. Four or five applications were required on each side to get all the material onto the screen. After each application the material was pressed into the screen by rolling a glass rod over it with a firm hand. Drying was carried out at 350°C so that it could be accomplished quickly thereby preventing the Teflon from settling out of the mix.

A 1.6 mg/cm^2 waterproofing Teflon film was sprayed onto one side of the electrode (1). Finally, the chloroplatinic acid was reduced under a stream of hydrogen at room temperature for 2 hr.

By initially incorporating chloroplatinic acid rather than platinum black into the electrode, the catalyst was not subjected to high temperatures which could cause sintering. A second advantage of adding the platinum in solution is that more uniform distribution of catalyst in the final electrode structure is assured than if materials of varying densities were mixed together.

Electrodes with varying platinum content[3] were prepared and evaluated on hydrogen, oxygen, and air in ambient temperature, 5*N* sulfuric acid electrolyte fuel cells. A Kordesch-Marko (2) interrupter bridge was employed to monitor performance.

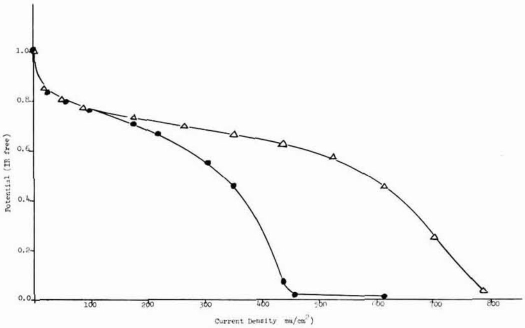

Fig. 1. IR free performance curves for standard and new silica containing electrodes on air at ambient temperature. Anodes, standard electrodes with 34 mg Pt/cm^2; cathodes, △ = new silica containing electrode with 10 mg Pt/cm^2, ● = standard electrode with 34 mg/cm^2; electrolyte: 5*N* H_2SO_4.

Excellent performances (0.8v IR free at 350 ma/cm^2) were obtained on hydrogen with platinum loadings of 1.0 mg/cm^2, and on oxygen with platinum loadings of 4.0 mg/cm^2. It was, however, as air electrodes that these new electrodes showed superiority. Figure 1 shows the IR free polarization curves for a test electrode with 10 mg platinum/cm^2 (also containing 0.15g silica, 0.15g graphite, and 0.12 cc T-30) and for a representative standard electrode (1) containing 34 mg platinum/cm^2. At low current densities (up to 100 ma/cm^2) performance of the test electrode paralleled those of standard electrodes, while at higher current densities the performance of this electrode, was significantly better. This electrode had a limiting current density of 800 ma/cm^2.

At current densities where standard electrodes show major polarization attributed to mass transport limitations, this new electrode, with less than one third the catalyst content, showed very little polarization. At 450 ma/cm^2 the IR free difference in potential between the two electrodes was 0.6v.

This improved performance is most probably attributable to a very highly porous electrode structure which allows for rapid mass transport of air to the catalytically active sites. Incorporation of a high surface area material such as silica into a fuel cell electrode makes the attainment of such a structure possible.

Manuscript received Oct. 14, 1966.

Any discussion of this paper will appear in a Discussion Section to be published in the December 1967 JOURNAL.

REFERENCES

1. L. W. Niedrach and H. R. Alford, *This Journal,* **112,** 117 (1965).
2. K. Kordesch and A. Marko, *ibid.,* **107,** 480 (1960).

---

[1] Present address: Avco Space Systems Division, Avco Corporation, Lowell, Massachusetts.

[2] The graphite served the dual purpose of imparting structural stability and conducting current in electrodes with low platinum contents.

[3] With lower platinum loadings (<6 mg/cm^2) more graphite was used, *e.g.*, electrodes with 1.0 mg Pt/cm^2 contained 0.3 g graphite.

Further Observations on the Oxidation of Zirconium in Dry Oxygen

E. Hillner

Bettis Atomic Power Laboratory, Westinghouse Electric Corporation, Pittsburgh, Pennsylvania

In a previous investigation on the high-temperature oxidation performance of pure zirconium, it was demonstrated that crystal bar (iodide process) zirconium will exhibit a transition in rate kinetics from cubic to parabolic behavior after extended exposure periods whereas high-grade sponge material undergoes a cubic-to-linear change under these same conditions (1). Both materials were found to behave in almost an identical manner in all other aspects of the oxidation reaction. Further investigations were undertaken at this laboratory in an attempt to substantiate the previously observed variance in posttransition behavior between sponge and crystal bar zirconium, and to initiate a limited parametric study involving the possible origins of this deviation.

Experimental

The primary concern associated with the initial study (1) involved the choice of specimen geometry (0.05 cm diameter wire). The present investigation employed platelet specimens of both materials, ~2.5 x 1.25 x 0.38 cm. Due to the size and weight of these coupons, the constant modulus helical spring balance employed in the first study could not be used; instead, the new specimens were placed in a molybdenum boat, in the center of a tubular zircon vacuum chamber, which in turn was externally heated with the aid of a horizontally mounted, split-tube, resistance-wound furnace. The loading and weighing of specimens was performed by two different schedules. In the first scheme, four specimens (two sponge and two crystal bar zirconium) were loaded into the boat, evacuated to below 10^{-5} Torr, heated in 400 Torr predried oxygen for a specified length of time, cooled to room temperature, weighed on a Mettler semi-automatic microbalance, and returned to the vacuum chamber for additional exposure. Thus, this method of collecting kinetic data involved the repeated heating, cooling, and weighing of the same specimens after various exposure times. Specimens handled in this manner are henceforth designated as having undergone "discontinuous weight determinations." In the second schedule, the specimens were exposed for only one time cycle, cooled, weighed and then discarded. A freshly prepared group of platelets was then employed for the next exposure time, etc. Data from this latter group are indicated by the term "continuous weight determinations." In order to expedite the comparison of the current information with that presented in (1), all test results generated in this study have been obtained at the highest test temperature of the referenced experiments, *i.e.*, 850°C. Oxygen pressure was maintained at 400 Torr for each exposure, and at least two experimental runs were carried out for each test condition. Detailed chemical analyses of the two zirconium materials are presented in (1).

Results

The kinetics of oxidation can be described by the empirical equation

$$(\Delta W)^n = kt$$

where ΔW is the weight gain per unit area of original surface, t is the time, n and k are constants for a given temperature. To determine the applicable rate equation from weight gain data, the empirical equation is more conveniently used in its logarithmic form

$$\log \Delta W = 1/n \log k + 1/n \log t$$

in which case, a plot of ΔW against t on logarithmic coordinates yields a straight line having a slope of $1/n$. The average results for each test condition are plotted in this manner in Fig. 1. The open symbols represent specimens that were chemically polished in

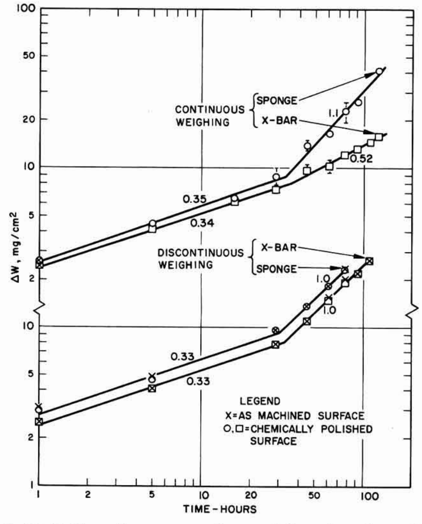

Fig. 1. Oxidation of sponge and crystal bar zirconium, 400 Torr O_2, 850°C, 0.38 cm thick specimens.

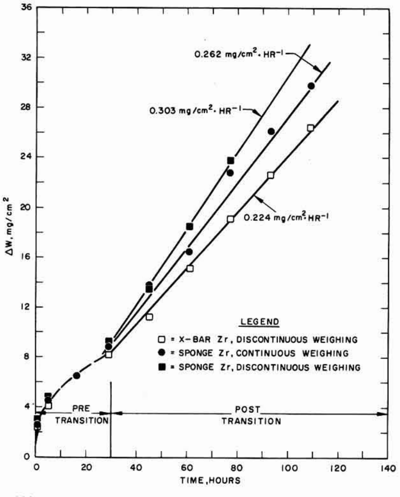

Fig. 2. Weight gain as a function of time for three of the four curves depicted in Fig. 1.

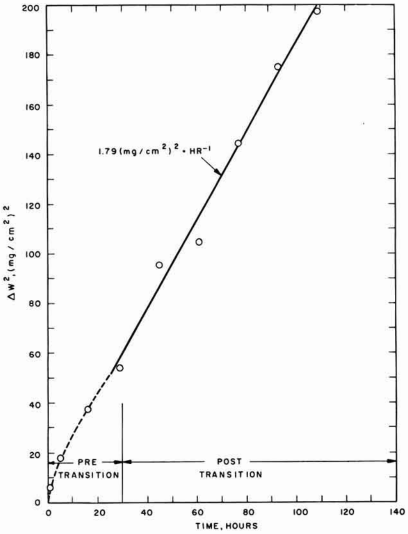

Fig. 3. Square of the weight gain as a function of time; continuously weighed X-bar specimens.

solutions of 45 v/o HNO_3 + 5 v/o HF + 50 v/o H_2O prior to exposure whereas the "X" 's indicate the data generated with specimens whose surfaces were machined to a 64 rms finish, degreased and rinsed in ethyl alcohol before each test. The numerical values indicate the calculated slopes on the log-log plot. Values for n in the pretransition kinetic region were obtained directly from Fig. 1; k_c was determined from a plot of the cube of the weight gain against time. The corresponding values for posttransition oxidation performance were obtained by replotting the data on linear coordinates (Fig. 2, 3). (One group of data, X-bar under continuous weighing conditions, required a replot of the square of the weight gain against time.) Table I compares the results generated in this limited study with those of the parent investigation.

Discussion and Conclusions

The data shown in Table I appear to indicate no significant alteration in the oxidation characteristics of the two materials as a consequence of the change in specimen geometry. At first glance it may appear that the pretransition rate constants (k_c) cluster into two groups; one group with an average value of 0.28, the other at approximately 0.47. It should be recalled, however, that the cubic rate constant is obtained from the cube of the weight change ($\Delta W^3 = k_c t$); a variation in the weight gain data of ~12% can account for the differences noted in the pretransition rate constants. Thus, the observed values are within the uncertainty band associated with data acquisition since it has been established previously (1) that the reproducibility in weight gain data in this series of experiments was no better than 10-15%. The same discussion can be applied to the apparent variations noted in the two posttransition parabolic rate constants (k_p) determined from the square of the weight gain. A weighing bias of ~14% can account for the observed differences in the latter values.

Once again, it has been demonstrated that for the method of continuous weight gain determination, the pretransition oxidation performances of high-grade sponge zirconium and crystal bar zirconium are alike in all respects. It has also been substantiated that, for continuously weighed specimens, the posttransition kinetics of sponge zirconium will follow a linear rate equation whereas crystal bar zirconium exhibits parabolic rate behavior. It has been postulated previously that this disparity in posttransition oxidation behavior may be related to the initial oxygen level of the two materials (1). Since the data generated in ref. (1) were obtained in 50 Torr oxygen pressure and those of the present study in 400 Torr oxygen, the oxidation performance of either grade of zirconium appears insensitive to oxygen pressure in the range 50-400 Torr. These results confirm the work of other investigators who found no pressure effect on zirconium oxidation (2, 3).

The major conclusion drawn from this limited study involves the sensitivity of crystal bar zirconium in the posttransition kinetic region to the method of obtaining weight change information. Thus, the information presented in Table I and Fig. 1 clearly shows that crystal bar zirconium will oxidize in accordance with a posttransition parabolic rate equation when weight gain information is obtained by either continuous measurements at test temperature (1) or by employing different specimens for each datum point. When a fixed group of identical specimens was used to obtain the entire kinetic curve by means of interrupted weight determinations on the same samples, linear posttransition behavior was observed. The crystal bar pretransition region and the entire kinetic behavior of sponge zirconium appears unaffected by the mode of weight change measurement. A possible explanation for this behavior may involve the enhanced susceptibility to oxide film breakdown due to the thermal cycling imposed on those specimens subjected to repeated heating and cooling during interrupted weight gain determinations.

Table I. Comparison of the oxidation behavior of high-grade sponge and crystal bar (iodide) zirconium at 850°C

			Sponge Zr**		X-Bar Zr**	
Parameter	Units	Type of weight gain determination	0.056 cm dia Wire (1)	0.38 cm Thick plate	0.056 cm dia Wire (1)	0.38 cm Thick plate
n (pretrans)*	—	Continuous	3.1	2.9	3.0	2.9
n (pretrans)*		Discontinuous	—	3.0	—	3.0
k_c (pretrans) cubic	$(mg/cm^2)^3 \cdot min^{-1}$	Continuous	0.55	0.29	0.41	0.26
k_c (pretrans) cubic	$(mg/cm^2)^3 \cdot min^{-1}$	Discontinuous	—	0.45	—	0.28
ΔW_{Trans}‡	mg/cm^2	Continuous	9.0	8.8	8.7	8.0
ΔW_{Trans}‡	mg/cm^2	Discontinuous	—	9.2	—	8.0
t_{Trans}‡	hours	Continuous	35	34	32	34
t_{Trans}‡	hours	Discontinuous	—	32	—	33
n' (posttrans)*	—	Continuous	1	1	2	2
n' (posttrans)*		Discontinuous	—	1	—	1
k_L (posttrans linear)*	$mg/cm^2 \cdot hr^{-1}$	Continuous	0.29	0.26	N/A	N/A
		Discontinuous	—	0.30	—	0.23
k_p (posttrans parabolic)*	$(mg/cm^2)^2 \cdot hr^{-1}$	Continuous	N/A	N/A	3.8	1.8
		Discontinuous	—	N/A	—	N/A

* For pretransition: $\Delta W^n = k_c t$.
For posttransition. $\Delta W^{n'} = k_L t$ (when $n' = 1$) or $\Delta W^{n'} = k_p t$ (when $n' = 2$).
** All chemically etched surfaces.
‡ Trans—at transition.
N/A = not applicable.

As a final observation, it can be seen from Fig. 1 and Table I that the quantity of residual fluorides or other contaminants that may be associated with the chemical polishing of zirconium surfaces does not affect the subsequent long-term oxidation behavior of the metal to any significant degree.

Acknowledgment

The author greatly appreciates the kind encouragement of and helpful discussions with Doctors B. Lustman, J. Hino, and J. N. Chirigos. This work has been performed under AEC Contract AT-11-1-GEN-14.

Manuscript received Sept. 30, 1966.

Any discussion of this paper will appear in a Discussion Section to be published in the December 1967 JOURNAL.

REFERENCES

1. E. Hillner, *Electrochem. Technol.*, **4**, 132 (1966).
2. H. A. Porte, J. G. Schnizlein, R. C. Vogel, and D. F. Fischer, *This Journal*, **107**, 506 (1960).
3. R. E. Westerman, *ibid.*, **111**, 140 (1964).

Brief Communications

The Diffusion Layer on a Rotating Disk Electrode

John Newman

Inorganic Materials Research Division, Lawrence Radiation Laboratory,
and Department of Chemical Engineering, University of California, Berkeley, California

In a recently published work (1), the author treated the current distribution on a rotating disk under conditions where ohmic potential drop, surface overpotential, and concentration variations near the electrode must all be taken into account. The diffusion layer, which is then characterized by a nonuniform current density and concentration at the surface, was handled by a power-series expansion in r, the radial distance from the axis of rotation

$$c = c_\infty \left[1 + \sum_{m=0}^{\infty} A_m (r/r_o)^{2m} \theta_m(\zeta) \right] \qquad [1]$$

where c is the concentration of the reactant, c_∞ is the bulk concentration, r_o is the radius of the electrode, and θ_m represents functions of $\zeta = y(a\nu/3D)^{1/3}\sqrt{\Omega/\nu}$, where y is the normal distance from the disk, $a = 0.51023$, ν is the kinematic viscosity, D is the diffusion coefficient, and Ω is the rotation speed of the disk.

The functions θ_m and, in particular, the derivatives $\theta_m'(0)$ at the surface were obtained by a finite-difference solution of the differential equations

$$\theta_m'' + 3\zeta^2\theta_m' - 6m\zeta\theta_m = 0 \qquad [2]$$

subject to the boundary conditions

$$\theta_m = 1 \text{ at } \zeta = 0 \text{ and } \theta_m = 0 \text{ at } \zeta = \infty$$

Subsequent numerical difficulties were encountered which required accurate values of the derivatives $\theta_m'(0)$.

As suggested by the work of Rosner (2), one can use the equations in section 58 of Levich's book (3) to obtain the concentration at the surface in terms of an integral over the concentration derivative at the surface

$$c(r,o) = c_o(r) = \frac{1}{\Gamma(2/3)} \int_o^r \frac{J(r')\,r'\,dr'}{(r^3 - r'^3)^{2/3}} \qquad [3]$$

where $J(r) = -\partial c/\partial\zeta$ at $\zeta = 0$. Substitution of a power-series expansion for c into Eq. [3] yields an expression for $\theta_m'(0)$

$$\theta_m'(0) = -\frac{3\Gamma\left(\frac{5}{3}\right)\Gamma\left(\frac{2m+3}{3}\right)}{2\Gamma\left(\frac{4}{3}\right)\Gamma\left(\frac{2m+2}{3}\right)} \qquad [4]$$

The gamma functions necessary to evaluate $\theta_m'(0)$ from Eq. [4] are given (4) to 15 significant figures. Values of $\theta_m'(0)$ are in satisfactory agreement with those tabulated in Table I of ref. (1). At the same time direct use of Eq. [3] or its inverse (2) provides a possibility of avoiding the numerical difficulties encountered in the earlier work (1).

Acknowledgment

This work was supported by the United States Atomic Energy Commission.

Manuscript received Dec. 6, 1966.

Any discussion of this paper will appear in a Discussion Section to be published in the December 1967 JOURNAL.

REFERENCES

1. John Newman, *This Journal*, **113**, 1235 (1966).
2. D. E. Rosner, *ibid.*, **113**, 624 (1966).
3. V. G. Levich, "Physicochemical Hydrodynamics," Prentice-Hall, Inc., Englewood Cliffs, N. J. (1962).
4. "Handbook of Mathematical Functions," Milton Abramowitz and I. A. Stegun, Editors, p. 3, National Bureau of Standards, Washington (1964).

Large Amplitude A-C Polarography of Aqueous Cd(II)

J. D. McLean and Andrew Timnick

Department of Chemistry, Michigan State University, East Lansing, Michigan

Theoretical treatment of a-c polarographic data has been limited to the condition that the amplitude of the applied a-c voltage, $\Delta E_{\text{p-p}}$, be no larger than $16/n$ mv peak to peak, n being the number of electrons transferred in the reduction process (1). Several formulas have been derived for large amplitudes for the special case of very small frequencies ($k_h >> \omega D$), but these are of very limited use (2). Here, k_h is the heterogeneous rate constant for electron transfer, ω is the angular frequency of the applied alternating potential, and D is the diffusion coefficient. Recently, Smith extended the theoretical treatment to $70/n$ mv p-p and derived an expression by which currents and phase angles could be calculated (3). No experimental verification was presented.

The work reported in this note was in progress when the most recent information appeared (3). Even though this work does not directly test Smith's equations it was undertaken to test the extent of applicability of existing equations developed for low amplitudes, by determining the effect of large amplitudes on experimentally determined k_h values for aqueous solutions of Cd(II).

All data were obtained at $E_{1/2}{}^R$, the reversible d-c half-wave potential, since maximum deviation in quantities measured to evaluate k_h would be expected at this d-c potential. Several supporting electrolytes were employed, to obtain a variation in the value of k_h.

The solutions used were prepared from A.C.S. reagent grade chemicals without further purification. A 0.0100M Cd(II) stock solution was prepared from $Cd(NO_3)_2 \cdot 4H_2O$ and standardized by EDTA titration (4).

Current and phase-angle measurements were obtained at maximum drop size, with an a-c polarograph constructed in this laboratory using the circuits of Smith (5) with modifications in the phase-angle detecting circuit (6). A Hewlett-Packard Model 202A signal generator provided all a-c potentials. A Sargent S-30260 potentiometer was employed to measure all d-c potentials applied to the cell. A Tektronix Model 502 oscilloscope was employed to measure the amplitude of the alternating potential applied to the cell. A Sargent Model S.R. recorder was employed to measure the d-c currents, rectified a-c currents, and signals proportional to the phase angle.

Phase angles were corrected for the uncompensated solution resistance and double-layer charging current of the supporting electrolytes according to the method of Bauer and Elving (7).

The polarographic cell was constructed so that prepurified nitrogen, which had been further purified by bubbling through an acid vanadous column, could be either bubbled through the solution by way of a coarse frit at the cell bottom or blown over the top of the solution. The cell was equipped with three electrodes: dropping mercury electrode, saturated calomel electrode, and a platinum wire auxiliary electrode. The side arm of the reference electrode was separated from the polarographic solution by an isolation compartment with a fine frit. The auxiliary electrode was also separated from the polarographic solution with a similar isolation compartment. The isolation compartments contained the supporting electrolyte.

All measurements were made in a constant temperature room which had an ambient temperature of 24 ± 1°.

Instrument performance was tested at large amplitudes through the frequency range 30-1200 Hz by determining the resistance and capacitance values for known value components of a dummy cell. Tests were run at 10, 50, and 100 mv peak to peak, and all results were within an experimental error of the order of 3%. The double-layer capacity, C_{dl}, and uncompensated solution resistance, R_t, for the supporting electrolytes 1.0M Na_2SO_4, 1.0M H_2SO_4, and 1.0M KNO_3 were determined at both 10 and 100 mv. The resistances and double-layer capacitances measured at 10 mv for the individual supporting electrolytes did not vary by more than 3% from those measured at 100 mv over the frequency range investigated. The values measured at 10 and 100 mv are listed in Table I, as well as the half-wave potentials at which they were measured. The $E_{1/2}{}^R$ for Cd(II) in each supporting electrolyte was determined from the log = 0 intercept of a log $(i_d - i)/i$ vs. $E_{d\text{-}c}$ plot. The diffusion coefficients listed in Table I were determined in this laboratory during a previous study (6) and were calculated by the Lingane-Loveridge equation (9).

Table I. Experimental constants for evaluation of k_h in various supporting electrolytes

Supporting electrolyte	$E_{1/2}{}^R$ vs. SCE, v	$C_{d.l.}$, μf		R_t, ohms		$D \times 10^6$, cm²/sec*
		10 mv	100 mv	10 mv	100 mv	
1.0M Na_2SO_4	−0.606	0.833	0.834	77.2	78.7	5.51
1.0M H_2SO_4	−0.597	0.952	0.956	58.9	60.4	7.03
1.0M KNO_3	−0.585	1.14	1.14	76.4	78.0	10.20

* $D = D_O{}^\beta D_R{}^\alpha$ where α and β are transfer coefficients.

Table II. Variation of heterogeneous rate constant with changing amplitude of applied a-c potential for 5.0×10^{-4}M Cd (II) in various supporting electrolytes evaluated at $E_{1/2}{}^R$

$E_{p\text{-}p}$, mv	1.0M Na_2SO_4 slope $\times 10^2$	1.0M Na_2SO_4 k_h, cm/sec	1.0M H_2SO_4 slope $\times 10^2$	1.0M H_2SO_4 k_h, cm/sec	1.0M KNO_3 slope $\times 10^3$	1.0M KNO_3 k_h, cm/sec
10	2.62	0.06	1.32	0.14	3.35	0.67
20	2.32	0.07	1.36	0.14	2.27	1.00
30	2.40	0.07	1.47	0.13	2.51	0.90
40	2.30	0.07	1.41	0.13	2.48	0.91
50	2.32	0.07	1.39	0.13	2.50	0.90
60	2.24	0.07	1.28	0.15	2.20	1.03
70	2.24	0.07	1.20	0.16	1.82	1.24
80	2.15	0.08	1.23	0.15	1.46	1.55
90	2.10	0.08	1.19	0.16	1.50	1.51
100	2.11	0.08	1.06	0.18	1.13	2.00

The dependence of the heterogeneous rate constant on the applied a-c potential is tabulated in Table II, for various supporting electrolytes. The heterogeneous rate constants were obtained by use of the expression

$$\cot \Phi = 1 + \frac{1}{k_h} (D\omega/2)^{1/2} \qquad [1]$$

where Φ is the corrected phase angle (8). This is the correct expression for the special case when $E_{d\text{-}c} = E_{1/2}{}^R$ and under the restriction that the amplitude of the applied alternating voltage be less than $16/n$ mv p-p. By plotting cot Φ vs. $\omega^{1/2}$ (see Fig. 1 and 2), one can readily calculate k_h from the slope of the linear

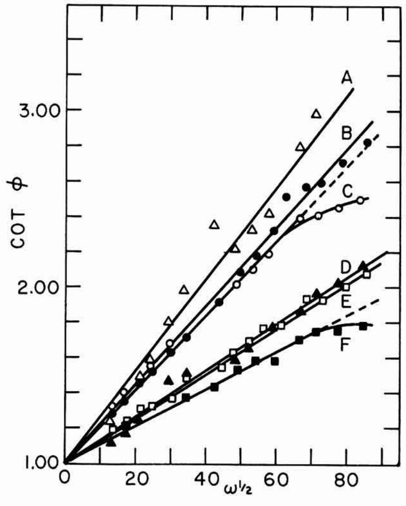

Fig 1. Effects of increasing amplitude of the applied a-c potential on cot Φ vs. $\omega^{1/2}$ evaluated at $E_{1/2}{}^R$ for 5.0×10^{-4}M Cd(II) in sulfate media. Curves A, B, and C are for 1.0M Na_2SO_4: A, $\Delta E_{p\text{-}p} = 10$ mv; B, $\Delta E_{p\text{-}p} = 60$ mv; C, $\Delta E_{p\text{-}p} = 100$ mv. Curves D, E, and F are for 1.0M H_2SO_4: D, $\Delta E_{p\text{-}p} = 10$ mv; E, $\Delta E_{p\text{-}p} = 60$ mv; F, $\Delta E_{p\text{-}p} = 100$ mv.

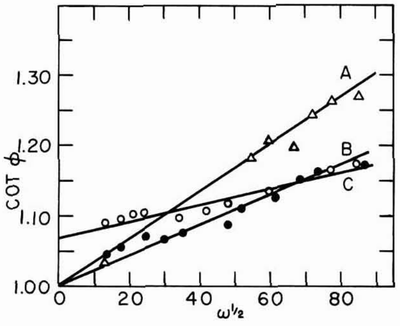

Fig. 2. Effects of increasing amplitude of the applied a-c potential on plots of cot Φ vs. $\omega^{1/2}$ evaluated at $E_{1/2}{}^R$ for 5.0 x 10^{-4}M Cd(II) in 1.0M KNO_3. A, $\Delta E_{p\text{-}p} = 10$ mv; B, $\Delta E_{p\text{-}p} = 60$ mv; C, $\Delta E_{p\text{-}p} = 100$ mv.

portion of the plot, if a value for $D^{1/2}$ is known. The values used for the plots were obtained by making phase-angle measurements on 5.0 x 10^{-4} M Cd(II) in various supporting electrolytes at fourteen different frequencies between 30 to 1200 Hz and at the d-c potential equal to $E_{1/2}{}^R$.

From Table II it can be seen that, if k_h is between 0.05 and 0.20 cm/sec, its value, as determined by the low amplitude equation, does not vary markedly to the limit of amplitudes tested up to a frequency of 800 Hz. Although the k_h values show good agreement, some deviations in the data become apparent above 60 mv as is shown in Fig. 1. These deviations occur as a distinct falling off from linearity of the cot Φ vs. $\omega^{1/2}$ plots at frequencies above 800 Hz, with the magnitude of the error increasing directly with the frequency. In all of these plots, the intercept is cot $\Phi = 1$ at 0 frequency, as is predicted by Eq. [1].

In a recent monograph (3), Smith presents theoretical a-c polarograms and a-c polarographic phase angles for a specific hypothetical system for $\Delta E_{p\text{-}p}$ of 10, 40, 60, and 80 mv. He demonstrates that cot Φ should decrease with increasing values of $\Delta E_{p\text{-}p}$ at the d-c potential equal to $E_{1/2}{}^R$. Although the magnitudes of these changes cannot be compared directly with our experimental values due to differences in constant parameters involved, one can see that the changes follow the same pattern. Smith's theoretical figures as well as our experimental data indicate that the changes are relatively small if the heterogeneous rate constant is in the range 0.01 to 0.20 cm/sec as is the case for Cd(II) in sulfate media.

Heterogeneous rate constants for Cd(II) in 1.0M KNO_3 calculated from slopes obtained from Fig. 2 show much greater variation than the values obtained in sulfate media. This is primarily due to the fact that the heterogeneous rate constant in this medium is considerably faster, and thus changes in the slope produce a much greater change in the value of k_h. Rate constants of the order of 1.0 cm/sec or faster are difficult to determine accurately by the a-c method we employ. Figure 2 data were included to demonstrate what might be expected if large amplitudes are employed on these systems. Although the values of k_h show deviation as $\Delta E_{p\text{-}p}$ increases, no deviation from theoretical behavior, that is linearity of the plot of cot Φ vs. $\omega^{1/2}$ and intercept of cot $\Phi = 1$ as $\omega \rightarrow 0$, is observed until $\Delta E_{p\text{-}p}$ exceeds 60 mv. At this point, the cot Φ intercept at $\omega \rightarrow 0$ becomes greater than 1.00 in violation of theory. Again, the error becomes increasingly large as $\Delta E_{p\text{-}p}$ increases.

The results obtained for the aqueous Cd(II) system indicate that if the heterogeneous rate constant for the electron transfer is between 0.05 and 0.20 cm/sec, low amplitude equations can be used to calculate k_h values for $\Delta E_{p\text{-}p}$ up to 70 mv, which is considerably beyond the previously predicted limit of $\Delta E_{p\text{-}p} = 16/n$ mv, which would be 8 mv for Cd(II).

Acknowledgment

The authors are grateful to the Socony Mobil Oil Company and The Electrochemical Society for the support of this work.

Manuscript received Nov. 21, 1966.

Any discussion of this paper will appear in a Discussion Section to be published in the December 1967 JOURNAL.

REFERENCES

1. H. Matsuda, Z. *Elektrochem.*, **62**, 977 (1958).
2. B. Breyer and H. H. Bauer, "Alternating Current Polarography and Tensammetry," Chap. 2, Interscience Publishers, New York (1963).
3. D. E. Smith, "Electroanalytical Chemistry," Vol. I, Chap. I, A. J. Bard, Editor, Marcel Dekker, Inc., New York (1966).
4. G. Schwarzenbach, "Complexometric Titration," Interscience Publishers, New York (1957).
5. D. E. Smith, *Anal. Chem.*, **35**, 602 (1963).
6. J. K. Frischmann, Ph.D. thesis, Michigan State University, East Lansing, Mich. (1966).
7. H. H. Bauer and P. J. Elving, *J. Am. Chem. Soc.*, **82**, 2091 (1960).
8. R. Tamamushi and N. Tanaka, *Z. Physik. Chem.*, **21**, 89 (1959).
9. J. J. Lingane and B. A. Loveridge, *J. Am. Chem. Soc.*, **72**, 439 (1950).

Recrystallization of Supported Platinum

J. F. Connolly, R. J. Flannery, and B. L. Meyers

Research and Development, American Oil Company, Whiting, Indiana

Measurements of surface areas electrochemically (1) and by x-ray diffraction show that supported platinum crystallites grow rapidly when in contact with a conducting solution. This effect indicates that the type of dispersion necessary to make platinum an economic direct-hydrocarbon-fuel-cell catalyst may be difficult to maintain.

The crystallite growth was first observed during attempts to extend the conditions for electrochemical platinum-area measurements (1) to higher temperatures. Results are summarized in Table I. Platinum area losses range from 5 to 90% of the initial area depending on such factors as initial crystallite size, temperature, and type of support.

Area losses are not due to poisoning because they are detected in roughly the same measure by both x-rays and the electrochemical method. Furthermore, they cannot be attributed to permanent platinum dissolution because: platinum determinations made before and after treatment usually agreed within the reproducibility of the method (2%); analyses of the soaking liquids after the highest temperature runs showed a pickup of only 0.1% of the platinum originally in the samples; integrated x-ray diffraction intensities increased in all cases where they were measured.

There are no detectable area losses due to heating in air or argon at these temperatures, or even 100°C

Table I. Summary of results

Support[j]	Support area, m^2/g	Wt, % Pt	Initial x-ray cryst. size,[k] Å	Initial electrochem. Pt area, m^2/g Pt	% Pt area lost x-ray[l]	% Pt area lost electrochemical[m]
ACG	11	4.1	30	45	80[a]	60[a]
ACG	11	8.6	40	45	65[a]	70[a]
ACG	11	8.6	40	45	5[e]	10[e]
ACG	11	8.6	40	45	70[f]	90[f]
ACG	11	8.6	40	45	15[g]	10[g]
ACG	11	16.6	30	25	75[a]	60[a]
ACG	11	16.6	30	25	85[b]	80[b]
ACG	11	16.6	30	25	80[c]	75[c]
ACG	11	16.6	30	25	90[d]	90[d]
ACG	11	5.2	45	—	50[i]	—
ACG	11	8.9	100	35	10[a]	30[a]
ACG	11	8.9	100	35	20[h]	30[h]
ACG	11	8.9	100	35	20[b]	40[b]
SB	60	9.7	30	40	75[a]	55[a]
PC62	200	8.7	60	70	10[a]	5[a]
PC62	200	8.7	60	70	20[b]	15[b]
B_4C	11	11.1	30	25	55[a]	45[a]
SiC	<1	1.2	125	—	10[c]	—
SiC	<1	1.2	125	—	15[d]	—
Al_2O_3	2	2.1	145	—	40[c]	—
Al_2O_3	2	2.1	145	—	55[d]	—
Al_2O_3	15	9.0	140	—	30[c]	—
Al_2O_3	15	9.0	140	—	40[d]	—
Al_2O_3	85	1.2	40	—	40[c]	—
Al_2O_3	85	8.9	80	—	55[c]	—
Al_2O_3	85	8.9	80	—	55[d]	—

[a] Open circuit in 95% H_3PO_4 at 150°C for 60 hr.
[b] Open circuit in 95% H_3PO_4 at 190°C for 60 hr.
[c] Open circuit in 50% $CaCl_2$ at 150°C for 60 hr.
[d] Open circuit in 50% $CaCl_2$ at 190°C for 60 hr.
[e] Open circuit in 90% H_3PO_4 as 105°C for 60 hr.
[f] Open circuit in 65% $CaCl_2$ at 150°C for 60 hr.
[g] Open circuit in H_2O (150 μmho/cm) at 165°C for 60 hr.
[h] Open circuit in 95% H_3PO_4 at 150°C for 480 hr.
[i] 0.10-1.0v in 85% H_3PO_4 at 145°C for 6 hr. This sample was bonded with 40% Teflon. All other samples are in powdered form.
[j] ACG → Am. Cyanamid graphite (3), SB → Schawinigen Black, PC → Stackpole Carbon Co., B_4C → Boron carbide from Norton Co., NC → National Carbon Co.
[k] Dimension perpendicular to 111 plane, calculated from the Scherrer equation, employing the Warren method for instrumental broadening (2). The dimension perpendicular to the 200 plane, as measured for a few samples, was about 20% less. The 311 plane was used for the 1.2% Pt on Al_2O_3 sample.
[l] 100 [1-(initial crystallite size)/(final crystallite size)].
[m] 100 [1-(final electrochemical area)/(initial electrochemical area)].

higher. Thus, the rate of area loss is orders of magnitude higher than that of the losses experienced in "sintering." A possible mechanism would be "electrorecrystallization," *i.e.*, local cells may be formed between large and small platinum crystallites, with the smaller crystallites acting as anodes because of their higher surface energies. Complex platinum ions would then be transported through the solution while electrons pass through platinum-platinum contacts, or through a conducting support, or through both. The transport of platinum complexes through the solution with no necessity for electron flow between crystallites would also be conceivable.

Experimental

The technique for making electrochemical measurements of the surface area of carbon-supported platinum (1) has been simplified by using powdered rather than Teflon-bonded samples, and by substituting a charge measurement in the "double layer" region for the oxide arrest as a measure of the support effect.

Teflon bonding of powders, in addition to being tedious, requires that they be subsequently anodized extensively (1) to reactivate the platinum surface. We have found that tightly confining a powdered sample between porous tantalum plates (Kennametal) in a tantalum holder gives reproducible results for samples with supports like NC60[1] and ACG.[1] Hard supports like PC62[1] and B_4C may be used in the same way, so long as a three- or fourfold dilution with a low-surface-area graphite like NC60 is used to promote electrical contact. The NC60 has practically no effect on the measurement. Because the holder exposes only 0.8 cm^2 of the porous tantalum plates (Fig. 1) the currents must be held below 20 ma to avoid excessive IR drops. IR drops are further minimized by drawing 0.1-0.2 cc of electrolyte through the holder after assembly to thoroughly wet the sample and porous tantalum plates.

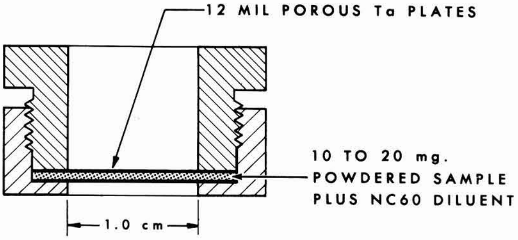

Fig. 1. Tantalum holder for powdered samples

The change from Teflon-bonded to powdered electrodes resulted in the higher area carbons giving somewhat more O_2 evolution activity at 1.3-1.4v (*vs.* a reversible hydrogen electrode in the same solution) than is desirable. Therefore, as a measure of the support contribution, the charge consumption from 0.55 to 0.35v was substituted for the charge consumption in the oxygen arrest.[2] We then obtain equations for platinum surface area analogous to Eq. [5] and [6] of ref. (1), *i.e.*,

$$r' = Q_{C,D}/Q_{C,H} \qquad [1]$$

$$A_{Pt} = (r'Q_{T,H} - Q_{T,D})/(r'k_H - k_D) \qquad [2]$$

where A_{Pt} is the platinum area in contact with solution, $Q_{C,D}$ and $Q_{C,H}$ are charges consumed on the carbon support from 0.55 to 0.35v and 0.05 to 0.30v, $Q_{T,D}$ and $Q_{T,H}$ are the total charges consumed on the electrode from 0.55 to 0.35v and 0.05 to 0.30v, and k_D and k_H are constants which give the charge consumption on platinum per square centimeter of platinum from 0.55 to 0.35v and 0.05 to 0.30v. The quantities $Q_{C,D}$ and $Q_{C,H}$ are measured at the same *dv/dt* (usually 10 to 20 mv/sec) on the nonplatinized carbon support while $Q_{T,D}$ and $Q_{T,H}$ are similarly measured on the platinized electrode; k_D and k_H are measured on bright platinum of known roughness.

For the supports listed in Table I, $r' = 1.00 \pm 0.05$. Using this value for r' and $k_H = 0.19$ mc/cm² and $k_D = 0.005$ mc/cm² reduces Eq. [2] to

$$A_{Pt} \cong 5.4(Q_{T,H} - Q_{T,D}) \qquad [3]$$

Equation [3] was used to calculate the electrochemical areas in Table I. The potential-time sequence for each measurement is shown in Fig. 2.

There is a misprint in ref. (1). The equations for calculating the fractions of the total charge consumptions which are due to the carbon support should be

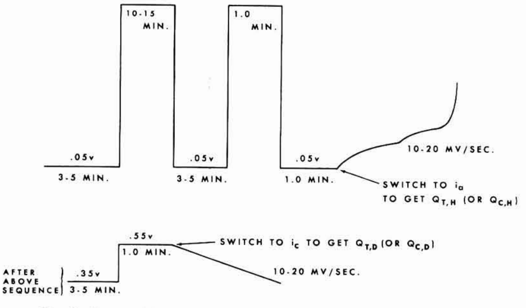

Fig. 2. Potential sequence for Pt surface area measurement

---

[1] See Table I footnote j.

[2] Of course, in those cases where oxide stripping is suitable and the hydrogen arrest is unuseable (*e.g.*, palladium area measurements on moderate area carbons), then a charge measurement in the double layer region can correct for the support contribution in the oxide reduction arrest.

$$\frac{Q_{\mathrm{C,O}}}{Q_{\mathrm{T,O}}} = r\left(1 - \frac{k_0}{k_{\mathrm{H}}}\frac{Q_{\mathrm{T,H}}}{Q_{\mathrm{T,O}}}\right) \Big/ \left(r - \frac{k_0}{k_{\mathrm{H}}}\right) \qquad [4]$$

$$\frac{Q_{\mathrm{C,H}}}{Q_{\mathrm{T,H}}} = \left(\frac{Q_{\mathrm{T,O}}}{Q_{\mathrm{T,H}}} - \frac{k_0}{k_{\mathrm{H}}}\right) \Big/ \left(r - \frac{k_0}{k_{\mathrm{H}}}\right) \qquad [5]$$

For the simplified procedure used in this note Eq. [4] has little meaning, while Eq. [5] reduces to

$$\frac{Q_{\mathrm{C,H}}}{Q_{\mathrm{T,H}}} \cong \frac{Q_{\mathrm{T,D}}}{Q_{\mathrm{T,H}}}$$

Reference (1) also contains the doubtful claim: "there should be no lower limit on the size of the platinum crystallites which can be detected." However, very small crystallites probably grow at rates large enough to interfere with electrochemical surface-area measurements made at room temperature.

Acknowledgment

The authors thank L. Granatelli for making the platinum analyses and R. F. Waters for platinizing the electrodes.

Manuscript received Oct. 20, 1966; revised manuscript received Dec. 9, 1966.

Any discussion of this paper will appear in a Discussion Section to be published in the December 1967 JOURNAL.

REFERENCES

1. J. F. Connolly, R. J. Flannery, and G. Aronowitz, *This Journal*, **113**, 577 (1966).
2. H. P. Klug and L. E. Alexander, "X-Ray Diffraction Procedures," p. 506, John Wiley & Sons, Inc., New York (1954).
3. R. G. Haldeman, W. P. Colman, S. H. Langer, and W. A. Barber, "Fuel Cell Systems," p. 106, American Chemical Society, Washington, D. C. (1965).

Extended Abstract Book Publication Program for the Society's 1967 Fall Meeting in Chicago, Ill.

The Board of Directors has provided that the National Office shall assist Divisions with the mechanics of publishing Extended Abstracts for sessions involving 15 or more papers at our National Meetings. The Divisions will handle the technical editing of the abstracts following which the Society Office will arrange for the printing and distribution of the books, thus relieving Division representatives of this responsibility. Each Division program will be the subject of a separate Extended Abstract Book. This means that each author who submits a paper for presentation at our meeting should do three things:

1—Submit *three* copies of the usual 75-word abstract of the paper for publication in the printed program of the meeting;

2—Simultaneously submit *three* copies of an extended abstract of the paper of 500-1000 words (see instructions below); and

3—Send the 75-word abstract and the 500-1000-word extended abstract to The Electrochemical Society, 30 East 42 St., New York, N. Y., 10017, *not later than May 15, 1967.*

Notification of acceptance for meeting presentation, along with scheduled time, will be mailed to authors with general instructions no earlier than two months before the meeting. Those authors who require more prompt notification are requested to submit with their abstract a self-addressed post card with full author-title listing on the reverse.

The Extended Abstract Books will be published by photo-offset reproduction *from typewritten copy submitted by the author.* Special care should therefore be given to the following typing instructions so as to establish uniformity in printing:

1—Abstracts are to be 500-1000 words in length (two pages single spaced), and are to contain (to whatever extent practical) all significant experimental data to be presented during oral delivery.

2—Please send an *original* and *two copies* of the abstract typed SINGLE SPACE. Use white bond paper, size 8½ x 11 inches, with 1¼ inch margins on all sides.

3—Title of paper should be in capital letters. Author(s) name and affiliation should be typed immediately below. It is not necessary in the heading or body to designate paper as "Extended Abstract," or to quote the Divisional Symposium involved.

4—All copy, including figures, symbols, and corrections, must be in black ink. No handwritten corrections, please. Submit graphs on onion skin without grids, or on graph paper specifically designed for offset reproduction; strip-on tape is acceptable.

5—Figures should be pasted in within the typing dimensions indicated. Submit only the important illustrations. Avoid use of half tones except where absolutely necessary. Captions should be typed not wider than figure dimensions and pasted in proper place in the abstract. Figure caption should appear at bottom of figure. Table title should appear at top of table.

6—Mail to The Electrochemical Society *unfolded.*

7—Please note that the extraordinarily low price, per volume, of Extended Abstracts is made possible only through your strict adherence to these instructions. Any deviation threatens this low cost.

Members and JOURNAL subscribers will receive notice of Extended Abstracts Books to be scheduled for publication. The notices will be accompanied by order blanks for the copies desired. Orders should be submitted with remittance. The advance orders will be necessary for estimating numbers of books to be printed and will be mailed to purchasers prior to the Chicago meeting. Some extra copies will be available at the meeting but the advance-paid order is the only way to be assured of getting copies.

SOLID STATE SCIENCE

Manganese-Activated Luminescence in the $MgO-Al_2O_3-Ga_2O_3$ System

Jesse J. Brown

Chemical and Metallurgical Division, Sylvania Electric Products Inc., Towanda, Pennsylvania

ABSTRACT

Manganese-activated phosphors were prepared by solid state reactions throughout the spinel crystalline solution region in the $MgO-Al_2O_3-Ga_2O_3$ system. The best ultraviolet-excited phosphor examined, $(Mg_{0.90},Mn_{0.01})Ga_{2.06}O_4$, is characterized by a peak emission wavelength at 512 nm, a 50% peak intensity band width of 36 nm, and a quantum efficiency equivalent to that of Zn_2SiO_4:Mn. Al^{3+} for Ga^{3+} substitutions in $MgGa_2O_4$ lead to phosphors with improved cathodoluminescence, decreased photoluminescence, longer peak emission wavelength, and longer cathodoluminescence decay characteristics. These data are discussed in view of temperature, crystal structure, and related literature.

The mineral spinel, $MgAl_2O_4$, is only one of a large class of isostructural AB_2O_4 compounds that have become known as spinels. Ideally the spinel structure consists of a face-centered cubic close-packed array of oxygen anions with metal cations filling the interstices. The unit cell contains 32 oxygen ions or eight AB_2O_4 molecules. This gives rise to 96 interstices per unit cell of which 32 are octahedral (B) sites and 64 tetrahedral (A) sites. Normally only 16 of the B and 8 of the A sites are filled with cations. There are three general classifications of spinels, the normal spinel in which the A ions are in tetrahedral sites and the B in octahedral, the random or intermediate spinel in which the A and B ions are randomly distributed in the 8 tetrahedral and 16 octahedral sites, and the inverse spinel in which the 8 tetrahedral sites are occupied by B ions and the 16 octahedral sites occupied randomly by A and B ions. It is well established that the equilibrium cation distribution in spinels is dependent on temperature and pressure as well as composition.

Originally it was the purpose of this investigation to attempt to incorporate Mn^{2+} selectively in octahedral and tetrahedral sites in basically the same spinel compound. A logical choice for this study was the crystalline solution series between the compounds $MgGa_2O_4$ and $MgAl_2O_4$ in the $MgO-Al_2O_3-Ga_2O_3$ ternary system since Mn^{2+} has an octahedral site preference larger than Ga^{3+} but smaller than either Mg^{2+} or Al^{3+}. However, when the intense uv-excited green luminescence of $MgGa_2O_4$:Mn was observed, major emphasis was shifted to the empirical optimization of formulation variables and characterization of spectral properties of phosphors throughout the ternary system.

Literature

Moller and King (1) prepared various gallate compounds, including $MgGa_2O_4$ spinel, and presented characteristic x-ray diffraction data. More recently Schmalzried (2) established the phase relationships in the $MgO-Ga_2O_3$ system. Twenty mole % Ga_2O_3 and 2 mole % MgO were found to be soluble in $MgGa_2O_4$ at 1200°C. At 1000°C, the solubility of Ga_2O_3 decreased to 10% and of MgO to about 1%. The population of Mg^{2+} in octahedral sites in $MgGa_2O_4$ was found to vary from 0.90 at 900°C to 0.84 at 1400°C, indicating the influence of temperature on cation distribution in this spinel compound. More recently Weidenborner *et al.* (3) determined the detailed structure of magnesium gallate from single crystals grown from a molten lead-oxygen-fluoride melt. Their results confirmed the partially inverted nature of $MgGa_2O_4$, that it belongs to the space group Fd3m with $a_o = 8.286 \pm 0.003Å$, and that 16 ± 2% of the Mg^{2+} are in tetrahedral sites and 81 ± 1% in octahedral. Since the single crystals used in this study were annealed slowly from 1200° to 850°C, the data must be assumed to correspond to a temperature of 850°C or slightly higher.

The $MgO-Al_2O_3$ phase relations have been studied by several people (4-7). This system resembles the $MgO-Ga_2O_3$ system in that considerable Al_2O_3 is soluble in $MgAl_2O_4$ spinel, but only trace amounts of MgO. Datta and Roy (8,18) have reported that the cation distribution in $MgAl_2O_4$ is a function of temperature and pressure and becomes more normal at high temperatures. Saalfeld (9) has found that the vacancies associated with the $MgAl_2O_4$ crystalline solution series in the $MgO-Al_2O_3$ system prefer to locate on octahedral cation sites. Hummel and Sarver (10) prepared cathodoluminescent phosphors by activating $MgAl_2O_4$ by Mn^{2+} and isoelectronic Fe^{3+}.

Hill *et al.* (11) established the phase relationships in the $Ga_2O_3-Al_2O_3$ system which showed extensive crystalline solution at high temperatures and the formation of an intermediate solid solution series below 800°C. Katz and Roy (12) studied the phase relationships in the $MgAl_2O_4-Ga_2O_3$ binary join and found extensive crystalline solution of Ga_2O_3 in $MgAl_2O_4$. These data were used to estimate the extent of crystalline solution within the ternary system.

Based on the above references, the probable phase relationships in the $MgO-Al_2O_3-Ga_2O_3$ system were constructed as shown in Fig. 1.

Green-emitting $ZnGa_2O_4$:Mn is the only gallate compound reported by Leverenz (13) in his extensive treatment of luminescent materials.

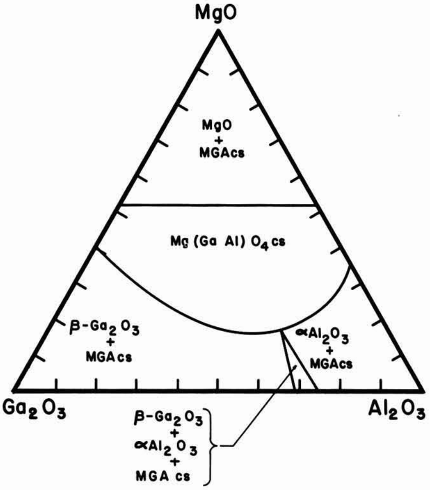

Fig. 1. (a, b, c, d). 1400°C isothermal section of the MgO-Ga_2O_3-Al_2O_3 ternary system and probable T-X diagrams of associated binary systems (2, 4, 5, 6, 7, 11, 12).

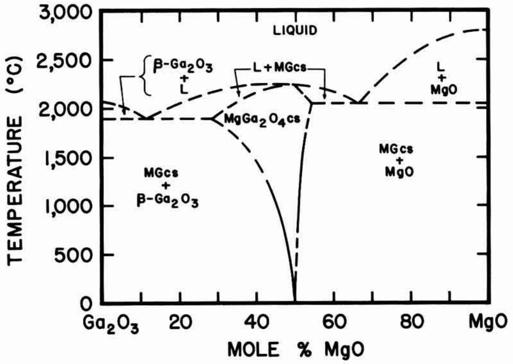

b

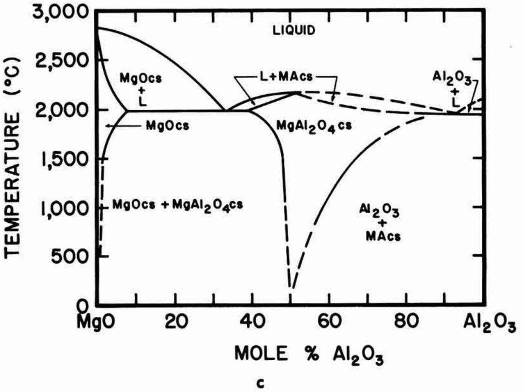

c

Experimental Procedure

Sample preparation.—The raw materials used in this investigation consisted of luminescent grade basic magnesium carbonate, $MgCO_3 \cdot Mg(OH)_2$, and manganese carbonate, $MnCO_3$, aluminum hydroxide, $Al_2O_3 \cdot nH_2O$, and 99.999% pure gallium oxide, Ga_2O_3. Weight loss measurements were conducted on the magnesium and aluminum compounds in order to compensate batch calculations for sorbed water. Appropriate proportions of the raw materials were weighed to an accuracy of ±0.1 mg on an analytical balance. Each preparation was hand mixed under acetone in a glass mortar and pestle for 10 to 20 min and allowed to air dry. Samples to be used for subsolidus equilibria studies were heat treated twice in air at the desired temperature for 17 hr each, with an intermediate light mixing. This procedure was necessary to insure complete reaction and homogeneity. Preparations used for luminescence studies were heat-treated only once in air at the desired temperature for 8 to 17 hr, then reheated at a slightly lower temperature for 1 hr in a very mildly reducing atmosphere. In all cases, fused silica or sintered alumina crucibles were used. Noble metal containers were unsatisfactory because the gallium tended to amalgamate with the crucible metal.

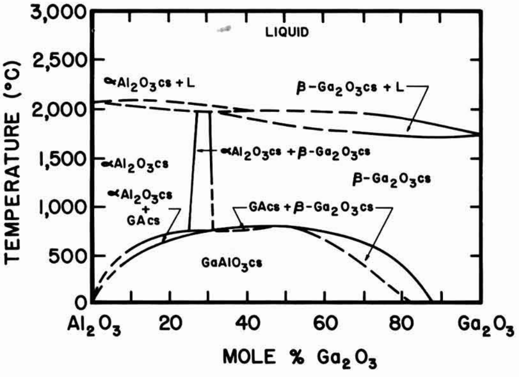

d

Compositions were periodically analyzed quantitatively by atomic absorption and wet chemical methods in order to confirm the formulated compositions. A typical result is shown in Table I.

A Norelco x-ray diffractometer employing nickel-filtered CuKα radiation, operating at 40 kv and 15 ma was used with a scanning rate of 1°-2θ/min for routine phase identification and 1/8°-2θ/min for more precise lattice parameter measurements.

Luminescence.—All fluorescence excitation and emission spectra and peak height measurements were obtained with a Perkin-Elmer spectrofluorimeter as previously described (14).

Cathodoluminescence spectra were obtained using a demountable cathode-ray tube operating at 12 kv anode potential and 6 μa beam current over a standard scan TV raster of 1 in.^{2} area. Brightness under these conditions were measured with an eye-corrected Weston foot-Lambert meter.

Experimental Results

The MgO-Ga_2O_3 *system.*—Table II lists the compositions, x-ray diffraction, and luminescence data for preparations throughout the MgO-Ga_2O_3 system. In all cases the samples were heat-treated in two steps. The first heat-treatment at 1400°C/17 hr in air formed the host lattice with manganese incorporation. Qualitative data indicated that the highest practical

Table I. Comparison of formulated and analyzed ingredients in a typical preparation

Element	Weight per cent		
	Formulated	Atomic absorption	Chemical analysis
Mg	9.5	10.0	10.18
Ga	62.5	62.0	63.42
Mn	0.25	0.25	No data

Table II. Phase equilibria and luminescence data of phosphors prepared throughout the MgO-Ga_2O_3 system

Composition, mole % MgO	Ga_2O_3	MnO	Phase assemblages	a_o of $MgGa_2O_4$ spinel phase, A	Relative fluorescence peak height	Cathodoluminescence Brightness, ft-L	Color coordinates x	y
—	99	1	β-Ga_2O_3	—	—			
9	90	1	β-Ga_2O_3 + $MgGa_2O_{4cs}$	8.27	3			
19	80	1	β-Ga_2O_3 + $MgGa_2O_{4cs}$	8.274	18			
29	70	1	β-Ga_2O_3 + $MgGa_2O_{4cs}$	8.272	39			
39	60	1	β-Ga_2O_3 + $MgGa_2O_{4cs}$	8.271	75			
44	55	1	β-Ga_2O_{3tr} + $MgGa_2O_{4cs}$	8.272	89	8.0	0.103	0.664
45	54	1	$MgGa_2O_{4cs}$	8.275	95	8.0	0.101	0.671
46	53	1	$MgGa_2O_{4cs}$	8.277	100	7.0	0.111	0.671
47	52	1	$MgGa_2O_{4cs}$	8.279	92	7.0	0.112	0.678
49	50	1	$MgGa_2O_{4cs}$	8.282	70	5.5	0.112	0.678
59	40	1	$MgGa_2O_{4cs}$ + MgO	8.288	13			
69	30	1	$MgGa_2O_{4cs}$ + MgO	8.289	11			
79	20	1	$MgGa_2O_{4cs}$ + MgO	8.290	9			
89	10	1	$MgGa_2O_{4cs}$ + MgO	8.292	5			
99	—	1	MgO	—	—			

reaction temperature eventually provided the brightest phosphors. Typical preparations at this point had a pink body color and very weak green and red emission bands when excited by 253.7 nm radiation.

The second heat-treatment, carried out at 1200°C/1 hr in a 2% H_2 — 98% N_2 by volume gas mixture, provided preparations with a white body color and bright blue-green luminescence. For maximum phosphor brightness, it was found necessary to cool the samples to below 500°C in the protective atmosphere. Brightness was found to be dependent on the time, temperature, and atmosphere of the second heat-treatment, with the conditions specified above being optimum for 25g samples.

It is evident from Table II that magnesium gallate crystalline solution is the phase responsible for the luminescence in the MgO-Ga_2O_3 system. Manganese-activated MgO and β-Ga_2O_3 are nonluminescent under these conditions of preparation. It is also evident from Fig. 2 and Table II that these phosphors are efficiently excited only by 253.7 nm radiation. Cathodoluminescence measurements indicated typical light outputs of about 7.0 ft-L and color coordinates of $x \cong 0.110$ and $y \cong 0.670$.

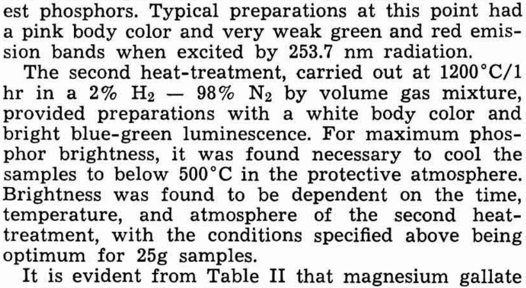

Fig. 2. Excitation and emission spectra of $MgGa_2O_4$:Mn

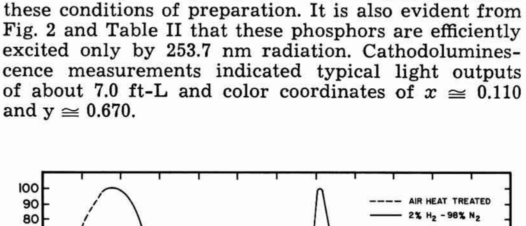

Fig. 3. Variation of fluorescence brightness and spinel lattice parameter a_o with composition in the MgO-Ga_2O_3 system.

Table III. Comparison of fluorescence characteristics and efficiency of $MgGa_2O_4$:Mn with Zn_2SiO_4:Mn and $MgWO_4$

	Zn_2SiO_4:Mn NBS 1028	$MgWO_4$ NBS 1027	$MgGa_2O_4$:Mn
Peak wavelength, nm	536	501	512
Band width at ½ I_{max}, nm	45	152	36
Relative peak height	253	100	326
Color coordinates			
x	0.277	0.234	0.116
y	0.686	0.320	0.679
% Absorption at 253.7 nm	94.2	96.0	84.7
Relative quanta × 10^{-6} [eg $\int \lambda_o I_o d\lambda$]	2.78	7.57	1.93
Emitted energy [eg $\int \rho(\lambda) d\lambda$]	1.12	3.58	0.87
Energy efficiency	35	43 (19)	34
Quantum efficiency	81	85 (19)	81

The excitation and emission spectral energy distribution curves for $MgGa_2O_4$: Mn are shown in Fig. 2. It can be noted that the excitation spectrum peaks near 253.7 nm making this phosphor especially suited for application in fluorescent lamps. The emission peaks sharply at 512 nm with a half width of 36 nm. Following the method of Palumbo and Wisnieski (16), the fluorescence quantum efficiency of $MgGa_2O_4$: Mn was found to be equivalent to that of NBS 1028 zinc orthosilicate (with high manganese concentration) as shown in Table III. Also shown in Fig. 2, for sake of comparison, are the emission bands present prior to the second heat-treatment. The green emission is increased about 50 times by mild reduction, whereas the red band completely disappears.

Figure 3 shows the variation of the spinel a_o lattice parameter and fluorescence peak height with composition. The abrupt breaks in both curves near 48 and 62 mole % Ga_2O_3 signify the limits of $MgGa_2O_4$ crystalline solution. These are in good agreement with Schmalzried's (2) data when one realizes that the preparations of the present study contain 1 mole % manganese activator. Optimum fluorescence is obtained within the crystalline solution region at approximately 53 mole % Ga_2O_3. Crystalline solution of MgO in $MgGa_2O_4$ decreases the fluorescence more markedly than Ga_2O_3 substitutions. The brightness curves outside of the crystalline solution region approximates linearity because of dilution effects from the second phase.

Table IV and Fig. 4 show the effect of manganese concentration on phosphor brightness and peak emis-

Table IV. Effect of Mn^{2+} variations on $MgGa_2O_4$ phosphor

Sample No.	Composition, moles MgO	Ga_2O_3	MnO	$\frac{\text{Moles MnO}}{\text{Moles MgO + MnO}}$	% Relative peak height	Peak wavelength, nm	% Peak height decrease at 100°C
1	100	100	—	—	—	—	—
2	99	100	0.1	0.001	80	510.5	—
3	98	100	0.5	0.005	96	510.5	8.5
4	97	100	1.0	0.010	100	510.5	11.0
5	96	100	2.0	0.020	77	513.5	19.0
6	94	100	3.0	0.030	53	514.5	>20
7	93	100	4.0	0.040	42	515.5	—
8	92	100	5.0	0.050	29	516.5	—

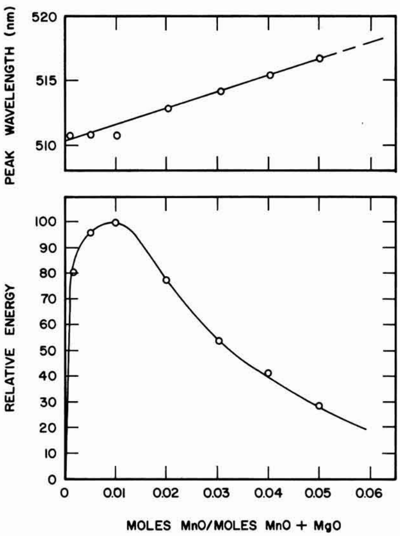

Fig. 4. Variation of peak wavelength (top) and brightness (bottom) with manganese concentration in $MgGa_2O_4$.

sion wavelength. Compositions were adjusted for manganese additions so that the Mn^{2+} could substitute for Mg^{2+} (or Ga^{3+}) and maintain the same approximate vacancy concentration. The top curve in Fig. 4 shows the variation of peak wavelength with increasing manganese additions. The apparent linear relationship is not surprising in view of the isomorphous $MgGa_2O_4$ and $MnGa_2O_4$ structures. The bottom curve shows the variation of peak intensity with manganese content. Concentration quenching, common to many Mn^{2+}-activated phosphors can be observed. Optimum fluorescence brightness is obtained at approximately 0.01 moles MnO.

The extreme right-hand column of Table IV shows the per cent peak height decrease observed between 25° and 100°C. This property was obtained by mounting a small furnace in the sample chamber of the spectroradiometer. These data confirm the general knowledge that low Mn^{2+} levels usually improve the temperature dependence of a phosphor. A very slight emission broadening and peak wavelength shift (towards shorter wavelengths) was observed, especially at high manganese levels.

Figure 5 shows the temperature dependence of $MgGa_2O_4$:Mn (sample 4, Table IV) measured up to 400°C with a HPMV plaque tester (17). The curve was found to be completely reversible up to at least 250°C, eliminating the possibility of the brightness decrease being caused by a chemical reaction.

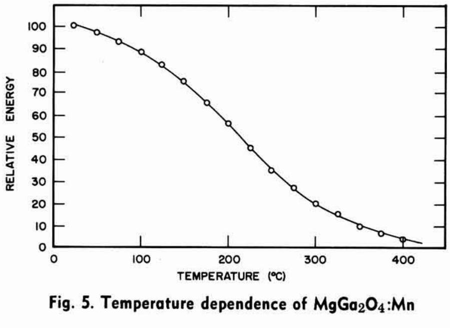

Fig. 5. Temperature dependence of $MgGa_2O_4$:Mn

Table V. Compositions and luminescence and x-ray data for preparations throughout the spinel crystalline solution series in the MgO-Ga_2O_3-Al_2O_3 systems

	Composition, mole %				253.7 nm Excited		CR excited			Lattice parameter
No.	MgO	Al_2O_3	Ga_2O_3	MnO	Pk ht	Peak λ	Ft-L	x	y	a_o, A
1	50	—	50	0.5	100	510.0	5.5	0.116	0.673	8.279
2	45	—	55	0.5			4.0	—	—	
3	40	—	60	0.5			3.7	0.102	0.631	
4	35	—	65	0.5			3.0	—	—	
5	30	—	70	0.5			3.0	0.101	0.609	
6	50	10	40	0.5	64	512.0	9.5	0.134	0.706	8.249
7	45	12.5	42.5	0.5			8.8	0.123	0.692	
8	40	15	45	0.5			7.5	—	—	
9	35	17.5	47.5	0.5			6.0	0.106	0.682	
10	30	20	50	0.5			4.5	—	—	
11	25	22.5	52.5	0.5			4.5	—	—	
12	20	25	55	0.5			2.3	0.122	0.697	
13	50	25	25	0.5	31	517.5	9.5	0.148	0.712	8.160
14	45	27.5	27.5	0.5			10.0	—	—	
15	40	30	30	0.5			10.2	0.146	0.714	
16	35	32.5	32.5	0.5			10.0	—	—	
17	30	35	35	0.5			10.0	0.132	0.696	
18	25	37.5	37.5	0.5			8.0	—	—	
19	20	40	40	0.5			8.5	0.136	0.702	
20	50	40	10	0.5	7	523.0	8.8	0.173	0.727	8.122
21	45	42.5	12.5	0.5			8.8	—	—	
22	40	45	15	0.5			9.0	0.166	0.720	
23	35	47.5	17.5	0.5			9.0	—	—	
24	30	50	20	0.5			9.0	0.162	0.721	
25	25	52.5	22.5	0.5			10.0	—	—	
26	20	55	25	0.5			9.9	0.145	0704	
27	50	50	—	0.5	—	—	8.0	0.225	0.724	8.083
28	45	55	—	0.5			8.9	0.216	0.730	
29	40	60	—	0.5			7.1	—	—	
30	35	65	—	0.5			7.3	0.222	0.730	
31	30	70	—	0.5			6.9	—	—	

These high-temperature data are important because they indicate that this phosphor, correctly formulated, can be used in fluorescent lamps (which generally operate below 100°C) without significant changes in brightness or other spectral characteristics.

The MgO-Al_2O_3 *binary system.*—Phosphors prepared throughout the spinel crystalline solution region of this system were excited only by cathode rays. The results of samples prepared at 1400°C are shown in Table V. Brightness appears to be maximum at approximately $(Mg_{0.90},Mn_{0.01})Al_{2.06}O_4$, and there is little change in color coordinates throughout the series. In general, these data are in agreement with those of Hummel and Sarver (10).

The Al_2O_3-Ga_2O_3 *binary system.*—Manganese-activated phosphors were prepared throughout the Al_2O_3-Ga_2O_3 system at 1400°C. Significant luminescence was not observed. X-ray diffraction powder data agreed essentially with the phase diagram of Hill *et al.* (11). Compositions in the intermediate crystalline solution region were not prepared because of their low-temperature stability range.

The MgO-Al_2O_3-Ga_2O_3 *ternary system.*—The compositions, lattice parameters, fluorescence, and cathodoluminescence data for preparations throughout the

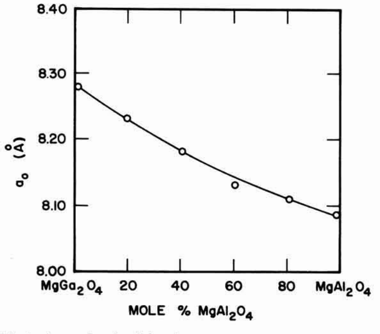

Fig. 6. Variation of spinel lattice parameter a_o *vs.* composition on the $MgGa_2O_4$-$MgAl_2O_4$ join.

spinel crystalline solution region in the MgO-Al_2O_3-Ga_2O_3 ternary system are listed in Table V. All compositions were heat-treated at 1400°C/17 hr in air and second fired at 1200°C/1 hr in a 2% H_2-98% N_2 atmosphere. The data plotted in Fig. 6 illustrate the variation of the a-axis of the spinel unit cell with composition throughout the $MgGa_2O_4$-$MgAl_2O_4$ join. The continuous variation of this parameter confirms the existence of a crystalline solution series. The decrease of a_o from 8.279Å for $MgGa_2O_4$ to 8.083Å for $MgAl_2O_4$ reflects the relative sizes of the trivalent cations, *e.g.*, the Goldschmidt radius of Ga^{3+} is 0.62Å and Al^{3+} is 0.57Å. The following luminescence results were obtained:

1. Photoluminescence.—As Al^{3+} replaces Ga^{3+} in the spinel structure, the manganese-activated ultraviolet excited peak wavelength increases and brightness decreases (Fig. 7). Magnesium aluminate is practically inert.
2. Cathodoluminescence.—The general trend of peak wavelength observed for ultraviolet excitation is also evident for cathode-ray excitation. (Brightness data are too erratic for a trend to be observed.)

Figure 8 illustrates the variation of brightness (ft-L) and chromaticity coordinates (x,y) throughout the ternary crystalline solution region. These results indicate (*i*) brightness is maximum near the center of the region (*e.g.*, near 40MgO, $30Ga_2O_3$, $30Al_2O_3$), and (*ii*) x and y increase as the Al^{3+} content increases.

Figure 9 illustrates the effect of increasing $MgAl_2O_4$ concentrations on the decay characteristics of this phosphor. A persistent "tail" develops at about 50% $MgAl_2O_4$ and becomes progressively longer at higher $MgAl_2O_4$ concentrations. These decay curves were found to vary somewhat depending on the composition of the atmosphere of the second heat-treatment.

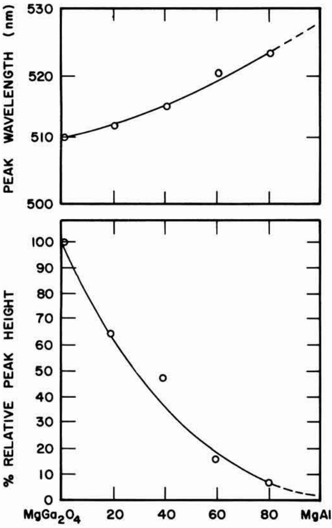

Fig. 7. Variation of ultraviolet excited peak wavelength (top) and brightness (bottom) with composition on the $MgGa_2O_4$-$MgAl_2O_4$ join.

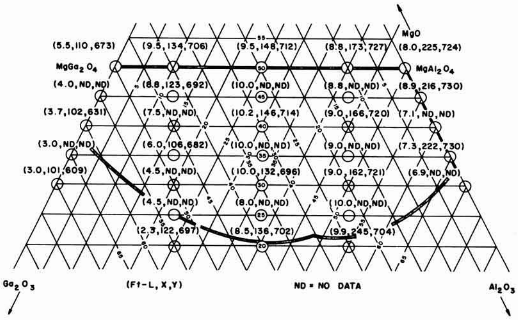

Fig. 8. Cathodoluminescence brightnesses and chromaticity coordinates of phosphors prepared throughout the spinel crystalline solution region in the MgO-Al_2O_3-Ga_2O_3 system.

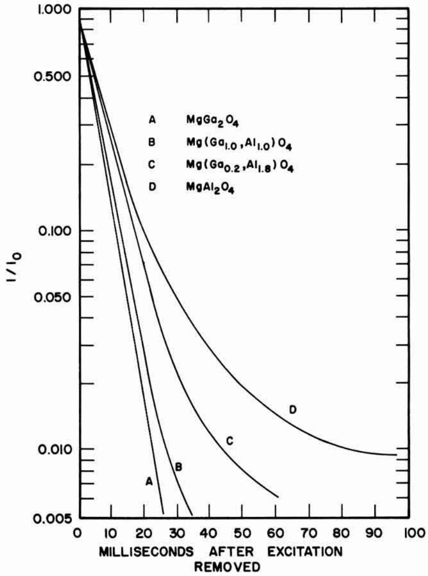

Fig. 9. Cathodoluminescence decay of phosphors throughout the $MgGa_2O_4$-$MgAl_2O_4$ join.

Discussion

Although both $MgGa_2O_4$ and $MgAl_2O_4$ crystallize with the spinel structure, they differ in their cation distributions as previously pointed out. The green emission of manganese in both of these compounds suggest tetrahedral oxygen coordination of Mn^{2+}. Furthermore, the pink body color and absence of luminescence after only air heat-treatments of $MgGa_2O_4$ suggest the possibility of manganese entering the structure as Mn^{3+}. The presence of Mn^{3+} after air heat-treatment is strengthened by the reflectance spectra of $MgGa_2O_4$:Mn measured before and after reduction as shown in Fig. 10. The broad absorption band in the blue-green region of the spectrum present only in the air-fired sample appears to be similar to

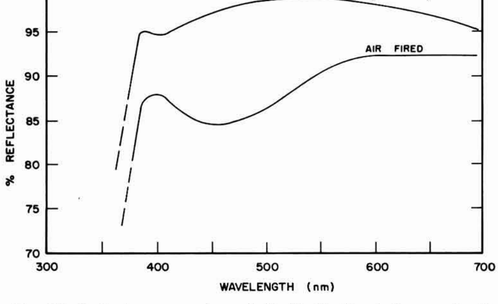

Fig. 10. Reflectance spectra of $MgGa_2O_4$:Mn before and after reduction.

that shown by Rabatin and Gillooly (15) to be characteristic of Mn^{3+}. Another qualitative indication of this mechanism was the significant green fluorescence developed after only air heat-treatments in preparations where small amounts of Si^{4+} or Ge^{4+} were substituted for Ga^{3+}. This probably resulted from the tetravalent cations forcing more of the manganese into the divalent state in order to balance the electrostatic charges.

Jagodzinski and Saalfeld (4) have shown that vacancies are distributed only over octahedral sites in $MgAl_2O_4$. If it is assumed that this is also the case for $MgGa_2O_4$, and that the population of Mg^{2+} ions in octahedral sites is about 0.84 at 1400°C (2), then the optimum phosphor composition can be approximated as follows

$$(\overset{2+}{\mathrm{Mg}}_{0.06},\overset{3+}{\mathrm{Ga}}_{0.93},\mathrm{Mn}_{0.01})^{\mathrm{IV}}(\overset{2+}{\mathrm{Mg}}_{0.84},\square_{0.03},\overset{3+}{\mathrm{Ga}}_{1.13})^{\mathrm{VI}}\mathrm{O}_4$$

Summary

1. Magnesium gallate activated by divalent manganese has been found to be an efficient ultraviolet excited phosphor with a peak emission wavelength at 512 nm. The optimum phosphor composition was determined to be $(Mg_{0.90},Mn_{0.01})(Ga_{2.06})O_4$.

2. Al^{3+} for Ga^{3+} substitutions in the spinel lattice rapidly decrease the fluorescence brightness, but increase the cathodoluminescence light output. The peak emission shifts from 512 to 525 nm and the decay characteristics become increasingly longer with Al^{3+} substitutions.

Acknowledgments

The author wishes to thank Mr. D. T. Palumbo and Dr. R. W. Mooney for many stimulating discussions during the course of this investigation. X-ray diffraction data were obtained by Dr. C. W. W. Hoffman. Procedures for the quantitative analyses of Mg, Ga, and Mn in magnesium gallate by wet chemistry methods were developed by Mrs. A. R. Mikus and by atomic absorption methods by Mr. J. L. Seeley. Sample preparations were carried out with the assistance of Messrs. J. D. Deysher and O. B. Bullock.

Manuscript received Aug. 25, 1966; revised manuscript received Oct. 14, 1966. This paper was presented at the Cleveland Meeting, May 1-6, 1966.

Any discussion of this paper will appear in a Discussion Section to be published in the December 1967 JOURNAL.

REFERENCES

1. T. Moller and G. L. King, *J. Am. Chem. Soc.*, **75**, 6060 (1953).
2. H. Schmalzried, *Z. physik. Chem.*, **28**, 203 (1961).
3. J. E. Weidenborner, N. R. Stemple, and Y. Okaya, *Acta Cryst.*, **20** [6], 761 (1966).
4. H. Jagodzinski and H. Jagodzinski, *Z. Kristallogr.*, **110**, 197 (1958).
5. H. Saalfeld and H. Jagodzinski, *ibid.*, **109**, 87 (1957).
6. A. M. Alper, R. N. McNally, P. G. Rebbe, and R. C. Doman, *J. Am. Ceram. Soc.*, **45** [6], 263 (1962).
7. D. M. Roy, R. Roy, and E. F. Osborn, *Am. J. Sci.*, **251**, 337 (1953).
8. R. K. Datta and R. Roy, *Nature*, **191**, 169 (1961).
9. H. Saalfeld, *Ber. Dtsch. Keram. Ges.*, **39**, 52 (1962).
10. F. A. Hummel and J. F. Sarver, *This Journal*, **111** [2], 252 (1964).
11. V. G. Hill, R. Roy, and E. F. Osborn, *J. Am. Ceram. Soc.*, **35** [6], 136 (1952).
12. G. Katz and R. Roy, *ibid.*, **48**, 450 (1965).
13. H. W. Leverenz, "An Introduction to Luminescence of Solids," John Wiley & Sons, Inc., New York (1950).
14. W. Slavin, R. W. Mooney, and D. T. Palumbo, *J. Opt. Soc. Am.*, **51**, 93 (1961).
15. J. G. Rabatin and G. R. Gillooly, *This Journal*, **111** [5], 542 (1964).
16. D. T. Palumbo and R. J. Wisnieski, "Efficiencies of Lamp Phosphors," In press.
17. R. W. Mooney, *This Journal*, **105**, 456 (1958).
18. R. K. Datta and R. Roy, Geol. Soc. Amer., Special paper No. 68, 159 (1961).
19. A. Bril and W. Hoekstra, *Philips Research Rept.*, **16**, 356 (1961).

Fluorescence of Eu^{3+}-Activated Garnets Containing Pentavalent Vanadium

G. Blasse and A. Bril

Philips Research Laboratories, N. V. Philips' Gloeilampenfabrieken, Eindhoven-Netherlands

ABSTRACT

$NaCa_2Mg_2V_3O_{12}$ has garnet structure and shows a broad emission band with a maximum at about 500 nm under short-wave uv excitation. Eu^{3+} is introduced according to the substitution $Ca^{2+} + Mg^{2+} \rightarrow Eu^{3+} + Li^{+}$. Unlike the emission of the usual Eu^{3+}-activated garnets (like YAG) the Eu^{3+} emission shows strong $^5D_0$-$^7F_2$ transitions in this case. The energy transfer from the vanadate group to the Eu^{3+} ion is not very efficient. This is ascribed to the small value of the overlap of the Eu^{3+} and V^{5+} orbitals, the V-O-Eu angles being 90° and 120°.

Rare earth activated garnets have been studied extensively. Usually the composition of the host lattice is $A_3B_5O_{12}$ (A = Y,Gd; B = Al, Ga). The formula $\{Y_3\}[Al_2](Al_3)O_{12}$ gives more insight into the crystal chemistry of the garnets: { } represents a dodecahedral site, [ ] an octahedral site, and ( ) a tetrahedral site. Recently Bayer (1) described garnets containing pentavalent vanadium, *e.g.*, $\{Na\,Ca_2\}[Mg_2](V_3)O_{12}$. Since a number of vanadates [*e.g.*, YVO_4 (2) and $Ca_3(VO_4)_2$ (3)] appear to be suitable host lattices for rare earth activated phosphors, we studied the fluorescence of unactivated and Eu^{3+}-activated $NaCa_2Mg_2V_3O_{12}$.

Experimental

Materials with composition $\{NaCa_{2-\delta}Eu_\delta\}[Li_\delta Mg_{2-\delta}](V_3)O_{12}$ were prepared by firing intimate mixtures of Na_2CO_3, $CaCO_3$, Eu_2O_3, Li_2CO_3, $MgCO_3$, and NH_4VO_3 at 750°C in O_2 several times. X-ray powder diagrams were obtained using CuKα radiation.

The performance of the optical measurements has been described in detail elsewhere (4).

Results

Compositions $\{NaCa_{2-\delta}Eu_\delta\}[Li_\delta Mg_{2-\delta}](V_3)O_{12}$ proved to be single-phased garnets up to $\delta = 0.4$. For higher values of δ a second phase with zircon structure was found in the x-ray diagrams. These materials were not studied further. The lattice parameter of the garnet phase did not change more than 0.01Å going from $\delta = 0$ to $\delta = 0.4$ and amounted to $a = 12.45$Å for $\delta = 0$, in good agreement with Bayer's results (1).

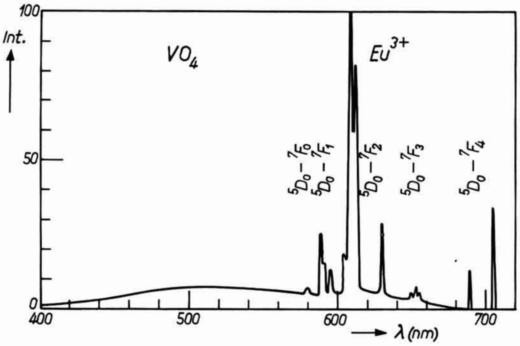

Fig. 1. Spectral emission under short wavelength u.v. excitation of $NaCa_{1.9}Eu_{0.1}Li_{0.1}Mg_{1.9}V_3O_{12}$.

Under short-wave u.v. excitation $NaCa_2Mg_2V_3O_{12}$ shows a white emission at room temperature (quantum efficiency about 30%; this value may be a lower bound due to the low reaction temperature). Even at the highest Eu^{3+} concentration ($\delta = 0.40$), we observed this host lattice emission in addition to the characteristic Eu^{3+} emission. Figure 1 presents the emission for the composition with $\delta = 0.10$. Table I gives the ratio of Eu^{3+} emission to total emission for several values of δ. The excitation spectrum of the fluorescence and the diffuse reflection spectrum for the material with $\delta = 0.10$ are given in Fig. 2. These spectra do not change with the activator concentration.

Discussion

Emission.—Figure 1 shows the host lattice emission as well as the activator emission. The former consists of a very broad band extending from approximately 400 to 700 nm with a maximum at roughly 500 nm, which must be due to transitions in the vanadate group. Vanadate emission at room temperature has been reported earlier for compounds of the type $M_2V_2O_7$ (M = Mg, Zn, Cd, Ca, Sr, Ba) (5).

The emission of the Eu^{3+} ion consists of the well-known transitions from ^5D_o down to the ^7F manifold. It is interesting to note that in the vanadium garnet the red lines (^5D_o — $^7F_2$) have the strongest intensity. In the aluminum and gallium garnets (*e.g.*, YAG), however, the red and orange lines (^5D_o — $^7F_1$) have comparable intensity (6), which is not surprising, because the Eu^{3+} ion occupies a site which has an approximate center of symmetry, if only the nearest neighbors, *viz.*, the eight O^{2-} anions are considered. For a strict center of symmetry the red fluorescence due to the ^5D_o — $^7F_2$ transition is forbidden. Blasse, Bril, and Nieuwpoort (7) have noticed that the intensity ratio of the red and orange lines can be drastically changed by chemical variations of the next-nearest neighbors of the Eu^{3+} ion. The present results are another example of this effect. Contrary to the situation with the anions, the cation neighbors of the dodecahedral site in the garnet structure of $Y_3Al_5O_{12}$ lack inversion symmetry. In $NaCa_2Mg_2V_3O_{12}$, where the tetrahedral Al^{3+} ions are replaced by V^{5+} ions and the octahedral Al^{3+} ions by Mg^{2+} ions, this lack of inversion symmetry seems to be of more importance.

Table I. Ratio of the quantum efficiency of the Eu^{3+} emission to the total quantum efficiency for materials $NaCa_2Mg_2V_3O_{12}$: Eu, Li

Composition	Ratio
$NaCa_2Mg_2V_3O_{12}$	0
$NaCa_{1.96}Eu_{0.04}Li_{0.04}Mg_{1.96}V_3O_{12}$	0.1
$NaCa_{1.9}Eu_{0.1}Li_{0.1}Mg_{1.9}V_3O_{12}$	0.2
$NaCa_{1.8}Eu_{0.2}Li_{0.2}Mg_{1.8}V_3O_{12}$	0.4
$NaCa_{1.6}Eu_{0.4}Li_{0.4}Mg_{1.6}V_3O_{12}$	0.6

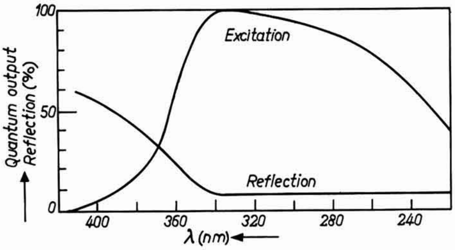

Fig. 2. Relative excitation spectrum of the fluorescence and diffuse reflection spectrum of $NaCa_{1.9}Eu_{0.1}Mg_{1.9}V_3O_{12}$.

This is an indication again that the intensity alterations seem to be dependent on the state of polarization of the oxygen ions, as noted earlier (7): in $NaCa_2Mg_2V_3O_{12}$ the anions are much more strongly polarized than in YAG because in $NaCa_2Mg_2V_3O_{12}$ each O^{2-} ion has one highly charged and small V^{5+} ion as one of its neighbors. The crystal field splittings are not strongly influenced by this effect, as follows from a comparison of the Eu^{3+} emission of YAG : Eu (6) and $NaCa_2Mg_2V_3O_{12}$: Eu, Li. The ^5D_o — $^7F_1$ transition contains three lines and the ^5D_o — $^7F_2$ transition four lines in both cases. The splittings are of the same order of magnitude.

In this connection we note that the anomalous behavior of the Curie temperature of V^{5+}-substituted yttrium iron garnet (the Curie temperature does not change if the paramagnetic ions are replaced by diamagnetic ions) has also been ascribed to an influence of the V^{5+} ions on the chemical bonding (8).

Excitation and reflection.—Since the reflection spectra do not change very much in the investigated region of δ(0-0.4), the absorption in the u.v. region is ascribed to the vanadate groups of the host lattice. The excitation is most efficient at the wavelength of the absorption edge (see Fig. 2). From Table I it is seen that the energy transfer from vanadate group to Eu^{3+} activator is not very efficient. This is contrary to the energy transfer from vanadate group to Eu^{3+} ion in Eu^{3+}-activated YVO_4 and $Ca_3(VO_4)_2$, where the transfer is very efficient (2, 3). Elsewhere we have argued that transfer of this type is exchange-regulated and therefore strongly dependent on the crystal structure, the O^{2-} ions playing a role (9). Unfortunately the structure of $Ca_3(VO_4)_2$ is not known. In YVO_4 : Eu the V-O-Eu angle is 170°, whereas in $NaCa_2Mg_2V_3O_{12}$: Eu,Li the V-O-Eu angle is 90° or 120° (10). This means that the wave function overlap of the vanadium and europium ions is larger in YVO_4 than in $NaCa_2Mg_2V_3O_{12}$, σ-bonding being involved in the 180° case and π-bonding in the 90° case. Therefore the vanadate → Eu^{3+} ion transfer should be more efficient in YVO_4 than in $NaCa_2Mg_2V_3O_{12}$, in agreement with the experimental results. That there is still considerable energy transfer from vanadate group to Eu^{3+} ion in the garnet may be due to direct overlap of the orbitals of the V^{5+} and Eu^{3+} ion. Each V^{5+} ion is surrounded by six dodecahedral ions, of which two are at a distance equal to one quarter of the cell edge, *i.e.*, only 3.1Å in the present case. Direct overlap is a well-known phenomenon in magnetic exchange theories as is the angle-dependence of the overlap of wave functions of cations separated by anions (11). The strong magnetic interaction between Cr^{3+} ions in $ZnCr_2O_4$, for instance, is ascribed to direct overlap of t_{2g} wave functions of the Cr^{3+} ions (Cr^{3+} — Cr^{3+} distance 2.9Å).

Manuscript received Aug. 8, 1966; revised manuscript received Oct. 17, 1966.

Any discussion of this paper will appear in a Discussion Section to be published in the December 1967 JOURNAL.

REFERENCES

1. G. Bayer, *J. Am. Chem. Soc.*, **48**, 600 (1965).
2. F. C. Palilla, A. K. Levine, and M. Rinkevics, *This Journal*, **112**, 776 (1965).
3. L. H. Brixner and P. A. Flournoy, *ibid.*, **112**, 303 (1965).
4. A. Bril and W. L. Wanmaker, *ibid.*, **111**, 1363 (1964).
5. Y. Kotera and T. Sekine, *Bull. Chem. Soc. Japan*, **27**, 13 (1954).
6. L. G. Van Uitert, R. C. Linares, R. R. Soden, and A. A. Ballman, *J. Chem. Phys.*, **36**, 702 (1962); J. A. Koningstein, *Phys. Rev.*, **136**, A717 (1964).
7. G. Blasse, A. Bril, and W. C. Nieuwpoort, *J. Phys. Chem. Solids*, Int. Conf. on Luminescence, Budapest, 1966.
8. S. Geller, G. P. Espinosa, H. J. Williams, R. C. Sherwood, and E. A. Nesbitt, *J. Appl. Phys.*, **35**, 570 (1964); *Appl. Phys. Letters*, **3**, 60 (1963).
9. G. Blasse and A. Bril, *J. Chem. Phys.*, In press; G. Blasse, *J. Chem. Phys.*, In press.
10. S. Geller and M. A. Gilleo, *J. Phys. Chem. Solids*, **3**, 30 (1957).
11. J. B. Goodenough, "Magnetism and the Chemical Bond," p. 202, Interscience Publishers, New York (1963).

Fluorescence and Cathodoluminescence of Eu^{+3} in Some Alkali and Alkaline Earths-Yttrates and Gadolinates as Hosts

L. H. Brixner

Pigments Department, Experimental Station,
E. I. du Pont de Nemours & Company, Wilmington, Delaware

ABSTRACT

Efficient fluorescence of Eu^{+3} was measured in alkali yttrate and gadolinate hosts of the type ABO_2, where A is Li or Na; B, Y or Gd, under both ultraviolet and electron excitation. The optimum Eu^{+3} concentration was determined for each host; the concentration *vs.* fluorescent intensity curves are presented, as well as some fluorescent emission spectra. Some alkaline earth compounds were also studied as hosts.

Although the fluorescence of Eu^{+3} in such hosts as Gd_2O_3 and $CaWO_4$ was studied as early as 1909 by Urbain (1), it was not until the advent of the laser concept that europium has been more extensively investigated in all conceivable solid hosts as well as in liquid systems. Stimulated emission was first observed from Eu^{+3} in a chelate (2) and later also in Y_2O_3 (3) as a solid state host. In some of our own experiments (4), we failed to observe laser action from Eu^{+3} in $Ca_3(VO_4)_2$, despite the fact that energy exchange between the host lattice and Eu^{+3} was demonstrated. Van Uitert (5) showed that energy exchange also occurs in the host $GdVO_4$. This composition, or rather the isostructural YVO_4, became of interest recently when Levine *et al.* (6) found that europium in this type of host also shows very efficient cathodoluminescence. It was probably this finding which initiated a renewed search for other novel host structures for Eu.

Most previous work was either done with compositions where the rare earths (Y or Gd for instance) have a cationic function (vanadates, molybdates, tungstates, etc.) or with the rare earth oxide itself. A number of rare earth compounds where the rare earth constitutes the anionic portion, such as SrY_2O_4 (7) or $LiYO_2$ (8), have been described recently, and it was the purpose of this study to investigate these compounds as hosts for Eu^{+3}.

Experimental

The constituent components were generally of the best commercially available purity and were given no further purification treatment. The preparation techniques were essentially identical to those described in detail in (9). Occasional analytical checks were carried out for compositions after complete reaction employing x-ray fluorescence techniques. X-ray powder patterns were taken to confirm the structures obtained with those well documented in the literature; only minor lattice parameter deviations could be observed when appreciable portions of Y^{+3} were substituted by Eu^{+3}. For the Gd hosts, the parameters were essentially unchanged when Eu was introduced. The procedures for obtaining the spectra upon optical excitation have already been described (9). To study the emission characteristics under electron excitation we used an available electron microprobe analyzer. The advantage here was the fact that as many as 11 samples could be excited and studied under absolutely identical conditions. These were generally an excitation current of 0.002 μA, a voltage of 20 kv, using a S-11 response-type detector tube (No. 6199) together with a red filter. The samples were powder compacts pressed into 1/8 diameter holes of a 1 in. diameter brass support plate. The inspection area was approximately 540 μ^2.

The first system which was studied in detail was $LiY_{1-x}Eu_xO_2$. As can be seen from Fig. 1, the optimum fluorescent emission occurred around 6 mol % Eu^{+3} for both ultraviolet and electron excitation. Although different in gradients, the two curves show

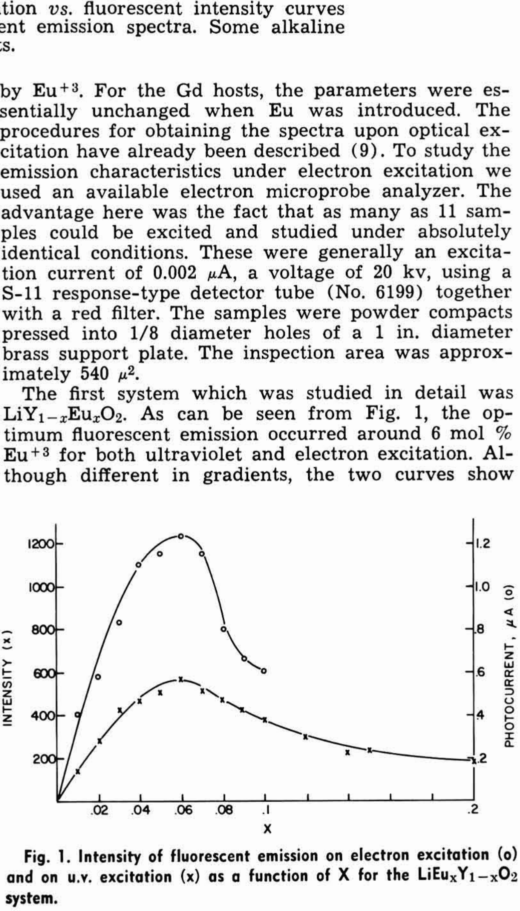

Fig. 1. Intensity of fluorescent emission on electron excitation (o) and on u.v. excitation (x) as a function of X for the $LiEu_xY_{1-x}O_2$ system.

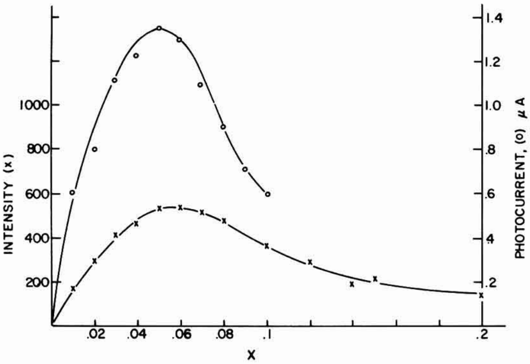

Fig. 2. Intensity of fluorescent emission on electron excitation (o) and on u.v. excitation (x) as a function of X for the $LiEu_xGd_{1-x}O_2$ system.

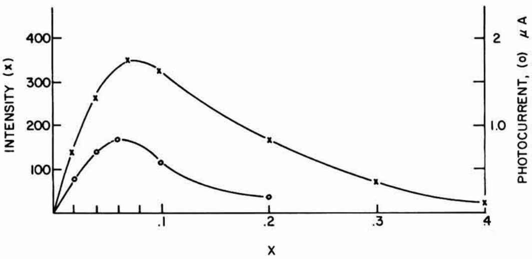

Fig. 3. Intensity of fluorescent emission on electron excitation (o) and on u.v. excitation (x) as a function of X for the $Eu_xY_{1-x}NaO_2$ system.

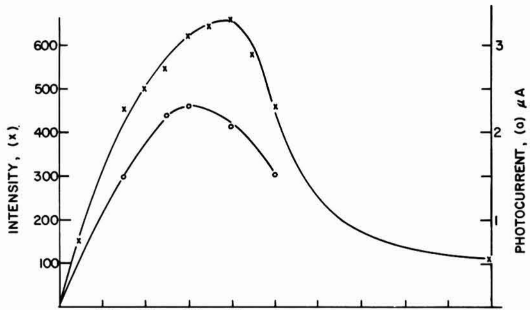

Fig. 4. Intensity of fluorescent emission on electron excitation (o) and on u.v. excitation (x) as a function of X for the $NaEu_xGd_{1-x}O_2$ system.

fundamentally the same characteristics of a steep rise to the optimum emission point and then gradual drop of emission intensity until eventually complete concentration quenching occurs. Figures 2, 3, and 4 show the same results for the corresponding systems: $LiGd_{1-x}Eu_xO_2$, $NaY_{1-x}Eu_xO_2$, and $NaGd_{1-x}Eu_xO_2$. All attempts to prepare any compositions between both Y_2O_3 and Gd_2O_3 and the alkali oxides of K, Rb, and Cs failed completely.

For the purpose of a comparison, the peak intensities of the investigated compositions are summarized in Table I. In the last column marked Lum/o, we have something of a "Figure of Merit," giving the efficiency based on the equivalent Eu concentration. The term is derived from the over-all intensity divided by the % Eu present in this composition. The location of the peak emission of all compounds is at about 613 mμ as specifically demonstrated for $LiEu_{0.07}Y_{0.93}O_2$ in Fig. 5. The halfwidth of the predominant 613 mμ line narrowed to 3Å at 77°K.

Table I. Comparison of peak emission for some Li and Na yttrates and gadolinates

Composition	Opt. inten. under uv excitation (2537A)	Opt. inten. under electron excitation	% Eu	Lum/o
$LiEu_{0.06}Y_{0.94}O_2$	570	1.24	6.93	82.25
$LiEu_{0.05}Gd_{0.95}O_2$	540	1.35	3.88	139.20
$NaEu_{0.07}Y_{0.93}O_2$	350	0.85	7.17	48.81
$NaEu_{0.08}Gd_{0.92}O_2$	660	2.30	5.74	115.00

Concerning ternary compositions between the alkaline earth oxides and Y_2O_3 and Gd_2O_3, Schwarz (7) had already demonstrated that only SrO and BaO formed compounds of the types AB_2O_4 ($A = Sr^{+2}$, Ba^{+2}; $B = Y^{+3}$, Ln^{+3}). In our own experiments, we also failed to form compounds with CaO or with MgO, ZnO, and CdO. For these reasons, we studied only SrY_2O_4 and BaY_2O_4 as host compositions for Eu^{+3}.

Although the substitutional elements are the same as in the previously discussed compounds, due to the different environmental symmetry as well as the different crystal field influence on the Stark splitting, the fluorescent emission spectra for Eu^{+3} in these hosts could be expected to be different and therefore it seemed of interest to study it. The most striking difference becomes apparent in Fig. 6, where a complete reversal of the intensity in the 590 and 610 mμ region can be observed. Such shifts of the bulk of the emission intensity are, of course, associated with the corresponding change of symmetry. Unfortunately the structures of neither host are well enough known to establish from group theory the number of possible components which each transition would be allowed to have. Under monoclinic symmetry the $^5D_o \rightarrow {}^7F_1$

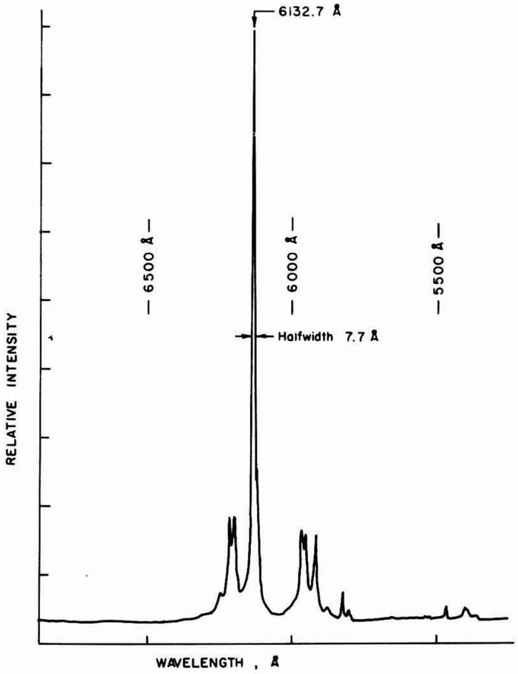

Fig. 5. Fluorescent emission spectrum of $LiEu_{0.07}Y_{0.93}O_2$ at 300°K.

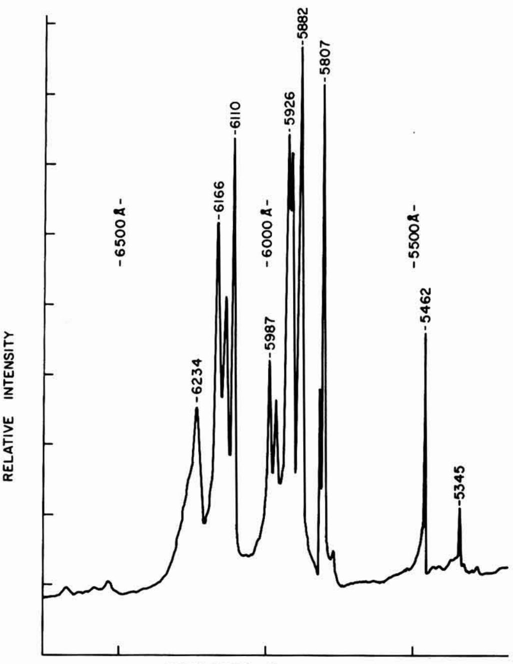

Fig. 6. Fluorescent emission spectrum of $SrEu_{0.20}Y_{1.80}O_4$ at 300°K.

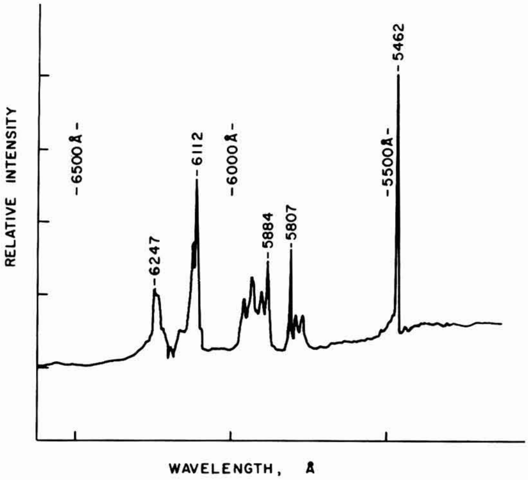

Fig. 7. Fluorescent emission spectrum of $BaEu_{0.14}Y_{1.86}O_4$ at 300°K.

transition can, for instance, exhibit a maximum of three components, all of which are clearly resolved in the spectrum of $Gd_{0.5}Eu_{0.5}NbO_4$ (10). For this case, the bulk of the emission also shifts from the $^5D_0 \rightarrow {}^7F_2$ transition to the $^5D_0 \rightarrow {}^7F_1$ transition in going to the more symmetrical $Ba_2La_{0.9}Eu_{0.1}NbO_6$. Similar observations have also been made for organic Eu compounds (11). Figure 7 shows the corresponding spectrum for $BaEu_{0.14}Y_{1.86}O_4$ where the same type of reversal can be seen. The over-all intensities were also much weaker than in the alkali-rare earth oxide hosts. For the purpose of a comparison we did determine the complete fluorescent emission characteristics as a function of the Eu concentration in both hosts. In $BaEu_xY_{2-x}O_4$, the optimum occurred at $x = 0.14$, and in $SrEu_xY_{2-x}O_4$, at $x = 0.20$. The observed intensities of emission at the optimum x were 78 for the Ba and 52 for the Sr compounds, compared with 570 for $LiEu_{0.06}Y_{0.94}O_2$.

In summary, we can state that the Li and Na rare earth oxides of Y_2O_3 and Gd_2O_3 make interesting and efficient hosts for Eu^{+3}, but the location of the emission prevents them from being useful as good red phosphors. The alkaline earth compounds SrY_2O_4 and BaY_2O_4 showed completely different fluorescent emission characteristics and were furthermore substantially less efficient as hosts for Eu^{+3}.

Manuscript received June 3, 1966; revised manuscript received Oct. 24, 1966.

Any discussion of this paper will appear in a Discussion Section to be published in the December 1967 JOURNAL.

REFERENCES

1. G. Urbain, *Am. Chem. Phys.*, **18**, 293 (1909).
2. H. Samelson and A. Lempicki, *Applied Phys. Letters*, **5**, 173 (1964).
3. N. C. Chang, *J. Appl. Phys.*, **34**, 3500 (1963).
4. L. H. Brixner and P. A. Flournoy, *This Journal*, **112**, 303 (1965).
5. L. G. van Uitert, R. R. Soden, and R. C. Linares, *J. Chem. Phys.*, **36**, 1793 (1962).
6. A. K. Levine and F. C. Palilla, *Appl. Phys. Letters*, **5**, 108 (1964).
7. H. Schwarz, *Z. Naturforsch.*, **19B**, 955 (1964).
8. K. S. Vorres, Rare Earth Conferences II, 147 (1964).
9. L. H. Brixner, *This Journal*, **111**, 690 (1964).
10. L. H. Brixner, International Conference on Luminescence, Budapest (1966), Preprints, Section D-9, p. 3.
11. N. J. Rose and E. Abramson, *J. Chem. Phys.*, **42**, 1849 (1965).

Resistivity Inhomogeneities in Silicon Crystals

R. G. Mazur

Research Laboratories, Westinghouse Electric Corporation, Pittsburgh, Pennsylvania

ABSTRACT

The extent of small-scale radial resistivity inhomogeneity in several n-type silicon crystals has been quantitatively determined with high spatial resolution by the spreading resistance resistivity measurement technique. Typical results for Czochralski, float-zone refined, crucible-less, web-grown and vapor-deposited epitaxial silicon are given, showing that appreciable nonuniformity in local resistivity exists in many crystals. The usefulness of the spreading resistance technique in rapid evaluation of the degree of resistivity inhomogeneity of individual silicon samples is illustrated.

In the last few years a number of publications have dealt with a variety of microdefects and inhomogeneities in silicon single crystals. This work has recently been reviewed by John, Faust, and Stickler (1). The various crystallographic defects have been extensively studied with high spatial resolution by several techniques. Optical and infrared microscopy, scanning electron microscopy, and x-ray diffraction microscopy have given a linear spatial resolution on the order of 10^{-4} cm, while transmission electron microscopy has utilized a much higher spatial resolution capability of about 10^{-7} cm.

Resistivity or impurity concentration inhomogeneities have also been observed qualitatively with 10^{-4} cm linear resolution using several preferential etching and plating techniques. However, quantitative measurements on electrically active inhomogeneities have been limited by the spatial resolution of the standard potential probe resistivity measurement techniques. While certain situations allow a high linear spatial resolution through a one-dimensional approach, *e.g.*, the study of diffusion profiles by incremental etch and four-point probe (2), the general case is strongly affected by the fact that resistivity is a volume property. Standard potential probe limitations are most obvious when minimum volumes sampled are compared with those of the "visual" techniques mentioned above. Light microscopy, scanning electron microscopy, and x-ray diffraction microscopy all provide a volume resolution of *ca.* 10^{-12} cm^3 and transmission electron microscopy utilizes a volume resolution of 10^{-18} cm^3 or better. In contrast, the incremental anodic oxidation, etch and four-point probe technique involves a minimum volume of about 5×10^{-8} cm^3. The one- or two-point potential probe technique requiring a bar-sample of at least $5.0 \times 10^{-2} \times 10^{-2}$ cm^2 cross-sectional area gives an average resistivity over a volume of 5×10^{-7} cm^3, if the probes are moved in 1×10^{-3} cm increments along the length of the bar. There is obviously a difference of several orders of magnitude in the spatial resolution of resistivity fluctuations by the standard methods as opposed to the essentially visual techniques. Recent developments in the spreading resistance resistivity measurement technique (3) have enabled us to begin a study of fine-scale resistivity fluctuations in silicon with a sampling volume of 10^{-10} cm^3 or less. This paper provides preliminary data on fine-scale resistivity inhomogeneities observed in typical Czochralski, float-zone refined, crucible-less, web-grown and vapor-deposited epitaxial silicon, showing that significant variations do exist in many crystals. The data also suggest a tentative procedure for assessing the microscale quality of silicon by the spreading resistance technique.

The data reported are not considered extensive enough for a judgment of the relative worth of material produced by the various growth processes as the total number of samples examined to date is small and the degree of correlation between raw material fine-scale resistivity homogeneity and final device performance is not accurately established.

Experimental

All of the material examined to date has been n-type silicon. The samples used were not especially selected in any way so that, aside from their limited number, they represent a good cross section of single crystal silicon commonly available. Sample resistivities ranged from a few tenths of an ohm-centimeter to several hundred ohm-centimeters. This initial study has been limited to radial resistivity variation as much as it is possible to do so on the scale involved.

Spreading resistance resistivity measurements can be made by measuring the resistance between a pair of probe-contacts (obviating the need for any other contacts to the sample) or with a single spreading resistance probe and some form of relatively large-area contact to the sample for current return. This latter mode provides maximum spatial resolution, and all data reported here were obtained with a single probe. The base contact used was ultrasonically soldered tin-indium (50:50). Base contact resistance was separately checked for each sample to insure that it was negligibly small compared to the spreading resistance on that sample.

Each sample was polished with 0.3μ alumina in a water slurry on a rough glass plate to produce the surface finish for which the calibration curve relating spreading resistance and sample resistivity had been previously established. Certain samples were also checked after several minutes etching in CP4A.[1]

After preparation each sample was probed radially at intervals of 0.1 mm over a span of 5.0 mm located approximately midway between the center and edge of the crystal. A second set of measurements was then made, covering a 0.5 mm interval midway in the first 5 mm span in steps of 0.01 mm. The raw values of measured spreading resistance were then computer processed to

(*i*) convert the local spreading resistance values to local resistivities (ρ_i), using a predetermined calibration curve;

(*ii*) calculate the average resistivity of each set of measurements ($\bar{\rho}_i$);

(*iii*) calculate the standard deviation ($s = \sqrt{\Sigma^n{}_{i=1}(\bar{\rho}_i - \rho_i)^2/n-1}$) of the n individual values of resistivity ρ_i about the average $\bar{\rho}_i$;

(*iv*) tabulate the individual deviations of the ρ_i from $\bar{\rho}_i$;

(*v*) reject any raw data which led to a deviation ($\bar{\rho}_i - \rho_i$) greater than $4s$;

(*vi*) if such rejection of "spurious" data was necessary, the amended data was reprocessed through steps (*i*) to (*iv*);

---

[1] 120 cc 40% HF, 120 cc acetic acid, 200 cc HNO_3.

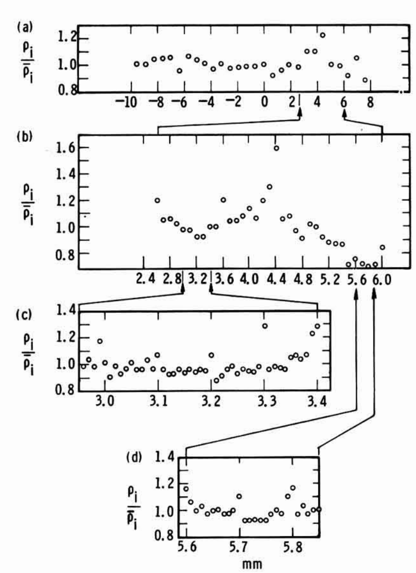

Fig. 1. Typical radial resistivity inhomogeneity in float-zone silicon, plotted as $\rho_i/\bar{\rho}_i$ vs. relative radial position, where $\bar{\rho}_i$ is in each case the local average resistivity. (a) Standard potential probe profile; (b), (c), (d), spreading resistance probe profiles; (b) 0.1 mm scale; (c) and (d) 0.01 mm scale.

(*vii*) calculate values of the ratio of local resistivity, ρ_i, to the average resistivity, $\bar{\rho}_i$, for each point probed (in order to allow direct comparison of resistivity fluctuations in samples of varying nominal resistivity);

(*viii*) plot these values of ρ_i/ρ_i *vs.* the radial position

(*ix*) calculate $s/\bar{\rho}_i$ for each sample, in an attempt to characterize the various materials checked by a single quantitative parameter as well as by the pictorial results produced by the digital plotter.

Results and Discussion

Figure 1 is an illustration of some results obtained with the procedure described above. The sample is a rather typical float-zone crystal of 1 ohm-cm average resistivity. Figure 1a is a radial resistivity profile obtained by a standard one-point traveling potential probe technique covering a span of 18 mm more or less centered on the crystal. The potential probe was moved in 0.5 mm increments. The average resistivity of these 0.5 mm sections is seen to vary from about 0.9 to 1.2 times the over-all average resistivity of the crystal. Figure 1b gives a spreading resistance-derived resistivity profile on the same sample as in Fig. 1a. The arrows indicate the section of the 1a sample examined. The spreading resistance probe measurement was made at intervals of 0.1 mm. The resulting values of $\rho_i/\bar{\rho}_i$ show that the resistivity fluctuations in this material are more extreme than was indicated by the standard traveling probe potential profile, with local resistivities ranging from 0.7 to > 1.3 times the average resistivity of the material probed in Fig. 1b. Figure 1c and 1d are plots of $\rho_i/\bar{\rho}_i$ of two separate sections of the material covered in Fig. 1b, now at intervals of 0.01 mm.

Figure 2a is a plot of $\rho_i/\bar{\rho}_i$ for a 10 ohm-cm Czochralski crystal, probed at 0.1 mm intervals over a span of 5 mm. It can be seen that the local resistivity varies from about 0.85 to about 1.15 times the average resistivity of this 5 mm section of the crystal. For the data in Fig. 2a, $s/\bar{\rho}_i = 0.067$. Thus, local resistivities 6.7% greater or less than the average resistivity in this 5 mm section of silicon have a probability of occurrence of 0.32; with 1% of the volumes sampled then having a probable resistivity 2.5 $(s/\bar{\rho}_i)$ or about 17% greater or less than the sample's average resistivity.

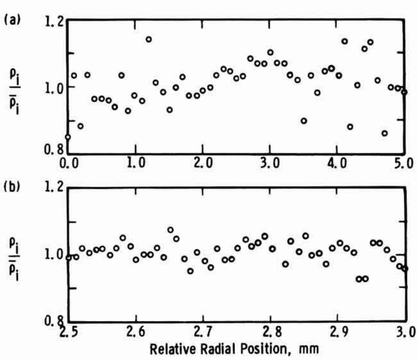

Fig. 2. $\rho_i/\bar{\rho}_i$ vs. relative radial position in a 10 ohm-cm Czochralski crystal. (a) 0.1 mm scale, $s/\bar{\rho}_i = 0.067$; (b) 0.01 mm scale, $s/\bar{\rho}_i = 0.031$.

Figure 2b gives the values of $\rho_i/\bar{\rho}_i$ measured in the central region of the 2a sample with a 0.01 mm spacing. The local resistivity variation on this finer scale is seen to be less than that observed on the 0.1 mm scale. The lesser range of local resistivity values on the 0.01 mm scale is reflected in a smaller value of fractional standard deviation of 0.031 for the data in Fig. 2b.

Another Czochralski crystal, a 14 ohm-cm (average resistivity) sample, clearly illustrates in Fig. 3 several features of this type of measurement. While the fine-scale data of Fig. 3b, as well as the point-to-point variation of $\rho_i/\bar{\rho}_i$ in Fig. 3a, show the material to be relatively uniform on the fine-scale, a long-period and very large variation in resistivity is apparent from the data of Fig. 3a, which shows a variation of almost a factor of two in resistivity over a 4 mm span of this crystal. This type of profile is also indicated nonpictorially by the relative values of fractional standard deviation, these being 0.024 for the 0.01 mm scale data of Fig. 3b and 0.185 for the 0.1 mm data in Fig. 3a, a ratio of $s/\bar{\rho}_i$ (0.1 mm) to $s/\bar{\rho}_i$ (0.01 mm) of about 8.

An interesting point illustrated by the sample depicted in Fig. 3 is that, while the fractional standard deviation obviously fails to characterize accurately the material in detail completely, it fails safe; that is,

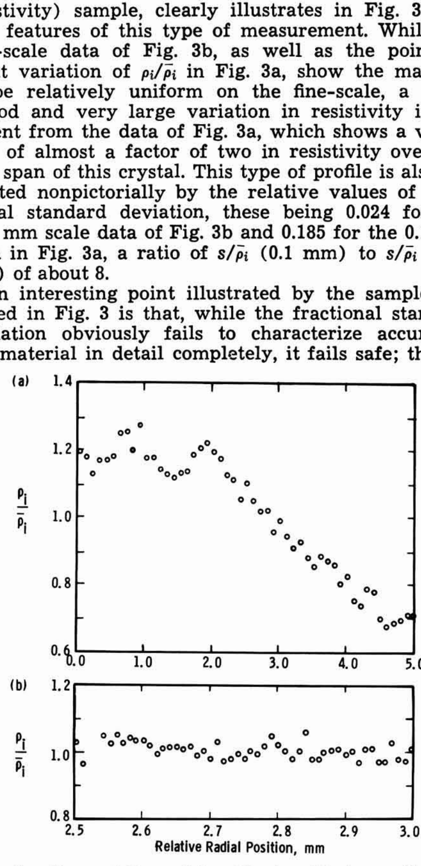

Fig. 3. $\rho_i/\bar{\rho}_i$ vs. relative radial position in a 14 ohm-cm Czochralski crystal with a long-term resistivity gradient. (a) 0.1 mm scale, $s/\bar{\rho}_i = 0.185$; (b) 0.01 mm scale, $s/\bar{\rho}_i = 0.024$.

the material is clearly indicated to be defective or questionable in some way by a high value of $s/\bar{\rho}_i$ on any scale.

Figure 4 is a plot of fine-scale (0.01 mm probe intervals) made on a sample of 175 ohm-cm Czochralski crystal before and after etching the sample for several minutes in CP4A. The purpose of this experiment was to determine how much of the fine-scale, point-to-point spreading resistance variation was due to inherent fluctuations in resistivity in the material and how much was the result of scratches or other polishing artifacts on the alumina-polished surface. Figure 4a (the polished surface) apparently has the same scatter as that of the etched sample (Fig. 4b). The quantitative measure of homogeneity, the fractional standard deviation, bears out the qualitative picture: values of $s/\bar{\rho}_i$ of 0.038 (for the polished surface) and 0.032 (for the etched surface) are not significantly different. Thus, the observed fine-scale fluctuations in resistivity are not due to the surface finish.

Figure 5 shows some results obtained on a 0.7 ohm-cm float-zone crystal. Figure 5a is the 0.1 mm scale data, with $s/\bar{\rho}_i = 0.06$; Fig. 5b gives the 0.01 mm scale data on the center section of the polished sample shown in Fig. 5a, with $s/\bar{\rho}_i = 0.022$; Fig. 5c shows 0.01 mm scale data on a sample of this same material etched for several minutes in CP4A. The value of $s/\bar{\rho}_i = 0.029$ for the etched sample of Fig. 5b again demonstrates that the variations in resistivity observed in this work are real and do not reflect a variable surface finish.

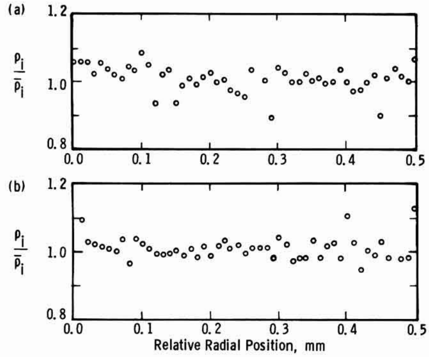

Fig. 4. $\rho_i/\bar{\rho}_i$ vs. relative radial position in a 175 ohm-cm Czochralski crystal as a function of surface finish. (a) alumina-polished surface, 0.01 mm scale, $s/\bar{\rho}_i = 0.038$; (b) chemically polished surface, 0.01 mm scale, $s/\bar{\rho}_i = 0.032$.

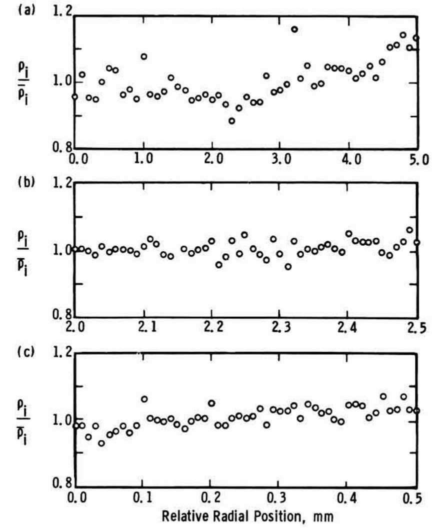

Fig. 5. $\rho_i/\bar{\rho}_i$ in a 0.7 ohm-cm float-zone crystal as a function of relative radial position and surface finish. (a) 0.1 mm scale, alumina-polished surface, $s/\bar{\rho}_i = 0.060$; (b) 0.01 mm scale, alumina-polished surface, $s/\bar{\rho}_i = 0.022$; (c) 0.01 mm scale, chemically polished surface, $s/\bar{\rho}_i = 0.029$.

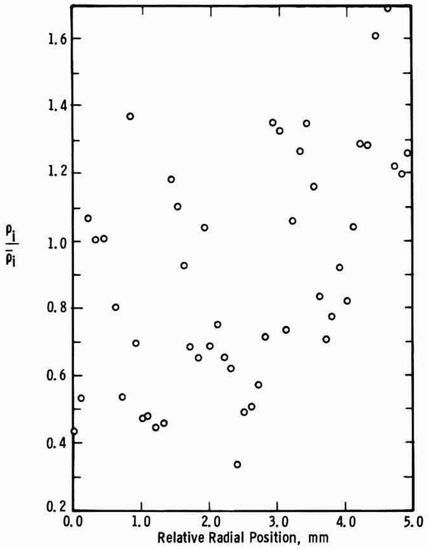

Fig. 6. $\rho_i/\bar{\rho}_i$ vs. relative radial position in a 250 ohm-cm float-zone crystal, 0.1 mm scale, $s/\bar{\rho}_i = 0.37$.

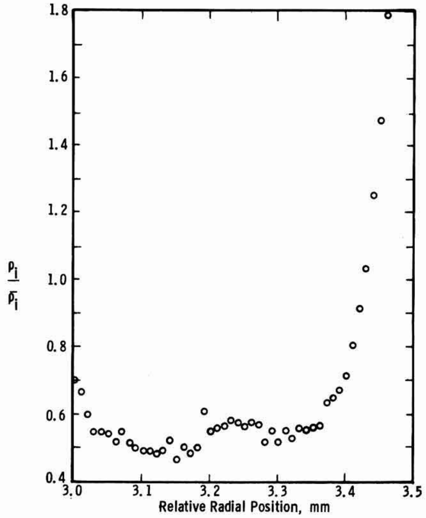

Fig. 7. $\rho_i/\bar{\rho}_i$ vs. relative radial position in a 250 ohm-cm float-zone crystal, 0.01 mm scale, $s/\bar{\rho}_i = 0.42$.

Figure 6 illustrates an extreme situation. This is a 250 ohm-cm float-zone crystal which has a 0.1 mm scale fractional standard deviation of 0.37; with a corresponding range of local resistivities varying by a factor of about 6. Figure 7 shows a small section of this material on the 0.01 mm scale. While the resistivity fluctuation over distances of a few tenths of a millimeter is quite small, the beginning of a high ρ region at the end of the section shown leads to an over-all value of $s/\bar{\rho}_i = 0.42$. As before, it is apparent

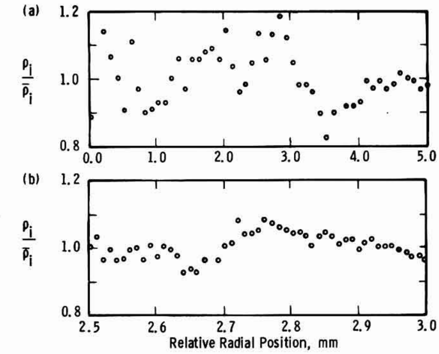

Fig. 8. $\rho_i/\bar{\rho}_i$ vs. relative radial position in a 44 ohm-cm crucible-less pulled silicon crystal. (a) 0.1 mm scale, $s/\bar{\rho}_i = 0.079$; (b) 0.01 mm scale, $s/\bar{\rho}_i = 0.037$.

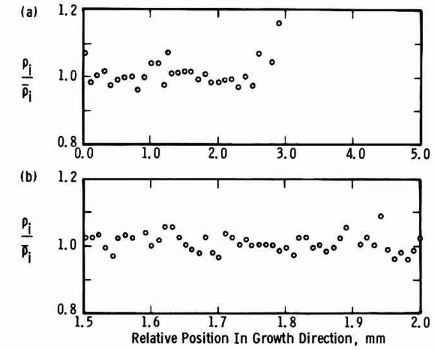

Fig. 9. $\rho_i/\bar{\rho}_i$ vs. relative position in growth direction in a 0.31 ohm-cm silicon web: (a) 0.1 mm scale, $s/\bar{\rho}_i = 0.039$; (b) 0.01 mm scale, $s/\bar{\rho}_i = 0.027$.

that the value of the fractional standard deviation of ρ_i is a "fail-safe" parameter in evaluating crystal quality in that it is necessary for the material to be uniform on both the macroscopic and microscopic scale to satisfy the condition $s/\bar{\rho}_i << 1$.

Figure 8 shows a sample of crucible-less silicon with a resistivity of 44 ohm-cm. Here the fractional standard deviation of the 0.1 mm scale data is 0.079. The fractional standard deviation of the 0.01 mm scale data (Fig. 8b) is 0.037. From this and other specimens, it is apparent that the crucible-less silicon, in this respect, as in many others, is often midway between the float-zone and Czochralski crystals.

Figure 9 shows a web sample with a resistivity of 0.31 ohm-cm. Figure 9a shows a 3 mm section of the material probed at 0.1 mm intervals, with a fractional standard deviation in the resistivity values of 0.039. Figure 9b shows the fine-scale data taken at 0.01 mm intervals with a fractional standard deviation of 0.027. These data indicate that this web material is at least as uniform as the float-zone material on the coarse scale and is as uniform or more uniform than either float-zone or Czochralski material on the fine-scale. Note also the near unity value of the ratio $s/\bar{\rho}_i$ (coarse) to $s/\bar{\rho}_i$ (fine-scale).

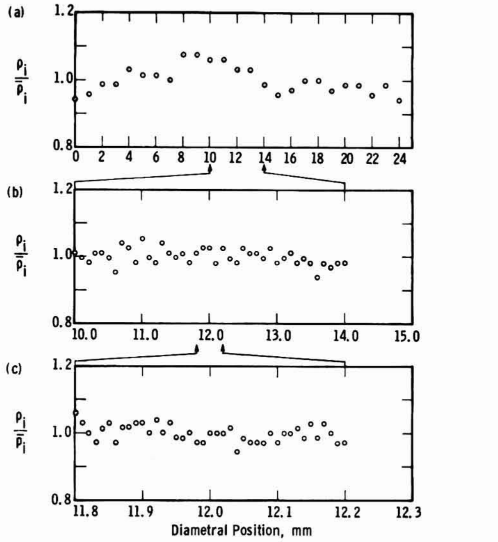

Fig. 10. $\rho_i/\bar{\rho}_i$ vs. diametral position coordinate in a 28 ohm-cm vapor-deposited epitaxial crystal: (a) 1.0 mm scale, $s/\bar{\rho}_i = 0.039$; (b) 0.1 mm scale, $s/\bar{\rho}_i = 0.023$; (c) 0.01 mm scale, $s/\bar{\rho}_i = 0.025$.

Figure 10 shows a sample of 28 ohm-cm, n-type epitaxial silicon produced in our laboratories. It may be seen that the epitaxial sample, at least produced under the conditions used here, is very uniform in resistivity, both across the whole of the diameter of a 25 mm slice, and on the fine-scale as well, with the total scatter of all of the resistivity values lying in the range of plus or minus 7%.

Where a comparison may be made, these results agree with those of Benson (4) relating to radial resistivity variations in Czochralski crystals. They also provide experimental support for a model involving convection currents in the liquid as the primary cause of resistivity inhomogeneities in melt-grown silicon (5). If this model is indeed an accurate one, the greater resistivity homogeneity of silicon web and epitaxial silicon may be then understood as the result of the rapid growth rate of web from its supercooled melt and, in the case of the vapor-grown epitaxial material, as due to the complete absence of a liquid phase.

Summary and Conclusions

The quantitative results of these measurements are summarized in Table I. Note especially the values given for the ratio s (0.1 mm scale) to s(0.01 mm scale). The tabulated data suggest that two parameters

Table I. Quantitative results of measurements

Growth process	Over-all average resistivity, $\bar{\rho}$ (ohm-cm)	s/ρ_i, 0.1 mm scale	s/ρ_i, 0.01 mm scale	Surface finish	s, 0.1 mm scale / s, 0.01 mm scale
Czochralski	10	0.067	0.031	Alumina polish	2.2
Czochralski	14	0.185	0.024	Alumina polish	7.7
Czochralski	175		0.038	Alumina polish	—
Czochralski	175		0.032	Chemical polish	—
Float-zone	0.7		0.029	Chemical polish	—
Float-zone	0.7	0.060	0.022	Alumina polish	2.7
Float-zone	250	0.37	0.42	Alumina polish	0.88
Crucible-less	44	0.079	0.037	Alumina polish	2.1
Web	0.31	0.039	0.027	Alumina polish	1.4
Vapor-deposited	28	0.023	0.025	Alumina polish	0.92

may be conveniently used to establish crystal quality insofar as resistivity inhomogeneity is concerned. These are the fine-scale (0.01 mm scale) fractional standard deviation of resistivity and the ratio of the coarse-scale value of fractional standard deviation to the fine-scale value. With these parameters determined in accordance with the procedures used in this work, a low value of $s/\bar{\rho}_i$ (0.01 mm scale) and a near-unity value of the ratio of $s/\bar{\rho}_i$ (0.1 mm) to $s/\bar{\rho}_i$ (0.01 mm) indicates uniform resistivity silicon. It is essential to note that both criteria must be met to rate material as truly homogeneous.

In conclusion, while this work cannot support a final judgment of the relative worth of material produced by the various growth processes, it does show that significant variations in local resistivity do exist in at least some silicon samples and that the spreading resistance technique may be used to advantage in investigating the problem of resistivity inhomogeneity in silicon. Further work must be done, especially in comparing device yields to crystal "quality" as defined above, to determine the real importance of these measurements.

Manuscript received Aug. 18, 1966; revised manuscript received Oct. 24, 1966. This paper was presented at the Cleveland Meeting, May 1-6, 1966.

Any discussion of this paper will appear in a Discussion Section to be published in the December 1967 JOURNAL.

REFERENCES

1. H. F. John, J. W. Faust, Jr., and R. Stickler, *IEEE Trans. Parts, Materials and Packaging*, September 1966.
2. E. Tannenbaum, *Solid-State Electron*, **2**, 123 (1961).
3. R. G. Mazur and D. H. Dickey, *This Journal*, **113**, 255 (1966).
4. K. E. Benson, *Electrochem. Tech.*, **3**, 332 (1965).
5. A. Mueller and M. Wilhelm, *Z. Naturforschung*, **19a**, 254-263 (1964).

The Solidification of Bi_2Te_3 and Its Solid Solutions with Bi_2Se_3 and Sb_2Te_3 under the Influence of Ultrasonic Agitation

H. E. Bates and Martin Weinstein

Tyco Laboratories, Inc., Waltham, Massachusetts

ABSTRACT

The effect of ultrasonic agitation during solidification was studied for three systems: Bi_2Te_3, 0.8 Bi_2Te_3-0.2 Bi_2Se_3, and 0.25 Bi_2Te_3-0.75 Sb_2Te_3. Reduction in grain size was most pronounced in 0.8 Bi_2Te_3-0.2 Bi_2Se_3; the other compositions showed relatively little refinement. A definite tendency for alignment of acicular grains with low intensities of ultrasonic irradiation was noted in all three systems. Compressive fracture stress was increased by agitation for all three systems with considerable anisotropy of strength, relative to the growth direction, occurring in agitated and unagitated material. Highest fracture strength was found in 0.8 Bi_2Te_3-0.2 Bi_2Se_3, 7000 *vs.* 5000 psi for unagitated material. Reduction in length was about equal at 3%. Seebeck coefficient and resistivity were measured as functions of temperature and found to exhibit a difference between agitated and unagitated material which correlated with the amount of grain refinement observed. This is a result of the crystallographic anisotropy of electrical properties in Bi_2Te_3 alloys, reflected by the degree of misorientation caused by ultrasonic agitation.

During the course of investigating the effects of ultrasonic energy on the solidification of thermoelectric materials (1, 2), experiments were carried out with Bi_2Te_3 and some of its technologically interesting alloys. It was of specific interest to observe the effect of ultrasonic agitation on the solidification behavior of these materials because of their highly anisotropic nature.

Other investigators (3-5) have observed coarsening of acicular crystallites in solidified eutectic structures with sonic and ultrasonic vibrations. These are the only instances of the effects of vibration on the solidification of crystals having strong acicular growth habits. In addition Bi_2Te_3 alloys are susceptible to segregation during freezing, requiring either elaborate zone-leveling techniques to produce homogeneous ingots or preparation of thermoelements by powder metallurgical techniques which introduce a number of difficulties with contamination (6) and sintering and grain size effects (7, 8). The results of our investigations with PbTe materials indicated the possibility of considerably enhancing the mechanical properties and improving the homogeneity of cast ingots of Bi_2Te_3 and related alloys.

Thus, the purpose of the present work was to explore the effect of ultrasonic agitation during solidification of a class of alloys exhibiting highly anisotropic growth and to observe the consequences of this method of preparation on the mechanical and electrical properties of these alloys.

Experimental

The experimental procedures and apparatus have been described in detail previously (1, 2). The assembly used to solidify the melts with ultrasonic agitation is shown in Fig. 1.

A charge of 50-75g was sealed under vacuum in the quartz tube. A resistance furnace was lowered over the tube and heated until the charge had melted, as indicated by a thermocouple attached at the base of the tube. After a short period at a temperature 30°-40° above the melting point, the piezoelectric transducer, epoxied to the base of the quartz pedestal, was energized. The furnace was then raised by a motorized hoist so that solidification proceeded upward from the bottom of the ingot at a rate defined by the rate of removal of the furnace. As the freezing interface moved upward, the input frequency to the piezoelectric crystal was varied slightly to maintain a resonant condition. The input power was also increased gradually to compensate for increasing attenuation of the ultrasonic energy in the solidified portion of the

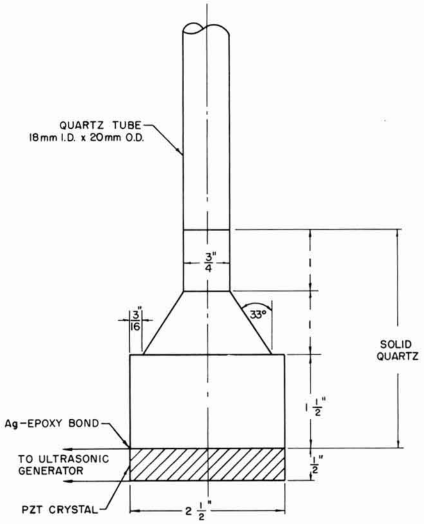

Fig. 1. Piezoelectric transducer, quartz concentrator, and crucible assembly.

melt. Energy intensities varied from 1-9 w/cm^2 at frequencies of approximately 21 and 33-35 kc. Solidification rates were varied from 6.3 x 10^{-3} to 14.1 x 10^{-3} mm/sec.

Results

The effect of ultrasonic agitation during solidification was to cause some reduction in grain size in all three materials. The most interesting result was the varying responses to agitation of three materials of identical structure. Bismuth telluride is rhombohedral with atoms arranged in a sequence Te-Bi-Te-Bi-Te . . . Te with adjacent Te atoms probably bonded only by van der Wall's forces (9). This structure accounts for the anisotropic transport processes and easy cleavage of Bi_2Te_3. Bismuth selenide and antimony telluride form complete isomorphous pseudobinary solid solutions with Bi_2Te_3.

Macrophotographs (Fig. 2) show the gross structure of two ingots of 0.8 Bi_2Te_3-0.2 Bi_2Se_3, the one on the left directionally solidified, the one on the right directionally solidified with 8 watts/cm^2 of ultrasonic agitation for approximately two-thirds of its length. Both were grown at the same rate of 1.1 iphr. The coarse acicular grain structure of the unagitated ingot is plainly visible, while in the lower half of the agitated ingot the grains cannot be resolved. The various bands in the agitated ingot are the result of changes in the frequency of the ultrasound to maintain resonance and of turning off the ultrasonic input for a short period at one point. The microstructures of these ingots are shown in Fig. 3 and 4. It is interesting to note here that the very finest grains found in the agitated material were still basically acicular. Figure 3 is not truly representative of the structure of the unagitated material since none of the very large grains are shown. The bismuth telluride-bismuth selenide showed the greatest reduction in grain size of all three systems. The average grain size (length) in the agitated material was approximately 30 times less than that of the unagitated, directionally solidified material.

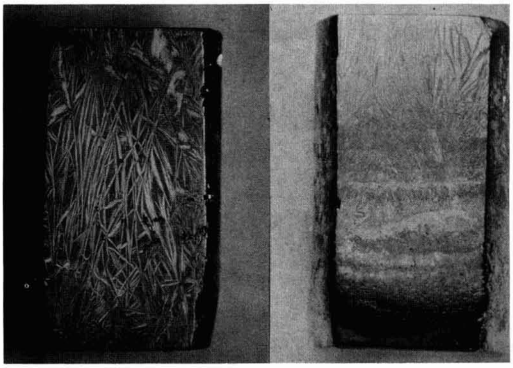

Fig. 2. Macrostructure of 0.8 Bi_2Te_3-0.2 Bi_2Se_3 ingots: (a) directionally solidified; (b) directionally solidified with ultrasonic agitation. Magnification 1½X.

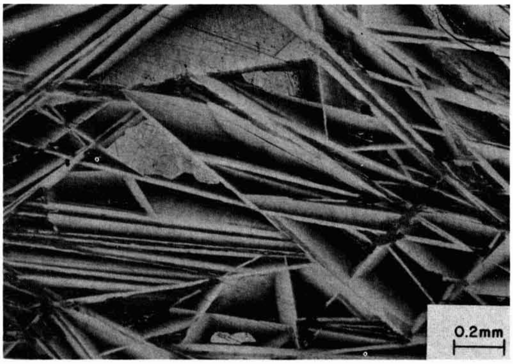

Fig. 3. Microstructure of directionally solidified 0.8 Bi_2Te_3-0.2 Bi_2Se_3. Magnification *ca.* 35X.

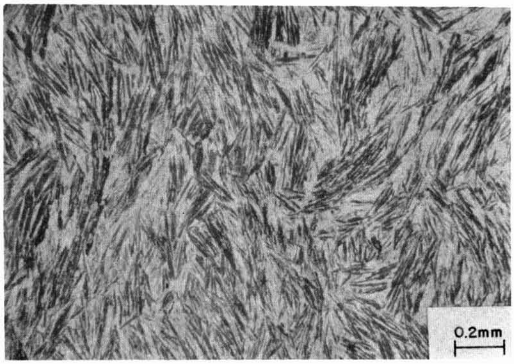

Fig. 4. Ultrasonically agitated 0.8 Bi_2Te_3-0.2 Bi_2Se_3. Magnification *ca.* 35X.

The structure of the unagitated Bi_2Te_3 was virtually identical to that of the Bi_2Te_3-Bi_2Se_3 shown in Fig. 3. A transverse section at the bottom of an agitated ingot of Bi_2Te_3 is shown in Fig. 5. The ultrasonic energy intensity was approximately 6 w/cm^2 and growth rate 1.1 iphr. It is obvious that while the grains here are fairly long, they are considerably more "blocky" than those in the Bi_2Te_3-Bi_2Se_3. The top of an ingot similarly prepared is shown in Fig. 6; the grains are very needle-like here. The top ends of the ingots, which were 1.5 to 1.75 in. long, received substantially less agitation than the bottom portions because of increased attenuation in the solidified portion of the ingot. The intensity applied to the top section may have been about 1w/cm^2 or less. This is a clear example of the application of increasing ultrasonic energy tending to promote an increasingly equiaxed structure. Grain size reduction in the lower portions of agitated ingots was of the order of 10 or 12:1. An

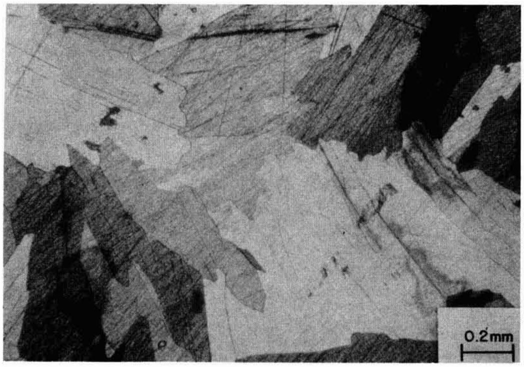

Fig. 5. Microstructure of Bi_2Te_3 solidified with ultrasonic agitation; bottom section of ingot. Magnification *ca.* 35X.

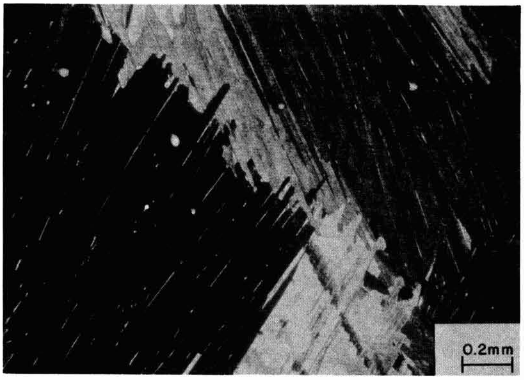

Fig. 6. Microstructure of top section of Bi_2Te_3 of Fig. 5, transverse section. Magnification *ca.* 35X.

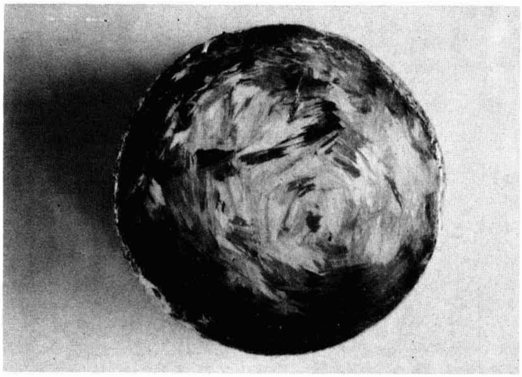

Fig. 7. Macrostructure of Bi_2Te_3 ingot showing crystallite alignment by low intensity vibrations in top section. Magnification 1½X.

Fig. 8. Microstructure of directionally solidified 0.25 Bi_2Te_3-0.75 Sb_2Te_3. Magnification *ca.* 35X.

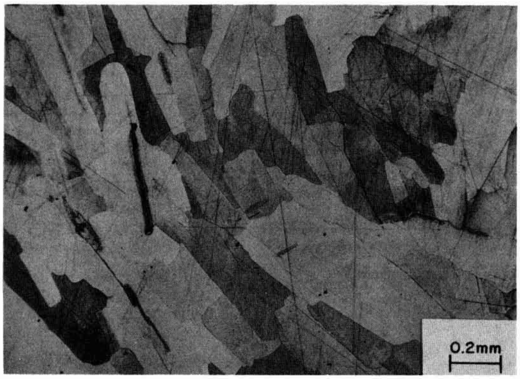

Fig. 9. Ultrasonically agitated 0.25 Bi_2Te_3-0.75 Sb_2Te_3. Magnification 35X.

interesting phenomenon was observed in the top sections of agitated ingots of all three materials. particularly bismuth telluride and bismuth-antimony telluride. An example from Bi_2Te_3 is shown in Fig. 7. The grains in this case tend to line up with their long axes roughly parallel to the circumference thus giving the somewhat spiral appearance to the gross structure. This was apparently the result of low intensity radial vibrations of the system. Such an effect of low intensity vibrations could be of benefit in producing an oriented structure in the materials so as to take advantage of the anisotropic thermoelectric properties.

Bismuth-antimony telluride, when solidified quickly, grows in acicular grains which are severely segregated on a microscale. We found this in water-quenched material and to some extent in ingots grown at more than two inches/hr. Solidification at 0.9 iphr produced the microstructure of Fig. 8. This unagitated ingot exhibited a wide range of grain sizes, the majority tending to a length/diameter (l/d) ratio of about three. Significant grain refinement was difficult to achieve in this system. Figure 9 shows the microstructure of the agitated material. (Ultrasonic energy intensity was 8-9 w/cm^2.) The grains retain approximately the same l/d ratio, while a reduction in average size of about 6-8:1 has occurred. A tendency to greater ratios of length to width in the grains of the top section was found in both agitated and unagitated ingots. The grains of the agitated ingots showed an alignment with the side of the crucible similar to that in Bi_2Te_3.

Compressive strength.—The compressive fracture strengths were measured on samples cut parallel and perpendicular to the growth direction of the ingots as shown in Table I. Samples were mainly in the shape of rectangular blocks about 0.25 in. on a side by 0.4-0.5 in. long. A Hounsfield Type W Tensometer was used for the tests. The agitated material showed

Table I. Compressive fracture strength parallel to growth direction

Material	Compressive fracture strength, psi	Total strain at fracture, in/in
Bi_2Te_3 (agitated)	3,500	0.03
Bi_2Te_3 (unagitated)	2,500	0.02
0.8 Bi_2Te-0.2 Bi_2Se_3 (agitated)	7,000	0.030
0.8 Bi_2Te_3-0.2 Bi_2Se_3 (unagitated)	5,000	0.026
0.25 Bi_2Te_3-0.75 Sb_2Te_3 (agitated)	6,500	0.016
0.25 Bi_2Te_3-0.75 Sb_2Te_3 (unagitated)	2,300	0.08

a definite increase in strength over the unagitated for all three materials.

Considerable anisotropy of strength was found in all the materials. Fracture strength perpendicular to the growth direction was 50-60% of that parallel to the growth direction in unagitated samples. In the agitated samples strength perpendicular to the growth direction was 70-80% of that parallel. Grains grow in these materials as a rule with their cleavage planes parallel to the heat flow. In the unagitated, directionally solidified ingots the grains were generally aligned with the growth direction. Thus, compression parallel to the growth direction was also parallel to the cleavage plane.

Compression perpendicular to the growth direction is averaged over all angular orientations of the cleavage plane with respect to the compression direction. Thus in compressing perpendicular to the growth direction some favorably oriented grains reach the critical shear stress for slip or cleavage in the basal plane at a fairly low over-all stress level. In compressing parallel to the growth direction, where the cleavage planes are essentially all parallel to the stress axis, the over-all stress level must approach the critical shear stress for slip and/or cleavage. The samples of agitated material, however, with decreased orientation of the grains with the growth direction, exhibit strengths more nearly equal in the two directions. That the agitated materials showed generally higher strengths may be attributed to their finer grain sizes. A fine grain size increases the strength by limiting the propagation of slip or cleavage in any given grain through the interference of the more numerous grain boundaries.

Electrical properties.—Measurements of the Seebeck coefficient and resistivity as functions of temperature were made parallel to the growth direction on all ingots. The results of these measurements are shown as α^2/ρ (volt^2/°C — ohm cm) in Fig. 10-12 for 0.8 Bi_2Te_3 — 0.2 Bi_2Se_3 + 0.04% CuBr (n-type), Bi_2Te_3 + 0.04% Pb (p-type), and 0.25 Bi_2Te_3 — 0.75 Sb_2Te_3 + 0.05% Pb + 0.03% Cd (p-type). The values shown are in generally good agreement with those reported by most other authors for these materials.

The curves reflect the effect of the ultrasonic agitation in disturbing the orientation of the grains with the growth direction. With the cleavage planes generally oriented in the growth direction, the unagitated materials exhibit higher electrical efficiency factors. Madigan (10) predicted a reduction of 28% in the figure of merit of randomly oriented polycrystalline rods of Bi_2Te_3 *vs.* oriented single crystals, while Piwkowski (8) finds differences of 25-60% in the figure of merit of single crystal compared with pressed and sintered Bi_2Te_3.

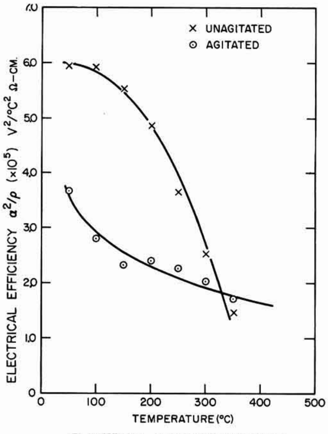

Fig. 10. Electrical efficiency factor of 0.8 Bi_2Te_3-0.2 Bi_2Se_3 measured parallel to growth direction.

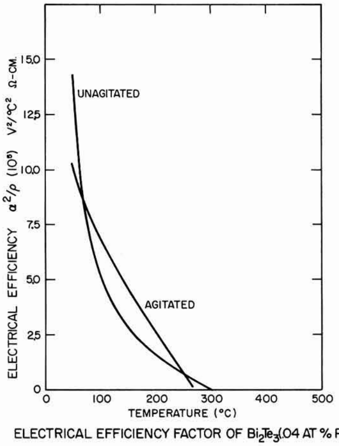

Fig. 11. Electrical efficiency factor of Bi_2Te_3 (0.04 a/o Pb) measured parallel to growth direction.

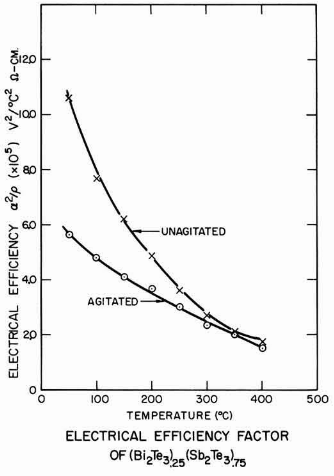

Fig. 12. Electrical efficiency factor of 0.25 Bi_2Te_3-0.75 Sb_2Te_3 measured parallel to growth direction.

The sharper decrease of α^2/ρ with increasing temperature for the unagitated Bi_2Te_3 — Bi_2Se_3 and Bi_2Te_3 —Sb_2Te_3 can be attributed to somewhat poorer chemical homogeneity than the agitated material. This is ultimately reflected in a less regular behavior than that exhibited by the agitated material.

Conclusions

1. Significant grain refinement was obtained in the Bi_2Te_3 — Bi_2Se_3 system by ultrasonic agitation of the melt during solidification. Little refinement was observed in the Bi_2Te_3 and Bi_2Te_3 — Sb_2Te_3 systems.
2. A tendency for alignment of acicular grains parallel to the crucible wall was noted at low ultrasonic intensities.
3. The Seebeck coefficient and resistivity as a function of temperature exhibit a difference between agitated and unagitated material which correlates with the amount of grain refinement. This is a result of the crystallographic anisotropy of electrical properties in Bi_2Te_3 alloys, reflected by the degree of misorientation caused by ultrasonic agitation.

Acknowledgments

The authors wish to thank Mr. E. J. Sherwin for his expert experimental aid. This work was performed under Contract NObs-86015 for the Bureau of Ships, Department of the Navy.

Manuscript received Aug. 18, 1966. This paper was presented at the Cleveland Meeting, May 1-6, 1966.

Any discussion of this paper will appear in a Discussion Section to be published in the December 1967 JOURNAL.

REFERENCES

1. M. Weinstein, *Trans. AIME*, **230**, 321 (1964).
2. H. E. Bates and M. Weinstein, *This Journal*, **112**, 693 (1965).
3. M. J. Berger and W. Rostoker, *Foundry*, **81** [7], 100 (1953).
4. R. S. Richards and W. Rostoker, *Trans. ASM*, **48**, 884 (1956).
5. R. G. Garlick and J. F. Wallace, *Trans. AFS*, **67**, 366 (1959).
6. R. A. Horne, "Direct Conversion of Heat to Electricity," J. Kaye and J. Walsh, Editors, John Wiley & Sons, Inc., New York (1960).
7. C. Kolm and J. J. Giacalone, "Properties of Elemental and Compound Semiconductors," H. C. Gatos, Editor, Interscience Publishers, New York (1960).
8. T. R. Piwkowski, *Adv. Energy Conv.*, **4**, 247 (1964).
9. M. H. LaChance and E. E. Gardner, *ibid.*, **1**, 133 (1961).
10. J. R. Madigan, *J. Appl. Phys.*, **33**, 3564 (1962).

Nucleation and Growth of Crystals in Gels

J. Dennis and H. K. Henisch

Materials Research Laboratory, The Pennsylvania State University, University Park, Pennsylvania

ABSTRACT

Because the crystals in any one-growth system grow competitively, nucleation control is one of the keys to the practical exploitation of the gel-growth technique. The paper discusses some of the principal factors on which nucleation in gels depends and shows how nucleation can be controlled by programming of the reagent concentrations, by trace impurities, and by varying the gel structure. Multiple reseeding procedures are described which permit the growth of larger crystals than can be obtained with single growth stages.

Studies of nucleation have in the past been hampered by the lack of sufficiently simple systems on which meaningful experiments could be performed and by the general difficulty of controlling the processes involved. For such studies, the gel method (1, 2) offers new opportunities. The crystals grow within the gel, in the same localities in which they nucleate and in chemical environments which can be locally analyzed. Once nucleation has taken place, the growth has been shown to be diffusion controlled (2). This paper describes the results of nucleation experiments and shows how they can be at least qualitatively understood in terms of critical radius theory. It also provides an explanation for the photonucleation phenomena previously reported (1) and describes procedures which promote orderly growth through nucleation control.

The growth procedures are simple, even though the associated chemical and diffusion processes are not. Gels of 1.06 g/cm^3 density are made from solutions of sodium metasilicate, in the presence of varying acid concentrations. The acid in question may be one of the reagents participating in the formation of the crystal material. The other reagent is placed as a solution on top of the gel and allowed to diffuse. Alternatively, a nonacid reagent may be added to the sodium silicate solution before gelling, in addition to an acid which then serves only to adjust the *p*H. There are various possibilities, as the following examples will make clear:

(*a*) Growth of calcium tartrate crystals:
Present in the gel: tartaric acid, (initially *p*H 2.7), Diffusing into the gel: calcium chloride (initially 1*N*).

(*b*) Growth of lead iodide crystals, PbI_2:
Present in the gel: lead acetate and acetic acid, (initially *p*H 4.0), Diffusing into the gel: potassium iodide (initially 0.1*N*, increasing to 0.5*N*).

(*c*) Growth (3) of lead hydroxy iodide crystals, $PbI(OH)$:
Present in the gel: acetic acid and potassium iodide (initially *p*H 8.5), Diffusing into the gel: lead acetate (initially 0.2*N*).

It has already been shown that a variety of crystals suitable for solid-state experimentation can be produced in similar ways. The method is especially useful for substances which, because of their low solubilities or low dissociation temperatures (or both) cannot readily be grown by other methods. Since the crystals in any one growth system grow competitively, control of the nucleation process is in many cases a key to the practical utility of the method.

Heterogeneous and Homogeneous Nucleation

The most readily accountable form of nucleation is "heterogeneous," in the sense that it depends on the presence of foreign substrates. It is easy to demonstrate (*e.g.*, by dispersing inert crystalline powders) that it can take place in a gel. There is no reason for expecting heterogeneous nucleation in a gel to be generically different from corresponding process in simple solution, but the frequency of its occurrence is not the same. Thus, most of the accidentally present dust grains which would ordinarily be eligible as nuclei in solution are immobilized by the presence of the gel, perhaps because they are embedded in small cells. In such circumstances, very thin layers of crystal may grow on them, but insufficient material would be available to permit growth beyond submicroscopic size. Alternatively, since the gelling process itself is believed to depend on the presence of foreign nucleation centers, most of the available substrates may be used up by the time gelling is complete. What ever the mechanism, the immobilization of unwanted nucleation centers is believed to be one of the important factors governing the success of the gel method.

Heterogeneous nucleation can be utilized for epitaxial growth and may become important in connection with the growing interest in heterojunctions. In passing, heterojunctions of $PbI_2/PbI(OH)$ and $CaC_4H_4O_6/CuC_4H_4O_6$ have been gel-grown in this way.

There are, however, reasons for believing that much and sometimes most of the nucleation observed in reasonably low dust content gel media is "homogeneous," *i.e.*, that it depends on the formation of critical

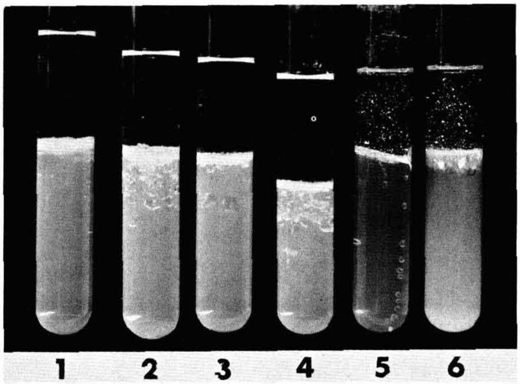

Fig. 1. Experiments on nucleation control: 1, 2, 3, 4, calcium tartrate, 5, 6, lead iodide; 1, 2, *p*H 3.5; 3, *p*H 2.5; 4, *p*H 2.8; 5, 6, *p*H 4.1. Artificial nuclei present in tubes 2, 3, 4 and 6; the round objects in tube 5 are bubbles.

nuclei. This follows in part from the enormous supersaturations which prevail in the gel, from the distribution of crystals in any given growth system, and from the time-sequence of their appearance. If nucleation were heterogeneous, the final distribution should in the normal way be uniform, corresponding to a uniform dust-distribution, but this is not in fact observed. There is, in principle, the possibility (4) that the diffusing reagent may create its own foreign substrates by reacting with impurities in the resident reagent, thereby creating a nonuniform distribution of nuclei. However, this would involve rather specialized conditions and, as a general mode of operation, seems unlikely. Epitaxial growth on a foreign substrate generally calls for lower supersaturations than homogeneous nucleation, and a corresponding demonstration is shown on Fig. 1. Tubes 1 and 2 contain, above the gel, the same solution of $CaCl_2$. The gel in tube 1 is free of deliberately added foreign nuclei and is seen not to support any crystal formation because the $CaCl_2$ concentration is too low. Some accidental unwanted dust grains are undoubtedly present but are evidently immobilized by the gel. Tube 2 contains heterogeneous nuclei in the form of fine titanium dioxide dust and supports copious nucleation. The number of crystals formed is still much smaller than the total number of TiO_2 grains present, showing that, in the presence of very high dust concentrations, the gel cannot immobilize all the potential nucleation centers. Tubes 5 and 6 provide the same demonstration for PbI_2. A similar difference can be observed by varying the *p*H in the gel. One would expect the homogeneous nucleation of calcium tartrate to be sensitive to the acidity of the gel, considering that the material is appreciably soluble in tartaric acid. In fact, crystal formation in a clean system is rare below *p*H 3. In the presence of artificial nuclei, *p*H is still an important factor but crystals appear in gels which are considerably more acidic. Tubes 3 and 4 on Fig. 1 show this, the acidities being 2.5 and 2.8, respectively.

Nucleation Control through Concentration Programming

The above considerations lead (in low dust-content gel media) to a simple method of nucleation control. The concentration of the diffusing reagent is initially kept below the level at which nucleation is known to occur. It is then increased in a series of small steps, which can be optimized for any system as regards magnitude and timing. At some stage, a few nuclei begin to form. As the concentration of the diffusant increases, these nuclei act as sinks, and the resulting establishment of radial diffusion patterns reduces concentrations and appears thus to inhibit the formation of additional nuclei. Subsequent increases of reagent concentration lead to faster growth but not, in general, to new nucleation. The existing crystals are thus able to grow noncompetitively and their quality is correspondingly good. It has been found empirically that frequent small steps are more beneficial than a few large concentration increases. The method has been successfully applied to the control of nucleation in several systems (Table I), and has yielded crystals of larger size and a higher degree of perfection than those produced without programming. The size increase amounts to approximately a factor of 3, except for calcium tartrate for which nucleation is rare enough even without programming to reduce the importance of the competitive growth limitation.

Table I. Effect of concentration programming on crystal size

Crystal	Typical sizes: largest linear dimensions, mm	
	Without programming	With programming
Calcium tartrate	~12	~12
Cuprous tartrate	1	3
Lead iodide	3	15
Thallium iodide	0.5	1.5
Calcium carbonate (aragonite spherulites)	0.5	1.5
Cadmium oxalate	2	5

It remains to be shown that the method can be more generally applied, the present indications being that it can.

Effect of Trace Impurities and Molecular Volume

The theory of homogeneous nucleation via critical nucleus formation in solution is still only imperfectly understood (5, 6). Under the simplifying assumptions envisaged by the Kelvin equation and the Gibbs-Duhem relationship, the radius r_c of the critical nucleus forming in a solution would be given by

$$r_c = \frac{2\sigma V_s}{kTS}$$

where V_s is the molecular volume of the solute, S the supersaturation, and σ the surface energy per unit area (closely related to the surface tension and identical with it under simplest conditions). By analogy with other interface parameters, σ is expected to be selectively sensitive to the presence of contaminants, especially since the free energy of nucleus formation (7) depends on σ^3. It is certainly true that solution processes can be affected sensitively by the presence of contaminants in the low ppm range (8). For the calcium tartrate system, the most potent contaminant

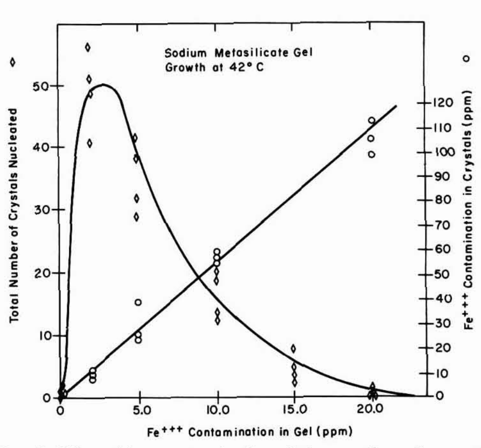

Fig. 2. Effect of iron contamination of the growth medium on the nucleation and composition of calcium tartrate crystals.

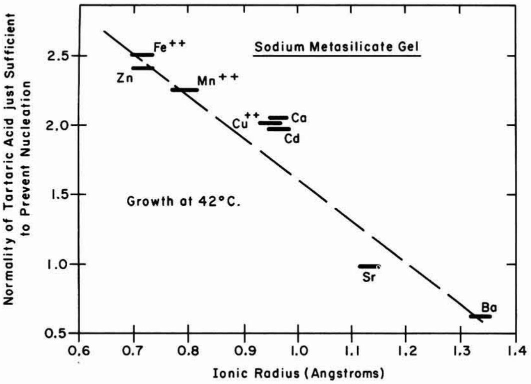

Fig. 3. Effect of molecular volume on critical nucleus formation of tartrates.

was found to be iron. Results which show its effect are given in Fig. 2 and the relationship is evidently not simple. A very small concentration of ferric ions promotes nucleation; larger concentrations inhibit it, whereas the uptake of iron by the crystal itself (spectroscopically determined) increases uniformly as expected. That the growing crystals become enriched in contaminant appears to be a peculiarity associated with iron. There is, of course, infinite scope for investigations of this kind, using different combinations of crystals and potential contaminants. General predictions cannot as yet be made.

The previously reported observations of photonucleation can, in all likelihood, be understood in similar terms, *i.e.*, as an indirect effect of light on σ. It has long been known (9) that light (especially uv) dissociates tartaric acid with the production of CO_2, which can easily be shown to enhance the nucleation of calcium tartrate crystals. This can be demonstrated convincingly by comparing a series of growth systems, maintained in darkness, but with different amount of CO_2 additive in the gel.

In a manner similar to that demonstrated above, a correlation can be established between nucleation frequency and the molecular volume of the solute, as suggested by the approximate calculation of the critical radius. For this purpose it is actually convenient to use, as an index of comparison, not the probability of nucleation as such, but the normality of the acid on the gel which is just sufficient to suppress nucleation. Its correlation with the ionic radius of the metal is shown in Fig. 3 for a series of tartrates grown under otherwise identical conditions. The radius may be taken as a relative measure of molecular volume.

Effect of Gel Structure

If the views expressed above are correct, then one would expect nucleation to be more difficult in gels of smaller cell size. In order to test this, it is necessary to have some method whereby gels can be compared from this point of view, at least in a semiquantitative manner. Quantitative work on hydrogels is, of course, hampered by their complicated structure and, in particular, by the fact that not only the mean cell dimensions but also the size distribution about this mean can vary. However, by allowing a compound of large molecular volume to diffuse, an empirical relative measure of effective cell size can be obtained. In the present case, this was done by observing the diffusion of methyl-blue in gels of varying Si:Al ratio. The diffusion process is monitored by making light absorption measurements as a function of distance from the gel surface. As Fig. 4 shows, diffusion becomes more difficult as the amount of Al increases, and it is reasonable to conclude that this is due to progressively diminishing cell sizes. Al certainly has this effect on the cell dimensions of dehydrated gels, as Plank and Drake (10) have demonstrated.

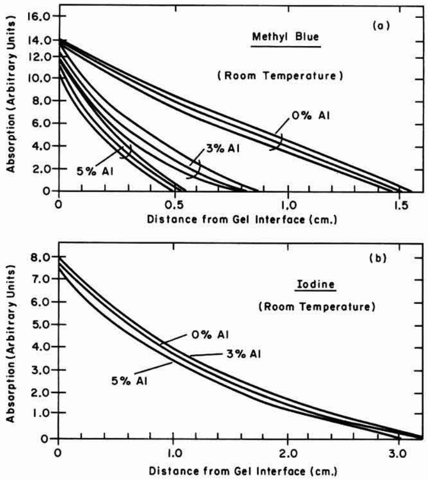

Fig. 4. Effect of alumina content on the diffusion of methyl blue and iodine in sodium metasilicate aluminate gels, assessed by optical absorption measurements.

Table II shows how, under a standard set of conditions, the number of crystals nucleated depends on gel composition and thus evidently on the cell size. The expected correlation is observed and Table II, incidentally, gives an impression of the extent to which the results vary between growth tubes of the same composition and thermal history. It is, however, necessary to check that the various gels used do not present different diffusion conditions to the reagents involved in crystal formation. When the diffusants are very small compared with the cell size, the cell size should have no material effect on the diffusion process. Figure 4 shows that (for iodine) this is indeed correct, and the comparison implied by Table II is therefore valid.

Reseeding Procedures

Once nucleated, the crystals grow until they reach a constant size. It has already been shown that this size is determined by the progressive exhaustion of the reagents (1). Replenishment of at least one (the diffusing) reagent is a simple matter, but the removal of the waste products of the reaction is not. If, therefore, a crystal of larger size is required, it must be reseeded into another gel. This is done first by gelling a small amount of sodium metasilicate in a tube, resting the seed on the gel surface thus formed, and covering it first with additional sodium metasilicate solution and, after second gelling, with the diffusing reagent. In the course of transferring the crystal from one growth system to another, its surfaces are generally damaged and possibly contaminated, resulting in polycrystalline growth. To prevent this, the temperature is

Table II. Standard set of conditions.

Crystal	0% Al	3% Al	5% Al	6% Al	8% Al
Calcium tartrate	65, 75, 107, 93	30, 14, 19, 24	7, 0, 13, 6		0, 0, 0, 2
Copper tartrate	536, 324, 342, 441	67, 57, 78, 30		13, 5, 44, 22	
Lead iodide	8, 7, 7, 10	3, 4, 0, 0	0, 0, 0, 0		0, 0, 0, 0

Table III. Weights of three crystals each of calcium and copper tartrate after re-seeding

Crystal	Initial	Weight in mg 1st Seeding	2nd Seeding	3rd Seeding	4th Seeding
Calcium tartrate	137.2	354.0	820.5	939.2	1104.0
	175.6	401.4	873.5	1083.1	1204.1
	139.4	347.0	685.4	803.1	952.3
Copper tartrate	21.2	43.3	63.5	78.4	96.3
	18.7	37.8	69.6	84.4	101.1
	18.4	30.2	66.0	81.7	103.4

raised immediately after reseeding in order to dissolve a portion of the seed, as is usual in all seeding procedures. When the temperature is subsequently lowered, growth proceeds in the normal way until the reagents are once again exhausted. The process can then be repeated. In a series of steps it is thus possible to grow considerably larger crystals than can ordinarily be obtained in a single growth system. The method has not yet been widely applied, but the principle is illustrated below on the basis of calcium and copper tartrate. Table III shows the weights of particular crystals after successive reseeding stages. With care, their high degree of optical perfection can be fully maintained throughout this procedure.

Acknowledgment

This work was supported by contract No. DA 49-083 OSA-3140 with the Advanced Research Projects Agency.

Manuscript received Oct. 12, 1966.

Any discussion of this paper will appear in a Discussion Section to be published in the December 1967 JOURNAL.

REFERENCES

1. H. K. Henisch, J. Dennis, and J. I. Hanoka, *J. Phys. Chem. Solids*, **26**, 493 (1965).
2. H. K. Henisch, J. I. Hanoka, and J. Dennis, *This Journal*, **112**, 627 (1965).
3. H. K. Henisch and J. Dennis, *This Journal*, **112**, 1240 (1965).
4. V. Vand, Private communication.
5. J. W. Gibbs, "Collected Works," p. 78, Longmans Green, Inc., London (1928).
6. D. Turnbull, *Solid State Phys.*, **3**, 225 (1956).
7. A. Van Hook, "Crystallization," p. 107, Reinhold Publishing Corp., New York (1961).
8. M. B. Ives and J. J. Plewes, *J. Chem. Phys.*, **42**, 293 (1965).
9. H. A. Spoehr, *Biochem. Z.*, **57**, 95 (1914).
10. C. J. Plank and J. C. Drake, *J. Coll. Sci.*, **2**, 399 (1947).

Characteristics of the Surface-State Charge (Q_{ss}) of Thermally Oxidized Silicon

B. E. Deal, M. Sklar, A. S. Grove, and E. H. Snow

Research and Development Laboratories, Fairchild Semiconductor, Palo Alto, California

ABSTRACT

The nature of the surface-state charge (Q_{ss}) associated with thermally oxidized silicon has been studied experimentally using MOS structures. The effects of oxidation conditions, silicon orientation, annealing treatments, oxide thickness, and electric field were examined, as well as the physical location of the surface-state charge. The results indicate that the surface-state charge can be reproducibly controlled over a range 10^{10}-10^{12} cm^{-2}, and that it is an intrinsic property of the silicon dioxide-silicon system. It appears to be due to an excess silicon species introduced into the oxide layer near the silicon during the oxidation process.

In much of the early work on the properties of semiconductor surfaces, experimental results were interpreted within the framework of two quantities: fast and slow surface states (1). "Fast surface states" are electronic states within the forbidden gap of the semiconductor, located at the surface, which are in good electrical communication with the semiconductor bulk. Because of this, they can act as surface recombination centers. Their density per unit area for both clean germanium and silicon surfaces has been generally found to be of the same order as the surface atom density. If the semiconductor is covered by an adsorbed layer, or an oxide, the density of fast states has been found to decrease to 10^{11}-10^{12} cm^{-2}. "Slow states," in contrast, have been attributed to ionic contamination within an oxide covering the semiconductor surface. Because of their relatively large distance from the semiconductor, they are in poor electrical communication with it. Their density is a strong function of the ambient and surface treatment of the sample, but generally ranges in the neighborhood of 10^{12}-10^{13} cm^{-2}.

In the past several years, the thermally oxidized silicon surface has been investigated very intensively, partly due to its extreme technological importance and partly to the ease with which its characteristics can be studied (2). As a result of these investigations, a detailed picture of this system has emerged which is not explainable strictly within the framework of fast and slow surface states.

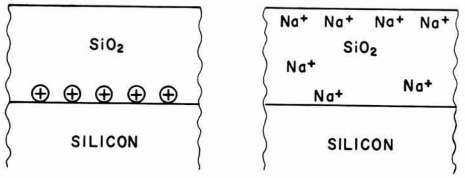

(a) SURFACE-STATE CHARGE, Q_{ss} (b) MOBILE IMPURITY IONS

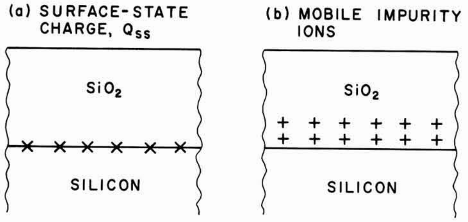

(c) FAST SURFACE STATES (d) TRAPS IONIZED BY RADIATION

Fig. 1. Charges or states associated with the silicon dioxide-silicon system.

An idealized representation of the current picture of the thermally oxidized silicon system is depicted in Fig. 1. Fast surface states have been identified, but in many cases their density has been found to be less than 5 x 10^{10} cm^{-2} (3), considerably lower than in other systems, thus leading to the low surface recombination velocity of passivated silicon devices (4). While slow surface states, in the customary sense, have not been evident, ionic space charges within the oxide have been observed. These were found to result from either contamination by relatively mobile ions such as sodium (5, 6), or from exposure to ionizing radiation (7). They are evidently in poor electrical contact with the underlying silicon even when located very near the oxide-silicon interface.

These charges within the oxide, which have generally been found to be positive, induce a negative charge in the silicon, and thereby lead to the tendency of thermally oxidized silicon surfaces to be n-type, as observed already in the earliest experiments (8). On the other hand, it has been shown (3) that even oxides grown in such a manner that ionic contamination was precluded are characterized by a positive charge, apparently located in the oxide, near the oxide-silicon interface. This charge, which has been designated the surface-state charge, and whose density per unit area is denoted by Q_{ss} (3), is the subject of the present paper.

The characteristics of the surface-state charge as established in the earlier study, were the following: (*i*) Its density Q_{ss} is reproducible. For one particular set of conditions [oxidation at 1200°C, in dry O_2; (111) silicon orientation] its density is ~2 x 10^{11} cm^{-2}. (*ii*) Its density is independent of the impurity concentration in the silicon, and of the oxide thickness over a wide range. (*iii*) Its density is independent of the band bending or surface potential in the silicon over at least the middle 0.7 ev of the energy gap. (*iv*) Its density is stable under elevated temperature—bias test conditions of the kind that would lead to rearrangement of sodium contamination in the oxide, or to annealing of radiation-induced space charges.

These characteristics are difficult to reconcile with the conventional picture of slow and fast states at a semiconductor surface. Therefore, a study was undertaken to examine in detail the nature of the surface-state charge. The present paper contains a summary of an extensive experimental investigation dealing with the effect of oxidation conditions, silicon orientation, annealing treatments, oxide thickness, and electric fields on Q_{ss} and with its spatial distribution in the oxide. The primary means of evaluation was the capacitance-voltage method of analysis using metal-oxide-semiconductor (MOS) structures.

Experimental

Materials.—Silicon used in these studies was single crystal Czochralski type. It was obtained from the Kollstan Semiconductor Elements Company of Westbury, New York, in the form of circular slices approximately 2 cm in diameter and lapped on both sides to a thickness of 250μ. Dislocation count was specified to be less than 100 cm^{-2}. Both p- and n-type dopants (boron and phosphorus) were included, the concentrations being ~10^{16} cm^{-3} for most of the experiments. Various surface orientations were studied, including (111), (110), and (100).

Aluminum used for field plates and back contacts was obtained from Cominco Products, Inc., Spokane, Washington, and was specified as 99.9999% pure. A separate analysis indicated the sodium content was 1 ppm or less. Gases used for oxidation and annealing (O_2, N_2, and argon) were obtained in a liquid form from Air Reduction Company, Richmond, California. Total water content was less than 5 ppm in each gas. Special tests indicated other impurities such as hydrocarbons or hydrogen were extremely low, *i.e.*, less than 2 ppm. A molecular sieve trap was used to remove any excess water or hydrocarbons in all gases. Deionized water used for rinsing samples and for wet oxidations had a resistivity at 25°C of 16 megohm-cm and an initial sodium content of less than 0.002 ppm. Although this latter value increased upon storage in the Pyrex or quartz bubbling flask, the analysis of the distillate from the exit end of the oxidation tube indicated 0.030 ppm Na or less.

Procedure.—Immediately prior to oxidation, the silicon slices used for MOS device fabrication were cleaned in both organic and inorganic solvents using ultrasonic agitation. They were then chemically polished in a 4HF:10HNO_3 solution followed by a quench in acetic acid. Approximately 50μ per side were removed during this operation. Appropriate deionized water rinses were used between the various cleaning and polishing steps. Samples used for thickness measurements were mechanically polished resulting in the removal of 30μ per side. The same cleaning as mentioned above was carried out following mechanical polishing.

The oxidation procedure was essentially the same as described earlier (9). Slices were placed flat on a thin quartz boat and inserted in a tube furnace with separate systems being used for n- and p-type samples. Either dry oxygen or wet oxygen (oxygen bubbled through 95°C H_2O) was used as the oxidizing ambient, with the time and temperature of oxidation depending on the specific experiment. Various pulling rates were employed, the standard one being very rapid (less than 3 sec through the 50 cm from the center of the furnace to the end of the tube).

In certain cases, the samples were annealed in either nitrogen or argon following oxidation. Each oxidation contained a slice for thickness evaluation in addition to those samples used for MOS device fabrication and evaluation. Oxide thicknesses were determined on the special test slices using multiple beam interferometry (10). Accuracy of this method was found to be ±40Å for oxides greater than 2000Å and ±20Å for thicknesses less than 2000Å. After oxidation or annealing, the back oxide was removed from selected samples and MOS capacitance-voltage plots obtained using a gold pressure contact probe. The other samples were metallized with aluminum on the top surface after first removing 50-100Å of oxide in a 10:1 H_2O:HF solution to eliminate contamination. The thickness of the aluminum field plate was 2000-5000Å. The back oxide was then removed and aluminum evaporated on the bare silicon. Top field plates 375μ in diameter on 1250μ centers were then prepared by photoresist operations. Finally, the slices were heat treated at 550°C for 2-5 min in dry nitrogen. Most electrical measurements were made on the slice but in certain cases the slices were scribed and broken into individual dice 1250μ square.

Evaluation.—The majority of the electrical evaluations in this investigation involved the determination of the surface-state charge density Q_{ss}. This measurement was accomplished by determining the shift of an experimental MOS capacitance-voltage curve along the voltage axis from the ideal theoretical curve calculated on the basis of assuming no fast surface states or oxide charges and no work function difference between metal and semiconductor. The resulting voltage shift ΔV is related to Q_{ss} by the expression (3)

$$\Delta V = Q_{ss} \frac{x_o}{K_o \epsilon_o} - \Phi_{MS}$$

where Q_{ss} is the surface-state charge density per unit area, $K_o\epsilon_o/x_o$ is the oxide capacitance per unit area, and Φ_{MS} is the metal-semiconductor work function or barrier energy difference. The latter value for aluminum/SiO_2/n-type silicon (10^{16} cm^{-3}) is —0.25v, while for aluminum/SiO_2/p-type silicon (10^{16} cm^{-3}) it is —0.95v (11). In the majority of the experiments, the experimental C-V curve was identical in shape to the theoretical curve so that the shift along the voltage axis was parallel within experimental error.

In general, C-V plots were obtained on a number of units from each slice. The measurements were made by automatically plotting capacitance *vs.* voltage on an X-Y recorder. Capacitance measurement frequency was about 100 kc and measurements were at 25°C. Reproducibility of Q_{ss}/q values was always better than 5×10^{10} cm^{-2} for a particular condition of sample preparation.

Results

Oxidation conditions.—The temperature of oxidation in dry oxygen was found to affect the value of Q_{ss} significantly. A certain reproducible value of Q_{ss} was obtained at any given temperature. This was the case whether the oxide was prepared at that particular temperature, *e.g.*, 1000°C, or prepared at another temperature and then given a final treatment in dry oxygen at 1000°C. This effect was observed with both n-type and p-type silicon.

Typical MOS C-V plots for samples prepared by dry O_2 oxidation of n-type silicon at four different temperatures are shown in Fig. 2. The effect of oxidation temperature on Q_{ss} is clearly demonstrated by the displacements of the different plots from the theoretical curve. More complete data showing the effect of temperature on Q_{ss} are shown in Fig. 3. Both n-type and p-type values are included for temperatures ranging from 550° to 1250°C. All oxide thicknesses for this particular graph are 0.20μ. Above 920°C, the oxides were prepared at the temperature indicated. Below 920°C, the oxides were first prepared at 1200°C and then immediately subjected to the lower temperature for a sufficiently long time (previously determined) that the steady state value of Q_{ss} was reached. This time varied from less than 10 min at 900°C to nearly 1 hr at 550°C. It should be re-emphasized that the values presented in Fig. 3 were obtained by quenching the oxidized silicon slice from the oxidation temperature as described previously.

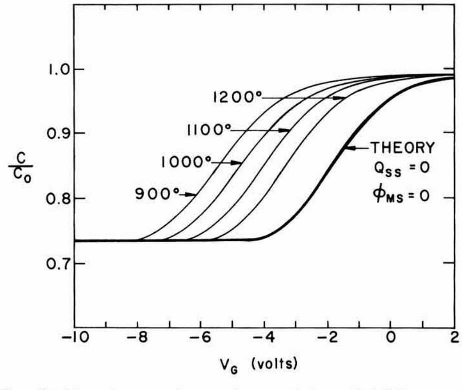

Fig. 2. Capacitance-voltage characteristics of MOS structures prepared by oxidation in dry oxygen at various temperatures [$x_o = 0.20\mu$; $N_D = 1.4 \times 10^{16}$ cm^{-3}; (111) orientation].

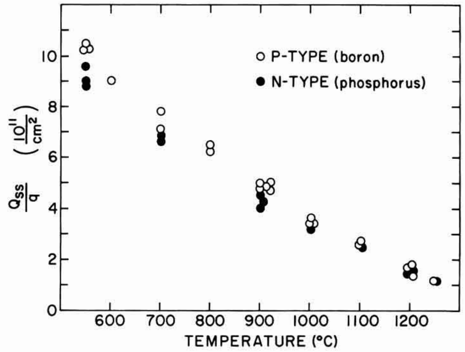

Fig. 3. Effect of oxidation temperature on the surface-state charge density Q_{SS}—dry oxygen [$x_o = 0.20\mu$; N_A, $N_D = 1.4 \times 10^{16}$cm^{-3}; (111) orientation].

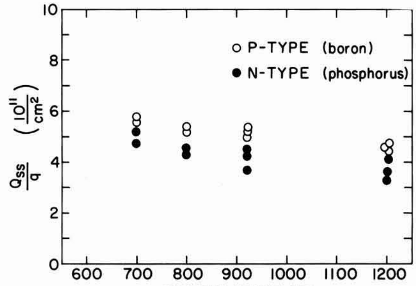

Fig. 4. Effect of oxidation temperature on the surface-state charge density Q_{SS}—wet oxygen (95°C H_2O) [$x_o = 0.20\mu$; N_A, $N_D = 1.4 \times 10^{16}$ cm^{-3}; (111) orientation].

The effect of oxidation temperature on Q_{ss} for the case of oxides prepared in wet oxygen (95°C H_2O) was not nearly so pronounced: Q_{ss} was found to be nearly unchanged between 700° and 1200°C, increasing only slightly with decreasing temperature. Typical data are shown in Fig. 4. Note that at the higher temperatures the Q_{ss} values for wet O_2 are considerably higher than those for dry O_2 oxides, but dry O_2 values are higher below 900°C. Results identical to those shown in Fig. 4 were obtained by oxidation in wet argon (95°C H_2O). By oxidizing under bias in order to exclude contamination, Goetzberger (12) found $Q_{ss}/q = 4 \times 10^{11}$ cm^{-2} for 1000°C, steam oxidation, in agreement with these data.

The increased values of Q_{ss} at lower oxidation temperatures (for dry O_2 oxidation) are directly related to another effect, namely, the dependence of Q_{ss} on pull rate from the oxidation furnace. Typical data are given in Table I for various pull rates from a 1200°C oxidation in dry oxygen. It is evident that the slower the rate of pull, the higher the Q_{ss} value. These observations are easily explained by the fact that the slower the rate of pull, the more time the sample is exposed to oxygen in the lower temperature range, which results in increased Q_{ss} values. The rapid pull ($t < 3$ sec) evidently does not permit sufficient exposure of the samples to oxygen in this temperature range and therefore results in the Q_{ss} value corresponding to the oxidation temperature.

Silicon orientation.—It has been shown (13-15) that silicon orientation affects the surface-state charge density Q_{ss} of MOS devices, *i.e.*, the value of Q_{ss} decreases in the order (111)>(110)>(100). Results obtained in the present study, which are in agreement

Table I. Dependence of surface-state charge density (Q_{SS}) on pull rate in dry O_2 following thermal oxidation

(Samples were oxidized at 1200°C for 60 min. $x_o = 0.2\mu$. Silicon was p-type, boron doped, $C_B = 1.4 \times 10^{16}$ cm^{-3}, (111) orientation. Distance from center to end of tube was 54 cm.)

Pulling time (min)	Pulling rate (cm/min)	Q_{ss}/q (cm^{-2})
<0.05	>1065	1.9×10^{11}
0.167	319	2.8
0.50	106	5.6
1.0	53.3	7.3
2.8	19.0	8.9
34.0	1.6	9.8

Table II. Dependence of the surface-state charge density and the linear oxidation rate constant on silicon orientation

Oxide type	Temp (°C)	Silicon orientation	Q_{ss}/q (cm^{-2})	B/A (μ/hr)
Dry O_2	1200	(111)	1.7×10^{11}	1.12
		(110)	0.6	0.90
		(100)	0.2	0.56
Dry O_2	920	(111)	4.7	0.021
		(110)	2.1	0.018
		(100)	1.7	0.012
Wet O_2 (95°C H_2O)	1200	(111)	4.0	14.40
		(110)	1.7	12.0
		(100)	1.2	7.2
Wet O_2 (95°C H_2O)	920	(111)	5.6	0.406
		(110)	3.6	0.37
		(100)	3.4	0.21

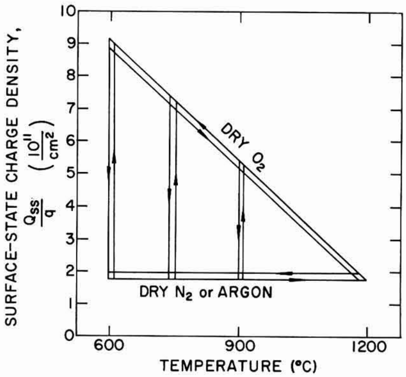

Fig. 5. Illustration of the reversibility of heat treatment effects on the surface-state charge density Q_{ss}.

with those of ref. (13-15), are summarized in Table II, for both dry and wet O_2 oxidation at 1200° and 920°C.

A similar effect of orientation on oxidation kinetics was noted in earlier investigations (9, 16). In particular, it is now known (17) that the silicon orientation influences the linear rate constant B/A, which is proportional to the chemical reaction rate constant at the oxide-silicon interface (17-19). This effect is also indicated in Table II. It is evident that the values of B/A and of Q_{ss} for the three orientations follow similar trends.

Annealing treatments.—A wide variety of annealing effects on the surface condition of thermally oxidized silicon has been reported (20-25).

The effect on Q_{ss} due to annealing in oxygen at temperatures other than that of initial oxidation was already described above. This effect is summarized in Part A of Table III. Here, values of Q_{ss} are listed for three conditions of oxygen anneal after 1200°C oxidation: slow pull in O_2, anneal at 900° and at 550°C. These results are compared with the 1200°C standard. Both (111) and (100) orientations are included. It can be inferred from earlier work (21, 24) that the higher Q_{ss} values resulting after certain oxidation conditions can be significantly reduced by annealing in an inert ambient. The inert ambient effect is shown in Part B of Table III. Data are presented for both wet and dry oxygen oxidations followed by inert ambient anneals for two silicon orientations. It can be noted that regardless of the original oxidizing ambient, the final Q_{ss} value will be approximately that of 1200°C dry O_2 if the sample is subsequently annealed in dry argon or nitrogen.

Part C of Table III also demonstrates the fact that the final oxidation or annealing treatment determines the Q_{ss} value. In this case samples have been given combination oxidation treatments, *i.e.*, first dry O_2 followed by wet O_2 or conversely wet O_2 and then dry O_2. Standard dry O_2 and wet O_2 data are also included for comparison. In each case the value of Q_{ss} was characteristic of the final oxidizing ambient.

These results are best summarized by reference to the "dry oxygen triangle" illustrated in Fig. 5. Here Q_{ss} is plotted against oxidation temperature. As temperature decreases, Q_{ss} increases and we may move in either direction along the diagonal line labeled "dry O_2." Thus, an oxidized sample may be prepared at any temperature and then subjected to dry oxygen at any other temperature, with the resulting value of Q_{ss} being that associated with the final temperature. The time required for attaining steady state increases with decreasing temperature, being less than 5 min at 1200°C and approximately 1 hr at 550°C.

Another characteristic of the "dry oxygen triangle" is that associated with annealing in an inert ambient. As is indicated in the figure by the lower plot marked "N_2 or Argon", any Q_{ss} value resulting from a previous oxidation at a given temperature can be reduced to a constant value approximating that af 1200°C dry oxygen. This is accomplished by subsequently annealing the structure in dry high purity nitrogen or argon for times characteristic of the particular temperature. These times are similar to those mentioned above for oxygen. Both of these effects are reversible.

The lines shown in Fig. 5 are based on data for (111) p-type silicon; the effect with n-type silicon is approximately the same. A similar relationship exists for (100) silicon, where the Q_{ss} values are reduced by a factor of 2-3 from that of an MOS structure prepared from (111) silicon under identical conditions.

The purity of the gases used in the annealing experiments was found to be extremely critical, especially in the case of the inert ambients argon or nitrogen. For instance, gaseous sources of argon gave nonreproducible increases of Q_{ss} values at the lower temperatures. This was believed to be due to contamination of the gas, although the impurities involved were not identified. Only by use of freshly evaporated liquid argon were reproducible results obtained.

Table III. Dependence of surface-state charge density on annealing treatments and silicon orientation

	Oxide type	Oxidation temperature (°C)	Annealing ambient	Annealing temperature (°C)	Annealing time	Q_{ss}/q (cm^{-2}) (111)	(100)
(A)	Dry O_2	1200	—	—	Std. fast pull (<3 sec)	1.7×10^{11}	0.2×10^{11}
	Dry O_2	1200	O_2	—	Slow pull (2 min)	7.4	2.0
	Dry O_2	1200	O_2	900	10 min	4.6	1.7
	Dry O_2	1200	O_2	550	90 min	10.0	4.2
(B)	Dry O_2	1200	—	—	Std. fast pull	1.7	0.2
	Dry O_2	1200	N_2	1200	10 min	1.8	0.0
	Dry O_2	920	—	—	Std. fast pull	4.7	1.7
	Dry O_2	920	Argon	920	30 min	1.9	0.7
	Wet O_2	920	—	—	Std. fast pull	5.6	3.4
	Wet O_2	920	N_2	920	20 min	2.0	0.8
(C)	Dry O_2	1200	—	—	Std. fast pull	1.7	—
	Dry O_2	1200	Wet O_2	1200	1 min	5.0	—
	Wet O_2	1200	—	—	Std. fast pull	4.7	—
	Wet O_2	1200	Dry O_2	1200	20 min	2.1	—

Table IV. Values of Q_{SS} for various thickness of dry O_2 oxides prepared at 1200° and 920°C

Two orientations, (111) and (100) for both p- and n-type silicon (10^{16} cm^{-3}) are included.

Silicon type	Oxidation temperature (°C)	(111) Orientation Oxide thickness (μ)	(111) Orientation Q_{ss}/q (cm^{-2})	(100) Orientation Oxide thickness (μ)	(100) Orientation Q_{ss}/q (cm^{-2})
p-type	1200	0.205	1.7×10^{11}	0.195	0.2×10^{11}
		0.415	1.9	0.410	0.2
		0.635	1.8	0.630	0.1
p-type	920	0.061	4.0×10^{11}	0.030	0.9×10^{11}
		0.100	4.6	0.080	1.4
		0.205	4.7	0.161	1.4
		0.263	4.7	0.201	1.7
		0.331	4.6	0.258	1.6
n-type	1200	0.200	1.4×10^{11}	0.195	0
		0.405	1.7	0.400	0
		0.620	1.8	0.610	0
n-type	920	0.205	3.8×10^{11}	0.154	0.4×10^{11}

Table V. Values of Q_{SS} for various thicknesses of wet O_2 (95°C H_2O) prepared at 1200° and 920°C

Two orientations, (111) and (100), for both p- and n-type silicon (10^{16} cm^{-3}) are included.

Silicon type	Oxidation temperature (°C)	(111) Orientation Oxide thickness (μ)	(111) Orientation Q_{ss}/q (cm^{-2})	(100) Orientation Oxide thickness (μ)	(100) Orientation Q_{ss}/q (cm^{-2})
p-type	1200	0.200	4.0×10^{11}	0.180	1.1×10^{11}
		0.410	4.5	0.400	1.7
		0.620	5.3	0.600	1.4
p-type	920	0.082	4.5×10^{11}	0.056	1.9×10^{11}
		0.170	5.4	0.120	2.6
		0.345	6.7	0.245	3.6
		0.550	6.6	0.415	3.5
n-type	1200	0.200	3.3×10^{11}	0.190	0.6×10^{11}
n-type	920	0.185	3.7	0.127	1.7×10^{11}

Oxide thickness.—Measurements of the effect of oxide thickness on Q_{ss} were extended to include samples prepared in both dry and wet oxygen at 1200° and 920°C, and for (111) and (100) oriented p- and n-type silicon. Oxide thicknesses ranged from less than 0.01μ to over 0.6μ. The resulting Q_{ss} values are given in Tables IV and V. It can be noted that the values of Q_{ss} are relatively constant over the entire thickness range.

The orientation effect is again quite evident from the data in Tables IV and V, with the Q_{ss} ratio between (111) and (100) samples being approximately 2-3:1 for any given condition.

It should be emphasized that unless the correction for work function difference Φ_{MS} is made, an erroneous dependence of Q_{ss} on thickness would be obtained. That this correction is necessary is evident from Fig. 6 where the voltage shift ΔV is plotted as a function of oxide thickness for four different oxidation conditions. It is evident that conditions (A), (B) and (D) have widely different slopes reflecting the different Q_{ss} values, but that they have identical intercepts, *i.e.*, Φ_{MS} values. Conditions (B) and (C) have identical slopes, *i.e.*, Q_{ss} values, but different intercepts, reflecting the difference in Φ_{MS} for p- and n-type silicon (11). These results are in close agreement with data presented by Ko and Locher (26) who demonstrated the constancy of Q_{ss} with oxide thickness and the effect of metal work function in a similar manner.

Electric field[1].—It has been shown that ionic contamination within the SiO_2 layer can be rearranged in minutes at 150°C (5). On the other hand, the characteristics of MOS structures prepared as described above have been demonstrated to be stable at 150°C, under applied fields of ±75 v/μ for 3600 hr (3), and also under various other test conditions (27). Recently, an apparent increase in Q_{ss} has been reported (28, 29) due to application of negative fields (metal negative) at higher temperatures. This effect was investigated in further detail.

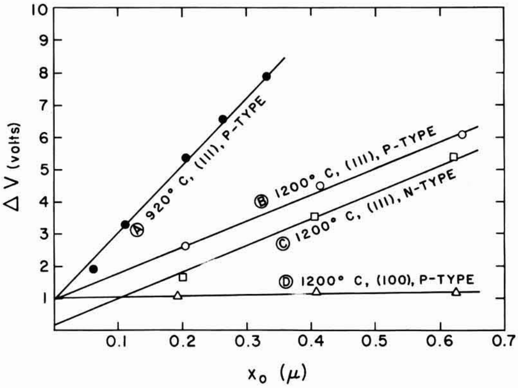

Fig. 6. Displacement ΔV between experimental and theoretical capacitance-voltage characteristics as a function of oxide thickness x_o. In each case the slope is proportional to Q_{SS} while the intercept equals $-\Phi_{MS}$.

Negative fields of 50 to 275 v/μ were applied across the oxide at temperatures of 300°-450°C for times of 2 min or more. Typical results are shown in Fig. 7, where the plots in Fig. 7(a) are for a 0.2μ dry oxide on p-type silicon, while Fig. 7(b) is for the same type of oxide on n-type silicon. In each case, the theoretical curve is labeled (A), the original experimental curve is labeled (B) while the curve resulting after application of the negative field is labeled (C). It can be noted that for each conductivity type the resulting curve displays a sharp break near the intrinsic point. Other experiments using current-voltage measurements on gate-controlled p-n junction diodes (4) have definitely related this phenomenon to an increase in fast surface state density N_{st}. The approximate N_{st} values can be estimated as indicated in Fig. 7 to be about 5 x 10^{11} cm^{-2}, while the resulting increase in Q_{ss} values are about 5-7 x 10^{11} cm^{-2}. If no fast states were observed after application of the negative field, the resulting curves (due only to a change in Q_{ss}) would be represented by the dotted lines in Fig. 7, labeled (D).

Several interesting observations were made concerning the effect of negative fields on the C-V characteristics of MOS structures. These effects were similar for p- or n-type silicon with (111) or (100) orientations, and for wet or dry oxides prepared at high or low temperatures. First, an increase in Q_{ss} was generally accompanied by an increase in N_{st} of about equal magnitude. Second, the total change of C-V characteristics would saturate in 1 to 3 min at 400°C for a given applied field. At 300°C, the time required to reach the same saturated or steady-state value was about 8 hr. These times are about four orders of magnitude longer than those required for the rearrangement of sodium contamination. Third, the total change in C-V characteristics at a given field was proportional to the initial Q_{ss} value. Finally, the results obtained with different oxide thicknesses show the effect to be proportional to the applied field rather than the applied voltage.

Examples of some of the above observations are indicated in Fig. 8 and 9. In Fig. 8, the steady state values of $Q_{ss}/q + N_{st}$, corresponding to the total displacement of the midpoints of the C-V plots from the

---

[1] The phenomenon discussed in this section has locally been referred to as Drift VI.

13

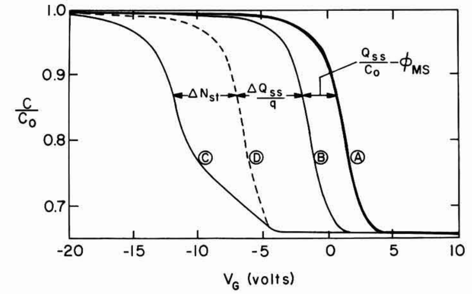

(a) P-TYPE SILICON

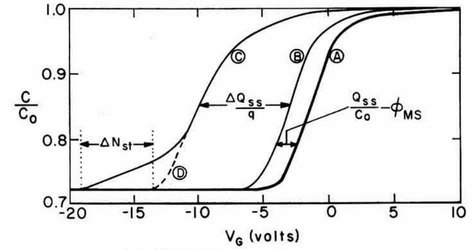

(b) N-TYPE SILICON

Fig. 7. Illustration of the effect of heat-treatment under negative gate bias on the capacitance-voltage characteristics [—200 v/μ for 2 min at 400°C].

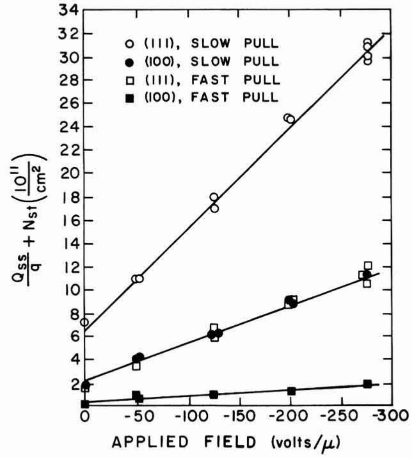

Fig. 8. Steady-state values of $Q_{ss}/q + N_{st}$ as a function of applied field for four different MOS structures with various initial Q_{ss} values [1200°C dry O_2 oxidation; $x_o = 0.20\mu$; p-type, $N_A = 1.4 \times 10^{16}$ cm^{-3}].

theoretical value [see Fig. 7 (a)] are shown for four structures as a function of applied field. The linear dependence of change in the C-V curve with applied field is readily seen, as well as the dependence on the initial Q_{ss} value. In Fig. 9, similar plots are shown for oxides of three different thicknesses on n-type silicon. Here the total change in C-V characteristics reflects only ΔQ_{ss}, but the ΔN_{st} term would just double the change. It is obvious from this plot that the change is dependent on field, not voltage, across the oxide.

An attempt was made to move the charge in the opposite direction by application of a positive field. Small decreases in Q_{ss} were indeed noted, even on structures with low initial Q_{ss} values. It was also noted that in cases where the C-V characteristics had been shifted by a negative field, they could be partially recovered toward the original value by the application of a positive voltage or by shorting the field plate to the silicon at 400°C.

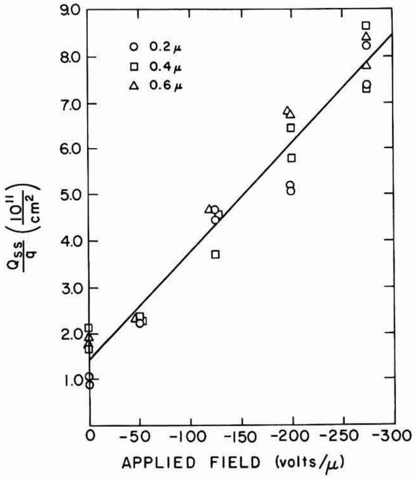

Fig. 9. Steady-state values of Q_{ss}/q as a function of applied field for MOS structures with various oxide thicknesses [1200°C dry O_2 oxidation; (111) orientation; n-type, $N_D = 1.4 \times 10^{16}$ cm^{-3}].

Spatial distribution of Q_{ss}.—The spatial distribution of Q_{ss} within the oxide can be inferred from etching experiments in which the conductance of an inverted surface is measured as a function of the amount of oxide removed.[2] However, one must use great care in the interpretation of these experiments. In particular, it should be noted that the inversion layer conductance will decrease as the oxide is removed even if Q_{ss} is located entirely at the oxide-silicon interface. The reason for this is that, because of the finite width of the surface depletion region in the silicon, Q_{ss} will induce part of its image charge on the outer surface of the oxide and only part in the silicon. As the oxide becomes thinner compared to the depletion region width, more and more of the image charge will be induced on the outer surface and correspondingly less in the silicon. This is clearly true in the case of a metallized surface where the charge at the outer surface is in the form of electrons in the metal. In the case of a bare oxide, it is reasonable to assume that the charge at the outer surface is in the form of ions adsorbed onto the surface from the etch solution.

If we assume Q_{ss} to be uniformly distributed over some finite width d near the oxide-silicon interface, then the charge distribution in an oxidized, high resistivity p-type silicon surface will be as shown in Fig. 10 where Q_G is the charge per unit area induced on the outer surface of the oxide, Q_n is the charge per unit area in the inversion layer,[3] Q_B is the charge per unit area in the surface depletion region and $x_{d\,max}$ is the depletion region width. The condition of charge neutrality requires that

$$Q_G + Q_{ss} + Q_n + Q_B = 0$$

and the condition of zero voltage drop across the system requires that

$$\frac{Q_G x_o}{K_o} + \frac{Q_{ss} d}{2K_o} - \frac{Q_B x_{d\,max}}{2K_s} = 0$$

---

[2] Similar experiments have been used to determine the spatial distribution of sodium ions (5) and of radiation-induced space-charge (30).

[3] Most of the inversion layer charge will be within a distance from the Si-SiO$_2$ interface of the order of $(°KT/q)E_s$ where $E_s = Q_s/K_s\epsilon_0$ is the surface field. For the case considered, this distance is about 30Å and is therefore negligible.

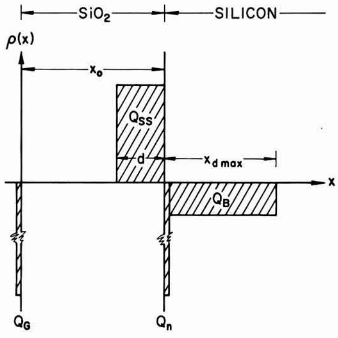

Fig. 10. Charge distribution due to Q_{ss} in a thermally oxidized, p-type silicon structure.

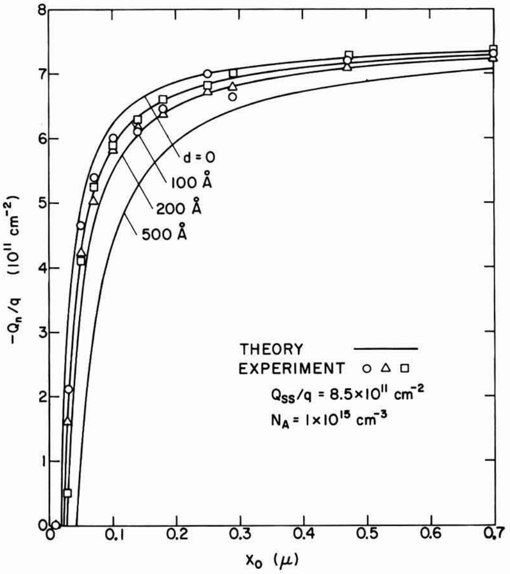

Fig. 11. Inversion layer charge density as a function of remaining oxide thickness. Theory is based on various assumed spatial distributions of Q_{SS}; experimental points are based on channel conductance measurements.

If Q_G is eliminated between these two equations, we obtain for the charge in the inversion layer

$$-Q_n = Q_{ss}\left(1-\frac{d}{2x_o}\right) + Q_B\left(1+\frac{K_o x_{d\,max}}{2K_s x_o}\right)$$

Since Q_B and $x_{d\,max}$ can be calculated for any given doping level (3), one can plot a family of theoretical curves of $-Q_n$ *vs.* x_o with d as a parameter. This is done in Fig. 11 for the case of $Q_{ss}/q = 8.5 \times 10^{11}$ cm^{-2} and $N_A = 10^{15}$ cm^{-3}.

Experimentally, Q_n can be determined directly by measuring the small-signal source-drain conductance of an MOS transistor which is given by $g = -\mu_{eff}\, Q_n Z/L$, where Z/L is a known geometrical factor and μ_{eff} is the effective inversion layer mobility which has been previously determined (31). Experiments have been performed in which Q_n was measured as the oxide was etched away in steps. Some typical results are plotted in Fig. 11 along with the corresponding theoretical curves. By comparing experiment and theory it can be concluded that d lies between 0 and 200Å, although the method is not sufficiently sensitive to allow a more precise determination. Similar results were obtained on other samples with Q_{ss}/q values ranging between 2×10^{11} and 1×10^{12} cm^{-2}. These findings are not in agreement with the results of a similar experiment by Lindmayer (25). The discrepancy appears to be due to his neglecting the factors discussed above.

Discussion

On the basis of the above experimental results, it is possible to enumerate certain characteristics of the surface-state charge.

Its density Q_{ss} is independent of the band bending or surface potential over at least the middle 0.7 ev of the energy gap. This can be concluded from the fact that experimentally observed capacitance-voltage characteristics are displaced in a parallel manner from the ideal theoretical characteristics (3).

Its density is stable under moderate temperature-bias tests (3).

Its density is practically independent of the impurity type and concentration in the silicon in the range 10^{14} to 10^{17} cm^{-3} (3), although n-type Si shows a slightly lower density than p-type (see Fig. 3 and 4).

Its density is independent of the oxide thickness for a given preparation condition (see Tables IV and V and Fig. 6).

Most of the charge is located within not more than 200Å of the oxide-silicon interface as demonstrated by etching experiments (see Fig. 11).

Its density can be significantly, reproducibly, and reversibly varied by changing the ambient (*i.e.,* dry oxygen or water vapor) and temperature of oxidation. The surface-state charge density is dependent only on the final oxidation step (see Fig. 5).

Heat treatment in inert ambients reduces Q_{ss} to approximately its lowest value, that found after oxidation in dry oxygen at 1200°C (see Fig. 5).

The orientation of the silicon influences Q_{ss} significantly (13-15). The variation follows approximately the variation of the surface reaction rate constant for oxidation (see Table II).

Under negative fields applied at temperatures well in excess of that required to move sodium contamination in the oxide, Q_{ss} can be increased (28-29). This increase saturates at a value proportional to both the initial Q_{ss} and the applied field (see Fig. 8 and 9); and it is also accompanied by an apparent increase in the density of fast surface states (see Fig. 7).

The most important conclusion that can be made on the basis of these facts is that the surface-state charge is not an extraneous contamination, such as sodium ions, but is a phenomenon intrinsically connected with the silicon dioxide-silicon interface. This is supported by the relative immobility of the surface-state charge, and more importantly, by its high degree of reproducibility.

The lack of variation of this charge with surface potential taken together with the observation that the charge is located within 200Å of the interface indicates that this charge must be related to energy levels which are outside of the middle 0.7 ev of the silicon energy gap. It is quite possible, in fact, that the energy levels are outside of the entire silicon energy gap, but are located within the forbidden gap of the silicon dioxide as illustrated in Fig. 12.

The fact that the charge is practically independent of doping type and concentration rules out the possibility that it is due to doping impurities from the silicon being incorporated into the oxide during its formation. On the contrary, the silicon orientation dependence strongly suggests that it is a silicon species in the oxide that is responsible for the surface-state charge.[4]

---

[4] For the purposes of this discussion, we make no attempt to distinguish between an excess of silicon and a deficit of oxygen. It should be noted that oxygen vacancies generated as a result of reaction between the metal gate electrode of an MOS structure and the silicon dioxide layer have been proposed in an entirely different context as an explanation for the low temperature instability (32).

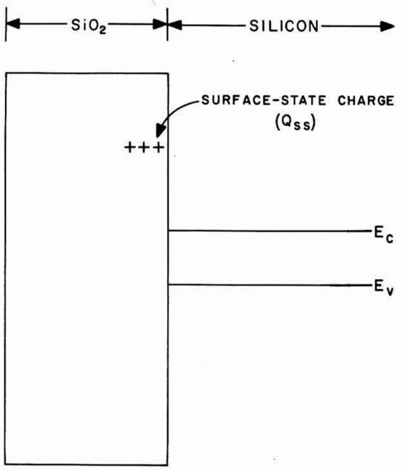

Fig. 12. Energy band structure of the Si-SiO_2 system, in flat-band condition, showing proposed energy levels associated with the surface-state charge.

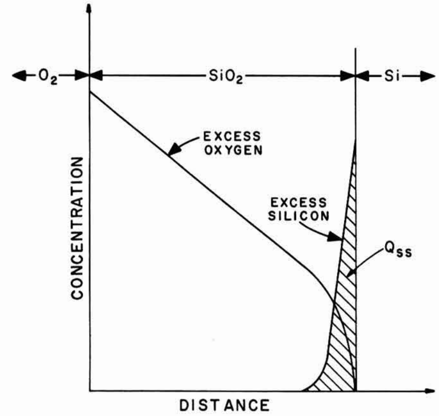

Fig. 13. Schematic illustration of the proposed distribution of excess species in an oxide film during formation.

This possibility is further supported by the fact that the strongest effect on Q_{ss} is due to variations in the oxidation conditions. Although it is well known that thermal oxidation of silicon proceeds by the inward motion of an excess of the oxidizing species, there must be an excess of silicon present near the oxide-silicon interface in order to react with the oxidant. Should this excess silicon be ionic,[5] it could indeed lead to a positive charge near the interface with many of the observed characteristics.

This possibility makes the variation of Q_{ss} with oxidation conditions plausible. It is also consistent with the observed increase in surface-state charge density on application of a negative field at high temperatures: it is known (35) that during anodic oxidation it is the silicon species that moves, under the influence of negative fields, toward the outer oxide surface. It might be then that in this case also, the negative field near the interface aids the entry of excess silicon into the oxide. This would be consistent also with the resulting increase in fast surface state density: vacancies in bulk silicon are known to act as recombination centers. Thus, should silicon be injected from the interface into the oxide, an enhanced concentration of vacancy-like irregularities would result which might lead to increases in surface recombination rates and in fast surface state densities.

It is interesting to note that a similar hypothesis has been advanced by Brody and Handy (36) in order to resolve discrepancies in measurements on tunnel sandwiches involving the Al-Al_2O_3 interface. Also, Heine and Sperry (37) have shown evidence for the existence of excess ionic aluminum incorporated into the aluminum oxide near the oxide-metal interface.

Thus, in summary, it appears that the surface-state charge (Q_{ss}) can best be explained as being due to excess silicon ions in a narrow region next to the silicon, which are introduced into the oxide, as illustrated schematically in Fig. 13, during the process of oxidation.

Acknowledgment

The authors wish to thank P. J. Fleming for his assistance with the measurements and G. E. Moore for his continued suggestions and encouragement throughout this investigation.

Manuscript received Aug. 19, 1966.

Any discussion of this paper will appear in a Discussion Section to be published in the December 1967 JOURNAL.

REFERENCES

1. See Chap. 9 in A. Many, Y. Goldstein, and N. B. Grover, "Semiconductor Surfaces," John Wiley and Sons, New York (1965).
2. For a comprehensive review of silicon oxidation studies prior to 1965 see "Integrated Silicon Device Technology, Volume VII. Oxidation," Technical Report No. ASD-TDR-63-316, Research Triangle Institute, June (1965).
3. A. S. Grove, B. E. Deal, E. H. Snow, and C. T. Sah, *Solid-State Electronics,* **8,** 145 (1965).
4. A. S. Grove and D. J. Fitzgerald, *ibid.,* **9,** 783 (1966).
5. E. H. Snow, A. S. Grove, B. E. Deal, and C. T. Sah, *J. Appl. Phys.,* **36,** 1664 (1965).
6. E. Yon, W. H. Ko, and A. B. Kuper, *IEEE Trans. Electron Devices, ED-13,* 276 (1966).
7. For a review of radiation effects on surfaces, see J. P. Mitchell and D. K. Wilson, *Bell Syst. Tech. J.,* **46,** 1 (1967).
8. M. M. Atalla, E. Tannenbaum, and E. J. Scheibner, *ibid.,* **38,** 749 (1959).
9. B. E. Deal, *This Journal,* **110,** 527 and 1292 (1963).
10. S. Tolansky, "Multiple-Beam Interferometry of Surfaces and Films," Clarendon Press, Oxford, England (1948).
11. B. E. Deal, E. H. Snow, and C. A. Mead, *J. Phys. Chem. Solids,* **27,** 1873 (1966).
12. A. Goetzberger, *This Journal,* **113,** 138 (1966).
13. Y. Sasaki, Private communication, Nov. 11, 1964.
14. J. F. Delord, D. G. Hoffman, and G. Stringer, *Bull. Am. Phys. Soc.,* **10,** 546 (1965).
15. P. Balk, P. J. Burkhardt, and L. V. Gregor, *Proc. IEEE,* **53,** 2133 (1965).
16. J. R. Ligenza, *J. Phys. Chem.,* **65,** 2011 (1961).
17. W. A. Pliskin, *IBM, J. Research Dev.,* **10,** 198 (1966).
18. B. E. Deal and A. S. Grove, *J. Appl. Phys.,* **36,** 3770 (1965).
19. P. J. Burkhardt and L. V. Gregor, *Trans. Met. Soc. AIME,* **236,** 299 (1966).
20. H. S. Lehman, *IBM J. Research Dev.,* **8,** 422 (1964).
21. A. B. Kuper and E. H. Nicollian, *This Journal,* **112,** 528 (1965).
22. P. Balk, Paper presented at the San Francisco Meeting of the Society, Abst. No. 109, May 9-13, 1965.
23. E. Kooi, *IEEE Trans. Electron Devices, ED-13,* 238 (1966).
24. A. G. Revesz and K. H. Zaininger, *ibid.,* 246 (1966).
25. J. Lindmayer, *Solid-State Electronics,* **9,** 225 (1966).
26. W. H. Ko and R. Locher, "Recent News" Paper

---

[5] Ionized silicon was one of several possibilities suggested in this context by Donovan (2) and by Revesz (33). Without specifying the species leading to the surface-state charge, Lindmayer (34) developed a model which treats the interface between oxide and silicon as a heterojunction. This model, although appealing, seems inconsistent with the experimental results; the heterojunction picture leads to the conclusion that the charge transfer from oxide to silicon should be a function of the impurity concentration and type in the silicon much as is the case in an ordinary p-n junction. This, however, is in contradiction to the experimental observations.

presented at the Cleveland Meeting of the Society, May 1-6, 1966.
27. P. Lamond, J. Kelley, and M. Papkoff, Paper Presented at the Washington, D. C., Meeting of the IEEE Electron Device Group, Oct. 1964.
28. Y. Miura and Y. Matukura, *Jap. J. Appl. Phys.*, **5**, 180 (1966).
29. A. Goetzberger, "Recent News" Paper presented at the Cleveland Meeting of the Society, May 1-6, 1966.
30. A. S. Grove and E. H. Snow, *Proc. IEEE*, **54**, 894 (1966).
31. O. Leistiko, Jr., A. S. Grove, and C. T. Sah, *IEEE Trans. Electron Devices, ED-12*, 248 (1965).
32. J. E. Thomas and D. R. Young, *IBM J. Research Dev.*, **8**, 368 (1964).
33. A. G. Revesz, *IEEE Trans. Electron Devices, ED-12*, 97 (1965).
34. J. Lindmayer, *Solid-State Electronics*, **8**, 523 (1965).
35. E. A. Benjamini, E. F. Duffek, C. A. Mylroie, and F. Schulenburg, "Recent News" Paper presented at the New York Meeting of the Society, Oct. 1-4, 1963.
36. T. P. Brody and R. M. Handy, "Hot Electron Emission Controlled by Bolometric Layers," Fourth Quarterly Report, Contract No. DA-44-009-AMC-357(x), Sept. 30, 1964.
37. M. A. Heine and P. R. Sperry, *This Journal*, **112**, 359 (1965).

A Nitric Oxide Process for the Deposition of Silica Films

Myron J. Rand

Bell Telephone Laboratories, Inc., Allentown, Pennsylvania

ABSTRACT

A new process for vapor depositing thin films of silica on a heated substrate is described. The reagents are hydrogen ($\geqq$95%), nitric oxide (1-4%), and silicon tetrachloride or tetrabromide (0.1-1%). The chloride system is useful at 950°-1200°C and the bromide at 775°-950°C, so that the latter may serve to coat Ge as well as Si. The over-all reaction is believed to be $2NO + 2H_2 + SiX_4 \rightarrow SiO_2 + N_2 + 4HX$ and is probably mostly homogeneous. For the more commonly used film thicknesses the nitric oxide process is three to five times more rapid than either the steam or carbon dioxide reactions. Rate curves are presented for various temperatures and concentrations. The apparent temperature coefficient of deposition rate decreases markedly in the upper part of the temperature range for both the Cl and Br systems. Improved film thickness uniformity may be obtained as a practical result. The films produced are transparent, vitreous, smooth, and tightly adherent. Physical tests indicate they are amorphous silica with less short-range order than in thermal oxides. Films from the chloride system regularly produce Si surface charges of 3-6 x 10^{11}/cm^2 in MOS capacitor tests. Breakdown voltages equal those of steam oxides. Limited bias-aging experiments have shown shifts similar to those of steam oxides. The films are satisfactory masks for boron and phosphorus diffusions; Kodak Photoresist adheres very well.

In principle, deposition of silicon dioxide films from the vapor phase has several advantages in planar semiconductor device processing over the more conventional thermal oxide formation by reaction of a silicon substrate surface with steam or wet oxygen. Since no silicon is consumed, junction movement is minimized, as is pileup or depletion of dopants at the substrate-oxide interface. It is easier to produce thick films by vapor deposition, since the rate is not diffusion-limited. The process is also more practical for producing doped films for diffusion sources. Finally, materials other than silicon may be coated; an example is the deposition of silica for an etching mask with nonfluoride-containing etches.

Nevertheless, deposited oxide film processes are uncommon in device production, with the exception of low-temperature pyrolytic oxides from organosilanes used by necessity for germanium coating. Recently there has been experimental-scale interest in oxides from the hydrogen-carbon dioxide-silicon tetrahalide system (1-4). The slow acceptance of deposited oxides from this (and other) systems appears to arise from the difficulties of producing uniform thicknesses, the fact that growth rates are not significantly faster than for thermal oxides for the more useful film thicknesses, the possibility of introducing carbon into the film or substrate, the evidence for some substrate etching reaction occurring, and unfamiliarity with film quality.

This paper presents a novel system for silica film deposition from mixtures of hydrogen, nitric oxide, and silicon tetrachloride or tetrabromide. It was originally devised to improve two of the five conditions mentioned above, those of growth rate and possible carbon contamination. As it happens, the other three are affected favorably also. This report summarizes some sixty runs in apparatus ranging from a single-slice vertical-flow tube to a ten-slice machine with provision for continuous rotation of each substrate independently. Films up to 1.5μ thick have been deposited.

The NO-H_2 *System*

Silica vapor deposition employing oxides of nitrogen was investigated primarily because of the large free energy change available to drive the reaction. In addition, any trace codeposition of silicon nitride which may occur should be tolerable, since it is a good insulator and diffusion barrier also. Nitric oxide, rather than N_2O or NO_2, was chosen for superior thermal stability to confine the reaction to a zone very close to the heated substrate and thus avoid deposition of particulate silica both on the slice and in the cooler parts of the system. NO has an additional advantage: it is a good intermediate in chain reaction mechanisms because it is readily either oxidized or reduced. As an example, it is known that NO may transform the chain initiation or termination steps in the H_2-Cl_2 reaction from heterogeneous to homogeneous (5).

The standard free energy change for the NO process is shown in Fig. 1, with the corresponding reactions for the CO_2 process included. At all temperatures the NO process has much greater driving energy. The reaction as written assumes that the ultimate reduction product of the NO is nitrogen. Other possibilities are N_2O, hydroxylamine, ammonia, and hydrazine; in $\geqq$95% hydrogen ambient at the 800°-1200°C used in this work only ammonia is considered a rea-

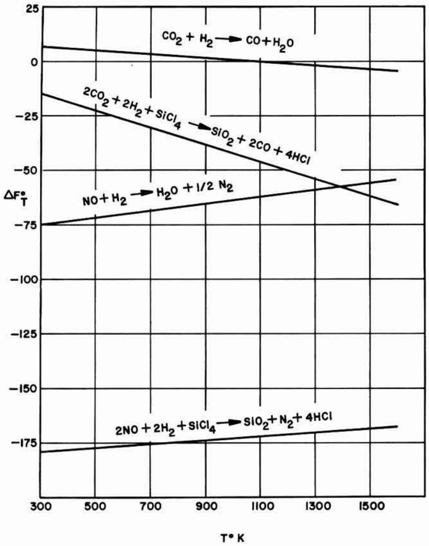

Fig. 1. Standard free energies of nitric oxide and carbon dioxide process reactions at various temperatures.

sonable alternative to nitrogen, and even ammonia is extensively dissociated at equilibrium at these temperatures.

The NO-H_2 reaction has been investigated at temperatures below 500°C (6, 7), where it must be catalyzed and where substantial amounts of ammonia may be formed. At the other extreme it has been studied extensively under conditions providing an abundance of atomic hydrogen, in flames (>1500°C) or with mercury photosensitization; here the reaction is homogeneous. The only recent study of the intermediate zone is that of Graven (8) in the range 850°-1060°C. The reaction was predominantly homogeneous; a complex rate expression was proposed, but the reaction mechanism could not be determined unequivocally.

The multislice deposition apparatus used for much of the work reported here employed an r.f.-heated molybdenum susceptor as the major hot surface. By monitoring the moisture content of the exhaust gases, the reaction between hydrogen and 2% NO in this apparatus was observed to begin at 400°-500°C and increase steadily as the temperature was raised. At 1000°C, at a flow rate which would displace the reactor volume about once a minute, the moisture content of the exhaust was 5000 ppm, or a reaction "efficiency" of 25%. By scrubbing the exhaust gas with dilute HCl and back-titrating it was established that less than 2% of the NO present was reduced to ammonia.

At present we believe that in excess hydrogen NO reacts at 800°-1200°C to produce nitrogen and water; that the reaction is mostly homogeneous, with some surface catalysis possible in the lower part of the range; and that it is a chain reaction of unknown mechanism, proceeding by unstable intermediates probably including atomic hydrogen, N_2O, nitroxyl (HNO), and perhaps HO_2. Needless to say, the addition of the silicon tetrahalide multiplies the complexity. The nitric oxide process for silica film deposition may be regarded as

$$2\left[NO + H_2 \rightarrow \frac{1}{2} N_2 + H_2O\right] \qquad [1]$$

$$2H_2O + SiX_4 \rightarrow SiO_2 + 4HX \qquad [2]$$

only if it is borne in mind that there are many possible routes to SiO_2 other than reaction [2]

Nothing in the foregoing discussion should limit the process to silicon halides; it should be adaptable to oxide deposition in any system with volatile metal halides. To date only silica deposition has been attempted.

Experimental

The deposition area of the apparatus most frequently used has already been described (4); in any event, the reactor design is not important to the success of the process. Each apparatus geometry has different gas dynamics and should be calibrated for the effect of total flow rate. Nitric oxide (Matheson Company) contained ~0.1% each of N_2, N_2O, and NO_2. When passage through Ascarite (which removes NO_2) and a —78° trap did not influence deposition rates the gas was thereafter used without purification. Reactant concentrations ranged from 0.25% NO-0.05% SiX_4 to 4.2% NO-1.0% SiX_4. Total flow rates were such as to displace the reactor volume about once a minute. The bromide system was studied over the range 790°-950°C, the chloride system 950°-1200°C. Substrates coated include Si and Ge of various resistivities, Mo, Ta, and fused silica.

Instead of bringing the substrates to temperature in hydrogen and then introducing the other reactants, it was found advantageous to adjust the gas ambient first and then heat the substrate. Using this method the substrate etching which often plagues the carbon dioxide process was not observed. There are several possible etching reactions, but at temperatures at which their rates become significant the nitric oxide process has already sealed the surface with a continuous silica film. With any method of ambient adjustment, however, the NO process definitely gives less trouble with etching than the CO_2 process.

Deposition Rates

Figures 2 and 3 are Arrhenius plots showing rates of silica film deposition for typical reactant concentrations for the chloride and bromide systems. Rates for the CO_2 process from ref. (1, 2, 4) are included also. Activation energy for the Cl system is 65 kcal (2.8 ev)/mole, and for the Br system 55 kcal (2.4 ev)/mole. Since activation energies for the NO-Cl and CO_2-Cl processes are about the same, it is possible that the rate-determining slow step for the two is the same. If so, this could only be the gas-phase hydrolysis of $SiCl_4$. It would then be a mistake to assume that this reaction, at elevated temperature, is very rapid simply because it is rapid in the liquid phase at room temperature.

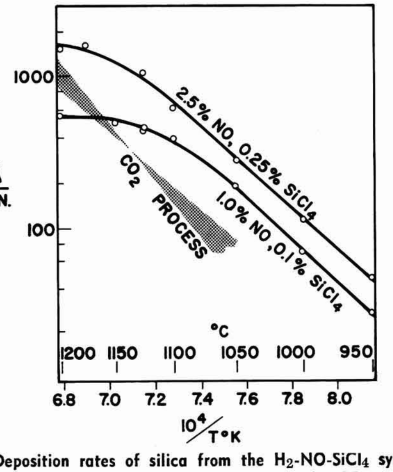

Fig. 2. Deposition rates of silica from the H_2-NO-$SiCl_4$ system. The shaded area shows the range of results for the CO_2 process from ref. (1), (2).

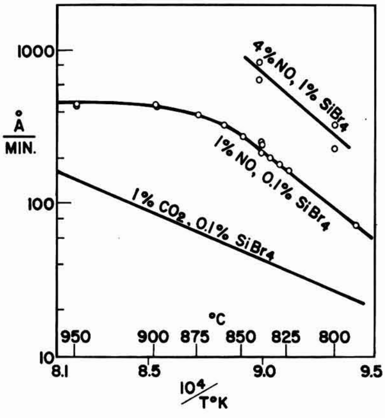

Fig. 3. Deposition rates of silica from the H_2-NO-$SiBr_4$ system

Table I. Time (minutes) required for a 5000Å SiO_2 film

Temperature, °C	Steam	CO_2-$SiCl_4$	2.5% 0.25% NO - $SiCl_4$	1% 0.1% CO_2-$SiBr_4$	1% 0.1% NO-$SiBr_4$
825	—	—	—	143	30
900	—	—	—	58	12
950	112	>350	114	38	11
1050	44	83	17	—	—
1100	35	28	7	—	—
1200	19	5	3.2	—	—

Table I compares the time required to grow a 5000Å film by steam, CO_2, and NO processes at various temperatures. The NO process has a speed advantage of 3 to 5 times over competing processes under usual operating conditions.

The shape of the Arrhenius plots requires comment. In the lower parts of the temperature ranges studied the expected linear dependence of log rate *vs.* $1/T$ is found. Results are little affected by transport rate, *i.e.*, total flow rate, and should thus be close to true kinetic rates. However, at higher temperatures the deposition rate levels off to an extent which is influenced by concentration. Here there is evidently serious depletion of silicon halide in the reaction zone, and the reaction is becoming diffusion-controlled. At still higher temperatures the apparent rate actually decreases, and particulate silica is embedded in the deposited films. The interpretation is that now the reaction zone has moved out far enough from the substrate to allow some of the silica formed to escape deposition and instead be carried away by the gas flow.

The tendency of the deposition rates to level off may be used to advantage in improving the thickness uniformity of oxides from the NO system. If nonuniformity is due to temperature inhomogeneity of the substrate, it may be minimized by operating under conditions where the apparent temperature coefficient of deposition rate is low. An oxide thickness variation of only ±5% across a 1 in. diameter slice may be obtained, for example, at 950° in the bromide system. The same equipment, used for the CO_2 process under identical conditions, produced ±17% variation in oxide thickness. The deposition of particulate silica imposes an upper temperature limit to the use of this expedient. Film uniformity is also aided by high total flow rate and by low reactant concentrations.

Film Properties

The nitric oxide process reliably produces clear, vitreous, tightly adherent silica films which are amorphous by electron diffraction. Electron microscopy shows fewer surface features than with any other process yet examined; the NO-Br system film appears particularly smooth.

Some other film properties are given in Table II. The etch rate and residual halogen content are of the same order as those of CO_2 process oxides. The slightly high refractive index, considered along with the absorption spectrum, opens the possibility that the films are slightly oxygen-deficient. (The high refractive index of the NO-Br system film can be accounted for by its Br content, however.) The SiO stretching vibration appears at a frequency lower than in thermal oxides, and the absorption band is considerably broadened. The NO oxide is evidently more truly amorphous, *i.e.*, has less short-range order. Instead of oxygen deficiency, an alternative explanation is that the films contain small amounts of codeposited silicon nitride. The absorption maximum of the nitride is ~850 cm^{-1}, and its refractive index near 2.0.

No hydroxyl has been detected in the Cl system films; small amounts are sometimes seen in the Br system films, but this is common in films made at 850° by any deposition process where water is a possible product.

Kodak KPR Photoresist adheres very well to NO process oxides. Patterns etched in the silica and examined at 500X have shown no evidence of resist-film lifting at the edges.

The electrical properties given in Table II have been measured on three MOS capacitors on each of 16 slices, these made in ten separate runs. The NO-Cl oxides, as made, produce a lower Si surface charge than does routinely produced steam oxide. NO-Br oxides run about twice as high as steam; these have not yet been subject to experiments on treatments to reduce the charge. Both systems produce films with acceptable insulating properties. Breakdown voltage is not polarity-dependent, and is usually sharp. A few capacitors showed "channels" (current limiting) which did not then break down further up to 2 x 10^7 v/cm.

Tests as masks against boron and phosphorus diffusion have been made with patterns etched in 0.4-0.5μ thick films made with 1% NO-0.1% $SiCl_4$ at 1100°. Conditions for the B diffusion were: B_2O_3 predeposition 18 min, 870° in N_2, later followed by 135 min drive-in at 1200° in 90% N_2-10% O_2. For phosphorus P_2O_5 in O_2 for 45 min at 1040° was used. Junctions were delineated by angle-lapping and staining. There was no instance of dopant leaking through the film, or of any mechanical film failure.

Planar transistors made with the NO process film as the first oxide were indistinguishable from those with

Table II. Properties of NO-process silica

	Steam, 1050°	NO-$SiCl_4$, 1100°	NO-$SiBr_4$, 850°
Relative etch rate, P etch*	1	1.8	3.8
Halogen content, %	0	0.5	2.6
Refractive index, 546 mμ	1.455-1.460	1.48-1.50	1.49-1.51
Water contact angle	35-40°	40°	55°
I.r. transmission minimum, cm^{-1}**	1089	1065	1064
Half-band width, cm^{-1}	85	110-170	113-121
MOS capacitor results:			
Surface charge/cm^2***	5-8 × 10^{11}	3-5 × 10^{11}	1-2 × 10^{12}
Av. dielectric constant 0.5 mc	3.9	3.7	3.8
Breakdown v/cm	6-8 × 10^6	5-10 × 10^6	5-7 × 10^6

* Ref (9).
** 0.6μ thick film.
*** As made, *i.e.*, no subsequent heat-treatment.

conventional processing in such tests as breakdown voltages, leakage currents, gain, capacitance, frequency cutoff, and saturation voltage. Extended aging tests are not yet available. A limited study of drift in films 1700-2100Å thick was made using MOS structures. After 1 hr at 100°C with a field of 10^6 v/cm (field plate positive), the surface charge density was increased by 2-4 x 10^{11}/cm^2. Freshly grown 1050° steam oxides with field plates deposited in the same evaporation equipment showed increases of 3-4 x 10^{11}/cm^2 under the same drift conditions.

Acknowledgment

The aid of J. Drobek and H. E. Nigh in the physical evaluation of the films is acknowledged with thanks.

Manuscript received Aug. 1, 1966; revised manuscript received Oct. 17, 1966. This paper was presented at the Philadelphia Meeting Oct. 9-14, 1966.

Any discussion of this paper will appear in a Discussion Section to be published in the December 1967 JOURNAL.

REFERENCES

1. W. Steinmeier and J. Bloem, *This Journal*, **111**, 206 (1964).
2. S. K. Tung and R. E. Caffrey, *Trans. Met. Soc. AIME*, **233**, 572 (1965).
3. K. H. Maxwell and L. H. Rabouin, *Electrochem. Tech.*, **3**, 37 (1965).
4. M. J. Rand and J. L. Ashworth, *This Journal*, **113**, 48 (1966).
5. P. G. Ashmore and J. Chanmugam, *Trans. Faraday Soc.*, **49**, 254 (1953).
6. S. Sourirajan and J. L. Blumenthal, *Int. J. Air Water Pol.*, **5**, 24 (1961).
7. R. J. Ayen and M. S. Peters, *Ind. Eng. Chem. Process Design Develop.*, **1**, 204 (1962).
8. W. M. Graven, *J. Am. Chem. Soc.*, **79**, 3697 (1957).
9. W. A. Pliskin and R. P. Gnall, *This Journal*, **111**, 872 (1964).

Physical Description of the Anisotropic Stress Effect in the Silicon P-N Junction Cantilever Transducer

Lewis K. Russell and Wilhelm H. Legat

Components Division, Semiconductor Operation, Raytheon Company, Mountain View, California

ABSTRACT

A silicon p-n junction device using the anisotropic stress effect has been constructed. The device exhibits a change in reverse leakage current on application of a bending force. The device consists of a narrow bar of silicon into which a sharp notch is cut electrolytically. On the opposite surface, a shallow p-n junction is produced by diffusion. Sensitivity to bending is achieved when mechanical damage is produced at the surface of the shallow junction in a controlled fashion. The corresponding change in the forward and reverse characteristics of the device after scribing is described. Methods of testing the device and changes in operating characteristics are discussed.

A theory of device operation is proposed. This theory presents a model of generation of dislocation loops from Frank-Read sources produced during the plastic deformation phase. The dislocation loops, on application of stress, enter the depletion region of the junction creating a generation current according to the Sah-Noyce-Shockley generation-recombination theory. A mathematical model of the device is developed. Operating characteristics are then compared with the mathematical model. The sensitizing operation produces noise sources within the device. The spectrum of these sources is described and the intensity is compared to device sensitivity during the scribing operation. Device noise is reduced by a decrease in the emitter perimeter. Operating characteristics of the device are discussed. These include linearity of the stress-leakage current curve, change of sensitivity with voltage, deflection with applied force, a-c impedance, junction capacity, mechanical stiffness, effective minority carrier lifetime, and fundamental vibration frequency.

In 1962, Wilhelm Rindner reported extreme changes in the electrical characteristics of p-n junctions when they were anisotropically stressed by a diamond stylus (1). He called the effect "the anisotropic stress effect" (ASE). Similar stress on the emitter-base junction of transistors will drastically modify the collector characteristics causing a large decrease in current gain (2). Indeed, any solid-state device wherein a shallow junction is anisotropically stressed will show changes in operating characteristics. Besides transistors, the devices which have been investigated include: 4-layer diodes (3) and avalanche transistors which showed changes in their negative resistance regions, field-effect transistors (3) where large impedance and transconductance changes were seen, and tunnel diodes (4) where large excess current changes were observed.

A distinct and separate stress effect was reported by Goetzberger and Finch (5) who observed a reversible change in diode breakdown voltage when the shallow junction was stressed by a stylus of material softer than silicon. Like Rindner, Goetzberger and Finch used a stylus to apply force to the junction.

Description of the Device

Figure 1 shows a sketch of a stress transducer that does not require the use of a stylus but depends entirely on the stress created at the junction by bending the device about a sharp notch running beneath the

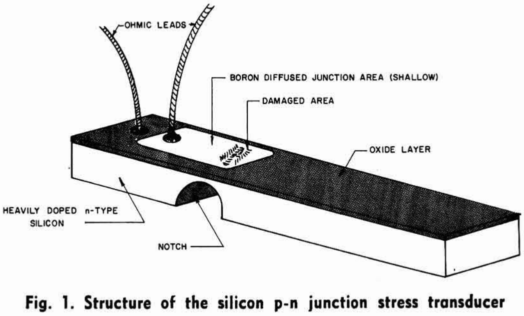

Fig. 1. Structure of the silicon p-n junction stress transducer

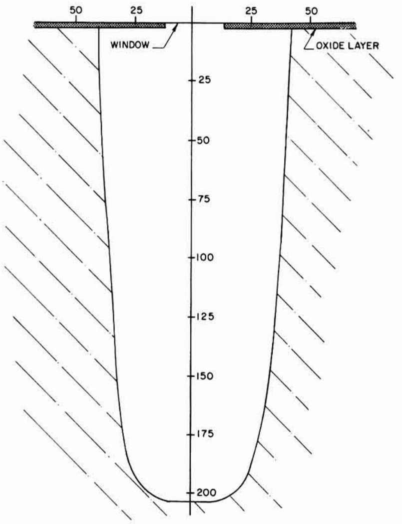

Fig. 2. Typical notch profile, in microns.

junction area. When one fastens one end of the device and bends the free end down, tension will be created at the shallow junction, ($\lesssim 0.5\mu$ deep). Bending in the opposite direction will create compression at the junction. Experimentally, it was seen that the bending occurred only in the vicinity of the notch. The high stress necessary for the anisotropic stress effect is thus produced. The range of reverse-bias operation of the device is controlled completely by the choice of starting material resistivity. If a low voltage device is desired which has voltage variations about a reference level of 1-2v, a material resistivity of about 0.01 ohm-cm is necessary as indicated in Fig. 1. Other devices were made having material resistivities as high as 50 ohm-cm. These devices were better suited for study of the effect whereas the low resistivity devices have better noise properties and are better suited for practical applications. A complex relationship exists between device sensitivity (current change per unit bending moment), applied voltage, and substrate resistivity; it has been determined empirically from measurement of many samples to be $S = 2.4V^{155}\ \rho^{-0.8}$ where S is sensitivity in μa/gcm, V is in volts, and ρ is resistivity in ohm-cm.

The junction was formed by diffusing phosphorus into n-type silicon or boron into p-type silicon to a depth of roughly ½μ. Suitable metallic contacts were sintered into the n- and p-regions to form ohmic contacts. Gold wires of roughly 1 mil diameter were ball-bonded onto the metal contacts leaving enough lead-length to permit easy testing.

The bridge of silicon running above the apex of the notch is typically 25μ thick. This thickness and even the notch shape may be varied to meet the demands of sensitivity and mechanical stiffness. A typical notch shape is shown in Fig. 2. Depth to width ratios of 2.5 are easily obtained by electrolytic etching. One can see in the figure the presence of a thin oxide layer with a 25μ window. Etching occurs through this window which acts as a virtual cathode in that all ionized particles must pass through this window. By varying the electrical field intensity one may vary the notch shape. The notch shape may also be varied by changing the window size and the length of time of etching.

Sensitization

Early in our work to develop the intrinsic stress transducer, we discovered that no measurable anisotropic stress effect could be produced by stress concentration alone (6). At about the same time it was discovered that physical damage occurred to the surface of p-n junctions that were stressed by diamond stylii. It thus seemed reasonable that some method of sensitization was required to produce the desired effect. Various methods of treating the surface of the junction were attempted, including damage by high-speed electrons, damage by sandblasting, damage by ultrasonic scribing, and damage by scribing with a diamond stylus under a controlled pressure. Of these four methods the last was most satisfactory and most controllable.

The damaged area shown in Fig. 1 is produced by scribing with a diamond stylus under a controlled pressure while displaying the characteristics of the diode on a Tektronix 575 curve-tracer. Scribing is continued until a given degradation of the reverse characteristic of the diode is obtained. Figure 3 shows a drawing of the reverse characteristic of a typical diode with a high resistivity before and after

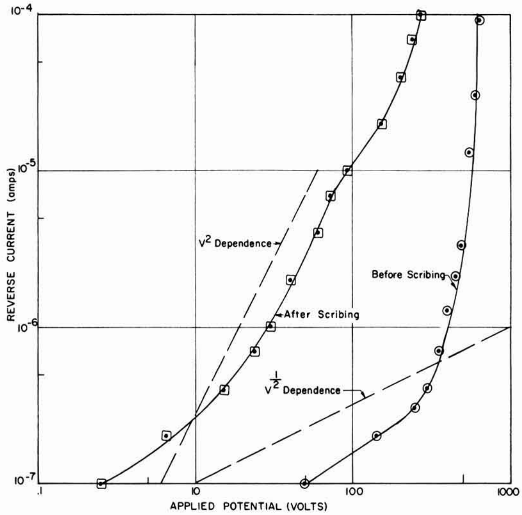

Fig. 3. Reverse characteristics of a typical transducer diode

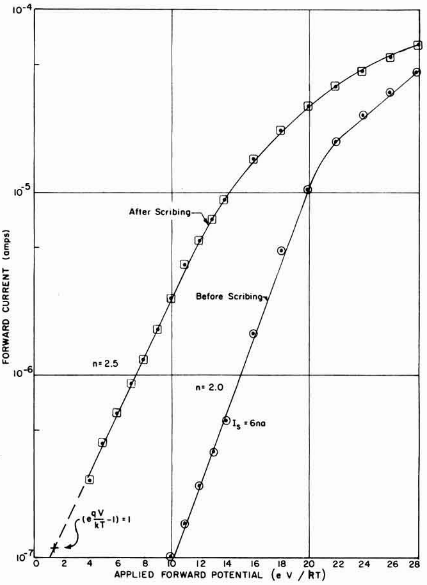

Fig. 4. Forward characteristics of a typical transducer diode

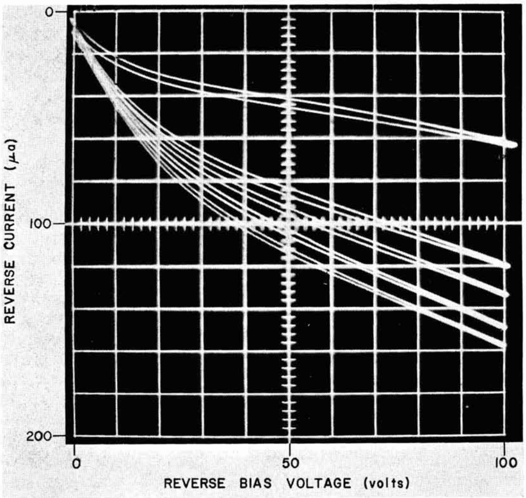

Fig. 5. Multiple exposure oscillograph of the reverse characteristics of a transducer diode under forward loads of 0, 9,000, 12,000, 14,500, and 17,000 dynes at a distance of 2 mm from the notch.

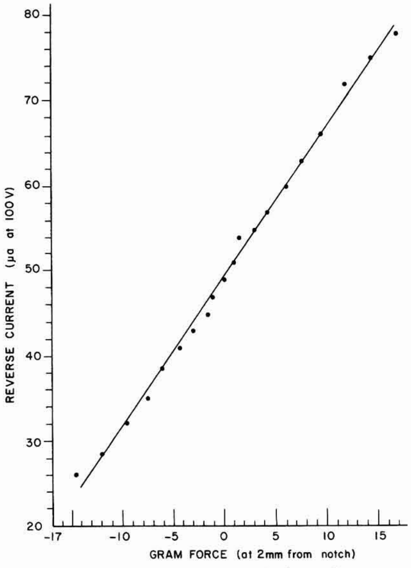

Fig. 6. Linearity of the transducer diode under static test.

scribing. Before scribing the leakage current is very small; after scribing a large leakage current is seen. We have deliberately destroyed some of the rectifying properties of the diode, principally, the high impedance in the reverse bias condition. Figure 4 shows that the forward current increased by about an order of magnitude up to an applied forward potential of about 15 ev/kT. In both forward and reverse bias conditions, the amount of change is proportional to the amount of damage sustained by the junction. With little damage, there would be little change in the operating characteristics.

Response

Figure 5 shows a multiple exposure oscillograph of a typical transducer under forward loads of from 9,000 to 17,000 dynes. The top curve is the zero load curve. Forward load refers to the fact that bending occurs in such a way as to produce compression at the junction. Under reverse load, tension would be created at the junction, and the characteristics of the device under load would fall above the zero load line. Thus, forward load produces an increase in reverse current and reverse load produces a decrease in reverse current. Figure 6 best illustrates the difference. Here, reverse current is plotted against gram force at a distance of 2 mm from the notch. One notices that a reverse current of 50 μa at 100v bias is obtained when the device is unstressed. At a forward load of 9800 dynes, reverse current has risen to 67 μa. The corresponding reverse load produces a reverse current of 32 μa.

In the earliest devices made, we could obtain an initial sensitivity of about 2 μa/dyne-cm. Under testing and high current heating, this sensitivity dropped to about 0.86 nanoamp/dyne-cm. This represents a factor of 2000 change. At this final sensitivity little further sensitivity degradation of the device was seen. More recent devices have not shown this much decrease of sensitivity, but some annealing is observed after the sensitizing process. We have also seen experimentally that temperatures on the order of 500°C will accelerate this annealing process. Complete annealing, however, is not possible even at temperatures up to 800°C, and usually 0.17% of the initial sensitivity remains at this temperature.

Figure 7 shows a typical graph of the reduction of reverse leakage current over a period of continuous testing at high dissipation levels. The device was reverse biased at 100v. The top curve shows the initial current-force characteristic. The slope of this curve from 1 to 3½g force shows a 25 μa/g sensitivity. The 40 mw dissipation is shown by the arrow. After 2 hr of testing, the sensitivity dropped to 16 μa/g. The 20 mw power dissipation point is shown by the arrow on this curve. After 6 hr of continuous testing, the sensitivity had dropped to 5 μa/g. After 10 hr, the sensitivity was 2 μa/g, and further reduction of device stress sensitivity was slight. The 5 mw point is shown on the diagram.

This sensitivity degradation or annealing of the anisotropic stress effect was at first considered to be a serious flaw in the device design. However, after the initial annealing is accomplished, the characteristics remain stable over long periods of time. This type of Joule heat annealing has also been shown to exist in germanium tunnel diodes which were degraded by indentation with a stylus and by 2 Mev

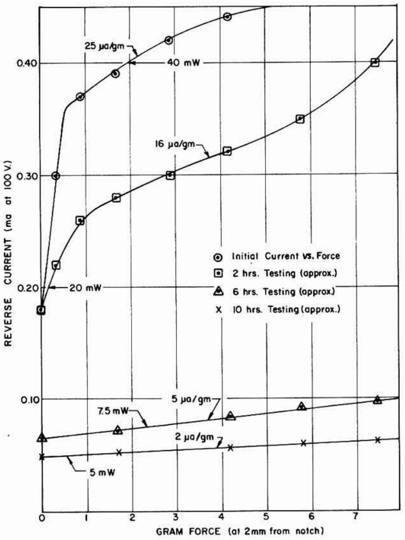

Fig. 7. Decrease of reverse current sensitivity over a period of continuous testing at high dissipation levels (100v reverse bias).

electrons (7). Stability was tested by bending the device in forward and reverse directions continuously at 120 Hz for a period of 11 months. During this time further degradation of the device characteristics was not observed. This test was performed at room temperature. Temperatures up to 100°C did not seem to cause further deterioration of the device characteristics, *i.e.*, sensitivity.

Theory of Device Operation

Several models of the anisotropic stress effect have been proposed up to this time (4, 8, 9). These models include piezoresistance, internal field emission, band bending, and generation-recombination. These models have all been examined in detail by Rindner (3, 10). The piezoresistance and internal field emission models predict a reverse current change with applied force having the wrong temperature dependence, whereas band bending has been shown (9) to produce a smaller effect in the reverse bias condition of silicon (111) diodes than is seen experimentally. As stated earlier, no stress sensitivity was detected by using the notch alone; sensitivity was seen only after the sensitization was accomplished. The fact that ASE sensitivity can be annealed out strongly suggests that the major mechanism contributing to the effect is one that is also affected by high temperature. The best model having the correct temperature dependence and strong stress sensitivity is the generation-recombination model. This model was first proposed by Rindner in 1963 (8) and is the model which best describes the results obtained with the present transducer.

In the early work using the diamond stylus visible damage was seen on the surface of the semiconductor even at very low forces. Rindner, in his discussion of stylus type anisotropic effect, also indicates a limit to complete reversibility of the effect, *i.e.*, when a certain load on the stylus was exceeded, the zero stress curve had shifted in the direction of increasing current. Thus the junction and the electrical characteristics of the junction show permanent deterioration. Surface damage of this type is very likely to produce dislocations which extend deep into the body of the semiconductor material. These dislocations have been postulated to be loops which are pinned to the damage at the surface or to internal defects. Annealing of the damaged surface at the plastic flow temperature and subsequent etching with CP4 shows the typical rosette pattern of dislocation loops attaching to pinning points at the surface (11). These rosette patterns have long been known to exist in lithium fluoride crystals which have been indented by small particles (12).

Pariiski, Landau, and Startsev investigated the jumping of dislocation loops in LiF single crystals when the pinning points were etched away (13). They found that energy was stored in the dislocation loops, and when the pinning points were removed the loops would reduce in size, collapsing toward the center, until the loop intersection with the surface encounters another pinning point or blocking point which retards further jumping. Jumping occurs with subsequent etchings until the dislocation loop completely annihilates itself. These specimens were etched at room temperature without application of any external load to the crystal. These researchers determined a lower limit of the dislocation velocity during the jump. This minimum velocity was given as about 500 μ/sec. They conclude that the velocity might be much higher than this.

Chaudhuri *et al.* (14) have investigated the velocity of dislocations in semiconductors. They propose an activation energy for dislocations in silicon of 2.17 ev which appears to be independent of stress level and temperature. Using the equation for the velocity of a dislocation held by pinning points (locks) proposed by van Bueren (15) and reasonable stress values, one would predict velocities of from 3 to 3000 cm/sec at room temperature. For example, a loop 1000Å in length and a stress level of 1.075 x 10^8 dynes/cm^2 (less than two orders of magnitude below the theoretical yield strength of silicon) would produce a velocity of 250 cm/sec. Detailed calculation of dislocation velocity using van Beuren's equation may be found in the appendix.

Direct experimental measurement of these velocities are made extremely difficult because the loops are, first of all, quite small, and second, they encounter obstacles in the form of other loops and flaws which again pin the moving loop and retard or stop its forward motion. Celli *et al.* (16) have proposed a model of dislocation motion which considers the effect of dragging points. With reasonable assignment of parameters the theory is able to agree with experimental values of dislocation velocity. Although dislocation velocities of the magnitude proposed here have not been observed by direct experiment, some indirect evidence does exist that very high dislocation velocities are achieved in crystals at room temperature, *e.g.*, in LiF. The experimental difficulties of growing sufficiently pure dislocation free silicon crystals have restricted all experiments to crystals having a high density of dragging points and hence quite low dislocation velocities. Since we have been unable to detect any significant ASE due to bending stress alone, we have been forced to conclude that damage, and hence dislocations, have a key role in the effect. To our knowledge we know of no other experiments wherein anisotropic stress has been applied to a shallow p-n junction in the absence of damage and where the ASE has been demonstrated. If one now assumes the existence of such dislocation loops pinned to the surface at the damaged region created by the scribe line (the results of Rindner seem to indicate this is possible), one may extend or diminish the loop size by compressing or extending the material between the pinning points as shown in Fig. 8. Kabler (17) has indicated that the loop is probably a half-hexagon where loop growth is accomplished by motion parallel to the surface of the 60° segments and motion perpendicular to the surface of the bottom segment. In Fig. 8, 9, and 10 the depletion layer is shown as roughly symmetrical about the junction. This corresponds to the low-voltage transducer design wherein a shallow diffusion is made into an already heavily doped crystal. The dimensions are not accurate since the figures are intended to illustrate the dislocation motion only.

Another mechanism by which dislocations may enter the depletion region is as follows. Deformation

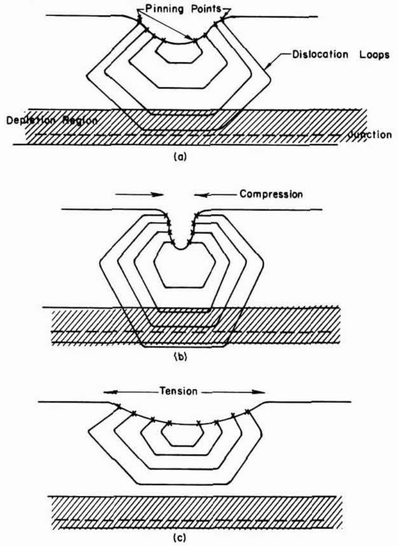

Fig. 8. Motion of dislocation loops created by plastic deformation (scribing): (a) no stress; (b) compression at surface; (c) tension at surface.

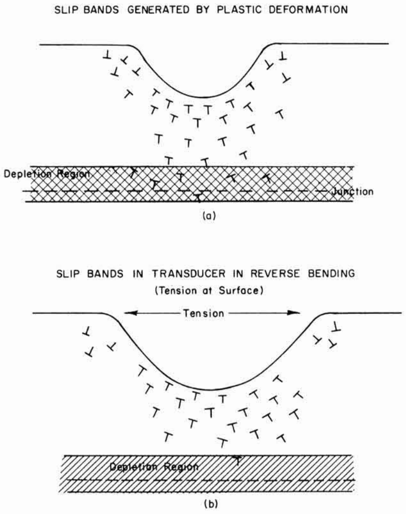

Fig. 9. Motion of slip bands created by plastic deformation: (a) no stress; (b) tension at surface.

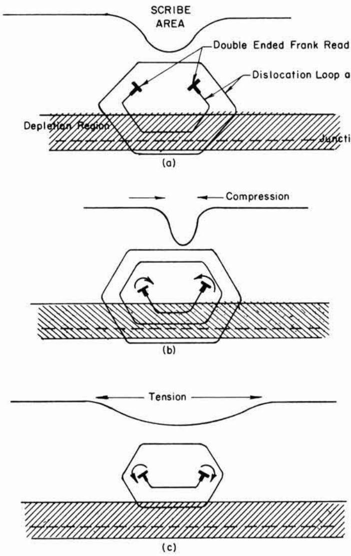

Fig. 10. Motion of dislocation loops and rings emanating from a double-ended Frank-Read source: (a) no stress; (b) compression at surface; (c) tension at surface.

bands are known to be generated by plastic deformation. These bands are formed mostly in crystals by compression or tension rather than in bending or twisting. Slip bands are formed across the deformation bands without interruption apart from bending to follow the curvature of the lattice as shown diagramatically in Fig. 9. On forward bending, compression is created at the surface, and the slip bands, under compression, migrate deeper into the body of the material. Thus more dislocations enter the depletion region of the p-n junction. Reverse bending causes tension at the junction as shown. The slip bands migrate toward the surface pulling the dislocation lines out of the depletion region. As seen in Fig. 9, the number of dislocations at any point is proportional to the radius of curvature at that point. An increase in the radius of curvature at the surface will cause the dislocations to pull in toward the scribe line.

The two theories of reversible movement of dislocations in and out of the depletion region may not be the only ones possible. In creating the anisotropic stress effect, both theories of dislocation movement may apply. The movement of dislocation lines and loops is further complicated by Frankel defects and foreign atoms lying inside the crystal bulk. Thus the theories presented here are not complete answers but merely steps toward solving a complicated phenomenon. A third theory involves a merging of the two previous theories. In Fig. 9 the parallel dislocation lines may, under stress, rotate forming dislocation loops. Pairs of dislocation lines may act as double-ended Frank-Read sources (18). After plastic deformation, dislocation loops may already have been generated by the dislocation line pairs. Many of these loops enter the depletion region causing the degraded reverse characteristic. Figure 10 shows a diagram illustrating the process. Under compression the loops radiate further outward and more loops are formed by the line pairs. When the compression is relieved, the dislocation loops collapse toward the Frank-Read sources as in the diagram. Tension causes further collapse of the loops and even the collapse of rings that have been formed. This pulls more loops and rings out of the depletion region. This effect is known as the Bauschinger effect (19). When the device is under forward pressure, compression is applied to the scribed area and an increase in reverse leakage current is observed. This corresponds to an increase in the number of dislocation loops in the depletion region. In Fig. 10 only one double-ended Frank-Read source is shown. In reality, there may be many Frank-Read sources packed close together under the scribe line, the density of sources being proportional to the amount of plastic damage sustained by the crystal during the sensitizing process. One must recognize that this theory is very incomplete and has not been proven by an extensive program of metallurgical experiments.

We have endeavored, using x-ray diffraction studies, to determine whether room temperature scribing with a diamond stylus would produce any dislocations in silicon. The silicon slices were cut from an ingot doped with antimony to a resistivity of roughly 0.01 ohm-cm. They were lapped to 15 mils thickness and chemically polished to a final thickness of 11 mils. Scribing was performed in the $(1\bar{1}0)$ direction and perpendicular to the $(1\bar{1}0)$ direction with forces of 2000, 4000, and 8000 dynes. X-ray micrographs were taken following scribing with the diffracting plane lying in the $(10\bar{1})$, $(1\bar{1}0)$, and the $(0\bar{1}1)$ planes of the slice. If the Burgers vector of a generated dislocation lies in the diffracting plane it will almost disappear from the micrographs, whereas if it is perpendicular to the dif-

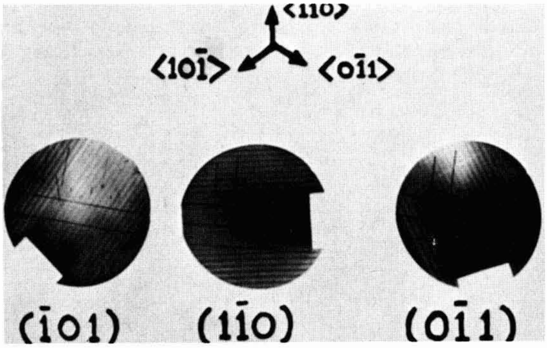

Fig. 11. X-ray micrographs of a silicon wafer scribed with a 1μ diameter diamond hemisphere under forces of 2000, 4000, and 8000 dynes along the $\langle 111 \rangle$ direction and perpendicular to the $\langle 111 \rangle$ direction. Diffractiongraphs were taken with the plane of diffraction parallel to the $(\bar{1}01)$, $(1\bar{1}0)$, and $(0\bar{1}1)$ planes of the crystal.

fraction plane it will exhibit maximum contrast. Figure 11 shows the existence of dislocations due to room temperature scribing. In the center micrograph the short 2000 dyne/cm² line has all but disappeared. The diffraction plane is here almost parallel to the dislocation Burgers vector. In the two side micrographs the diffraction plane lies at 30° to the Burgers vector of the long lines. Here the 2000 dyne/cm² line shows much reduced contrast. Further diffraction experiments have been completed and will be reported in the near future (20).

It is known that dislocations act as acceptors in silicon producing trapping levels in the forbidden region between the valence band and the conduction band. Depending on the position of the Fermi level, the acceptor sites are filled to some degree, and the dislocation line is negatively charged. This negative line charge is neutralized by a cylindrical space charge of fixed donors around the dislocation. It has been confirmed (21) that dislocations produce recombination centers in germanium and that the minority carrier lifetime is drastically decreased by the existence of these recombination centers. Indeed, at room temperature, p-type germanium has a lifetime of $\tau = 0.7/N_d$. In n-type, the lifetime is $\tau = 2.5/N_d$ where N_d is the dislocation density. One would expect similar relationships to exist for silicon.

Up to now the argument has been to link the reversible motion of dislocation loops with reversible changes in the leakage current of the back biased diode. Justification for this linkage can be made by using the Sah-Noyce-Shockley model of carrier generation and recombination in p-n junctions and its effect on p-n junction characteristics (22). for medium to large reverse bias ($V > kT/q$) the generation current is given by Eq. [1].

$$J_{gr} = \frac{qn_i W}{2\sqrt{\tau_{no}\tau_{po}}} \left[\cosh\left\{ \left(\frac{E_t - E_i}{kT} \right) + \ln \sqrt{\frac{\tau_{po}}{\tau_{no}}} \right\} \right]^{-1} \quad [1]$$

where W is the space charge layer width, τ equals minority carrier lifetime, E_t the energy level of the traps, and E_i the energy of the intrinsic Fermi level. τ_{no} and τ_{po} are the electron and hole minority carrier lifetimes. When the trap levels lie at mid-band the first term in the hyperbolic cosine is 0 and the term in square brackets is given by expression [2].

$$\cosh\left\{ \ln\sqrt{\frac{\tau_{po}}{\tau_{no}}} \right\} = 1/2 \left(\exp\left[\ln\sqrt{\frac{\tau_{po}}{\tau_{no}}} \right] + \exp\left[-\ln\sqrt{\frac{\tau_{po}}{\tau_{no}}} \right] \right) = 1/2 \left(\sqrt{\frac{\tau_{po}}{\tau_{no}}} + \sqrt{\frac{\tau_{no}}{\tau_{po}}} \right) \quad [2]$$

As a simplifying assumption, let us consider this to be true (Rindner has found the effective trapping level in germanium to be 0.09 ev from the intrinsic Fermi level). Using this simplifying assumption, Eq. [1] now becomes

$$J_{gr} = + \frac{qn_i W}{4} \left(\frac{1}{\tau_{po}} + \frac{1}{\tau_{no}} \right) \quad [3]$$

We see that the generation recombination current is dependent upon depletion layer width and lifetime. Investigators of ASE in Japan have been successful in demonstrating up to a 30% decrease in minority carrier lifetime under both uniaxial and anisotropic stress for both germanium and silicon (23, 24). They attributed the reduction in lifetime to strain fields and expressed total lifetime as a function of two components, the stress independent and the stress dependent lifetimes, in the following fashion:

$$\frac{1}{\tau_n} = \frac{1}{\tau_{no}} + \frac{1}{\tau_\sigma}$$

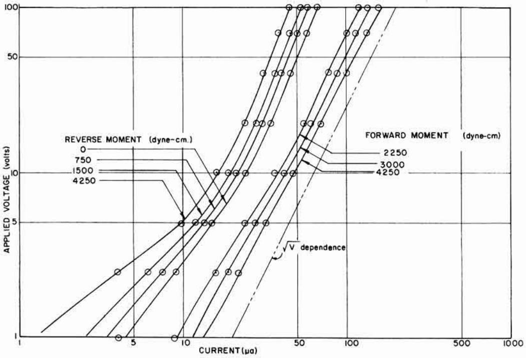

Fig. 12. Reverse characteristics of a typical transducer diode under stress.

where τ_σ has the following dependence

$$\tau_\sigma = \frac{1}{vAN}$$

where v is the thermal velocity of minority carriers, cm/sec^{-1}, A the capture cross section for minority carriers, cm², and N the number of recombination centers, cm^{-3}.

Assuming v and A constant throughout our measurements we may obtain J_{gr} as a function of N. Thus for an N-type substrate with a p-type diffusion the lifetime of minority carriers in the surface layer will be

$$\tau = \left[\frac{1}{\tau_{no}} + vAN \right]^{-1}$$

Since the p-n junction is formed by using a constant impurity source high-temperature diffusion for a very short time, it will closely approximate a step junction, especially at the higher voltages and for shallow junctions. For a 0.5μ junction the voltage at which the cube root dependance becomes a square root dependance is about 2v (26). Using the step-function equation for depletion layer width given by Eq. [4]

$$W = \left[\frac{2\kappa\epsilon_0 V'}{q(N_D - N_A)} \right]^{1/2} \quad [4]$$

and considering only the effect of the change of minority carrier lifetime given by the equation above we have

$$J_{gr} = \frac{qn_i}{4} \left[\frac{2\,\kappa\epsilon_0 V'}{q(N_D - N_A)} \right]^{1/2} \left(\frac{l}{\tau_{no}} + vAN \right) \quad [5]$$

where V' is the applied voltage plus the built-in voltage.

Thus, for reverse voltages greater than kT/q the generation-recombination current is proportional to the density of recombination centers in the depletion region and proportional to the square root of the applied voltage. Figure 12 shows the square root voltage dependence for our device under various forward and reverse load conditions and for reverse bias. Figure 6 shows clearly that the current-force relationship was quite linear which would suggest that recombination center density is linearly proportional to the applied bending moment. Note that an approxi-

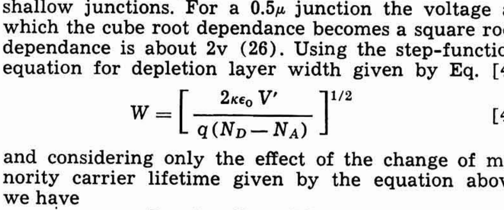

Fig. 13. Transducer noise measurement set-up

mate square-root voltage dependence is maintained for both forward and reverse bending moment for voltages above 5v. Below this voltage the slope changes somewhat for the reverse moment curves in the direction of lower resistance approaching an inverse cube-root dependence.

For the moment it is not clear whether the change in τ_σ is due to a change in A or a change in N. Certainly a strain field would change A, but on the other hand dislocation loops have been shown to exist in silicon, they have been shown to move rapidly as a function of the motion of the pinning points in LiF, and we show here that ASE is seen in the bending mode only when damage is present. With this assemblage of facts it does not seem too unreasonable to postulate that the change in $1/\tau_\sigma$ is due to N, and that the change in N is due to the reversible movement of dislocation loops into the depletion region as previously discussed.

Noise

Electrical noise generated at the junction was investigated using the apparatus shown in Fig. 13. The transducer diode was biased at its normal operating voltage (around 1.0v for the low-voltage variety and 45.0v for the high-voltage type). Using this set-up the noise current-frequency spectrum was found to be approximately (1/f) from 1 to 100 kHz both before and after the sensitizing operation although scribing increased the noise current over the entire range by roughly a factor of 10 as shown in Fig. 14. Indeed, scribing changes the noise current from about 6 na to about 60 na on typical units as may be seen from Fig. 15. The oxide layer offers some protection as can be seen by the increase of noise after oxide removal. Much of the noise eliminated by the oxide layer is below 100 Hz and is due to slow states in the thin air grown oxide present after the removal of the thermal oxide. The noise current generated by scribing is (1/f) flicker noise due to reverse leakage current. As was mentioned earlier, scribing degrades the reverse characteristic lowering the resistance, and increasing the leakage. Fonger (27) has shown that this type of noise current is directly proportional to leakage current. We have observed this type of behavior as may be seen from Fig. 16.

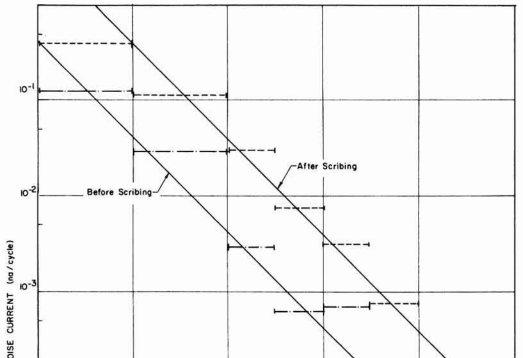

Fig. 14. Noise current spectrum of a typical transducer diode

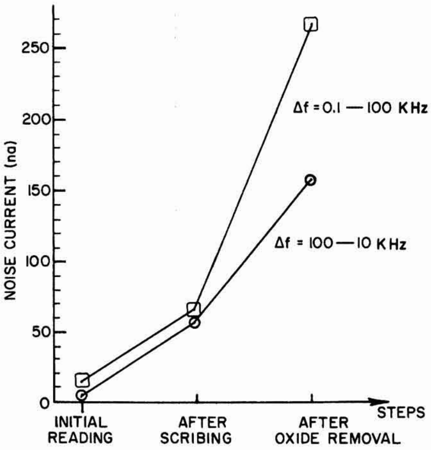

Fig. 15. Noise current increase in the transducer diode after scribing and oxide removal.

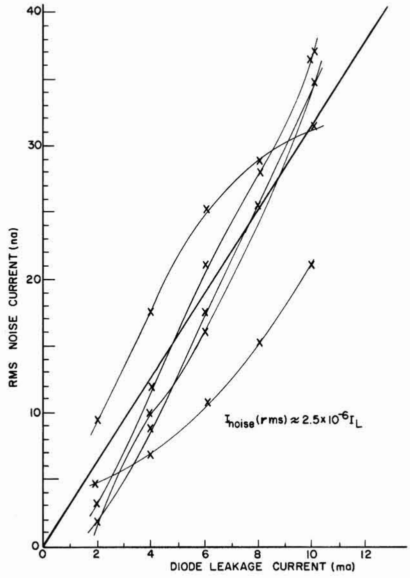

Fig. 16. Variation of diode noise current with reverse leakage current.

With the protective oxide present the transducer is insensitive to gaseous ambients. Gas cycles using dry N_2, wet N_2, O_2, and air were applied to the surface without a change in noise current. CCl_4 was also tried as an atmosphere, but it did not change the (1/f) spectrum or intensity. Contact noise has been shown to be responsible for flicker noise by Montgomery (28).

An experiment involving four ohmic contacts on the diode showed that contact noise was responsible for only 20% of the total (1/f) noise. About half of the total noise is located at the perimeter of the junction where it intersects the oxide layer. Reduction of this perimeter correspondingly reduced the (1/f) noise. This noise is also leakage noise generated by channeling under reverse bias.

Since the sensitivity of the transducer increases with scribing as well as the noise it was at first thought that the signal-to-noise-current ratio might remain

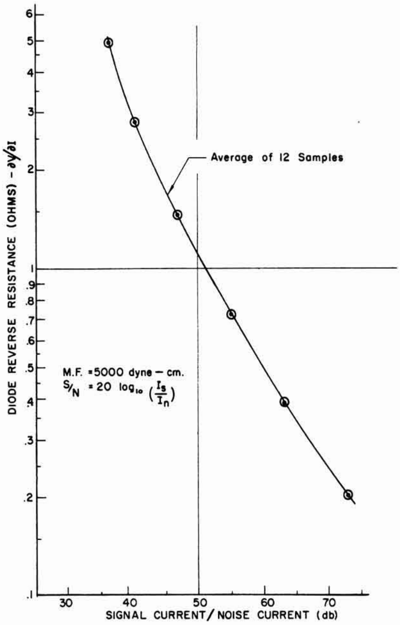

Fig. 17. Change in signal-to-noise ratio as a function of diode reverse resistance.

constant during the process. However, an experiment revealed that the signal-to-noise ratio actually slowly increased with scribing as shown in Fig. 17. In the figure the reverse resistance is the slope of the reverse-biased current-voltage trace taken at the operating voltage. The increase in S/N ratio is perhaps due to the relative decrease in importance of nonscribe-related noise sources. A device with 75db signal-to-noise ratio was obtained under a 5000 dyne-cm variation.

An analysis of stress created at the junction in a direction parallel to the surface and perpendicular to the notch indicates a stress maximum of 3.6×10^9 dynes/cm^2 for a bending moment of 5000 dyne-cm. Beyond this stress the more fragile units would fracture. The pressure and shape of the notch seriously complicates an analysis of the stresses at the junction itself although methods of analysis exist (29). A typical notch had a mechanical stiffness of 3.3×10^5 dynes/cm.

A recent analysis of dislocation velocity (14) in silicon indicates a room temperature velocity for these stress levels above 100 cm/sec. For a movement of 0.1μ a frequency of 10 MHz is theoretically possible. The maximum frequency of vibration of the free end of the transducer is however related to the geometry of the device. Typical units had a 10 kHz self-resonance, and no attempt was made to increase this value. Mechanical stiffness for the 10 kHz resonance was about 3×10^5 dynes/cm.

Effective junction lifetime using the method of Lederhandler and Giacolleto (30) was found to be in the range of 1 μsec before stress was applied. One must remember here that this already represents the lifetime of a seriously degraded junction. This lifetime corresponds to that obtained by Matsuo (31) using a stylus pressure of almost 30g. A simple equivalent circuit of the diode under reverse bias is a variable resistor with a zero-stress resistance of 500 ohms in parallel with a capacitor of about 200 pf capacity. Impedances calculated using this model are in close agreement to measurements taken on a typical transducer diode from d.c. to 1 MHz.

Manuscript received Nov. 22, 1965; revised manuscript received Oct. 14, 1966. This paper was presented at the San Francisco Meeting, May 9-15, 1965.

Any discussion of this paper will appear in a Discussion Section to be published in the December 1967 JOURNAL.

REFERENCES

1. W. Rindner, *J. Appl. Phys.*, **33**, 2479 (1962).
2. W. Rindner and R. Nelson, *Proc. IRE*, **50**, 2106 (1962).
3. W. Rindner, G. Doering, and R. Wonson, *Solid State Electronics*, **8**, 227 (1965).
4. W. Bernard, W. Rindner, and H. Roth, *J. Appl. Phys.*, **35**, 1860 (1964).
5. A. Goetzberger and R. H. Finch, *ibid.*, **35**, 1851 (1964).
6. W. H. Legat and L. K. Russell, *Solid State Electronics*, **8**, 709 (1965).
7. W. Rindner, H. Roth, and W. Bernard, *J. Appl. Phys.*, **36**, 3625 (1965).
8. W. Rindner and I. Braun, *ibid.*, **34**, 1958 (1963).
9. R. Edwards, Trans. IEEE-ED11, 286 (1964). J. J. Wortman, J. R. Hauser, and R. M. Burger, *J. Appl. Phys.*, **35**, 2122 (1964).
10. W. Rindner, *J. Appl. Phys.*, **36**, 2513 (1965).
11. W. Rindner and R. F. Tramposch, *ibid.*, **34**, 758 (1963). R. F. Tramposch and W. Rindner, *Appl. Phys. Letters*, **3**, 42 (1963).
12. J. J. Gilman and W. G. Johnston, "Dislocations and Mechanical Properties of Crystals," J. Wiley & Sons, Inc., New York (1957).
13. Z. B. Pariiski, A. I. Landau, and V. E. Startsev, *Soviet Phys. Solid State*, **5**, 1002 (1963).
14. A. R. Chaudhure, J. R. Patel, and L. G. Rubin, *J. Appl. Phys.*, **33**, 2736 (1962).
15. H. G. van Bueren, "Imperfections in Crystals," North-Holland Publishing Co. (1960).
16. V. Celli, M. Kabler, T. Ninomiya, and R. Thomson, *Phys. Rev.*, **131**, 58 (1963).
17. M. N. Kabler, *ibid.*, **131**, 54 (1963).
18. A. H. Cottrell, "Dislocation and Plastic Flow in Crystals," Oxford Press (1953).
19. N. F. Mott, "Dislocations and Mechanical Properties of Crystals," Lake Placid Conference, John Wiley & Sons, Inc., New York (1957).
20. E. M. MacKenna, W. H. Legat, and L. K. Russell, To be published.
21. G. K. Wertheim and G. L. Pearson, *Phys. Rev.*, **107**, 694 (1957).
22. C. T. Sah, R. N. Noyce, and W. Shockley, *Proc. IRE*, **45**, 1228 (1957).
23. Y. Matukura, *Japanese J. Appl. Phys.*, **3**, 256 (1964).
24. T. Imai, M. Uchida, H. Sato, and A. Kobayashi, *ibid.*, **4**, 102 (1965).
25. Y. Matukura and Y. Miura, *ibid.*, **4**, 72 (1965).
26. "Integrated Silicon Device Technology—Vol. II" AD423148-Defense Documentation Center (unclassified).
27. W. H. Fonger, "Transistors L" RCA Laboratories, Princeton (1956).
28. H. C. Montgomery, *Bell Syst. Tech. J.*, **31**, 950 (1952).
29. H. Neuber, "Kerbspannungslehre," J. Springer, Berlin (1958).
30. S. R. Lederhandler and L. J. Giacoletto, *Proc. IRE*, **43**, 477 (1955).
31. K. Matsuo, *J. Phys. Soc. Japan*, **19**, 1490 (1964).

APPENDIX

Calculation of dislocation velocities at room temperature under high stress.—Van Bueren has derived an expression for the velocity of a dislocation line pinned between two points in a crystalline lattice (15). The resulting expression is given below.

$$v = \nu_0 \, b \exp(-E/kT) \sinh(\tau b^2 l/kT)$$

where ν_0 is the lattice vibrational frequency, b the distance of line travel (minimum of one lattice constant), τ stress level, l length of dislocation line between pinning points, and E activation energy for the motion of a dislocation; k and T have their usual meaning.

When $b^2 l >> kT$ we have $\sinh(\tau b^2 l/kT) \approx \frac{1}{2} \exp(\tau b^2 l/kT)$ and our equation becomes

$$v = \frac{\nu_0 b}{2} \exp\left(\frac{\tau b^2 l}{kT} - \frac{E}{kT}\right)$$

Consider a dislocation loop 1000Å long between the two pinning points. If we subject the loop to a stress of 10^8 dynes/cm^2 the resulting dislocation velocity should be found as shown below:

for $b = 5.4 \times 10^{-8}$ cm; $b^2 = 2.916 \times 10^{-15}$ cm^2
$\nu_0 = k\theta_0/h = 1.376 \times 10^{13}$ (sec)$^{-1}$ (θ_0 = Debye temperature)
$k = 1.38 \times 10^{-16}$ ergs/°K $= 8.625 \times 10^{-5}$ ev/°K
$T = 300$°K; $kT = 4.14 \times 10^{-14}$ dyne-cm $= 0.0258$ ev
$E = 2.17$ ev (14)

Since $\tau b^2 l/kT = 70.42$ and $E/kT = 83.86$, the exponential term equals 8.23×10^{-5}.

Also $\nu_0 b/2 = 3.72 \times 10^5$ which yields $v = 3.06$ cm/sec.

If we increase the stress level slightly (say by only 1%) a large increase in dislocation velocity results.

We now have

$$\tau = 1.01 \times 10^8 \text{ dynes/cm}$$

$$\tau b^2 l/kT = 71.121$$

and the exponential term becomes 8.83×10^{-6}. This gives a resultant $v = 3.28$ cm/sec, *i.e.*, almost a 10% increase in velocity. Calculations of 5, 7.5, and 10% increases in stress yield velocities as shown below:

% Increase	Velocity, cm/sec
1.0	3.28
5.0	18.0
7.5	250.0
10.0	3.120.0

Since τ and l exhibit the same behavior in the equation, a slight change in the length of the dislocation loop would produce the same effect on the dislocation velocity. We also observe that the distance of travel of the loop (b) profoundly affects the dislocation velocity. The distance of travel will of course be limited by crystalline imperfections preventing its forward travel. When such an imperfection is encountered by a loop, a great deal more energy is needed to overcome this barrier than is necessary for simple unhindered forward travel.

The velocity calculated above is instantaneous velocity between imperfections as opposed to average velocity taken over large distances and times. Average velocity is the quantity reported in experiments on various materials. Chaudhuri *et al.* (14) report that the distances over which the dislocations accelerate before encountering imperfections are small compared to the distances necessarily involved in making an experimental measurement of dislocation velocity.

Chemical Etching of Germanium in the System HF-H_2O_2-H_2O

B. Schwartz[1]

Bell Telephone Laboratories, Incorporated, Murray Hill, New Jersey

ABSTRACT

The etching of germanium in the system HF-H_2O_2-H_2O has been studied, and comparisons are made with results obtained from the HF-HNO_3-H_2O system. Strong crystal-orientation influences and relatively high apparent activation energies are observed; surface reactivity and subsequent removal of reaction products are consequently proposed as rate limiting in the etching reaction. On the basis of equilibrium in the adsorption-dissociation steps, an equation is derived which describes the rate data obtained over the entire concentration and temperature ranges studied. Evidence is presented to show that divalent germanium is the prime oxidation state leaving the (100) and (111) surfaces. $GeOF_2$ is postulated as one of the reaction products leaving the (110) surface.

The use of semiconductor materials in the fabrication of active electronic devices has resulted in much work on the chemistry of these materials. Most of the effort has been spent on the problems of impurity content, stoichiometry, and thermodynamics in the formation of single crystals of these materials (1-3). Another important aspect is the etching of the single crystals to obtain the desired electrical and geometrical characteristics (4).

When an elemental semiconductor is etched in an aqueous system, somewhere in the process oxidation of the element must occur in order to produce a removable product. For that reason, an oxidizing agent is always present in the solution[2] when either silicon (6, 7) or germanium (8-11) is etched. In most cases nitric acid is used as the oxidizing agent and hydrofluoric acid is added as the means of forming a soluble or gaseous reaction product (6, 8, 11). However, the etching of germanium in the system HF-HNO_3-H_2O is beset with many difficulties, such as uncontrollable induction periods and passivating films (9, 11). Another etching system for germanium that has found practical application is HF-H_2O_2-H_2O (10). This paper reports the results of a study of the etch rate of single-crystal germanium in aqueous solutions of HF and H_2O_2 as a function of the composition and temperature of the etchant. The influence of crystallographic orientation and conductivity type of the germanium specimens on the etch rate is discussed. A kinetic model is developed, based on adsorption-dissociation isotherms, which describes mathematically the etch-rate data obtained. A comparison is made of equilibrium constants for both peroxide and fluoride adsorption and dissociation reactions. From the order of the reaction, relative to H_2O_2 and HF concentrations, postulations of the desorbing species are made.

Experimental Procedure

The etch rates were determined by measuring the decrement in thickness of both n- and p-type germanium dice of approximately 3 ohm-cm resistivity after subjecting them to the etchant under the chosen conditions of time and temperature. The thickness of each die was measured at its center with a double-pointed micrometer that could be read to ±0.0001 in., and the reading was estimated to the next decimal place. Three dice were etched simultaneously in each

---

[1] The data used in this paper were obtained while the author was employed at Hughes Aircraft Company.

[2] Although it has been observed that water will dissolve germanium, Harvey and Gatos (5) determined that it was necessary to have dissolved oxygen in the water or the etching would not proceed.

experiment; all three were of the same conductivity type, but the major faces of each displayed only one of the three low-index planes. All of the dice were approximately 0.025 in. thick, but the surface areas were $1.25x10^{-2}$, $1x10^{-2}$, and $1.6x10^{-2}$ in.^{2} for the (111)-, (110)-, and (100)-oriented samples, respectively. All dice were pre-etched in a solution of HF-HNO_3-H_2O-$HC_2H_3O_2$ to produce a specular surface free of work damage.

The etching solutions were prepared by weighing out the required amounts of the reagents in polyethylene bottles. Although it has been found that solutions so made and stored are stable (8), no solutions were allowed to stand overnight, and all solutions were used within ½ hr to 4 hr after preparation. In order to ensure an adequate supply of reagents of constant concentration, several 1-lb bottles of the specific reagent (HF or H_2O_2) were thoroughly mixed in a large container. The concentrations of these master batches were determined, and the original bottles were then refilled from these master batches.

Since H_2O_2 is catalytically decomposed by many metals and metallic ions, it was considered necessary to take precautions to exclude these from contact with the etching solutions. Thus neither platinum nor stainless-steel equipment could be used, and all experiments were conducted in polyethylene ware. The etchant was allowed to equilibrate thermally in a constant temperature bath before any samples were introduced. The quoted temperature was the initial temperature of the solution and, unless otherwise stated, was 25°C. Because of the poor heat-transfer characteristics of polyethylene beakers, the experiments were run under essentially adiabatic conditions.

All of the samples were contained in a small, perforated basket, which was agitated violently while immersed in the etching solution. Quenching was achieved by rapidly transferring the basket to a large beaker containing 250 ml of water. Approximately 20 ml of etchant was used for each measurement and was discarded immediately afterward; fresh solution was used for each determination. The conditions of etching were chosen such that the concentrations of reagents in the etching solution were depleted to a negligible extent.

Experimental Results

Figure 1, a plot of thickness change as a function of time, using differently oriented specimens, shows that there are no apparent induction periods in this system; thus, explicit etch-rate numbers can be quoted. In general, the rate numbers obtained in this work were comparable, to within ±5%, to the numbers obtained by Bloem and van Vessem (10).

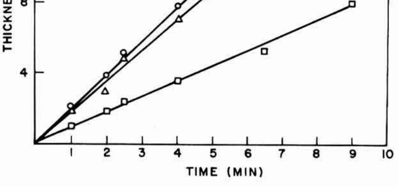

Fig. 1. Thickness change as a function of time, using a solution of 50% HF, 50% H_2O_2. The samples were n-type and were □ (100), ○ (110), and △ (111)-oriented, respectively. The solutions were made using 49.05% HF and 29.0% H_2O_2.

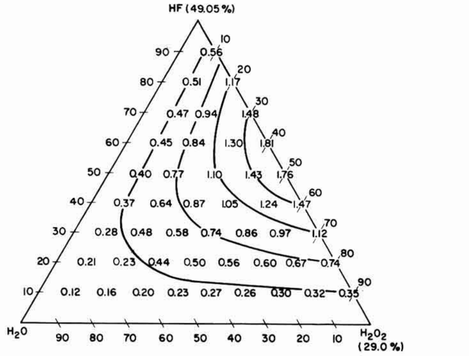

Fig. 2. Etch rate, in mils/min, as a function of etch composition. Samples were n-type, (111)-oriented, and the initial temperature was 25°C.

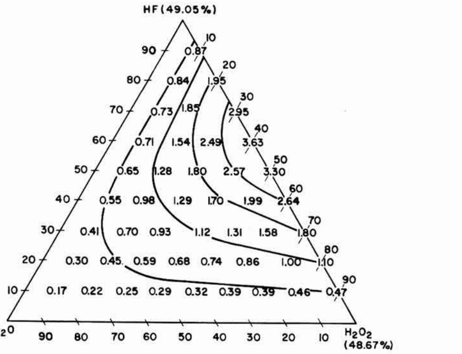

Fig. 3. Etch rate, in mils/min, as a function of etch composition. Samples were n-type, (111)-oriented, and the initial temperature was 25°C.

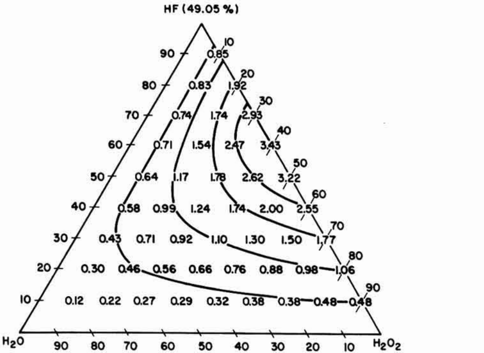

Fig. 4. Etch rate, in mils/min, as a function of etch composition. Samples were p-type, (111)-oriented, and the initial temperature was 25°C.

Figures 2, 3, and 4 are triaxial plots of etch rates at 25°C as a function of etchant composition, using (111)-oriented specimens. For ease in displaying the data,[3] the axes were left in weight-per cent units and normalized to 100% of the concentrated solutions used. The H_2O axis represents added water, not total water in the system. Also it should be noted that both standard-concentrated H_2O_2 (29.0% in Fig. 2) and

---

[3] Conversion of the scales to mol fraction units compresses the region of representation considerably but yields basically the same isoetch-rate contours.

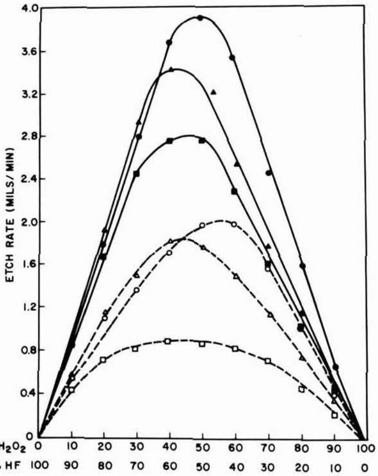

Fig. 5. Etch rates vs. normalized etch composition, using only the zero-added-water data. The solid curves were obtained using 49.05% HF, 48.67% H_2O_2 solutions, and the dashed curves were obtained with 49.05% HF, 29.0% H_2O_2 solutions. Orientations were ○ (110), □ (100), △ (111), and all samples were p-type.

special high-concentration H_2O_2 (48.67% in Fig. 3 and 4) were used as reagents for this study. Figures 2 and 3 show that a change from 29 to 49% H_2O_2 had practically no effect on the isoetch-rate contour but changed only the magnitude of the etch rates. A comparison of the data in Fig. 3 and 4 shows that, within experimental error, n- and p-type germanium of the same crystallographic orientation etched at the same rate in comparable etching solutions.

When all of the triaxial plots are examined, it is seen that in the regions of high H_2O_2 concentrations the isoetch-rate curves are essentially parallel to constant HF lines. Conversely, in regions of high HF concentrations the isoetch-rate curves indicate that the H_2O_2 concentration is the important rate-controlling factor.

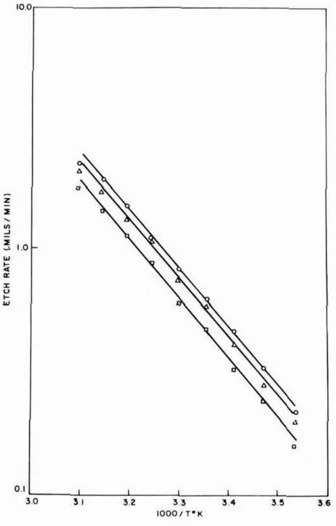

Fig. 6. *Influence of temperature on the etch rate of n-type* samples. The curves were obtained using 10% HF, 90% H_2O_2. The solution was made from 49.05% HF and 48.67% H_2O_2. Orientations were ○ (110), □ (100), and △ (111).

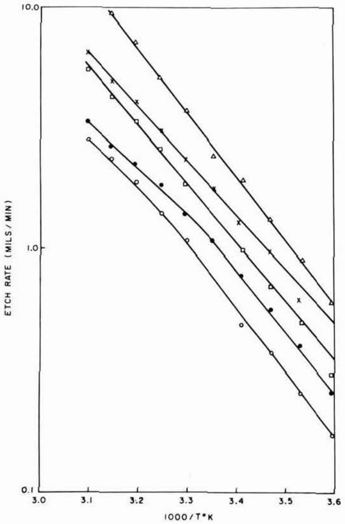

Fig. 7. Influence of temperature on the etch rate of (100)-oriented, n-type samples. Solution concentrations were: ○, 15% HF-55% H_2O_2-30% H_2O; ●, 55% HF-15% H_2O_2-30% H_2O; □, 20% HF-80% H_2O_2; X, 80%HF-20% H_2O_2; △, 35% HF-65% H_2O_2. Solutions were made using 49.05% HF and 48.67% H_2O_2.

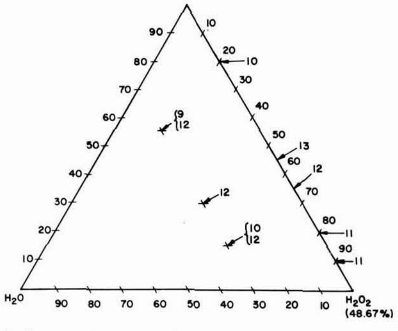

Fig. 8. Temperature dependences, in kcal/mol, as a function of *solution composition.*

Whereas Fig. 3 and 4 show that conductivity type had no apparent effect on the etch rate, Fig. 5 shows that orientation influences the etch rate strongly in both the 49 and the 29% H_2O_2 systems.

A study of the influence of temperature on the etch rate yielded curves shown in Fig. 6 and 7. Although the different orientations etch at different rates, the slopes of the lines drawn through the points in Fig. 6 are essentially the same. The breaking curves of Fig. 7 are typical of data obtained when there appears to be a shift in the rate-controlling step. A summary of the "apparent" activation energies as a function of etch composition is given in Fig. 8. The magnitude of the temperature dependences (9-13 kcal/mol) and the effect of orientation on the etch rates, together with the fact that etch rates in this system are much lower than in the HNO_3 system (11), suggest that over the entire composition region the etching reaction is surface controlled and not diffusion controlled.

Figure 9 is a plot of the effect of dilution with water on the etch rate of (110)-oriented dice; it is a two-dimensional representation of the three-dimensional etch-rate surface obtained with these reagents. The line drawn is the curve of 2:1 mol ratio of HF to

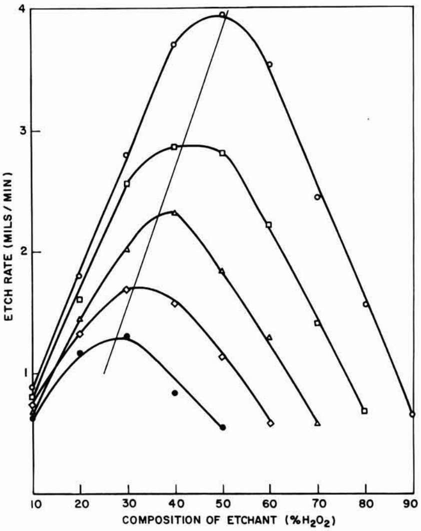

Fig. 9. Influence of added water on the etch rate of p-type, (110)-oriented germanium. Dilutions were ○, zero; □, 10%; △, 20%; ◇, 30%; and ●, 40% added water. Reagent concentrations were 49.05% HF and 48.67% H_2O_2.

H_2O_2, and it appears to agree very well with the etch-rate maxima. This might indicate the following stoichiometry

$$Ge + 2HF + H_2O_2 \rightarrow GeF_2 + 2H_2O \qquad [1]$$

or

$$Ge + 4HF + 2H_2O_2 \rightarrow GeF_4 + 4H_2O \qquad [2]$$

as the over-all reaction equation. However, as can be inferred from Fig. 5, the line that could be drawn through the maxima of the (111) and (100) etch rates would be displaced to mol ratios greater than 2:1. An analysis of the raw data showed that the ratios could be as high as 3:1, as indicated by Bloem and van Vessem (10). This ratio would then suggest the stoichiometry

$$Ge + 6HF + 2H_2O_2 \rightarrow H_2GeF_6 + 4H_2O \qquad [3]$$

Miuller and his co-workers (12), studying the dissolution of germanium in acidic and basic solutions of hydrogen peroxide, found that the etching rate increased with increasing acid or base concentration. The dissolution rate passed through a maximum and then decreased as more additive was put in the etching solution. In fact, if enough acid or base was added to the solution, the etching action would cease. Supin (13) has also studied the dissolution of germanium in hydrogen peroxides of various pH and found similar effects.

In order that the influence of an acid diluent on the etch rate in this system might be seen, a comparison was made between the etching rates of n-type (110)-oriented germanium in solutions that were diluted with pure water, glacial acetic acid, or concentrated sulfuric acid. Figure 10 shows the results of these experiments: curve I resulted when 20% acetic acid was added; curve II shows the effect when 20% sulfuric acid was added; and curve III indicates the effect of 20% added water; curve IV shows the effect of adding only 10% water, and curve V is the etching rate with no added diluent. Note the similarity of curves II and V; the etch rate appears to remain the same whether the solution was diluted with H_2SO_4 or not. However, dilution with acetic acid results in a definite increase in the etch rate. In both cases of dilution in acid, though, more etching was achieved than with an equivalent water-diluted system. It appears that the etch-rate surface generated by the composition-rate plot for acid-diluted HF-H_2O_2 etches would probably have less of a gradient in the direction of the diluent until critical added-acid concentrations were reached. Then a very marked decrease in etch rates would occur owing to the presence of large concentrations of diluent in the system.

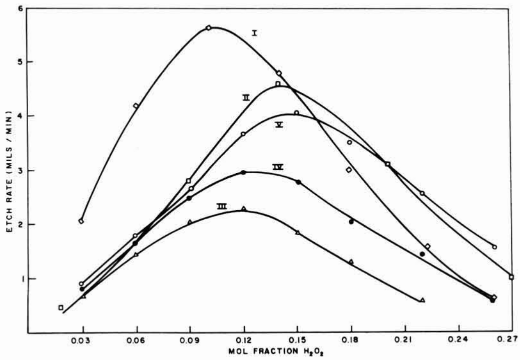

Fig. 10. Influence of acid diluent on the etch rate of (110)-oriented, n-type samples. Curve I, 20% added glacial $HC_2H_3O_2$; II, 20% added concentrated H_2SO_4; III, 20% added H_2O; IV, 10% added H_2O; V, zero added H_2O. Reagent concentrations were 49.05% HF and 48.67% H_2O_2.

Discussion of the Kinetics Model

In the introduction it was noted that dissolution of an elemental semiconductor proceeds in stepwise fashion: oxidation of the element followed by complexing of the oxidized form. Laidler (14) points out that a heterogeneous reaction occurring on a solid surface involves five consecutive steps:

1. Diffusion of the reacting molecules to the surface.
2. Adsorption of the reactants on the surface.
3. Reaction on the surface.
4. Desorption of the products.
5. Diffusion of the desorbed products into the main body of the surrounding medium.

Since the present study deals with the dissolution of a solid in a liquid, these five steps must be considered. In the system Si-HF-HNO_3-H_2O it was shown (6, 7) that, in a specific etchant-composition region, diffusion was the dominant kinetic factor in the dissolution. In the system Ge-HF-HNO_3-H_2O it was observed (11) that control by diffusion was only of secondary importance, and it was postulated that step 4 was the most important part of the sequence. In the system Ge-HF-H_2O_2-H_2O the high-temperature dependence and strong crystallographic orientation effects clearly indicate that, over the entire composition region studied, the rate-controlling factors are involved in one or more of steps 2, 3, and 4, while steps 1 and 5 play only minor roles.

Camp (8) considered the system of r-sequential steps involved with rate control at a Ge-HF + H_2O_2 solution interface and derived a relationship which fitted his temperature data quite well

$$R = \frac{1}{\displaystyle\sum_{1}^{r} \frac{e^{E_i/kT}}{a_i C_i^{p_i}}} \qquad [4]$$

where R = etch rate, E_i = activation energy of i^{th} step, C_i = concentration of reagent involved in i^{th} step, p_i = power to which C_i enters i^{th} reaction, a_i = constant associated with i^{th} reaction, k = Boltzmann constant, T = absolute temperature. For his derivation Camp used the expression

$$R_j = \theta_j a_j C_j^{p_j} \exp\left(-E_j/kT\right) \qquad [5]$$

where θ_j was the fraction of the surface on which the j^{th} or rate-limiting reaction took place; he assumed rate control by only one reagent at a time.

It was found that Eq. [4] qualitatively fitted the temperature data shown in Fig. 6 and 7 and also the data displayed in Fig. 5, which were obtained by varying the reagent concentrations and holding the temperature constant. However, if the data of Fig. 2, 3, and 4 are converted to mol fraction or molality units and replotted as a function of varying only one reagent at a time (Fig. 11 and 12), then Eq. [4] no longer describes the shapes of the curves obtained.

Laidler (14) has considered the case where a diatomic molecule is first adsorbed and then dissociated on a surface

$$A_2 + 2S \rightleftharpoons 2(S - A) \qquad [6]$$

He found that at equilibrium the fraction of surface sites covered, θ, was

$$\theta = \frac{a_\theta C_{A_2}{}^{1/2}}{1 + a_\theta C_{A_2}{}^{1/2}} \qquad [7]$$

where a_θ = constant of proportionality. His analysis can be extended so that if there are two diatomic molecules simultaneously in equilibrium with activated surface sites, *i.e.*

$$X_2 + 2S \overset{K_X}{\rightleftharpoons} 2(S - X) \qquad [8]$$

$$Y_2 + 2S \overset{K_Y}{\rightleftharpoons} 2(S - Y) \qquad [9]$$

then the fractions of the surface covered by each activated species would be

$$\theta_X = \frac{K_X{}^{1/2} C_{X_2}{}^{1/2}}{1 + K_X{}^{1/2} C_{X_2}{}^{1/2} + K_Y{}^{1/2} C_{Y_2}{}^{1/2}} \qquad [10]$$

$$\theta_Y = \frac{K_Y{}^{1/2} C_{Y_2}{}^{1/2}}{1 + K_X{}^{1/2} C_{X_2}{}^{1/2} + K_Y{}^{1/2} C_{Y_2}{}^{1/2}} \qquad [11]$$

and the fraction of unoccupied sites would be

$$(1 - \theta_X - \theta_Y) = \frac{1}{1 + K_X{}^{1/2} C_{X_2}{}^{1/2} + K_Y{}^{1/2} C_{Y_2}{}^{1/2}} \qquad [12]$$

Laidler (14) also considered the generalized bimolecular surface-catalyzed gas-phase reaction

$$A + B + S_2 \rightleftharpoons ABS_2 \rightarrow \text{reaction products} \qquad [13]$$

and he arrived at the expression

$$R = k' C_A C_B C_{S_2} \qquad [14]$$

where k' = rate constant, C_A = concentration of reagent A, C_B = concentration of reagent B, C_{S_2} = concentration of bare dual sites at adsorption-desorption equilibrium.

The following is an attempt to apply the surface adsorption-dissociation concepts to the aqueous system under study here. If we assume an n-component system in steady state with the surface reaction or desorption step as rate limiting, then an equation analogous to Laidler's expression for the j^{th}, or rate-controlling, step can be written as

$$R_j = a_j e^{-E_j/kT} C_{S_m} \prod_{1}^{n} C_i{}^{p_i} \quad {}^{4} \qquad [15]$$

where C_i = concentration of each of the reagents in solution, p_i = stoichiometry with which each of the reagents is involved in the rate-limiting step, C_{S_m} = a surface-concentration function that describes the nature of the surface on which the j^{th} reaction takes place (the adsorption and dissociation steps on the surface are assumed to be in equilibrium with the reagents in solution).

For the system Ge-HF-H_2O_2-H_2O, Eq. [15] becomes

$$R = a'[H_2O_2]^{p_1}[HF]^{p_2} C_{S_m} \qquad [16]$$

where a' contains the water and the activation terms, which are assumed to be constant factors at constant temperature. Note that Eq. [15] reduces to Camp's original expression, Eq. [5], if indeed the reaction steps are sequential and the rate-controlling step involves only one reagent. Therefore Laidler's surface-concentration function should be Camp's fraction of the surface on which the rate-limiting reaction can proceed and

$$R = \theta a'[H_2O_2]^{p_1}[HF]^{p_2} \qquad [17]$$

Let us assume that X_2 and Y_2 in Eq. [8] and [9] represent the peroxide and fluoride reagents, respectively; the pair of adsorption and dissociation steps might then be

$$H_2O_2 + 2Ge \overset{K_1}{\rightleftharpoons} 2(Ge - OH) \qquad [18]$$

and

$$HF_2^- + 2Ge \overset{K_2}{\rightleftharpoons} (2Ge \cdot HF_2)^- \quad {}^{5} \qquad [19]$$

For constant [HF], and if we assume that H_2O_2, the rate-limiting reagent, acts only on the unoccupied surface sites, then Eq. [17] becomes

$$R = (1 - \theta_1 - \theta_2) a''[H_2O_2]^{p_1}[HF]^{p_2} \qquad [20]$$

Substitution of corrected Eq. [12] into Eq. [20] results in

$$R = \frac{a''[H_2O_2]^{p_1}[HF]^{p_2}}{1 + K_1{}^{1/2}[H_2O_2]^{1/2} + K_2{}^{1/2}[HF]^{1/2}} \quad {}^{6} \qquad [21]$$

For constant $[H_2O_2]$ and if we assume that HF, the rate-limiting reagent, acts only on the oxidized surface sites, then Eq. [17] becomes

$$R = \theta_1 a'''[H_2O_2]^{p_1}[HF]^{p_2} \quad {}^{7} \qquad [22]$$

Substitution of corrected Eq. [10] into [22] results in

$$R = \frac{a''' K_1{}^{1/2}[HF]^{p_2}[H_2O_2]^{p_1 + 1/2}}{1 + K_1{}^{1/2}[H_2O_2]^{1/2} + K_2{}^{1/2}[HF]^{1/2}} \qquad [23]$$

Although Eq. [15] is the general rate expression governing the over-all system, the assumption that there are two different rate-limiting situations results in two specific rate equations. In that part of the etchant composition region where $[H_2O_2]$ is rate limiting, it is the oxidation of bare germanium that is assumed to be the important step and Eq. [21] is believed to be the rate expression describing the situation. When [HF] is rate determining, Eq. [23] is believed to be the appropriate rate expression. One approach to the generation of a single relationship which describes the entire system is to use the mathematical technique of linear combination of the component parts. This results in

$$R = \frac{b[H_2O_2]^{p_1}[HF]^{p_2}}{1 + K_1{}^{1/2}[H_2O_2]^{1/2} + K_2{}^{1/2}[HF]^{1/2}} + \frac{b' K_1{}^{1/2}[H_2O_2]^{p_2 + 1/2}[HF]^{p_2}}{1 + K_1{}^{1/2}[H_2O_2]^{1/2} + K_2{}^{1/2}[HF]^{1/2}} \qquad [24]$$

or

$$R = (b + b' K_1{}^{1/2}[H_2O_2]^{1/2}) \frac{[H_2O_2]^{p_1}[HF]^{p_2}}{1 + K_1{}^{1/2}[H_2O_2]^{1/2} + K_2{}^{1/2}[HF]^{1/2}} \qquad [25]$$

---

[4] It should be noted that $a_j \exp(-E_j/kT)$ is equivalent to k' of Eq. [14] by the Arrhenius equation.

[5] According to Sidgwick (16), the predominating anionic species in hydrofluoric acid solutions is HF_2^-. The symbol $(_2Ge \cdot HF_2)^-$ is to be regarded as an abbreviation for a possible bridged structure of the form $Ge \cdot F\text{-}H\text{-}F \cdot Ge^-$.

[6] Note that [HF] has been used in the denominator in order to simplify the analysis. The fluoride species of importance is not really known. A more rigorous derivation might require use of $[HF_2^-]$ or $[H_2F_2]$, but this would merely be a correction of K_2 by a factor of 20 or 2, respectively. The former number comes from the fact that the concentration of the bifluoride ion is approximately 5% of the total hydrogen fluoride in solution.

[7] The reason a'' and a''' are used and are to be distinguished from the generalized a' is that now two different rate-controlling reagents are being considered separately and the specific rate constants for these reactions do not necessarily have to be equal.

Let us now consider the results of applying some specific sets of conditions to Eq. [25].

Case I.—If [HF] is held constant at different parametric values and $[H_2O_2]$ is considered to be the independent variable, then

(*A*) when

$$1 + K_1^{1/2}[H_2O_2]^{1/2} << K_2^{1/2}[HF]^{1/2} \quad [26]$$

and if $b'\sqrt{K_1[H_2O_2]}$ is also small then

$$R \propto [H_2O_2]^{p_1} \quad [27]$$

(*B*) when

$$1 + K_2^{1/2}[HF]^{1/2} << K_1^{1/2}[H_2O_2]^{1/2} \quad [28]$$

and if b' is small then

$$R \propto [H_2O_2]^{p_1 - 1/2} \quad [29]$$

Case II.—If $[H_2O_2]$ is held constant at different parametric values and [HF] is considered to be the independent variable, then

(*A*) when

$$1 + K_2^{1/2}[HF]^{1/2} << K_1^{1/2}[H_2O_2]^{1/2} \quad [30]$$

then

$$R \propto [HF]^{p_2} \quad [31]$$

(*B*) when

$$1 + K_1^{1/2}[H_2O_2]^{1/2} << K_2^{1/2}[HF]^{1/2} \quad [32]$$

then

$$R \propto [HF]^{p_2 - 1/2} \quad [33]$$

Application of the Kinetics Model

It is readily seen that the curves in Fig. 11 can be expressed by the relationships shown in Eq. [26] through [29] if p_1 is unity. Similarly, the curves of Fig. 12 can be expressed by the relationships shown in Eq. [30] through [33] if p_2 is greater than unity but less than 2.[8] And finally, the data in Fig. 5 can be described by Eq. [25] since, when the concentration of either of the reagents is zero, the rate is zero.

Consideration of the appropriate data on all three orientations studied made possible an evaluation of p_1 and p_2 as a function of orientation; the results are shown in Table I.

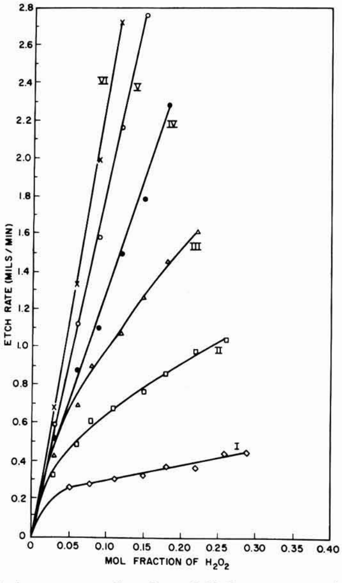

Fig. 11. Etch rate as a function of H_2O_2 concentration at constant HF concentration. The HF mol fractions were: I, 0.05; II, 0.09-0.11; III, 0.14-0.16; IV, 0.18-0.21; V, 0.23-0.26; and VI, 0.28-0.31. Samples were p-type, (100)-oriented.

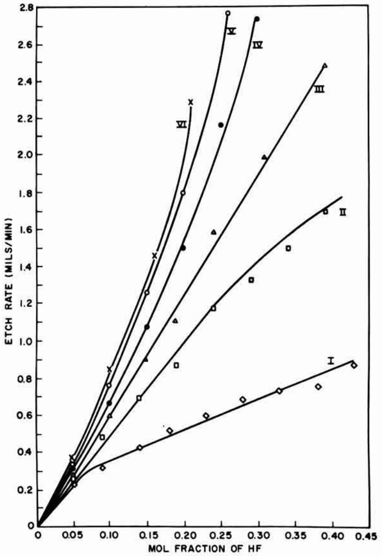

Fig. 12. Etch rate as a function of HF concentration at constant H_2O_2 concentration. The H_2O_2 mol fractions were: I, 0.03; II, 0.06; III, 0.08-0.09; IV, 0.11-0.12; V, 0.15; and VI, 0.18. Samples were p-type, (100)-oriented.

Equation [29] and the data from Table I lead to the prediction that at low [HF] and relatively high $[H_2O_2]$ the etch rate for the (100) surface should vary as the square root of the peroxide concentration. When the data from curves I and II of Fig. 11, which are an approximation to these reagent concentration conditions, are used, the predicted square-root dependence is indeed obtained. In a similar manner, Eq. [33] predicts a $(p_2 - 1/2)$ dependence of the etch rate on [HF] at low $[H_2O_2]$. From curve I of Fig. 12, the etch rate is found to be dependent on [HF] to the 0.7 power, in excellent agreement with the value predicted using the (100)-data in Table I.

Although Eq. [25] appears to express the over-all etching situation, it contains at least four parameters that can be manipulated in any attempt at a detailed quantitative evaluation. Since the raw data are limited in quantity and precision, it is simpler to take Eq. [21] and [23] and attempt order-of-magnitude calculations to determine if the assumptions made in the analysis are reasonable. With each of the two equations considered separately as the working relationship, the etch-rate data for all three orientations of the p-type series were analyzed using an IBM 7094 computer[10] to determine the best values for a, K_1, and K_2. The computer analysis consisted of determining the root-mean-squared deviation of calculated from measured etch rates for each of the experimental con-

Table I. Results of evaluation[9]

Orientation	p_1	p_2
(100)	1	>1
(111)	1	>1
(110)	>1	>1

---

[8] When the data in curves IV, V, and VI of Fig. 12 are used, p_2 appears to be about 1.3.

[9] In most cases the value for p_2 was approximately 1.2 – 1.3. For the (110) orientation p_1 is identical to p_2. When both HF and H_2O_2 concentrations were simultaneously high, it was observed that p_2 could go as high as 1.9.

[10] The entire computer program and analysis were developed by M. Yamin.

Table II. Summary of results

Orientation	From use of Eq. [21] a''	From use of Eq. [21] K_1/K_2	From use of Eq. [23] a'''	From use of Eq. [23] K_1/K_2
(100)	2×10^4	3	1×10^2	10
(111)	2×10^4	3	1×10^2	10
(110)	2×10^4	3	2×10^2	5

ditions. This computation was performed for 1000 combinations of a, K_1, and K_2, covering a predetermined range for each constant. The particular combination of a, K_1, and K_2 which minimized the root-mean-square deviation was selected. The parameter ranges were determined initially by a hand calculation where the data from two experimental points were used in solving a pair of simultaneous equations. Table II summarizes the results of the computer analysis. These results show that in all cases the peroxide adsorption reaction is favored over the fluoride adsorption reaction. It is also seen that $a'' >> a'''$ by two orders of magnitude, and this is consistent with the assumption that $b >> b'$.

The agreement between experiment and theory can be seen in Fig. 13 and 14, which are computer-generated plots of calculated *vs.* measured etch rates for the (111)-oriented specimens using Eq. [21] and [23], respectively. On the basis of any normal standards for predicting rates in heterogeneous kinetics, this is a surprisingly good correlation, considering that all 45 points covering the entire composition region studied are being examined in each case. The predicted rate is less than a factor of two away from the experimentally measured value at any given point.

The data of Table I indicate that for the (100) and (111) orientations the etch rate is first order with respect to the hydrogen peroxide concentration. This means that the rate-controlling step involves formation or removal of divalent germanium on or from the surface, as described, for example, in Eq. [1]. For the (110) orientation, the superlinearity, evidenced by the higher value of p_1, indicates that some tetravalent germanium is also being formed. However, the fact that for the (110) orientation p_1 and p_2 were equal and greater than 1 but less than 2 leads to the postulation of the reaction stoichiometry

$$Ge + 2HF + 2H_2O_2 \rightarrow GeOF_2 + 3H_2O \qquad [34]$$

GeF_2 as a chemical entity has been isolated and identified (16, 17), but the existence of $GeOF_2$ has never been demonstrated; the analogous $GeOCl_2$ has been obtained (17). In all cases it is believed that once the reaction product leaves the surface of the solid and diffuses into the bulk of the solution, continued fluoridation to the GeF_4 or H_2GeF_6 form takes place.

Earlier in this paper, in discussion of Fig. 9, comments were made about reaction stoichiometry based on the maximum etch rate and solution concentration. Although at first it would appear that these results were being contradicted by the stoichiometries resulting from the kinetics analysis, in reality they are two different situations. The former relationship is the efficiency of the system as a function of concentration. The latter relationship is the rate-limiting process taking place only on the surface and therefore should be considered as truly kinetics limiting.

It has been shown that Eq. [15] can be reduced to Camp's original expression, Eq. [5]. Using an analysis similar to his, it is possible to obtain a temperature-dependence relationship of the form

$$R = \frac{1}{\displaystyle\sum_{1}^{r} \frac{e^{E_i/kT}}{a_i \prod_{1}^{n} C_h^{p_h}}} \qquad [35]$$

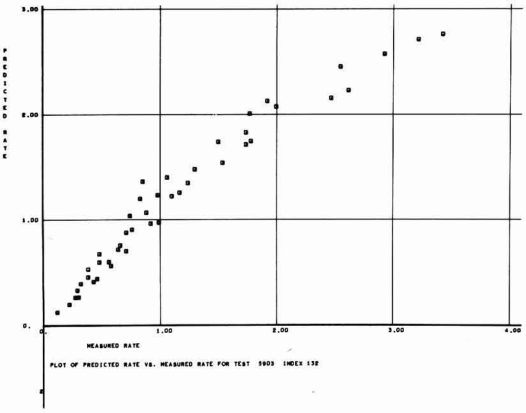

Fig. 13. Computer-generated plot of calculated etch rate *vs.* measured etch rate for (111)-oriented, p-type specimens with Eq. [21] as the generating function. Both coordinates are in units of mils/min.

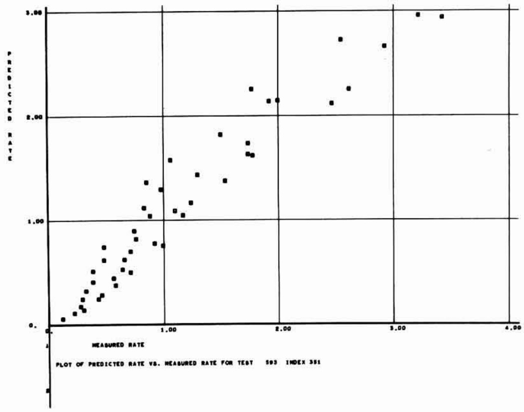

Fig. 14. Computer-generated plot of calculated etch rate *vs.* measured etch rate for (111)-oriented, p-type specimens with Eq. [23] as the generating function. Both coordinates are in units of mils/min.

Although the j^{th} reaction may be the rate-limiting step at a given temperature, it does not necessarily hold that this step is rate limiting at all temperatures. In fact, another step in the sequence could become the slow step at an elevated temperature and the rate limitation would shift from the j^{th} to the k^{th} step. In order for this to occur there would have to be a higher activation energy[11] associated with the k^{th} step than with the j^{th} step, and breaking curves of the form observed by Camp and also seen in Fig. 7 would then result.

Reaction Mechanism

The question naturally arises as to what is the actual mechanism by which the above-described surface reactions take place. Unfortunately, no answers can be provided at this time. In fact, the existence of the intermediate reaction products hypothesized above still needs to be verified experimentally. It is interesting to speculate, however, about certain aspects of the mechanism implied by the kinetics postulated. Why is the "adsorbed fluoride" not the final form of

---

[11] It is interesting to note the relationship between rate and activation energy in Eq. [35]. Because of the inverse-sum effect, the temperature dependence of the rate becomes low when the activation energy is high. This is a good example of how dangerous it is to attempt to get a true activation energy from a semi-logarithmic plot of rate *vs.* reciprocal of temperature.

the intermediate? A suggested answer (18) might be that ultimately at least two fluorine atoms are needed on each germanium atom and the adsorption of the charged anionic form of the fluoride reduces the possibility that a second fluorine may come to that site. If this is so, then it is possible that the acid-dilution effects seen in Fig. 10 are in reality merely influencing the concentration of HF_2^- ions, which in turn influence the concentration of "inactive" sites on the surface. However, this approach to the possible reaction mechanism still does not give any understanding of why the particular orientations act the way they do.

Conclusions

The major conclusion reached in this study is that the $Ge\text{-}HF\text{-}H_2O_2\text{-}H_2O$ etching system is etch-rate limited by a surface-reaction or product desorption step. The application of Laidler's gas-phase adsorption-dissociation isotherm concepts to this liquid system yields results qualitatively in agreement with the experimental data, and consistent with the relationships previously obtained by Camp.

Evidence has been presented which shows that divalent germanium is the major reaction product leaving the surface. There is also strong kinetic evidence for postulating the formation of $GeOF_2$ as a reaction product leaving the (110) surface. However, it is believed that the ultimate reaction product found in solution would probably be GeF_4 or H_2GeF_6.

A comparison of the equilibrium constants for the peroxide and bifluoride adsorption-dissociation reactions shows that the peroxide reaction is favored over the bifluoride reaction.

Although different orientations appear to have different reaction stoichiometries, no firm mechanism explaining these results can be presented at this time.

Acknowledgments

The author would like to express his appreciation to Mr. J. Estlick and Miss J. Werner, of the Hughes Aircraft Company, for their assistance in obtaining the rate data; and his deep indebtedness to Mr. H. Robbins, of the Bell and Howell Company, for the time and effort which he spent on this problem. Also, stimulating discussions with many of his colleagues, D. L. Klein, M. Yamin, P. C. Milner, B. G. Cohen, J. Klerer, K. L. Lawley, and I. Amron, to name only a few, were of invaluable assistance.

After this paper was accepted for publication, one of the reviewers questioned the legitimacy of using the technique of linear combinations in going from Eq. [21] and [23] to Eq. [24]. Since we have assumed that the system is in steady state, by definition

$$R = R_1 = R_2 = R_3 = \ldots . = R_r \qquad \text{(a)}$$

Therefore, also by definition

$$R = \frac{1}{r} \sum_{1}^{r} R_i \qquad \text{(b)}$$

which is a linear combination of the component reactions. For Eq. [24] I have chosen to use only two terms of the sum and the $1/r$ factor is included in the constants b and b^1.

Manuscript received May 31, 1966; revised manuscript received Nov. 2, 1966. This paper was presented in part at the Houston Meeting, Oct. 9-13, 1960.

Any discussion of this paper will appear in a Discussion Section to be published in the December 1967 JOURNAL.

REFERENCES

1. B. Schwartz, "Vapor Deposition," C. F. Powell, J. H. Oxley, and J. F. Blocher, Jr., Editors, John Wiley & Sons, Inc., New York (1966).
2. "Semiconductors," N. B. Hannay, Editor, Reinhold Publishing Corp., New York (1959).
3. R. K. Willardson and H. L. Goering, Editors, "Compound Semiconductors," Reinhold Publishing Corp., New York (1962).
4. P. J. Holmes, Editor, "The Electrochemistry of Semiconductors," Academic Press Inc., New York (1962).
5. W. W. Harvey and H. C. Gatos, *This Journal*, **105**, 654 (1958).
6. B. Schwartz and H. Robbins, *ibid.*, **106**, 505 (1959).
7. D. L. Klein and D. J. D'Stefan, *ibid.*, **109**, 37 (1962).
8. P. R. Camp, *ibid.*, **102**, 586 (1955).
9. M. C. Cretella and H. C. Gatos, *ibid.*, **105**, 487 (1958).
10. J. Bloem and J. C. van Vessem, *ibid.*, **109**, 33 (1962).
11. B. Schwartz and H. Robbins, *ibid.*, **111**, 196 (1964).
12. R. L. Miuller, A. V. Danilov, T. P. Markova, V. N. Mel'nikov, A. B. Nikol'skii, and S. M. Repinskii, *Leningr. Universitet, Vestnik, Ser. Fiz. i. Khim*, **15**, 80 (1960).
13. G. S. Supin, *Zhur Prikl. Khim.*, **32**, 478 (1959).
14. K. J. Laidler, "Chemical Kinetics," McGraw-Hill Book Co., New York, (1950).
15. S. Glasstone, "Textbook of Physical Chemistry," D. Van Nostrand Co., Inc., Princeton (1946).
16. N. V. Sidgwick, "The Chemical Elements and their Compounds," Clarendon, Oxford (1950).
17. O. H. Johnson, *Chem. Rev.*, **51**, 431 (1952).
18. D. L. Klein, Private communication.

Reflection X-Ray Topography of GaAs Deposited on Ge

Eugene S. Meieran

Fairchild Semiconductor, Division of Fairchild Camera & Instrument Corporation, Palo Alto, California

ABSTRACT

Reflection x-ray topography is well suited to the study of defects in epitaxial films deposited on single crystal substrates. In particular, since GaAs and Ge have lattice parameters that are almost, but not quite equal, certain reflecting planes can be used with suitable radiation to allow separate topographs of the GaAs epitaxial film and Ge substrate to be taken. In this way, the various types of defects appearing in the epitaxial film can be analyzed to show whether or not they were influenced by growth conditions or by substrate preparation. During our investigation, growth pyramids due to imperfections or contamination in the substrate, and dislocation networks, probably due to mismatch between film and substrate lattice parameters, were observed. The latter were observed in both the film and substrate, but occurred only for films more than about 2μ thick.

Germanium is structurally an ideal substrate material for the epitaxial deposition of GaAs, since single crystal Ge is relatively inexpensive, the technology of wafer preparation is well known, and the lattice parameter is within 0.1% of that of GaAs. Several types of epitaxial reactors for such deposition have been described in the literature (1, 2). In addition, studies by means of optical microscopy of the perfection of the GaAs layer have been conducted (3). It is the purpose of this paper to describe how x-ray topography, using reflection Berg-Barrett geometry (4), can be used to characterize, separately and nondestructively, both the substrate Ge and the epitaxial GaAs film. The comparison of topographs of the film and substrate can aid in understanding the propagation of defects into the film from the substrate, or the formation of defects in the film or substrate separately.

Experimental

Sample preparation.—The GaAs films were grown by the water transport method (5) on chemically polished (111) Ge wafers, doped with As to a carrier

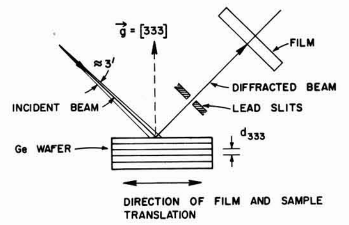

a) (333) reflection, Cu Kα_1 radiation

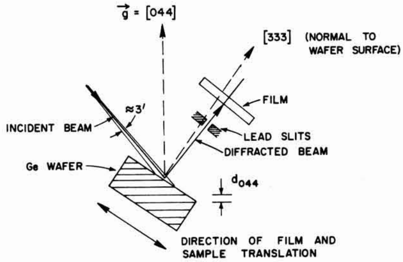

b) (044) reflection, Cu Kα_1 radiation

Fig. 1. Crystal alignment for taking (333) and (044) topographs

concentration of about 1 x 10^{19}/cc. All films described in this paper were doped to about 1 x 10^{18} carriers/cc and ranged between 1 and 15μ thick. The surface of the wafer after deposition consists of a central region covered with single crystal GaAs deposition, a narrow surrounding region covered with polycrystalline GaAs, and pure Ge on which no deposition took place.

X-ray technique.—The difference in lattice parameters a_o between GaAs and Ge, 5.6576 *vs.* 5.6534Å, is the important parameter in the x-ray technique. According to Bragg's law

$$\lambda = 2d \sin \theta$$

so

$$\frac{\Delta\theta}{\tan\theta} = \frac{\Delta d}{d} = \frac{\Delta a}{a_o}$$

and transposing

$$\Delta\theta = \frac{\Delta a}{a_o} \tan\theta = \frac{0.0042}{5.65} \tan\theta = 7.42 \times 10^{-4} \tan\theta$$

where d is the interplanar spacing of the crystal and 2θ the angle between incident and diffracted beams. Consequently, for any particular set of reflecting planes, in order to take separate topographs of Ge and GaAs, $\Delta\theta$ should be as large as possible. For this reason, and because surface defects only rather than bulk defects are to be studied, CuKα_1 radiation is used with reflection geometry. For convenience in comparing the topographs to normal optical micrographs, the topographs should be as undistorted as possible, while for maximum resolution, the diffracted beam should be normal to the recording film. For all these reasons, (333) symmetric and {044} asymmetric reflections are useful. All the pertinent data for these two reflections are given in Table I, and the geometries involved for (111) wafers are shown in Fig. 1. The geometries necessary for other wafer orientations, such as {100} or {110}, can be derived similarly. For intensity purposes, the (333) reflection is more useful and allows faster topographs to be taken, while from the point of distortion, the {044} is more useful.

It is seen from Table I that a beam divergence of less than 5 min of arc is needed to resolve the four peaks due to the Kα_1 Kα_2 doublets from both GaAs and Ge. Therefore, the divergence slits were set to 3 min of arc. Then, in order to examine large regions of the sample, both the sample and recording film (film firmly attached to the sample) were translated through the direct beam, in a manner similar to Lang scanning (6).

The actual apparatus used was a Lang camera, modified for taking reflection topographs. Since the counter window used for aligning the sample is wide, the 2θ setting of the counter arm need only be approximate. However, the actual sample setting is critical and must be set to within a few seconds of arc. The alignment of the wafer for (333) reflections does not depend on the rotation of the wafer about its normal, since the reflecting planes are parallel to the wafer surface. However, for asymmetric reflections, where the reflection planes must be rotated to the vertical position, a Laue photograph is useful. For the purposes described here, a 100μ spot focus and Cu target of a Jarrell Ash Microfocus x-ray unit was used, operating at 35 kv and 6.5 ma. The beam divergence slits were set to 0.5 mm wide, and were placed 50 cm from the focal spot of the x-ray tube. Ilford nuclear plates emulsion L-4, 50μ thick, were used and required an exposure time of about 1 hr for 1-cm scan.

Results

The optical micrograph of a thick film chosen to illustrate some of the defects observed is seen in Fig. 2a. Pyramidal defects and "fish scale" are seen, as is the polycrystalline boundary between the single crystal film and the film free region. The film-free area at the bottom of the micrograph is almost defect free. Figure 2b shows the (333) reflection topograph using only the beam diffracted from the Ge, while Fig. 2c shows the (333) reflection topograph using only the GaAs. The polycrystalline boundary region between the single crystal GaAs and the undeposited region is clearly seen in both Fig. 2b and 2c, as are the pyramidal defects which appear as white dots. As reported elsewhere for Si (7, 8), it appears that the pyramids nucleate at the epitaxial film-substrate interface and grow larger as the film grows thicker. Also seen in both topographs is evidence of slip in the Ge and GaAs along the three <110> directions in the (111) surface plane. (The <110> directions do not seem to meet at 60° due to distortion in angles, as seen in Fig. 1a.) None of this slip corresponds to the "fish scale" of Fig. 2a. The region of Ge free from film appears defect free, in agreement with Fig. 2a.

For comparison purposes, Fig. 2d is an (044) topograph of the same region of the sample. For this topograph, the divergence slits were opened slightly so that both the GaAs and Ge peaks record simultaneously. Again, the various types of defects mentioned above are visible. As schematically shown in Fig. 1b, there is very little angular distortion in this topograph.

The question of whether the strain field in the Ge is plastic, due to slip in the Ge, or elastic, due to the slip in the GaAs and the adherence of the GaAs to the Ge, can be answered by Fig. 3. Figure 3a shows the surface of a Ge wafer from which the deposited GaAs film was etched away in a small region. Again, numerous pyramidal type defects can be seen both

Table I. Interplanar spacings and 2θ values for (333) and (044) reflections from Ge and GaAs, for CuKα_1 and CuKα_2 radiation

	a_o	d_{333}	$2\theta_{333}$, Kα_1	$2\theta_{333}$, Kα_2	d_{044}	$2\theta_{044}$, Kα_1	$2\theta_{044}$, Kα_2
GaAs	5.6534	1.0880	90° 8.3′	90° 25.3′	0.9994	100° 50.4′	101° 10.8′
Ge	5.6576	1.0888	90° 3.1′	90° 20.3′	1.0001	100° 44.4′	101° 4.8′

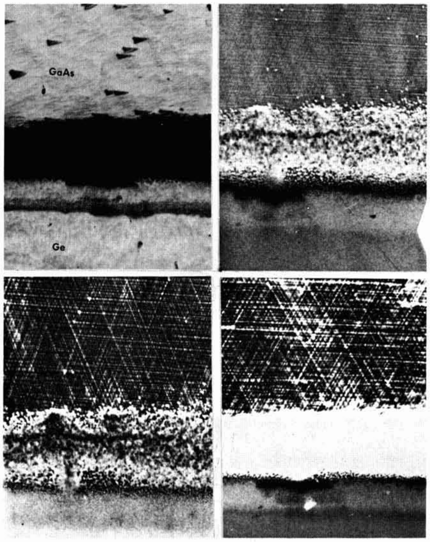

Fig. 2. GaAs deposited on (111) Ge substrates: a (top left) optical micrograph; b (top right) (333) Ge topograph; c (bottom left) (333) GaAs topograph; d (bottom right) (044) GaAs and Ge topograph. Magnification *ca.* 5X.

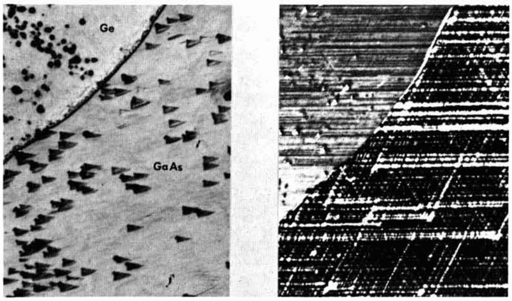

Fig. 3. GaAs deposited on (111) Ge: a (left) optical micrograph; b (right) (044) GaAs and Ge topograph. Magnification *ca.* 5X.

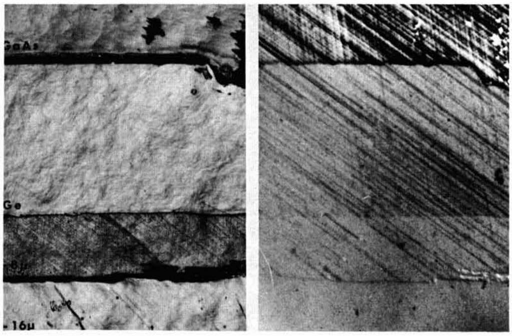

Fig. 4. GaAs deposited on (111) Ge substrate, with GaAs film etched away from part of the sample and steps etched into the Ge. a (left) optical micrograph; b (right) (333) Ge topograph. Magnification *ca.* 15X.

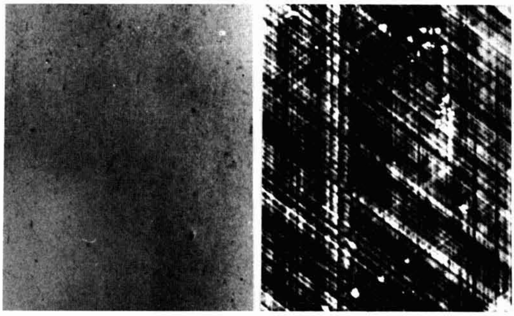

Fig. 5. GaAs deposited on (111) Ge substrate by HCl transport. (333) Ge + GaAs topographs: a (left) 1μ thick film; b (right) 15μ thick film. Magnification *ca.* 10X.

in the remaining film and on the Ge. Figure 3b shows an (044) topograph which records both GaAs and Ge peaks. The strain in the Ge remains even though the GaAs has been removed, and is therefore plastic strain. This is in agreement with the work of Amick (3), who by optical techniques saw strain patterns in the Ge substrate which resembled those seen in Fig. 2 and 3.

The depth of strain field in the Ge was estimated by taking a wafer, removing the GaAs film, and then etching steps about 8μ deep into the Ge itself, as shown in the optical micrograph Fig. 4a. The Ge topograph, Fig. 4b, shows that the strain lines disappear after about 15μ of Ge is removed, so that the depth of the strain in Ge corresponds roughly to the thickness of the epitaxial film, about 15μ thick in this example.

It is apparent that the strain is due to large amounts of plastic deformation or slip that occurs during either film growth or sample cooling from the deposition temperature. The slip is probably due to mismatch in lattice parameters between substrate and film. This was indirectly confirmed by taking x-ray topographs of GaAs deposited on GaAs, where the film and substrate resistivities corresponded roughly to the GaAs on Ge case. No evidence of large-scale slip was observed. Unfortunately, a comparison of theoretical values of dislocation density necessary to accommodate mismatched lattices (10) with experimental observations is not possible. This is due to the lack of resolution of the x-ray technique ($\approx 2\mu$) in comparison to the required theoretical dislocation spacing of less than 0.1μ. However, it can be stated that the dislocations forming the networks observed in Fig. 2, 3, and 4 are spaced much closer than 2μ apart, since individual dislocations cannot be resolved. These latter observations were confirmed by transmission electron microscopy. A sample with a thick GaAs film was etched to remove the film and chemically thinned from the backside to enable transmission samples to be made which showed the strained surface. The electron micrographs showed dislocation clusters in which the dislocations were spaced $\approx 0.1\mu$ apart. The dislocations ran in the $<110>$ directions.

No dislocation networks were observed in films less than about 2μ thick, in agreement with theoretical considerations proposed by Van der Merwe (10). For example, Figs. 5a and 5b are topographs of the GaAs layer deposited on two identical Ge substrates. Figure 5a shows a film about 1μ thick, while Fig. 5b shows a 15μ thick film, made under identical deposition conditions except for duration of deposition. No slip is seen in Fig. 5a while slip similar to Fig. 2, 3, and 4 is seen in Fig. 5b. These two films were deposited by HCl transport rather than H_2O transport, but no structural differences in films have been observed to depend on the transporting medium.

Conclusions

1. Reflection x-ray topography can be used to image separately and nondestructively the GaAs films and the Ge substrates on which they have been deposited.
2. For films thicker than a few microns both the substrate and film contain dislocation networks, probably due to the mismatch between lattice parameters.

3. In cases where slip occurs, the depth of the strain in the Ge is of the same order of magnitude as the thickness of the epitaxial film, about 15μ.

Acknowledgments

The author wishes to thank Dr. Bruce Cairns for growing the epitaxial films; R. Warncke and R. Jiminez for assistance in the laboratory; and Doctors I. Blech and H. Sello for many valuable and interesting discussions.

Manuscript received Aug. 19, 1966; revised manuscript received Oct. 25, 1966.

Any discussion of this paper will appear in a Discussion Section to be published in the December 1967 JOURNAL.

REFERENCES

1. N. Goldsmith and W. Oshinsky, *RCA Rev.*, **24**, 546 (1963).
2. N. Holonyak, Jr., D. C. Jillson, and S. F. Bevaqua, "Metallurgy of Semiconductor Material XV," p. 49, Interscience (John Wiley & Sons), New York (1959).
3. J. A. Amick, *RCA Rev.*, **24**, 555 (1963).
4. C. S. Barrett, "Structure of Metals," McGraw-Hill Book Co., New York (1952).
5. P. H. Robinson, *RCA Rev.*, **24**, 574 (1963).
6. A. R. Lang, *J. Appl. Phys.*, **30**, 748 (1959).
7. J. E. Lawrence and R. Tucker, *ibid.*, **36**, 3095 (1965).
8. G. R. Booker, *Phil. Mag.*, **11**, 1007 (1965).
9. J. A. Amick, "Single Crystal Films," p. 281, Francombe and Sato, Editors, Pergamon Press, New York (1964).
10. J. H. van der Merwe, ref. (9), p. 139.

Technical Notes

Chemical Polishing of Cadmium Sulfide

M. V. Sullivan and W. R. Bracht

Bell Telephone Laboratories, Incorporated, Murray Hill, New Jersey

The usual crystal form of CdS is the wurtzite structure which is in the hexagonal crystal system. When crystal faces, which are perpendicular to the c axis, are examined one notices striking differences in some of the physical, electrical, and chemical properties. These differences may be attributed to the fact that on one face the surface Cd atoms have only three S atoms as nearest neighbors, whereas the S atoms have four Cd atoms as nearest neighbors. On the opposite face the order is reversed. Thus, one face appears to be rich in Cd, whereas the other appears to be rich in S. The Cd-rich face (00.1) is commonly referred to as the A face. The opposite face $(00.\bar{1})$ appears to be rich in S and is referred to as the B face. The difference in etching characteristics of these two faces has been noted many times (1-4). Although several etchants for CdS are described in the literature, none produces a high polish on the B face.

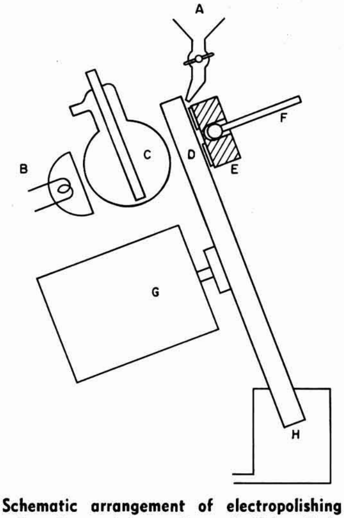

Fig. 1. Schematic arrangement of electropolishing equipment: A, dropping funnel containing etchant; B, light; C, heat absorber; D, rotating disk; E, polishing block holding 3 or more specimens; F, support rod for polishing block; G, motor drive; H, drip pan.

It is well known that stirring of the etchant often influences etching rates. Advantage has been taken of this effect in order to improve the flatness and smoothness of polished semiconductor surfaces (5, 6). A known etchant is selected and fed between the semiconductor being polished and a large flat surface moving parallel to the semiconductor. The result is a stirring action which accelerates the etching on elevated areas of the surface being polished and thus produces a relatively flat, smooth surface. The present work describes the application of this polishing technique to CdS.

Experimental

A schematic drawing of the equipment is shown in Fig. 1. It is similar to that developed for polishing other semiconductors (5, 6). Undoped CdS in the range of 1-10 ohm-cm with a Hall mobility of 300-380 cm^2/v-sec was cut perpendicular to the c axis, producing A (00.1) and B $(00.\bar{1})$ faces, and perpendicular to the a axes producing the six equivalent sides of the hexagonal unit prism. The A and B faces can be distinguished from each other by a 60-sec etch in 50% HCl.[1] This produces a mat finish on the B face and a bright finish on the A face. The slices were mounted on block E as shown in Fig. 1 and lapped with 5μ Al_2O_3. Disk D is 12 in. in diameter and covered with PAN-W Pellon cloth. The HCl etchant is fed at the rate of about 15 cc/min from supply A to the region between the driven disk (rotating about 50 rpm) and the free-running polishing block E. Light, if required, is supplied by a Sylvania Sun Gun, B, and the majority of the radiant heat is removed in the water-filled flask C.

Results and Discussion

The etching rate as a function of concentration is shown in Fig. 2. In the lower range (10-20%) the removal rate was inconveniently slow, and near the upper limit (40-50%) the intensive stirring could not control the rapid etching rate and preferential etch-

---

[1] All concentrations of HCl are expressed as a volume per cent of the standard 37-38% assay HCl.

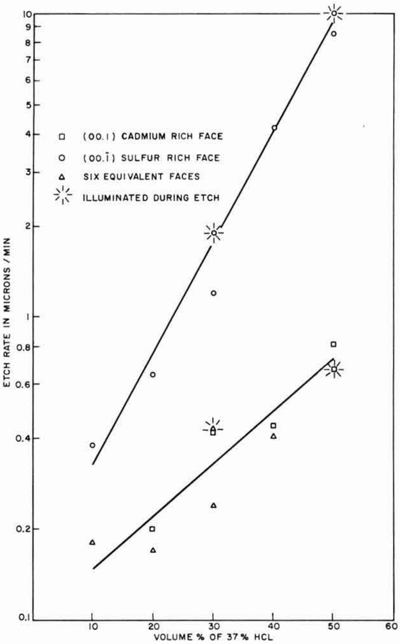

Fig. 2. Etch rate for CdS in various concentrations of concentrated (37-39%) HCl and H_2O.

ing appeared. This preferential etching occurred on the A-face (00.1) at a slightly lower HCl concentration than on the B-face (00.$\bar{1}$) or on any of the six equivalent faces of the hexagonal unit prism. A practical concentration limit for routine work seems to be 30% HCl since this composition can be used on all of the principal faces with excellent results. Figure 3A illustrates an A-face polished in a high concentration of HCl while Fig. 3B is typical of any face polished in the 30% composition.

Figures 4A and 4B are interference photographs of the A and the B face, respectively, of a slice of CdS polished in 30% HCl. A major portion of the surfaces is flat to within ±0.1 mil (±2.5μ). Figures 5A and 5B are profiles of the same surfaces taken on at Talysurf, model 3. Irregularities in the surface of the A-face are consistently less than 500Å and on the B-face less than 250Å. Occasionally it is more difficult to polish the A-face of a particular crystal of CdS, but only rarely is any difficulty encountered on any other crystal face.

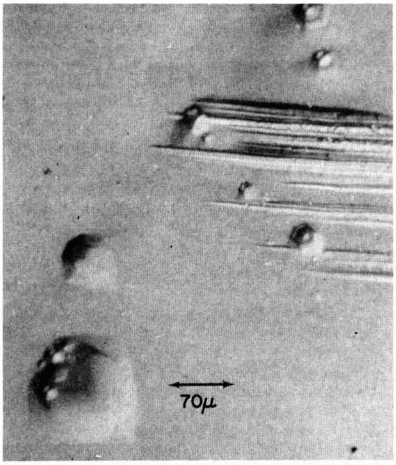

Fig. 3A. Interference contrast photograph of an A (00.1) face polished in 50% HCl. Preferential etching results in poor polishing at this concentration of HCl.

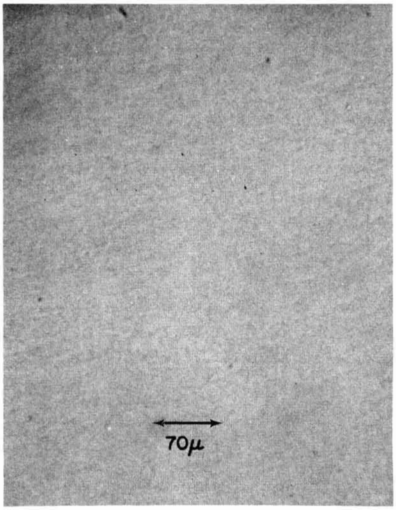

Fig. 3B. The A (00.1) face polished in 30% HCl. The B (00.$\bar{1}$) face and the six equivalent faces of the hexagonal unit prism appear similar to the A (00.1) face when polished in 30% HCl. The field of view in Fig. 3A and 3B is about 0.017 x 0.019 in.

The data in Fig. 2 indicate that there may be a slight effect of light on the etch rate as calculated from thickness measurements. On two faces there was an increase in rate and on the third face a slight decrease. Illumination on the A face appeared to produce a slight beveling effect indicating a greater etch rate at the edges of the slice.

In the chemical polishing of GaAs (6) it was found that the etch rate varied directly with pressure. Since polishing is usually a slow process, this acceleration due to pressure was very desirable. In the case of CdS, any significant increase in pressure over that required to maintain the polishing block close to the wheel

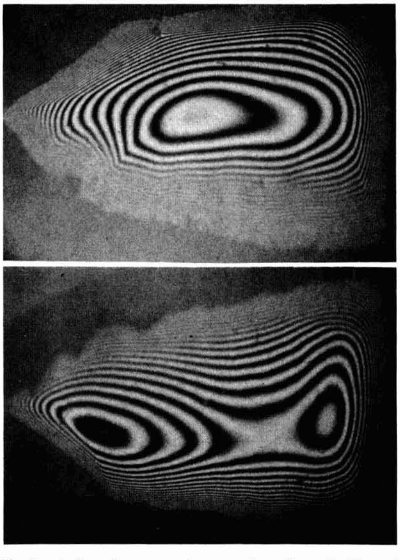

Fig. 4A (top) Interference photograph using thallium light of a polished A (00.1) face. Each fringe represents 2700Å difference in elevation and the field of view is about 0.25 x 0.36 in. Fig. 4B (bottom) Same for the B (00.$\bar{1}$) face.

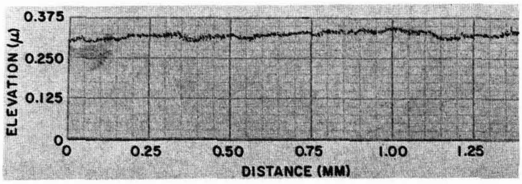

Fig. 5A. Profile of the specimen from Fig. 4A as taken on Talysurf Model 3.

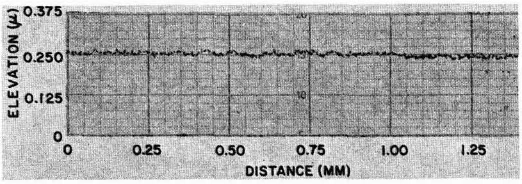

Fig. 5B. Profile of the specimen from Fig. 4B as taken on Talysurf Model 3.

(about 50 g/cm^2) caused scratching of the surface.

The epitaxial films which have been grown on CdS polished in this manner are more perfect than those which have been grown on mechanically polished or chemically polished (HCl without "planar intensive stirring") CdS.

Summary

The chemical polishing of CdS with HCl ordinarily gives a bright surface on the A face and a satin finish on the B face, but neither surface has the "polished" finish which is most desirable for device applications. The addition of planar intensive stirring to the chemical polishing has resulted in smooth, flat damage-free surfaces on all of the principal faces including both the A and the B faces. The recommended polishing solution is 30% concentrated (37-38%) HCl in water.

Manuscript received Oct. 24, 1966; revised manuscript received Nov. 21, 1966.

Any discussion of this paper will appear in a Discussion Section to be published in the December 1967 JOURNAL.

REFERENCES

1. D. Coster, K. S. Knol, and J. A. Prins, *Z. Phys.*, **63**, 345 (1930).
2. D. C. Reynolds and S. J. Czyzak, *J. Appl. Phys.*, **31**, 94 (1960).
3. R. Zare, W. R. Cook, Jr., and L. R. Shiozawa, *Nature*, **189**, 217 (1961).
4. E. P. Warekois, M. C. Lavine, A. N. Mariano, and H. C. Gatos, *J. Appl. Phys.*, **33**, 690 (1962); Erratum, *ibid.*, **37**, 2203 (1966).
5. M. V. Sullivan, D. L. Klein, R. M. Finne, L. A. Pompliano, and G. A. Kolb, *This Journal*, **110**, 412 (1963).
6. M. V. Sullivan and G. A. Kolb, *ibid.*, **110**, 585 (1963).

Addendum to Precipitates Induced in GaAs by the In-Diffusion of Zinc

J. F. Black and E. D. Jungbluth

General Telephone & Electronics Laboratories, Bayside, New York

(Vol. 114, No. 2, pp. 181-187)

The purpose of this communication is to clarify some of the procedures and qualify several of the results described in this recently published paper (1).

The infrared (IR) absorption (more accurately called IR attenuation) of diffused samples was frequently referred to in terms such as "strong IR absorption," or "reduced IR transmission," or "opaque to IR." These phrases were intended to denote IR attenuation over and above that which could be attributed to free carrier absorption.

A progressive increase in (excess) IR attenuation was described for several samples listed in Table I of the paper. This increase in IR attenuation was ascribed to increasing degrees of precipitation. Under illumination normal to the plane of diffusion the different thickness of the diffused layers in these samples would, alone, have caused strong differences in IR attenuation. Therefore, in this work comparisons of the IR attenuation were conducted on polished profile sections of equal thickness (75μ) cut from each sample. These comparisons were made with the aid of slotted masks, positioned and fixed under the microscope, over each profile section so that only the diffused layer was exposed to the IR illumination. When these masks were not used, or when they were not properly positioned, the IR radiation passing through the relatively transparent undiffused portion of the section interfered with the observations of IR transmission through the diffused layer. Recent measurements have shown, however, that the concentration of zinc at the boundary of the precipitate containing layers varied significantly from sample to sample (these measurements are described below). Consequently, the variation in IR attenuation through the diffused layers can only be approximately equated with variations in the degree of precipitation in each sample.

Diffused samples were sectioned normal to the diffusion plane for junction delineation by etching. Since etching did not generally produce a sharp line at the p+ p junction (for 600 X magnification), it was usually difficult to resolve a separation as small as 1μ between p+ p and p-n junctions. This meant that even though a p+ p junction occurred at a zinc concentration greater than 1 x 10^{19} atoms/cm^3 in an n-doped sample, if the p+ p junction was no more than 1μ away from the p-n junction it would appear that only one junction was present. In such a case, for example in our 5.9 x 10^{18} n-doped samples, the p+ p junction would be judged to occur at the same concentration as the p-n junction; 5.9 x 10^{18} atoms/cm^3. This amplification of our previous comments shows that our data are consistent with other recent measurements (2) of etched profile sections of p+ p and p-n junctions in zinc diffused GaAs. Extrapolation of these other junction measurements suggests that the p+ p junction in zinc diffused GaAs occurs at a zinc concentration of about 2 x 10^{19} atoms/cm^3.

Additional determinations of diffusion profiles performed with the electron beam microprobe showed somewhat higher zinc values at the p+ p boundary than before. On three additional samples the zinc concentration at the boundary of the layer of high etch pit density was 8 x 10^{18} atoms/cm^3 (24 hr at 700°C), 1.2 x 10^{19} atoms/cm^3, (2 hr at 800°C), and 1.0 x 10^{19} atoms/cm^3 (2 hr at 900°C). On each analysis the instrument "noise" level was equivalent to $\pm$ 5 x 10^{18} zinc atoms/cm^3. These analyses were obtained with a Philips Model AMR-3 Electron Probe Microanalyzer using a flexible mica crystal to achieve optimum focussing of characteristic x-rays and a 30 kv beam, at a sample current of 0.18 μa and counting over a period of 100 sec.

The discussion (1) of the excess IR attenuation in the diffused layers led to the conclusion that, for a zinc concentration of 5 x 10^{18} atoms/cm^3 at the boundary of the layer, the excess IR attenuation amounted to more than 300 cm^{-1}. This excess was proposed to be due to the presence of the submicroscopic precipitation. It would appear that the magnitude of this excess absorption must now be revised downward because the boundary zinc concentration may in general be higher than 5 x 10^{18} atoms/cm^3. However, even if the zinc concentration were as high as 2 x 10^{19} atoms/cm^3, which seems possible according to recent measurements, we must still account for excess IR attenuation amounting to about 200 cm^{-1}.

Acknowledgment

The authors wish to express their gratitude to W. J. Sutkowski for the electron probe analysis.

REFERENCES

1. J. F. Black and E. D. Jungbluth, *This Journal*, **114**, 181 (1967).
2. A. Herzog, *Solid-State Elec.*, **9**, 721 (1966).

Brief Communication

Study of Impurity Heterogeneities in InSb by Means of a Permanganate Etchant

A. F. Witt

Department of Metallurgy and Center for Materials Science and Engineering, Massachusetts Institute of Technology, Cambridge, Massachusetts

Heterogeneities of the impurity distribution in semiconductors (coring and striations) can be revealed by several different techniques like autoradiography, resistivity measurements, and etching. Of these, etching is the method most frequently used because of its relative simplicity and the good resolution that can be obtained.

In InSb impurity striations are commonly investigated with dilute or modified CP-4 etchants. This reagent gives good resolution if the semiconductor surface is properly prepared and adequate optical facilities are available. Like most etchants it suffers from a major disadvantage: the etching process is accompanied by gas evolution which frequently leads to severe pitting and demands careful control if optimum resolution is to be obtained. The background of the etched surface is not very smooth and thus requires relatively long exposure times for microphotography with a resulting deterioration of the photographic resolution.

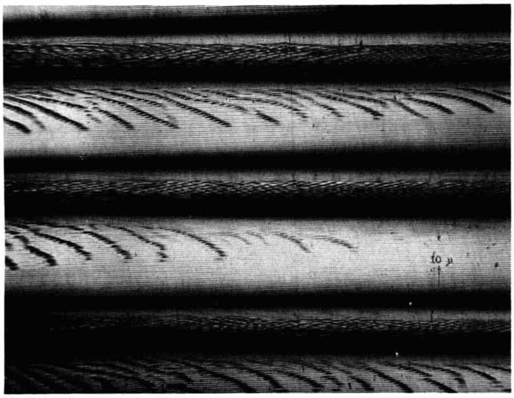

Fig. 1. Vibrational tellurium striations in InSb

A permanganate nongas-evolving etchant was developed (1 HF, 1 CH_3COOH, 1 $KMnO_4$ 0.05M) which has striking advantages over modified CP-4 etchants. For optimum results the semiconductor surface to be investigated is either immersed into the etchant or alternately the etchant is applied with a cotton applicator for a period of 4 to 6 min. (Heating or agitation is not required.) Since the oxidation process with $KMnO_4$ is not accompanied by any gas evolution the etching time is not critical and pitting is completely absent. This particular etching solution leads to a very smooth background and reveals striations with extremely high resolution. From our investigations we conclude that the ultimate resolution of striations is limited by the resolution of the optical system (about 0.2μ) rather than by that of the etchant. As a consequence of the increased reflectivity of the specimen (smoothness) it is possible to decrease the exposure times for microphotography from several minutes to fractional seconds and thus to preserve optimum resolution.

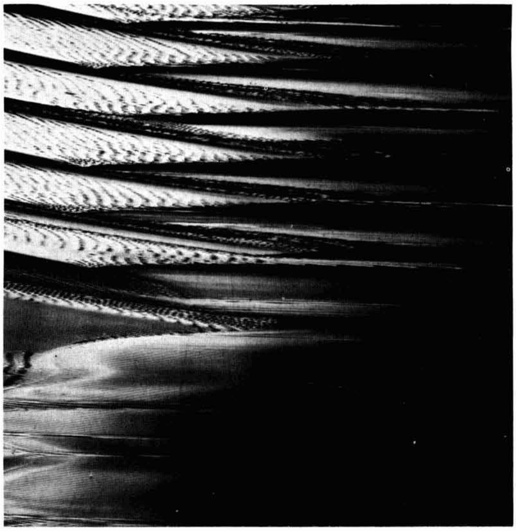

Fig. 2. Impurity striations in InSb as revealed with permanganate etch on a (211) plane.

Figures 1 and 2 show two typical instances of InSb surfaces etched with the new nongas-evolving etchant. Resolution of this magnitude could not be achieved with the standard etchants. It is most likely that the same etchant or some modified composition could be used for other materials.

Manuscript received Dec. 12, 1966.

Any discussion of this paper will appear in a Discussion Section to be published in the December 1967 JOURNAL.

ELECTROCHEMICAL SOCIETY NEWS

MARCH
1967

The Kalita Humphreys Theater—designed by architect Frank Lloyd Wright.

Dallas: 41 Sessions in Technical Program

Thin Films Interest High

At Dallas in the Spring, 218 papers will fill the week-long meeting from May 7-12. Thirteen symposia from six divisions assure a quick pace, with four sessions often running concurrently.

Strong interest continues in the subject of thin films. Three divisions sponsor the Monday and Tuesday sessions on Growth Mechanisms in Thin Films. It will be remembered that the Electronics Division sponsored a thin film session in Buffalo, followed by the Dielectrics and Insulation Division in Philadelphia, now joined by the Electrothermics and Metallurgy Division for Dallas.

Anodic Oxides, Rectification and Conduction Mechanisms will concern Dielectrics and Insulation Division attendees on Wednesday and Thursday. Included among 39 papers to be presented are several of special note. General Electric's D. A. Vermilyea (Abstract No. 22) reports experimental data suggesting that protons may be the charge carriers responsible for capacitance phenomena observed with anodic films on Ta, Nb, Sb, Ti, and W. IBM author T. W. Hickmott (Abstract No. 24) presents a model in explanation of observed large photovoltage and photocurrents with illuminated Nb-Nb$_2$O$_5$-Au diodes, and predicts also that a low work function counterelectrode should eliminate evidence of double injection in Nb-Nb$_2$-O$_5$ diodes.

At the Electronics Semiconductor sessions, which run Wednesday through Friday, symposia on Passivation, Epitaxy, and P-N Junctions are scheduled. During this last, MIT authors A. F. Witt and H. C. Gatos (Abstract No. 95) describe a technique to measure growth rate within angstroms per second in various parts of a single crystal, employing high-frequency vibrations.

Electrochemical Oxidation of Organic Compounds will include 12 papers, presented Monday and Tuesday, sponsored by the Electro-Organic Division. At one session, Case Institute authors B. Epstein and T. Kuwana (Abstract No. 113) postulate a general mechanism describing the electro-oxidation of phthalhydrazides in alkaline media, and note the contribution of optical spectroscopy in this determination. Industrial Electro-Organic Processes, also sponsored by the Electro-Organic Division, will present a number of authors including J. E. Slager and L. W. Staal, Miles Laboratories (Abstract No. 121) who have reduced p-hydroxy propiophenone with sodium-lead alloy, 3, 4 to yield 40-lb batches of 3,4 bis (para hydroxyphenyl) hexandiol 3, 4 at current efficiencies up to 50%.

Beef-Barbecue, Dallas Society Feature

At the Society's Dallas Meeting, Monday evening will be a special treat for city folk—a western-style beef barbecue on a 100-acre dude ranch some 20 minutes by bus from the hotel. Well-known Walter Jetton, LBJ's barbecue chef, will prepare beef and spare ribs for meeting attendees, while western entertainment is supplied by Texas Jim Boyd and His Men of the West.

Society social functions begin informally on Sunday evening with a kaffee-klatch. The Society's business and luncheon meeting will be held on Tuesday, and Dr. H. J. Read will be featured speaker on Tuesday evening at a banquet and reception. Wednesday's social function will enable members to spend several hours together in a musical atmosphere, with refreshments.

On Tuesday, May 9th, Texas Instruments, Inc., will host a plant tour for 100 meeting registrants. The firm's germanium production line will be toured, with special attention to automated assembly and testing operations.

Fifty registrants will have the opportunity, on Wednesday, May 11th, to tour Ling-Temco-Vought, Inc., which recently acquired Wilson Co., Chicago meat packers. Ling-Temco can be credited with design of a number of aircraft and special vehicles, including the scout rocket, the Lance missile, the 7-A attack bomber, and the well-known XC-142, a vertical take off and landing experimental vehicle. Visitors will tour all these facilities plus engineering design and wind tunnels.

Dallas Meeting

THE ELECTROCHEMICAL SOCIETY

May 7, 8, 9, 10, 11, and 12, 1967

Sunday through Friday

CONDENSED TECHNICAL PROGRAM

Monday, May 8, 1967

Joint Symposium: Dielectrics and Insulation—Electronics—Electrothermics & Metallurgy (Abstracts 1-11) 9:00 A.M.-12:30 P.M.; 2:00-5:00 P.M. (North Ballroom, second floor)

Electro-Organics (Abstracts 109-116) 9:00 A.M -12:00 M.; 2:00-5:00 P.M. (Sam Houston Room, second floor)

Electrothermics & Metallurgy (Abstracts 206-214) 9:00-11:40 A.M.; 2:00-4:30 P.M. (Ballroom Foyer, second floor)

Theoretical Electrochemistry (Abstracts 164-176) 9:00 A.M.-12:05 P.M.; 2:00-5:00 P.M. (S. F. Austin Room, second floor)

Tuesday, May 9, 1967

Joint Symposium: Dielectrics and Insulation—Electronics—Electrothermics & Metallurgy (Abstracts 12-20) 9:00 A.M.-12:00M.; 2:00-5:30 P.M. (North Ballroom, second floor)

Electro-Organics (Abstracts 117-125) 9:00 A.M.-12:15 P.M.; 2:00-5:10 P.M. (Sam Houston Room, second floor)

Electrothermics & Metallurgy (Educational Lecture) 4:30-5:30 P.M. (Ballroom Foyer, second floor)

Industrial Electrolytics (Abstracts 141-152) 9:00-11:40 A.M.; 2:00-4:55 P.M. (W. B Travis Room, second floor)

Theoretical Electrochemistry (Abstracts 177-184) 9:00 A.M.-12:00M.; 2:00-4:55 P.M. (S. F. Austin Room, second floor)

Wednesday, May 10, 1967

Dielectrics and Insulation (Abstracts 21-33) 9:00 A.M.-12:00M.; 2:00-6:00 P.M. (Ballroom Foyer, second floor)

Electronics—Semiconductors (Abstracts 83-99) 9:00-11:50 A.M.; 2:00-5:10 P.M. (South Ballroom, second floor)

Electro-Organics (Abstracts 126-134) 9:00 A.M.-12:00M.; 2:00-5:05 P.M. (Sam Houston Room, second floor)

Industrial Electrolytics (Abstracts 153-163) 9:00 A.M.-12:00M.; 2:00-4:55 P.M. (W. B. Travis Room, second floor)

Theoretical Electrochemistry (Abstracts 185-193) 9:00-11:55 A.M.; 2:00-4:40 P.M. (S. F. Austin Room, second floor)

Thursday, May 11, 1967

Dielectrics and Insulation (Abstracts 34-49) 9:00 A.M.-12:10 P.M.; 2:00-5:30 P.M. (Ballroom Foyer, second floor)

Electronics—Luminescence (Abstracts 68-78) 9:00-11:50 A.M.; 2:00-4:25 P.M. (W. B. Travis Room, second floor)

Electronics—Semiconductors (Recent News Papers) 9:00 A.M.-12:00M.; 2:00-5:00 P.M. (South Ballroom, second floor)

Electro-Organics (Abstracts 135-140) 9:00 A.M.-12:00M. (Sam Houston Room, second floor)

Theoretical Electrochemistry (Abstracts 194-205) 9:00 A.M.-12:00M.; 2:00-5:00 P.M. (S. F. Austin Room, second floor)

Friday, May 12, 1967

Dielectrics and Insulation (Abstracts 50-67) 9:00 A.M.-1:20 P.M. (S. F. Austin Room, second floor); 9:00 A.M.-12:00M.; 2:00-3:50 P.M. (Ballroom Foyer, second floor)

Electronics—Luminescence (Abstracts 79-82) 9:00 A.M.-12:00M. (W. B. Travis Room, second floor)

Electronics—Semiconductors (Abstracts 100-108) 9:00 A.M.-12:10 P.M. (South Ballroom, second floor)

GENERAL INFORMATION

Meeting Headquarters is the Sheraton-Dallas Hotel, Southland Center, Dallas, Texas 75221. Technical sessions and social functions will be held in the headquarters hotel, which also has reserved its rooms for The Electrochemical Society members and guests. In addition, the Society has arranged with the Statler-Hilton Hotel for a large block of rooms to accommodate fully the anticipated attendance. The Statler-Hilton Hotel is located at 1914 Commerce Street, about four and one-half blocks from the Sheraton-Dallas. Taxis and a daytime shoppers' bus provide transportation between these hotels for those who do not wish to walk.

Reservation cards for both hotels have been mailed to Society members permitting a choice between the Sheraton-Dallas and the Statler-Hilton.

Request by letter for room reservations should be mailed to: Reservations Manager, Sheraton-Dallas Hotel, Southland Center, Dallas, Texas 75221. Not all those who request the Sheraton-Dallas can be accommodated there, so late reservations may be transferred to the Statler-Hilton Hotel. Please state that you will be attending The Electrochemical Society meeting. If your wife will be attending also, be sure to so state on your request for reservations.

Rates per day at the Sheraton-Dallas Hotel are: single, $11.50-17.50; two-people, $16.00-22.00; suites (1 bedroom) $42.00, (2 bedroom) $59.00.

Rates per day at the Statler-Hilton are: single, $11.00-15.50; double, $17.00-22.50; twin, $18.00-27.00; suites (one bedroom) $35:50, 39.50, and 49.50; (two bedrooms) $58.00 and 69.00.

Headquarters location of The Electrochemical Society is the Pecos Room, third floor, Sheraton-Dallas Hotel.

Dallas Section Headquarters is in the Prairie Room, second floor.

Ladies Headquarters is the Green Room, third floor.

REGISTRATION

The Registration Desk will be located on the lobby floor in the area adjacent to the escalators, Sunday, May 7, through Friday, May 12, 1967.

The registration schedule is:

Sunday, May 7—3:00-9:30 P.M.
Monday, May 8—8:00 A.M.-5:00 P.M.
Tuesday, May 9—8:00 A.M.-5:00 P.M.
Wednesday, May 10—8:00 A.M.-5:00 P.M.
Thursday, May 11—8:00 A.M.-5:00 P.M.
Friday, May 12—8:00 A.M.-12:00M.

Registration fees are:
Technical Session Registration (men and women)

Members	$10.00
Nonmembers Speakers and Coauthors	10.00
Nonmembers	20.00*
Student Members	Complimentary
Student Nonmembers	2.00
Last Day Registrants	5.00
Ladies Registration Fee for Social Events	5.00

* If a nonmember fills out an application form and subsequently is elected to membership in the Society, the difference between the nonmember and member registration fee will be applied to his first year's dues.

1967 FALL MEETING
at the
Sheraton Towers
Chicago, Illinois
October 15, 16, 17, 18, 19, and 20, 1967

Sessions probably will be scheduled:

Battery Division—General Session; Nonaqueous Electrolyte Batteries; Zinc Electrodes.

Corrosion Division—General Session; Properties of Oxide Corrosion Products.

Dielectrics and Insulating Division—General Session; Capacitor Technology; Contact Failure Arising from the Formation of Insulating Films; Electrets.

Electrodeposition Division—General Session; Dielectro- and Electrophoretic Deposition.

Electronics Division — Semiconductors—General Session; Materials Characterization Problems.

Electrothermics & Metallurgy Division—General Session; Protective Coating Technology.

Papers are now being solicited for the meeting to be held in Chicago, Ill., October 15-20, 1967. **Triplicate copies of the usual 75-word abstract, as well as of an extended abstract 500-1000 words** (see notice on p. 244 of this issue for typing instructions), are due at The Electrochemical Society, Inc., 30 East 42 St., New York, N. Y. 10017, *not later than May 15, 1967* in order to be included in the program. (Papers sponsored solely by the Corrosion Division do not require an extended abstract.)

Please indicate on 75-word abstracts for which Division's Symposium the paper is to be scheduled. Underline the name of the author who will present the paper. No paper will be placed on the program unless an author will present it in person, or has designated a qualified person to present it. Should clearance of a paper be required by the author's employer, such should be obtained before the paper is submitted.

Notification of acceptance for meeting presentation, along with scheduled time, will be mailed to authors with general instructions no earlier than two months before the meeting. Those authors who require more prompt notification are requested to submit with their abstract a self-addressed post card with full author-title listing on the reverse.

Presentation of a paper at a technical meeting of the Society does not guarantee publication in the JOURNAL OR ELECTROCHEMICAL TECHNOLOGY.

An author who wishes his paper considered for publication in the JOURNAL OR ELECTROCHEMICAL TECHNOLOGY should send triplicate copies of the manuscript to the Managing Editor of the appropriate publication, 30 East 42 St., New York, N. Y. 10017. Concerning papers to be published in the JOURNAL see notice on per page charge on p. 292C of the November issue.

All papers presented at meetings become the property of The Electrochemical Society, and may not be published elsewhere, either in whole or in part, unless permission for release is requested of and granted by the Society. Papers already published elsewhere, or submitted for publication elsewhere, are not acceptable for oral presentation except on invitation by a Divisional program Chairman.

SYMPOSIA

The Dielectrics and Insulation—Electronics—Electrothermics & Metallurgy Divisions have planned a Joint Symposium on Growth Mechanisms in Thin Films on Monday and Tuesday in the North Ballroom, second floor.

The Dielectrics and Insulation Division has scheduled symposia on Anodic Oxides Wednesday and Thursday, Conduction Mechanisms in Dielectric Films Friday morning, and Failure Mechanisms in Thin Films all day Friday. All sessions are in the Ballroom Foyer except the one on Conduction Mechanisms in Thin Films on Friday morning which is in the S. F. Austin Room, second floor.

The Electronics Division—Semiconductor Group has scheduled symposia on Passivation Wednesday morning, P-N Junctions Wednesday afternoon, a General Session and Recent News Papers on Thursday, and Epitaxy Friday morning, all sessions in the South Ballroom, second floor.

The Electro-Organic Division has scheduled symposia on Electrochemical Oxidation of Organic Compounds all day Monday and Tuesday morning, Industrial Electro-Organic Processes Tuesday morning and Tuesday afternoon, and Electrochemistry in Nonaqueous Media all day Wednesday and Thursday morning in the Sam Houston Room, second floor.

The Industrial Electrolytic Division has scheduled symposia on Production and Uses of Mercury Cell Sodium Amalgam Tuesday morning, Current Distribution and Electrode Design Tuesday afternoon and all day Wednesday, all in the W. B. Travis Room, second floor.

The Theoretical Electrochemistry Division has scheduled a symposium on Structure and Characteristics of Surface Reaction Products on Tuesday and Wednesday and General Sessions on Monday and Thursday, in the S. F. Austin Room, second floor.

The Electrothermics & Metallurgy Division has scheduled a symposium on Carbide Composites on Monday. Two Educational Lectures are scheduled on Materials in Space, the first Monday afternoon, the second Tuesday afternoon, in the Ballroom Foyer, second floor.

BOARD AND COMMITTEE MEETINGS

Sunday, May 7, 5:00 P.M.—**Council of Local Sections,** London Room, third floor.

Sunday, May 7, 5:00 P.M.—**Technical Committee,** Brazos Room, third floor.

Monday, May 8, 2:00 P.M.—**Publication Committee,** O'Henry Room, third floor.

Monday, May 8, 4:00 P.M.—**Joint Editorial Staff** Meeting, ***Electrochemical Technology*** and ***Journal of the Electrochemical Society***, Pioneer Room, third floor.

Monday, May 8, 5:00 P.M.—**Membership Committee,** London Room, third floor.

Monday, May 8, 5:00 P.M.—**Honors and Awards Committee,** O'Henry Room, third floor.

Wednesday, May 10, 12:00M.—**Chairmen of Future Meetings** Luncheon, Brazos Room, third floor.

Wednesday, May 10, 7:30 P.M.—**Board of Directors,** Vaquero Room, second floor.

DIVISION LUNCHEON AND BUSINESS MEETINGS, AND COCKTAIL PARTY

Monday, May 8, 12:15 P.M.—**Electro-Organic** Division Luncheon and Business Meeting, Trinity Room, third floor.

Monday, May 8, 12:15 P.M.—**Electrothermics & Metallurgy** Division Luncheon and Business Meeting, place to be announced.

Tuesday, May 9, 12:30 P.M.—**The Electrochemical Society** Luncheon and Business Meeting, South Ballroom, second floor.

Wednesday, May 10, 12:15 P.M.—**Dielectrics and Insulation** Division Luncheon and Business Meeting, North Ballroom, second floor.

Wednesday, May 10, 12:15 P.M.—**Industrial Electrolytic** Division Luncheon and Business Meeting, Pioneer Room, third floor.

Wednesday, May 10, 12:15 P.M.—**Theoretical Electrochemistry** Division Luncheon and Business Meeting, Trinity Room, third floor.

Thursday, May 11, 5:15 P.M.—**Electronics** Division Business Meeting and Cocktails, North Ballroom, second floor.

GENERAL FUNCTIONS

Sunday Evening Kaffee Klatsch

On Sunday evening, May 7, coffee will be served from 8:00 to 10:00 P.M. in the Ballroom Foyer, second floor, to give early arrivers an opportunity to chat with old and new friends.

Symposia Chairmen Breakfasts

Special breakfasts will be held for Symposia Chairmen Monday through Friday, May 8 through 12. On the day in which he presides at technical session, each Symposium Chairman should be in the Trinity Room, third floor, at 7:45 A.M. for a complimentary breakfast.

Monday Evening Barbecue

On Monday, May 8, there will be a western-style barbecue featuring LBJ's barbecue cook, Walter Jetton. Buses will leave the Sheraton-Dallas Hotel at 5:30 P.M. and travel northwest of Dallas for barbecued beef and ribs. The buses will return to the Sheraton-Dallas at 9:30 P.M.

Tuesday Evening Banquet and Reception

A banquet honoring Dr. H. J. Read will be held at 6:45 P.M., Tuesday, May 9, in the South Ballroom, second floor. A reception with cocktails being served will be held following President Read's address.

Wednesday Evening Mixer

On Wednesday evening there will be a general get-together in the North Ballroom, second floor, from 8:00 to 10:00 PM. Free beer and chips will be served to the strains of music from Old Mexico.

PLANT TOURS

Tuesday Afternoon Plant Tour

A tour Tuesday afternoon, May 9, is scheduled through Texas Instruments. Parts of the Semiconductor Division and the Central Research Laboratories will be visited. Participation will be limited to 100 visitors (Noncitizens require advance authorization); transportation is complimentary. Buses leave the Sheraton-Dallas at 1:30 P.M., returning about 4:00 P.M.

Wednesday Afternoon Plant Tour

A tour Wednesday afternoon, May 10, is scheduled through Ling-Temco-Vought, Inc., including engineering design, wind tunnel testing, production, assembly, and flight testing for aircraft and components. Participation will be limited to 50 visitors (Noncitizens require advance authorization): transportation is complimentary. Buses leave the Sheraton-Dallas at 1:30 P.M., returning about 4:00 P.M.

DALLAS

Dallas was born in 1841 when John Neely Bryan established a trading post and persuaded others to settle on the banks of the Trinity River. Today little more than 100 years later, the city has grown to its present position as the cultural, financial, sports, and business center of the Southwest. Dallas is first in Southern United States, east of Los Angeles, in manufacturing employment, wholesale sales, banking business, insurance sales and administration, and convention business, and is noted for its aggressive citizenship, its clean skyline, women's fashions, and expanding, diversified economy. The unique Apparel Mart and modern downtown stores have rightly earned Dallas the title, "Fashion Queen of the Southwest".

Dallas is famous for beautiful homes and gardens, its Symphony, the Dallas Civic Opera and Civic Ballet, The Owen Fine Arts Center at SMU, the Theater Center designed by Frank Lloyd Wright, and the seven museums at State Fair Park are within a few minutes of the downtown area. Twenty Colleges and universities and the Southwest Center for Advanced Studies are in the Dallas metropolitan area.

In sports Dallas is known as the home of the SMU Mustangs, the NFL Cowboys, and the New Year's Day Cotton Bowl football game and pageant.

Industrial firms near Dallas of interest to meeting attendees include Society Sustaining Members Mobil Oil Co., Inc., and Texas Instruments, Inc.

An information desk will be located in the registration area where detailed information about Dallas will be available. Advice will be provided about transportation, restaurants, shopping, theaters, museums, nightclubs, sports, and other activities.

LADIES' PROGRAM

Women on route to Dallas frequently are not sure what to wear, so may we help you. Texas weather can be unpredictable and, of course, is quite different from northern and eastern climates. The normal day-time temperature for May is 72.9°F. However, the temperature may rapidly change from the 80's to the lower 60's. It is recommended to bring spring cottons, light woolen for an unexpected "norther," and possibly a light-weight coat for air conditioned hotels and other buildings. Hats are still favored, but one is no longer conspicuous without one. Don't forget your walking shoes for the tours and shopping. All convention activities are informal. Note: Leave your iron, needle, and thread at home; these will be available in the Ladies' Headquarters in the Green Room on the third floor.

Sunday, May 7—The Ladies' Headquarters in the Green Room on the third floor will open at 3:00 P.M., and the hostesses will be happy to help you make your plans for the week and answer any questions you may have. Sunday evening you are invited to attend the "Kaffee Klatsch" with your husband.

Monday, May 8—Fruit juice, coffee, and do-nuts will be served in the Ladies Headquarters' each morning, Monday through Friday, from 9:00 to 10:00 A.M. On Monday, the group will leave the Sheraton-Dallas at 10:15 A.M. after a view of the city from the Southwestern Tower. You will then have an opportunity to sample Helen Corbitt's excellent cuisine and enjoy informal fashion modeling in the lovely Zodiac Room at the world famous Neiman-Marcus. After luncheon and the style show, you may shop or browse around at your leisure. Monday evening the ladies are invited to attend an informal western barbecue with their husbands. Nationally known Walter Jetton will feature his recipes made famous during LBJ's ranch affairs. Buses leave the Sheraton-Dallas at 5:30 P.M. and will return approximately 9:30 P.M.

Tuesday, May 9—No definite plans have been made following the coffee hour. Members of the Ladies' Committee will be on hand to make suggestions and take small groups to visit places of special interest and shopping tours. Ladies are invited to attend the banquet and the reception in the Ballroom, second floor, at 6:45 P.M.

Wednesday, May 10—This is a big day for the ladies. The bus will leave the Sheraton-Dallas at 10:00 A.M. for a sightseeing tour of Dallas. This will be a guided tour in an air-conditioned bus following the winding course of Turtle Creek to the quiet of the Southern Methodist University campus. The tour will then continue to White Rock Lake and pass the palatial home of H. L. Hunt. Lunch will be at a Mexican restaurant. The group will then proceed to the famous one-of-kind Apparel Mart which together with the downtown stores has made Dallas Fashion Queen of the Southwest. The group will tour the Mart, see costume collection, and the Dallas Museum of Fashion. At 4:30 P.M. the bus will return to the Sheraton-Dallas Hotel.

Thursday, May 11—The ladies will leave the Sheraton-Dallas at 10:15 A.M. to visit the Dallas Theater Center. The Center which is jutting out of the small tree-studded cliffs on the east bank of Turtle Creek is a massive Frank Lloyd Wright creation, the only theater he ever designed. The theater's revolving stage offers repertory company productions year around, and the group will have an opportunity to observe the inside atmosphere of the theater under Paul Bakers' direction. A lunch buffet will be served. The bus will return to the Sheraton-Dallas in the early afternoon.

Friday, May 12—This will be the final Coffee Hour in the Green Room of the Sheraton-Dallas.

COST OF VARIOUS FUNCTIONS

(other than registration)

Please buy tickets as early as possible.

Sunday Evening Kaffee Klatsch	Complimentary
Symposia Chairman Breakfast	Complimentary
Wednesday Evening Mixer	Complimentary
Monday Barbecue	$5.00 plus 75¢ transportation
Tuesday Society Luncheon	3.75
Tuesday Reception and Banquet, per Person	9.00
Division Luncheons	3.75
Ladies Activities:	
Monday	4.00
Wednesday	4.00
Thursday	3.00
Texas Instruments Trip	Complimentary
Ling-Temco-Vought Trip	Complimentary

JES and ET

Copies of the February, March, and April issues of the ***Journal of The Electrochemical Society*** will be available in the registration area. The price of a single copy of the Journal is $1.70 to members, $2.25 to nonmembers.

Copies of the November-December, January-February, and March-April issues of ***Electrochemical Technology*** will be available in the registration area. The price of a single copy of ET is $1.40 to members, $2.85 to nonmembers.

DISCUSSION

No recording will be made of oral discussion. Those contributing to the discussion of a paper and desiring their remarks to be published should send the discussion to the Managing Editor of the ***Journal of The Electrochemical Society*** or of ***Electrochemical Technology***, 30 East 42 St., New York, N. Y. 10017. The discussion will then be referred to the author for reply. Publication of the discussion and the comments of the authors depends on publication of the paper in the ***Journal*** or in ***Electrochemical Technology***.

Written discussion of a published paper should be submitted within two months following publication of the article. A Discussion Section is published annually in ***Electrochemical Technology***.

EMPLOYMENT POSTERS

Companies which desire to recruit employees at the Dallas Meeting will have posters to this effect on a Bulletin Board adjacent to the Registration Desk. Companies are requested to confine their announcements to this bulletin board.

Note

Photographing of lantern slides, charts, etc., will be permitted unless specifically prohibited by the speaker. Photo flash and photo floods are prohibited. Tape recordings except on behalf of the Society are prohibited.

EXTENDED ABSTRACTS

Extended Abstracts books of papers presented at the Dallas Meeting are available: Dielectrics & Insulation, Electronics, Electrothermics & Metallurgy $2.00; Dielectrics and Insulation $3.00; Electronics $3.00; Electro-Organic $3.00; Industrial Electrolytics $2.00; Theoretical Electrochemistry $3.00. Bound volume of books $15.00.

DALLAS MEETING ROOM SCHEDULE, MAY 7-12, 1967

	Monday		Tuesday		Wednesday		Thursday		Friday	
Meeting of:	A.M.	P.M.	A.M.	P.M.	A.M.	P.M.	A.M.	P.M.	A.M.	P.M.
Joint Symposium, Dielectrics and Insulation—Electronics—Electrothermics & Metallurgy	A	A	A	A						
Dielectrics and Insulation					C	C	C	C	C/E	C
Electronics—Luminescence							F	F	F	
Electronics—Semiconductors					B	B	B	B	B	
Electro-Organic	D	D	D	D	D	D	D			
Electrothermics & Metallurgy	C	C		C						
Industrial Electrolytic			F	F	F	F				
Theoretical Electrochemistry	E	E	E	E	E	E	E	E		

A—North Ballroom
B—South Ballroom
C—Ballroom Foyer

D—Sam Houston Room
E—S. F. Austin Room
F—W. B. Travis Room

All meeting rooms are on the second floor

Dallas Meeting

THE ELECTROCHEMICAL SOCIETY

May 7, 8, 9, 10, 11, and 12, 1967

Sunday through Friday

DIELECTRICS AND INSULATION—ELECTRONICS—ELECTROTHERMICS & METALLURGY

Monday A.M., May 8, 1967

Joint Symposium on Growth Mechanisms in Thin Films, with A. Miller presiding

(NORTH BALLROOM, second floor)

9:00 A.M.—"Some Growth Effects in Thin Films" by K. L. Chopra (Abstract No. 1)

9:50 A.M.—"The Heteroepitaxial Deposition of Si and Ge" by I. B. Cadoff (Abstract No. 2)

10:40 A.M.—Ten-minute intermission

10:50 A.M.—"Epitaxial Growth of Germanium on Single Crystal Spinel" by D. J. Dumin (Abstract No. 3)

11:10 A.M.—"Mechanism of Vapor Growth and Properties of $GaAs_{1-x}P_x$" by I. Akasaki and T. Hara (Abstract No. 4)

11:30 A.M.—"A Theoretical Analysis of Silicon Growth from $SiCl_4$" by J. J. Grossman (Abstract No. 5)

11:50 A.M.—"Formation of Single Crystal Germanium Thin Films on Insulating Substrates by Electron Beam Zone Melting" by C. T. Naber (Abstract No. 6)

12:10 P.M.—"The Anomalous Dielectric Behavior of Silicon Nitride Films" by R. C. G. Swann, T. P. Cauge, and R. R. Mehta (Abstract No. 7)

Monday P.M., May 8, 1967

Joint Symposium on Growth Mechanisms in Thin Films (cont'd), with D. Seraphim presiding

(NORTH BALLROOM, second floor)

2:00 P.M.—"Vapor Quenched Films and Related Phenomena" by S. Mader (Abstract No. 8)

2:50 P.M.—"Structures of Gold-Aluminum Systems" by Choh-Yi Ang (Abstract No. 9)

3:40 P.M.—Ten-minute intermission

3:50 P.M.—"Molybdenum-Gold Contact Technology" by J. A. Cunningham (Abstract No. 10)

4:40 P.M.—"Channel Formation in Low Density Tantalum Films through the Action of Oxygen" by B. H. Vromen (Abstract No. 11)

Tuesday A.M., May 9, 1967

Joint Symposium on Growth Mechanisms in Thin Films (cont'd), with W. R. Sinclair presiding

(NORTH BALLROOM, second floor)

9:00 A.M.—"Polycrystalline II-VI Films: Deposition Methods and Physical Properties" by F. V. Shallcross (Abstract No. 12)

9:50 A.M.—"The Deposition and Structure of Oriented Films of CdS and ZnO" by N. F. Foster (Abstract No. 13)

10:40 A.M.—Ten-minute intermission

10:50 A.M.—"Thin Film Active Devices" by J. L. Moll (Abstract No. 14)

11:40 A.M.—"Oriented Overgrowth in Vacuum Co-evaporated CdS Thick Films" by S. M. Zalar (Abstract No. 15)

12:15 P.M.—The Electrochemical Society Luncheon and Business Meeting, South Ballroom, second floor

Tuesday P.M., May 9, 1967

Joint Symposium on Growth Mechanisms in Thin Films (cont'd), with N. F. Mott presiding

(NORTH BALLROOM, second floor)

2:00 P.M.—"Motion of Electrons in Noncrystalline Materials" by N. F. Mott (Abstract No. 16)

3:00 P.M.—"Structure and Properties of Dielectric Films" by C. Weaver (Abstract No. 17)

3:50 P.M.—Ten-minute intermission

4:00 P.M.—"Growth Phenomena in the Formation of Dielectric Films by Sputtering" by M. H. Francombe (Abstract No. 18)

4:50 P.M.—"Preparation and Properties of Vanadium Dioxide Films" by J. B. MacChesney, J. F. Potter, and H. J. Guggenheim (Abstract No. 19)

5:10 P.M.—"Amorphous Metal Oxide Films Prepared by Reactive Sputtering" by M. L. Lieberman (Abstract No. 20)

DIELECTRICS AND INSULATION

Wednesday A.M., May 10, 1967

Anodic Oxides, Rectification and Conduction Mechanisms, with P. F. Schmidt presiding

(BALLROOM FOYER, second floor)

9:00 A.M.—"On the Mechanisms of Electrolytic Rectification" by P. F. Schmidt (Abstract No. 21)

9:20 A.M.—"Anodic Films, Protons, and Electrolytic Rectification" by D. A. Vermilyea (Abstract No. 22)

10:00 A.M.—"Ionic Transport and Membrane Potentials in Amorphous Oxides" by R. H. Doremus (Abstract No. 23)

10:35 A.M.—Ten-minute intermission

10:45 A.M.—"Electroluminescence and Conduction in Anodic Films" by T. W. Hickmott (Abstract No. 24)

11:10 A.M.—"Asymmetric Conduction in Thin Film Tantalum/Tantalum Oxide/Metal Structures" by N. Schwartz and N. N. Axelrod (Abstract No. 25)

11:40 A.M.—"Conduction Mechanisms in Ta Thin Film Capacitors" by I. F. M. Walker (Abstract No. 26)

12:15 P.M.—Dielectrics and Insulation Division Luncheon and Business Meeting, North Ballroom, second floor. Dr. A. R. Von Hippel of MIT will speak on "The Circuitous Route of Electrochemistry from Empiricism to Insight As Seen by an Outsider."

Wednesday P.M., May 10, 1967

Anodic Oxides, Rectification and Conduction Mechanisms (cont'd), with D. M. Smyth presiding

(BALLROOM FOYER, second floor)

2:00 P.M.—"Conduction and Stoichiometry in Heat-Treated Anodic Oxide Films" by D. M. Smyth and G. A. Shirn (Abstract No. 27)

2:20 P.M.—"Conduction Mechanism in Annealed Ta/Ta_2O_5 Structures" by Kurt Lehovec (Abstract No. 28)

2:40 P.M.—"Oxygen Evolution on Semiconducting TiO_2" by P. J. Boddy (Abstract No. 29)

3:00 P.M.—"On the Rectification of Anodic Oxide Films of Titanium" by F. Huber (Abstract No. 30)

3:20 P.M.—"Equilibrium Properties of the Space Charge Injected into an Insulator by an Electrolyte" by J. M. Hale (Abstract No. 31)

3:40 P.M.—"The Dynamic Current-Voltage Characteristics of Porous Anodic Oxides on Aluminum" by C. E. Michelson (Abstract No. 32)

4:00 P.M.—Ten-minute intermission

4:10 P.M.—Panel Discussion. Discussors include above speakers and J. O'M. Bockris, B. E. Conway, P. L. DeBruyn, M. J. Dignam, A. V. Hippel, S. K. Kurtz, J. Ross MacDonald, S. R. Pollack, R. Stratton, D. G. Thomas, and L. Young.

Thursday A.M. May 11, 1967

Anodic Oxides, Growth Mechanisms (cont'd), with L. Young presiding

(BALLROOM FOYER, second floor)

9:00 A.M.—"Review of Mechanism of High-Field Ionic Conduction in the Growth of Anodic Oxide Films" by L. Young (Abstract No. 34)

9:20 A.M.—"The Movement of Atoms During the Anodic Oxidation of Tantalum" by J. P. S. Pringle (Abstract No. 35)

10:00 A.M.—"A Model for Ionic Conduction and Dielectric Behavior in Anodic Oxide Films on Valve Metals" by M. J. Dignam (Abstract No. 36)

10:40 A.M.—Ten-minute intermission

10:50 A.M.—"Mechanism of Anodic Aluminum Oxide Formation in Phosphate Solutions" by J. J. Randall, Jr. (Abstract No. 37)

11:10 A.M.—"The Mobilities of Tantalum and Oxygen Ions in Anodic Films Formed in Phosphoric Acid" by G. P. Klein (Abstract No. 38)

11:30 A.M.—"Oxygen Transport in the System Tantalum/Anodic Ta_2O_5/O_2 in the Temperature Range 200°-500°C" by C. A. Steidel (Abstract No. 39)

11:50 A.M.—"Current Decay during Constant Voltage Anodization of Ta, Al, and Si" by Rudolf Dreiner (Abstract No. 40)

Thursday P.M., May 11, 1967

Anodic Oxides, Growth Mechanisms (cont'd), with M. J. Dignam presiding

(BALLROOM FOYER, second floor)

2:00 P.M.—"An Ellipsometric Study of Oxygen-Containing Films on Platinum Anodes" by A. K. N. Reddy, M. A. Genshaw, and J. O'M. Bockris (Abstract No. 41)

2:20 P.M.—"An Ellipsometric Determination of the Dependence of the Refractive Index on Field Strength in Tantalum Oxide" by J. L. Ord (Abstract No. 42)

2:40 P.M.—"Electrochemical Study of Anodic Oxide Layer on Tantalum" by A. Tvarusko, N. Ibl, and M. Wiedmer (Abstract No. 43)

3:00 P.M.—"Effect of Formation Rate on the Structure of Anodic Films on Aluminum" by C. G. Dunn (Abstract No. 44)

3:20 P.M.—"Information on Anodic Oxide Films on Valve Metals from Reanodization Data" by C. G. Dunn (Abstract No. 45)

3:40 P.M.—Ten-minute intermission

3:50 P.M.—"Growth, Composition, and Vacuum-Radiation Stability of Anodically Formed Aluminum Oxide Films" by T. R. Beck, D. W. Hamilton, and R. B. Gillette (Abstract No. 46)

4:10 P.M.—"Far Infrared Analysis of Sulfuric-Anodized Anodic Aluminas" by G. A. Dorsey, Jr. (Abstract No. 47)

4:30 P.M.—"The Growth, Stability, and Breakdown of Anodic Oxide Films on Cobalt, Chromium, and Vanadium" by J. R. Wilson, I. A. MacDonald, and J. T. N. Atkinson (Abstract No. 48)

4:50 P.M.—"Gas Phase Anodization of Tantalum" by T. A. Jennings, W. McNeill, and R. E. Salomon (Abstract No. 49)

5:10 P.M.—"Electrochemical Variables in the Anodic Synthesis of CdS Films" by G. Serad, D. G. Husted, and W. McNeill (Abstract No. 49A)

Friday A. M., May 12, 1967

Conduction Mechanisms in Dielectric Films, with L. V. Gregor presiding

(S. F. AUSTIN ROOM, second floor)

9:00 A.M.—"Electronic Conduction Mechanisms in Thin Films" by J. Simmons (Abstract No. 50)

9:30 A.M.—"I-V Characteristics of Mo-Si_3N_4-Metal Structures" by J. R. Yeargan and H. L. Taylor (Abstract No. 51)

9:50 A.M.—"Theory of Charge Distribution in MOS Oxide" by H. P. Caban-Zeda and A. B. Kuper (Abstract No. 52)

10:10 A.M.—"The Activation Energies of Conduction in Ta Anodic Films" by G. J. Korinek (Abstract No. 53)

10:30 A.M.—Ten-minute intermission

Stress in Thin Films, with E. Klokholm presiding

10:40 A.M.—"Strain in Metal Films On Single Crystal Quartz Substrates" by K. Haruta, J. L. Hokanson, and W. J. Spencer (Abstract No. 54)

11:20 A.M.—"The Intrinsic Stress in Evaporated Thin Films" by E. Klokholm (Abstract No. 55)

12:00 M.—"Residual Stresses in Electrodeposited Nickel Films" by S. Tan and E. Klokholm (Abstract No. 56)

12:40 P.M.—"Electrical Evaluation of Deposited Tantala Films" by J. R. Szedon, M. H. Francombe, S. A. Zeitman, and R. M. Handy (Abstract No. 56A)

Friday A.M., May 12, 1967

Failure Mechanisms in Thin Films, with N. Schwartz presiding

(BALLROOM FOYER, second floor)

9:00 A.M.—"Techniques for Studying Failure in Thin Films" by J. W. Faust, Jr. (Abstract No. 57)

10:00 A.M.—"Detection of Flaws and Flaw Breakdown in Anodic Tantalum Oxide by Differential Interference Microscopy" by N. N. Axelrod (Abstract No. 58)

10:20 A.M.—"Tin Whiskers and Filamentary Growths on a Thin Film Conductor in Response to Direct Current Flow" by R. B. Marcus and M. H. Rottersman (Abstract No. 59)

10:40 A.M.—Ten-minute intermission

10:50 A.M.—"Relationship between Dielectric Breakdown and Edge Structure of Evaporated Aluminum Electrodes" by S. W. Chaikin and G. A. St. John (Abstract No. 60)

11:10 A.M.—"Correlation of Physical and Electrical Properties with Intermetallic Reactions of Al and PbSn Bonds with Au/NiCr Thin Films" by J. Boros, J. W. Kanz, and W. L. Robinson (Abstract No. 61)

11:30 A.M.—"Electromigration in Metal Films" by W. E. Mutter (Abstract No. 62)

Friday P.M., May 12, 1967

Failure Mechanisms in Thin Films (cont'd), with P. White presiding

(BALLROOM FOYER, second floor)

2:00 P.M.—"The Dielectric Strength of Silicon Dioxide Films as Used in Semiconductor Devices" by J. A. Baldrey and R. V. Mariner (Abstract No. 63)

2:20 P.M.—"Failure of Solid Tantalum Capacitors due to Anodic Electronic Activation" by G. P. Klein (Abstract No. 64)

2:40 P.M.—"Field Induced Growth of Crystalline Tantalum Oxide" by Julius Klerer (Abstract No. 65)

3:00 P.M.—Ten-minute intermission

3:10 P.M.—"Gold-Induced Break-Away Oxidation of Tantalum" by W. O. Freitag (Abstract No. 66)

3:30 P.M.—"Construction of Nonpolar Electrolytic Capacitors" by J. C. W. Kruishoop (Abstract No. 67)

ELECTRONICS—LUMINESCENCE

Thursday A.M., May 11, 1967

General Session, with Paul Goldberg presiding

(W. B. TRAVIS ROOM, second floor)

9:00 A.M.—"Rare Earth Activated Phosphors," Keynote Address by F. C. Palilla (Abstract No. 68)

9:50 A.M.—"Effects of Photon Absorption at Low Temperature in Distinct UV-Absorbing Groups" by S. G. Polick and H. N. Hersh (Abstract No. 69)

10:15 A.M.—Twenty-minute intermission

10:35 A.M.—"Europium Luminescence in $InBO_3$ and Related Orthoborates" by F. J. Avella and C. S. Wiggins (Abstract No. 70)

11:00 A.M.—"Intensities of the Eu^{3+} $^5D_0 \rightarrow {}^7F_2$ Transitions in Rare Earth Vanadates" by Ojars Sovers and Gleb Gashurov (Abstract No. 71)

11:25 A.M.—"Characterization of Energy Transfer Interactions between Rare Earth Ions" by L. G. Van Uitert (Abstract No. 72)

11:50 A.M.—"The Energy Levels of Eu^{3+} and the Brightness of YVO_4:Eu^{3+} at High Temperature" by D. T. Palumbo and J. E. Mathers (Abstract No. 73)

Thursday P.M., May 11, 1967

General Session, with D. J. Bracco presiding

(W. B. TRAVIS ROOM, second floor)

2:00 P.M.—"Terbium Activated Lanthanum Silicate Phosphors" by T. E. Peters (Abstract No. 74)

2:25 P.M.—"Effects of Charge Compensation on the Optical Spectra of Tb^{3+} in CaF_2:Tb^{3+}" by R. L. Amster (Abstract No. 75)

2:50 P.M.—"Mixed Valence Europium Phosphors" by W. A. McAllister (Abstract No. 76)

3:15 P.M.—Twenty-minute intermission

3:35 P.M.—"Methods for Trace Analysis of Rare Earths" by J. F. Cosgrove, D. W. Oblas, and D. J. Bracco (Abstract No. 77)

4:00 P.M.—"A New Analog-Computing Spectroradiometer" by R. E. Shrader (Abstract No. 78)

5:15 P.M.—Electronics Division Business Meeting and Election of Officers, North Ballroom, second floor. Beer provided for Electronic Division Members; cash bar also available.

Friday A.M., May 12, 1967

General Session, with Willi Lehmann presiding

(W. B. TRAVIS ROOM, second floor)

9:00 A.M.—"Spectro Characteristics and Efficiency of GaAs Light Diodes" by Richard Klein, William Agosto, Lawrence Murray, and Henry Kressel (Abstract No. 80)

9:25 A.M.—"Particle Size and Morphology of Zinc Sulfide Precipitates" by R. A. Brown (Abstract No. 81)

9:50 A.M.—"Zinc Oxide Phosphors" by Willi Lehmann (Abstract No. 82)

10:15 A.M.—Twenty-minute intermission

10:35 A.M.—Recent News Papers

ELECTRONICS—SEMICONDUCTORS

Wednesday A.M., May 10, 1967

Passivation, with B. E. Deal presiding

(SOUTH BALLROOM, second floor)

9:00 A.M.—"Films of Silicon Nitride-Silicon Dioxide Mixtures" by T. L. Chu, C. H. Lee, and J. R. Szedon (Abstract No. 83)

9:20 A.M.—"The Epitaxial Growth of Aluminum Nitride" by T. L. Chu, D. W. Ing, and A. J. Noreika (Abstract No. 84)

9:40 A.M.—"Some Applications of Silicon Oxy-Nitride as a Semiconductor Surface Protectant" by J. E. Mann and P. Walker (Abstract No. 85)

10:00 A.M.—"Redistribution of Donor and Acceptor Impurities in Silicon during the Deposition and Subsequent Reheat of Pyrolytic Silicon Nitride" by T. P. Cauge, R. R. Mehta, and R. C. G. Swann (Abstract No. 86)

10:20 A.M.—Ten-minute intermission

10:30 A.M.—"Thin Film Boron Nitride" by M. J. Rand and J. F. Roberts (Abstract No. 87)

10:50 A.M.—"Interface State Analysis with the MOS Conductance Technique" by E. H. Nicollian and A. Goetzberger (Abstract No. 88)

11:10 A.M.—"The Analysis of the Channel Current Associated with Silicon Planar P^+N Junction" by Masaya Ohta (Abstract No. 89)

11:30 A.M.—"Selective Vapor Phase Etching of Semiconductors" by J. W. Blair, E. C. Teague, and E. G. Alexander (Abstract No. 90)

Wednesday P.M., May 10, 1967

P-N Junctions, with Elizabeth Tarrants presiding

(SOUTH BALLROOM, second floor)

2:00 P.M.—"Gaseous Diffusion into Silicon" by W. G. Dautzenberg, Y. W. Hsueh, and B. R. Wilkins (Abstract No. 91)

2:20 P.M.—"Phosphorus Diffusion in Silicon Using Phosphine" by M. S. R. Heynes and P. G. G. van Loon (Abstract No. 92)

2:40 P.M.—"An Efficient Boron Trichloride Diffusion System" by R. C. Thomas, J. W. Sprague, and E. L. Marcy (Abstract No. 93)

3:00 P.M.—"A Liquid Antimony Diffusion System" by F. L. Gittler (Abstract No. 94)

3:20 P.M.—Ten-minute intermission

3:30 P.M.—"Impurity Distribution in Single Crystals, IV. Crystal Growth Characteristics of InSb Pulled from the Melt as Revealed by High-Frequency Impurity Striations" by A. F. Witt and H. C. Gatos (Abstract No. 95)

3:50 P.M.—"Measurement of Epitaxial Doping Density **vs.** Depth" by D. R. Decker (Abstract No. 96)

4:10 P.M.—"Semiconductor Doping by High Energy 1-2.5 Mev Ion Implantation" by S. Roosild, R. Dolan, and B. Buchanan (Abstract No. 97)

4:30 P.M.—"Secondary Breakdown Capability of Epitaxial Transistors" by P. J. Kannam, F. G. Ernick, and J. Marino (Abstract No. 98)

4:50 P.M.—"$NP\nu N$ Transistor Collector Breakdown Voltage **vs.** Epitaxial Layer Thickness" by H. R. Gates, B. V. Gokhale, and E. G. Grochowski (Abstract No. 99)

Thursday A. M., May 11, 1967

General Session and Recent News, with K. F. Greenough presiding

(SOUTH BALLROOM, second floor)

9:00 A.M.—"Dielectrically Isolated Matched Transistor Pairs" by W. C. Rosvold, W. H. Legat, and L. K. Russell (Abstract No. 99A)

9:20 A.M.—"Characterization of Anomalous Growth Observed in Electron Beam Irradiated Silicon" by David Sivertsen, Olin Cecil, and Rolf Haberecht (Abstract No. 99B)

9:40 A.M.—Recent News Papers

Thursday P.M., May 11, 1967

Recent News (cont'd) with L. Bailey presiding

(SOUTH BALLROOM, second floor)

2:00-5:00 P.M.—Recent News Papers

5:15 P.M.—Electronics Division Business Meeting and Election of Officers, North Ballroom, second floor. Beer provided for Electronic Division Members; cash bar also available.

Friday A.M., May 12, 1967

Epitaxy, with William Cox presiding

(SOUTH BALLROOM, second floor)

9:00 A.M.—"Epitaxial Growth of Sulfur Doped $GaAs_{1-x}P_x$ Alloys and Their Physical Properties" by I. Akasaki, M. Hashimoto, and T. Hara (Abstract No. 100)

9:20 A.M.—"Epitaxial GaAs Films Deposited under Near-Equilibrium Conditions in Ultra-High Vacuum" by P. Hudock (Abstract No. 101)

9:40 A.M.—"Heterojunction Formation by the Low-Temperature Vapor Growth of GaAs" by D. K. Jadus, G. O. Ladd, and D. L. Feucht (Abstract No. 102)

10:00 A.M.—"Growth of Single Crystals of InAs-GaAs" by H. Olsen, H. Robbins, and R. K. Willardson (Abstract No. 103)

10:20 A.M.—Ten-minute intermission

10:30 A.M.—"Growth Rate and Doping in the $GeCl_4$-H_2 System" by V. J. Silvestri (Abstract No. 104)

10:50 A.M.—"A Surface Reaction Approach to the Growth Kinetics of Epitaxial Silicon from $SiCl_4$" by E. G. Alexander (Abstract No. 105)

11:10 A.M.—"Low-Temperature Epitaxial Growth of Silicon in Ultra-High Vacuum" by R. N. Thomas, A. J. Noreika, and M. H. Francombe (Abstract No. 106)

11:30 A.M.—"Epitaxial Growth of Silicon on Sapphire" by P. Rai Choudhury and R. R. Fergusson (Abstract No. 107)

11:50 A.M.—"Extraction of III-V Intermetallic Compounds from Metallic Matrices" by S. Z. Beer (Abstract No. 108)

ELECTRO-ORGANICS

Monday A.M., May 8, 1967

Electrochemical Oxidation of Organic Compounds, with A. K. Hoffmann presiding

(SAM HOUSTON ROOM, second floor)

9:00 A.M.—"Electroorganic Reactions and the Role of Intermediates" by B. E. Conway, L. Marincic, and E. J. Rudd (Abstract No. 109)

9:45 A.M.—"Galvanostatic Studies of the Mechanism of Oscillatory Behavior during the Anodic Oxidation of Formaldehyde" by H. F. Hunger (Abstract No. 110)

10:30 A.M.—"The Electrochemical Oxidation of Aromatic Hydrocarbons in Methylene Chloride" by A. J. Bard, K. S. V. Santhanam, and John Phelps (Abstract No. 111)

11:15 A.M.—"Electrochemical Oxidation of Crystalline Aromatic Hydrocarbons" by J. M. Hale (Abstract No. 112)

12:15 P.M.—Electro-Organic Division Luncheon and Business Meeting in the Trinity Room

Monday P.M., May 10, 1967

Electrochemical Oxidation of Organic Compounds (cont'd), with A. K. Hoffmann presiding

(SAM HOUSTON ROOM, second floor)

2:00 P.M.—"Organic Electrooxidation Studies and Optical Spectroscopy" by Barry Epstein and Theodore Kuwana (Abstract No. 113)

2:45 P.M.—"Electroorganic Reactions: (a) Anodic Cyanations and (b) Electrochemical Reactions of Methylenecyclopropenes" by S. Andreades and E. W. Zahnow (Abstract No. 114)
3:30 P.M.—"The Specific Cleavage of Tyrosyl-Peptide Bonds by Electrolytic Oxidation" by L. A. Cohen and S. Isoe (Abstract No. 115)
4:15 P.M.—"The Electrochemical Formation of Carbonium and Iodonium Ions from Alkyl and Aryl Iodides" by L. L. Miller and A. K. Hoffmann (Abstract No. 116)

Tuesday A. M., May 9, 1967

Electrochemical Oxidation of Organic Compounds (cont'd), with A. K. Hoffmann presiding

(SAM HOUSTON ROOM, second floor)

9:00 A.M.—"The Anodic Alkoxylation of Amines" by N. L. Weinberg and E. A. Brown (Abstract No. 117)
9:45 A.M.—"Oxidation of Aromatic Amines" by S. Wawzonek and T. W. McIntyre (Abstract No. 118)
10:30 A.M.—Fifteen-minute intermission

Industrial Electroorganic Processes, with Charles Wright presiding

10:45 A.M.—"The Present Status of Industrial Electroorganic Chemistry," Introductory Remarks by Sherlock Swann, Jr. (Abstract No. 118A)
11:00 A.M.—"Electrochemistry of Organo-Aluminum Compounds" by Herbert Lehmkuhl (Abstract No. 119)
11:45 A.M.—"The Electrolytic Production of Metal Alkyls" by W. H. Thomas and E. M. Marlett (Abstract No. 120)
12:30 P.M.—The Electrochemical Society Luncheon and Business Meeting in the South Ballroom, second floor

Tuesday P.M., May 9, 1967

Industrial Electroorganic Processes, with Charles Wright presiding

(SAM HOUSTON ROOM, second floor)

2:00 P.M.—"Commercial Application of the Electroreduction of a Ketone to Pinacol" by J. E. Slager and P. W. Staal (Abstract No. 121)
2:35 P.M.—"Anodic Coupling of Organic Anions" by S. Wawzonek and Tsung-yuan Su (Abstract No. 122)
3:10 P.M.—Fifteen-minute intermission
3:25 P.M.—"Electrochemical Reduction of Cyanoalkyldimethylsulfonium Ions" by J. H. Wagenknecht and M. M. Baizer (Abstract No. 123)
4:00 P.M.—"Concerning the Mechanism of the Intramolecular Electrolytic Reductive Coupling of Bis-Activated Olefins at a Mercury Cathode" by J. P. Petrovich, J. D. Anderson, and M. M. Baizer (Abstract No. 124)
4:35 P.M.—"Reductive Coupling of Olefinic Compounds by an Alkali Metal Amalgam" by F. A. Matsuda, M. Kawamata, and Y. Hirata (Abstract No. 125)

Wednesday A. M., May 10, 1967

Electrochemistry in Nonaqueous Media, Principles, with T. B. Reddy presiding

(SAM HOUSTON ROOM, second floor)

9:00 A.M.—"Electrochemistry in Nonaqueous Solvents of Intermediate Dielectric Constant" by I. M. Kolthoff (Abstract No. 126)
9:50 A.M.—"Kinetics and Thermodynamics of Electrode Reactions in Aprotic Solvents" by J. N. Butler (Abstract No. 127)
10:30 A.M.—Ten-minute intermission
10:40 A.M.—"Electrical Double Layer in Nonaqueous Solutions" by Richard Payne (Abstract No. 128)
11:20 A.M.—"Electrochemical Power Systems in Nonaqueous Solvents" by Raymond Jasinski (Abstract No. 129)

Wednesday P.M., May 10, 1967

Electrochemistry in Nonaqueous Media (cont'd), Specific Solvents, with J. N. Butler presiding

(SAM HOUSTON ROOM, second floor)

2:00 P.M.—"Precise Polarography in Ethylenediamine and Acetic Acid" by W. B. Schaap (Abstract No. 130)
2:35 P.M.—"Electrochemistry in Pyridine" by P. J. Elving and R. F. Michielli (Abstract No. 131)
3:10 P.M.—Ten-minute intermission
3:20 P.M.—"Influence of the Solvent System on the Orientation of Ambient Molecules in the Coordination Sphere of Metal Ions" by F. Farha, Jr., and R. T. Iwamoto (Abstract No. 132)
3:55 P.M.—"Thermodynamic Studies in Dimethyl Sulfoxide" by W. H. Smyrl and C. W. Tobias (Abstract No. 133)
4:30 P.M.—"Dimethylformamide as a Solvent for Electrochemistry, A Review" by R. E. Visco (Abstract No. 134)

Thursday A. M., May 11, 1967

Electrochemistry in Nonaqueous Media (cont'd), with A. J. Bard presiding.

(SAM HOUSTON ROOM, second floor)

9:00 A.M.—"Electrochemistry in Formamide: The Double Layer at the Mercury-Formamide Interface" by G. H. Nancollas, D. S. Reid, and C. A. Vincent (Abstract No. 135)
9:35 A.M.—"Electrochemistry in Propylene Carbonate" by David Boden (Abstract No. 136)

End of Invited Papers

10:10 A.M.—Ten-minute intermission
10:20 A.M.—"Parasitic Reactions during Lithium Deposition from Nonaqueous Electrolytes" by R. G. Selim (Abstract No. 137)
10:45 A.M.—"Electrochemical Studies on Lead in Organic Electrolytes" by M. L. B. Rao (Abstract No. 138)
11:10 A.M.—"Inorganic Separators for Nonaqueous Electrolyte Batteries" by M. P. Strier and F. E. Littman (Abstract No. 139)
11:35 A.M.—"Conductance Measurements in Aqueous and Acetone Solutions by an A-C Potentiometric Method" by F. P. Anderson, R. W. Guelke, M. C. B. Hotz, A. H. Spong, and H. C. Brookes (Abstract No. 140)

INDUSTRIAL ELECTROLYTICS

Tuesday A.M., May 9, 1967

Production and Uses of Mercury Cell Sodium Amalgam, with R. N. Hyer presiding

(W. B. TRAVIS ROOM, second floor)

9:00 A.M.—Introductory Remarks
9:10 A.M.—"Formation of Sodium Dithionite from Sodium Amalgam and Sulfur Dioxide in Nonaqueous Media" by R. G. Rinker and Scott Lynn (Abstract No. 141)
9:35 A.M.—"The Influence of Quaternary Ammonium Salts on the Reactivity of Sodium Amalgam" by J. D. Littlehailes and B. J. Woodhall (Abstract No. 142)
10:00 A.M.—"Performance Characteristics of a Sodium-Bismuth Cell" by H. Shimotake and E. J. Cairns (Abstract No. 143)
10:25 A.M.—"Sodium Peroxide from Sodium Amalgam" by C. K. Bon, M. P. Neipert, and D. L. Schechter (Abstract No. 144)
10:50 A.M.—"Economic Studies on the Amalgam Type Chlorine Cell" by Fumio Hine (Abstract No. 145)
11:15 A.M.—"Mechanism of Electrolytic Perchlorate Production" by M. P. Grotheer and E. H. Cook (Abstract No. 146)
12:30 P.M.—The Electrochemical Society Luncheon and Business Meeting in the South Ballroom, second floor

Tuesday P. M., May 9, 1967

Current Distribution and Electrode Design, with Scott Lynn presiding

(W. B. TRAVIS ROOM, second floor)

2:00 P.M.—Introductory Remarks
2:05 P.M.—"Analysis of Current Density Distribution in a Propagating Stress Corrosion Crack" by T. R. Beck and E. A. Grens, II (Abstract No. 147)
2:30 P.M.—"Instabilities of the Current Distribution in Smeared Transition Zones between Two Electrical Conducting Phases" by K. J. Euler (Abstract No. 148)
2:55 P. M.—"Gas Phase Transport Processes—Their Influence on Electrode Current Density Distribution" by H. J. R. Maget (Abstract No. 148A)
3:15 P.M.—"Current Distribution on a Rotating Disk below the Limiting Current" by John Newman (Abstract No. 149)
3:40 P.M.—"Current and Potential Distribution in Cylindrical Geometries: Engineering Applications" by Leonard Nanis (Abstract No. 150)

4:05 P.M.—"An Investigation into the Causes of Leakage Current in Diffused Indium Antimonide Diodes" by J. A. Baldrey and P. J. Marston (Abstract No. 151)
4:30 P.M.—"Development of a High Speed Indium Antimonide Photodiode" by J. A. Baldrey, P. J. W. Noble, and P. J. Marston (Abstract No. 152)

Wednesday A.M., May 10, 1967

Current Distribution and Electrode Design (cont'd), with C. A. Hampel presiding

(W. B. TRAVIS ROOM, second floor)

9:00 A.M.—Introductory Remarks
9:05 A.M.—"Hydrogen-Oxygen Fuel Cells" by A. Winsel (Abstract No. 153)
9:30 A.M.—"Current Distribution in Porous Electrodes: The Hydrazine Electrode Operating under Forced Flow" by S. Szpak and T. Katan (Abstract No. 154)
9:55 A.M.—Twenty-minute intermission
10:15 A.M.—"The Influence of Microcrystalline Properties on the Activity of Platinum Based Electrocatalysts for the Oxidation of Propane" by J. Giner, J. M. Parry, and S. M. Smith (Abstract No. 155)
10:40 A.M.—"Current Distribution in Porous Electrodes" by R. J. Brodd (Abstract No. 156)
10:45 A.M.—Panel Discussion on Future Goals of the Industrial Electrolytic Division, with R. M. Hunter presiding
12:15 P.M.—Industrial Electrolytic Division Luncheon and Business Meeting in the Pioneer Room, third floor

Wednesday P.M., May 10, 1967

Current Distribution and Electrode Design (cont'd), with L. E. Vaaler presiding

(W. B. TRAVIS ROOM, second floor)

2:00 P.M.—"Porosity and Pore-Size Distribution in Zinc Electrodes" by F. Przybyla and F. J. Kelly (Abstract No. 157)
2:25 P.M.—"Structure of Mercuric Oxide Cathodes in Primary Alkaline Cells" by F. Przybyla and F. J. Kelly (Abstract No. 158)
2:50 P.M.—"Lithium Wick Electrode" by D. A. J. Swinkels and S. B. Tricklebank (Abstract No. 159)
3:15 P.M.—"Metal to Graphite Connections in Industrial Electrolytic Applications" by S. J. S. Parry, J. R. Anton, and M. W. Voelker (Abstract No. 160)
3:40 P.M.—"Contact Resistance of Graphite Lead-In Rods" by W. E. Sloka and L. E. Vaaler (Abstract No. 161)
4:05 P.M.—"Mercury Cell Anode and Anode Stem Design" by H. A. Sommers (Abstract No. 162)
4:30 P.M.—"A Valve Electrode for Use in Fused Salts" by D. A. J. Swinkels (Abstract No. 163)

THEORETICAL ELECTROCHEMISTRY

Monday A.M., May 8, 1967

General Session, with S. Schuldiner presiding

(S. F. AUSTIN ROOM, second floor)

9:00 A.M.—"The Sulfur Cathode in Liquid Ammonia Electrolytes" by W. S. Harris (Abstract No. 164)
9:25 A.M.—"Electrolysis of Nitrate Melts and Related Processes" by H. E. Bartlett and K. E. Johnson (Abstract No. 165)
9:50 A.M.—"Electrolysis of Carbon Dioxide Using a Solid Oxide Electrolyte" by W. H. Smart and J. Weissbart (Abstract No. 166)
10:15 A.M.—"A Generalized Expression for the Tafel Slope and the Kinetics of Oxygen Reduction on Noble Metals and Alloys" by D. S. Gnanamuthu and J. V. Petrocelli (Abstract No. 167)
10:40 A.M.—Ten-minute intermission
10:50 A.M.—"Kinetic Isotope Effects in Oxygen Electrode Reactions, II. Experimental Study of H/D Isotope Effects in the Electrochemical Reduction of Oxygen" by J. D. E. McIntyre, M. Salomon, and W. F. Peck, Jr. (Abstract No. 168)
11:15 A.M.—"Static Behavior of the Oxygen-Peroxide Couple on Platinum" by H. B. Urbach, R. J. Bowen, and J. H. Harrison (Abstract No. 169)
11:40 A.M.—"The Dynamic Behavior of the Oxygen-Peroxide Systems on Platinum" by R. J. Bowen, H. B. Urbach, and J. H. Harrison (Abstract No. 170)

Monday P.M., May 8, 1967

General Session (cont'd), with C. E. Enke presiding

(S. F. AUSTIN ROOM, second floor)

2:00 P.M.—"The Relation between Hydrogen Coverage and Potential of the Hydrogen Electrode" by T. C. Franklin, Takuji Itoh, Masahiko Naito, and Jerry Barrett (Abstract No. 171)
2:25 P.M.—"Diffusion Control in Hydrogen Discharge on Platinum" by Frank Ludwig and Ernest Yeager (Abstract No. 172)
2:50 P.M.—"Potentiostatic Current-Potential Measurements on a Platinum Electrode in a High-Purity Closed System" by Sigmund Schuldiner, T. B. Warner, and B. J. Piersma (Abstract No. 173)
3:20 P.M.—Ten-minute intermission
3:30 P.M.—"The Structure and Catalytic Activity of Platinized Platinum" by D. F. A. Koch (Abstract No. 174)
4:00 P.M.—"The Electrochemical Activation of Platinum Electrodes" by S. D. James (Abstract No. 175)
4:30 P.M.—"On the Activity of Platinum Catalysts in Solution, I. Effects of Thermal Treatment and Chemical Etching on the $Pt\text{-}O_{ad}/H_2$ Specific Reaction Rate" by T. B. Warner, Sigmund Schuldiner, and B. J. Piersma (Abstract No. 176)

Tuesday A.M., May, 8, 1967

Structure and Characteristics of Surface Reaction Products, with D. A. Vermilyea presiding

(S. F. AUSTIN ROOM, second floor)

9:00 A.M.—Introductory Remarks
9:05 A.M.—"LEED Studies, CO Adsorption on the Tungsten (112) Face" by C. C. Chang and L. H. Germer (Abstract No. 177)
9:45 A.M.—"Interaction of Oxygen with Rhodium Single Crystal Surfaces" by C. W. Tucker, Jr. (Abstract No. 178)
10:25 A.M.—Ten-minute intermission
10:35 A.M.—"Chemisorbed Gas Structures in Heterogeneous Catalysis" by R. L. Park (Abstract No. 179)
11:15 A.M.—"High Energy Electron Diffraction and X-Ray Emission Analysis of Surfaces and Their Reaction Product" by P. B. Sewell (Abstract No. 180)
11:55 A.M.—"The Structure of Thin Electrodeposited Layers" by E. H. Boult and H. R. Thirsk (Abstract No. 180A)
12:30 P.M.—The Electrochemical Society Luncheon and Business Meeting in the South Ballroom, second floor.

Tuesday P.M., May 9, 1967

Structure and Characteristics of Surface Reaction Products (cont'd), with M. W. Breiter presiding

(S. F. AUSTIN ROOM, second floor)

2:00 P.M.—"Characterization of the Nickel-Oxygen Interface by Surface Potential Measurements" by T. Delchar (Abstract No. 181)
2:40 P.M.—"Infrared Studies of Protective Films Formed by Acetylenic Corrosion Inhibitors" by G. W. Poling (Abstract No. 182)
3:20 P.M.—Fifteen-minute intermission
3:35 P.M.—"Mass Spectrographic Methods for Studying Surfaces" by W. M. Hickam (Abstract No. 183)
4:15 P.M.—"Characterization of Surface Reaction Products by Mass Spectroscopy" by R. K. Willardson (Abstract No. 184)

Wednesday A.M., May 10, 1967

Structure of Characterization of Surface Reaction Products (cont'd), with F. G. Will presiding

(S. F. AUSTIN ROOM, second floor)

9:00 A.M.—"A Study of the Formation of Anodic Oxide Films on Platinum" by J. L. Ord (Abstract No. 185)
9:40 A.M.—"Electrochemical Characterization of the Surface Composition of Platinum Alloys and Copper Adlayers on Platinum" by M. W. Breiter (Abstract No. 186)
10:20 A.M.—Fifteen-minute intermission
10:35 A.M.—"Characterization of Thin Reaction Product Films by Ellipsometry" by Jerome Kruger (Abstract No. 187)

11:15 A.M.—"Identification and Characterization of Electrochemical Reaction Products by X-ray Diffraction" by Jeanne Burbank (Abstract No. 188)

12:15 P.M.—Theoretical Electrochemistry Division Luncheon and Business Meeting in the Trinity Room

Wednesday P.M., May 10, 1967

Structure and Characterization of Surface Reaction Products (cont'd), with Jerome Kruger presiding

(S. F. AUSTIN ROOM, second floor)

2:00 P.M.—"On the Passivity of Iron-Chromium Alloys" by R. P. Frankenthal (Abstract No. 189)

2:30 P.M.—"The Oxidation State of Reduced CO_2" by S. B. Brummer and K. Cahill (Abstract No. 190)

3:00 P.M.—"A Study of Initial Film Formation on Nickel Metal Using Linear Sweep Voltammetry" by R. F. Scarr (Abstract No. 191)

3:30 P.M.—Ten-minute intermission

3:40 P.M.—"Crystal Morphology and Mechanism of Growth of α-Fe_2O_3 Blade-Like Platelets on Iron" by R. L. Tallman and E. A. Gulbransen (Abstract No. 192)

4:10 P.M.—"Crystal Morphology and Mechanism of Growth of α-Fe_2O_3 Whiskers on Iron" by R. L. Tallman and E. A. Gulbransen (Abstract No. 193)

Thursday A.M., May 11, 1967

General Session (cont'd), with R. E. Meredith presiding

(S. F. AUSTIN ROOM, second floor)

9:00 A.M.—"Overpotential-Time Variation for Galvanostatic Charging with Potential Dependent Capacitance" by Leonard Nanis and Philippe Javet (Abstract No. 194)

9:25 A.M.—"Short-Pulse Techniques, II. Perturbation Times in Alkali-Halide Systems" by B. J. Piersma, Sigmund Schuldiner, and T. B. Warner (Abstract No. 195)

9:50 A.M.—"Cathodic Polarization of the Manganese Dioxide Electrode in Alkaline Electrolyte" by A. Kozawa and R. A. Powers (Abstract No. 196)

10:20 A.M.—Ten-minute intermission

10:30 A.M.—"Coordination Chemistry of Hydrated Nickel Oxides in Alkaline Electrolyte: Crystal Field Considerations in the Formation of Higher Oxides" by F. P. Kober and M. A. Aia (Abstract No. 197)

11:00 A.M.—"Controlled Potential Coupling of Acetone to Pinacol" by E. C. French and R. M. Hurd (Abstract No. 198)

11:30 A.M.—"The Electrode Kinetics of the Reduction and Oxidation of Antimony" by L. L. Wikstrom and Ken Nobe (Abstract No. 199)

Thursday P.M., May 11, 1967

General Session (cont'd), with T. C. Franklin presiding

(S. F. AUSTIN ROOM, second floor)

2:00 P.M.—"A Rapid Solid-Electrochemical Method for Determining Diffusion Coefficients in Metals" by D. O. Raleigh (Abstract No. 200)

2:25 P.M.—"Effect of Hydrogen Absorbed by Electrode and Electrolyte on Hydrogen Coverage" by D. J. BenDaniel and F. G. Will (Abstract No. 201)

2:50 P.M.—"The Practical Implications of the Finite Contact Angle Meniscus in Fuel Cells" by B. D. Cahan and J. O'M. Bockris (Abstract No. 202)

3:20 P.M.—Ten-minute intermission

3:30 P.M.—"A Model for Wetproofed Porous Electrodes" by Ralph Brown and L. A. Horve (Abstract No. 203)

4:00 P.M.—"Compatibility of H_2O_2 with Spacecraft Reaction Control Systems" by U. M. Robinson (Abstract No. 204)

4:30 P.M.—"The Role of Copper in the Pitting of Aluminum" by H. L. Craig, Jr., R. D. Dewey, and J. R. Scott (Abstract No. 205)

ELECTROTHERMICS & METALLURGY

Monday A.M., May 8, 1967

Carbide Composites, with W. C. Hagel presiding

(BALLROOM FOYER, second floor)

9:00 A.M.—Introductory Remarks

9:05 A.M.—"Cr_3C_2 Fiber Reinforced Modified Nichrome Produced by a Controlled Solidification Method" by H. E. Bates, F. Wald, and Martin Weinstein (Abstract No. 206)

9:30 A.M.—"Precipitated Carbides in Alloy Systems" by J. B. Newkirk and J. Marcantonio (Abstract No. 207)

9:55 A.M.—"Characteristics of Commercial Carbide Powders" by R. E. Riley (Abstract No. 208)

10:15 A.M.—Ten-minute intermission

10:25 A.M.—"Carbide-Graphite Composites" by K. V. Davidson, R. E. Riley, and J. M. Taub (Abstract No. 209)

10:45 A.M.—"Preparation and Properties of Continuous Boron Carbide Filaments for Reinforced Composites" by J. J. Higgins and J. J. Gebhardt (Abstract No. 210)

11:15 A.M.—"Diffusion of Carbon in Zirconium Carbide" by S. Sarian and J. M. Criscione (Abstract No. 211)

12:15 P.M.—Electrothermics & Metallurgy Luncheon and Business Meeting. Place to be announced

Monday P.M., May 8, 1967

Carbide Composites (cont'd), with L. M. Litz presiding

(BALLROOM FOYER, second floor)

2:00 P.M.—"A Film-Thickness Determination of Nitrogen Diffusion in Zirconium Nitride" by C. J. Rosa and W. C. Hagel (Abstract No. 212)

2:25 P.M.—"The Formation of Titanium Carbide Film on Iron by Vapor Plating" by Takehiko Takahashi, Kohzoh Sugiyama, and Kensuke Tomita (Abstract No. 213)

2:50 P.M.—"Production and Characteristics of Submicron Carbides of Refractory Metals" by Ernst Neuenschwander (Abstract No. 214)

3:30 P.M.—Educational Lecture on Materials in Space, sponsored by the Electrothermics and Metallurgy Division. Speaker to be announced.

Tuesday P.M., May 9, 1967

Educational Lecture, with W. E. Kuhn presiding

(BALLROOM FOYER, second floor)

4:30 P.M.—Educational Lecture on Materials in Space, sponsored by the Electrothermics & Metallurgy Division. Speaker to be announced.

INDEX TO AUTHORS

(The number in the right hand column is the abstract number used in the Technical Program and Abstracts.)

SHERATON DALLAS HOTEL

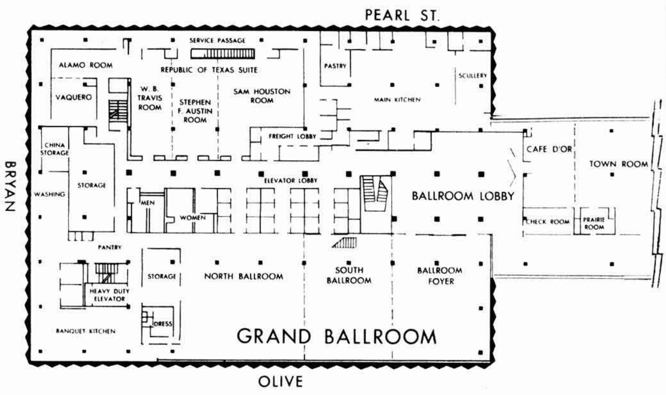

SECOND FLOOR

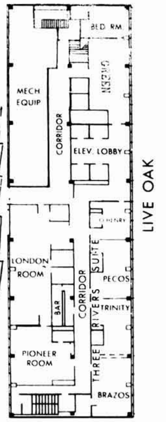

THIRD FLOOR

Abstracts*

Joint Symposium
DIELECTRICS AND INSULATION
ELECTRONICS—
ELECTROTHERMICS & METALLURGY

Abstract No. 1

Some Growth Effects in Thin Films

K. L. Chopra, Ledgemont Lab., Kennecott Copper Corp., Lexington, Mass. (Invited Paper)

The influence of deposition parameters on the growth of thin films is reviewed. The effects of the presence of an electric field and electrostatic charges during deposition, and that of the kinetic energy of the impinging atoms on the growth and structural changes of the resulting films are discussed at length.

Abstract No. 2

The Heteroepitaxial Deposition of Si and Ge

I. B. Cadoff, Dept. of Metallurgy and Materials Sciences, School of Engineering, New York University, New York, N. Y.

Single crystal deposits of germanium and silicon have been grown on substrates of different composition from the deposited material. The orientation relationships that exist between the film and substrate suggest that the growth is epitaxial which in these cases is referred to as heteroepitaxial. The discussion of these heteroepitaxy configurations will be divided into two subcategories, the cases where the basic crystal structures of deposit and substrate are similar, *e.g.*, Ge on Si and the cases where they are of different crystal classes, *e.g.*, Si on Al_2O_3. A summary of the preparation techniques and observed crystallographic relationships will be presented along with a model for heteroepitaxial overgrowth.

Abstract No. 3

Epitaxial Growth of Germanium on Single Crystal Spinel

D. J. Dumin, RCA Laboratories, Princeton, N. J.

The electrical properties of germanium films grown epitaxially on cubic spinel via the pyrolysis of germane have been measured as a function of substrate orientation, growth temperature, and film thickness. Mobilities of the order of 200-300 cm^2/v-sec have been obtained on 5-10μ, p-type, 0.1 ohm cm germanium grown on (100) and (111) spinel. The films were deformed and under compressive stresses of the order of 10^9 dynes/cm^2.

Abstract No. 4

Mechanism of Vapor Growth and Properties of $GaAs_{1-x}P_x$

I. Akasaki and **T. Hara,** Matsushita Research Institute Tokyo, Inc., Ikuta, Kawasaki, Japan

$GaAs_{1-x}P_x$ crystals have been prepared using $AsCl_3$, PCl_3, and Ga sources. The growth rate is proportional to the feed rate of trichlorides. The growth rate profiles for GaAs and GaP differ from each other, but the molar fraction in $GaAs_{1-x}P_x$ grown at a certain temperature is equal to that in trichlorides fed into the system. The influence of substrate orientation on the growth rate decreases with increasing x. The ionization energy of donor in $GaAs_{1-x}P_x$ varies abruptly with the composition.

Abstract No. 5

A Theoretical Analysis of Silicon Growth from $SiCl_4$

J. J. Grossman, Douglas Aircraft Co., MSSD, 3000 Ocean Park Blvd., Santa Monica, Calif. 90406

Steinmaier's thermodynamic analysis of silicon growth by the hydrogen reduction of silicon tetrachloride is shown to give two possible solutions. These are compared with the exact thermodynamic calculation for the two reactions Steinmaier used

$$\begin{array}{ll} SiCl_4 + Si & 2SiCl_2 \\ SiCl_4 + 2H_2 & Si + 4HCl \end{array}$$

as well as one in which $SiHCl_3$ is formed by the reaction

$$\begin{array}{ll} SiCl_4 + HCl & SiHCl_3 \end{array}$$

The results of Steinmaier (without $SiHCl_3$) are fortuitously similar to the latter results. Finally the effect of diffusion through a boundary layer is compared with the thermodynamic calculations and the similarity is emphasized.

Abstract No. 6

Formation of Single Crystal Germanium Thin Films on Insulating Substrates by Electron Beam Zone Melting

C. T. Naber, Research Div., McDonnell Co., St. Louis, Mo. 63166

Vacuum deposited Ge films on insulating substrates were recrystallized by electron beam zone melting. Similar crystallization effects were observed in Ge films deposited on both single crystal sapphire and polycrystalline alumina. Crystal grains as wide as 0.2 mm and as long as 5.0 mm were obtained in Ge films on sapphire. The electron beam processed regions of the films which contained relatively large crystal grains exhibited n-type conductivity, while the regions which contained relatively small crystal grains exhibited p-type conductivity. The Hall mobilities of the electron beam processed films ranged between 50 cm^2/(v-sec) and 1200 cm^2/(v-sec).

Abstract No. 7

The Anomalous Dielectric Behavior of Silicon Nitride Films

R. C. G. Swann, T. P. Cauge, and **R. R. Mehta,** ITT Semiconductor Research Dept., Palo Alto, Calif.

Silicon nitride was deposited onto silicon wafers by the rf glow discharge reaction of ammonia and silane. Anomalous dielectric effects have been observed in these films at thicknesses that would be applicable to MNS transistors. The model proposes that high internal film stresses, which were known to exist in other deposited films, are responsible for the anomalous behavior. Three different substrate temperatures have been used for the study of film thickness dependence of dielectric constant, dielectric voltage breakdown, loss factor, and surface state densities.

Abstract No. 8

Vapor Quenched Films and Related Phenomena

S. Mader, IBM Watson Research Center, P. O. Box 218, Yorktown Heights, N. Y. 10598

Deposition of films on cold substrates (quenching from the vapor phase) introduces a high amount of

---

* An asterisk by a name indicates which author will present the paper.

structural disorder. A survey is given of metastable structures produced by vapor quenching, in particular of those found in binary metal mixtures as a function of the atomic size factors. With size factors larger than 10% concentrated alloys of close packed metals are amorphous. The relative stability and annealing characteristics of such structures are discussed.

Abstract No. 9

Structures of Gold-Aluminum Systems

Choh-Yi Ang, Autonetics Div., North American Aviation, Inc., Anaheim, Calif. 92803

The gold-aluminum metallurgical bonds in many integrated circuits have been found to be a major source of defects and structural anomalies which led to device failures under high reliability testing conditions. In order to investigate the phenomena associated with bond failure, all the known intermetallic compounds, including the "purple plague," of the gold-aluminum system were prepared to serve as standards for metallographic, x-ray, and electron microprobe analyses. Bulk diffusion couples were also constructed for studying rate processes and phase transformations. Activation energies for the growth of certain phases were obtained, based on limited observations. Certain mechanical properties were also determined. The experimental observations are utilized to formulate a hypothesis for the mechanism of gold-aluminum bond failures.

Abstract No. 10

Molybdenum-Gold Contact Technology

J. A. Cunningham, Texas Instruments Inc., P. O. Box 5012, Dallas, Texas 75222

The technology of applying the bimetal contact system MoAu to integrated circuits is discussed and reviewed. Early sublimed Mo technology and device problems are discussed and contrasted with the presently used triode-sputtering deposition equipment. Film resistivities, adhesion, deposition rates, ohmic contact problems, and etching properties are presented. The application of molybdenum-gold to "air-oxide" isolated integrated circuits is reviewed. An approach to large-scale integration using Mo-Au-Mo multilayer interconnections is presented. Finally, a variety of experiments with RF-sputtered MoAu films are discussed.

Abstract No. 11

Channel Formation in Low Density Tantalum Films through the Action of Oxygen

B. H. Vromen, Bell Telephone Laboratories, Inc., Murray Hill, N. J.

Freshly sputtered low density tantalum films, exposed to 60μ of oxygen, show a considerable ($\sim 50\%$) resistance increase, reaching 50% completion in 1.5 sec. From the anodization behavior of low density films overlaid by normal density tantalum and from electron micrographs it is inferred that the channels, typical of low density tantalum, are produced during the oxygen reaction. As the sputter voltage is raised from 1000 to 5000v a smooth transition in properties from low to normal density occurs. Structurally the change is toward larger crystallites and smaller aggregates, separated by finer channels.

Abstract No. 12

Polycrystalline II-VI Films: Deposition Methods and Physical Properties

F. V. Shallcross, RCA Laboratories, Princeton, N. J. 08540

Techniques for preparation of polycrystalline films of II-VI compounds on amorphous and polycrystalline substrates are reviewed. The relations between deposition parameters, structure, and electrical properties of the films are discussed. Major emphasis is given to vacuum-deposited CdS and CdSe films intended for use as semiconductors in thin-film insulated-gate field-effect devices. Nonvacuum techniques and materials suitable for other applications are considered briefly.

Abstract No. 13

The Deposition and Structure of Oriented Films of CdS and ZnO

N. F. Foster, Bell Telephone Laboratories, Inc., Murray Hill, N. J.

(No abstract available)

Abstract No. 14

Thin Film Active Devices

J. L. Moll, Stanford University, Stanford, Calif.

A number of active thin film devices have been proposed. These include the tunnel emitter, metal base transistor, thin film transistor, and tunnel triode. The operation of these devices depends critically in some cases on the physical and electrical properties of the film and in some cases on the electrical nature of the interface.

Abstract No. 15

Oriented Overgrowth in Vacuum Co-evaporated CdS Thick Films

S. M. Zalar, Westinghouse Research Labs., Churchill Boro., Beulah Road, Pittsburgh, Pa. 15235

Stoichiometric, well oriented and pizeoelectrically active CdS thick films ($5\text{-}20\mu$) have been produced by the de Klerk and Kelly technique of vacuum co-evaporation. The mechanism of oriented overgrowth in CdS films, co-evaporated on amorphous (glass) and metallic substrates, is analyzed in terms of equivalent partial pressures, and compared with the direct evaporation of CdS. The topography and texture of CdS thick films have been investigated by optical microscopy and electron diffraction. (Sponsored by the U. S. Army Electronics Command, Fort Monmouth, N. J.)

Abstract No. 16

Motion of Electrons in Noncrystalline Materials

N. F. Mott, Cavendish Lab., University of Cambridge, Cambridge, England

(No abstract available)

Abstract No. 17

Structure and Properties of Dielectric Films

C. Weaver, Dept. of Natural Philosophy, University of Stratholyle, Glasgow, Scotland

A survey of the existing information on the structure of vacuum-deposited dielectric films is given. Attention is drawn to the existence of stresses which can cause crazing effects and to recrystallization during ageing. Losses in dielectric films are consistently higher than for the corresponding bulk material, and this may be attributed to the high defect concentration. Particular emphasis is laid on the measurements at very low frequencies which show conclusive evidence of space-charge polarization effects in alkalid halides and similar materials.

Abstract No. 18

Growth Phenomena in the Formation of Dielectric Films by Sputtering

M. H. Francombe, Westinghouse Research Labs., Pittsburgh, Pa. 15235

The various factors affecting the growth of oxide and nitride dielectric films prepared by reactive and rf sputtering are reviewed in relation to the features of these preparative methods. Formative conditions such as deposition rate, substrate temperature, ambient atmosphere, and substrate structure, which influence the stoichiometry and crystal structure of the films are discussed. The results of recent studies on the growth of the amorphous and crystalline forms of the oxides Ta_2O_5, Nb_2O_5, TiO_2, and ZrO_2, and of the nitrides Si_3N_4 and AlN are presented together with a brief evaluation of those structural properties which affect critically the measurement of dielectric properties. [This work was supported in part under Contract No. AF 33(615)-3814.]

Abstract No. 19

Preparation and Properties of Vanadium Dioxide Films

J. B. MacChesney, J. F. Potter, and **H. J. Guggenheim,** Bell Telephone Laboratories, Inc., Murray Hill, N. J.

Phase equilibria of the vanadium-oxygen system have been restudied in the composition range VO_2-V_2O_5 in order to establish the conditions required for stable existence of the VO_2 phase. Using this knowledge, it was possible to prepare films of VO_2 exhibiting transition in conductivity between semiconducting and metallic states. Amorphous films of V_2O_5 were first prepared by vapor deposition of vanadyl trichloride at temperatures below 127°C in 1 atm of CO_2. Reduction of these to VO_2 was accomplished by heating in controlled atmospheres of appropriate partial oxygen pressure at temperatures between 500° and 550°C. The resulting thin film (0.1-1.0μ) exhibited a sharp drop (three orders of magnitude) in resistance at the expected transition temperature, 67°C.

Abstract No. 20

Amorphous Metal Oxide Films Prepared by Reactive Sputtering

M. L. Lieberman, R&D Labs., Corning Glass Works, Corning, N. Y.

An apparatus has been developed which is suitable for deposition of mixed metal oxide films by multicathodic reactive sputtering. Use of refrigerated substrates has resulted in amorphous single and mixed metal oxide films. In particular, single metal oxides of lead, bismuth, tin, and tellurium and mixed metal oxides of lead and bismuth have been prepared. Crystallization of the films has produced metastable phases. The refractive indices and extinction coefficients of the various films are presented.

DIELECTRICS AND INSULATION

Abstract No. 21

On the Mechanisms of Electrolytic Rectification

P. F. Schmidt, Bell Telephone Laboratories, Inc., Allentown, Pa.

A literature survey of papers dealing with electrolytic rectification and related topics is given for the period 1959-1966. Experiments on current flow in the system Si/SiO_2/electrolyte are then presented, which indicate the importance of absorbed water for the electrical properties of this system.

Abstract No. 22

Anodic Films, Protons, and Electrolytic Rectification

D. A. Vermilyea, General Electric R & D Center, Schenectady, N. Y. 12301

Electrolytic rectification, or the passage of electric current from electrolytic solutions through anodic films on a metal substrate, occurs mainly at flaws in thick films on all metals. For thin films on certain metals conduction also occurs through the bulk of the film. In the latter situation, there is also often a pronounced increase in electrical capacitance of the film. One interpretation of the capacitance increase is that a proton space charge is developed in the oxide film. The evidence which supports the proton space charge hypothesis, and the relationship between such space charge and electrolytic rectification are the subject of this talk.

Abstract No. 23

Ionic Transport and Membrane Potentials in Amorphous Oxides

R. H. Doremus, General Electric R & D Center, Schenectady, N. Y. 12301

To aid in understanding the electrical conductance and potential across amorphous oxide films, some experimental and theoretical results on ionic transport in bulk oxide glasses are reviewed. Results on alkali and hydroxyl ion movement in fused silica are perhaps the most pertinent; results on other glasses help to test theories and to show the effects of additives and hydration of the glass. The relation of electrical potentials across ion-exchanging glasses to ionic properties is also discussed.

Abstract No. 24

Electroluminescence and Conduction in Anodic Films

T. W. Hickmott, General Electric R&D Center, Schenectady, N. Y. (Present address: IBM, Route 52, East Fishkill Facility, Hopewell Junction, N. Y. 12533)

Measurements of electroluminescence under forward bias, photoresponse, and current-voltage characteristics of Nb-Nb_2O_5-Au diodes, with oxide thicknesses between 50 and 3500Å, show that both electrons and holes contribute to conduction. A simple model is discussed in which hole injection and conduction, occurring in an impurity band, are governed by the counterelectrode metal.

Abstract No. 25

Asymmetric Conduction in Thin Film Tantalum/Tantalum Oxide/Metal Structures

N. Schwartz and **N. N. Axelrod,** Bell Telephone Laboratories, Inc., Murray Hill, N. J.

Asymmetric conduction in a thin film tantalum/tantalum oxide/metal structure depends strongly on the method of preparation of the individual elements as well as on the conditions under which the structure is measured. Some of the factors which need to be considered are: (1) the gas and alloy metal content of the sputtered tantalum film; (2) the structural perfection of the tantalum film; (3) the nature of the metal counterelectrode; and (4) ambient factors such as the presence of moisture during measurement. The principal results from these investigations can be explained on the basis of flaws in the anodic oxide. Evidence exists, however, that some degree of asymmetric conduction exists in nominally flaw-free films.

Abstract No. 26

Conduction Mechanisms in Tantalum Thin Film Capacitors

I. F. M. Walker, Northern Electric Co., Ltd., R & D Labs., Ottawa, Ont., Canada

The results of a preliminary investigation into conduction mechanisms in tantalum thin film capacitors are presented and discussed. The results obtained are indicative of space charge limited current with an exponential trap distribution. Measurements of photoconductivity are also discussed and, it is shown that these are in agreement with the proposed conduction mechanism.

Abstract No. 27

Conduction and Stoichiometry in Heat-Treated Anodic Oxide Films

D. M. Smyth, and **G. A. Shirn,** R&D Labs., Sprague Electric Co., North Adams, Mass. 01247

The properties of heat-treated, anodic oxide films on tantalum and niobium are reviewed and further evidence is presented that the dielectric properties are determined by an exponential gradient of electronic conduction across the oxide film. The activation energy of conduction has been found to be a function of the local conductivity and hence varies with position in the film. The implications of this on the mechanism of conduction are discussed.

Abstract No. 28

Conduction Mechanism in Annealed Ta/Ta_2O_5 Structures

Kurt Lehovec, R&D Labs., Sprague Electric Co., North Adams, Mass.

Smyth and co-workers have published a series of papers on measurements of capacitance and loss angle of annealed Ta/Ta_2O_5 structures and have derived conductivity profiles from these data. Various interpretations will be discussed which include the following aspects: (*i*) the oxygen vacancy distribution during annealing which is frozen-in at room temperature; (*ii*) ionization equilibria of the oxygen vacancies to provide an exponential profile of electron conductivity; (*iii*) exchange of electrons between tantalum and oxygen vacancies by tunneling; (*iv*) loss mechanism by partial alignment of dipoles consisting of ionic defects as observed by Breckenridge for alkali halides; and (v) electron extraction from the oxide through the tantalum anode and/or electrode injection from the cathode at anodic bias voltages.

Abstract No. 29

Oxygen Evolution on Semiconducting TiO_2

P. J. Boddy, Bell Telephone Laboratories, Inc., Murray Hill, N. J. 07971

Semiconducting n-type TiO_2 evolves oxygen under strong anodic polarization despite the presence of an exhaustion layer. Addition to the solution of species more oxidizable than water causes no increase in current at a given potential; hence electron emission over the surface barrier is unimportant. The data may be interpreted in terms of electron tunneling from oxide ions in the crystal surface as the rate-determining step, followed by faster electrochemical processes.

Abstract No. 30

On the Rectification of Anodic Oxide Films of Titanium

F. Huber, Radio Corp., of America, Somerville, N. J.

The phenomenon of electrolytic rectification in anodic oxide films has been studied extensively for the system metal-metal oxide-electrolyte for many years. This paper describes experimental results on the rectification of the electrical current in anodic oxide films, especially TiO_2 sandwiched between two metallic electrodes. The rectification of the electric current is interpreted on the basis of a p-n junction within these oxide films. In addition, these junctions can exhibit photovoltaic effects and can be used for the fabrication of field effect devices.

Abstract No. 31

Equilibrium Properties of the Space Charge Injected into an Insulator by an Electrolyte

J. M. Hale, Cyanamid European Research Institute, 91, Route de la Capite, Cologny, Geneva, Switzerland

The contact between an insulator and an oxidizing or reducing electrolyte is studied quantum mechanically. The descriptions of the space charge layer provided by various theoretical models are critically examined in the light of available experimental information and it is shown that models based on the approximations either of a nondegenerate, or of a wholly degenerate surface are inadequate. Effects arising from the underlying metallic substrate in the case of a thin film, or from current flow, are described qualitatively.

Abstract No. 32

The Dynamic Current-Voltage Characteristics of Porous Anodic Oxides on Aluminum

C. E. Michelson, Olin Mathieson Chemical Corp., 275 Winchester Ave., New Haven, Conn. 06504

Rapid voltage reduction across porous anodic coatings results in zero current and a relatively long time is required for recovery to the new equilibrium current. The recovery time is dependent on the voltage change, rate of change, and electrolyte temperature. Capacity measurements show that physical thinning occurs only when current begins to increase late in the recovery period. This behavior appears inconsistent with the conventional pore base dissolution mechanism of porous oxide growth.

There is no Abstract No. 33

Abstract No. 34

Review of Mechanism of High-Field Ionic Conduction in the Growth of Anodic Oxide Films

L. Young, Electrical Engineering Dept., University of British Columbia, Vancouver 8, B.C., Canada

The development of the theory of ionic conduction in anodic oxide films is traced briefly, and the modifications required to take account of recent developments, in particular, the structural changes leading to variable amounts of oxygen ion movement and the growth of nonuniform films in some electrolytes, are discussed.

Abstract No. 35

The Movement of Atoms during the Anodic Oxidation of Tantalum

J. P. S. Pringle, Atomic Energy of Canada Ltd., Chalk River Nuclear Lab., Chalk River, Ont., Canada

A method has been developed for stripping thin uniform layers from anodic oxide films on tantalum. By combining this method with radioactive or nuclear methods of analysis, excellent accuracy can be achieved in measuring the concentration profiles of atomic species within the oxide. Computer analysis of these profiles then gives the parameters of the mathematical functions which describe them. These various techniques have been used to study the movement of atoms during the anodic oxidation of tantalum. Results are presented and discussed.

Abstract No. 36

A Model for Ionic Conduction and Dielectric Behavior in Anodic Oxide Films on Valve Metals

M. J. Dignam, Dept. of Chemistry, University of Toronto, Toronto, Ont., Canada

Recent data relating to the anodic oxidation of valve metals requires a major revision in the theories of conduction and dielectric behavior for these systems. In this paper, a model for these systems, which predicts results consistent with the data, is presented. Although similar to that presented previously, the present model treats the oxide film as a "homogeneous" glass, that is a random three-dimensional network. The nature of the mass and charge carrying defects which are to be expected for such a system is discussed and predictions based on their properties examined against experimental data. The apparent coupling between ionic conduction properties and dielectric phenomena is attributed to a contribution by the polarization of the oxide to the local field at the mobile defect. As was the case for the previous model, transient conduction phenomena are attributed principally to dielectric relaxation phenomena.

Abstract No. 37

Mechanism of Anodic Aluminum Oxide Formation in Phosphate Solutions

J. J. Randall, Jr., R&D Labs., Sprague Electric Co., North Adams, Mass. 01247

The amount of oxide formed per unit charge passed during the anodization of aluminum in aqueous and nonaqueous phosphate-containing electrolytes has been found to be dependent on anodizing temperature and current density as well as on the rate at which the solution is agitated during the oxidation. Current efficiencies less than 100% are due to the formation of soluble aluminum species, the extent of which is dependent on the hydrogen ion concentration at the oxide-solution interface. The fraction of a film which grows by cation transport was found by the use of a P^{32} tracer to be constant at 0.27 ±0.02 for films formed to over a wide range of thicknesses with widely varying amounts of dissolution occurring during film formation.

Abstract No. 38

The Mobilities of Tantalum and Oxygen Ions in Anodic Films Formed in Phosphoric Acid

G. P. Klein, P. R. Mallory & Co., Inc., Lab. for Physical Science, Northwest Industrial Park, Burlington, Mass.

Anodic tantalum oxide films which were formed in solutions containing phosphate ions exhibited re-formation characteristics (voltage *vs.* time at constant current) after annealing in vacuum (10^{-5} mm Hg, 3-500°C) which indicated the presence of a duplex layer structure. Tantalum oxide containing phosphate ions was found to lose oxygen while stoichiometric oxide and oxide formed in solutions of sulfate or nitrate ions was not reduced to the same extent under the given annealing conditions. These differences in the re-formation characteristics of tantalum oxide provided a means to determine the relative mobilities of tantalum and oxygen ions through voltage measurements. Cationic transport fractions of tantalum ions were found to be n_{Ta} 5+ = 0.50 ± 0.10 depending on formation conditions.

Abstract No. 39

Oxygen Transport in the System Tantalum/Anodic Ta_2O_5/O_2 in the Temperature Range 200°-500°C

C. A. Steidel, Bell Telephone Laboratories, Inc., Murray Hill, N. J.

Studies were made of the oxygen transport through anodic tantalum oxide on sputtered β-tantalum in the range between 200°-500°C by monitoring the resistance of the oxide covered tantalum with time. The oxygen flux is a constant until the tantalum reaches saturation, and it is proportional to reciprocal oxide thickness. Short circuit current measurements of oxygen flux using porous carbon electrodes agree with resistance measurements of the tantalum films. Evidence is presented to prove that the mobile ionic species in the oxide in the temperature range 350°-500°C is an oxygen vacancy.

Abstract No. 40

Current Decay during Constant Voltage Anodization of Ta, Al, and Si

Rudolf Dreiner, R&D Labs., Sprague Electric Co., North Adams, Mass. 01247

Ta, Al, and p-type Si samples were anodized at constant current. After predetermined potentials had been reached, the formations were continued at these potentials. The current decay during the constant voltage phase was analyzed. Over the range investigated the results can be described adequately by Faraday's law and a single barrier type relation $i = i_1 \exp (BF)$, with (i) the ionic current and (F) the field. The relations $i = i_2 \exp (\gamma\sqrt{F/KT})$ and $i = i_3 \exp [q(\alpha+{}^{\beta}F)F/_{KT}]$, which were recently discussed in literature, are compared with these experimental data.

Abstract No. 41

An Ellipsometric Study of Oxygen-Containing Films on Platinum Anodes

A. K. N. Reddy, M. A. Genshaw, and J. O'M. Bockris, The Electrochemistry Laboratory, The University of Pennsylvania, Philadelphia, Pa. 19104

Ellipsometry is applied to study the oxidation of platinum in sulfuric acid solution. Steady-state and transient measurements show that oxide film formation commences when the potential is anodic to 0.95v. The film is light absorbing, revealing its electronic conductivity. The film thickness increases linearly with potential. A mechanism of film growth based on place exchange is developed.

Abstract No. 42

An Ellipsometric Determination of the Dependence of the Refractive Index on Field Strength in Tantalum Oxide

J. L. Ord, Dept. of Physics, University of Waterloo, Waterloo, Ont., Canada

The dependence of the refractive index of tantalum oxide on the forming field was studied using a computer-operated following ellipsometer. If an effective field model is used to describe the field acting on the charge carriers, the measured changes in the refractive index are adequate to account for the deviation from a linear dependence of log i on E. The changes in the refractive index are attributed to small field-produced density or concentration changes within the oxide.

Abstract No. 43

Electrochemical Study of Anodic Oxide Layer on Tantalum

A. Tvarusko,* N. Ibl, and **M. Wiedmer,** Swiss Federal Institute of Technology, Zurich, Switzerland

Oxide layers of 10-60Å were grown on tantalum at low, constant currents (0.4-40 μa/cm^2). The nature of current flow through these layers was studied. The slope of the voltage-time curve shows a more or less pronounced change of slope at voltages between 1.5 and 3v *vs.* SCE, depending on the pretreatment. A large effect is observed with contaminated surfaces. The results of four different types of experiments indicate that under these conditions a large portion of the current is electronic. The measurements of the galvanostatic transients (obtained by applying either a current step or an "illumination step") are discussed in more detail.

Abstract No. 44

Effect of Formation Rate on the Structure of Anodic Films on Aluminum

C. G. Dunn, General Electric R&D Center, P.O. Box 8, Schenectady, N. Y. 12301

Oxide formation on aluminum at a constant rate of voltage increase of 10 v/min in an oxalic acid electrolyte results in porous type films on aluminum which differ from results reported for the constant voltage method of formation. Pore diameter does not remain constant; it increases with increasing voltage according to transmission electron microscope data. With fresh aqueous ammonium pentaborate the structure depends on both electrolyte concentration and rate of anodic oxidation.

Abstract No. 45

Information on Anodic Oxide Films on Valve Metals from Reanodization Data

C. G. Dunn, General Electric R&D Center, P.O. Box 8, Schenectady, N. Y. 12301

A constant rate of voltage increase method is described for the formation and study of anodic oxide films on valve metals. Information on formed or formed and treated films is obtained from the constant or variable ionic currents that are required to produce dense oxide during reanodization studies of dense films, porous films, chemically thinned films, mechanically deformed films, and films physically modified by thermal treatments.

Abstract No. 46

Growth, Composition, and Vacuum-Radiation Stability of Anodically Formed Aluminum Oxide Films

T. R. Beck, Boeing Scientific Research Labs., P. O. Box 3981, Seattle, Wash. 98124, **D. W. Hamilton** and **R. B. Gillette,** The Boeing Co., Aerospace Group, P. O. Box 3707, Seattle, Wash. 98124

A 1200v, 1.7μ thick, nonporous aluminum oxide film has been produced by anodizing in a dilute solution of ammonium tartrate in ethanol. This film, in contrast to porous anodic films, is extremely stable in vacuum-ultraviolet, proton, and alpha particle radiation environments. The nonporous film is composed of two distinct layers with different IR spectra and is considerably enriched in aluminum with respect to Al_2O_3. Implications to growth mechanisms are discussed.

Abstract No. 47

Far Infrared Analysis of Sulfuric-Anodized Anodic Aluminas

G. A. Dorsey, Jr., Dept. of Metallurgical Research, Kaiser Aluminum & Chemical Corp., Trentwood, Wash.

Far infrared absorptions of anodic coatings are attributed to Al-O-Al (or Al-$\underset{\text{H}}{\text{O}}$-Al) linkages. Also, an empirical relationship is used to interpret these data in terms of alumina crosslinking. The effects of anodizing time and current density are examined as are the effects of sealing, the latter also influencing alumina cross-linking. Apparently, during anodizing, there is a relatively short period during which an appreciable quantity of barrier layer converts into porous layer. Sealing yields a similar conversion.

Abstract No. 48

The Growth, Stability, and Breakdown of Anodic Oxide Films on Cobalt, Chromium, and Vanadium

J. R. Wilson, I. A. MacDonald, and **J. T. N. Atkinson,** Metallurgical Engineering Dept., Queen's University, Kingston, Ont., Canada

Anodic oxide films have been grown on pure polycrystalline cobalt, chromium, and vanadium by both galvanostatic and potentiostatic techniques. The films have been identified by diffraction methods and by cathodic charging curves. Variables investigated included electrolyte constitution and temperature, the foreign anion concentration, cell geometry, and specimen temperature. The failure of the anodic films has been related to the presence of anions "grown into" the film and identified by infrared transmission spectroscopy.

Abstract No. 49

Gas Phase Anodization of Tantalum

T. A. Jennings, W. McNeill, and **R. E. Salomon,*** Pitman-Dunn Research Laboratories, Frankford Arsenal, Philadelphia, Pennsylvania

The anodic oxidation of tantalum in the gas phase was studied by using an electro-magnetic ion cathode. Oxide films were prepared at constant current densities of 0.5 ma/cm^2 and 1.0 ma/cm^2. Growth characteristics of anodic tantalum oxide films, in the gas phase, were found to be similar to those for anodic tantalum oxide films in liquid electrolytes and also to those for tantalum oxide films prepared by thermal oxidation. The form of the growth rate law was found to be current density dependent and suggested that growth characteristics are influenced by the energy dissipated by ion bombardment.

Abstract No. 49A

Electrochemical Variables in the Anodic Synthesis of CdS Films

G. Serad, D. G. Husted, and **W. McNeill,** Pitman-Dunn Research Laboratories, Frankford Arsenal, Philadelphia, Pa.

(No abstract available)

Abstract No. 50

Electronic Conduction Mechanisms in Thin Films

J. Simmons, Standard Telecommunications Laboratory, London Rd., Harlow, Essex, England

(No abstract available)

Abstract No. 51

I-V Characteristics of Mo-Si_3N_4-Metal Structures

J. R. Yeargan and **H. L. Taylor,** The University of Texas, Austin, Texas 78712

I-V data form a straight line over as much as four decades on a Schottky plot for thin films of vapor deposited silicon nitride in a metal-insulator-metal configuration. Thickness variations, activation energies, and different metals for electrodes indicate a bulk limited process. Current variation with temperature is typical of thermal emission processes. These considerations suggest a transport mechanism similar to the Poole-Frenkel effect. (This work supported by NASA Grant NGR-44-012-043 and the Joint Services Electronics Program under Grant AF-AFOSR-766 66 and AF-AFOSR-766 67.)

Abstract No. 52

Theory of Charge Distribution in MOS Oxide

H. P. Caban-Zeda* and **A. B. Kuper,** Case Institute of Technology, Cleveland, Ohio 44106

Steady-state distribution, $N(x)$, of charged impurities in homogeneous oxide in MOS is calculated by solving the continuity equation and Poisson's equation assuming that neutral impurity is initially at M surface and moves between blocking electrodes. Three cases are solved: (*i*) cation mobile, fully ionized, (*ii*) cation mobile, recombining with anion near the M/O interface, (*iii*) anion and cation both mobile. Bias applied, plates shorted, and plates floating are considered. Results will be compared with Na and Br distributions in SiO_2 on Si obtained by radiotracer analysis after diffusion and drift. (Supported by Research Grant NGR 36-003-067, NASA, Electronics Research Center, Cambridge, Mass.

Abstract No. 53

The Activation Energies of Conduction in Ta Anodic Films

G. J. Korinek, Rare Metals Dept., CIBA Corp., Summit, N. J. 07901

The knowledge of the activation energy of the conduction process is necessary for the determination of the conduction mechanism. The conduction as a function of temperature has been measured for a number of Ta anodic and nonanodic oxides. The activation energies have been determined and are compared with some of those available in the literature. The relationship between the activation energy of conduction and the quality of the oxide film is discussed.

Abstract No. 54

Strain in Metal Films on Single Crystal Quartz Substrates

K. Haruta, J. L. Hokanson, and **W. J. Spencer,** Bell Telephone Laboratories, Inc., Allentown, Pa.

Strain in thin metal films deposited on single crystal quartz plates was studied by measuring deformations in the crystalline substrate. Intensity variations in transmission x-ray diffraction give a measure of the curvature and strain gradient of the crystal lattice due to the adherent metal film. Investigations were carried out on several metal films under a variety of plating and annealing conditions.

Abstract No. 55

The Intrinsic Stress in Evaporated Thin Films

E. Klokholm, IBM Watson Research Center, Yorktown Heights, N. Y.

The sign and the magnitude of the intrinsic stresses observed in evaporated metal films cannot be predicted from *a priori* knowledge. In an effort to correlate the observed intrinsic stress, S, with other physical parameters, S in a variety of metal films has been measured. The stress was measured *in situ* by the cantilevered substrate technique. The films were evaporated from an electron bombarded source in vacuums of 10^{-6} to 10^{-7} Torr onto glass susbtrates at room temperature. The data obtained indicate that films of metals with high melting temperatures, T_m, generally have larger intrinsic stresses. For metals with $T_m \cong 2000°C$, $S \cong 10^{10}$ dynes/cm^2; $T_m \cong 1500°C$, $S \cong 5 \times 10^9$ d/cm^2; $T_m \cong 1000°C$, $S \cong 2 \times 10^9$ d/cm^2, and for metals such as Sn with very low T_m the stress at room temperature is less than 10^8 d/cm^2.

Abstract No. 56

Residual Stresses in Electrodeposited Nickel Films

S. Tan and **E. Klokholm,** IBM T. J. Watson Research Center, Yorktown Heights, N. Y. 10598

The bending beam technique has been used to measure the residual stresses in electroplated nickel films. Cu-Be, Cu, and Ag evaporated on glass were used as substrates. The deposition rate was varied from 7 to 48 Å/sec. The stresses were found to be independent of deposition rate. The initially tensile stress decreased with thickness and became compressive before levelling off. The thickness at which the stress was zero depended on the saccharin content of the bath.

Abstract No. 56A

Electrical Evaluation of Deposited Tantala Films

J. R. Szedon, M. H. Francombe, S. A. Zeitman, and **R. M. Handy,** Westinghouse Research Laboratories, Pittsburgh, Pa. 15235

Dielectric films produced by d-c sputtering of tantalum in an oxygen ambient were deposited on unheated silicon substrates. Film thicknesses were established interferometrically. Electrical measurements were performed using capacitor structures with aluminum as the metallic electrode. Several unusual electrical effects have been observed in these structures. An increase of the dielectric constant from 16 to 22 resulted from a short annealing process (425°C, 1 min in nitrogen). Instabilities in both the current-voltage and the capacitance-voltage behavior of the units were observed in the 25°-150°C range. Several charge instability mechanisms appear to be involved. At room temperature, instability appeared to involve charge exchange across the oxide-silicon interface. This mode of instability has been observed earlier in Al-Si_3N_4-Si units. At elevated temperatures ionic conduction effects were induced for a limited range of electrical field stress. The responsible ionic species have not been identified. [This work was sponsored in part by the Air Force Avionics Lab., Wright-Patterson Air Force Base under Contract AF 33(615)-3390.]

Abstract No. 57

Techniques for Studying Failure in Thin Films

J. W. Faust, Jr. (present address: Materials Research Lab., Pennsylvania State University, University Park, Pa.) R&D Center, Westinghouse Electric Corp., Pittsburgh, Pa. 15235

Many of the techniques used to study failures in bulk material may be used to study failures in thin films. In some cases, however, the sample preparation technique is quite different. This talk deals with the detection and identification techniques for failures in thin films. Failures may be compositional variations or crystallographic defects. The various techniques available for studying these failure mechanisms are discussed in terms of what techniques can be used for various types and what the limitations of each technique are. Optical, electron microscopic, x-ray diffraction and topography, electron diffraction, microprobe, and mass spectrographic (both conventional and solid source spark) techniques are some of the ones that are taken up. Examples will be given as illustrations. Wherever possible, results of several techniques on the same specimen are given.

Abstract No. 58

Detection of Flaws and Flaw Breakdown in Anodic Tantalum Oxide by Differential Interference Microscopy

N. N. Axelrod, Bell Telephone Laboratories, Inc., Murray Hill, N. J.

In situ observation by differential interference microscopy has been used to demonstrate that flaws exist in anodic tantalum oxide films ($\sim$2500Å) formed from sputtered β-tantalum films. These flaws are sites of irreversible processes upon the application of cathodic voltages. The oxide flaws are formed primarily at sharp prominences in the sputtered metal film surface. The irreversible breakdown processes depend on the metallic counterelectrode used. Photographed sequences and further applications of the technique are discussed.

Abstract No. 59

Tin Whiskers and Filamentary Growths on a Thin Film Conductor in Response to Direct Current Flow

R. B. Marcus and **M. H. Rottersman,** Bell Telephone Laboratories, Inc., Murray Hill, N. J.

Whiskers and filamentary growths have been observed to grow from tin films deposited on nickel/chromium films in response to a d-c current flow through the film. The filaments grow on the conductive film surface towards the negative electrode during application of power with densities of $\sim$10 w/cm^2 of film surface. These growths were observed in terminations for tantalum nitride resistor structures when subjected to excessive d-c power loads. A number of experimental techniques including electron microscopy and diffraction show that the migrating material is in the liquid state during growth, and that electrotransport appears to be the driving force for the migration. The migrating material is mostly tin which flows through channels in the conducting film caused by dissolution of the nickel and chromium in the tin.

Abstract No. 60

Relationship between Dielectric Breakdown and Edge Structure of Evaporated Aluminum Electrodes

S. W. Chaikin and **G. A. St. John,** Stanford Research Institute, Menlo Park, Calif.

The edges of aluminum electrodes evaporated through masks influence breakdown of dielectrics in crossovers and capacitors. We have studied aluminum film edges by electron microscopy (replica, transmission, cross section). For 2000-4000Å films with mask-to-substrate spacing af 2 mils, observed penumbras exceed calculated penumbras by 50-75%. The cause is probably low sticking of aluminum atoms to the nonmetallic substrate and reflection under the mask. The slope of a typical edge is a gentle 5-10%. The occurrence of edge breakdown is probably due to field enhancement by the sharp edge; an enhancement factor of 3 has been calculated.

Abstract No. 61

Correlation of Physical and Electrical Properties with Intermetallic Reactions of Al and PbSn Bonds with Au/NiCr Thin Films

J. Boros, J. W. Kanz, and **W. L. Robinson,** Autonetics, 3370 Miraloma Ave., Anaheim, Calif. 92803

Sensitive four-point electrical resistance measurements have been used to detect potential failure mechanisms in both ultrasonic (Al wire) and solder (Pb-Sn) bonds on Au/NiCr thin-film hybrid microcircuits. Such bond structures have been subjected to sufficient thermal stress to simulate field service and worst-case processing conditions. Correlation was obtained between resistance changes and the results of microprobe, metallographic, and mechanical bond strength measurements.

Abstract No. 62

Electromigration in Metal Films

W. E. Mutter, IBM Components Div., East Fishkill Facility, Hopewell Junction, N. Y. 12533

Electromigration is observed in aluminum film test stripes in the range of 0.5 to 2.0 x 10^6 amp/cm^2 at ambient temperatures of 100°-150°C. Substantial evidence is presented to show that mass transport of aluminum does occur and that it can lead to eventual electrical opens in thin film conductors. A mechanism of conductor failure based on the condensation of mobile vacancies at favorable sites is developed and related to the experiments. More limited observations on electromigration in films of molybdenum, copper, gold, and silver fall in line with theoretical expectations based on self-diffusion at low temperatures and published electromigration data on bulk samples at much higher temperatures.

Abstract No. 63

The Dielectric Strength of Silicon Dioxide Films as Used in Semiconductor Devices

J. A. Baldrey* and **R. V. Mariner,** Texas Instruments Ltd., Manton Lane, Bedford, England

Measurements have been made of the dielectric strength of silicon dioxide films as formed by different techniques and after having been subjected to the boron and phosphorus diffusion cycles typical of silicon device manufacture. At room temperature, maximum dielectric strength is 5 mega-volts/cm, but practical results are limited by point defects in the oxide and thickness of the contact metal the lowest limit being 1.5 Mv/cm. As temperature is increased under constant voltage stress, the maximum usable dielectric strength is found to be 2 Mv/cm at 150°C and 1 Mv/cm at 400°C.

Abstract No. 64

Failure of Solid Tantalum Capacitors due to Anodic Electronic Activation

G. P. Klein, Lab. for Physical Science, P. R. Mallory & Co., Inc., Northwest Industrial Park, Burlington, Mass.

Electronic conductivity of anodic oxide films on tantalum was found to be caused, among other things, by thin layers of intimately adhering semiconductor oxides, such as manganese dioxide, deposited by pyrolytic techniques or by reactive sputtering. Uniform electronic activation was observed in electrolytes on reapplication of the original formation voltage. Defective sites in the anodic oxide film showed electronic conductivity below the level at which uniform activation occurred. The steady increase in leakage current in solid electrolyte tantalum capacitors is attributed to a similar mechanism of anodic electronic activation when these capacitors are polarized at elevated temperatures and voltages above about 60% of the formation voltage.

Abstract No. 65

Field Induced Growth of Crystalline Tantalum Oxide

Julius Klerer, Bell Telephone Laboratories, Inc., Murray Hill, N. J. 07971

Anodic d-c field growth of crystalline tantalum oxide on tantalum foil in a nitric acid solution has been reported in the literature. Attempts to form crystalline oxide on sputtered tantalum film, utilizing techniques which were successful with tantalum foil, produced negative results. Formation of crystalline β-Ta_2O_5, however, did occur when the amorphous oxide was scintillated in the dilute nitric acid solution. The scintillation voltage for Ta_2O_5 films formed from various types of sputtered tantalum was investigated as a function of dielectric thickness, temperature, and electrolyte type and concentration. Results to be presented indicate that the scintillation field of the oxide in nitric acid as the electrolyte, is inversely proportional to the oxide thickness, and is also dependent on the composition of the sputtered tantalum. In addition the evidence suggests that nucleation of the crystalline oxide is due to localized breakdown. Equations have been obtained relating scintillation voltage to thickness of oxide film formed.

Abstract No. 66

Gold-Induced Break-Away Oxidation of Tantalum

W. O. Freitag, Univac Div., Sperry Rand Corp., Blue Bell, Pa.

Tantalum films undergo break-away oxidation in air at 200°-450°C when in direct contact with gold resulting in failure of resistor-conductor networks. An interlayer of another metal prevents this, provided that enough interlayer is present to form a diffusion barrier for the gold. Other metals have been tested for their effect on the oxidation of sputtered tantalum films. Gold accelerates the oxidation at 425°C, Cu and Pd permit the Ta to oxidize as rapidly or almost as rapidly as Ta alone; Ni, Co, Cr, and Mo do not.

Abstract No. 67

Construction of Nonpolar Electrolytic Capacitors

J. C. W. Kruishoop, Philips Research Labs., N. V. Philips' Gloeilampenfabriken, Eindhoven, The Netherlands

A new type of electrolytic capacitor is described, which lacks the undesirable rectifying properties of the conventional one. The electrolyte in such a nonpolar capacitor has to meet some new additional requirements, namely, absence of hydrogen ions and self-healing properties in the cathodic direction as well as in the anodic direction. An explanation of the cathodic self-healing process is given for one special electrolyte, anhydrous $Ca(NO_3)_2$ in dry pyridine, but there are many more examples of suitable nonpolar electrolytes.

ELECTRONICS—LUMINESCENCE

Abstract No. 68

Rare Earth Activated Phosphors

F. C. Palilla, Bayside Labs., General Telephone & Electronics Laboratories, Inc., Bayside, N. Y.

(No abstract available)

Abstract No. 69

Effects of Photon Absorption at Low Temperature in Distinct UV-Absorbing Groups

S. G. Polick and **H. N. Hersh,** Zenith Radio Corp., 6001 W. Dickens Ave., Chicago, Ill. 60639

This study is concerned with what happens when uv photons are absorbed by distinct groups such as WO_4 and VO_4. Experiments at 78°K on undoped YVO_4 and $GdVO_4$, using uv light, indicate that the absorbed energy is partitioned into two fractions, one of which gives rise to immediate host fluorescence, the other of which is stored (to be released radiatively if subsequently stimulated properly). This is not contemplated by the usual charge-transfer model of the absorption process. Data are presented on the efficiency of this process and on results with other uv-absorbing groups.

Abstract No. 70

Europium Luminescence in $InBO_3$ and Related Orthoborates

F. J. Avella* and **C. S. Wiggins,** General Telephone & Electronics Laboratories. Inc., 208-20 Willets Point Blvd., Bayside, N. Y. 11360

Indium orthoborate is an effective host for Eu^{3+} when excited by cathode rays. With that mode of excitation, the luminous efficiency of $InBO_3{:}Eu$ is superior to that of the Eu activated rare earth orthoborates and comparable to that of $YVO_4{:}Eu$. Variations observed in spectral details among the orthoborate phosphors are related to effects of crystal symmetry on Eu^{3+} electronic transitions.

Abstract No. 71

Intensities of the Eu^{3+} $^5D_0 \rightarrow {}^7F_2$ Transitions in Rare Earth Vanadates

Ojars Sovers and **Gleb Gashurov,*** General Telephone & Electronics Laboratories, Inc., 208-20 Willets Point Blvd., Bayside, N. Y. 11360

Intensities of the two uv-excited $^5D_0 \rightarrow {}^7F_2$ emission lines in europium-doped vanadates are calculated theoretically. For the series of phosphors (Sc, Lu, Y, Gd)$VO_4{:}Eu^{+3}$, it is reasonable to assume that variation of the Eu^{+3} wave functions, as well as differences in energy-transfer mechanisms, are slight and do not affect the emission intensities. Variation of crystal field at the europium ion is the dominant effect, and is described by a single parameter, $B_2{}^3$. Ratios of $^5D_0 \rightarrow {}^7F_2$ intensities are obtained from ratios of $|B_2{}^3|^2$ calculated from point charge models of these four vanadates. Agreement between theory and experiment will be discussed.

Abstract No. 72

Characterization of Energy Transfer Interactions between Rare Earth Ions

L. G. Van Uitert, Bell Telephone Labs., Inc., Murray Hill, N. J. 07971

Energy transfer between rare earth (RE) ions in $Na_{0.5}RE_{0.5}WO_4$ has been examined. Transfer from Tb to Eu, Dy, and Er and from Eu to Nd is predominately by dipole-dipole interactions. Transfer from Tb to Sm involves 3-body interactions and transfer from Tb to Nd is either by dipole quadruple or 3-body interactions. Conditions for energy migration between Tb ions and exchange enhancement of transfer are also discussed.

Abstract No. 73

The Energy Levels of Eu^{3+} and the Brightness of $YVO_4:Eu^{3+}$ at High Temperature

D. T. Palumbo and **J. E. Mathers,** Sylvania Electric Products Inc., Towanda, Pa. 18848

The energy levels of Eu^{3+} in luminescent systems ($LaCl_3$, Y_2O_3, ScO, $GdVO_4$, YVO_4) are derived from excitation spectra and compared with literature values. A correlation is made of the temperature dependence of luminescence in $GdVO_4$ and YVO_4 with the intensity of the $^5D_1$, $^5D_2$, and $^5D_3$ absorptions. Data are given to show that the emission intensity at high temperature increases with the $^5D_1$, $^5D_2$, and $^5D_3$ absorption intensities.

Abstract No. 74

Terbium Activated Lanthanum Silicate Phosphors

T. E. Peters, General Telephone & Electronics Laboratories, Inc., 208-20 Willets Point Blvd., Bayside, N. Y. 11360

The synthesis and luminescent properties of terbium activated lanthanum silicates are described. The compositional phases observed in the SiO_2-La_2O_3 system are in general agreement with the observations reported in the literature; discrepancies between investigators can be attributed to the complexities of the lattices and the sensitivity of composition to synthesis parameters. Optimum luminescence efficiencies are obtained with SiO_2/La_2O_3 ratios of 1.8 to 2.2 corresponding to the composition $La_2Si_2O_7$. Luminescence response to short ultraviolet and cathode-ray excitation is compared to Zn_2SiO_4:Mn and (Zn,Cd)S:Ag, respectively.

Abstract No. 75

Effects of Charge Compensation on the Optical Spectra of Tb^{3+} in $CaF_2:Tb^{3+}$

R. L. Amster, General Telephone & Electronics Laboratories, Inc., 208-20 Willets Point Blvd., Bayside, N. Y. 11360

The excess positive charge of trivalent terbium in $CaF_2:Tb^{3+}$ can be compensated in ways which lead to a variety of local symmetries about the Tb^{3+}. Compensation by monovalent cations in Ca^{++} sites promotes cubic symmetry whereas compensation by oxide ions in F^- sites produces trigonal symmetry. Charge neutrality brought about by interstitial F^- ions leads to environments of intermediate symmetries. The intensity ratio of Tb^{3+} emisisons at 541 and 489 nm serves as a measure of the RE ion environment.

Abstract No. 76

Mixed Valence Europium Phosphors

W. A. McAllister, Advanced Development Dept., Westinghouse Electric Corp., Bloomfield, N. J.

Replacement of lanthanum in $LaPO_4$:Eu phosphors by barium-lithium pairs ($La_{1-2x}Ba_xEu_xLi_xPO_4$) leads to interesting emission characteristics. (1) Line emission typical of Eu^{+3} for all ultraviolet excitation but most pronounced at short wavelength. (2) A blue band for excitation wavelengths greater than 266nm, for certain values of x. (3) An ultraviolet band prominent under the same conditions favoring the blue emission. Results of x-ray and microscopic examination indicate that the line emission is due a Eu^{+3} center which receives energy from the host, the bands representing centers which are excited directly and having Eu^{+2} as activator.

Abstract No. 77

Methods for Trace Analysis of Rare Earths

J. F. Cosgrove, D. W. Oblas, and **D. J. Bracco,** General Telephone & Electronics Laboratories, Inc., 208-20 Willets Point Blvd., Bayside, N. Y. 11360

The emergence of rare earth activated materials in luminescence and laser applications has posed new demands on methods of detection of rare earths at trace levels. This paper evaluates several instrumental methods applied to rare earth activated phosphors and the raw materials used in their synthesis. Emphasis is on the effectiveness of comprehensive analysis at trace levels. The results include determinations made possible by recent innovations in the techniques of mass spectroscopy, absorption and emission spectroscopy, activation analysis and optical fluorescence excited by x-rays.

Abstract No. 78

A New Analog-Computing Spectroradiometer

R. E. Shrader, RCA Laboratories, Princeton, N. J.

The recent wide-spread use of commercial and concomitant accelerated research on line-emitting phosphors has made necessary the development of improved spectroradiometric equipment for the study of the luminescence of such phosphors. This paper describes recently constructed equipment which has the following capabilities: automatic correction of detector output for all system-defects over six overlapping 3000Å-wide range, with provision for use to 10μ; interchangeability of gratings and/or detectors suitable for each wavelength range; resolution to 0.25 amp in the visible (4000-7000Å); analog determination of colorimetric X, Y, and Z in the visible; integration of $\int W(\lambda)\,d\lambda$ or $\int W(\nu)\,d\nu$, or $\int \frac{W(\lambda)}{\lambda}\,d\lambda$ over any selected range; band-spread analog recorder-drive from 10 to 300 Å/in., or 0.1 to 2.0 ev/in.; continuous recording of $\int \frac{W(\lambda)}{\lambda}\,d\lambda$ to permit evaluation of total photons in each resolved line or complex. The method of achievement, purpose and advantage of each of the many functions of the instrument will be dealt with in some detail. In addition, the mathematics of analog integration of $\int (\bar{x}, \bar{y}, \text{ or } \bar{z})\,d\lambda$ for line spectra are discussed.

Abstract No. 79

There is no Abstract 79

Abstract No. 80

Spectro Characteristics and Efficiency of GaAs Light Diodes

Richard Klein, William Agosto, Lawrence Murray, Electronic Components and Devices RCA, Somerville, N. J., and **Henry Kressel,** RCA Sarnoff Research Lab., Princeton, N. J.

Incoherent electroluminescent spectra and quantum efficiency of GaAs diodes were measured as functions of dopant, doping level, junction gradient, current density, and temperature. I-V and C-V characteristics were taken and the electrical, optical, and physical parameters were correlated. Injection mechanisms, including impurity state tunneling are discussed in relation to the diode parameters. Measurements of the photoluminescent spectra were carried out and correlated with the results obtained by other methods.

Abstract No. 81

Particle Size and Morphology of Zinc Sulfide Precipitates

R. A. Brown, Radio Corp. of America, Electronic Components and Devices, Lancaster, Pa. 17604

The influence of various factors (*e.g.*, pH, rate of addition of hydrogen sulfide, temperature, concentration of the zinc solution) on the particle size and crystal morphology of ZnS obtained by normal precipitation methods has been investigated. Precipitation from strongly acid solution results in the formation of aggregates, of the order of 1-5μ, which are irregular, globular masses. Some preliminary experiments are reported regarding the effect of the various preparatory conditions on the size and morphology of ZnS:0.015% Ag phosphors.

Abstract No. 82

Zinc Oxide Phosphors

Willi Lehmann, Westinghouse Research Labs., Pittsburgh, Pa. 15235

Zinc oxide may emit in four different bands, the uv near-edge emission, the common green band (possibly involving sulfur), a yellow-orange band due to selenium, and a red to near-infrared band due to ammonia. Up to about 10% of the ZnO can be replaced by CdO with a corresponding shift of the emission bands toward lower energies. The possibility of impurity activation due to anion substitution cannot be excluded.

ELECTRONICS—SEMICONDUCTORS

Abstract No. 83

Films of Silicon Nitride-Silicon Dioxide Mixtures

T. L. Chu, C. H. Lee, and **J. R. Szedon,** Westinghouse Research Labs., Pittsburgh, Pa. 15235

A series of amorphous films of silicon nitride-silicon dioxide mixtures have been deposited on silicon substrates by the pyrolysis of silane in an ammonia-oxygen mixture. The effect of the reactant composition on the composition of the film has been studied. The physical properties of these films, such as density, dielectric constant, dissolution rate, infrared absorption, etc., are discussed as a function of their composition. The electrical characteristics of MIS structures prepared from these films will be compared with those of MNS structures. (This work was supported in part by U.S. Naval Air Development Center, Johnsville, Pa., under Contract N 62269-67-C-0189.)

Abstract No. 84

The Epitaxial Growth of Aluminum Nitride

T. L. Chu, D. W. Ing, and **A. J. Noreika,** Westinghouse Research Labs., Pittsburgh, Pa. 15235

Aluminum nitride films have been deposited on the basal plane of hexagonal silicon carbide substrates by chemical transport and ammonolysis techniques. The transport technique was carried out in a sealed tube, and the films obtained exhibited only fiber structures. The ammonolysis technique was carried out in a gas flow system, and the films obtained were single crystalline and epitaxial with respect to the substrate. The deposition processes and the properties of the films are discussed. [This work was supported by the Research and Technology Division, Air Force Command, under Contract AF 33(615)-3624.]

Abstract No. 85

Some Applications of Silicon Oxy-Nitride as a Semiconductor Surface Protectant

J. E. Mann and **P. Walker,** TRW Semiconductors, 14520 Aviation Boulevard, Lawndale, Calif. 90260

A silicon oxy-nitride compound has been reactively sputtered on a variety of transistor, zener, and varicap structures, both as a surface protectant replacement for silicon dioxide and as a final surface and/or device sealant. Results have shown improvement in device leakage stability through power aging and salt spray tests in different package designs, including molded packages and on chip-on-substrate devices. Radiation environment tests have shown this nitride compound to be superior to silicon dioxide.

Abstract No. 86

Redistribution of Donor and Acceptor Impurities in Silicon during the Deposition and Subsequent Reheat of Pyrolytic Silicon Nitride

T. P. Cauge, R. R. Mehta, and **R.C.G. Swann,** ITT Semiconductor Research Dept., Palo Alto, Calif.

Redistribution of gallium, boron, and phosphorus in silicon after deposition of silicon nitride is measured using the MOS method. Large changes in surface concentration can be induced during film deposition. Such effects cannot be stimulated thermally, since the temperature and duration of deposition are relatively small, and therefore an alternative mechanism is presented to explain the phenomenon. Subsequent reheat promotes a behavior governed by thermal diffusion, and theoretical impurity distributions agree with those measured experimentally. Values of surface state density and silicon nitride dielectric constant are correlated with the redistribution phenomenon.

Abstract No. 87

Thin Film Boron Nitride

M. J. Rand and **J. F. Roberts,** Bell Telephone Laboratories, Inc., Allentown, Pa.

Vitreous thin films of boron nitride have been deposited on Si, Ta, SiO_2, etc., at 600°-900°C by a diborane-ammonia chemical vapor deposition reaction which is described. Physical, chemical, and electrical properties have been investigated, and the films have been tested for potential applications such as semiconductor surface protection, boron diffusion source, insulator, and thin-film varistor. BN film shows strongly nonohmic high-field conductivity which is stable and polarity-independent. At room temperature a plot of log current density *vs.* the square root of field strength is linear over eight decades of current.

Abstract No. 88

Interface State Analysis with the MOS Conductance Technique

E. H. Nicollian and **A. Goetzberger,** Bell Telephone Laboratories, Inc., Murray Hill, N. J.

Typically in an MOS capacitor, equivalent parallel conductance caused by interface state loss changes by an order of magnitude between 5 and 100 kHz while the largest capacitance dispersion is only 14%. This makes the conductance far more accurate to use than capacitance for extracting interface state properties. Interface state densities down to the $10^9 cm^{-2}$-ev^{-1} range have been measured using the conductance technique. Interface state density and capture cross section as functions of surface potential can be obtained with a simplified technique based on an experimentally verified interface state equivalent circuit. A set of three universal curves which aid in the analysis is presented.

Abstract No. 89

The Analysis of the Channel Current Associated with Silicon Planar P^+N Junction

Masaya Ohta, Hitachi Musashi Works, 1450 Josuihoncho, Kodairashi, Tokyo, Japan

The collector junction channel current of gold diffused silicon NPN transistor is investigated. The knee in the I-V characteristics of the collector junction can be found after high stress operation. The flat part of this knee nearly coincides with the applied voltage of high stress operation and the convex part appears in the C-V curve of the collector junction in response with this knee. We propose a new model for channel current explaining these phenomena.

Abstract No. 90

Selective Vapor Phase Etching of Semiconductors

J. W. Blair,* E. C. Teague, and **E. G. Alexander,** Texas Instruments Inc., P.O. Box 5012, Dallas, Texas 75222

Results are reported of selective etch experiments performed on silicon, germanium, and gallium arsenide samples partially masked by SiO_2. HCl or HBr etchants in H_2, He, Ar, or N_2 comprised the etching systems. Plausible explanations of the vapor etch "edge effect," undercutting, and effect of mask geometry are given in terms of relative adsorption strengths, mobility of etchant molecules, and mass action principles. A technique for reducing these effects is presented.

Abstract No. 91

Gaseous Diffusion into Silicon

W. G. Dautzenberg, Y. W. Hsueh*, and **B. R. Wilkins,** Molecular Electronics Div., Westinghouse Electric Corp., P.O. Box 7377, Elkridge, Md. 21227

Diffusion experiments using gaseous dopants on silicon in an open-tube system have been performed. Arsine, diborane, and phosphine were used as the sources of impurities for diffusion. Various gas concentrations, as well as diffusion temperatures and time cycles, were the main factors of controlling the diffusion parameters. Dopant concentrations in the gases were varied from 100 ppm to 1% in oxidizing conditions. The temperature range was 815°-1280°C. Results indicated that the gaseous system, from the point of view of operational simplicity, reproducibility, cleanliness, and uniformity, is superior to conventional liquid and solid source systems. Analysis of some results are presented.

Abstract No. 92

Phosphorus Diffusion in Silicon Using Phosphine

M. S. R. Heynes and **P. G. G. van Loon,** ITT Semiconductors, 3301 Electronics Way, W. Palm Beach, Fla.

Phosphine (PH_3) was used as a diffusion source in both reducing and oxidizing conditions. Erratic results were obtained in reducing conditions using up to 1% PH_3. In oxidizing conditions, solid solubility limited results were reproducibly obtained from 750° to 1200°C with PH_3 concentrations from 0.1 to 1.0%. The presence of water in the system from the oxidation of PH_3 does not appear to be of significance. No difficulty was experienced in applying phosphine diffusion to device fabrication.

Abstract No. 93

An Efficient Boron Trichloride Diffusion System

R. C. Thomas, J. W. Sprague, and **E. L. Marcy,** Semiconductor Products Dept., General Electric Co., Syracuse, N. Y.

The importance of ambient conditions control in boron diffusion has led to the design of a "tight" system. A tight system provides the stability and accurate control required in the addition of hydrogen, oxygen, and boron trichloride to the nitrogen diffusion ambient. The source is a high pressure cylinder of ¼% boron trichloride in nitrogen. One system can provide the full range of surface concentration from 10^{17} to solid solubility limit. Quartz ware design is consistent with maximum reproducibility of diffusion.

Abstract No. 94

A Liquid Antimony Diffusion System

F. L. Gittler, Bell Telephone Laboratories, Inc., Allentown, Pa.

A liquid diffusion system using $Sb(C_2H_5O)_3$ has been developed. This system is suitable for high concentration buried layers in integrated circuits and base layer diffusions in pnp transitors. Epitaxial layers grown on slices diffused with $Sb(C_2H_5O)_3$ show low stacking faults, no haze or defects commonly found by use of the solid source. Diffusion coefficients and energy of activation were calculated. Correlation of oxygen concentration with sheet resistivity variation is presented.

Abstract No. 95

Impurity Distribution in Single Crystals, IV. Crystal Growth Characteristics of InSb Pulled from the Melt as Revealed by High-Frequency Impurity Striations

A. F. Witt and **H. C. Gatos,** Dept. of Metallurgy and Center for Materials Science and Engineering, MIT, Cambridge, Mass.

It was found that during crystal growth from the melt it is possible to introduce high frequency vibrations in the melt (5-50 Hz) without altering the growth characteristics of the crystal. If an impurity is present, these vibrations are incorporated into the crystal in the form of very sharp impurity striations superimposed on the regularly appearing impurity heterogeneities. Knowing the frequency of the vibrations, the separation of the resulting striations in the crystal can serve as an accurate measure of crystal growth on a microscale. This novel technique was employed for the study of the microscopic growth rate and its variations in the different parts of single crystals of InSb. In crystals grown in the <111> direction large differences were observed between the "core" and the "off core" regions. Furthermore it was possible to relate the usually observed impurity heterogeneities to specific differences in the microscopic rate of crystal growth. Several aspects of crystal growth as revealed by the above internal time constant are discussed.

Abstract No. 96

Measurement of Epitaxial Doping Density vs. Depth

D. R. Decker, Bell Telephone Laboratories, Inc., Reading, Pa.

The determination of epitaxial doping density *vs.* depth from capacitance-voltage measurements on diffused diodes is derived for the general case. These calculations extend the useful range of the capacitance-voltage technique and allow profiling of epitaxial doping in depth through the use of deep-diffusion test diodes. Experimental comparison of the deep-diffusion and shallow-diffusion characterization techniques shows that the deep-diffusion technique extends the capability of capacitance-voltage measurements with accuracy comparable to the shallow junction measurements (5-15%) to depths needed for practical devices.

Abstract No. 97

Semiconductor Doping by High Energy 1-2.5 Mev Ion Implantation

S. Roosild, R. Dolan, and **B. Buchanan,** Air Force Cambridge Research Labs., Office of Aerospace Research, Bedford, Mass.

The formation of junctions in silicon through the use of mono-energetic ions in the energy range from 1 to 2.5 Mev has been studied. Boron and nitrogen ions were used. Results are presented on the annealing temperatures required to place these ions into substitutional states, on the distribution of these ions in the host material, and on the electrical characteristics of the p-n or n-p junctions obtained.

Abstract No. 98

Secondary Breakdown Capability of Epitaxial Transistors

P. J. Kannam, F. G. Ernick, and **J. Marino,** Semiconductor Div., Westinghouse Electric Corp., Youngwood, Pa.

Transistors with $V_{CEO} = 150v$, $f_t = 30$ mc, $h_{FE} = 20$ at 20Å and $V_{CE}(sat) = 0.5v$ at 20Å were fabricated using an epitaxial collector, epitaxial base and diffused emitter. The impurity profile was determined by the spreading resistance technique and the design was optimized by computer methods. The base width in the range of 2-15μ and the base resistivity in the range of 0.1 to 10 ohm-cm were used for device fabrication. The electrical characteristics were tested, and the dependence of secondary breakdown and f_t on base width and base resistivity was established.

Abstract No. 99

NP ν N Transistor Collector Breakdown Voltage vs. Epitaxial Layer Thickness

H. R. Gates, B. V. Gokhale, and **E. G. Grochowski.** IBM Components Division, East Fishkill Facility, Hopewell Junction, N. Y.

Infrared interference has been used to determine correlation between epitaxial thickness and collector breakdown in NP$_\nu$N transistors. The precise correlations obtained give an equation for collector-base breakdown of the form

$$BV_{cbo} = bh + A$$

where h is the infrared thickness. The constant, A, includes the translational effect of the collector-base junction depth and substrate outdiffusion. The constant b was equal to 19.7 volts/micron throughout the experimental range of BV_{cbo} — 90 to 175v. This relationship is predicted from the ionization integral including effects of charged gold centers on the electric field.

Abstract No. 99A

Dielectrically Isolated Matched Transistor Pairs

W. C. Rosvold, W. H. Legat, and **L. K. Russell,** Raytheon Co., 350 Ellis St., Mountain View, Calif. 94040

Very uniform matching of electrical parameters is achieved by using adjacent transistors on a common, dielectrically isolated, polycrystalline silicon substrate. This novel approach utilizes the anisotropic properties of [100] orientation silicon for the precision shaping of the isolated active areas. Because of this only one polycrystal layer is necessary to achieve dielectric isolation. Adjacent transistors are separated from the wafer on their common substrate which yields the highest probability for the matching of the difficult parameters such as V_{BE} tracking and h_{FE}. Typical parameters are presented.

Abstract No. 99B

Characterization of Anomalous Growth Observed in Electron Beam Irradiated Silicon

David Sivertsen, Olin Cecil, and **Rolf Haberecht,** Materials R&D Lab., Texas Instruments Inc., Dallas, Texas

An anomalous growth of silicon observed in electron irradiated areas and reported previously by us is characterized in this work. Several theories are postulated as possible explanations for the mechanism responsible for hill formation. Several indirect methods are used to characterize the structure of the electron irradiated region. Impurities such as lithium and boron were diffused into the substrate after the peaks were formed to compare diffusion characteristics in exposed and unexposed areas. Chemical etching procedures were used to determine the distribution of dislocations in exposed and unexposed areas.

Abstract No. 100

Epitaxial Growth of Sulfur Doped $GaAs_{1-x}P_x$ Alloys and Their Physical Properties

I. Akasaki, M. Hashimoto, and **T. Hara,** Matsushita Research Institute Tokyo, Inc., Ikuta, Kawasaki, Japan

$GaAs_{1-x}P_x$ alloys doped with sulfur above 10^{18} cm^{-3} have been prepared over the whole range of x using epitaxial technique. The electron mobility varies largely with the composition. The effective electron mass in GaAs obtained from the plasma minimum is about 0.08 m. The minimum value of infrared reflectivity rises with the increase of x. In GaP-rich alloys plasmons interact with optical phonons. The obtained mass in GaP is about 0.34 m, which agrees with that reported to date.

Abstract No. 101

Epitaxial GaAs Films Deposited under Near-Equilibrium Conditions in Ultra-High Vacuum

P. Hudock, General Telephone & Electronics Laboratories Inc., Bayside, N. Y.

Epitaxial films of GaAs have been deposited on single-crystal GaAs substrates by using a sublimation technique under near equilibrium conditions in ultra-high vacuum. Epitaxial GaAs films are easily achieved at temperatures as low as 600°C by performing the depositions in background pressures of 5 x 10^{-10} Torr or less. The relative rates of growth for four GaAs orientations are $\{311\} > \{100\} > \{110\} > \{111\}$, in agreement with the growth factor for crystallization on these orientations. With the use of near-equilibrium conditions, impurities can be transported from the source material to the epitaxial layers with approximately the same carrier concentrations. The resistivity of the epitaxial films approached that of the source crystals for both 0.01 and 2 x 10^4 ohm·cm material. The temperature dependence of the mobility for the epitaxial GaAs films is similar to that for the GaAs source crystals.

Abstract No. 102

Heterojunction Formation by the Low-Temperature Vapor Growth of GaAs

D. K. Jadus, G. O. Ladd, and **D. L. Feucht,** Electrical Engineering Dept., Carnegie Institute of Technology, Pittsburgh, Pa.

Gallium arsenide has been grown epitaxially on germanium at temperatures as low as 475°C using a close-spaced growth system. The grown n-type GaAs has a carrier concentration in the range of 10^{14}-10^{17}/cm^3 and a room temperature Hall mobility of approximately 10^3 cm^2/v-sec. The formation of a thin n-layer in the Ge near the interface, due to arsenic diffusion, has been retarded by the use of a heavily diffused p region and low growth temperatures. A heterojunction transistor fabricated using this system possessed a β greater than unity even though the base region was more heavily doped than the emitter. [This work was supported in part by the Air Force Cambridge Research Laboratories under contract AF-19-(628)-5811 and the U. S. Army Research Office-Durham under contract DA-31-124-ARO(D)-131.]

Abstract No. 103

Growth of Single Crystals of InAs-GaAs

H. Olsen, H. Robbins, and **R. K. Willardson,** Bell & Howell Research Center, 360 Sierra Madre Villa, Pasadena, Calif. 91109

Single crystals of $InAs_{1-x}$-$GaAs_x$ have been grown from the melt for values of x ranging from 0.01 to 0.99. Three different techniques have been used successfully: (*i*) Czochralski, using a magnetic coupled crystal pulling unit completely sealed in quartz to maintain the arsenic pressure, (*ii*) Czochralski, using B_2O_3 encapsulation to prevent the loss of arsenic, and (*iii*) growth on GaAs seed plates from an indium- or gallium-rich solution of InAs-GaAs. [This research was supported in part by the U. S. Naval Ordnance Laboratory, Corona, Calif., under Contract Number N123(62738)55582A.]

Abstract No. 104

Growth Rate and Doping in the $GeCl_4$-H_2 System

V. J. Silvestri, IBM Thomas J. Watson Research Center, Yorktown Heights, N. Y. 10598

The reduction of $GeCl_4$ with H_2 has been used extensively for epitaxial deposition of Ge although details of this process are not well known. Results of experimental and theoretical studies on the analogous $SiCl_4$-H_2 reaction have indicated that at normal epitaxial deposition temperatures the Si systems generally in use approximate equilibrium ones and are mass-transport controlled. To gain more insight into the $GeCl_4$-H_2 reaction, growth rate, and doping conditions in a Ge epitaxial system have been investigated in the present work and the following results were obtained: (*i*) The growth rate for a given Ge/H_2 gas phase ratio is independent of time at substrate temperatures between 600° and 850°C. (*ii*) The growth rate increases linearly with increase in Ge flux for Ge/H_2 ratios between 4 x 10^{-4} and 1 x 10^{-2}. (*iii*) The growth rate remains constant for different H_2 linear gas stream velocities at constant Ge flux. These growth rate data indicate that for substrate temperatures above 600°C the $GeCl_4$-H_2 reaction approaches equilibrium and that it is mass-transport limited. In agreement with this hypothesis it was also observed that the boron concentration in epitaxial Ge layers deposited at 700°, 800°, and 830°C increased linearly with B_2H_6 content in the gas phase and that it did not change for the three different substrate temperatures.

Abstract No. 105

A Surface Reaction Approach to the Growth Kinetics of Epitaxial Silicon from $SiCl_4$

E. G. Alexander, Texas Instruments Inc., P.O. Box 5012, Dallas, Texas 75222

The kinetics of the hydrogen reduction of silicon tetrachloride to produce epitaxial silicon films are considered in terms of surface adsorption and reaction. A mechanism involving reaction between adjacently adsorbed unlike species describes the observed growth kinetics up to intermediate values of $SiCl_4$ concentration. Etching conditions predominate when, at high concentrations of $SiCl_4$, hydrogen is virtually excluded from the surface. The observed silicon growth or etching rate is shown to be the difference between two much larger terms, indicating considerable refluxing occurs at the surface. Examples show that this surface approach complements alternative explanations based primarily on gaseous diffusion and thermodynamics.

Abstract No. 106

Low-Temperature Epitaxial Growth of Silicon in Ultra-High Vacuum

R. N. Thomas, A. J. Noreika, and **M. H. Francombe,** Westinghouse Research Labs., Pittsburgh, Pa. 15235

A systematic study has been made of the oriented growth of "thick" films of silicon on the clean (111)-7 surface of silicon, as characterized by *in-situ* LEED observations. Crystals prepared by web and Czochralski growth were used as substrates. The crystalline perfection of films grown by sublimation in the temperature range 300°-650°C has been correlated with parameters such as deposition rate, film thickness, and substrate surface perfection using transmission electron microscopy on chemically thinned samples. The sensitivity of LEED pattern details to changes in crystal perfection of the grown layers is discussed.

Abstract No. 107

Epitaxial Growth of Silicon on Sapphire

P. Rai Choudhury, Sperry Semiconductor, 38 Main St., Norwalk, Conn., and **R. R. Fergusson,** Northern Electric Company Ltd., Research and Development Labs., Ottawa, Ont., Canada

Oriented films of silicon were deposited on single crystal sapphire substrates by the pyrolytic decomposition of silane. Three methods of substrate preparation were investigated; namely, high temperature heating in hydrogen, etching in o-phosphoric acid and vapor etching with silicon. Etching with silicon at high temperatures was found to be the most satisfactory in that it resulted in a flat surface and the etching was non-preferential. The temperature and the flow rate dependence of the etch rate by silicon were measured and the results analyzed in terms of possible etching reaction mechanisms and the quality of the etched surface. Thin films of silicon were then deposited on substrates prepared by the methods mentioned above. The quality of the deposits were evaluated by optical microscopy, x-ray and electrical measurements.

Abstract No. 108

Extraction of III-V Intermetallic Compounds from Metallic Matrices

S. Z. Beer, Westinghouse Research Labs., Pittsburgh, Pa. 15235

Crystals of III-V and other intermetallic compounds are often grown from metallic solutions. The extraction of the desired product from the metallic matrix may prove quite troublesome. While the metal can frequently be dissolved away from the product with aqueous solutions of acids or bases, this is not always possible because of the reactivity of the nonmetallic substance with water. In many such instances it was found that a solution of 85-100g of mercuric chloride in dry N, N-dimethylformamide at 80°-120°C is a clean, rapid, and safe reagent. Other mercuric halides or cyanide can be used. The high solubility of the mercuric salts in the solvent and the high temperature at which the reaction can be run makes the reagent useful for many metals and nonmetals. Silicon and selenium are attacked by the addition of ammonium fluoride.

ELECTRO-ORGANICS

Abstract No. 109

Electroorganic Reactions and the Role of Intermediates

B. E. Conway, L. Marincic, and **E. J. Rudd,** Dept. of Chemistry, University of Ottawa, Ottawa, Ont., Canada

The role of intermediates in selected electrochemical organic reactions will be considered and the relation to reaction pathways illustrated. Results of studies with C^{14}-labelled simple organic molecules will be considered in relation to chemisorption of intermediates in the case of the Kolbe and formate oxidation reactions. The intermediates in ketone reduction will be considered in relation to (*a*) the steady-state reduction behavior and mechanism at mercury, platinum, and nickel, and (*b*) the behavior in H/D isotopically substituted solvents.

Abstract No. 110

Galvanostatic Studies of the Mechanism of Oscillatory Behavior during the Anodic Oxidation of Formaldehyde

H. F. Hunger, U.S. Army Electronics Command, Fort Monmouth, N. J.

Galvanostatic studies of formaldehyde half-elements in sulfuric acid at room temperature were made. Coulometric analysis of the voltage transients indicates a reaction mechanism with a catalytic decomposition reaction as the coupling step. Above +0.8v the participation of the oxidized platinum surface becomes evident. Adsorption experiments support these findings. Oscillations occur after a critical amount of organic species has been adsorbed. High Tafel slopes and estimates of the adsorbed amount indicates the presence of multilayers.

Abstract No. 111

The Electrochemical Oxidation of Aromatic Hydrocarbons in Methylene Chloride

A. J. Bard, K. S. V. Santhanam, and **John Phelps,** Dept. of Chemistry, University of Texas, Austin, Texas

The electrochemical oxidation of several aromatic hydrocarbons, including 9,10-diphenylanthracene, rubrene, 1,3,6,8-tetraphenylpyrene, anthracene, and tetracene at a platinum electrode in methylene chloride solutions containing 0.2*M* tetra-n-butylammonium perchlorate was investigated using cyclic voltammetric and coulometric techniques. Electron spin resonance was also employed in solution analysis. The results show that the oxidations proceed by a one-electron abstraction, and that stable solutions of the cation radicals can be obtained for hydrocarbons substituted in positions of high electron density. The general utility of methylene chloride as a solvent and further applications to electrochemical studies is also discussed.

Abstract No. 112

Electrochemical Oxidation of Crystalline Aromatic Hydrocarbons

J. M. Hale, Cyanamid European Research Institute, 91 Route de la Capite, Cologny, Geneva, Switzerland

A study is made of the heterogeneous oxidation (corrosion) of an insulating crystal by an oxidizing electrolyte. It is assumed that the abstraction of an electron from the valence band of the crystal by the oxidant is the rate-determining step in this process. The theory describing electron transfers at insulator electrodes then predicts the relative rates of attack, by one electrolyte on a series of similar solids, and by a variety of electrolytes on the same solid. Comparison of the corrosion rates of the aromatic hydrocarbons supports the theoretical conclusions.

Abstract No. 113

Organic Electrooxidation Studies and Optical Spectroscopy

Barry Epstein and **Theodore Kuwana,** Dept. of Chemistry, Case Institute of Technology, University Circle, Cleveland, Ohio

Because of complications in organic electrode reactions, it is advantageous to employ different electrochemical and supporting, concurrent nonelectrochemical methods to elucidate mechanism details. A comparative study, using many methods, of oxidation of some phthalhydrazides at platinum electrodes in alkaline solutions is discussed, as is the oxygen effect on coulometric results. Optical methods have been extensively used to obtain supporting information. Approaches to following concentration and determining spectra of products and unstable species are presented.

Abstract No. 114

Electroorganic Reactions: (a) Anodic Cyanations and (b) Electrochemical Reactions of Methylenecyclopropenes

S. Andreades and **E. W. Zahnow,** Central Research Dept., Experimental Station, E. I. du Pont de Nemours and Co., Wilmington, Del. 19898

Anodic oxidations of cyanide ion in the presence of various organic substrates at controlled potentials will be described. The following examples illustrate cyanations achieved in 50-96% yields.

$$\mathrm{Et_4N}^{\oplus}\,\overset{\ominus}{\mathrm{CN}} \xrightarrow[+2.0\ \mathrm{v.\ (S.C.E.)}]{\mathrm{CH_3CN}} \mathrm{Et_2NCH(CH_3)CN} + \mathrm{CH_2{=}CH_2}$$

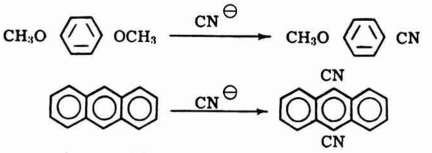

Mechanisms of these reactions are discussed. In the second part of the talk, electrochemical reactions of methylenecyclopropenes and tetracyanoquinodimethanes are described.

Abstract No. 115

The Specific Cleavage of Tyrosyl-Peptide Bonds by Electrolytic Oxidation

L. A. Cohen and **S. Isoe,** National Institute of Health, Bethesda, Md.

Electrolytic oxidation of peptides or proteins containing tyrosine results in conversion of the phenolic system to a dienone spirolactone coupled with hydrolytic cleavage of the following peptide bond. A continuous flow electrolytic cell was developed for the oxidative cleavage of milligram quantities of protein, at potentials as low as 1.5v. Electrolytic oxidation of an enzyme, ribonuclease, results in the cleavage of five of the six tyrosyl-peptide bonds known to be present.

Abstract No. 116

The Electrochemical Formation of Carbonium and Iodonium Ions from Alkyl and Aryl Iodides

L. L. Miller and **A. K. Hoffmann,** Colorado State University, Fort Collins, Colo., and American Cyanamid Company, Stamford, Conn., respectively

The electrochemical oxidation of organic iodies has been studied in lithium perchlorate, acetonitrile solution at a platinum electrode. It has been discovered that alkyl iodides can be oxidized and are converted via alkyl carbonium ions to *N*-alkyl acetamides. Cations produced in the oxidation of aryl iodides do not undergo carbon-iodine bond scission, but will attack aromatic molecules to form diaryliodonium ions.

Abstract No. 117

The Anodic Alkoxylation of Amines

N. L. Weinberg and **E. A. Brown,** American Cyanamid Co., Stamford, Conn., and Bristol Laboratories of Canada Ltd., Candiac, Canada, respectively

The anodic methoxylation of 2,6-dimethoxypyridine afforded 2,3,3,6,6-pentamethoxy-1,4-cyclohexadiene and 2,3,5,6-tetramethoxypyridine. N-methylpyrrole gave 1-methyl-2,2,5,5-tetramethoxy-3-pyrroline. N,N-dimethylaniline gave N-methoxy-methyl-N-methylaniline and N,N-bis(methoxymethyl) aniline in contrast to the dimeric products reported previously. Alkoxylation occurred preferentially at the alkyl rather than at the benzylic carbon in the electrolysis of N,N-dimethylbenzylamine, N-benzyl-N-methylethanolamine, and N-benzyldiethanolamine. Several mechanisms are discussed including the possible role of adsorption of the substrate on the anode.

Abstract No. 118

Oxidation of Aromatic Amines

S. Wawzonek and **T. W. McIntyre,** Dept. of Chemistry, University of Iowa, Iowa City, Iowa

The electrochemical oxidation of aromatic amines was studied in various aprotic solvents, methanol, and aqueous mixtures of these solvents. Polarographic studies in acetonitrile indicated that aniline and substituted anilines were oxidized in a one electron step. Exceptions to this behavior were *p*-nitroaniline and 2,4-dinitroaniline which showed two electron steps. In the presence of pyridine all of the anilines gave two electron waves. Electrolytic oxidation on a large scale in the various solvents gave the corresponding azo compounds.

Abstract No. 118A

The Present Status of Industrial Electroorganic Chemistry

Sherlock Swann, Jr., Dept. of Chemistry, University of Illinois, Urbana, Ill.

(No abstract available)

Abstract No. 119

Electrochemistry of Organo-Aluminum Compounds

Herbert Lehmkuhl, Max-Planck-Institut für Kohlenforschung, 433 Mülheim-Ruhr, Kaiser Wilhelm Platz 1, Germany

The electrochemical cleavage of alkali-organoaluminum compounds of the general type $M[AlR_3X]$ ($M =$ alkali-metal, $X =$ alkyl, hydrogen or halogen) can be carried out in various ways: (*i*) In the presence of trialkylaluminum a high-purity aluminum is deposited at the cathode; using an anode of normal, impure aluminum this process may be used for refining aluminum or for electroplating other metals with aluminum. (*ii*) Using anodes of metals, which are able to form stable alkylmetals, the corresponding alkylmetals are formed. (*iii*) By electrolysis of sodium-tetraalkyl-aluminum metallic sodium is produced at the cathode.

Abstract No. 120

The Electrolytic Production of Metal Alkyls

W. H. Thomas and **E. M. Marlett,** Ethyl Corp., P. O. Box 341, Baton Rouge, La.

(No abstract available)

Abstract No. 121

Commercial Application of the Electroreduction of a Ketone to Pinacol

J. E. Slager and **P. W. Staal,** Chemicals Div., Miles Laboratories, Inc., Elkhart, Ind. 46514

The bimolecular reduction of ketones to diols by magnesium or aluminum amalgrams and sodium lead has been the subject of many publications. More recently the electrolytic reductive coupling has been investigated on a laboratory scale. We were interested in producing 3,4 bis(para hydroxyphenyl) hexanediol-3,4. The electrochemical reductive coupling of p-hydroxy propiophenone was investigated. The final commercial cell had a 75 gallon capacity yielding 40-45 lb per batch. The problems involved in the scale-up of the process are discussed.

Abstract No. 122

Anodic Coupling of Organic Anions

S. Wawzonek and Tsung-yuan Su, Dept. of Chemistry, University of Iowa, Iowa City, Iowa

Anodic coupling of organic anions offer a facile method for the preparation of potentially important bifunctional organic compounds. The Kolbe reaction and the related Brown Walker synthesis have been applied to sodium levulinate and sodium monomethyl adipate. Oxidation of the anion from nitroparaffins has led to the formation of dinitroparaffins. The same reaction in the presence of nitrite ion has given the crossed coupled product, the 1,1-dinitroparaffin. Anodic oxidation of the sodium derivatives of ethyl esters of malonic acetoacetic and phenyl acetic acid leads to the dimeric esters and of β-diketones to tetraketones.

Abstract No. 123

Electrochemical Reduction of Cyanoalkyldimethylsulfonium Ions

J. H. Wagenknecht* and **M. M. Baizer,** Central Research Dept., Monsanto Co., St. Louis, Mo.

The study of the polarographic reductions of cyanoalkyldimethylsulfonium ions in anhydrous dimethyl sulfoxide indicates that the cyanoalkyl anions formed react with the sulfonium ion to form nonreducible species. This causes an abnormally low polarographic diffusion current. The reduction of cyanomethyldimethylsulfonium ion to the cyanomethyl anion occurs in one step, whereas cyanoethyldimethylsulfonium ion and cyanopropyldimethylsulfonium ion have an initial one electron reduction wave leading to the cyanoalkyl radical. The formation of the anion occurs at more negative potentials.

Abstract No. 124

Concerning the Mechanism of the Intramolecular Electrolytic Reductive Coupling of Bis-Activated Olefins at a Mercury Cathode

J. P. Petrovich, J. D. Anderson, and **M. M. Baizer,** Central Research Dept., Monsanto Company, St. Louis, Mo.

A polarographic study of the esters, $C_2H_5OCOCH=CH(\overset{|}{\underset{|}{C}})_nCH=CHCO_2C_2H_5$, showed that reduction at a D. M. E. occurs at a more positive potential for those members of the series that formed cyclic products on macro-electrolysis than for those that gave linear saturated material or model compounds such as ethyl crotonate and diethyl 2-heptene-1, 7 dioate. On the basis of this polarographic data as well as micro-coulometry and controlled potential macro-electrolysis, a concerted reduction-cyclization mechanism is proposed for the bis-activated olefins studied.

Abstract No. 125

Reductive Coupling of Olefinic Compounds by an Alkali Metal Amalgam

F. A. Matsuda, M. Kawamata, and **Y. Hirata,** Central Research Lab., Toyo Koatsu Industries, Inc., Kuden-cho, Totsuka-ku, Yokohama, Japan

Our laboratory has developed a high yield process using alkali metal amalgams in the presence of catalysts for the nonelectrolytic reductive coupling of α,β-monoolefinic nitriles, carboxylates, amides, and ketones. It furnishes a method not only for obtaining hydrodimers in high yield but also for preparing a variety of polyfunctional compounds.

Abstract No. 126

Electrochemistry in Nonaqueous Solvents of Intermediate Dielectric Constant

I. M. Kolthoff, Dept. of Chemistry, University of Minnesota, Minneapolis, Minn.

(No abstract available)

Abstract No. 127

Kinetics and Thermodynamics of Electrode Reactions in Aprotic Solvents

J. N. Butler, Tyco Laboratories, Inc., Bear Hill, Waltham, Mass. 02154

The experimental problems involved in electrochemical, thermodynamic and kinetic studies in aprotic organic solvents are discussed. Purification of solvents and electrolytes usually involves a combination of chemical treatment and vacuum distillation. Some stable, reversible, reference electrodes are the amalgam/metal ion, silver/silver chloride, or thallium amalgam/thallous chloride systems. Liquid junction potentials may be corrected by extrapolation procedures; or a constant ionic medium (usually tetraethylammonium perchlorate) may be used. Combination of potentiometric and calorimetric measurements yields enthalpies, entropies, and free energies. Electrode kinetic measurements are hampered primarily by the high resistance of most aprotic electrolytes. Galvanostatic pulse methods, coulostatic methods, and Faradaic rectification are suggested as experimental techniques to avoid errors due to ohmic overpotential.

Abstract No. 128

Electrical Double Layer in Nonaqueous Solutions

Richard Payne, Air Force Cambridge Research Labs., Energetics Branch, L. G. Hanscom Field, Bedford, Mass. 01730

Results of recent double layer measurements in nonaqueous solvents including dimethylsulfoxide, propylene carbonate, ethylene carbonate, 4-butyrolactone, 4-valerolactone and the formamides are presented. The occurrence of capacity humps similar to those found in aqueous solutions is discussed in relation to preferential orientation of solvent dipoles and their reorientation in the applied field. The close similarity of specific adsorption of ions from aqueous and nonaqueous solutions is discussed in terms of solvation and specific metal-ion interactions.

Abstract No. 129

Electrochemical Power Systems in Nonaqueous Solvents

Raymond Jasinski, Tyco Laboratories, Inc., Bear Hill, Waltham, Mass.

Batteries employing the alkali or alkaline earth metals as negative plates, are in principle, capable of energy densities in excess of 100 watt hr/lb. The realization of this performance, of course, also requires an active positive plate material of low equivalent weight and high positive potential, as well as a conductive electrolyte which is thermodynamically compatible with the electrodes. This paper reviews progress made on batteries operating at ambient temperature with electrolytes based on organic solvents. Liquid ammonia and fused salt electrolyte systems are not considered.

Abstract No. 130

Precise Polarography in Ethylenediamine and Acetic Acid

W. B. Schaap, Dept. of Chemistry, Indiana University, Bloomington, Ind.

Both the experimental techniques and the theory of polarography in nonaqueous solvents of low dielectric constant have been studied in detail. Resistance-corrected half-wave potentials have been obtained in anhydrous ethylenediamine ($D = 12.5$) and in glacial acetic acid ($D = 6.1$) over wide ranges of concentration of supporting electrolytes. Factors considered include ion-pair formation, complex-ion formation, activity coefficients, and liquid-junction potentials. In ethylenediamine, simple ion pairing is the predominant factor at supporting electrolyte concentrations below 0.1M, while in glacial acetic acid ion-paired complex species were detected.

Abstract No. 131

Electrochemistry in Pyridine

P. J. Elving and **R. F. Michielli,** The University of Michigan, Dept. of Chemistry, Ann Arbor, Mich.

After consideration of the purification and properties of pyridine, its use as a solvent for electrolysis, potentiometry, conductometry and polarography will be summarized with emphasis on phenomena, which result from its strong Lewis-base character and low dielectric constant, and on the more or less unique features associated with inorganic and organic electrode processes in pyridine, e.g., reduction of bivalent cations in 1*e* steps and levelling effect on Brønsted acids which are converted to pyridinium salts.

Abstract No. 132

Influence of the Solvent System on the Orientation of Ambient Molecules in the Coordination Sphere of Metal Ions

F. Farha, Jr., and **R. T. Iwamoto,** Dept. of Chemistry, University of Kansas, Lawrence, Kansas

In solvents containing both the hydroxy and the nitrile groups (hydracrylonitrile and alcohol-aliphatic nitrile mixtures), electrochemical, and visible and infrared spectral data indicate that the particular functional group which coordinates to copper(II) ion is determined by the polar characteristic of the medium. In a polar medium, the mode of coordination favored is that which results in the formation of the more polar of the two possible solvated species. In a nonpolar medium, the reverse is true. The influence of the solvent system on the orientation of 3-butenenitrile and 3-dimethylaminopropionitrile in the coordination sphere of copper(I) and silver ion also has been investigated.

Abstract No. 133

Thermodynamic Studies in Dimethyl Sulfoxide

W. H. Smyrl and **C. W. Tobias.** Dept. of Pharmaceutical Chemistry, University of California, San Francisco, and Dept of Chemical Engineering, University of California, Berkeley, Calif., respectively

Activity coefficients of lithium chloride in dimethyl sulfoxide have been determined in the cell

$$\mathrm{Pt(s)/Li(s)/LiCl(solution)/TlCl(s)/Tl_{(Hg)}(l)/Pt(s)}$$

For concentrations lower than 0.12*M*, the activity coefficients of lithium chloride may be represented by

$$\ln \gamma_{\mathrm{LiCl}} = -\frac{\alpha z_+ |z_-| I^{1/2}}{1 + I^{1/2}} + 2\beta_{\mathrm{LiCl}}\, m_{\mathrm{LiCl}}$$

The standard cell potentials are 2.4212, 2.4176, and 2.4137v at 25°, 30°, and 35°, respectively.

Abstract No. 134

Dimethylformamide as a Solvent for Electrochemistry, A Review

R. E. Visco, Bell Telephone Laboratories, Inc., Murray Hill, N. J.

The physical properties and methods of purification of dimethylformamide are reviewed. Results of electrochemical experiments on organic and inorganic electroactive species are reviewed and comparisons are made with results in other solvents. The anodic process of DMF oxidation at platinum electrodes is discussed and comparisons made with chemical oxidation of DMF.

Abstract No. 135

Electrochemistry in Formamide: The Double Layer at the Mercury-Formamide Interface

G. H. Nancollas, D. S. Reid, and **C. A. Vincent,** Dept. of Chemistry, State University of New York at Buffalo, Buffalo, N. Y.

Capacitance measurements have been made at a dropping mercury electrode in formamide solutions of lithium, sodium, potassium, rubidium and cesium chlorides as a function of applied potential, temperature, and concentration. Interfacial tensions have also been measured and, for potassium chloride and cesium chloride, the results are used to calculate the relative surface excesses of anion and cation. A components of charge analysis has been made, and the data are discussed in terms of the enthalpy changes associated with ionic solvation and specific adsorption.

Abstract No. 136

Electrochemistry in Propylene Carbonate

David Boden, The Electric Storage Battery Co., Yardley, Pa.

A study has been made of the response of glass electrodes to the concentration of lithium ion in propylene carbonate solutions containing K^+, $NH_4{}^+$, Mg^{++} and $(C_2H_5)_4N^+$ ions. Plots of potential *vs.* log C_{Li^+} all show the same general shape, a linear portion almost independent of the lithium ion concentration follower by a linear portion where the electrode behaves reversibly towards lithium ion. The point at which reversible behavior begins is observed to depend on the size and concentration of the competing ion. This is explained by a thermodynamic treatment.

Abstract No. 137

Parasitic Reactions during Lithium Deposition from Nonaqueous Electrolytes

R. G. Selim, P. R. Mallory Co. Inc., Lab. for Physical Science, N. W. Industrial Park, Burlington, Mass.

Observations are presented concerning seven reduction processes which have been observed when a platinum electrode is cathodized in a propylene carbonate-$LiClO_4$ solution. The results are discussed in terms of surface limited and mass transport limited processes, and correlated with the impurity concentrations. A review is presented of major problem areas in which further work is required before data concerning lithium electrodeposition can be satisfactorily interpreted.

Abstract No. 138

Electrochemical Studies on Lead in Organic Electrolytes

M. L. B. Rao Lab. for Physical Science, P. R. Mallory & Co. Inc., Northwest Industrial Park, Burlington, Mass. 01803

Galvanostatic anodic charge and cathodic discharge curves have been obtained for lead and lead alloys in two organic electrolytes: propylene carbonate, 1M in $LiAlCl_4$, and γ-butyrolactone, 0.5M in LiCl. Charging curves exhibited periodic (oscillatory) voltage phenomenon followed by passivation. Discharge curves of pre-anodized electrodes showed a single plateau corresponding to the reduction of $PbCl_2$ to Pb. Utilization efficiencies calculated from charge and discharge coulombs ranged from 10 to 100% depending on the current density, alloy composition, and electrolyte. The differences in observed behavior have been explained, and the suitability of $Pb/PbCl_2$ electrodes for rechargeable organic electrolyte cells is discussed.

Abstract No. 139

Inorganic Separators for Nonaqueous Electrolyte Batteries

M. P. Strier, and **F. E. Littman,** Missile & Space Systems Div., Astropower Lab., Douglas Aircraft Co., Newport Beach, Calif. 92663

The severe self-discharge problem encountered with lithium-copper chloride and lithium-copper fluoride batteries was attacked through the use of Astropower inorganic separators. The resistivities of inorganic separators in 1M $LiClO_4$ solutions in the organic solvents γ-butyrolactone and propylene carbonate were evaluated. A number of experimental cells were built to evaluate the effectiveness of different separators in nonaqueous batteries. The use of the appropriate inorganic separator results in a marked improvement in the efficiency of both $LiCuCl_2$ and Li-CuF cells. Further improvements in efficiency were obtained by the use of chelating agents in conjunction with certain separators. The use of inorganic ion exchange materials was attempted as well.

Abstract No. 140

Conductance Measurements in Aqueous and Acetone Solutions by an A-C Potentiometric Method

F. P. Anderson (South African Council for Scientific and Industrial Research), **R. W. Guelke, M. C. B. Hotz,*** **A. H. Spong** and **H. C. Brookes,** University of Cape Town Dept. of Chemistry, Rondebosch, S. Afr.

A four-electrode A. C. circuit is described that eliminates many of the errors inherent in conventional two-electrode methods. A small alternating current is passed between the outer electrodes and the potential difference between two probe electrodes is measured against a reference voltage derived from a transformer. The method is shown to be virtually frequency independent using aqueous KCl solutions and the accuracy of the results tested on aqueous NaCl solutions. Applicability to non-aqueous solvents is demonstrated by measurements on solutions of perchloric acid, three alkali perchlorates and lithium chloride in anhydrous acetone.

INDUSTRIAL ELECTROLYTICS

Abstract No. 141

Formation of Sodium Dithionite from Sodium Amalgam and Sulfur Dioxide in Nonaqueous Media

R. G. Rinker, Chemical and Nuclear Engineering Dept., University of California, Santa Barbara, Calif., and **Scott Lynn,** Research Lab., The Dow Chemical Co., Pittsburg, Calif. (present address: Chem. Engrg. Dept., Univ. of California, Berkeley, Calif.)

The formation of sodium dithionite, $Na_2S_2O_4$, was studied in hydrocarbons, alcohols, ethers, amides and dimethyl sulfoxide, using sulfur dioxide and sodium amalgam (0.3% Na by weight in Hg) as raw materials. Direct contact in dimethyl formamide gave yields of $Na_2S_2O_4$ exceeding 90% and in dimethyl sulfoxide, 80%. Reaction mechanisms involved stabilized, radical-ion species of SO_2. Some dispersion of the amalgam and over-reduction of the SO_2 were encountered. (Work done at the Dow Chemical Co. Research Lab., Pittsburg, Calif.)

Abstract No. 142

The Influence of Quaternary Ammonium Salts on the Reactivity of Sodium Amalgam

J. D. Littlehailes and **B. J. Woodhall,** Imperial Chemical Industries Limited, Petrochemical & Polymer Lab., The Heath, Runcorn, Cheshire, England.

During work on related topics we found that quaternary ammonium salts, specifically those with the general cation structure $RMe_3\overset{\oplus}{N}$, catalyzed the reaction of sodium amalgam with water. The reaction is catalyzed by other quaternary ammonium salts only to the same degree as by, for example, alkali metal salts, presumably due to a conductivity effect. The unique character of the cations $\overset{\oplus}{RNMe_3}$ is supported by electrochemical measurements. Kinetic measurements have been performed and are reported, with mechanistic discussion.

Abstract No. 143

Performance Characteristics of a Sodium-Bismuth Cell

H. Shimotake and **E. J. Cairns,** Chemical Engineering Div., Argonne National Lab., Argonne, Ill. 60439

A sodium-bismuth cell represented by

$$Na_{(l)}/Na^+/Na(Bi)_{(l)}$$

has been built. A 30 a/o Na-Bi alloy was used as the cathode metal, and the molten salt mixture of NaI-NaCl-NaF (53.2-31.6-15.2 m/o) as the electrolyte. The cell temperature was varied from 535° to 615°C. Cell discharge current densities of 440 and 1100 ma/cm^2 at 0.5 and 0.15v, respectively, have been achieved. (Work performed under the auspices of the A.E.C.)

Abstract No. 144

Sodium Peroxide from Sodium Amalgam

C. K. Bon, M. P. Neipert, and **D. L. Schechter,** Electrochemical and Inorganic Chemical Research Lab., The Dow Chemical Co., 1705 Bldg., Midland, Mich. 48640

(No abstract available)

Abstract No. 145

Economic Studies on the Amalgam Type Chlorine Cell

Fumio Hine Kyoto University at Uji, Uji, Kyoto, Japan

The coefficient, α, of the well-known formula

$$\text{Plant cost} = \text{Constant (Plant size)}^{\alpha}$$

for the amalgam process chlorine plant has been calculated and was about 0.926 instead of usual value, 0.6. The chlorine plant cost depends on the operating current density, and the manufacturing cost is related to the electric power cost. Thus, the operating current density has an optimum which is a function of the annual fixed charge and the power cost.

Abstract No. 146

Mechanism of Electrolytic Perchlorate Production

M. P. Grotheer and **E. H. Cook,** Hooker Chemical Corp., Niagara Falls, N. Y.

The proposed mechanism for the electrolytic formation of sodium perchlorate from sodium chlorate involves mass transport of the chlorate ion to the anode surface where it reacts with an adsorbed oxygen species. Thie adsorbed oxygen species is an intermediate in the oxygen evolution reaction. Competition exists between the reaction to form perchlorate from chlorate and the reaction to produce molecular oxygen. Factors supporting the proposed mechanism include the effects of current density, sodium chlorate concentration, condition of the anode surface and polarization studies.

Abstract No. 147

Analysis of Current Density Distribution in a Propagating Stress Corrosion Crack

T. R. Beck, Boeing Scientific Research Labs., P. O. Box 3981, Seattle, Wash. 98124, and **E.A. Grens, II,** Dept. of Chemical Engineering, University of California, Berkeley, Calif. 94720

The purpose of this work was to develop a quantitative model for the kinetic and mass transport processes in a propagating stress corrosion crack. Analysis of the problem led to a system of simultaneous differential equations which with their appropriate boundary conditions were solved by computer implemented numerical methods. Current density distribution along the walls of the crack was calculated. Results of the calculations are compared to experimental data for stress corrosion cracking of titanium alloy.

Abstract No. 148

Instabilities of the Current Distribution in Smeared Transition Zones between Two Electrical Conducting Phases

K. J. Euler, VARTA-Aktiengesellschaft, Frankfurt/Main, Federal Republic of Germany

In the transition zone between phases of different conduction types, the electrical current is not only unevenly distributed, but also, in many cases, local or temporal instabilities occur. Most of these effects are already observed, but until now no theoretical treatment has been published. As a straight forward extension of the linear mathematical treatment of the current distribution in porous electrodes, an explanation of two classes of instabilities can be given. Beneath these purely electrical instabilities, a number of more complicated cases have to be regarded. These are local instabilities caused by overlapping singularities, *e.g.*, spots of minor density or conductivity, local and temporal instabilities caused by thermal breakthroughs, and instabilities caused by hydrodynamical eddies. Moreover the current distribution shows local and temporal fluctuations as the result of the granular structure of the transition. These instabilities have many aspects and influence many physical and technical phenomena, of which here only the electrochemical properties of porous electrodes are looked for.

Abstract No. 148A

Gas Phase Transport Processes—Their Influence on Electrode Current Density Distribution

H. J. R. Maget, Direct Energy Conversion Operation, General Electric Co., Lynn, Mass.

No abstract available

Abstract No. 149

Current Distribution on a Rotating Disk below the Limiting Current

John Newman, Inorganic Materials Research Div., Lawrence Radiation Lab., and Dept. of Chemical Engineering, University of California, Berkeley, Calif.

The uniform current density on a rotating disk electrode at the limiting current is not achieved at lower currents because the edge of the disk is more accessible than the center as a result of the ohmic potential drop in the solution. The current distribution is calculated for well-stirred solutions and also for lower rotation speeds where surface overpotential, concentration overpotential, and ohmic drop are all significant. The current density at the center can vary between 50 and 100% of the average current density, and the ohmic potential drop to the center of the disk is 27.3% greater for the uniform current than for the primary current distribution.

Abstract No. 150

Current and Potential Distribution in Cylindrical Geometries: Engineering Applications

Leonard Nanis, School of Chemical Engineering, University of Pennsylvania, Philadelphia, Pa.

The mathematical treatment of the potential-space problems which are of use for electrochemical engineering applications can be made to yield information on (*i*) local current density and (*ii*) electrode resistance useful in cell design. In addition, the spatial variation of potential may be used to obtain knowledge of the regional effects of electrode conditions on the general field, useful in estimation of limits of application. In a cylindrical coordinate system, solutions are obtained by the use of Fourier-Bessel (Hankel) transformation applied to the Laplace equation

$$\frac{\partial^2\psi}{\partial r^2} + \frac{1}{\mathrm{r}}\frac{\partial\psi}{\partial \mathrm{r}} + \frac{\partial^2\psi}{\partial Z^2} = 0$$

in combination with particular Weber-Schafheitlin integral relations to account for boundary conditions. A disk electrode at constant potential and with constant current density are considered as special cases. The results are used in applications drawn from plating and fuel cell design.

Abstract No. 151

An Investigation into the Causes of Leakage Current in Diffused Indium Antimonide Diodes

J. A. Baldrey and **P. J. Marston,** Texas Instruments Ltd., Manton Lane, Bedford, England.

Measurements have been made of the reverse leakage current of indium antimonide diodes as a function of temperature. The results are analyzed in terms of surface leakage, impurity atoms in the depletion region, and of thermal generation of current carriers.

Abstract No. 152

Development of a High Speed Indium Antimonide Photodiode

J. A. Baldrey, P. J. W. Noble (Present Address: Allen Clarke Research Center, Plessey Co., Ltd., Towcester, Northants, England), and **P. J. Marston,** Texas Instruments Ltd., Manton Lane, Bedford, England.

This paper describes the developemnt of a high speed indium antimonide photodiode capable of operating at frequencies up to 3 gigahetrz. Results will be given for D^x and N.E.P. of the final device system.

Abstract No. 153

Hydrogen-Oxygen Fuel Cells

A. Winsel, VARTA-Ag, P. O. Box 5029, 6 Frankfurt/Main, Federal Republic of Germany

DSK-electrodes are, as in the case of other gas diffusion electrodes, penetrated by two distinct pore systems, one of which at a given gas pressure is completely filled with gas, while the other is filled with electrolyte. In both of these pore systems the respective phases (gas, liquid) are able to move independently under the influence of a hydrostatic pressure gradient. Assuming an isotropic porous body in the macroscopic part and using a predetermined pore distribution function, hydrodynamic relationships for the movement of the electrolyte and the gas phase, respectively, have been derived, however, employing for this derivation certain simplifications. From this the pressure and concentration distribution, respectively, for a gas diffusion electrode under load have been calculated for both phases. Experimental methods for determining the characteristic specific flow resistances are finally discussed.

Abstract No. 154

Current Distribution in Porous Electrodes: The Hydrazine Electrode Operating under Forced Flow

S. Szpak and **T. Katan,** Materials Sciences Lab., Lockheed Palo Alto Research Lab., Palo Alto, Calif.

Experimental results on current distribution in porous electrodes operating under forced flow are presented. The regime of validity of a simple model (monotubular reactor) with respect to a complex structure is established. The importance of the i/η relationship on the distribution functions is stressed and illustrated by comparison of the calculated current density distribution with that obtained experimentally, and the effect of the direction of flow on current distribution for a complex reaction is shown. Practical implications are noted.

Abstract No. 155

The Influence of Microcrystalline Properties on the Activity of Platinum Based Electrocatalysts for the Oxidation of Propane

J. Giner, J. M. Parry, and **S. M. Smith,** Tyco Laboratories, Inc., Waltham, Mass.

The intrinsic activity of platinum based catalysts towards the oxidation of propane has been measured in terms of the rate of oxidation of strongly adsorbed intermediates of the reaction, using a galvanostatic pulse technique. Linear Tafel plots with a slope of $2RT/F$ were obtained. The intrinsic activities defined by the extent of parallel displacement of the Tafel plots have been related to the microcrystalline properties of the catalysts measured by x-ray techniques. (This work was supported by the U.S. Army Engineer Research and Development Laboratories, Fort Belvoir, Va.)

Abstract No. 156

Current Distribution in Porous Electrodes

R. J. Brodd, Consumer Products Div., Research Lab., Union Carbide Corp., P. O. Box 6116, Cleveland, Ohio

The various experimental and calculated current distributions are reviewed as applied to chlorine electrolysis. Where possible the experimental and calculated current distributions are compared. The effects of porosity, current density, polarization characteristics, and electrical resistivity on current distribution and electrode performance are discussed.

Abstract No. 157

Porosity and Pore-Size Distribution in Zinc Electrodes

F. Przybyla and **F. J. Kelly,** Research Lab., Mallory Battery Co. of Canada Ltd., 2333 North Sheridan Way, Sheridan Park, Ont., Canada

Experimental results have been obtained showing the relationship between particle-size distribution and pore-size distribution in the porosity range 45-75%. It has been found that anode performance at any given total porosity is dependent on pore-size distribution. Within a given temperature/current density range a calculable total porosity, pore-size distribution, and compromise BET surface area are shown to ensure optimum anode performance.

Abstract No. 158

Structure of Mercuric Oxide Cathodes in Primary Alkaline Cells

F. Przybyla and **F. J. Kelly,** Research Lab., Mallory Battery Co. of Canada Ltd., 2333 North Sheridan Way, Sheridan Park, Ont., Canada

Measurements have been made of fractional potential differences across a zinc/potassium hydroxide/mercuric oxide cell under discharge. A considerable degree of cathodic polarization was detected and was overcome by modifying the microstructure of the mercuric oxide-graphite cathode. Cathodes of improved structure were evaluated over a range of temperature and current density, and the increase in cathode performance evaluated as a function of cathode porosity and mercuric oxide particle size.

Abstract No. 159

Lithium Wick Electrode

D. A. J. Swinkels and **S. B. Tricklebank,** Allison Div., General Motors Corp., P. O. Box 894, Indianapolis Ind. 46206

The delivery of liquid reactants to electrodes in electrochemical systems under zero g conditions or even against gravity can be accomplished by using capillary forces. Metal wicks have been used for control of the Li-LiCl interface in the Li-Cl$_2$ system at 650°C. Theoretical predictions of wicking depth and wicking rate have been demonstrated experimentally under various conditions.

Abstract No. 160

Metal to Graphite Connections in Industrial Electrolytic Applications

S. J. S. Parry, J. R. Anton, and **M. W. Voelker,** Great Lakes Carbon Corp., Graphite Products Division, P. O. Box 667, Niagara Falls, N. Y. 14302

One problem in the application of power to mercury cells is the electrical and mechanical stability of the anode stems or pins. A primary requirement is that the connection between bus bar and anode have a low electrical resistance that is relatively constant over the life of the pin. An evaluation of the use of threaded connections, pressed lead powder, pressed copper amalgam, and cast alloy as the method of binding the copper to the graphite, has been made by measuring voltage drop as a function of time at operating temperature. By suitable preparation it is possible to produce a low resistance joint that is electrically stable and mechanically dependable over several months at cell operating temperatures.

Abstract No. 161

Contact Resistance of Graphite Lead-In Rods

W. E. Sloka and **L. E. Vaaler,** Union Carbide Corp., Carbon Products Division, Parma Technical Center, 12900 Snow Rd., Parma, Ohio.

The graphite-to-graphite contact resistances of three commonly used graphite lead-in rod connections were measured. The connections were made with (*i*) straight metric threads, (*ii*) National Course threads, and (*iii*) tapered pipe threads. The contact resistance was measured as a function of thread type, applied torque to the point of fracture, and socket depth. The width of the shoulder on the metric thread was also varied. Results indicate that a socket depth of one inch or greater is desirable. At a torque of 100 ft-lb, the contact resistance increases in the order, National Course thread, metric thread, tapered pipe thread. However, increasing the shoulder with the metric thread or increasing the torque to several hundred pounds on tapered pipe threads can change the relative values. Contact voltage drops as low as 20 mv at 1,000 amp appear to be attainable. An optimum graphite-to-graphite joint design is suggested.

Abstract No. 162

Mercury Cell Anode and Anode Stem Design

H. A. Sommers, 710 Berwyn-Baptist Rd., Devon, Pa.

The operation of mercury cells at current densities of up to 10,000 amp/m^2 and higher, about double that of five years ago, has made the design of anodes and anode stems of increasing importance to handle the greater amperage at minimum voltage drop. The anode-anode stem design and provision for anode adjustment of all of the mercury cells currently available are illustrated, described, and discussed.

Abstract No. 163

A Valve Electrode for Use in Fused Salts

D. A. J. Swinkels, Allison Div., General Motors Corp., P. O. Box 894, Indianapolis, Ind.

A valve electrode based on different principles from those used by Justi has been developed for use in fused salts. It is based on the relative wetting properties and electronic conduction properties of the two layers in a dual layer porous electrode. The specific electrode discussed here was developed as a chlorine electrode in fused LiCl at 650°C. Its use in the Li-Cl$_2$ battery and for the purification of Cl$_2$ are discussed.

THEORETICAL ELECTROCHEMISTRY

Abstract No. 164

The Sulfur Cathode in Liquid Ammonia Electrolytes

W. S. Harris, U.S. Naval Ordnance Laboratory, Corona, Calif. 91720

The electrochemical properties of elemental sulfur have been investigated in acid (NH_4SCN) liquid ammonia solutions. These acid solutions of sulfur were found to be reduced at high efficiency ($\sim$90%). The end product of reduction in acid solution is ammonium sulfide, thus utilizing 2 e^- per atom of elemental sulfur. Neutral solutions were less attractive. The investigations, which include use of solutions under static as well as dynamic conditions, indicate attractive possibilities for use of S as a cathode in liquid ammonia fuel cells and batteries.

Abstract No. 165

Electrolysis of Nitrate Melts and Related Processes

H. E. Bartlett (present address: Atomic Energy Board, Pretoria, S. Africa) and **K. E. Johnson** (present address: University of Saskatchewan, Div. of Natural Sciences, Regina, Sask., Canada) Sir John Cass College, London, England

The electrolysis of molten $NaNO_3$ gives rise to $NO_2 + O_2$ at the anode and first NO_2^- and O^{2-} and then, at more negative potentials, several products at the cathode including oxidized cathode metal in solution.

The formation of NO_2^- cannot be separated from the cathodic corrosion upon electrolysis of KNO_3 and both electrodes are corroded upon electrolysis of $NaNO_2$. The results are correlated with thermodynamic calculations, thermal decomposition, and metal reduction data.

Abstract No. 166

Electrolysis of Carbon Dioxide Using a Solid Oxide Electrolyte

W. H. Smart and **J. Weissbart,** Lockheed Missiles and Space Co., Lockheed Palo Alto Research Laboratory, Palo Alto, Calif.

Carbon dioxide was electrolyzed to oxygen and carbon monoxide at 700°-800°C in cells using ceramic electrolytes of composition $(ZrO_2)_{0.85}(CaO)_{0.15}$ and $(ZrO_2)_{0.82}(CeO_2)_{0.03}(CaO)_{0.15}$. The beneficial catalytic influence of water vapor contained in the inlet CO_2 stream was demonstrated by an increase of oxygen current efficiency from 19% (no water) to 100% at 785°C and 50 ma/cm^2 and from 15% (no water) to 75% at 790°C and 100 ma/cm^2. The variation of current efficiency with current density for the electrolysis of CO_2-H_2O mixtures was also studied. (This work was sponsored by the National Aeronautics and Space Administration, Ames Research Center.)

Abstract No. 167

A Generalized Expression for the Tafel Slope and the Kinetics of Oxygen Reduction on Noble Metals and Alloys

D. S. Gnanamuthu and **J. V. Petrocelli,** Ford Motor Co., Dearborn, Mich.

The usually employed expression for the Tafel slope is modified to take into account the potential which is effective in charge transfer within the double-layer. The exchange currents and cathodic Tafel slopes are obtained on noble metal electrodes having different number of holes in the d-band. Using the conventional and modified Tafel slopes, possible paths and rate-determining steps are suggested for the cathodic reduction of oxygen.

Abstract No. 168

Kinetic Isotope Effects in Oxygen Electrode Reactions, II. Experimental Study of H/D Isotope Effects in the Electrochemical Reduction of Oxygen

J. D. E. McIntyre, M. Salomon, and **W. F. Peck, Jr.,** Bell Telephone Laboratories, Inc., Murray Hill, N. J. 07971

An experimental study of the effects of H/D isotope substitution on the electrochemical reduction of oxygen in aqueous electrolytes is reported. Kinetic isotope effects were measured for the charge-transfer reactions and the surface-catalyzed decomposition of hydrogen peroxide formed as an intermediate electrolysis product. In alkaline solutions, a small normal primary isotope effect is observed. In acid solutions, the effect is large and inverse, confirming the existence of a solvent isotope effect predicted theoretically.

Abstract No. 169

Static Behavior of the Oxygen-Peroxide Couple on Platinum

H. B. Urbach, R. J. Bowen, and **J. H. Harrison,** U.S. Navy Marine Engineering Lab., Annapolis, Md.

The open circuit potential of platinum electrodes in alkaline electrolyte obeys the Nernst-equation for the oxygen-peroxide couple at low concentrations of peroxide. The experimental potential 0.762 volt RHE is in close agreement with the theoretical value of 0.752 volt. At high concentrations of peroxide a mixed potential is formed which is nearly independent of peroxide concentration but dependent upon the oxygen concentration.

Abstract No. 170

The Dynamic Behavior of the Oxygen-Peroxide Systems on Platinum

R. J. Bowen, H. B. Urbach, and **J. H. Harrison,** U.S. Navy Marine Engineering Lab., Annapolis, Md.

The cathodic behavior of oxygen-peroxide systems in alkaline environment ($pH = 14$) is determined by the reduction of oxygen to peroxide when the concentration of peroxide is relatively low, and by the reduction of peroxide to water when its concentration is relatively large. At low peroxide concentrations, Tafel slopes of ca. —2 RT/3F are observed. Increase of oxygen pressure translates these Tafel curves without rotation towards increased currents in direct proportion to the pressure. In contrast, peroxide concentration changes do not influence the Tafel slopes in low concentration ranges. Tafel slopes at high peroxide concentrations, ca. —200 mv, are, however, translated, without rotation in direct proportion to the concentration of peroxide.

Abstract No. 171

The Relation between Hydrogen Coverage and Potential of the Hydrogen Electrode

T. C. Franklin, Takuji Itoh, Masahiko Naito, and **Jerry Barrett,** Chemistry Dept., Baylor University, Waco, Texas

The equilibrium potential of a hydrogen electrode is given by the equation

$$E = E^{o} + \frac{RT}{nF} \ln \frac{\theta}{1 - \theta}$$

where θ is the fraction of the electrode surface covered by hydrogen. Plots relating θ to E were used to determine whether the adsorbed hydrogen is atomic ($n = 1$) or molecular ($n = 2$). It was found, for example, using a coulometric method of measuring θ that: (*i*) hydrogen on nickel in sodium hydroxide is atomic at low coverages and molecular at high coverages, and (*ii*) hydrogen on bright platinum in sulfuric acid is molecular.

Abstract No. 172

Diffusion Control in Hydrogen Discharge on Platinum

Frank Ludwig and **Ernest Yeager,** Dept. of Chemistry, Western Reserve University, Cleveland, Ohio 44106

Hydrogen overpotential measurements in acid solutions on rotating Pt disk electrodes indicate that diffusion control involving dissolved H_2 is predominant at moderate current densities. The current at constant potential is strongly dependent on rotation rate but the Tafel slope remains relatively constant at approximately 30 mv/decade. Kinetic control is predominant at higher current densities. Further evidence of substantial supersaturation of the solution adjacent to the electrode with H_2 has been obtained with the rotating disk-ring technique. [Research was partially supported by the Office of Naval Research.]

Abstract No. 173

Potentiostatic Current-Potential Measurements on a Platinum Electrode in a High-Purity Closed System

Sigmund Schuldiner, T. B. Warner, and **B. J. Piersma** (National Academy of Sciences Postdoctoral Resident Research Association at NRL. Present address: Eastern Baptist College, St. Davids, Pa.) U.S. Naval Research Laboratory, Washington, D. C. 20390

In a high-purity closed system, potential regions at which very slow reactions are rate-controlling were accurately separated and measured. Tafel regions and the possible reaction mechanism on a Pt electrode in helium-saturated 1M H_2SO_4 from the H_2 to the O_2 formation reactions were determined. Effects of dermasorbed H and O atoms on transient and steady-state reaction rates were shown. Maximum oxidizable and reducible impurity levels were quantitatively determined both in solution and as adsorbed species on the working electrode surface. It was shown that the impurity levels were very low. Very small additions of hydrogen or oxygen in the critical transition region from net cathodic to anodic reactions did not appear to have catalytic effects. However, at oxygen partial pressures above 10^{-7} atm, a poisoning effect was apparent.

Abstract No. 174

The Structure and Catalytic Activity of Platinized Platinum

D. F. A. Koch, Division of Mineral Chemistry, C.S.I.R.O., Melbourne, Australia

Platinum was deposited at controlled potentials in the range 0.0 to +0.15v (*vs.* SHE) from chloroplatinic acid onto a platinum substrate. The surface areas (by differential capacitance and hydrogen adsorption), the weight of the platinum per unit area, and the catalytic activity toward formaldehyde oxidation were determined on these deposits. The deposition potential critically influenced the surface area which in turn determined the catalytic activity. The catalytic activity for the anodic oxidation of formaldehyde was determined by the available surface area which decreased as the reaction rate was increased due to depletion of reactant within the fine pores of the deposit.

Abstract No. 175

The Electrochemical Activation of Platinum Electrodes

S. D. James, Brookhaven National Laboratory, Upton, N. Y. 11973

The various mechanisms proposed for the electrochemical activation of Pt electrodes are reviewed. Experimental results are described showing impurity desorption to be by far the most important result of conventional brief activation treatments. Literature evidence is cited for the view that a second type of activation exists produced by prolonged pre-oxidation and characterized by an exceptionally stable activity. This latter activation is probably associated with an oxide quite distinct from that formed in conventional brief anodizations. (This work was performed under the auspices of the U.S.A.E.C.)

Abstract No. 176

On the Activity of Platinum Catalysts in Solution, I. Effects of Thermal Treatment and Chemical Etching on the $Pt\text{-}O_{ad}/H_2$ Specific Reaction Rate

T. B. Warner,* Sigmund Schuldiner, and **B. J. Piersma,** U.S. Naval Research Laboratory, Washington, D. C. 20390

The effects of thermal treatment and chemical etching of platinum on the specific rate of the chemical reaction of chemisorbed oxygen with H_2 in electrochemically clean 1M H_2SO_4 solution were determined. On successive thermal treatments of bright Pt beads, which were heated to the melting point and then slowly recrystallized under high temperatures, the specific rate varied randomly from trial to trial. Where heating was more uniform, and the cooling rate slower, reaction of H_2 with $Pt\text{-}O_{ad}$ was usually faster. Repeated aqua regia etching of a given Pt bead caused monotonic improvement until a rate between 0.014 and 0.021 amp/cm^2 was attained. Rates on Pt wire electrodes, which probably differed from the flame-formed Pt beads both in average crystallite size and in number of defects (created by the drawing process and only partially removed by subsequent annealing), were highly variable, but considerably lower than on beads. Surfaces whose activity for the $Pt\text{-}O_{ad}/H_2$ reaction differed many-fold showed no differences in anodic charging curves nor did electrochemical rates of water oxidation at +0.617v and +0.587v (NHE) or reduction of hydrogen ions at +0.300v differ. It appears that many electrochemical reactions are insensitive to these differences in surface condition.

Because of its great sensitivity to catalyst pretreatments, the $Pt\text{-}O_{ad}/H_2$ reaction is identified as a "demanding reaction", especially useful for identifying and examining certain variables affecting contact catalysis in solution. Since impurity sorption is one such variable, the rate of this reaction is one of the most responsive cleanliness tests available.

Abstract No. 177

LEED Studies, CO Adsorption on the Tungsten (112) Face

C. C. Chang and **L. H. Germer,** Laboratory of Atomic and Solid State Physics, Engineering Physics, Cornell University, Ithaca, N. Y.

CO adsorbs on the clean tungsten (112) face with near unit sticking probability and desorbs with heat in three stages, the α, β_1 and β_2 at about 500°, 1000°, and 1100°K, respectively, with relatively small amounts in α and equal amounts in β_1 and β_2 totalling about one half monolayer at maximum coverage. Although room temperature adsorption produces only a diffuse diffraction pattern, the surface can be rearranged with heat to produce sharp P(2 x 1), C(6 x 4) and C(2 x 4) patterns. Work function change measurements and further diffraction pattern observations and flash-off experiments with a surface having various known oxygen surface structures yield information about surface reactivity and structure. (Supported by the National Aeronautics and Space Administration Contract No. NGR 33-010-029, the Advanced Research Projects Agency through the Materials Science Center, and American Iron and Steel Institute Con. No. 148.)

Abstract No. 178

Interaction of Oxygen with Rhodium Single Crystal Surfaces

C. W. Tucker, Jr., General Electric R&D Center, Schenectady, N. Y.

The earlier low-energy electron diffraction (LEED) work of the author on the interaction of oxygen and CO with platinum single crystal faces has been extended to rhodium. Generalizations which emerge regarding the behavior of the two metals and the types of structures which form are discussed. The three types of structures found are: (*a*) simple dilute structures, (*b*) high coverage coincidence lattices, and (*c*) mixed lattices containing metal and oxygen atoms.

Abstract No. 179

Chemisorbed Gas Structures in Heterogeneous Catalysis

R. L. Park, Sandia Laboratory, Albuquerque, N. Mex. 87115

Changes in surface structure during the oxidation of carbon monoxide on metals can be observed by low energy electron diffraction. There are, however, many ambiguities in the interpretation of these changes. Isotopic mixing studies impose a number of restrictions on possible reaction mechanisms. The results of such studies for nickel and palladium are discussed in terms of a mathematical model and compared with results of LEED studies. [This work was supported by the U. S. Atomic Energy Commission.]

Abstract No. 180

High Energy Electron Diffraction and X-Ray Emission Analysis of Surfaces and Their Reaction Product

P. B. Sewell, Division of Applied Chemistry, National Research Council, Ottawa, Ont., Canada

During the examination of surfaces and thin films by reflection high energy electron diffraction, x-rays are emitted from the specimen. To utilize this x-radiation for the analysis of thin surface layers, a low atomic number, crystal spectrometer has been attached to an ultra-high vacuum electron diffraction apparatus. The capability of this technique for thin film analysis is being investigated. In particular, oxygen Kα radiation from thin oxide films is being measured to calibrate the instrument for oxidation studies, and to determine the lower limit for the detection of oxygen in adsorbed gas layers.

Abstract No. 180A

The Structure of Thin Electrodeposited Layers

E. H. Boult and **H. R. Thirsk,** Dept. of Physical Chemistry, University of Newcastle-upon-Tyne, England

(No abstract available)

Abstract No. 181

Characterization of the Nickel-Oxygen Interface by Surface Potential Measurements

T. Delchar, General Electric R&D Center, Schenectady, N. Y.

Oxygen chemisorption on clean nickel surfaces has been investigated by measurement of changes in the nickel work function. These measurements have been used to elucidate the degree of ionicity of the nickel oxygen surface bond and also the kinetics of the transfer of oxygen adatoms into the metal lattice. The average barrier height for penetration is determined as 7 ± 1 kcal/mole. A model is proposed to account for the abnormally small pre-exponential rate factor for incorporation.

Abstract No. 182

Infrared Studies of Protective Films Formed by Acetylenic Corrosion Inhibitors

G. W. Poling, Texaco Research Center, Beacon, N. Y. 12508

Infrared spectra of surface films formed on iron and steel mirrors by propargyl alcohol, acetylene, and ethynyl-cyclohexanol acid corrosion inhibitors were recorded using a multiple reflectance technique. These spectra showed that the acetylenic molecules reacted at the metal surfaces in HCl solutions to produce protective polymer film coatings. Corrosion protection increased markedly as the polymer coatings grew from nearly two-dimensional, adsorbed layers to films 20-200Å thick. Saturated hydrocarbon material composed the majority of these films. Hydrogen evolved by the acid corrosion reaction probably participated in hydrogenating adsorbed acetylenic species. The polymer also contained several polar species including hydroxyl and carbonyl groups. Increased carbonyl content appeared to decrease the protectiveness of these films.

Abstract No. 183

Mass Spectrographic Methods for Studying Surfaces

W. M. Hickam, Westinghouse Research Labs., Pittsburgh, 15235

The use of the mass spectrograph in the study of surface and surface reactions frequently necessitates the development of miniature reaction and excitation systems. The development and use of two systems combined with the mass spectrograph are illustrated. One system combines levitation heating and melting with gas mass spectrometry for the analysis of gaseous reaction products and gases in metals. The second system utilizes a spinning sample electrode in the spark source mass spectrograph for the analysis of thin films.

Abstract No. 184

Characterization of Surface Reaction Products by Mass Spectroscopy

R. K. Willardson, Bell & Howell Research Labs., 360 Sierra Madre Villa, Pasadena, Calif. 91109

Mass spectroscopy is particularly useful in studies of reaction products on the surfaces of solids. It is applicable to all of the elements of the periodic table and for surface concentrations as low as 10^{11} atoms/cm^2. The various compounds which have formed on surfaces can also be identified. Analyses have been made using as little as 10^9 atoms of sample. Information on homogeneity and distribution of products can be obtained with resolutions on the order of one micron.

Abstract No. 185

A Study of the Formation of Anodic Oxide Films on Platinum

J. L. Ord, Dept. of Physics, University of Waterloo, Waterloo, Ont., Canada

The anodic oxidation of platinum was studied by analysis of electrical transients and optical measurements made with a computer-operated following ellipsometer. Platinum is one of the few metals on which ellipsometric studies of anodic oxidation are not complicated by pre-existing layers or layers produced by other reactions. The results show that in many ways the anodic oxidation of platinum is similar to the anodic oxidation of the passive metals. The thickness of the film measured optically is proportional to the Tafel slope determined by open-circuit transients.

Abstract No. 186

Electrochemical Characterization of the Surface Composition of Platinum Alloys and Copper Adlayers on Platinum

M. W. Breiter, Research and Development Center, General Electric Co., P. O. Box 8, Schenectady, N. Y. 12301

The application of voltammetric techniques is described. The amount of the platinum-rich and the gold-rich phase of heterogeneous platinum-gold alloys on the surface was determined as a function of bulk composition by periodic current-potential curves. Voltammetry with superimposed a-c voltage allowed to detect platinum atoms on the surface of platinum-chromium alloys. The transition from monolayer to multilayer properties was studied for adlayers of copper atoms on platinum in acidic solution.

Abstract No. 187

Characterization of Thin Reaction Product Films by Ellipsometry

Jerome Kruger, National Bureau of Standards, Washington, D. C. 20234

Ideally the ellipsometer should both measure the amount of surface reaction product and give some indication of its nature. In reality, these functions are limited by the insensitivity of the ellipsometric measurements to changes in refractive index for monolayer films, film inhomogeneity, and ambiguity in determining optical constants for absorbing films. Three experimental approaches designed to cope with these limitations are described as follows: 1) combination of ellipsometry with LEED and field electron emission, 2) thermal annealing of thin films, and 3) ellipsometric spectrometry.

Abstract No. 188

Identification and Characterization of Electrochemical Reaction Products by X-ray Diffraction

Jeanne Burbank, Naval Research Laboratory, Washington, D. C. 20390

X-ray diffraction examination of the surfaces of polycrystalline solids by reflection diffractometry, operation of the cell designed for simultaneous x-ray and electrochemical studies, and application of the Berg-Barrett topographic technique to polycrystalline surfaces are described. Silver and lead anodes are used for illustrating the kind of information readily obtained by these methods: identity of crystalline reaction products associated with electrochemical phenomena, physical characterization of reaction mechanisms involving multiphasic coatings, distinguishing between large grains and preferred orientation, and estimations of coating thickness and particle size.

Abstract No. 189

On the Passivity of Iron-Chromium Alloys

R. P. Frankenthal, Edgar C. Bain Lab. for Fundamental Research, United States Steel Corp., Research Center, Monroeville, Pa.

Electrochemical studies, as well as microscope observations, on an Fe-24% Cr alloy in H_2SO_4 have shown that at least two distinct, potential-dependent films are formed. The primary film, which is responsible for the initial passivation, is stable only within a few millivolts of the reversible activation potential. A secondary film, which forms at more positive potentials, grows to a thickness greater than 10Å and, with increasing potential and time, becomes very stable and resistant to reduction. The primary passivation process is reversible. The "thickness" of the primary film at the reversible activation potential corresponds to less than the equivalent of one O-atom per surface metal atom. From this "thickness" and from the *p*H dependence of the reversible activation potential (81 mv/*p*H), it is suggested that the primary passivation process forms a film containing chromium and oxygen ions and possibly also some constituent of the electrolyte solution.

Abstract No. 190

The Oxidation State of Reduced CO_2

S. B. Brummer* and **K. Cahill,** Tyco Laboratories, Inc., Waltham, Mass. 02154

The reduction of CO_2 on smooth Pt electrodes from 2M H_2SO_4 solutions at 40°C has been studied with potential step and galvanostatic pulse techniques. An oxidizable adsorbed product is formed from 0.45v *vs.*

RHE to below the hydrogen potential. This product occupies ~0.8 of a monolayer from 0.00 to 0.25v. Coverage declines above 0.25v and is zero above 0.45v. Current reversal techniques show that the oxidation of this product releases 1.2 electrons per covered cathodic H-atom deposition site, independent of time and potential adsorption. The adsorption kinetics of CO_2 were studied using anodic and cathodic H-atom charging. Possible chemical structures for reduced CO_2 are discussed. (This work was supported by the Office of Naval Research under Contract N00014-66-C0210.)

Abstract No. 191

A Study of Initial Film Formation on Nickel Metal Using Linear Sweep Voltammetry

R. F. Scarr, Consumer Products Div., Research Lab., Union Carbide Corp., P. O. Box 6116, Cleveland, Ohio 44101

The formation and removal of very thin films of the lower oxides of nickel in KOH electrolytes have been investigated using linear sweep voltammetry. Two regions of anodic activity have been observed corresponding to (*i*) a mixed process involving adsorbed hydrogen dissolution and β-$Ni(OH)_2$ formation, and (*ii*) formation of additional nickel oxide (not alpha-modification) by a different mechanism. These processes were correlated with electron micrographs of the surface at corresponding potentials. Evidence indicates that the hydrogen evolution-dissolution reaction is enhanced by the presence of nickel oxides.

Abstract No. 192

Crystal Morphology and Mechanism of Growth of α-Fe_2O_3 Blade-Like Platelets on Iron

R. L. Tallman and **E. A. Gulbransen,** Westinghouse Research Labs., Pittsburgh, Pa. 15235

The morphological structure of α-Fe_2O_3 blade-like platelets formed on iron at 450°C in atmospheres containing both water vapor and a trace of oxygen was studied. Electron diffraction patterns of individual blades showed the blade axis to be $[\bar{1}\bar{1}20]$. All of the patterns showed twinned crystals whose orientations are related by mirroring on the blade face plane, $(\bar{1}101)$. It is concluded that the growth mechanism involves the diffusion of iron ions along the twin plane interface to the tip where reaction occurs with oxygen. [This work was supported in part by the Office of Naval Research under Contract No. Nonr-4949(00).]

Abstract No. 193

Crystal Morphology and Mechanism of Growth of α-Fe_2O_3 Whiskers on Iron

R. L. Tallman and **E. A. Gulbransen,** Westinghouse Research Labs., Pittsburgh, Pa. 15235

The morphology of α-Fe_2O_3 whiskers formed on iron at 400° to 500°C in dry oxygen was studied. Diffraction patterns of individual whiskers and texture patterns of oxidized surfaces showed the whisker axis to be $[\bar{1}\bar{1}20]$. The axis indicated by the pattern is that resulting from axial twist. This is good evidence that the most simple oxide whiskers have a single screw dislocation. Arguments are presented for the view that the growth of a whisker occurs by diffusion of iron ions through the dislocation and reaction with oxygen at the tip. This work was supported in part by the Office of Naval Research under Contract No. Nonr-4949(00).

Abstract No. 194

Overpotential-Time Variation for Galvanostatic Charging with Potential Dependent Capacitance

Leonard Nanis and **Philippe Javet,** Institute for Direct Energy Conversion, University of Pennsylvania, Philadelphia, Pa.

The non-linear differential equation for the time variation of overpotential during galvanostatic charging is solved by introducing a close approximation for the second term of rate equation. The results obtained are in close agreement with known solutions, covering all values of transfer coefficient, and are simple in form. Further, the incorporation of potential dependent capacitance is readily accomplished. Computations for such cases are shown to have a considerable effect on the overpotential transient.

Abstract No. 195

Short-Pulse Techniques, II. Perturbation Times in Alkali-Halide Systems

B. J. Piersma (National Academy of Sciences-National Research Council Postdoctoral Resident Research Associate at NRL. Present address: Eastern Baptist College, St. Davids, Pa.), **Sigmund Schuldiner,** and **T. B. Warner,** U.S. Naval Research Laboratory, Washington, D. C. 20390

A new technique involving the perturbation of a system from equilibrium using very short galvanostatic pulses and miniature cells has been applied to study the electrical double layer at Pt electrodes. The perturbation time, the time required for the double layer to begin charging, was determined for hydrogen- and alkali metal-halide systems and for reversible hydrogen systems in several acids and NaOH. The perturbation time was essentially independent of charging current density and of the anion in solution, but was strongly dependent on the cation species and electrolyte concentration. Models to explain the absence of electrode polarization during the initial flow of charge into the double layer are discussed. A model which involves a very fast faradaic process and which is consistent with the experimental observations is proposed. It is suggested that the perturbation time, which is less than 100 nanosec for 1M solutions, represents the time required for movement of ions into or out of the compact double layer.

Abstract No. 196

Cathodic Polarization of the Manganese Dioxide Electrode in Alkaline Electrolyte

A. Kozawa and **R. A. Powers,** Union Carbide Corp., Consumer Products Division, Research Lab., P. O. Box 6116, Cleveland, Ohio 44101

The cathodic polarization of β- and γ-MnO_2 was measured at various constant currents in 9 M KOH and KOD electrolytes in the entire range of reduction from MnO_2 to $Mn(OH)_2$. Two limiting currents were observed at high current discharges of γ-MnO_2, one around $MnO_{1.75}$ and the other after $MnO_{1.5}$. The former was attributed to the kinetically limited process mainly due to formation of a lower oxide structure on the surface. Around $MnO_{1.9}$, a Tafel relation was observed for γ-MnO_2 and i_0 values were obtained. A few equations were derived for the proton diffusion process in the manganese dioxide and compared to the polarization data.

Abstract No. 197

Coordination Chemistry of Hydrated Nickel Oxides in Alkaline Electrolyte: Crystal Field Considerations in the Formation of Higher Oxides

F. P. Kober* and **M. A. Aia,** General Telephone & Electronics Laboratories, Inc., 208-20 Willets Point Blvd., Bayside, N. Y. 11360

It is generally assumed that the anodic polarization of $Ni(OH)_2$ in alkaline electrolyte results in the direct ionization of Ni(II) sites to form Ni(III) sites within the solid phase. We show, using crystal field considerations, that the formation of a Ni(III) d^7 complex is highly unfavorable thermodynamically; the heat of formation is on the order of 766 kcal/mole. As an alternative mechanism for any changes in electronic structure which occur at the nickel ion sites during the course of reaction, we propose the concept of "anodic site reduction," *i.e.*, charge transfer across the nickel-oxygen bond leading to electron pairing at the nickel ion sites. This charge transfer complex is shown theoretically to possess a reasonable degree of thermodynamic stability.

Abstract No. 198

Controlled Potential Coupling of Acetone to Pinacol

E. C. French, Continental Oil Co., Ponca City, Okla. and **R. M. Hurd,** North Texas State University, Denton, Texas

The electrochemical coupling reaction of acetone was studied in alkaline solution on a number of electrode materials, using controlled cathodic potentials. High overvoltage metals operating at potentials less active than 2100 mv (*vs.* SCE) and at less than ambient temperatures gave coupling efficiencies of up to 75 per cent. Other cathodes and different operating conditions gave lower yields. The role of the absorbed hydrogen atom in the mechanism of the reaction, while not clear, is probably reaction with an intermediate radical, rather than direct reductive attack on acetone itself.

Abstract No. 199

The Electrode Kinetics of the Reduction and Oxidation of Antimony

L. L. Wikstrom and **Ken Nobe,** Dept. of Engineering, University of California, Los Angeles, Calif. 90024

The electrode kinetics of antimony in both acid and alkaline solutions in the presence and absence of Sb(III) and Sb(V) were investigated. Kinetic parameters were determined for the redox reaction at the rest potential, for the deposition of antimony, and for the hydrogen evolution reaction. At the rest potential the over-all redox reaction was $Sb + 2H_2O = HSbO_2 + 3H^+ + 3e^-$ in acid solutions and $2Sb + 6\,OH^- = Sb_2O_3 + 3H_2O + 6e^-$ in alkaline solutions. Deposition of antimony was only observed for Sb(III).

Abstract No. 200

A Rapid Solid-Electrochemical Method for Determining Diffusion Coefficients in Metals

D. O. Raleigh, North American Aviation Science Center, 1049 Camino Dos Rios, Thousand Oaks, Calif. 91360

The diffusion coefficient of Ag in Ag-Au alloys at 400° was measured at five points in the alloy composition range 10-60 a/o Ag in a single day's experiment with one metal sample. Diffusion coefficients ranged 0.93 to 1.24×10^{-14} cm^2/sec. The method involves the measurement of diffusion-limited currents in the solid-electrolyte polarization cell Ag|AgBr|Au. Duplicate runs with polycrystalline and single crystal gold gave average agreement to 12%. Application to other systems will be discussed.

Abstract No. 201

Effect of Hydrogen Absorbed by Electrode and Electrolyte on Hydrogen Coverage

D. J. BenDaniel and **F. G. Will,** General Electric R&D Center, Schenectady, N. Y. 12301

An analysis is made of the effect of atomic hydrogen absorbed by the electrode and of molecular hydrogen absorbed by the electrolyte on the hydrogen coverage of the electrode as determined by nonsteady-state methods. The cases of anodic and cathodic voltage pulses and sweeps and the significant case of anodic charging curves are treated. A numerical evaluation of the results is made for the particular case of platinum electrodes in aqueous electrolytes for which reliable data on diffusion coefficients and solubilities could be obtained. The errors that are introduced in surface coverage determinations are found to be significantly larger than assumed previously. The theoretical results are compared to some experimental data obtained by other authors, and agreement within 20% is found.

Abstract No. 202

The Practical Implications of the Finite Contact Angle Meniscus in Fuel Cells

B. D. Cahan and **J. O'M. Bockris,** Electrochemistry Lab., University of Pennsylvania, Philadelphia, Pa.

The complete differential equation for gas electrode reactions at the F.C.A.M. in porous electrodes which includes diffusion, activation, resistance, and meniscus shape has been solved by digital computer for a number of variations of the basic parameters. The important variables for a given set of experimental conditions can thus be pinpointed readily. Theoretical and practical implications of the solution are discussed.

Abstract No. 203

A Model for Wetproofed Porous Electrodes

Ralph Brown and **L. A. Horve,** United Aircraft Corp., Pratt & Whitney Aircraft Division, SWEF, South Windsor, Conn.

Gas diffusion electrodes that are fabricated from codispersions of Teflon and catalyst particles form a structure consisting of flooded catalyst agglomerates which are covered by a thin film of electrolyte. The surrounding porous Teflon structure is gas-filled. A mathematical model was developed which considered the porous nature of the agglomerates. The model accounts for gas diffusion, activation and electrolyte ohmic polarization. In comparing this theory with data, more favorable results were obtained than when applying theories that do not consider the porous nature of the agglomerates.

Abstract No. 204

Compatibility of H_2O_2 with Spacecraft Reaction Control Systems

U. M. Robinson, LTV Astronautics Div., LTV Aerospace Corp., P. O. Box 6267, Dallas, Texas 75222

The Scout Launch Vehicle Reaction Control System and the Astronaut Maneuvering Unit Propulsion System manufactured by LTV Astronautics uses concentrated hydrogen peroxide as the monopropellant. As a consequence LTV has recently conducted an extensive investigation into factors which influence the stability of the hydrogen peroxide within propulsion systems. Through a series of laboratory tests the catalytic decomposition influences of propellant container surface finishes, surface passivation techniques, dissimilar metals, container surface to H_2O_2 volume ratios, and the selective influence of both anions and cations have been assessed.

Abstract No. 205

The Role of Copper in the Pitting of Aluminum

H. L. Craig, Jr., R. D. Dewey, and **J. R. Scott,** Reynolds Metals Co., Metallurgical Research Division, Fourth and Canal Streets, Richmond, Va. 23218

Double-refined (<100 ppm impurities) aluminum was pitted in chloride solutions of various *p*H values (1 to 10). Electron microprobe analysis detected an appreciable concentration of copper *within* the pits. The various aluminum specimens originally contained from <10 to 30 ppm of copper, homogeneously distributed throughout. This observation supports a new interpretation of the autocatalytic mechanism of pitting in aluminum. It also explains the often-observed evolution of hydrogen from "anodic" sites on the metal surface.

ELECTROTHERMICS & METALLURGY

Abstract No. 206

Cr_3C_2 Fiber Reinforced Modified Nichrome Produced by a Controlled Solidification Method

H. E. Bates, F. Wald, and Martin Weinstein, Tyco Laboratories, Inc., Hickory Drive, Waltham, Mass. 02154

Cr_3C_2 reinforced modified nichrome was produced by controlled precipitation from the melt. After evaluation of the phase equilibria in the quaternary Ni-Cr-Si-C system the composition 64.64 w/o Ni, 27.5 w/o Cr, 2.86 w/o C, and 5.0 w/o Si was chosen as the most suitable alloy structure for directional solidification. This alloy contains 22 w/o Cr_3C_2 aligned fibers in a 84.9 w/o Ni-8.7 w/o Cr-6.4 w/o Si matrix. The fibers have well-defined flat faces and in cross section indicate either orthorhombic or hexagonal habit. Fibers up to 3-5 mm long are plentiful and the majority have length/diameter ratios greater than 100. The mechanical properties of this composite are discussed. [This work was sponsored by the Advanced Metallurgical Studies Branch, Air Force Materials Lab., Wright-Patterson Air Force Base under Contract AF 33(615)-3106.]

Abstract No. 207

Precipitated Carbides in Alloy Systems

J. B. Newkirk and **J. Marcantonio,** Metallurgy Dept., University of Denver, Denver, Colo. 80210

Metal carbides that are precipitated in alloys by heat-treatment can have important effects on the physical behavior of the alloy. The purpose of this paper is to review what is known about the more important precipitated carbides with respect to their mode of occurrence, their crystal structures, thermodynamic properties, mechanism and kinetics of formation, and their effects on alloy properties. An x-ray analytical method for determining the composition of precipitated carbides is described, and new data obtained by this method are given.

Abstract No. 208

Characteristics of Commercial Carbide Powders

R. E. Riley, Los Alamos Scientic Lab. of the University of California, Los Alamos, N. Mex.

The data herein report the problems associated with the development of a procurement specification of commercial carbide powders through powder characterization. Presented is a discussion on the morphological types of structures observed on commercial NbC, TaC, and ZrC powders. Also given are the results obtained for the various parameters determined to characterize powders. Proposed is a technique whereby one can use these parameters in developing a procurement specification for a particular requirement.

Abstract No. 209

Carbide-Graphite Composites

K. V. Davidson, R. E. Riley, and **J. M. Taub,** Los Alamos Scientific Lab. of the University of California, Los Alamos, N. Mex.

The effect of the many process variables on the high-temperature properties of hot pressed carbide-graphite composites has received considerable attention over this past year. It was the intent of this program to evaluate these effects by holding certain variables constant. The investigative work includes data on the effect of composition, as well as the effect of binder content and contaminants in the as-received powders. Particular attention is given to the mechanisms which affected resistance to deformation at elevated temperatures. Some data are presented on the effect of pressure on deformation of extruded composites at high temperatures. Also presented are preliminary results on the effect of composition of TaC-graphite composites and solid solution and solid solution composites of TaC-NbC.

Abstract No. 210

Preparation and Properties of Continuous Boron Carbide Filaments for Reinforced Composites

J. J. Higgins and **J. J. Gebhardt,** Missile and Space Div., General Electric Co., P. O. Box 8555, Philadelphia, Pa. 19101

Boron carbide filaments are promising reinforcements for use in both resin and metal composites because of their potentially high strength, high elastic modulus, and low density. This paper discusses the preparation and properties of such filaments from the viewpoint of their ultimate usefulness in such applications. Continuous boron carbide filaments were vapor deposited on tungsten substrates having a boron precoat from mixtures of boron trichloride, methane, and hydrogen at 1 atm and temperatures between 1100° and 1200°C. Deposition rates were considerably less than for boron alone; a close relationship was seen between the stoichiometry of the feed gas, filament composition and mechanical properties. In extended runs, average strengths of 390,000 psi were achieved, with individual values as high as 474,000 psi (1-in. gauge). Elastic modulus values up to 62 x 10^6 psi were also characteristic of the product. In prototype epoxy resin composites of less than optimum uniformity and homogeneity, bend strengths up to 244,000 psi and moduli up to 54 x 10^6 psi were measured at 85 v/o filaments, indicating that efficient transfer of stress to the filaments occurred. [Work sponsored by Plastics and Composites Branch, MANC, Nonmetallic Materials Div., Air Force Materials Lab., Wright-Patterson Air Force Base, Ohio, Contract AF33(615)-1644.]

Abstract No. 211

Diffusion of Carbon in Zirconium Carbide

S. Sarian and **J. M. Criscione,** Union Carbide Corp., Parma Technical Center, Carbon Products Div., Parma, Ohio 44130

The self-diffusion coefficients of carbon-saturated ZrC have been measured in the temperature range of 1350°-2150°C using standard tracer techniques. Single and polycrystalline samples were used. The coefficients can be expressed by two equations

$$D^* - 1.32 \text{ x } 10^2 \exp\left(-\frac{113{,}200}{RT}\right) \text{ cm}^2\text{/sec}$$

representing volume diffusion, and

$$D^* \simeq 1.6 \exp\left(-\frac{90{,}000}{RT}\right) \text{ cm}^2\text{/sec}$$

representing short-circuit enhanced diffusion.

Abstract No. 212

A Film-Thickness Determination of Nitrogen Diffusion in Zirconium Nitride

C. J. Rosa and **W. C. Hagel,** Metallurgy Div., Denver Research Institute, University of Denver, Denver, Colo. 80210

Calculations of diffusion coefficients for nitrogen in zirconium nitride are given in terms of a unidirectional, two-phase, volume-diffusion model. These calculations require the knowledge of both the thicknesses of nitride films and of nitrogen diffusion coefficients in the underlying zirconium metal. The values obtained can be represented by $D_N^{ZrN} = 0.86 \text{ x } 10^{-5}$ exp $(—24{,}900/RT)$ cm^2/sec for the temperature range of 650°-850°C. Zirconium kinetics for extended exposures up to 900 hr are also included. The portion of nitrogen confined to the α-zirconium phase amounts to about 80 w/o of the total nitrogen consumed during the overall nitriding process. Evaluations based on initial nitriding kinetics show that the diffusion coefficients for nitrogen in α-zirconium may be expressed approximately as $D_N^{\alpha\text{-}Zr} = 5 \text{ x } 10^{-4}$ exp $(—38{,}000/RT)$ cm^2/sec for the temperature of 600°-825°C.

Abstract No. 213

The Formation of Titanium Carbide Film on Iron by Vapor Plating

Takehiko Takahashi, Kohzoh Sugiyama, and **Kensuke Tomita,** Dept. of Applied Chemistry, Faculty of Engineering, Nagoya University, Furo-Cho, Chikusa-Ku, Nagoya, Japan

When titanium tetrachloride carried by argon is reduced by spongy titanium and flowed over a carbon steel at 850°-1000°C, titanium carbide film is formed on the steel surface, and the thickness can be related linearly with root of time. If a mixture of hydrogen and propane is used as carrier, carbide film grows linearly to the time. Pre-electroplating of cobalt on the steel is effective to obtain a good carbide film.

Abstract No. 214

Production and Characteristics of Submicron Carbides of Refractory Metals

Ernst Neuenschwander, CIBA Limited, Rare Metals Dept., Basle, Switzerland

A process for the preparation of carbides of refractory metals with particle sizes in the range 100-1000Å is described and the products are characterized by chemical and x-ray analysis, electromicrographs, particle size distributions, and specific surface areas. Applications of submicron carbides in hot-pressing of pure carbide bodies, in hard metals, and as dispersoids in dispersion-hardened alloys are discussed.

Reports on ECS Summer Assistance Awards and Weston Fellowship Award for 1966

During the summer of 1966, the following graduate students received $800 each, representing three Summer Assistance Awards of The Electrochemical Society, one of which is known as the Edward Weston Fellowship, one the Colin Garfield Fink Fellowship, and one the ECS Summer Fellowship.

James McLean, Michigan State University, East Lansing, Mich., was awarded the Edward Weston Fellowship.

Stanley Piekarski, University of Kansas, Lawrence, Kansas, was designated recipient of the Colin Garfield Fink Fellowship.

Chung-Chiun Lui, Case Institute of Technology, Cleveland, Ohio, received the ECS Summer Fellowship Award.

The Summer Assistance Award is made "without regard to sex, citizenship, race, location, or financial need to a fellow or teaching assistant pursuing work between the degree of B.S. and Ph.D. on a subject in a field of interest to The Electrochemical Society." It is intended to cover a period during which the recipient has no financial support for the continuance of his work.

The Edward Weston Fellowship Report

Mr. McLean's report appears as a Brief Communication on page 239 of this issue.

Colin Garfield Fink Fellowship Report

A summary of Mr. Piekarski's report is as follows.

1,4 additions of various nucleophiles to quinones is a well-known reaction of quinones (1). However, no kinetic study of this reaction has been carried out, although Bishop, Porter, and Tong (2) have studied a similar reaction involving nucleophilic displacement of halide ions by sulfite ion in trimethylquinones. Bishop et al. (2), have shown that the reaction is subject to general acid catalysis. The present study is concerned with a detailed study of the kinetics of 1,4 addition of substituted anilines to o-quinones. All work reported was completed during the tenure of this fellowship.

Experimental Techniques.—The over-all reaction studied can be written as follows:

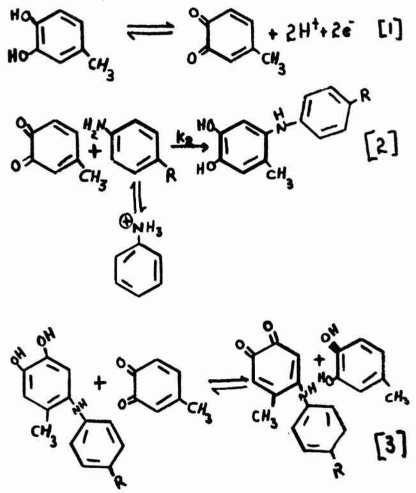

Figure 1 shows a cyclic voltammagram of catechol in 2.4M perchloric acid. On the initial voltage sweep an oxidation wave appears at +.63v vs. SCE. This corresponds to the oxi-

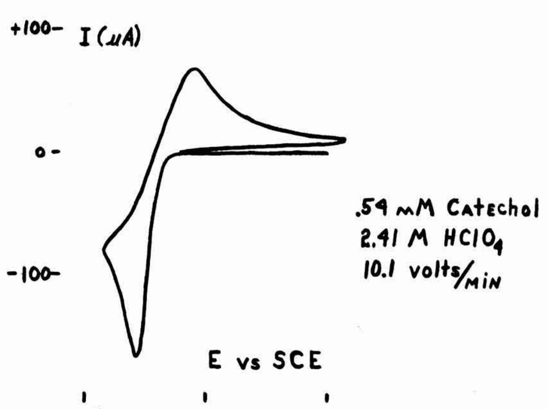

Fig. 1. Cyclic voltammetry of catechol

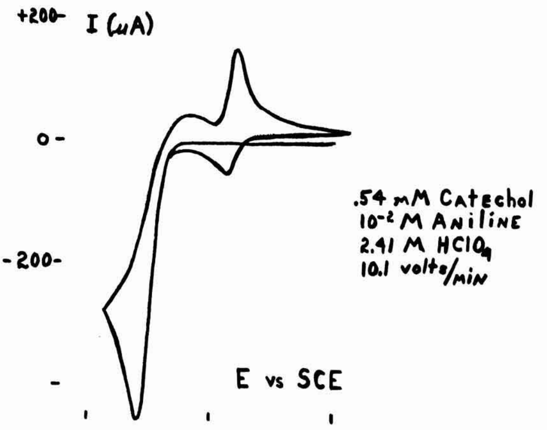

Fig. 2. Cyclic voltammetry of catechol in the presence of aniline

dation of catechol to o-quinone. On reversal of the direction of the voltage sweep, a cathodic wave is observed corresponding to the reduction of the o-quinone to catechol. Subsequent voltage sweeps show only this one redox couple. However, in the presence of aniline (Fig. 2) the cyclic voltammagram is very different. On the first anodic scan the same oxidation wave of catechol to o-quinone appears at +.63v. However, on reversal of the direction of voltage sweep, a large decrease in the cathodic wave corresponding to the reduction of o-quinone to catechol is observed. A new reversible couple is now observed which corresponds to the anilinoquinone-anilinocatechol couple.

Since the substituted catechol is more easily oxidized than the original catechol, reaction [3] will go to virtual completion, regenerating the original catechol and causing an increase in observed current. This current increase can be used to determine the rate of reaction [2]. Alberts and Shain (3) and Hawley and Feldberg (4) have developed a method for determining these rate constants by a potentiostatic method. In the absence of chemical reaction $it^{1/2}$ for the oxidation of catechol at a fixed potential anodic of E_p is a constant for a given concentration. However, in the presence of a substituted aniline $it^{1/2}$ will increase with time due to the regeneration of catechol in the vicinity of the electrode by reaction [2] and [3]. Hawley and Feldberg (4) have tabulated data for values of kt (k being first order or pseudo first order) as a function of n_{app}/n_o, where n_{app} is $it^{1/2}$ at time t_l in the presence of aniline, while n_o is $it^{1/2}$ at time t_l in the absence of aniline. A plot of various kt values versus t gives a straight line with zero intercept and slope of k. Table I shows a typical experiment and Fig. 3 is a plot of the data of Table I.

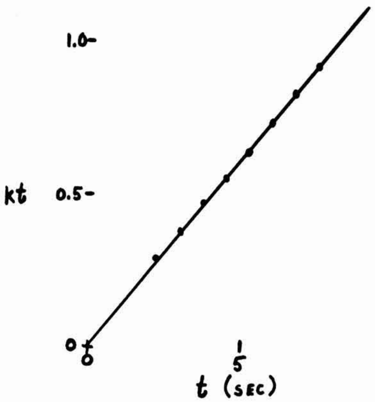

Fig. 3. Typical plot of kt vs. time. ● Experimental points (Table I)

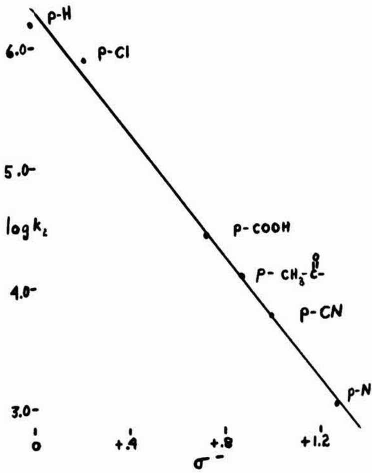

Fig. 4. Logarithms of rate constants (k_2) for the addition of para-substituted anilines to 4-methylcatechol in 0.945M sulfuric acid vs. σ^-. ●Experimental points (Table II), 25°C.

Table I. Typical Analysis of a Current-time Curve with ECC Complications.

t (sec)	$t^{1/2}$	i (μa current)	$n_{apparent}/n_o$	kt
2.25	1.50	58.7	1.240	.288
3.00	1.73	53.2	1.296	.374
3.75	1.93	49.4	1.343	.472
4.50	2.12	46.7	1.394	.551
5.25	2.28	44.7	1.436	.639
6.00	2.45	42.9	1.479	.738
6.75	2.60	41.4	1.517	.837
7.50	2.74	40.1	1.547	.922

6.75 mm Aniline + 0.3 mm 4 methylcatechol: pH 2.39; $E_{applied}$ = +0.57v vs. SCE; 30.0°C; $it^{1/2}_o$ = 71.0 μa $sec^{1/2}$; carbon paste electrode area = 0.32 cm^2; k_{obs} = 0.123 sec^{-1}.

Table II. Rate Constants (k_2) for Para-substituted Anilines.

para substituent	σ^-	ρK_a	k_2 (M^{-1} sec^{-1})*	log k_2
H	0	4.67	1.57 × 10^6	6.19
Cl	0.227	4.00	7.8 × 10^5	5.89
COOH	0.728	2.45	2.67 × 10^4	4.43
$CH_3-\overset{\overset{O}{\|}}{C}-$	0.874	2.05	1.22 × 10^4	4.09
CN	1.00	1.71	5.78 × 10^3	3.76
NO_2	1.27	1.00	1.01 × 10^3	3.01

* Average of at least 3 determinations.
$\rho = -2.60$ (determined by least-squares); 0.945M H_2SO_4; 25.0°C.

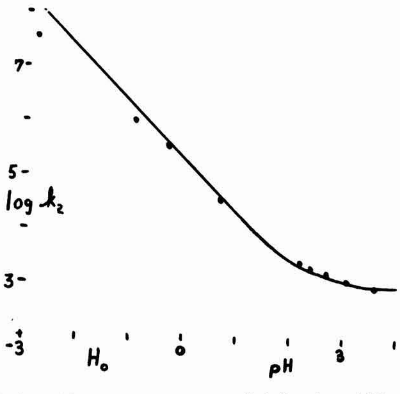

Fig. 5. Logarithm of rate constants (k_2) for the addition of aniline to 4-methylcatechol as a function of pH and H_o. ●Experimental points. Line is calculated from the equation $k_2 = 2.0 \times 10^5(H^+) + 1.1 \times 10^3$.

Results and Discussion

4-methyl-o-quinone.—A series of para substituted anilines were reacted with electrochemically generated 4-methyl-o-quinone in 0.945M H_2SO_4 at 25°C. The rate constant for the pseudo first-order reaction was calculated for each substituted aniline. Table II shows the data for these reactions. k_2 is k_{obs} divided by the concentration of aniline as free base in the solution assuming that the free base is the attacking nucleophile. The logarithm of these rate constants is plotted vs. σ^- in Fig. 4. σ^- rather than Hammett's σ was used since it has been found to give better correlations in many reactions of aniline (5). The value of ρ obtained is —2.60.

The 1,4 addition of aniline, p-nitroaniline, and p-aminoacetophenone to 4-methyl-o-quinone was studied as a function of the Hammett acidity function from H_o $+0.62$ to -2.80 in perchloric acid. If the reaction is acid catalyzed plots of log k_2 vs. H_o should be —1.0. The values obtained for the three anilines studied were -0.83 ± 0.02. It is not known at present whether the deviation of these slopes from unity is significant. Further studies are underway at this writing.

Aniline was chosen for a more complete study of the pH dependence of the reaction due to its convenient pK_a (4.61). The pH profile shows a slope of —0.80 from —2.80 to +0.62 as discussed above corresponding to the acid catalyzed reaction. At approximately pH 2 the curve begins to break and become pH independent. These data are shown in Fig. 5. The line plotted gives the theoretical behavior of the pH profile using rate constants determined in the curved region where both the catalyzed and uncatalyzed reactions are significant. The rate law was found to be

$$\frac{dP}{dt} = [2.0 \times 10^5 [H^+] + 1.1 \times 10^3] [\text{Aniline}] [\text{o-quinone}]$$

Further studies are also being carried out in the pH region of 2 to 3.6 (above pH 3.6 the reaction becomes too fast to measure by our present technique), to determine whether the reaction is general-acid-catalyzed. The results of further studies may change the numerical values of the rate equation.

As of this moment the following mechanism can be proposed although the position of the proton in the transition state will not be known until it is determined whether the acid catalysis is specific or general.

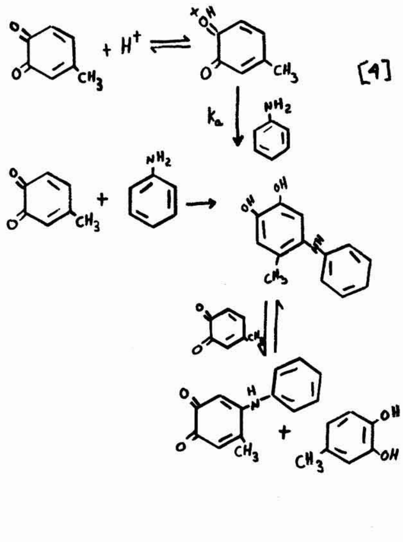

[1]

The rate law predicted from this scheme is: $dP/dt = [k_a(H^+)/K_{aq} + k_b][\text{o-quin}][\text{AN}]$ where K_{aq} is the acidity constant of the o-quinone. This rate law is of the same form as found in this study.

O-quinone.—Initial studies into the rate of 1,4-addition to unsubstituted o-quinone has shown that log k_2 vs. H_o is indeed —1.00 from —2.80 to +0.62.

References

1. L. Fieser, and M. Fieser, "Advanced Organic Chemistry," pp. 853-855, Reinhold Publishing Co., New York, (1961).
2. C. A. Bishop, R. F. Porter, and L. K. J. Tong, J. Am. Chem. Soc., **85**, 3991 (1963).
3. G. S. Alberts, and I. Shain, Anal. Chem., **35**, 1859 (1963).
4. M. D. Hawley, and S. Feldberg, J. Phys. Chem. In press.
5. J. E Leffler and E Grunwald, "Rates and Equilibria of Organic Reactions," p. 211, John Wiley & Sons Inc., New York (1963).

ECS Summer Fellowship Award

Mr. Lui's report is given below.

The bimetallic system bismuth-tellurium was studied by precise electromotive force measurements. The purposes of this study are to obtain information concerning the thermodynamic properties of this binary system and to determine the phase diagram of this system in detail.

It is desirable to apply emf measurement as a function of temperature and composition of the bimetallic concentration cell. A cell of the type

$$\text{Bi} \mid \text{BiCl}_3, \text{LiCl}, \text{KCl} \mid \text{Bi-Te}$$

was investigated.

In this study, a molten salt mixture of LiCl and KCl was used as the base of the electrolyte. The eutectic LiCl + KCl was purified according to Laitinen, Ferguson, and Osteryoung (1). The experimental work was performed in a dry box in which water was less than 0.5 ppm. and oxygen was less than 10 ppm (2).

Preliminary studies done by the author indicate the transference ions, i.e., the bismuth ions, are volatile from the melt. Therefore, a sealed isothermal cell has to be used. Within the cell, the equilibrium between the bismuth existing in the gas phase and the liquid phase can be reached at desired temperature, since an isothermal condition and sufficient quantity of bismuth chloride in the melt are provided.

Experimental work was performed during this period of study. The reference electrode was bismuth, and the second electrode was an alloy of bismuth and tellurium. The composition of the second electrode in this study consisted of approximately 50% tellurium by atomic weight. The total weight of each electrode was about 2.5g. Approximately 2g of bismuth chloride was added to the LiCl and KCl eutectic in each run. Result shows that this sealed isothermal cell is suitable for such a study. However, the inert gas which remained in the cell during the process of melting the electrolyte and of sealing the cell caused a volumetric expansion at high temperature. This expansion eventually cracked the glass cells. It is planned that the cell be sealed under a partial vacuum condition, and further measurements will be made under this modified condition.

References

1. H. A. Laitinen, W. S. Ferguson, and R. A. Osteryoung, This Journal, 104, 516 (1957).
2. M. S. Foster, C. E. Johnson and C. E. Crouthamel, "Helium-Purification Unit for High-Purity Inert-Atmosphere Boxes," ANL-6652, 1962.

BYLAWS
of
THE ELECTROCHEMICAL SOCIETY, INC.

(As Amended January 6, 1967)

The Board of Directors at its meeting on January 6, 1967, approved certain amendments to the Bylaws of the Society. The complete bylaws, as amended and adopted, are published herein.

BYLAWS

Article I

ORDER OF BUSINESS

Section 1. At the Annual Business Meeting of the Society, the order of procedure shall be as follows:

Approval of the minutes of the last meeting.
Reports of the Board of Directors, the Secretary, and the Treasurer.
Deferred Business.
New Business.
Report of Tellers of Election.
Address of the retiring President. (This may be presented at another session of the general meeting at the discretion of the President.)

Section 2. The Annual Business Meeting of the Society shall preferably be on the second day of a National Meeting.

Article II

NON-VOTING MEMBERSHIPS

Section 1. Student Member. A Student Member shall be a full-time undergraduate or graduate student registered for a degree in natural science or engineering. The applicant for Student Membership shall be recommended by two Active Members of the Society in good standing, and by a member of the senior staff of the college of his attendance. The Student Member shall submit suitable evidence of graduation to the Executive Secretary's office upon request. Upon graduation from college, unless he enters graduate school, the Student Member shall automatically become an Associate Member at the beginning of the next calendar year. He shall remain an Associate Member for three years and then automatically become an Active Member. If he enters graduate school as a full-time student he shall remain a Student Member as long as he remains in school. When he discontinues graduate studies, if he has completed three years of full-time graduate study he shall automatically become an Active Member at the beginning of the next calendar year. If he has completed less than three years of graduate study, he shall automatically become an Associate Member at the beginning of the next calendar year; then an Active Member after the equivalent of three years as Associate Member, each year of graduate study as a Student Member being credited as a substitute for one year as an Associate Member.

Section 2. Associate Member. An Associate Member shall have received an Engineering or Bachelor's degree with a major in natural science, but not yet have completed the requirement of three years of experience for Active Membership. In lieu of a scholastic degree, seven years of responsible professional experience in electrochemistry or allied subjects shall be required. An Associate Member shall automatically become an Active Member at the beginning of the next calendar year after he shall have acquired three years of professional experience in electrochemistry, or allied subjects. The applicant for Associate Membership shall be recommended by two Active Members of the Society in good standing.

Section 3. Contributing Memberships. Corporations, partnerships, and individual proprietorships who contribute financially to the support and development of the Society shall be entitled to membership which shall be defined by the Board of Directors as either Sustaining or Patron.

Article III

MEETINGS OF THE BOARD OF DIRECTORS

Section 1. The Board of Directors shall hold a regular meeting immediately preceding or during each National Meeting of the Society. The time and place for each regular meeting may be established by the Board of Directors at any previous regular or special meeting. In the absence of such action by the Board the time and place shall be set by the President, with the approval of the Executive Committee, in which instance at least thirty days notice of the time and place of such meeting shall be given to all those entitled to attend such meeting.

Section 2. Special meetings may be called by the President.

Section 3. All meetings of the Board of Directors shall be open to past Presidents. The President shall have authority to invite other persons to attend meetings who, in his judgment, will be of assistance to the Board in the transaction of its business.

Section 4. The order of business at all meetings of the Board of Directors shall be as follows:

1. Approval of the minutes of the last meeting (regular or special).
2. Communications from the President.
3. Communications from the Secretary.
4. Report of the Treasurer.
5. Reports of Committees.
6. Deferred Business.
7. New Business—Other than motions based on recommendations in committee reports. Such new business shall be submitted to the Secretary in writing at least thirty days prior to the meeting at which it is introduced in order to give adequate time for consideration by appropriate committees.
8. Adjournment.

Article IV

DUTIES OF OFFICERS

Section 1. The President shall preside at all meetings of the Society and at meetings of the Board of Directors. He may, at his discretion, represent the Society at any function to which no delegate has been named by the Board of Directors.

Section 2. The Secretary, besides performing the usual duties of that office, shall preserve the records of the Society, collect dues from members and all bills owing to the Society, and deliver the monies received to the Treasurer. He shall report to the Board of Directors at each of its meetings on the condition of the affairs of the Society.

Section 3. The Executive Secretary shall be responsible to the Secretary and shall perform such duties as are delegated to him by the Secretary.

Section 4. The Treasurer shall report to the Board of Directors at its meeting immediately preceding the business session of the annual meeting of the Society on the condition of the finances of the Society, and make such recommendations as will, in his opinion, tend to safeguard or improve the same.

Section 5. The Board of Directors shall report at the Annual Meeting on the general affairs of the Society.

Section 6. Funds budgeted for operation of the Society shall be disbursed on checks signed by any two of the following three officers: Executive Secretary, Secretary, or Treasurer or their agents as authorized by the Board of Directors. For disbursal of budgeted expenditures they may establish agents' funds under the control of the Secretary and Executive Secretary.

Article V

STANDING AND SPECIAL COMMITTEES

Section 1. The following Standing Committees shall be maintained in addition to the Admissions Committee established under Article III, Section 3, of the CONSTITUTION: Publication, Ways and Means, Finance, Membership (Personal and Contributing), Honors and Awards, Palladium Medal Award, F. M. Becket Memorial Award, Investment Advisory Panel, National Meeting, and Technical.

Section 2. The President may appoint special committees to conduct investigations or to represent the Society on special occasions.

Section 3. Unless otherwise specified, all committee appointments shall expire with the term of the President who made the appointments.

Section 4. Each committee shall report to the Board of Directors at least once a year.

Article VI

PUBLICATIONS

Section 1. The Society may publish or sponsor such publications as in the judgment of the Board of Directors will best carry out its objectives as stated in the CONSTITUTION of the Society.

Section 2. All such publications shall conform to the requirements of these Bylaws.

Section 3. No publication shall be issued or sponsored without prior approval of the Board of Directors.

Section 4. Society publications shall be made available to Society Members under conditions prescribed by the Board of Directors in conformity with these Bylaws. Society publications may also be made available to nonmembers under conditions approved by the Board of Directors.

Section 5. Subscription rates for the Society's journals shall be fixed by the Board of Directors not later than July 1 of each year for the ensuing year.

Prices for other publications issued by the Society, unless otherwise directed by the Board, shall be established by the Board of Directors.

Section 6. Financial arrangements for all Society publications shall be incorporated in the annual budget and shall be subject to the approval of the Board of Directors.

Article VII

PUBLICATION COMMITTEE

Section 1. The Publication Committee shall be composed of at least five members. It shall include a Chairman, the Secretary of the Society, and the Editor of each journal publication. The term of office, other than ex officio members, shall be three years.

Section 2. The Publication Committee shall: (a) be responsible for the adequacy of the publication program of the Society; (b) consult with editors of journal publications and recommend editorial policies to the Board; (c) appoint, subject to the approval of the Board of Directors, the editor of each Society publication and each publication sponsored by the Society; (d) undertake such other assignments relating to the publication program of the Society as may be delegated by the Board of Directors.

Section 3. Divisional Editors. The Editor of each journal publication shall appoint at least one Divisional Editor representing each Society Division for a three-year term, with the advice of the Chairman of the respective Division or Divisions. The Editor shall arrange with the Divisional Editors for review of all papers submitted for publication. Acting within the policies established, the Divisional Editors shall see that each paper submitted for publication is reviewed and make recommendations with respect to its publication to the Editor of the appropriate journal.

Section 4. Editorial Boards. The Editor acting as Chairman, and the Divisional Editors of the publication shall constitute the editorial board of each publication. They shall prescribe editorial policies for the publication consistent with the general policies established by the Publication Committee.

In order to provide consistency among publications, all Editorial Boards established under the Bylaws shall meet jointly at least twice a year during National Meetings under the chairmanship of the Publication Committee Chairman to coordinate and recommend general policies to the Publication Committee.

Article VIII

WAYS AND MEANS COMMITTEE

Section 1. The Ways and Means Committee shall act as an advisory group to the President and Board of Directors on all phases of the Society's business.

Section 2. The Ways and Means Committee shall be composed of seven members. Its Chairman shall be one of the Vice-Presidents. The other members shall be the two remaining Vice-Presidents, and four Active Members of the Society appointed by the President with the approval of the Board of Directors.

Section 3. The Ways and Means Committee may carry on its business through subcommittees composed of a Chairman, who shall be a member of the Ways and Means Committee, and such other members of the Society at large as the Chairman of such subcommittees may select.

Section 4. The Ways and Means Committee shall have the power to call on any of the officers of the Society or of its Sections or Divisions to furnish this Committee with such information as it may deem necessary to competently advise the President and Board of Directors as to policies to be followed in the conduct of the Society's affairs.

Section 5. The Ways and Means Committee shall report at appropriate intervals to the President and Board of Directors upon such items of the Society's business as have been referred to this committee for attention.

Article IX

FINANCE COMMITTEE

Section 1. A Finance Committee of five members shall be appointed by the President with the approval of the Board of Directors. This committee shall consist of the Treasurer who shall be Chairman, the Secretary, the Vice-President who is Chairman of the Ways and Means Committee, and two other members appointed from the active membership.

Section 2. The Finance Committee shall assist the Board of Directors in the preparation of a budget and advise the Board on matters of income, expense, and investment of all funds and all other financial operations of the Society.

Article X

MEMBERSHIP COMMITTEES

Section 1. Chairman, Personal Membership Committee. The President shall appoint, with the approval of the Board of Directors, the Chairman of the Personal Membership Committee.

Section 2. Personal Membership Committee. The President shall appoint a Personal Membership Committee consisting of at least one representative from each Division and at least one representative from each Local Section of the Society for the current term of office and the members shall serve until their successors have been appointed. The selection of these members shall be from a list of nominees submitted by each Division and Local Section, respectively.

Section 3. Contributing Membership Committee. The President shall appoint, with the approval of the Board of Directors, a Contributing Membership Committee to solicit Sustaining and Patron memberships from industry. The President shall, with the approval of the Board of Directors, appoint a Chairman of the Contributing Membership Committee.

Article XI

COMMITTEE FOR HONORS AND AWARDS

Section 1. The Honors and Awards Committee shall consist of nine members. The President of the Society shall be an ex officio member of the committee. Two members of the committee shall be appointed each year for four year terms by the President with the approval of the Board of Directors. The Chairman of the committee shall be designated by the President with the approval of the Board of Directors.

Section 2. Acheson Award. The Honors and Awards Committee shall submit recommendations to the Board of Directors for Acheson Medalists.

Section 3. Honorary Members. The Honors and Awards Committee may submit recommendations to the Board of Directors for Honorary Membership in the Society of individuals who, in the opinion of the committee, have made valuable contributions to electrochemistry or who deserve special recognition by the Society.

Section 4. Palladium Medal Award. The Palladium Medal Award Committee shall submit, through the Honors and Awards Committee, recommendations to the Board of Directors for the Palladium Medal Award.

Section 5. The Honors and Awards Committee shall, at the direction of the President with the approval of the Board of Directors, make recommendations for other awards and honors sponsored or administered by the Society and not otherwise designated in the CONSTITUTION and Bylaws.

Section 6. Nominations for Intersociety Awards. All requests by societies, organizations, or other groups for nominations shall be referred to the President, who shall evaluate them. The President shall refer those requests that he deems appropriate to the Society to the Chairman of the Honors and Awards Committee. Nominations or suggestions shall be arrived at by the Honors and Awards Committee by methods that are commensurate with the scope or importance of the award and with the time schedule involved. Nominations or suggestions shall be forwarded to the President for transmittal to the original source of the request.

Section 7. All future honors and/or awards by the Society other than Local Section honors and/or awards shall be subject to the approval of the Honors and Awards Committee.

Article XII

INVESTMENT ADVISORY PANEL

Section 1. The Investment Advisory Panel shall consist of five members appointed by the President with the approval of the Board of Directors for a term of five years. The Panel shall be rotating, with one new member appointed each year to replace the outgoing member, and it shall elect its own Chairman.

Section 2. It shall be the responsibility of this Panel to review the investments of the Society annually and to make suitable recommendations to the Treasurer, as Chairman of the Finance Committee, for appropriate revisions of the Society's investment portfolio.

Section 3. The Treasurer of the Society shall have the responsibility of reviewing and implementing the Panel's recommendations and of informing the Panel what additional monies have become available for investment.

Section 4. The Board of Directors is responsible for the judicious handling of the Society's assets. However, in the interest of expeditious operation, it may delegate to the Treasurer, with the advice of the Investment Advisory Panel, the execution of its investment policy.

Article XIII

NATIONAL MEETING COMMITTEE

Section 1. The National Meeting Committee of five members shall be appointed by the President with the approval of the Board of Directors. This committee shall consist of the Secretary, the Treasurer, who shall serve as Chairman, and three Past Local Chairmen of National Meetings.

Section 2. The National Meeting Committee shall recommend to the Board of Directors, cities, hotels, and dates for future meetings.

Section 3. The National Meeting Committee shall be responsible to the Board of Directors for the planning and operation of meetings in collaboration with Local Meeting Committees.

Article XIV

TECHNICAL COMMITTEE

Section 1. The Technical Committee shall be composed of the Division Chairmen, a Vice President, and the Secretary of the Society. It shall be presided over by the Vice-President, who shall be appointed by the President with the approval of the Board of Directors.

Section 2. This committee shall have the responsibility of insuring that the technical program of the Society as a whole is adequate and of arranging for appropriate and coordinated activities of the several Divisions to achieve this objective.

Section 3. Questions, or proposed legislation with reference to technical aspects of national, divisional, or local meetings of the Society or with reference to participation in intersociety affairs either by the Society itself or by one or more of its Divisions or Local Sections, shall be referred to the Technical Committee. The decisions of the Technical Committee with respect to such matters shall be reported to the Board of Directors.

Article XV

ACCOUNTS OF THE SOCIETY

The Board of Directors shall engage a public accountant, not later than June 1 each year, to audit the current accounts and financial statements of the Society. The report of such accountant shall be submitted in such form as to designate the source of all receipts by the Society and the disposition of all funds expended. It shall also include, as far as possible, a statement of the assets and liabilities of the Society so drawn up as to show clearly the net worth of the Society as of the close of the fiscal year for which the audit is made. The report of the auditor shall be submitted to the Board of Directors through the Treasurer of the Society.

In lieu of this report, the financial statement and a statement of examination by the auditor may be printed in the Society's Journal not later than two months after its approval by the Board. The general results of this audit shall be reported to the members of the Society at the Annual Meeting.

Article XVI

GUESTS AT MEETINGS

Section 1. Nonmembers may attend technical meetings and social functions of the Society. Requirements for registration of nonmembers shall be established by the Board of Directors.

Section 2. A Division inviting a foreigner to participate in a National Meeting shall appoint an official representative to serve as host for such visitor. In the event that the visitor for whom the host is designated is from a country whose citizens are subject to United States Department of State travel restrictions, the designated host shall also be responsible for the guest in accordance with State Department regulations.

Article XVII

DIVISIONS

Section 1. Any member of the Society may register for membership in any Division.

Section 2. The officers of the Division shall be a Chairman, one or more Vice-Chairmen, and a Secretary and a Treasurer. The offices of Secretary and Treasurer may be held by the same person. The above officers, together with two or more members of the Division shall constitute the Executive Committee of the Division.

The Division shall elect its officers and other members of the Executive Committee during a National Meeting of the Society or within thirty days thereafter. The officers and other committee members shall be elected for such terms as the Division Bylaws provide; their terms of office shall not exceed two years. An officer may be re-elected, however, if the Division Bylaws do not prohibit such re-election.

Section 3. A Division shall hold, if possible, at least one session a year at a National Meeting of the Society.

Section 4. The Society shall not be responsible for any debts contracted by the Divisions or by the officers thereof. Divisions may receive from the Society such financial assistance as the Board of Directors may determine to be proper, provided such request is accompanied by a financial statement covering the previous fiscal year. It is recommended that each Division submit a financial report within three months of the close of its fiscal year. Such funds shall be used for sending notices, for solicitation of papers, and for the legitimate work of the Divisions.

Section 5. The Board of Directors may recommend the dissolution of any Division of the Society, such recommendation to be submitted to a vote of the members present at an Annual Business Meeting of the Society.

Section 6. Divisions shall have the privilege of suggesting to the Secretary the names of eligible candidates for officers of the Society. Such suggestions shall be in the hands of the Nominating Committee prior to April 1. The Secretary shall transmit such suggestions to the Chairman of the Nominating Committee when he has been selected.

Section 7. It shall be the duty of the Executive Secretary of the Society to call to the attention of the officers of each Division all of the provisions of Article XVII at least once between January 1 and April 1 each year.

Section 8. If a Division of the Society can no longer function advantageously as a unit of the Society, it may request the Board of Directors for permission to dissolve. If such permission is granted, all funds which have been accumulated by the Division, including money in banking and other accounts and investments of all types, shall be transferred to The Electrochemical Society, Inc. If the Division has underwritten any continuing awards for which invested funds provide an adequate income, the Society may undertake to continue such awards at the discretion of the Board of Directors.

Article XVIII

REGULATIONS CONCERNING THE FORMATION AND CONDUCT OF LOCAL SECTIONS

Section 1. Geographical boundaries of the several Local Sections shall be set from time to time by the Board of Directors upon the advice of the Council of Local Sections. Members of the Society residing or having their principal place of business within said boundaries may become members of those Sections by complying with the Bylaws of those Sections. Members of the Society may become affiliated with any Section upon application to the Secretary of that Section. Only members of this Society are eligible for membership in the Local Sections.

Section 2. The following provisions shall apply to financial matters of common interest to the Local Section and the Society: (1) The expenses of each Local Section shall be borne by the members enrolled in said Section. The Society shall not be responsible for any debts contracted by a Local Section or by the officers thereof. (2) The Society will provide financial assistance to the several Sections by matching the per capita dues paid to the Section on a dollar for dollar basis, up to and including two dollars per member. If the assistance provided on this basis shall be less than fifty dollars, the amount shall be increased to fifty dollars on request. In order to provide equitable grants to each of the Sections, the following means of calculation shall apply:

> Each Local Section desiring financial support for the ensuing fiscal year must submit a request for support to the Executive Secretary prior to July 1. The basis of calculating local section membership shall be the paid-up members as of June 1 of the same year, and the total individual dues paid to the Section Treasurer for the past fiscal year.

Section 3. Each Local Section shall transmit promptly after each meeting to the Executive Secretary of the Society an abstract of its proceedings, including the titles and names of authors of all papers presented before it.

Section 4. When the Local Section is selected by the Society to act as host for a National Meeting, the Society will allocate not less than five hundred dollars in addition to out-of-pocket costs to the Section handling the many details associated with providing a suitable meeting.

Section 5. Before July 1 each year, each Section shall elect a Councilor to the Council of Local Sections. Such Councilor shall be an Active Member in good standing in the Society, and shall hold office for two years, beginning on July 1 immediately following his or her election, and each Section shall be entitled to two such Councilors. In addition, members of the Society not attached to any Local Section may be placed on the Council by petition of ten members of the Society. Not more than two such Councilors-at-Large may hold office at any one time. Such Councilors-at-Large can not be from any one locality for more than one two-year term in succession unless a Local Section has been formed in the interim and they thus become regular Councilors.

Section 6. The Council of Local Sections shall hold a meeting at each National Meeting of the Society. The duties of the Council of Local Sections shall be: (1) to consider problems affecting the welfare and operation of the Local Sections and to work toward their solutions; (2) to act as a clearing house on information, problems, and methods of organization of Local Sections; (3) to act as an advisory council to the Board of Directors of the Society on Local Section affairs; and (4) to make recommendations to the Board of Directors on such other matters relating to the interests of the individual members of the Society as the Councilors may become aware of from time to time.

Section 7. The Council of Local Sections shall elect one of its Local Section Councilors to the Board of Directors at each Spring Meeting of the Council for a two-year term, and he will be seated immediately at the next meeting of the Board of Directors. During the period a Councilor is a member of the Board of Directors, he shall continue to be a member of the Council. The Council shall also elect a Chairman, Vice-Chairman, and Secretary from its Local Section Councilors to conduct the necessary meetings and correspondence of the Council. Bylaws approved by the Board of Directors shall guide the formation and operation of the Council.

Section 8. Local Sections shall have the privilege of suggesting to the Secretary the names of eligible candidates for officers of the Society. Such suggestions shall be in the hands of the Nominating Committee prior to April 1 each year. The Secretary shall transmit such suggestions to the Chairman of the Nominating Committee when he has been selected.

Section 9. It shall be the duty of the Executive Secretary of the Society to call to the attention of the officers of each Local Section all the provisions of Article XVIII at least once between January 1 and April 1 each year.

Section 10. If a Local Section of the Society can no longer function advantageously as a unit of the Society, it may request the Board of Directors for permission to dissolve. If such permission is granted, all funds which have been accumulated by the Local Section, including money in banking and other accounts and investments of all types, shall be transferred to The Electrochemical Society, Inc. If the Section has underwritten any continuing awards for which invested funds provide an adequate income, the Society may undertake to continue such awards at the discretion of the Board of Directors.

Article XIX

DUES AND FEES

Section 1. The annual dues for Active Members shall be twenty dollars. The annual dues for Student Members shall be three dollars, and for Associate Members, thirteen dollars. Each member shall receive the JOURNAL OF THE ELECTROCHEMICAL SOCIETY.

Section 2. When individuals are elected to membership, they must elect to initiate their membership as of January 1 or July 1 of the year of election; or, if elected during the last quarter, January 1 of the year following election. In the case of a July 1 election for starting membership, dues will be prorated.

Section 3. Any Active Member who shall pay in one lump sum the amount indicated in the following table in accordance with his or her age at the time of payment shall be exempt from the payment of any further dues and shall be considered an Active Member during the remainder of his or her life.

Age	Amount
Through Age 35	$400
36-40	350
41-45	300
46-50	250
51-55	200
56-60	150
Above 60	100

Section 4. Corporations, partnerships, and individual proprietorships to qualify for membership in the Society shall contribute at least one hundred and thirty-five dollars per annum.

They shall be credited with multiple memberships for each one hundred and thirty-five dollars they contribute, and shall be called Sustaining Members. Those who contribute at least one thousand dollars per annum to the Society shall be designated as Patron Members.

Sustaining Members holding one membership only shall be entitled to designate a member as their representative. This individual or his duly authorized proxy shall be, while supported by a Patron or Sustaining Membership, entitled to all the privileges of membership for which the individual personally qualifies. The Sustaining Member shall receive one subscription to the JOURNAL and one bound volume and is free to designate the individual or organization receiving it.

Corporations, partnerships, and individual proprietorships holding Patron Membership shall be entitled to designate two members as their representatives. They shall be entitled to eight subscriptions to the JOURNAL and eight bound volumes.

Section 5. Emeritus Members shall be exempt from the payment of annual dues and shall have all the rights and privileges of an Active Member.

Section 6. Society Divisions and Local Sections may collect Division or Section dues as authorized by their respective Bylaws.

Article XX

APPEALS

Section 1. An appeal by a Division or Local Section from a decision of the Technical Committee may be made in writing to the President for presentation to the Board of Directors. The appeal must be signed by the Chairman, a Vice-Chairman, and two other members of the Executive Committee of the Division or Local Section.

Article XXI

AMENDMENTS

Section 1. Amendments to these Bylaws may be proposed by a member of the Board of Directors, seconded by another member of the Board of Directors and shall require a two-thirds roll-call vote of the entire Board for their adoption; mail votes shall be counted when received before the vote is counted. The text of the proposed amendments shall be transmitted to each member of the Board of Directors at least ten days before the meeting at which the vote on the same is to be taken.

PEOPLE

J. W. Faust, Jr. has been appointed Professor of Solid State Science in the Materials Research Laboratory of the Pennsylvania State University in University Park, Pa. He also holds a joint appointment in the School of Ceramic Science. He left the Westinghouse Research Laboratories to assume his new duties early in 1967. Dr. Faust joined the Westinghouse Research Laboratories 15 years ago to work on semiconductors. Although being best known in fields of crystal growth, etching, and the characterization of materials, he has worked on problems in practically every phase of semiconductor device production as consultant to the semiconductor manufacturing divisions of Westinghouse.

At Penn State, Dr. Faust will continue his studies in crystal growth, etching, and materials characterization in addition to teaching courses in at least some of these fields.

While at the Westinghouse Research Laboratories, he authored or coauthored over 55 scientific papers including sections of books and is the recipient of 10 U.S. patents with approximately as many more pending. He joined The Electrochemical Society in 1953 and was instrumental in building up the Electronics Division. He has held several national and local offices, and organized several symposia.

SECTION NEWS

Detroit Section

The Detroit Section held a dinner-meeting at Wayne State University's McGregor Memorial Conference Center on November 17, 1966. The speaker, Dr. Manuel M. Baizer of Monsanto Co., presented a lecture on "Electrolytic Reductive Coupling as a Synthetic Tool," which is summarized in the following abstract:

The utility of electrolytic reductive coupling as a means of synthesizing a variety of polyfunctional organic compounds was discussed. Activated olefins function as acceptors toward donors generated by electrolytic reduction of (a) other activated olefins—leading, e.g. to intermediates for Nylon 6,6, Nylon 6, plasticizers, amino-acids, (b) other activated olefinic groups in the same molecule—leading to a variety of carbocyclic and heterocyclic compounds, and (c) azo-compounds and Schiff bases—leading to heterocyclic nitrogen compounds.

A few years ago the discovery was made in Dr. Baizer's laboratory of a wholly electrolytic means of hydrodimerizing acrylonitrile to form adiponitrile which is used in the synthesis of Nylon 6,6. To exploit this process, the Monsanto Company has built the world's first and only large-scale plant facility for the electrolytic production of an organic chemical.

Vladimir Hospadaruk,
Second Vice-Chairman

Chicago Section

On January 26, 1967 the Chicago Section held a meeting at the Chicago Engineers Club in Chicago. Mr. N. Corey Cahoon, Vice-President of The Electrochemical Society and Senior Scientist in the Electrochemical Development Laboratory, Consumer Products Division, Union Carbide Corp., presented a talk on "Some Modern Techniques in Battery Research and Development." Mr. Cahoon's talk is described in the following abstract:

The development of new systems and improved methods of studying systems have contributed to the rapid growth of battery technology. Variations of electronic interrupter as well as potentiostatic sweep and similar techniques are examples of modern methods of measuring internal resistance and electrode polarization. Reaction product identification techniques utilizing DTA, xray, electron microscope and standard analytical methods are presented. The surface chemistry of powdered electrode materials is shown to be important in controlling the efficiency and operation of an electrode system.

James H. Lloyd,
Vice-Chairman

Indianapolis Section

Since Mr. Lowell F. Howard, Chairman, has moved from the Indianapolis area, the Office of Chairman has been filled for the 1966-67 season by Mr. George F. Fitzgibbon, formerly Vice-Chairman.

On December 6, 1966, the Indianapolis Section met at Atherton Center, Butler University. Guest speaker for the meeting was Mr. Edward M. Moss, Director of Engineering for the Capacitor Division of P. R. Mallory and Co., Inc., Indianapolis, who spoke on "Electrochemical Technology in Tantalum and Aluminum Capacitors." Mr. Moss pointed out that electrochemistry is the basic discipline involved in the processing of electrolytic capacitors. Following a description of the devices and a brief history of their development, he compared aluminum and tantalum capacitors with emphasis on the part electrochemical processing plays in determining device characteristics. Included was a discussion of the significance of etching, anodization, and electrolyte composition. Sample capacitors, color film and slides helped highlight the intricacy of modern capacitor construction and processing. The presentation was concluded with a brief review of recent advances in the industry, including miniturization for space use and the development of capacitors with increased volt-farad per unit volume characteristics.

The talk was followed by an active question and answer period.

Russell A. Foust, Jr.,
Secretary-Treasurer

South Texas Section

The South Texas Section was privileged to hear John L. Margrave speak on "High Temperature Fluorine Chemistry," at the meeting held on December 13, 1966, at the Geo Club in Houston.

Dr. Margrave, Professor of Chemistry at Rice University, illustrated novel techniques for the preparation and study of reactive fluorine-containing species generated in high temperature systems. Examples of these unique reactive species that were discussed include the subfluorides of boron, silicon, and carbon. The high temperature interaction between silicon metal and silicon tetrafluoride at low pressures yields silicon difluoride which appears to be a carbene-like molecule. Silicon difluoride, surprisingly, has a half-life of about two and one-half minutes in the gas phase at room temperature. However, at very low temperatures, it condenses irreversibly to form a polymeric species that is the silicon analogue of polytetrafluoroethylene. Condensation experiments of silicon difluoride with organic or inorganic substances have shown that a wide variety of new silicon-fluorine derivatives may be prepared. The techniques and resulting species thus described offer promises of vast new fields of chemical knowledge.

F. Olstowski,
Secretary-Treasurer

Call for Recent News Papers
Semiconductor Sessions

May 7-12, 1967, Dallas, Texas

The deadline date for the 75-word abstracts of Recent News Papers is Friday, March 31, 1967. Please send abstracts to: Harry Sello, Manager, Materials & Processes Dept., Fairchild Semiconductor R&D Labs., 4001 Junipero Serra Blvd., Palo Alto, Calif. 94304

The program will include contributions in the following areas relating to elemental, compound, and alloy semiconductors:

Materials Synthesis and Characterization
- Crystal Growth
- Epitaxy-homogeneous and heterogeneous
- Polycrystalline materials properties
- Diffusion
- Heterojunction formation and properties

Device Technology
- Ion implantation techniques
- Electron beam processing
- Diffusion and alloying
- Contact preparation and properties
- Surfaces and oxides
- Photomasking techniques
- Isolation techniques

Ten minutes, including discussion, are allotted to each Recent News Paper. If more time is necessary for your presentation, please consult with the Program Chairman.

OBITUARY

John T. Owen

The Society regrets to announce the passing of Dr. John T. Owen formerly of Bloomfield, N. J., on October 7, 1966. Dr. Owen was a life member of The Electrochemical Society for many years. His many friends will regret his passing as he was an inspiration to all those who came in contact with him. He participated in the activities of the Metropolitan New York Section of the Society.

Available
Spring

MEASUREMENT TECHNIQUES FOR THIN FILMS

**A methods symposium
published by
The Electrochemical Society, Inc.**

Original papers describing standard and special laboratory techniques applied to the measurement of thin films.

- Structural Properties
- Chemical Analysis
- Thickness
- Density
- Electrical Properties
- Optical Properties
- Stress Properties
- Acoustical Properties

Edited from selected papers presented by the Dielectrics and Insulation Division and by the Electronics Division at the 128th and 130th National Meeting, held October 1965 and October 1966.

- c. 560 pages
- 5½ x 8½ format
- never before published
- full subject index

please clip and return with remittance to
**The Electrochemical Society, Inc.
30 East 42 St., New York, N. Y. 10017**

Please enter my order for .... copies of Measurement Techniques of Thin Films, at $9.00 each. My check or money order is enclosed for $ .... (Payment must accompany order. No cash please. No discounts allowed.)

name

title

affiliation

mailing address

city

state zip code

country

Note: Remittances from outside the Continental United States must be by International Money Order or by bank draft on a New York bank.

**ULTRA-DRY, PURIFIED LITHIUM SALTS
$LiClO_4$, LiCl, LiBr, LiI, $LiAlCl_4$**

**for
fused salt chemistry
and electrolytes in
non-aqueous solvents**

AVAILABLE IN 200gm. AMPOULES

contact

ANDERSON PHYSICS LABORATORIES, INC.

Box 2680 Station A **Champaign, Illinois**
Phone (217) 356-1347

REPLACES:
SCREENING, SPRAYING, PAINTING

USE DRY
METALIZING—GLAZING—SEALING—
PLATING—BRAZING—RESISTIVE ETC.

TRANSFER TAPES OR TRANSFER PREFORMS

**Precise Thickness (range 0.0002 to 0.030 in.)
Exact Width (range 0.01 to 10.0 in.)**

For further information on Transfer Tapes and/or automatic, semi-automatic or manual Tape Transfer Machines write to

Vitta CORPORATION
WILTON, CONNECTICUT
TELEPHONE: (203) 762-8405

Chicago Meeting Symposia Plans—Fall 1967

Triplicate copies of the usual 75-word abstract, as well as of an extended abstract 500-1000 words(see page 244 for typing instructions) are due at The Electrochemical Society, Inc., 30 East 42 St., New York, N.Y., 10017, not later than May 15, 1967.

Battery Division Symposia Plans

The Battery Division is planning symposia on Nonaqueous Electrolyte Batteries and on Zinc Electrode Cells for the 1967 Fall Meeting to be held in Chicago, Ill., Oct. 15-20, 1967. A general session is also planned.

Nonaqueous Electrolyte Batteries

Papers dealing with properties of nonaqueous electrolytes and performance of primary and secondary cells utilizing nonaqueous electrolytes of the fused salt, organic-base, and ammonia-base electrolyte types are solicited. Inquiries and suggestions should be sent to the Symposium Chairman, Dr. M. Eisenberg, Electrochimica Corp., 1140 O'Brien Dr., Menlo Park, Calif. 94025.

Zinc Electrode Cells

Papers dealing with theory and technology of zinc electrodes are solicited. Dr. George Dalin, Yardney Electric Corp., 40-50 Leonard St., New York, N. Y., is Chairman.

Corrosion Division Symposium Plans

The Corrosion Division is planning a symposium on "Mechanical Properties of Oxide Corrosion Products" for the 1967 Fall Meeting to be held in Chicago, Ill., Oct. 15-20, 1967. There will be a number of invited papers, and contributed papers are also solicited.

Suggestions are most welcome, and should be directed to the Chairman, Dr. D. A. Vermilyea, General Electric Research and Development Center, Schenectady, N. Y. 12301.

Dielectrics and Insulation Division Symposia Plans

The Dielectrics and Insulation Division has planned three symposia and general sessions for the Chicago, Ill., Meeting, October 15-20, 1967.

Capacitor Technology

This symposium is divided into two separate sections. The first section will deal only with the Electrolytic Capacitor in all its forms, including liquid and solid electrolytic types.

Topics of interest are as follows:

(a) Properties of new capacitor materials as related to capacitor performance.

(b) Fundamentals of electrolytic capacitor behavior, equivalent circuits, failure mechanisms, etc.

(c) New or novel forms of electrolytic capacitors, advanced technology.

(d) New manufacturing processes and their impact on capacitor performance.

The second section of this symposium proposes to provide broader coverage of the stated subject. Papers should deal with work that is either recent or fundamental. Subjects of interest are as follows:

(a) New materials and techniques in film capacitors.

(b) The physics of dielectrics and their properties.

(c) Life and environmental testing.

(d) Characteristics of breakdown and failure mechanisms.

(e) Film capacitors in microcircuit devices.

(f) New or novel capacitor fabrication techniques.

Contact Failure Arising from the Formation of Insulating Films

This symposium will deal with all aspects of its stated subject. Topics of interest therefore include:

(a) Failure mechanisms and mediums, tarnish films, and metal migration.

(b) Characteristic properties of formed films.

(c) Testing and evaluation contact performance and failure.

(d) Methods of preventing failure.

(e) Semiconductor device contact failure.

Electrets

This symposium proposes to provide a survey of current work in the field. It will therefore cover all phases of the electret phenomena. The basic categories of work to be presented are:

(a) New or recent theoretical studies.

(b) Experimental investigations, methods techniques, and results.

(c) Application or practical devices.

Electrodeposition Division Symposium Plans

The Electrodeposition Division plans a symposium on Dielectro-and Electrophoretic Deposition for the 1967 Fall Meeting to be held in Chicago, Ill., October 15-20, 1967.

Invited papers during the first half day of the symposium will survey the fundamental physics of dielectrophoresis and electrophoresis, as well as their biophysical and biochemical aspects. Another half day of invited papers will be directed to applied aspects, including equipment and techniques, metallic and inorganic coatings and deposits, organic coatings and deposits, and biological applications. The symposium will conclude with a half day of contributed papers.

The symposium Chairmen are Herbert A. Pohl, Oklahoma State University, and William F. Pickard, Massachusetts Institute of Technology.

Inquiries and suggestions about the symposium should be addressed to J. V. Petrocelli, Applied Research Office, Ford Motor Co., P.O. Box 2053, Dearborn, Mich. 48121.

Electrothermics and Metallurgy Division Symposium Plans

Protective Coatings

A symposium on Protective Coatings is being organized by the Electrothermics and Metallurgy Division as part of the 1967 Fall Meeting of the Society to be held in Chicago, Ill., October 15-20, 1967. Sessions are being planned on Coatings for Super Alloys, Coatings for Refractory Metals and Coated Steel Products. A general session is also planned. Additional sessions may be scheduled depending on the nature of the papers submitted for presentation.

In each of the above areas papers stressing applied or basic research investigations on methods of inorganic coating application, or relating the behavior of coated bodies to processing variables are desired. It is the purpose of this symposium to stress coating application technology rather than the properties of coated bodies. Papers which deal solely with the properties of coated products or structures will be considered for inclusion in the program only if the exact nature of the coating is specifically characterized.

General Sessions

General sessions on subjects that come within the scope of activity of the Division are also planned for the 1967 Fall Meeting. To assist potential contributors to decide whether their papers fall within the field of interest of the Division, the following paragraph from the Division's tentative statement of scope is reproduced:

In general, the purpose of the Divi-

We offer an UNUSUAL opportunity for a

SENIOR PHYSICAL OR ELECTROCHEMIST

to manage a battery separator division responsible for government and industrial sales, production and development of new materials. Experience with AgZn, AgCd and NiCd battery systems required. Company is a staff owned research organization located in New York City. Proprietary technology offers individual significant financial potential. Reply to Box No. B-7, c/o The Electrochemical Society, Inc., 30 East 42 Street, New York, N. Y. 10017.

SYMPOSIA PLANS continued

sion is to aid and encourage the advancement of electrochemical science and industry concerned with specialty materials and processes. As specific examples of field in which the Division has maintained interest and activity, there may be cited: materials such as refractory metals and compounds, intermetallics, graphite, fused salts, and rare earth metals; equipment for the utilization of electrical energy and materials synthesis; processes using arcs, vacua, plasma, and electron and ion beams; and phenomena such as melting, vaporization, reaction, sintering, diffusion or oxidation occurring at high-temperatures, high pressures or involving high temperature materials.

Papers of both fundamental and applied nature are welcome.

Inquiries and suggestions concerning this symposium or the general session program should be sent to the Symposium Chairman, S. T. Wlodek, Graham Research Laboratories, Jones & Laughlin Steel Corp., 900 Agnew Rd., Pittsburgh, Pa. 15230.

NEW BOOKS

"Dielectric Behavior of Physically Adsorbed Gases," by R. L. McIntosh. Published by Marcel Dekker, Inc., New York, 1966. 160 pages; $9.75.

"In . . . (this volume) . . . the present state of knowledge concerning the dielectric behavior of physically adsorbed gas molecules on solid surfaces is reviewed," (book jacket). Measurements, calculations and interpretations of dielectric properties are discussed theoretically and with the use of specific examples in a clear and lucid manner.

The comments that can be made are not on the content of the book, but on

McGOVERN SENTER & ASSOCIATES, Inc.
MANAGEMENT CONSULTANTS
ONE HUNDRED THIRTY-FOUR MAIN STREET
STONEHAM, MASSACHUSETTS

OPTO-ELECTRIC DEVICES
INFRARED PROPERTIES
CRYSTAL IMPERFECTIONS
FAN IN — FAN OUT
NOISE PROTECTION
RECOMBINATION

1) Microwave IC R&D—Si & GaAs planar—Ph.D./M.S.
2) Device Research Physicist—Gunn effect—Ph.D. Phys./E.E.
3) Epitaxial Compound Materials—Ph.D. Ch./Ch.E.
4) Materials Evaluation—Elect. & phys. meas.—Ph.D./M.S. Phys.
5) Thick/thin film, Monolith. Device Engineers
6) Process Engineers—IC, trans., diode, rectifier
7) Reliability Engineers—B.S. Ch. with circuitry experience
8) Jr. Development Engineers—Diffusion, masking, metallizing
9) Device Development Engineers—New IC products
10) Test Equipment Engineers—Linear & Digital IC

To investigate the above positions in confidence, call (collect) Charles S. Langenfeld, (617) 438-9100 or forward your resume to him at the address above.

PHYSICAL CHEMIST

Sprague Electric, the nation's leading manufacturer of electronic components, has an opening in its corporate Research and Development Center for a Physical Chemist with either a B.S. or M.S. degree and 0-5 years' experience. Projects involved are study of the properties and reactions of metal and oxide surfaces in non-aqueous solutions, as well as development programs relating these to improve electrolytic capacitors. Excellent working conditions with the most modern facilities. Location is at North Adams, Mass., in the Berkshire Hills, famous summer and winter resort area, near Albany, N. Y. Sprague Electric provides comprehensive employee benefits, including a company-financed educational program toward advanced degrees.

Send your resume in confidence to:

John F. Miller
Corporate Manager
Recruitment and Staffing
Sprague Electric Company
1033 Marshall Street
North Adams, Mass. 01247

SPRAGUE®
THE MARK OF RELIABILITY

An Equal Opportunity Employer

Call for Recent News Papers Luminescence Session

May 7-12, 1967, Dallas, Texas

The deadline date for the 75-word abstracts of Recent News Papers is Friday, March 31, 1967. Please send abstracts to: Paul Goldberg, General Telephone & Electronics Laboratories, Inc., 208-20 Willets Point Blvd., Bayside, N. Y. 11361.

The program will include contributions in the following areas:

Luminescent Materials

Luminescence Phenomena

Instrumentation for Study of Luminescence

Ten minutes, including discussion are alloted to each Recent News Paper. If more time is necessary for your presentation, please consult with the Program Chairman.

---

whether it should have been published as a separate book. The entire contents of this book could have been published in approximately twenty pages of a standard scientific journal, received wider distribution and have cost less.

"Pharmaceutical Pharmacy," Volume 1, Theory and Application, Edited by L. G. Chatten. Published by M. Dekker & Co., New York, 1966. 504 pages; $14.50.

This volume is basically an introduction to the various areas of analytical chemistry with examples of specific interest and techniques for the analytical chemist in the pharmaceutical industry.

"Solid State and Semiconductor Physics," by John P. McKelvey. Published by Harper & Row, Inc., New York, 1966. 512 pages; $13.75.

Designed for senior undergraduate or beginning graduate courses, this textbook contains an extensive introduction to selected topics of general solid state physics necessary for an understanding of semiconductors.

Presupposing a knowledge of neither quantum mechanics nor statistical mechanics, the book discusses both subjects on an elementary level; thus, it will successfully serve students majoring in electrical engineering, metallurgy, or chemistry, in addition to physics majors, who need an understanding of semiconductor physics.

The first eight chapters cover space lattices and crystal symmetry, x-ray diffraction, dynamical behavior of periodic lattices, introduction to statistical mechanics, thermal properties of crystals, free-electron theory of transport effects in solids, and quantum behavior of electrons in periodic crystals. The principles covered in these chapters are applied to a systematic and detailed study of semiconductors (book jacket).

The above abstract sums up the content of this excellent introduction to its field. It can be heartily recommended as the first introduction to this field.

"Advances in Chromatography," Volumes 2 and 3, Edited by J. Calvin Giddings and Roy A. Keller. Published by Marcel Dekker, Inc., New York, 1966. Volume 2, 377 pages; $14.50; Volume 3, 271 pages; $11.50.

Volume 2 contains the following monographs: "Ion Exchange Chromatography of Amino Acids: Recent Advance in Analytical Determination," P. B. Hamilton, "Ion Mobilities in Electrochromatography," J. T. Edward, "Partition Paper Chromatography and Chemical Structure," J. Green and D. McHale, "Gradient Techniques in Thin-Layer Chromatography," A. Niederwieser and C. C. Honegger, "Geology—An Inviting Field to Chromatographers," A. S. Ritchie, "Extracolumn Contributions to Chromatographic Band Broadening," J. C. Sternberg, "Gas Chromatography of Carbohydrates," J. W. Berry, "Ionization Detectors for Gas Chromatography," A. Karmen, and "Advances in Programmed Temperature Gas Chromatography," L. Mikkelsen.

Volume 3 contains "The Occurrence and Significance of Isotope Fractionation During Analytical Separations of Large Molecules," P. D. Klein, "Adsorption Chromatography," C. H. Giles and I. A. Easton, "The History of Thin-Layer Chromatography," N. Pelick, H. R. Bolliger, and H. K. Mangold, "Chromatography as a Natural Process in Geology," A. S. Ritchie, "The Chromatographic Support," D. M. Ottenstein, "Electrolytic Conductivity Detection in Gas Chromatography," D. M. Coulson, and "Preparative-Scale Gas Chromatography," G. W. A. Rijnders.

Notice to Members

April 1 is Cut-off Date

Your attention is called to Article III, Section 9 of the Society Constitution which states: "Any member delinquent in dues after April 1 of each year shall no longer receive the Society's publications, and will not be allowed to vote in any Society election until such dues are paid. All members in arrears for one year after the first of April shall lose their membership status and can be reinstated only by action of the Board of Directors." Members who have not sent in 1967 payments will be mailed a second notice in February and are urged to make payment promptly in order to avoid delay in receipt of JOURNALS.

NEW MEMBERS

It is a pleasure to announce the following new members of The Electrochemical Society as recommended by the Admissions Committee and approved by the Board of Directors in December 1966.

Active Members

Anderson, L. B., Columbus, Ohio
Billinghurst, R. G., Windsor, Ont., Canada
Birke, R. L., Cambridge, Mass.
Brown, Jr., J. J., Towanda, Pa.
Burrows, B. W., Waltham, Mass.
Carr, W. N., Dallas, Texas
Cheskis, E. M., Niagara Falls, N. Y.
Chiku, Takewo, Nagoya, Japan
Emmenegger, F. P., Zurich, Switzerland
Fawcett, W. R., Guelph, Ont., Canada
Hamilton, W. S., Denton, Texas
Hancock, H. A., Saskatchewan, Alb., Canada
Handelin, C. B., Walnut Creek, Calif.
Heit, A. H., Mt. Holly, N. J.
Howard, W. G., St. Paul, Minn.
Hoyt, P. L., Garland, Texas
Lasater, R. M., Duncan, Okla.
Lockwood, R. A., Northridge, Calif.
Myre, O. E. L., New York City, N. Y.
Pan, P.-T., Beloit, Wis.
Rose, D. J., Los Altos, Calif.
Sherer, J. B., Garland, Texas
Spitzer, R. H., Argonne, Ill.
Stoneburner, D. F., Dayton, Ohio
Susek, J. L., Milwaukee, Wis.
Swann, R. C. G., Palo Alto, Calif.
Taylor, B. F., Stittsville, Ont., Canada
Tefteller, Jr., J. W., Dallas, Texas
Vromen, B. H., Plainfield, N. J.
Washington, E. L., Manchester, Conn.
Weinlein, C. E., Milwaukee, Wis.
Woerner, L. M., Freeland, Mich.

Associate Members

Gast, L. A., Dallas, Texas
Selser, M. J., Cupertino, Calif.

Student Associate Members

Furtado, A. W., Ann Arbor, Mich.
Gupta, P. C., Kingston, Ont., Canada
Myers, R. L., Madison, Wis.
Sedlak, J. M., Toronto, Ont., Canada
Taylor, D. F., Toronto, Ont., Canada

Transfer from Associate to Active Membership

Wikstrom, L. L., Bronx, N. Y.

ADVERTISER'S INDEX

Patron and Sustaining Members
of
THE ELECTROCHEMICAL SOCIETY

Patron Members

Aluminum Co. of Canada, Ltd., Montreal, Que., Canada

Dow Chemical Co.
Chemicals Dept., Midland, Mich.
Metals Dept., Midland, Mich.

General Electric Co.
Capacitor Dept., Hudson Falls, N. Y.
Chemical Laboratory, Knolls Atomic Power Laboratory, Schenectady, N. Y.
Chemical Systems and Processes Laboratory, Research and Development Center, Schenectady, N. Y. (3 memberships)
Direct Energy Conversion Operation, West Lynn, Mass.
Lamp Div., Cleveland, Ohio
Materials & Processes Laboratory, Large Steam Turbine-Generator Dept., Schenectady, N. Y.

The International Nickel Co., Inc., New York, N. Y.

Olin Mathieson Chemical Corp.
Chemicals Div., Research Dept., New Haven, Conn.

Union Carbide Corp.
Divisions:
Carbon Products Div., New York, N. Y.
Consumer Products Div., New York, N. Y.

Westinghouse Electric Corp.
Electronic Tube Div., Elmira, N. Y.
Lamp Div., Bloomfield, N. J.
Molecular Electronics Div., Elkridge, Md.
Semiconductor Div., Youngwood, Pa.
Research Laboratories, Pittsburgh, Pa.

Sustaining Members

Air Reduction Co., Inc., New York, N. Y.

Allen-Bradley Co., Milwaukee, Wis.

Allied Chemical Corp.
General Chemical Div., Morristown, N. J.

Aluminum Co. of America, New Kensington, Pa.

American Metal Climax, Inc., New York, N. Y.

American Potash & Chemical Corp., Los Angeles, Calif.

American Smelting and Refining Co., South Plainfield, N. J.

American Zinc Co. of Illinois, East St. Louis, Ill.

American Zinc, Lead & Smelting Co., St. Louis, Mo.

The M. Ames Chemical Works, Inc., Glens Falls, N. Y.

Ampex Corp., Redwood City, Calif.

Armco Steel Corp., Middletown, Ohio

Basic Inc., Bettsville, Ohio

Bell Telephone Laboratories, Inc., New York, N. Y. (2 memberships)

Bethlehem Steel Corp., Bethlehem, Pa. (2 memberships)

Boeing Co., Seattle, Wash.

Burgess Battery Co., Freeport, Ill. (2 memberships)

Burndy Corp., Norwalk, Conn.

Canadian Industries Ltd., Montreal, Que., Canada

Carborundum Co., Niagara Falls, N. Y.

Chrysler Corp., Detroit, Mich.

Cominco Ltd., Trail, B. C., Canada (2 memberships)

Continental Can Co., Inc., Chicago, Ill.

Corning Glass Works, Corning, N. Y.

Diamond Alkali Co., Painesville, Ohio

Wilbur B. Driver Co., Newark, N. J.

E. I. du Pont de Nemours & Co., Inc., Wilmington, Del.

Eagle-Picher Co., Chemical and Metals Div., Joplin, Mo.

Eastman Kodak Co., Rochester, N. Y.

Eltra Corp.
Prestolite Div., Toledo, Ohio
C&D Batteries, Conshohocken, Pa.

The Electric Storage Battery Co., Philadelphia, Pa. (2 memberships)

Engelhard Industries, Inc., Newark, N. J.

The Eppley Laboratory, Inc., Newport, R. I.

Esso Research and Engineering Co.
Engineering Technology Div., Florham Park, N. J.

Exmet Corp., Bridgeport, Conn.

Fairchild Semiconductor Corp., Palo Alto, Calif.

FMC Corp.
Inorganic Chemical Div., Buffalo, N. Y.
Inorganic Chemicals Div., South Charleston, W. Va.

Foote Mineral Co., Exton, Pa.

Ford Motor Co., Dearborn, Mich.

General Motors Corp.
Allison Div., Indianapolis, Ind.
Delco-Remy Div., Anderson, Ind.
Research Laboratories Div., Warren, Mich.

General Telephone & Electronics Laboratories, Inc., Bayside, N. Y.

Globe-Union, Inc., Milwaukee, Wis.

Sustaining Members (cont'd)

B. F. Goodrich Chemical Co., Cleveland, Ohio

Gould-National Batteries, Inc., Minneapolis, Minn.

Great Lakes Carbon Corp., New York, N. Y.

Harshaw Chemical Co., Cleveland, Ohio (2 memberships)

Hercules Powder Co., Wilmington, Del.

Hill Cross Co., Inc., West New York, N. J.

Hoffman Electronics Corp., Semiconductor Division,
El Monte, Calif.

Honam Electric Industrial Co., Kwangju City, Korea

Honeywell, Inc., Minneapolis, Minn.

Hooker Chemical Corp., Niagara Falls, N. Y.
(3 memberships)

HP Associates, Palo Alto, Calif.

Hughes Research Laboratories, Div. of Hughes Aircraft Co., Malibu, Calif.

International Business Machines Corp., New York, N. Y.

International Minerals & Chemical Corp., Skokie, Ill.

International Resistance Co., Philadelphia, Pa.

ITT Federal Laboratories, Div. of International Telephone & Telegraph Corp., Nutley, N. J.

Jones & Laughlin Steel Corp., Pittsburgh, Pa.

K. W. Battery Co., Skokie, Ill.

Kaiser Aluminum & Chemical Corp.
Metals Div. Research, Permanente, Calif.
Div. of Metallurgical Research, Spokane, Wash.

Kawecki Chemical Co., Boyertown, Pa.

Kennecott Copper Corp., New York, N. Y.

Leesona Moos Laboratories, Div. of Leesona Corp.,
Great Neck, N. Y.

Arthur D. Little, Inc., Cambridge, Mass.

Lockheed Aircraft Corp., Missiles & Space Div.,
Sunnyvale, Calif.

Mallinckrodt Chemical Works, St. Louis, Mo.

Metal Pumping Services, Inc., Cleveland, Ohio

P. R. Mallory & Co., Indianapolis, Ind.

Melpar, Inc., Falls Church, Va.

Miles Chemical Co., Div. of Miles Laboratories, Inc.,
Elkhart, Ind.

Mobil Oil Corp., Dallas, Texas

Monsanto Chemical Co., St. Louis, Mo.

M&T Chemicals Inc., Detroit, Mich.

Nalco Chemical Co., Chicago, Ill.

National Cash Register Co., Dayton, Ohio

National Lead Co., New York, N. Y.

National Steel Corp., Weirton, W. Va.

North American Aviation, Inc., El Segundo, Calif.

Northern Electric Co., Montreal, Que., Canada

Norton Co., Worcester, Mass.

Owens-Illinois Glass Co., Toledo, Ohio

Pennsalt Chemicals Corp., Philadelphia, Pa.

Phelps Dodge Refining Corp., Maspeth, N. Y.

Philips Laboratories, Inc., Briarcliff Manor, N. Y.

Pittsburgh Plate Glass Co., Chemical Div., Pittsburgh, Pa.

Potash Co. of America, Carlsbad, N. Mex.

Radio Corp. of America
Electronic Components and Devices, Lancaster, Pa.
RCA Victor Record Div., Indianapolis, Ind.

Republic Foil Inc., Danbury, Conn.

Reynolds Metals Co., Richmond, Va.

Shawinigan Chemicals Ltd., Montreal, Que., Canada

Sonotone Corp., Elmsford, N. Y.

Speer Carbon Co.
International Graphite & Electrode Div.,
St. Marys, Pa.

Sprague Electric Co., North Adams, Mass.

Stackpole Carbon Co., St. Marys, Pa.

The Standard Oil Company of Ohio,
Cleveland, Ohio

Stauffer Chemical Co., Dobbs Ferry, N. Y.

Texas Instruments, Inc., Dallas, Texas
Metals and Controls Corp., Attleboro, Mass.

3M Company, St. Paul, Minn.

Titanium Metals Corp. of America, Henderson, Nev.

Tyco Laboratories, Inc., Waltham, Mass.

Udylite Corp., Detroit, Mich. (4 memberships)

United States Borax & Chemical Corp.,
Los Angeles, Calif.

United States Steel Corp., Pittsburgh, Pa.

Univac, Div. of Sperry Rand Corp., New York, N. Y.

Universal-Cyclops Steel Corp., Bridgeville, Pa.

Upjohn Co., Kalamazoo, Mich.

Varian Associates, Palo Alto, Calif.

Western Electric Co., Inc., Chicago, Ill.

Wyandotte Chemicals Corp., Wyandotte, Mich.

Yardney Electric Corp., New York, N. Y.